CRANFIELD INSTITUTE OF TECHNOLOGY

COLLEGE OF AERONAUTICS

Ph.D. Thesis

R.S. LANGLEY

THE DYNAMIC ANALYSIS OF OFFSHORE MOORING TERMINALS

Supervisor: Dr.C.L. Kirk

February 1983

Then he got into the boat and his disciples followed him.
Without warning, a furious storm came up on the lake, so
that the waves swept over the boat. But Jesus was
sleeping. The disciples went and woke him, saying
"Lord, save us! We're going to drown!"
He replied, "You of little faith, why are you so afraid?"
Then he got up and rebuked the winds and the waves and it
was completely calm.
The men were amazed and asked, "What kind of man is this?
Even the winds and the waves obey him!"

Matthew 8 : 23-27

SUMMARY

This Thesis investigates the methods which are currently available for the dynamic analysis of Offshore Mooring Terminals, particular regard being paid to Single Point Mooring (SPM) Terminals. Various aspects of the problem are considered in turn, these being the random vibration of non-linear systems, the analysis of catenary mooring lines, buoy dynamics, ship motions, second order (or slow drift) forces and motions, and low frequency motions caused by instabilities. These various aspects are then applied to the dynamic analysis of a Single Buoy Storage (SBS) System and the effect of the method of analysis employed, the system dimensions and the environmental conditions on the computed response is investigated.

A Time Domain investigation of the stability of the SBS System in the presence of wind and current alone reveals that the system is only unstable for combinations of wind and current which are unlikely to occur in practise. A static offset position is then assumed and the calculation of the three-dimensional first and second order response to random waves is performed in the Frequency Domain, linear wave theory being used. The first order wave forces are calculated by using strip theory for the tanker and Morison's equation for the buoy. The second order response in surge, sway and yaw is calculated by a reflection coefficient method, these coefficients being obtained from published literature. The non-linear mooring system and the drag forces acting on the buoy are linearised using the equivalent linearisation method, due account being taken of the coupling between the first and second order response. The model developed for the first order response of the system allows the use of a spreading function in the incident wave spectrum.

The accuracy of linearisation techniques and the statistics of the second order force and response are also investigated.

CONTENTS

LIST OF FIGURES

NOTATION

The notation used in this Thesis is as defined in the main text.

ACKNOWLEDGEMENTS

The author would like to thank the following people for the assistance they have given him over the last two years:-

Dr.C.L.Kirk-for all his help in both academic and personal matters

My parents and brothers - for their continued encouragement

Mr.R.Thorne and Mr. and Mrs.M.L.Robinson - 'how beautiful on the mountains are the feet of those who bring good news'.

The Aircraft Design Ph.D. and Research students, both past and present, who have made working in the department an interesting and varied experience. In particular Mr.P.Bose, Dr.D.M.Ahn, Mr.M.Alavi, Mr.R.X.Chen, Mr.J.M.Shanks and Mr.R.Ghadimi.

Tricia Forrest-Holden - for her patience in typing this Thesis

My wife - for her moral support.

1.0 INTRODUCTION

1.1 The Development of Single Point Mooring Terminals

Single Point Mooring Terminals (SPM's) are, by definition, mooring terminals to which a vessel is moored by one point only, this being usually the bow or the stern. The purpose of such an arrangement is that the vessel is free to 'weathervane' about the mooring point and thus reduce the loads in the mooring system by presenting the least resistance to the oncoming wind, waves and current. These terminals were initially developed for use at ports where shallow water or cost prevented the provision of a jetty, and the environmental conditions were such that the hitherto used multipoint moorings, which did not allow weathervaning, were incapable of restraining the vessel. The earliest type of SPM to be used was the CALM system (see section 1.3.1), which consists of a catenary moored buoy to which the vessel moors via a bow hawser. Oil is transferred to the buoy through a floating hose and passes to seabed pipelines via flexible risers. This system was first used in 1960 in the Port of Miri, Sarawak, the maximum vessel size which could be moored being 3,000 DWT. So rapid was the subsequent development of this SPM that within a year systems capable of handling 100,000 DWT supertankers had been developed. Although originally designed for offloading and loading tankers near to a port, the system was soon being used to load tankers at offshore oilfields either as a temporary measure, until pipelines could be installed, or as a permanent transport facility at marginal fields where a pipeline was not cost effective. The severe environmental conditions encountered at these sites led to the development of a number of different types of SPM, some of which are discussed in section 1.3. About 300 such systems are in use at the present time and the first oil to be brought ashore from the North Sea in 1975 was transported in a super-tanker which was loaded at a CALM buoy in the Argyll Field.

The first SPM's which were used at offshore oil fields were intended to act as 'filling stations' only, and production time was lost whenever a tanker was not connected to the terminal. In an attempt to increase the production rate at some sites, a tanker acting as a buffer storage unit would be left permanently moored to the buoy, and shuttle tankers would then be loaded from this vessel. The fact that oil can be shipped from tanker to tanker at a much greater

rate than the production rate of most oilfields means that with this SPM the field can be continually on stream. The system was first adopted in 1964 in the Persian Gulf, a 45,000 DWT buffer storage tanker being permanently moored to a CALM via a bow hawser. To date, approximately 15 of these systems have been used worldwide, the most recent being that installed in the Indonesian Handil Field in 1977. The environmental conditions in which this type of system can be used effectively are severely limited - in even moderate seas there can be the danger of collision between the tanker and the buoy, which is known as 'buoy kissing'. In 1974 this problem was overcome with the installation of the first 'yoke' moored vessel in the Tunisian Ashtart Field. The bow hawsers were replaced with a yoke in the form of a rigid 'A'-frame, which was pivoted at the bow of the tanker in such a way as to allow relative heave motion between the vessel and the buoy. The connection at the buoy was via a swivel which afforded the tanker freedom to weathervane to face the incident environmental conditions. The oil was no longer transferred to the vessel via floating hoses, but was routed through the rigid yoke structure, an arrangement which overcame the frequently recurring problem of hose failure. This system is known as the Single Buoy Storage (SBS) system, eight of which are now in use around the world. The detailed dynamic analysis of this system is discussed in Chapters 8 and 9 of the present work. Yoke moorings have now been developed in which the yoke is connected to systems other than a catenary moored buoy, overviews of which have been given by Smulders and Remery (ref.1) and McLeod and Smulders (ref.2). Figures 1.1 and 1.2 summarise the yoke mooring systems which have been installed around the world to date, a description of the various types being given in section 1.4.

A recent expansion of the role of the yoke moored vessel has been the development of the Floating Production, Storage and Offloading System (FPSO), in which the permanently moored vessel not only acts as a storage system, but also houses production equipment. This obviates the need for the crude oil to be processed at either a fixed or floating production platform before being passed onto the SPM system, a property which holds particular interest for deep water or marginal fields. Of the sixteen yoke moored vessels which have been installed to date, four have housed processing equipment.

It is envisaged that as oil supplies become increasingly scarce, the short lived oil fields which are now considered to be 'marginal' will become economically viable. It is likely that FPSO's and yoke moored storage vessels, rather than fixed platforms and pipeline systems will be used to develop these fields, and thus the SPM can be expected to play an increasingly important role in the future.

1.2 Dynamic Characteristics of Single Point Mooring Terminals

Since SPM's are intended to be compliant systems, an understanding of their dynamic characteristics is essential at the design stage. The response of a SPM, with a tanker attached, can be categorised into the three sections given below.

1.2.1 First Order Motions

These are motions which have the same frequency range as the incident waves (0.2 - 1.6 rad/sec) and are a result of the first order dynamic subsurface pressure forces acting on the system. Typically the first order motions in the horizontal plane will be inertia dominated, whereas those in the vertical plane will be stiffness dominated. Well established mathematical models are available for the calculation of the first order response of floating bodies, and good agreement with model tests and full scale measurements can be obtained. The first order response of a mooring buoy and VLCC (very large crude carrier) are discussed in Chapters 4 and 5 respectively, and the analysis of these chapters is applied to the dynamic analysis of a SBS system in Chapter 8. Chapter 3 discusses the non-linear restoring forces which are provided by a catenary mooring system.

1.2.2 Second Order Motions

Second order, or 'slow drift', motions occur at frequencies which are well below that of the lowest frequency component of the incident wave spectrum. These motions are caused by non-linear effects which produce forces which are proportional to the product of two first order terms. In a random seastate, two first order terms x and y will have the form:-

$$x = \sum_n a_n \sin(\omega_n t + \varepsilon_n) \; ; \quad y = \sum_n a_n' \sin(\omega_n t + \varepsilon_n) \qquad (1.1)$$

The product of these two terms will then be:-

$$xy = \sum_n \sum_m a_n a'_m \sin(\omega_n t + \varepsilon_n)\sin(\omega_m t + \varepsilon_m)$$

$$= \sum_n \sum_m a_n a'_m \tfrac{1}{2}\{\cos[(\omega_n-\omega_m)t+\varepsilon_n-\varepsilon_m]-\cos[(\omega_n+\omega_m)t+\varepsilon_n+\varepsilon_m]\} \quad (1.2)$$

from the first term in which it can be seen that non-linear effects will product low frequency forces which have frequencies ranging from zero to the bandwidth of the incident wave spectrum. Physically, this can be thought of as a 'beating' or frequency modulation effect. Although the second order forces are not large, they will occur at the low natural frequencies of the surge, sway and yaw motions of the vessel and thus induce resonance. Damping in these modes, particularly surge, is light and thus large amplitude responses can be produced. Second order effects are discussed in detail in Chapter 6, and Chapter 8 contains an analysis method for the calculation of the second order response of a SBS system.

1.2.3 Limit Cycle Oscillations Caused by Instabilities

Due to the complex nature of the current forces which act on a VLCC, there is the possibility of a SPM system exhibiting unstable motions. The most commonly reported instance of this is the 'fish-tailing' motion of a tanker moored via a bow hawser. This effect can be explained physically by reference to Figure 1.3 (after ref.3). With the vessel in position (1), lifting forces due to current act to move the vessel to the left. This motion will continue until the bow hawser becomes taut (2), after which the lifting forces will cause the vessel heading to change. Once the angle of incidence of the vessel to the current passes through 0^o, the lift forces change sign and the vessel is moved to the right, as shown in stages (3) and (4). Eventually the tension in the bow hawser becomes such that the lift forces act to rotate, rather than translate, the vessel, and the vessel heading again passes through 0^o, causing a reversal in the lift force. The vessel moves to the left and the process is repeated. In this way, large amplitude low frequency motions of the vessel can be produced in the presence of current alone. A mathematical model of this effect, which is applicable to both a bow moored tanker and a SBS system is presented in Chapter 7.

Both instabilities and second order effects produce low frequency large amplitude motions in the horizontal plane, and in those systems which are unstable it is difficult to distinguish between these two phenomena in either model tests or full scale measurements. The coupling which can occur between these two effects is highly complex and is only amenable to study using time domain computer programs. In Chapter 7 it is shown that the SBS system tends, in general, to be stable which allows the slow drift analysis of Chapter 8 to be performed without reference to limit cycle oscillations.

1.3 Filling Station Single Point Mooring Terminals

1.3.1 The Catenary Anchor Leg Mooring (CALM) System

As previously mentioned, the CALM system which was installed in 1960 in the Port of Miri was the world's first SPM terminal. A typical CALM system is shown in Figure 1.4. The CALM consists of a cylindrical buoy of diameter 10-20m and depth 3-5m which is anchored to the seabed via four, six or eight catenary anchor lines. The loading tanker is moored to a turntable at the top of the buoy via one or more bow hawsers. At the centre of the turntable lies a fluid swivel, which is connected to a seabed manifold via flexible hoses, which can be arranged in a number of different configurations in an attempt to avoid snatch loads. Floating hoses lead from the fluid swivel to the midship manifold of the moored vessel, these hoses being allowed to drift freely when the vessel is not present. Many variations on the basic CALM design have now evolved, and a detailed discussion of these, along with the engineering aspects of the system has been given in ref.4.

A dynamic analysis of the CALM system, without the attached tanker, could be performed using the analysis in Chapters 3 and 4. The effect of the vessel could be included by using the analysis of Chapters 5, 6 and 7.

1.3.2 The Single Anchor Leg Mooring (SALM) System

The SALM system consists of a buoy moored to the seabed via one anchor chain, as shown in Figure 1.5. The SALM is similar to the CALM in that the tanker is moored to a turntable at the buoy with a bow hawser, but the oil is now transferred via a hose which rises to float on the surface from a product swivel on the seabed. When this system is used in deepwater the chain, or part of the chain, is replaced with tubular risers at the top of which is placed the product swivel. The

mooring system stiffness is provided by the pretension induced in the mooring chain by the excess buoyancy of the buoyancy unit. The first SALM was installed at Barga, Libya in 1969, and since then more than twenty others, each having variations upon the basic design, have been installed around the world. The main advantages of the SALM over the CALM are that the system is more easily extended to deeper water, and the fact that the problem of snatch loads in the underbuoy hoses is removed. Disadvantages are that the anchor base needs to be piled, and that the fluid swivels are submerged and thus less easily serviced. Detailed accounts of the historical and engineering developments of the SALM can be found in refs.4 and 5.

A dynamic analysis of this type of system could be performed using the analysis of Chapters 4,5,6 and 7.

1.3.3 The Fixed Tower

An alternative to the compliant SPM's described above is the fixed mooring tower. This takes the form of a jacket structure surmounted by a turntable, to which a loading vessel moors via bow hawsers. A typical fixed tower type SPM is shown in Figure 1.6. By attaching the riser pipes to the legs of the jacket structure, most problems caused by the dynamic response of these pipes are eliminated. The use of this type of system is limited to shallow water, since the cost of the jacket structure is roughly proportional to the cube of the water depth. To date, this system has proved popular in Italy only. More details can be found in refs.4 and 5.

1.3.4 The Articulated Tower

The articulated tower SPM (shown in Figure 1.7)has the advantages of the fixed tower as far as the riser pipes are concerned, whilst still being compliant. Buoyancy tanks within the structure provide a restoring force when the system is rotated about the universal joint which is built into the mooring base. The ballasting arrangement of the tower is such that the universal joint is kept under compression. The use of a floating hose between the tower and the tanker is avoided by the provision of a rigid boom, from which a hose is suspended to a bow manifold in the vessel. Further details of this system can be found in ref.4.

The dynamic response of the tower alone has been studied in three dimensions in ref.6. The first and second order motions of the

tower and attached tanker have been studied in two dimensions in ref.7. A complete three dimensional analysis of both the first and second order response of the system, as well as the study of instabilities, could be performed by utilising the analysis of Chapters 5,6 and 7.

1.4 Permanent Storage Single Point Mooring Terminals

1.4.1 The Single Buoy Storage (SBS) System

The SBS system is basically a CALM system in which the mooring hawsers have been replaced with a rigid yoke, as shown in Figure 1.8. The yoke is pivoted at the tanker along the horizontal axis and is connected to the buoy via a swivel which allows the tanker to weather-vane about the buoy. There are no articulations to allow independent roll and pitch motions of the buoy and the yoke, and thus the buoy swivel must be designed to withstand considerable bending moments. One reason for this design approach is that the oil is routed through the yoke structure, and passes through the swivel joint at the buoy. It is considered to be easier to increase the size of this swivel to take the large bending moments rather than to design a complicated 'universal' fluid swivel which may be prone to failure. Sagot and Heijst (ref.8) claim that further articulations between the buoy and the yoke would lead to large pitching motions of the buoy, which would be unacceptable for the underbuoy hoses. This arguement is questionable, since Bluewater Terminal Systems n.v. have successfully produced a yoke-CALM system in which the yoke and the buoy are allowed to pitch independently. The weathervaning motions of the vessel are catered for by a fluid swivel, whereas the buoy pitch motions are provided for by a short length of flexible hose, as shown in Figure 1.9. In both this and the conventional SBS system, the oil is transferred across the tanker hinges in flexible hoses. More details can be found in ref.4.

Since the SBS system requires no astern propulsion to prevent the tanker from colliding with the buoy, the yoke structure can be connected to either the bow or the stern of the vessel. The advantages in favour of a stern mooring have been listed by Smulders and Remery (ref.1) as follows:-

1) The stern mooring requires less structural modification to the vessel, since this portion of the ship tends to be of a stronger construction than the bow.

2) The centre of gravity of the vessel tends to be towards the stern, and thus a stern mooring will reduce the first order rotation

and vertical reactions induced in the yoke (see the results given in section 9.5.2).

3) A stern mooring will position the crew quarters upwind of storage tanks and vents.

4) Transportation to the operation site is easier when the buoy is connected to the stern of the vessel. Several tankers in which a stern mooring has been used have sailed to location under their own power.

5) Modifications to convert the tanker back to normal use are minimal.

Matched against these are the following disadvantages:

1) The mooring loads in the horizontal plane can be higher for a stern moored vessel (see section 9.5.2).

2) The stern is much closer to the sea surface than the bow of the vessel, and thus a stern mooring may lead to the shipping of water in rough weather. This rules out the use of a stern mooring where the design storm conditions have a significant wave height greater than around 10m.

Of the 14 yoke moorings that had been installed at the time of ref.1, 5 had been stern moored.

The dynamic response of the SBS system is analysed in detail in Chapters 8 and 9, this system being chosen as typical of the modern rigid yoke mooring terminals.

1.4.2 The Yoke-CALM System

This system, which has been discussed in the previous section, is shown in Figure 1.9. The system differs from the SBS in that there is an additional hinge between the yoke and the buoy, and thus an extra degree of freedom. The dynamic analysis of this system will be similar to that contained in Chapter 8 for the SBS, the only major difference occurring in the constraint equations. One less constraint is present, which results in an additional equation of motion.

1.4.3 The Yoke-SALM System

The Yoke-SALM, which is also known as the Single Anchor Leg Mooring Rigid Arm (SALMRA), is shown in Figure 1.10. The yoke-SALM is basically a SALM in which the mooring hawser has been replaced by a rigid yoke structure, which is pivoted horizontally at the tanker and connected to a triaxial universal joint/mooring swivel arrangement

on the top of the buoy. To date only one SALMRA has been installed, this being in the Santa Barbara Hondo Field. This system was developed by Exxon and Imodco and was installed in 1981 in 150m of water. Special care was taken to ensure that the system was capable of withstanding the earthquake loads which are likely to occur in that part of the world. The design storm considered had a significant wave height of 6.7m. More details of this system can be found in ref.9.

The dynamic analysis of the yoke-SALM could be performed along similar lines to that contained in Chapter 8 for the SBS system. Differences occur in the number of degrees of freedom (6 for the SALMRA, 8 for the SBS) and the restoring forces provided by the mooring system.

1.4.4 The Yoke Tower System

The first yoke tower system was installed in 122m of water in the Garoupa Field offshore Brazil, in 1980, (see Fig.1.11) and is a modified form of the articulated tower SPM - a fluid swivel at the top of the tanker allows for weathervaning motions of the vessel, and bearings between the yoke and the tower allow for differential roll and pitch motions. A novel feature is that there is an emergency discount device between the yoke and the tower, which allows the vessel to escape from impending collision or fire.

A second yoke tower system was installed in the North Sea Fulmar Field in 1981. In order to cope with the severe design storm conditions in this area, vessel size was increased from the 54,000 DWT of the Garoupa Field vessel to 210,000 DWT in an attempt to reduce the first order motions (see section 9.5.1). The use of this system in deep water is limited by the large bending moments which can occur in the tower. One possible way of overcoming this problem is to add an additional articulation to the tower, a modification which will significantly increase the cost. Further details can be found in ref.4.

Chakrabarti and Cotter (ref.10) have analysed the first order motions of the Yoke Tower system in two dimensions using standard methods. This work could be extended to a three dimensional analysis of both the first and second order response of the system, using the analysis of Chapters 5,6 and 8.

1.4.5 The SALS System

The SALS (Single Anchor Leg Storage) is fundamentally different from other yoke mooring systems in that the yoke structure houses a buoyancy chamber (see Figure 1.12). It is this buoyancy chamber which

produces the pretension in the riser, which in turn produces a restoring force when the vessel is displaced. The SALS was developed by SBM Inc. and first installed in the Spanish Castellon Field in 1977, in 116.7m of water. The fact that the buoyancy is provided by the yoke structure means that the riser can be fairly slender, which will reduce the wave forces acting on it and thus the induced bending moments. This makes the SALS applicable to deeper waters. The Castellon Field SALS used a chain link riser to which production and wellhead control lines were connected. A later SALS installed in the Malaysian Pulai Field in 1978 replaced this chain link system with a ring stiffened tubular structure of diameter 2m. In both systems the base of the riser is connected to an anchor base via a universal joint. Flexible jumper hoses are used to link the seabed manifold to the production line above this joint. A universal joint connects the riser to the yoke, and the product and wellhead control lines are passed through a multi-pass process and control swivel. Further information on the SALS can be found in refs.4 and 12.

Langley and Kirk (ref.11) have analysed the first and second order dynamic response of this system in two dimensions, and obtained reasonable agreement with model test results. Two buoyancy chamber configurations were considered - the conventional cylindrical chamber and a U-shaped chamber proposed for use in the North Sea. This analysis could be extended to three dimensions by use of the analysis of Chapters 5, 6 and 8.

1.4.6 The Imodco Bow Mooring System

This system, shown in Figure 1.13, remains as yet a proposal. The mooring yoke is replaced with a rigid attachment connected to the bow of the tanker, the base of which houses a swivel assembly to which catenary mooring lines are attached. This SBM can be considered as an extension of the SBS system for deep waters. As water depth increases, the size of the SBS buoy must increase in order to provide the required buoyancy for the mooring lines. This increase in the buoy size causes an increase in the wave forces and thus the structural loads within the system, placing a definite limit on the water depth in which a SBS system can be used. The Imodco system removes this problem by an arrangement in which the buoyancy forces required to support the mooring lines are provided by the vessel itself. Although Imodco claim that

this system is suitable for waterdepths up to 700m, it is yet to be tested, and it is possible that the vessels weathervaning abilities may not be equal to those of other types of permanent mooring system.

The first and second order responses of this system could be analysed using the analysis of Chapters 3,5,6,7 and 8.

1.5 Design Codes Relating to Single Point Mooring Terminals

The role of design rules and guidelines in the design of offshore structures can be summarised by stating the Foreword to the Det norske Veritas "Rules for the Design, Construction and Inspection of Offshore Structures", 1977:-

> "The intention of these Rules is to lay down minimum requirements regarding structural strength, serviceability, and inspection of offshore structures.
>
> The Rules are intended to be used where Det norske Veritas is requested to carry out surveillance of the design and construction of an offshore structure.
>
> Where Det norske Veritas is recognized as an inspection body by National Authorities, the Rules will serve as a supplement to any National Regulations that may exist.
>
> Where discrepancy may exist between National Regulations and these Rules, the former will apply".

The enforcement of various design rules is therefore a National affair. Usually, before an offshore structure can be installed, a Certificate of Fitness must be obtained from an independent body such as Lloyds or Det norske Veritas (DnV), which has led to the production of guidelines by these bodies. Concerning Dynamic Analysis, section 4.5.1.5 of the above mentioned DnV rules states that:-

> "Dynamic loading effects shall be determined by use of recognized methods of analysis and realistic assumptions as regards loadings, material properties and analytical methods".

This rather vague statement is clarified by more specific guidelines given in Appendix G of the rules. Of particular relevance to SPM's is section 4.5.1.6., which states:-

> "The effects of low frequency motions shall be thoroughly investigated as far as such phenomena may influence the loading effects."

In other words, the slow drift and unstable motions of the system must be closely examined.

In 1974 the American Bureau of Shipping (ABS) published "Rules for Building and Classing Single Point Mooring Terminals". This report dealt with the structural design and fabrication of SPM's, as well as giving design rules for catenary mooring chains and bow hawsers. In 1977 DnV published a tentative report "Rules for the Design,Construction and Inspection of Offshore Loading Systems", which concerned SPM's in relatively deep water. In the same year Flory et al, sponsored by the United States Coastguard, produced "Guidelines for Deep-water Port Single Point Mooring Design", which is an extensive report covering all aspects of filling station type SPM's. The American Petroleum Institute (API) specification 2F, Mooring Chain (1977), which was developed to serve as an inspection criteria for chain for drilling vessels, can also be applied to SPM mooring chains. As well as the more specific rules and guidelines, general guidelines such as the British DD55 : 1978 can be applied to the structural design of SPM systems.

In addition to the generally available material, individual companies in the field will have at their disposal a wealth of information based upon past designs and model tests, which should help to ensure a continuing improvement in the safety and reliability of all types of Single Point Mooring Terminal.

1.6 Analysis Methods for Single Point Mooring Terminals

1.6.1 Model Tests

One stage in the design process of a SPM terminal is the verification (or otherwise) that the system is able to withstand the environmental loads. Since SPM's are compliant, this must take into account the dynamic response of the system, which can be simulated using either a mathematical or a physical model. Physical model tests have been discussed at length by Newman (ref.13) and Pinkster and Remery (ref.14), and the specifications of the various model basins which are available throughout the world can be found in ref.3. The scaling factors which are used in model tests are based upon the Reynolds number,which represents the ratio of inertial forces to viscous forces, and the Froude number, which represents the ratio of inertial forces to gravitational forces. For a floating body under-

going oscillations of frequency ω, the Reynolds number is defined as $\omega\ell^2/\nu$, and the Froude number as $\omega(\ell/g)^{\frac{1}{2}}$, where ν is the kinematic viscosity of the fluid and ℓ is some typical dimension of the body. Ideally, these two numbers should have the same value for the model and the full scale structure, in which case the ratio $\ell^{\frac{3}{2}}g^{\frac{1}{2}}/\nu$ would remain constant. However, unless a centrifuge or a superfluid is used, g and ν will be fixed, while ℓ will change, which implies that under normal circumstances it is not possible to have both Reynolds number and Froude number similitude. Usually, Froude number scaling (between 1:50 and 1:70) is used, it being argued that viscous effects play a relatively small part for large offshore structures. Although this is true for the high frequency motions of SPM systems, the low frequency second order response is fairly sensitive to the level of viscous damping which is present (see section 9.4.8) and thus model tests are unlikely to produce an accurate representation of these motions.

Model testing is perhaps the most widely used method for SPM terminals, it's main advantage being that non-linear effects which are difficult to model theoretically can easily be incorporated into the model. These include breaking waves, the shipping of water on the deck of the vessel and non-linear mooring characteristics. Disadvantages of this type of testing are that it is expensive and cumbersome - to study the effect of a change in the dimensions of the system, for example, requires the construction of a new model. Also, results obtained for the second order response are likely to be suspect due to the above mentioned difficulties in scaling the viscous forces.

1.6.2 Theoretical Models

The various mathematical models which have been developed to study the dynamic response of SPM systems are described in section 1.7. Each of these models requires solution by a digital computer. The accuracy of a mathematical model is limited by the degree to which the structure and the fluid are idealised and also by the level of analysis which is employed. At the present stage there are some effects, such as the shipping of water on the deck, which cannot be simulated theoretically. All mathematical models contain some aspects which are based upon experimental results (e.g. the calculation of current loads on VLCC's is based on empirical formulae) and thus no model can

claim to be completely theoretical.

Once developed, the advantage of a computer based mathematical model is that the study of changes in the dimensions of the system and the environmental conditions requires only a change in the program input data, and thus parametric studies can be done at a much lower cost than in a model basin. Perhaps the ideal method of performing the dynamic analysis of a SPM system would be a short series of model tests, against which a mathematical model could be calibrated, followed by a computer based parametric study.

1.7 Literature Survey of the Dynamic Analysis of Single Point Mooring Terminals

Chapters 2 to 7 each concern some particular aspect of the dynamic analysis of SPM terminals, and specific literature surveys concerning these are to be found within the relevant chapter. The purpose of the present section is to summarise the published literature which is concerned with the complete dynamic analysis of a SPM system. Most of the published work which falls into this category deals with filling station type SPM's - of the 12 references listed below, only 2 deal with yoke moored tankers, while 7 deal with vessels moored by a bow hawser and 3 are concerned with the second order surge response of a vessel with a general mooring arrangement.

Much of the work done in this field before 1976 has been summarised in a review paper by Owen and Linfoot (ref.15) who cite 58 references. Large sections of this work have now been superceded by recent advances in the computation of current and wave drift forces acting on VLCC's. A later review paper, published in 1979 by Loken and Olsen (ref.16) provides a more up to date view of the state of the art as regards slow drift forces and motions. This paper cites 24 references. The 5 most recent papers on the dynamic analysis of filling station type SPM's are detailed below.

1) Wichers (1979,ref.17). This paper presents a time domain analysis of the limit cycle oscillations performed by a tanker moored by a bow hawser to a fixed point, in the presence of current and wind alone. The analytical results are compared with those of model tests and a reasonable level of agreement is found. Perhaps the greatest contribution made by this paper is in the semi-empirical formulae which are used to describe the viscous forces acting on a moving VLCC in the

presence of current. The author states that both first and second order wave forces, as well as the buoy motions, need to be included to complete the model.

2) Ratcliffe and Clarke (1980, ref.18). A three degree of freedom time domain model is presented for the horizontal motions of a tanker moored via a bow hawser to a fixed point. The exciting forces considered are those due to wind, current and second order wave effects (slow drift). Particular attention is paid to the role played by the wind, which is considered to be gusting, a harmonic series being used to describe the instantaneous wind speed. The model which is used to represent the slow drift forces is based upon the time history of the square of the wave height, although no details are given. This paper gives a brief note as to how the motions of the SPM terminal itself can be included.

3) Molin and Bureau (198), ref.19). A complete model of a tanker moored via a bow hawser to a mooring buoy is presented. The motions are broken down into the low frequency response in surge, sway and yaw and the high frequency response in all degrees of freedom. A time domain program for the surge, sway and yaw response produced by current, wind and slow drift forces is developed. To incorporate the first order response, the position of the tanker as given by the time domain program is 'frozen' at a particular time and used as a mean position about which the first order motions are calculated using frequency domain techniques. Although the mooring buoy motions are not included in the low frequency response, the first order response of this buoy is taken into account. In calculating the first order motions, non-linear drag forces are neglected. In this way the maximum hawser tension which is likely to occur when the tanker is at any point on its low frequency response can be estimated. The time histories of the slow drift forces are calculated using a state of the art 'reflection coefficient' method, due account being taken of the instantaneous vessel heading. These 'reflection coefficients' are the non-dimensionalised mean forces acting on the system in regular waves (see Chapter 6). The method of calculating the instantaneous current forces acting on the vessel differs from that of Wichers (ref.17), and is discussed in section 7.3.2.

4) Sørheim (1981, ref.20) The analysis of this paper follows that of Molin and Bureau (ref.19), except that a different formulation of the second order forces is used. The time histories of the second order forces are calculated from the time history of the wave profile using reflection coefficients whose dependence on the heading of the vessel is approximated by simple formulae. Although this method requires less computer time than that used by Molin and Bureau (ref.19) the results are liable to be far less accurate.

5) Oppenheim and Wilson (1982, ref.21) This paper presents a full time domain model of a floating vessel moored by any arrangement of mooring line. Particular regard is paid to the accurate determination of the stiffness properties of the mooring system. The spectra of the slow drift forces are calculated using reflection coefficients whose dependence on the heading of the vessel are approximated by simple formulae, and the time histories of the slow drift forces are calculated from these spectra using the 'Monte Carlo' method (see ref.22). Kaplan (ref.23) has pointed out that this method is in error as it leads to slow drift forces which have a Gaussian distribution, which is not the case in practise.

The above references are all concerned with the time domain analysis of SPM systems. In 1975 both Bowers (ref.24) and Pinkster (ref.25) presented frequency domain methods for calculating the second order surge response of a vessel moored in head seas by any general linear mooring arrangement. The Bowers method is based on the second order fluid potential, whereas the Pinkster method uses reflection coefficient techniques. Both these methods are discussed in Chapter 6. Roberts (1981, ref.26) has solved the same problem using the Fokker-Planck equation (see ref.27), although the solution involves certain assumptions about the incident wave spectrum which are unlikely to be true in practise.

Very little published literature concerning the dynamic analysis of yoke moored vessels is available. In 1978 Chakrabarti and Cotter (ref.10) presented a two-dimensional frequency domain analysis of the first order surge, heave and pitch motions of a yoke tower system. In 1982 Langley and Kirk (ref.11) presented a similar analysis of a SALS system, although in this case the second order surge response was included, a comparison being made between the

results obtained by the Bowers and Pinkster methods and by tank testing (ref.24 and 25). Although a considerable amount of published literature is available on various aspects of the dynamic analysis of SPM systems, this completes the material concerning the complete dynamic analysis of those systems which have been published to date.

1.8 The Scope of the Present Work

The present work examines in turn various aspects of the dynamic analysis of offshore mooring terminals, which are then applied to the dynamic analysis of a SBS system. This analysis is performed in the frequency domain, which allows a physical insight into the effect of various parameters on the first and second order response of the system. A chapter by chapter account of the work is given below.

Chapter 2 investigates the analysis methods which are currently available for solving the problem of the random vibration of non-linear systems. Offshore dynamics problems fall into this category since the ocean waves are random and non-linearities such as drag forces and non-linear mooring systems occur. The accuracy of various approximate methods of solution is evaluated by comparison with time domain results, and recommendations are made.

Chapter 3 investigates the non-linear stiffness properties of catenary anchoring systems. The stiffness curve for a single anchor line is found and used to construct the stiffness properties of a complete mooring system. A new method of linearising these stiffness properties in the horizontal plane, taking into account both first and second order motions, is also presented, the method being based on a linearisation technique discussed in Chapter 2.

Chapter 4 considers mooring buoy dynamics and derives the added mass, damping and stiffness matrices for a CALM/SBS type mooring buoy. The damping matrix contains terms which arise from the linearisation of the drag forces acting on the buoy, the linearisation method being discussed in Chapter 2. The inertia forces and moments acting on the buoy in regular waves are also derived.

Chapter 5 presents a summary of the techniques which are currently available for the calculation of first order ship motions. The strip theory method is discussed in detail and the first order wave forces, together with the added mass, potential damping and stiffness matrices

yielded by this method are given. Viscous effects acting in roll, surge, sway and yaw are also discussed.

Chapter 6 concerns the second order or 'slow drift' response of moored structures. The state of the art methods of calculating the mean drift forces in regular waves and the slowly varying forces in irregular waves are discussed, with some of the most commonly applied approximations. New work on the statistics of the slow drift forces is included, as well as a study of the sensitivity of the slow drift response to the type of wave spectrum considered and the shape of the 'reflection coefficient'.

Chapter 7 presents a time domain model for the unstable motions of a SPM system. This model is an extension of that developed by Wichers (ref.17) and is capable of dealing with either a tanker moored via a bow hawser to a fixed point, or a SBS system. The stability of the SBS system is investigated using this model. By including the mean drift forces, the use of the model is extended to the calculation of the static equilibrium position of stable systems.

Chapter 8 applies the analysis of the preceding chapters to the complete dynamic analysis of a SBS system. A fully three-dimensional model is presented, with the option of using either a unidirectional incident seastate or a spreading sea. Both the first and second order motions of the system are included in the model, due account being taken of the coupling caused by the non-linear mooring system and the drag forces acting on the buoy. The model is formulated in the frequency domain and differs from those which are to be found in the published literature in two regards - (1) No other model dealing with the three-dimensional first order response of a yoke moored tanker has been found in the published literature, and (2) No other work concerning the frequency domain solution of the coupled slow drift response of a moored vessel has been found. The advantage of dealing with the second order response in the frequency domain is that a physical insight into the effect of various parameters can be obtained, whereas with a time domain solution it is difficult to separate the effect of the various factors.

Chapter 9 presents the results of the analysis of Chapter 8 for a wide range of cases, from which various conclusions about the analysis methods used and the nature of the response of the system can be drawn.

2.0 ANALYSIS METHODS FOR SOLVING LINEAR AND NON-LINEAR OFFSHORE DYNAMICS PROBLEMS

2.1 Introduction

Due to the random nature of the offshore environment, the response of an offshore structure will be a random process which cannot be defined deterministically, i.e. it is not possible to state absolute maximum values. The problem for the offshore engineer is then to find functions which define this random process in sufficient detail for maximum expected values and other properties such as the number of cycles at a certain level (used in fatigue calculations) to be obtained. A random process $x(t)$ is often defined by its spectrum $S_x(\omega)$ or by its joint probability density function (jpdf) $p(\ddot{x},\dot{x},x)$, these descriptions being independent i.e. a process with a particular type of jpdf can have any shape of spectrum, and vice-versa. Although either can be used to find the mean squared value of the process, the peak value can only be estimated if the probability density function of the maxima of the process, $p_m(x)$, is known. Thus in order to completely define a random process it is sufficient to know $p(\ddot{x},\dot{x},x)$, from which $p_m(x)$ can be found, or alternatively to know both $S_x(\omega)$ and $p_m(x)$. The problem is then to find these functions for the response when the wave environment is defined as having a Gaussian profile and some specified spectrum (see Appendix A). The purpose of this chapter is to examine and evaluate the various techniques which are currently available and to note those which are applicable to the dynamic analysis of offshore mooring terminals. For simplicity a single degree of freedom system will be considered, which may be either linear or non-linear and which may have either Gaussian or non-Gaussian excitation. A summary of the methods of analysis which are discussed below is given in Figure 2.1.

2.2 Linear Systems

2.2.1 Spectral Analysis

A typical linear single degree of freedom system has the form:

$$\ddot{x} + 2\beta\omega_n\dot{x} + \omega_n{}^2x = F(t) \qquad (2.1)$$

where β is the damping ratio, ω_n is the natural frequency and $F(t)$

is the exciting force divided by the mass of the system. If the spectrum of F(t) is known to be $S_F(\omega)$ then the standard result for the spectrum of response is:-

$$S_x(\omega) = |H(i\omega)|^2 S_F(\omega) \tag{2.2}$$

$$H(i\omega) = (\omega_n^2 - \omega^2 + 2i\omega\,\omega_n\beta)^{-1} \tag{2.3}$$

From which the r.m.s. value of response can be found using:-

$$\sigma_x^2 = \int_0^\infty S_x(\omega)\,d\omega \tag{2.4}$$

In order to predict the maximum values of response it is necessary to know $p_m(x)$, which will depend upon the jpdf of F(t). The cases where F(t) is Gaussian and non-Gaussian are discussed below.

2.2.2 Gaussian Excitation

In offshore problems, forces which are directly proportional to wave height, such as inertia forces, have a Gaussian distribution. It is a standard result that the response of a linear system to Gaussian excitation is also Gaussian, in which case the following expression for the pdf of ν, the ratio of the peak values to the rms, has been given by Longuet-Higgins (ref. 28):-

$$p_m(\nu) = \frac{1}{\sqrt{2\pi}}\{\varepsilon\, e^{-\frac{1}{2}\nu^2/\varepsilon^2} + \nu\sqrt{1-\varepsilon^2}\, e^{-\frac{1}{2}\nu^2} \int_{-\infty}^{\frac{\nu\sqrt{1-\varepsilon^2}}{\varepsilon}} e^{-\frac{1}{2}t^2}\,dt\} \tag{2.5}$$

$$\varepsilon^2 = 1 - m_2^2/(m_4 m_0) \tag{2.6}$$

$$m_n = \int_0^\infty \omega^n S_x(\omega)\,d\omega \tag{2.7}$$

where ε is known as the 'spectral width parameter' and m_n is the nth spectral moment. For a narrow banded response with $\varepsilon \simeq 0$, equation (2.5) reduces to a Rayleigh distribution:-

$$p_m(\nu) = \nu e^{-\frac{1}{2}\nu^2} \tag{2.8}$$

for which it can be shown that the modal value of the highest peak in a group of N peaks is:-

$$\nu_{mode} = \sqrt{2\ell n N} \tag{2.9}$$

Another useful result is that the value of ν for which the probability of exceedance is α is:-

$$\nu_{max} = \sqrt{-2\ell n\{-\frac{1}{N}\ell n(1-\alpha)\}} \tag{2.10}$$

Given the spectrum of response and thus the rms value, equation (2.9) or (2.10) can be used to estimate the maximum response.

2.2.3 Non-Gaussian Excitation

If F(t) is highly non-Gaussian then it may be necessary to resort to the time domain in order to estimate the maximum response (see 2.3.1.3). For other cases, particularly if the system is lightly damped, the assumption that the response is Gaussian may yield sufficiently accurate results. One example of a non-Gaussian exciting force is the drag force acting on a slender offshore structure, which has an exponential peak distribution. In a typical offshore problem the exciting force will have a Gaussian component (e.g. the inertia forces) and a non-Gaussian component, making the determination of the peak distribution of the response very difficult, unless the Gaussian component dominates.

2.3 Non-Linear Systems

2.3.1 The Equivalent Linearisation Method of Spectral Analysis

A general non-linear single degree of freedom system has the form:-

$$\ddot{x} + r(\dot{x},x) = F(t) \tag{2.11}$$

where $r(\dot{x},x)$ is any non-linear function. Although spectral analysis methods are not directly applicable to non-linear equations, approximate spectral methods can be applied to (2.11) provided the non-linearities are not too great. One such method is the 'Equivalent Linearisation Method' which proceeds as follows. Equation (2.11) is replaced by a linear equation plus an error term:-

$$\ddot{x} + b_e\dot{x} + k_e x + \varepsilon = F(t) \tag{2.12}$$

$$\varepsilon = r(\dot{x},x) - b_e\dot{x} - k_e x \qquad (2.13)$$

The constants b_e and k_e are then chosen such that ε is minimised in the mean squared sense, i.e. such that:-

$$E\left[\frac{\partial \varepsilon^2}{\partial b_e}\right] = E\left[\frac{\partial \varepsilon^2}{\partial k_e}\right] = 0 \qquad (2.14)$$

where $E[y]$ represents the expected or average value of y. In order to evaluate (2.14) it is usually assumed that x(t) is Gaussian, which gives expressions for k_e and b_e in terms of σ_x and $\sigma_{\dot{x}}$ (the rms values of displacement and velocity respectively). These values are substituted into (2.12) and ε is neglected to yield the spectrum of response, via the method given in (2.2.1). From the spectrum of response, new values of σ_x and $\sigma_{\dot{x}}$ are calculated, yielding new values of k_e and b_e, and the process is repeated until convergence is achieved.

2.3.2 Gaussian Excitation

If the non-linearities in equation (2.11) are sufficiently small for a Gaussian response to be assumed, then the above spectral analysis can be used together with equation (2.9) or (2.10) to predict maximum response. Alternatively, if the exciting force is white noise then the Fokker-Planck equation yields an exact solution for the jpdf of displacement and velocity for a wide range of non-linear equations. For those equations not covered by the Fokker-Planck method, Caughey's Equivalent Non-Linear Differential Equation method can be used to yield an approximate solution for this jpdf. For highly non-linear equations whose excitation is not white noise, time domain methods must be used.

2.3.2.1 The Fokker-Planck Equation

The Fokker-Planck equation is a differential equation satisfied by the jpdf of a Markov Vector process, a Markov process being a one step memory process, i.e. one in which the value of t_n depends only upon the most recent value, that at time t_{n-1}. The derivation of this equation is based on the Chapman-Kolmogorov-Smoluchowski equation and is discussed at length by Lin (ref.27). If it is assumed that the displacement and velocity of a non-linear system subject to random

excitation form a Markov Vector process, then $p(\dot{x},x)$ satisfies the two dimensional Fokker-Planck equation, the form of which is considerably simplified when the exciting force is Gaussian white noise. An exact analytical solution to this equation is only known when the non-linear system has the form:-

$$\ddot{x} + \alpha f(H)\dot{x} + g(x) = N(t) \qquad (2.15)$$

$$H = \tfrac{1}{2}\dot{x}^2 + \int_0^x g(y)dy \qquad (2.16)$$

where N(t) is Gaussian white noise with spectral density S_o, and f(H) and g(x) are arbitrary functions. The solution for the jpdf is then:-

$$p(\dot{x},x) = C\exp\left[\frac{-\alpha}{\pi S_o} \int_0^H f(y)dy\right] \qquad (2.17)$$

where C is the normalisation constant, chosen to ensure that

$$\int_{-\infty}^{\infty}\int_{-\infty}^{\infty} p(\dot{x},x)d\dot{x}dx = 1.$$

Although white noise is unlikely in practice, it is often possible to approximate the exciting force by white noise, especially when the system is lightly damped and thus sensitive to only a narrow band of exciting frequencies, as shown in Figure 2.2. Roberts (ref. 26) has applied this approach to the slow drift motions of moored structures, and although it should be noted that the slow drift forces are far from Gaussian, his results agree well with time step integration methods for lightly damped systems. The mean squared values of response and velocity can be found from:-

$$\sigma_x^2 = \int_{-\infty}^{\infty}\int_{-\infty}^{\infty} x^2 p(\dot{x},x)d\dot{x}dx \; ; \quad \sigma_{\dot{x}}^2 = \int_{-\infty}^{\infty}\int_{-\infty}^{\infty} \dot{x}^2 p(\dot{x},x)d\dot{x}dx \qquad (2.18)$$

If the response is assumed to be narrow banded, then Lin (ref.27) gives the distribution of the maxima as:-

$$p_m(x) = -\frac{1}{M}\frac{d}{dx}\int_0^{\infty} \dot{x}p(\dot{x},x)d\dot{x} \qquad (2.19)$$

$$M = \int_0^\infty \dot{x} p(\dot{x},o) d\dot{x} \tag{2.20}$$

which can be used to estimate the maximum response.

2.3.2.2 Caughey's Equivalent Non-Linear Differential Equation

This method is an extension of the previous one and can be used for any non-linear differential equation of the type:-

$$\ddot{x} + r(\dot{x},x) = N(t) \tag{2.21}$$

where N(t) is Gaussian white noise of spectral density S_o. The equation is expressed in the form of (2.15) by introducing an error term and suitable functions f(H) and g(x):-

$$\ddot{x} = \alpha f(H)\dot{x} + g(x) + \varepsilon = N(t) \; ; \; H = \tfrac{1}{2}\dot{x}^2 + \int_0^x g(y)dy \tag{2.22}$$

$$\varepsilon = r(\dot{x},x) - \alpha f(H)\dot{x} - g(x) \tag{2.23}$$

The value of α is sought such that ε is minimised in the mean squared sense, i.e. such that:-

$$E\left[\frac{\partial \varepsilon^2}{\partial \alpha}\right] = 0 \Rightarrow E\left[2\alpha f^2(H)\dot{x}^2 - 2r(\dot{x},x)f(H)\dot{x} + 2g(x)f(H)\dot{x}\right] = 0 \tag{2.24}$$

The average values in equation (2.24) are found by noting that for any function $q(x,\dot{x})$:-

$$E\left[q(x,\dot{x})\right] = \int_{-\infty}^{\infty}\int_{-\infty}^{\infty} q(x,\dot{x})p(\dot{x},x)dxd\dot{x} \tag{2.25}$$

where $p(\dot{x},x)$ is given by equation (2.17). Use of (2.24) and (2.25) will yield an equation for α which in most cases will have to be solved numerically, although for some equations a closed solution is possible, as shown by Kirk (ref. 29). This method yields an approximate solution, the accuracy of which depends upon the magnitude of the error term ε.

2.3.2.3 Time Domain Analysis

For systems which cannot be solved by any of the above methods, it is necessary to resort to time step integration techniques, which can be used for any linear or non-linear system. These techniques result in a time history of response, which can then be analysed to determine various statistical properties and maximum values. In general terms the exciting force is represented as a Fourier series - in offshore problems this has the physical significance of representing the random sea state as a linear superposition of regular wave components. The wave spectrum is broken down as shown in Figure 2.3 and the total velocity potential (see Appendix B) is written as:-

$$\phi = \sum_n \frac{a_n g \cosh k_n(y+d)}{\omega_n \cosh k_n d} \operatorname{Sin}(k_n x - \omega_n t + \varepsilon_n) \qquad (2.26)$$

where a_n = amplitude of nth component = $\sqrt{2S_\eta(\omega_n)d\omega_n}$

k_n = $\omega_n^2/(g \tanh k_n d)$, the wave number of the component

ω_n = frequency of component (rads/sec)

ε_n = random phase angle of component, $0 < \varepsilon_n < 2\pi$

Having found ϕ, the time history of the force acting on the system can be found by using either Morison's equation (see Appendix C) or some other method for calculating the hydrodynamic loading. The equation of motion is then solved by time step integration (e.g. Newmark-Beta, Runge-Kutta methods), run times being sufficiently long for a steady state to be reached. Large amounts of computer time are needed for this method since a number of runs using different phase angles in equation (2.26) must be used to ensure that the results are statistically consistent.

2.3.3 Non-Gaussian Excitation

In practice most offshore problems will involve non-linear systems subject to non-Gaussian excitation, for which there is no exact analytical solution. Although r.m.s. values can be obtained via the Equivalent Linearisation method (section 2.3.1), peak values can only be estimated if either Gaussian white noise excitation is assumed (sections 2.3.2.1 and 2.3.2.2) or a Gaussian response is assumed (section 2.2.2). Usually the latter is preferred

and a linearised spectral analysis is used in conjunction with the work of Longuet-Higgins (ref.28). For cases where this would lead to large errors, time domain analysis (2.3.2.3.) must be used.

2.4 Application to a Particular Equation

2.4.1 The Equation Considered

A typical non-linear single degree of freedom system which may arise offshore is:-

$$\ddot{x} + 2\beta\omega_n(1+\gamma|\dot{x}|)\dot{x} + \omega_n^2(1+\delta x^2)x = F(t) \qquad (2.27)$$

This equation contains both linear and non-linear damping and stiffness terms. The linear damping may represent the potential damping due to wave generation, whereas the non-linear term may represent that due to viscous drag forces. The cubic non-linearity in the stiffness term is typical of that due to slack catenary moorings (see Chapter 4). By varying the parameters γ and δ the extent of the non-linearities can be altered, the linear equation (2.1) being obtained when $\gamma = \delta = 0$. It will be assumed that the system is lightly damped and that F(t) can be approximated to Gaussian white noise with spectral density S_o. As the equation is not of the form (2.15), it is not amenable to exact solution using the Fokker-Planck equation, but it can be solved approximately using Caughey's Equivalent Non-Linear Differential Equation Method. Results of this method for r.m.s.values of velocity and displacement are compared with those given by the Equivalent Linearisation method and Time Domain analysis in the following sections.

2.4.2 Caughey's Method

A suitable choice of the functions f(H) and g(x) when equation (2.21) has the form (2.27) is:-

$$g(x) = \omega_n^2(1 + \delta x^2)x; \qquad f(H) = H^{n/2} \qquad (2.28)$$

where n is 1 for all cases except when $\gamma = 0$, in which case it is zero. Using this form of g(x), equation (2.16) yields:-

$$H = \tfrac{1}{2}\dot{x}^2 + \tfrac{1}{2}\omega_n^2x^2 + \tfrac{1}{4}\omega_n^2\delta x^4 \qquad (2.29)$$

The error term, from equations (2.23), (2.27) and (2.28) is:-

$$\varepsilon = 2\beta\omega_n(1 + \gamma|\dot{x}|\dot{x}) - \alpha H^{n/2}\dot{x}$$

and application of equation (2.24) then yields

$$\alpha = 2\beta\omega_n E\left[(\dot{x}^2 + \gamma|\dot{x}|\dot{x}^2)H^{n/2}\right] / E\left[H^n x^2\right] \qquad (2.30)$$

Use of equation (2.25) and the fact that the integrands are even functions leads to:-

$$\alpha = \frac{2\beta\omega_n \int_0^\infty \int_0^\infty (\dot{x}^2+\gamma\dot{x}^3)H^{n/2} p(\dot{x},x)\,d\dot{x}dx}{\int_0^\infty \int_0^\infty H^n \dot{x}^2 p(\dot{x},x)\,d\dot{x}dx} \qquad (2.31)$$

where $p(\dot{x},x)$ is given by equation (2.17). Equation (2.31) is now solved for α: using an assumed value of α, $p(\dot{x},x)$ can be found which will then give a new value of α via equation (2.31), from which $p(\dot{x},x)$ can be recalculated etc., until convergence is achieved. The mean squared response and velocity of the system can then be found from:-

$$\sigma_{\dot{x}}^2 = 2\int_0^\infty\int_0^\infty \dot{x}^2 p(\dot{x},x)\,d\dot{x}dx \;;\quad \sigma_x^2 = 2\int_0^\infty\int_0^\infty x^2 p(\dot{x},x)\,d\dot{x}dx \qquad (2.32)$$

where a factor of $\frac{1}{2}$ has been introduced to account for the fact that the white noise will be considered over positive frequency only, in line with standard wave spectra.

2.4.3 Equivalent Linearisation Method

Use of equations (2.11), (2.13) and (2.27) gives the error term as:-

$$\varepsilon = 2\beta\omega_n(1 + \gamma|\dot{x}|)\dot{x} + \omega_n^2(1 + \delta x^2)x - b_e\dot{x} - k_e x \qquad (2.33)$$

Assuming that x and $\dot{x}$ are statistically independent so that $E\left[x\dot{x}\right] = 0$, and applying (2.14) leads to:-

$$b_e = 2\beta\omega_n + 2\beta\omega_n\gamma\, E\left[|\dot{x}|\dot{x}^2\right] / E\left[\dot{x}^2\right] \qquad (2.34)$$

$$k_e = \omega_n^2 + \omega_n^2 \delta E[x^4] / E[x^2] \tag{2.35}$$

If x and $\dot{x}$ are further assumed to be Gaussian so that:-

$$p(\dot{x},x) = \frac{1}{2\pi\sigma_x\sigma_{\dot{x}}} \exp\{-\tfrac{1}{2}(\frac{x^2}{\sigma_x^2} + \frac{\dot{x}^2}{\sigma_{\dot{x}}^2})\} \tag{2.36}$$

then equation (2.25) can be used to yield:-

$$b_e = 2\beta\omega_n + 2\beta\omega_n \sqrt{\frac{8}{\pi}}\,\sigma_{\dot{x}} \tag{2.37}$$

$$k_e = \omega_n^2 + 3\omega_n^2\delta\sigma_x^2 \tag{2.38}$$

The equations needed for this method are then completed by the following well known results for the response of a linear system to white noise:-

$$\sigma_{\dot{x}}^2 = \frac{\pi S_o}{2b_e} \; ; \; \sigma_x^2 = \frac{\pi S_o}{2b_e k_e} \tag{2.39}$$

The solution method is then iterative, as outlined in section 2.3.1.

2.4.4 Time Domain Analysis

The white noise spectrum is divided into a number of strips of width $d\omega$, and the exciting force represented as:-

$$F(t) = \sum_i \sqrt{2S_o d\omega}\; \mathrm{Cos}(\omega_i t + \varepsilon_i) \tag{2.40}$$

where ω_i is the mid frequency of the nth strip and ε_i is a random phase angle chosen from a rectangular distribution between 0 and 2π radians. Equation (2.40) is inserted into (2.27) and a 4th order Runge-Kutta integration routine used to give the time history of response.

2.4.5 Results and Conclusions

Figures 2.4 and 2.5 show the r.m.s. values of response and velocity obtained from equation (2.27) when $\beta = 0.2$, $\omega_n = 0.15$rad/s and $S_o = 0.1\ m^2s/rad$. These results were obtained for a range of values of δ and γ, the extreme values ($\delta = 0.008$, $\gamma = 0.8$) being

chosen so as to make the magnitude of the non-linear terms in (2.27) approximately twice that of the linear terms. The forcing function used in the time domain analysis had forty frequency components, equally spaced between 0 and 1 rad/s, and the results shown in the figures were obtained by averaging over five simulations, each of 250s duration and having a different set of random phase angles. Typical time histories of response are shown in Figures 2.6 to 2.9. The number of positive maxima, N, occurring in each group of five simulations was substituted into equation (2.9), to give the modal value of the maximum which would occur if the response were Gaussian. Figure 2.10 compares this value to the maximum value actually given by the time domain analysis. The following conclusions can be drawn from these results:-

a) As would be expected, Figure 2.4 shows that the r.m.s. response decreases as the damping (γ) and stiffness (δ) increase. Figure 2.5 shows that although the r.m.s.velocity decreases with an increase in damping (γ), it remains fairly constant as the stiffness (δ) increases. This is due to the fact that the increases stiffness reduces the amplitude but increases the frequency of response, thus having little effect on the response velocity. In fact, equation (2.39) states that for a linear system subject to white noise excitation, the r.m.s. velocity is independent of stiffness.

b) In theory, the Caughey and Equivalent Linearisation methods should show exact agreement for the linear case, $\delta = \gamma = 0$. In practice, there is a slight discrepancy due to the numerical integrations involved in equations (2.31) and (2.32), but this is only of the order of 1%. The time domain result at this point is within 0.3% of the exact result yielded by the Equivalent Linearisation method, which suggests that the method of time domain analysis used yields reliable results. From Figures 2.4 and 2.5 it can be seen that in all cases the Caughey method predicts a lower r.m.s. response than the Equivalent Linearisation method, the discrepancy between the two methods increasing as the non-linearities increase. This is probably due to the fact that equations (2.22), (2.28) and (2.29) used in the Caughey method lead to an overestimate of the damping.

c) The Equivalent Linearisation method and time domain results differ by a maximum of 10%, and in most cases the agreement is much closer than this. This figure is around 15% for the Caughey method. Since the Caughey method involves lengthy numerical integrations and would appear to yield less accurate results than the Equivalent Linearisation method, it's use is not recommended.

d) Figure 2.10 shows that equation (2.9) yields a good prediction for the maximum expected value, even when the equation is highly non-linear. It should be noted that (2.9) gives the modal value of the maximum occurring in a large number of time domain runs, whereas time domain results are given for one run only. Also, for the results quoted, the value of N was in the region of 100, whereas in an offshore situation this number is more likely to be of the order of 3000 (approximate number of wave peaks in a 12 hour storm), and thus the results in Figure 2.10 may be unrepresentative of the real situation.

e) Based on the above results it would appear that non-linear systems can be analysed effectively by using the Equivalent Linearisation method to find the r.m.s.response, and assuming a Gaussian response to predict maximum values. This is the method used for the analysis of the SBS system discussed in Chapter 8. It should be noted that the results given here are limited in nature, and care should be taken in applying them to equations other than of the form (2.27).

3.0 SLACK CATENARY MOORINGS

3.1 Introduction

An integral part of many offshore mooring systems is the slack catenary anchor line, which in it's simplest form comprises a heavy chain suspended from the vessel so as to have zero slope at the point where it touches the sea bed (see Figure 3.1). One advantage of this system, in view of the fact that most common makes of anchor have a very low resistance to vertical loads, is that the anchor need resist forces in the horizontal direction only. The line works on the principle that as the top end moves, chain is either lifted off or deposited on the seabed, thus changing the line tension and providing a restoring force. Both the CALM and SBS single point mooring systems (SPM) (see Sections 1.3.1. and 1.4.1.) incorporate a catenary moored buoy, in which four to twelve slack catenary lines, made of stud link chain, may be used. Typical dry weights for the chain used in these two types of system are 189 kg/m and 535 kg/m respectively. The anchoring system may consist of either piled foundations or one of the types of gravity anchors outlined in Figure 3.2.(after ref.30). In more elaborate systems, such as those required for very deep water, catenary lines may be multi-component, having varying mass per unit length and a distribution of buoyancy modules. This type of system has been discussed by Niedzwecki and Casarella (ref.31) and Ansori (ref. 32). Other systems, such as navigational and meteorological buoys, may use 'taut' moorings in which the anchor line does not have zero slope at the seabed, and the restoring forces are supplied by the elastic properties of the line, which is usually some form of nylon rope. Stiffness properties of slack moorings which become taut due to excessive top displacements have been discussed by Jain (ref. 33).

This chapter discusses the 'stiffness' or restoring force-deflection properties of single-component slack catenary mooring lines, which can often be accurately represented by a close fit cubic. Stiffness properties of complete mooring systems are then examined, and a possible design method is presented for a catenary moored buoy. The effect of mooring line non-linearities on the natural frequencies of the moored vessel are also discussed, together

with a method of linearising the restoring forces acting in the horizontal plane, for use in frequency domain analysis.

In the present mooring line analysis it is assumed that each of the cables behaves in a quasi-static manner when subjected to low frequency movements at the upper point. For very long cables in deep water it is possible that flexural wave propagation along the cables can have modifying effects on the restoring forces. In this thesis however such dynamic effects have been ignored, as the system considered is only in moderately deep water, d ≃ 85m.

3.2 Basic Properties of Slack Catenary Anchors

3.2.1 General Equations

The notation to be used in this section is shown in Figure 3.3 in which:

T_o = Horizontal component of top tension

T_v = Vertical component of top tension

T = Resultant top tension

y = Depth of catenary from attachment point to anchor

x = Horizontal projected length, from the lift off point to the top.

s = Length of suspended line.

ϕ = Angle to the horizontal, at the top.

The wetted weight per unit length of the line is denoted by P. For heavy lines (see Berteaux, ref.30) it is usually assumed that gravitational forces are much greater than those induced by the surrounding fluid, and the effect of waves and current is neglected, greatly simplifying the analysis and leading to the following five independent equations (see Berteaux, ref. 30 , or Muga and Wilson, ref. 34):-

$$T = (T_o^2 + T_v^2)^{\frac{1}{2}} \tag{3.1}$$

$$T_v = Ps \tag{3.2}$$

$$x = \frac{T_o}{P} \sinh^{-1}\left[\frac{Ps}{T_o}\right] \tag{3.3}$$

$$y = \frac{T_o}{P}\left\{\cosh\left[\frac{Px}{T_o}\right] - 1\right\} \tag{3.4}$$

$$P_s = T_o \tan \phi \tag{3.5}$$

From the above equations, the following four dependent equations can be derived:-

$$T = T_o + Py \tag{3.6}$$

$$T_v = (T^2 - T_o^2)^{\frac{1}{2}} \tag{3.7}$$

$$T_o = \left[T_v^2 - (Py)^2\right] / 2Py \tag{3.8}$$

$$y = \frac{T_o}{P} \left\{ \left[1 + \left(\frac{P_s}{T_o}\right)^2 \right]^{\frac{1}{2}} - 1 \right\} \tag{3.9}$$

It can be seen that, given P, there are seven unknowns and only five independent equations. Thus, to solve any catenary mooring problem at least two items must be known. Often these will be the water depth y and the required draft of the moored vessel, which will lead to T_v.

3.2.2 Stiffness Curves for a Single Catenary

In this section stiffness refers to the restoring forces produced by an inextensible mooring line. Having found the initial configuration of the catenary, the new configuration after the top has undergone some displacement must be found in order to calculate the stiffness properties. Let the top be displaced horizontally by a distance γ and vertically by a distance δ, and suppose that this causes a cable lift off of ν, as shown in Figure 3.4. Letting unprimed variables refer to the initial configuration and primed variables to the new position, it can be seen that:-

$$y' = y + \delta \tag{3.10}$$

$$x' = x + \gamma + \nu = x + \gamma + s' - s \tag{3.11}$$

Since (3.10) gives the new value of y, the problem reduces to finding the new value of the top tension T_v'. Now, from equations (3.1), (3.2) and (3.3) it follows that:-

$$x' = \frac{T_o'}{P} \sinh^{-1} \left(\frac{Ps'}{T_o'}\right) \quad (3.12)$$

$$Ps' = T_v' \quad (3.13)$$

$$T_o' = \left[T_v'^2 - (Py')^2\right] / 2Py' \quad (3.14)$$

which can be used to write equation (3.11) in a form in which the only unknown is T_v', i.e.

$$f(T_v') = 0 \quad (3.15)$$

This equation can then be solved numerically using a Newton-Raphson iteration procedure, i.e. if z_1 is the first approximation to T_v', then the next approximation, z_2, is given by:-

$$z_2 = z_1 - \frac{f(z_1)}{f'(z_1)} \quad (3.16)$$

where the functions f(z) and f'(z) are as follows:-

$$f(z) = \pi \ell n\{\theta + \sqrt{\theta^2 + 1}\} - x - \gamma - (z/P) + s \quad (3.17)$$

$$f'(z) = \frac{z}{P^2 y'} \ell n\{\theta + \sqrt{\theta^2 + 1}\} + \pi\psi\{\theta^2 + 1\}^{-\frac{1}{2}} - (1/P) \quad (3.18)$$

$$\pi = \left[z^2 - (Ry')^2\right] / (2P^2 y') \quad (3.19)$$

$$\psi = \{2Py' / \left[z^2 - (Py')^2\right]\} - \{4Py'z^2 / \left[z^2 - (Py')^2\right]^2\} \quad (3.20)$$

$$\theta = 2Py'z / \left[z^2 - (Py')^2\right] \quad (3.21)$$

Use of the above method for a range of values of γ and δ enables graphs of horizontal and vertical top tension against displacement to be drawn. Close fit cubics can then be fitted to these curves to give T_O and T_V as functions of the x and y displacements (assuming an x displacement with no y displacement and vice-versa). Examples of these curves, showing the closeness of fit, are shown in Figure 3.5. This figure relates to a chain with a wetted weight of 1604 N/m and a vertical top tension of 35 tonnes, in 125m of water. It can be seen that the vertical stiffness properties tend to be fairly linear,

whereas the horizontal properties are highly non-linear.

3.2.3 Stiffness Properties of a Complete Mooring System

Perhaps the simplest slack catenary mooring system is the cylindrical buoy, moored by n radial anchor chains, which is common to both the CALM and SBS single point mooring systems. This is shown in Figures 3.6, 3.7 and 3.8. This section will determine the stiffness properties of this system about an axis system with origin at the buoy's centre of gravity. Referring to Figures 3.6, 3.7 and 3.8, let:-

r = radius of buoy

h = height of the catenary attachment points above the buoy's centre of gravity (C.G.)

π_o = the angle the 'first' catenary makes with the x-axis

π_i = the angle the ith catenary makes with the x-axis
$= [2\pi(i-1)/n] + \pi_o$

$(b_1, b_2, b_3, \psi_1, \psi_2, \psi_3)$ = displacements of the buoy, as shown in Figure 3.8

The coordinates of the point of attachment of the ith cable, when the buoy is in the equilibrium position will be $x = r\cos\pi_i$, $y = r\sin\pi_i$ and $z = h$. The displacement of this point when the buoy has undergone a general displacement will be:-

$$\begin{bmatrix}\Delta x_i\\ \Delta y_i\\ \Delta z_i\end{bmatrix} = \begin{bmatrix}b_1\\ b_2\\ b_3\end{bmatrix} + \begin{bmatrix}\psi_1\\ \psi_2\\ \psi_3\end{bmatrix} \times \begin{bmatrix}r\cos\pi_i\\ r\sin\pi_i\\ h\end{bmatrix} = \begin{bmatrix}b_1+\psi_2 h-\psi_3 r\sin\pi_i\\ b_2+\psi_3 r\cos\pi_i-\psi_i h\\ b_3+\psi_1 r\sin\pi_i-\psi_2 r\cos\pi_i\end{bmatrix} \quad (3.22)$$

Resolving these displacements along the chain gives:-

$$X_i = -b_1\cos\pi_i - \psi_2 h\cos\pi_i - b_2\sin\pi_i + \psi_1 h\sin\pi_i \quad (3.23)$$

$$Y_i = b_3 + \psi_1 r\sin\pi_i - \psi_2 r\cos\pi_i \quad (3.24)$$

where X_i is the displacement of the cable top in a horizontal direction away from the anchor, and Y_i is the upwards displacement of this point.

From the single catenary analysis of the previous section, these displacements can be used to find the new top tensions in this chain, T_{o_i} and T_{v_i} say. The total restoring forces acting on the buoy can then be written as the vector:-

$$\underset{\sim}{F}_{tot} = \begin{bmatrix} -\sum_i T_{o_i}\cos\pi_i \\ -\sum_i T_{v_i}\sin\pi_i \\ \sum_i T_{v_i} \end{bmatrix} \tag{3.25}$$

and the restoring moments as:-

$$\underset{\sim}{M}_{tot} = \sum_i \left\{ \begin{bmatrix} r\cos\pi_i \\ r\sin\pi_i \\ h \end{bmatrix} \times \begin{bmatrix} -T_{o_i}\cos\pi_i \\ -T_{v_i}\sin\pi_i \\ T_{v_i} \end{bmatrix} \right\} = \begin{bmatrix} \sum_i (T_{v_i} r\sin\pi_i + hT_{o_i}\sin\pi_i) \\ \sum_i (hT_{o_i}\cos\pi_i + T_{v_i} r\cos\pi_i) \\ 0 \end{bmatrix} \tag{3.26}$$

In addition, there will be a restoring moment in yaw (ψ_3) given by $n(r/d)rT_o\psi_3$, which can be found by considering the displacement of a cable due to yaw alone, as shown in Figure 3.9. d and T_o are the initial span and horizontal tension in the cable respectively. In general, the stiffness characteristics of a complete mooring system tend to be more linear than those of a single line, since for a symmetrical system the non-linearities involving even powers of displacements will cancel. Another way of looking at this is that as the tightening, lifted cable stiffness increases, there is a somewhat smaller corresponding reduction in the stiffness of the slackening cable diametrically opposite. The above method is used in the next section to calculate the horizontal plane stiffness properties of the SBS and CALM systems.

3.3 A Design Method for Buoy Mooring Systems

In general, the following specifications must be met by catenary anchoring systems:-

a) If possible, no vertical force should be applied to the anchors i.e. the lines must not become taut, to avoid snatch loads, which can be many times greater than the mean cable load.

b) For certain structures the horizontal excursion must be limited to prevent damage to riser pipes, drill lines etc.

c) The system must be capable of withstanding the maximum forces which will be applied without exceeding 1/3 of the breaking load in any one line (ABS rules 1974, see section 1.5).

d) The stiffness properties must be chosen where possible so as to avoid the possibility of resonance, however this cannot always be achieved in practice.

In the following, a design procedure for SBS and CALM moorings is developed based mainly upon the horizontal properties of the system, since it is in this direction that wind, current and mean drift forces must be resisted. A note on the effect of the vertical properties of the mooring is given at the end of the section. It will be assumed that the maximum allowable span s_1, and horizontal excursion x_{max}, of a mooring line are given, and that from these it is required to find the initial configuration. Figure 3.1a, in which a subscript 1 relates to the extreme position and a '0' to the initial position, illustrates the problem. From equations (3.2), (3.3) and (3.8):-

$$x_o = \frac{T_o}{P}\sinh^{-1}\left[\frac{Ps_o}{T_o}\right] \quad ; \quad x_1 = \frac{T_1}{P}\sinh^{-1}\left[\frac{Ps_1}{T_1}\right] \qquad (3.27)$$

$$T_o = \left[(Ps_o)^2 - (Pd)^2\right]/2Pd \quad ; \quad T_1 = \left[(Ps_1)^2 - (Pd)^2\right]/2Pd \qquad (3.28)$$

Also, from the geometry of the system:-

$$s_1 - s_o + x_{max} + x_o = x_1 \qquad (3.29)$$

This then yields:-

$$s_1 - s_o + \frac{1}{2d}(s_o^2 - d^2)\sinh^{-1}\left(\frac{2ds_o}{s_o^2 - d^2}\right) + x_{max} = \frac{1}{2d}(s_1^2 - d^2)\sinh^{-1}\left(\frac{2s_1 d}{s_1^2 - d^2}\right) \qquad (3.30)$$

This equation can be non-dimensionalised by defining $r_1 = (s_1/d)$, $r_o = (s_o/d)$ and $x_r = (x_{max}/d)$ to give:-

$$f(r_o) = r_1 - r_o + \tfrac{1}{2}(r_o^2 - 1)\sinh^{-1}\left(\frac{2r_o}{r_o^2 - 1}\right) + x_r - \tfrac{1}{2}(r_1^2 - 1)\sinh^{-1}\left(\frac{2r_1}{r_1^2 - 1}\right) = 0 \qquad (3.31)$$

In this equation the only unknown is r_o, since r_1 and x_r have been specified. The equation can then be solved for r_o by the Newton-Raphson method, in the same way that (3.15) was solved for T_v'. This method requires the derivative of (3.31), which is:-

$$f'(r_o) = 1 + r_o \ell n\{g + (1 + g^2)^{\frac{1}{2}}\} + \tfrac{1}{2}g'(r_o^2 - 1)(g^2 + 1)^{-\frac{1}{2}} \quad (3.32)$$

$$g = 2r_o/(r_o^2 - 1) \quad (3.33)$$

$$g' = 2/(r_o^2 - 1) - 4r_o^2/(r_o^2 - 1)^2 \quad (3.34)$$

Once r_o has been found, the horizontal non-dimensional pre-tension required can be found from:-

$$(T_o/Pd) = \tfrac{1}{2}(r_o^2 - 1) \quad (3.35)$$

The load deflection curve about the initial position can then be found between (T_{o_i}/Pd) and x_{r_i} by moving the top of the cable a distance x_{r_i} from this position and solving (3.31) for the new value of r_{o_i}, which can then be applied to (3.35). Note that the form of this curve depends upon the initial position and thus upon the extreme position (defined by r_1 and x_r) which was specified. A cubic can be fitted to this curve in the form:-

$$(T_{o_i}/Pd) = ax_{r_i}^3 + bx_{r_i}^2 + cx_{r_i} + e \quad (3.36)$$

Comparison to the dimensional equation:-

$$T_{o_i} = Ax_i^3 + Bx_i^2 + Cx_i + D \quad (3.37)$$

where $x_i = x_{r_i}d$, shows that the relations between the dimensional and non-dimensional coefficients are $a = (Ad^2/P)$, $b = (Bd/P)$, $c = (C/P)$ and $e = (D/Pd)$. Using these stiffness properties for one line, the properties of a complete mooring system can be found, as discussed in section 3.2.3.

The non-dimensional equations given above have been used to construct the design tables shown in Figure 3.14. Each table gives the value of a non-dimensional quantity for various specified values of

s_1 and x_r. The first table indicates whether a horizontal displacement towards the anchor of $2x_r$ from the extreme position will carry the cable beyond the point at which it is vertical, a '1' indicating that this is the case. The purpose of this table is shown in Figure 3.11, where it can be seen that while the LHS cable is at it's maximum excursion, the RHS cable may become vertical, and thus lose all of it's horizontal stiffness. The next three tables give the non-dimensional values of cable length, horizontal span and horizontal tension, for the initial position. The four tables following these give the non-dimensional cubic coefficients for the stiffness properties of one cable about the initial configuration. The discrepancies between the values given in the table of (T_o/Pd) and those given in the table of (D/Pd) give an indication of the accuracy of the cubic fit. The remaining tables concern buoy systems having 4, 6 or 8 cables. F_{max} indicates the horizontal restoring force when the buoy is at the maximum excursion x_r. A possible buoy mooring design procedure, using these tables, is given below:-

a) Specify s_1 and x_r and the maximum horizontal force to be resisted. Also select the required number of cables.

b) Choose P, (and thus the chain diameter D_c) such that F_{max} can be restrained within the limits of x_r, using the tables.

c) Having found P, find T_o, s_o and x_o for the initial configuration, using the tables.

d) Find the maximum tension in the line at x_r, and check that this is less than 1/3 of the breaking load, using:-

$$\left.\begin{aligned}\text{Proof load} &= 0.014D_c^2(44-0.08D_c)/10\\ \text{Breaking load} &= 0.0211D_c^2(44-0.08D_c)/10\end{aligned}\right\}\text{in tonnes for } D_c \text{ in mm.}$$

These formulae have been taken from the API rules, 1977 (see section 1.5).

e) Check the system natural frequencies using the tables to give the stiffness coefficients.

f) If failed on (d) or (e) choose a new value of P, or a different number of cables.

The determination of the natural frequencies (e) is complicated by the fact that there is a non-linear restoring force, which makes the period of finite amplitude free vibration, amplitude dependent. The method of

finding this period is given in section 3.4. An example of the use of the design procedure outlined above is given in Chapter 9.

No account has been taken in this section of the vertical properties of the system. As the system displaces horizontally, the vertical component of top tension will be changed, causing a vertical displacement. This displacement then effects the horizontal stiffness properties of the system, and may cause a change in draft which will, in turn, change the current forces. For the type of system under investigation, it was found that at the maximum horizontal excursion, the vertical displacement was usually less than a metre, and may therefore be neglected.

3.4 The Effect of Non-Linearities on the Natural Frequencies

The equation of undamped free vibration in surge, of a buoy with catenary moorings can be written as a Duffing equation,

$$\ddot{x} + \alpha x + \beta x^3 = 0 \qquad (3.38)$$

where $\alpha = C/(M+Ma)$ and $\beta = A/(M+Ma)$, (M+Ma) being the mass plus added mass of the buoy with Ma assumed to be independent of frequency.

Writing $v = \dot{x}$, (3.38) can be written:-

$$v\frac{dv}{dx} = -\alpha x - \beta x^3 \qquad (3.39)$$

It will be assumed that the motion has the same characteristics as SHM in that $x = 0$ when $v = v_{max} = v_o$ say, and $x = x_{max} = a$ when $v = 0$. Integrating (3.39) then gives:-

$$\int_o^{v_o} v\,dv = \int_a^o (-\alpha x - \beta x^3)\,dx \Rightarrow a^2 = \frac{1}{\beta}\{-\alpha + (\alpha^2 + 2\beta v_o^2)^{\frac{1}{2}}\} \qquad (3.40)$$

Integrating (3.39) between the limits $x: 0 \to x$ and $v: v_o \to v$, it can be shown that:-

$$\frac{dx}{dt} = (v_o^2 - \alpha x^2 - \tfrac{1}{2}\beta x^4)^{\frac{1}{2}} \qquad (3.41)$$

Now, if T is the period of oscillation, such that $t = T/4$ when $x = a$, the above equation yields:-

$$\int_o^{T/4} dt = \int_o^a (v_o - \alpha x^2 - \tfrac{1}{2}\beta x^4)^{-\frac{1}{2}} dx \qquad (3.42)$$

Writing $x = a\sin\theta$ and using (3.40) to eliminate v_o then gives:-

$$T = 4\sqrt{2}\int_o^{\pi/2} (2\alpha + \beta a^2 + \beta a^2 \sin^2\theta)^{-\frac{1}{2}} d\theta \qquad (3.43)$$

This equation can be integrated numerically to give the period of free, undamped vibration. Typically, the dependence of the natural frequency on β is as shown in Figure 3.12. It can easily be shown that for the system:-

$$\ddot{x} + \alpha x + \gamma x^2 + \beta x^3 = 0 \qquad (3.44)$$

equations (3.40) and (3.43) become:-

$$v_o^2 = \alpha a^2 + 2\gamma a^3/3 + \tfrac{1}{2}\beta a^4 \qquad (3.45)$$

$$T = 4\sqrt{2}\int_o^{\pi/2} \{2\alpha+\beta a^2+\beta a^2\sin^2\theta+4a\gamma\sec^2\theta(1-\sin^3\theta)/3\}^{-\frac{1}{2}}d\theta \qquad (3.46)$$

It has been assumed that the motion is periodic in spite of the nonlinear stiffness, which is a reasonable assumption for moderately nonlinear stiffness. It is well known that nonlinear stiffness generates higher harmonic components (see Ref.35). Such effects have been ignored in this thesis.

3.5 Linearisation of Catenary Moorings in the Horizontal Plane

3.5.1 Formulation of the Problem

Figure 3.5 illustrates the fact that most catenary systems tend to be fairly linear in the vertical direction and yet highly non-linear in the horizontal plane. This horizontal non-linearity precludes the use of frequency domain techniques of dynamic analysis, unless some linearisation procedure is first applied (see section 2.3). In the following sections, the equivalent linearisation technique is applied to the horizontal stiffness properties of a catenary moored buoy, and the results obtained are used in Chapter 8, which contains the dynamic analysis of a SBS system.

It is assumed that the horizontal displacements of the buoy (see Figure 3.13) can be written:-

$$x = x_d + x_{sd} + x_m \quad ; \quad y = y_d + y_{sd} + y_m \qquad (3.47)$$

where the subscripts d and sd relate to the displacements caused by first and second order wave forces respectively (see Chapter 6). It is also assumed that these two types of displacement are statistically independend, and that, in the absence of more exact information (see section 6.4.3) they have Gaussian distributions. x_m and y_m are the static displacements caused by wind, current and mean drift forces.

The resultant displacement of the buoy in the horizontal plane is then:-

$$x_{res} = (x^2 + y^2)^{\frac{1}{2}} \tag{3.48}$$

and, assuming that the system has a cubic stiffness curve, defined by the coefficients k_1 and k_3, the resultant restoring force is:-

$$F_T = k_1(x^2 + y^2)^{\frac{1}{2}} + k_3(x^2 + y^2)^{3/2} \tag{3.49}$$

The restoring forces acting in the x and y directions are then:-

$$F_X = k_1x + k_3x(x^2 + y^2) \tag{3.50}$$

$$F_Y = k_1y + k_3y(x^2 + y^2) \tag{3.51}$$

from which it can be seen that there is a coupling between the non-linear terms.

3.5.2 Linearisation in the x-direction

Following the Equivalent Linearisation procedure (section 2.3.1) F_X is written:-

$$F_X = a_1x + a_2y + a_3 + \varepsilon \tag{3.52}$$

where ε is an error function defined by

$$\varepsilon = k_1x + k_3x(x^2 + y^2) - a_1x - a_2y - a_3 \tag{3.53}$$

The coefficients a_1, a_2 and a_3 are now found such that ε is minimised in the mean squared sense, i.e. such that:-

$$\left\langle \frac{\partial \varepsilon^2}{\partial a_1} \right\rangle = \left\langle \frac{\partial \varepsilon^2}{\partial a_2} \right\rangle = \left\langle \frac{\partial \varepsilon^2}{\partial a_3} \right\rangle = 0 \tag{3.54}$$

where $\langle x \rangle$ represents the ensemble average or expected value of x. It can be shown that (3.54) leads to the following matrix equation:-

$$\begin{bmatrix} \langle x^2 \rangle & \langle xy \rangle & \langle x \rangle \\ \langle xy \rangle & \langle y^2 \rangle & \langle y \rangle \\ \langle x \rangle & \langle y \rangle & 1 \end{bmatrix} \begin{bmatrix} a_1 \\ a_2 \\ a_3 \end{bmatrix} = \begin{bmatrix} k_1\langle x^2 \rangle + k_3\langle x^4 + x^2y^2 \rangle \\ k_1\langle xy \rangle + k_3\langle x^3y + xy^3 \rangle \\ k_1\langle x \rangle + k_3\langle x^3 + y^2x \rangle \end{bmatrix} \tag{3.55}$$

The coefficients a_1, a_2 and a_3 can then be found by matrix inversion. The method of calculating the mean values involved in equation (3.55) is given in section 3.5.4.

3.5.3 Linearisation in the y-direction

The restoring force in the y direction is written:-

$$F_Y = a_1 y + a_2 x + a_3 + \varepsilon \tag{3.56}$$

$$\varepsilon = k_1 y + k_3 y(x^2+y^2) - a_1 y - a_2 x - a_3 \tag{3.57}$$

Minimising ε in the mean squared sense then leads to:-

$$\begin{bmatrix} \langle y^2 \rangle & \langle xy \rangle & \langle y \rangle \\ \langle xy \rangle & \langle x^2 \rangle & \langle x \rangle \\ \langle y \rangle & \langle x \rangle & 1 \end{bmatrix} \begin{bmatrix} a_1 \\ a_2 \\ a_3 \end{bmatrix} = \begin{bmatrix} k_1\langle y^2 \rangle + k_3\langle y^4+x^2y^2 \rangle \\ k_1\langle xy \rangle + k_3\langle y^3x+yx^3 \rangle \\ k_1\langle y \rangle + k_3\langle y^3+x^2y \rangle \end{bmatrix} \tag{3.58}$$

from which a_1, a_2 and a_3 can be found.

3.5.4 Evaluation of the Average Terms

Let X and Y represent the time varying parts of x and y such that:-

$$x = x_d + x_{sd} + x_m = X + x_m \tag{3.59}$$

$$y = y_d + y_{sd} + y_m = Y + y_m \tag{3.60}$$

Substituting (3.59) and (3.60) into equations (3.55) and (3.58) reduces the problem of finding the average terms to that of finding the average value of a general term X^mY^n. As stated in section 3.5.1, it is assumed that X and Y are jointly Gaussian, in which case Lin (ref. 27) has shown that:-

$$p(X,,Y) = \frac{1}{2\pi\sigma_x\sigma_y\sqrt{1-\rho^2}} \exp\left\{\frac{\sigma_x^2X^2-2\sigma_x\sigma_y\rho XY+\sigma_x^2Y^2}{2\sigma_x^2\sigma_y^2(1-\rho^2)}\right\} \tag{3.61}$$

where $\rho = \langle XY \rangle / \sigma_x\sigma_y$. The mean values can then be calculated using:-

$$\langle X^mY^n \rangle = \int_{-\infty}^{\infty}\int_{-\infty}^{\infty} X^mY^n\, p(X,Y)dXdY \tag{3.62}$$

once the values of σ_x, σ_y and ρ for use in equation (3.61) have been found. The slow drift and direct wave induced motions are assumed to be statistically independent, so that:-

$$\sigma_x^2 = \langle x_d^2 \rangle + \langle x_{sd}^2 \rangle \tag{3.63}$$

$$\sigma_y^2 = \langle y_d^2 \rangle + \langle y_{sd}^2 \rangle \tag{3.64}$$

$$\langle XY \rangle = \langle x_dy_d + x_{sd}y_d + x_dy_{sd} + x_{sd}y_{sd} \rangle = \langle x_dy_d + x_{sd}y_{sd} \rangle \tag{3.65}$$

Since the equivalent linearisation procedure is an iterative technique for use in the frequency domain, it will now be assumed that some approximation to the response spectra is known. The terms on the RHS of (3.63) and (3.64) can then be found as the areas under the appropriate response spectra. In irregular waves, x_d and y_d can be written as:-

$$x_d = \text{Re} \sum_n a_n H(i\omega_n) e^{i\omega_n t} = \text{Re}\{a\} \quad (3.66)$$

$$y_d = \text{Re} \sum_n a_n G(i\omega_n) e^{i\omega_n t} = \text{Re}\{b\} \quad (3.67)$$

where a_n and ω_n are the amplitude and frequency of the n'th wave component, $H(i\omega_n)$ and $G(i\omega_n)$ are complex transfer functions, and Re denotes the real part. The product of x_d and y_d has the form:-

$$x_d y_d = \tfrac{1}{2}\text{Re}\{ab\} + \tfrac{1}{2}\text{Re}\{ab^*\}$$

$$= \tfrac{1}{2}\text{Re} \sum_n \sum_m a_n a_m \{H(i\omega_n)G(i\omega_m)e^{i(\omega_n+\omega_m)t} + H(i\omega_n)G^*(i\omega_m)e^{i(\omega_n-\omega_m)t}\} \quad (3.68)$$

where * denotes the complex conjugate.

The mean value of this product is then:-

$$\langle x_d y_d \rangle = \tfrac{1}{2}\text{Re} \sum_n a_n^2 H(i\omega_n) G^*(i\omega_n) \quad (3.69)$$

or, introducing the wave amplitude spectrum $S_\eta(\omega)$ such that $a_n = \sqrt{2S_\eta(\omega)d\omega}$:-

$$\langle x_d y_d \rangle = \text{Re} \int_o^\infty H(i\omega) G^*(i\omega) S_\eta(\omega) d\omega \quad (3.70)$$

Similarly, the mean value of the product of the slow drift responses can be written:-

$$\langle x_{sd} y_{sd} \rangle = \text{Re} \int_o^\infty \int_o^\infty P(i\omega_k) Q^*(i\omega_k) f(\omega, \omega_k) S_\eta(\omega) S_\eta(\omega+\omega_k) d\omega d\omega_k \quad (3.71)$$

where $P(i\omega_k)$ and $Q(i\omega_k)$ are complex transfer functions, and $f(\omega, \omega_k)$ is a wave reflection coefficient. An explanation of the form of (3.71) is given in Chapter 6.

3.5.5 Iterative Solution Technique

Initial values of σ_x, σ_y and ρ are assumed which are then used to find the linearised coefficients via equations (3.62), (3.61), (3.58) and (3.55). The linearised coefficients are then used in a frequency

domain analysis to yield the spectra of response. From equations (3.63), (3.64), (3.65), (3.70) and (3.71), new values of σ_x, σ_y and ρ are obtained, and the process is repeated until convergence is obtained.

4.0 BUOY DYNAMICS

4.1 Introduction

As discussed in sections 1.3 and 1.4, the catenary moored buoy is an integral part of several types of single point mooring systems. Since these systems tend to be used in locations which are exposed to severe weather conditions, the dynamic response characteristics of the buoy are of major concern in their design. Care must be taken to ensure that the buoy motions do not produce snatch loads in either the underbuoy hoses or the mooring lines, and also that the maximum expected excursions are within the limits of the oil transfer mechanisms (swivels etc). Unfortunately, the hydrodynamic loading acting on the buoy is extremely complex, i.e. waves may break over the top of the buoy, and viscous effects may produce flow separation and vortex shedding. Also, the buoy lies in the vicinity of the wave profile - an area where the results of linear wave theory tend to be least accurate, since this theory assumes that the wave profile is infinitely small. An estimate of the loading acting in the horizontal plane can be obtained from Morison's equation (see Appendix C), which states that the total force is the sum of a drag and inertia term:-

$$F_T = F_I + F_D = \tfrac{1}{4}C_m\pi\rho D^2 d_t\dot{u} + \tfrac{1}{2}\rho C_D d_t u_r|u_r| \qquad (4.1)$$

where D is the buoy diameter, d_t the buoy draft, $\dot{u}$ the fluid acceleration due to wave motion, u_r the relative fluid velocity due to waves, current and buoy motions, and C_m and C_D are the inertia and drag coefficients respectively. Equation (4.1) is an approximate formula for buoys with small draft, used for illustrative purposes only. In waves of amplitude 'a' and frequency ω, the ratio of maximum drag force to maximum inertia force on a fixed buoy in the absence of current can be shown to be:-

$$(F_D)_{max}/(F_I)_{max} = (\frac{2}{\pi})(\frac{C_D}{C_m})(\frac{a}{D}) \qquad (4.2)$$

The magnitude of this ratio for various values of (a/D) and (C_D/C_m) is shown graphically in Figure 4.1. Typical dimensions of the type of buoy used in single point mooring terminals are shown in Figure 4.2. For a 100 year North Sea design wave with a = 15m, the ratio (a/D)

will be approximately 1.5. Sharpkaya (ref. 36)has found experimental values of C_D and C_m for a fixed cylinder in an oscillating (T = 5.2725) stream, these values being found to depend upon the Reynolds number, the Keulegan-Carpenter number and the roughness characteristics of the cylinder. The applicability of these results to a cylinder moving in random waves is still the subject of some debate (see ref.37). In the case of a mooring buoy, values of around $C_D = 0.6$ and $C_m = 2.0$ would be predicted by these results. Reference to Figure 4.1 then shows that the maximum drag force is approximately 30% of the maximum inertia force, and thus viscous effects will play a large part in determining the flow pattern around the buoy. For this reason, the application of complex analytical techniques which assume potential flow, such as source-sink methods (see Chapter 5), to the problem of buoy dynamics may yield results which are less reliable than those predicted by the simpler, semi-empirical Morison's equation. One use of these techniques, however, is that they predict the frequency dependent added mass and potential damping coefficients which appear on the LHS of the equations of motion. Remery and Kokeel (ref. 38), Sabuncu and Calisal (ref. 39) and Garrison (ref.40) have presented non-dimensionalised results for these coefficients, which are applicable to many types of buoy.

The problem of buoy submergence can be examined by considering the transfer function $f(\omega)$ of heave motion, which can be found from linear theory. This function gives the ratio of the heave response of the buoy to the amplitude (a) of an incident wave of frequency ω. Letting h represent the height to which the buoy extends above the still water level, then either of the following three cases are possible (see Figure 4.3).

$$h < a[1 - f(\omega)] \quad ; \quad a[1 + f(\omega)] > h > a[1 - f(\omega)] ; \quad h > a[1 + f(\omega)] \tag{4.3}$$

In the first case submergence will always occur, whereas in the third case it will never occur. In the second case, submergence will depend upon the phase of the buoy motion relative to the wave profile. Typically, for the wave frequencies of interest (providing resonance does not occur), $f(\omega)$ lies between 0.8 and 1.2 (see Figure 20 of ref. 38), and the buoy moves in phase with the wave profile. To

avoid submergence in a 15m design wave, h would then need to be at least 3m, which is usually the case (see Figure 4.2). For this reason buoy submergence will not be considered in the following sections. It should be noted that buoy submergence can also be caused by breaking waves (see ref. 41), but this is beyond the scope of the linear theory and is thus neglected.

4.2 Added Mass and Potential Damping Matrices

Remery and Kokeel (ref. 38) have presented the results for the frequency dependent added mass coefficients of a floating buoy which are shown in Figure 4.5. An explanation of the notation used in this Figure is given in Figure 4.4. These results were obtained for a variety of diameter to draft ratios and a fixed water depth to draft ratio of 6, using source-sink methods. In reference (40), Garrison has given results for both the added mass and potential damping coefficients for a range of water depth to draft ratios and a specified draft to diameter ratio of 0.25. More recently, Sabuncu and Calisal (ref. 39) have given added mass and damping coefficients for a wide range of water depths and diameter to draft ratios, using a procedure outlined by Garret (ref. 42) who studied the scattering of waves by circular docks.

Inertial effects (both structural and added) due to the motions of the mooring chains, which will be induced by the buoy motions, are complex and will not be considered here. It is considered that these effects will be small when compared to the added mass forces acting on the buoy.

4.3 Drag Force and Linearised Damping Matrix

Figure 4.6 shows the degrees of freedom, reference axes and notation which will be used to determine the drag forces acting on a mooring buoy subjected to non-colinear waves and current. Using this Figure, the relative fluid velocities in the x and y directions at a point z above the origin of the axis system can be shown to be

$$r_x(z) = -\dot{b}_1 - \dot{\psi}_2 z - v_c(z)\cos\mu - u(z)\cos\theta \qquad (4.4)$$

$$r_y(z) \quad -\dot{b}_2 + \dot{\psi}_1 z - v_c(z)\sin\mu - u(z)\sin\theta \qquad (4.5)$$

where $u(z)$ and $v_c(z)$ are the wave and current velocities at z, and all

other notation is as shown in Figure 4.6

Although Morison's equation (Appendix C) strictly applies to the resultant relative velocity, the problem can be greatly simplified if it is applied independently to the relative velocities in the x and y directions. This is thought to be justified in view of the semi-empirical nature of this equation and the flexibility inherent in the choice of the drag coefficient C_D. The drag force acting on a strip of width dz can then be written:-

$$dF_x = \tfrac{1}{2}\rho C_D D r_x(z)|r_x(z)|dz \qquad (4.6)$$

$$dF_y = \tfrac{1}{2}\rho C_D D r_y(z)|r_y(z)|dz \qquad (4.7)$$

where D = buoy diameter and ρ = fluid density. The total forces and moments due to drag can then be written as

$$F_x = \int_{-d_t}^{s} dF_x \quad ; \quad M_x = -\int_{-d_t}^{s} z dF_y \qquad (4.8)$$

$$F_y = \int_{-d_t}^{s} dF_y \quad ; \quad M_y = \int_{-d_t}^{s} z dF_x \qquad (4.9)$$

where s and dt are as shown in Figure 4.6.

Tung and Wu (ref. 43) have given a linearisation procedure for drag force in the presence of current, using which, equations (4.6) and (4.7) can be written:

$$dF_x = \tfrac{1}{2}\rho C_D D \left[a_x(z)\{r_x(z)+v_c(z)\cos\mu\}+b_x(z)\right] \qquad (4.10)$$

$$dF_y = \tfrac{1}{2}\rho C_D D \left[a_y(z)\{r_y(z)+v_c(z)\sin\mu\}+b_y(z)\right] \qquad (4.11)$$

where $a_x(z)$, $b_x(z)$, $a_y(z)$ and $b_y(z)$ are linearisation coefficients, dependent upon the current velocity and the r.m.s. value of the time varying component of the appropriate relative velocity (see Appendix C). Substituting into (4.8) and (4.9), the drag forces and moments have the form:-

$$\begin{bmatrix} F_x \\ F_y \\ M_x \\ M_y \end{bmatrix} = -\begin{bmatrix} B_{11} & 0 & 0 & B_{15} \\ 0 & B_{22} & B_{24} & 0 \\ 0 & B_{24} & B_{44} & 0 \\ B_{15} & 0 & 0 & B_{55} \end{bmatrix} \begin{bmatrix} b_1 \\ b_2 \\ \psi_1 \\ \psi_2 \end{bmatrix} + \begin{bmatrix} F_{d_1} \\ F_{d_2} \\ M_{d_1} \\ M_{d_2} \end{bmatrix} + \begin{bmatrix} F_{c_1} \\ F_{c_2} \\ M_{c_1} \\ M_{c_2} \end{bmatrix} \qquad (4.12)$$

where the first matrix on the RHS of this expression is the linearised damping matrix, F_{d_i} and M_{d_i} are the linearised forcing functions due to the wave velocity and F_{c_i} and M_{c_i} are mean forces and moments. Detailed expressions for the terms on the RHS of equation (4.12) are given in Appendix F.

No reference to the viscous forces acting in heave has been found in the published literature, and it is therefore concluded that these effects are negligible if a damping disc is not used. The potential damping in heave is around 3% of critical, which is very low if resonance is likely to be a problem. It is expected, however, that considerable heave damping will be provided by the viscous forces acting on the mooring lines, although this is very difficult to quantify analytically.

4.4 Hydrostatic Stiffness

Since the buoy is surface piercing, hydrostatic restoring forces act in heave, roll and pitch. In heave, the stiffness is due to the increase or decrease in the displaced fluid caused by vertical motions of the buoy, and is given by:-

$$k_{33} = \pi\rho g D^2/4 \qquad (4.13)$$

Figure 4.7 shows the effect of a displacement ψ in either pitch or roll. The restoring moment can be written as:-

$$M = \psi\rho g\int_{-r}^{r} x^2 \ell dx = 2\psi\rho g\int_{-r}^{r} x^2(r^2-x^2)^{\frac{1}{2}}dx \qquad (4.14)$$

where ℓ is the width of a strip across the buoy at a distance x from the axis of rotation, as shown in Figure 4.7. Using (4.14) it can be shown that the roll and pitch stiffness coefficients are given by:-

$$k_{44} = k_{55} = \tfrac{1}{4}\pi\rho g r^4 = \pi\rho g D^4/64 \qquad (4.15)$$

Due to symmetry, no coupling occurs between heave, pitch and roll.

4.5 Inertia Forces

4.5.1 Surge and Sway

The inertia force acting in the horizontal plane can be calculated either by using source-sink numerical methods, or by using a simpler method based on the inertia term in Morison's equation. Although the results obtained by the former method will be exact within linear potential theory, they may be substantially different from the actual forces experienced by the buoy, due to the presence of viscous effects (see Section 4.1). For this reason the second, simpler approach is used here. The horizontal inertia force in regular waves is written as:-

$$F_1 = \rho V \left[1 + C_{a_1}\right] \dot{\bar{u}} \qquad (4.16)$$

where V is the volume of fluid displaced, C_{a_1} is a frequency dependent added mass coefficient, being equal to the added mass in surge or sway, divided by the mass of fluid displaced, and $\bar{u}$ is the average horizontal acceleration of the fluid which would occupy the region taken up by the buoy, were the buoy not present. This section will consider a wave travelling in the x-direction - for the general case the result obtained represents the resultant force, which can then by resolved into the x and y direction. The wave potential and horizontal acceleration are taken to be (see Appendix B):-

$$\phi = \frac{ag}{\omega} \frac{\cosh k(d+z)}{\cosh(kd)} \cos(\omega t - kx)$$

$$\dot{u} = a\omega^2 \frac{\cosh k(d+z)}{\sinh(kd)} \cos(\omega t - kx) \qquad (4.17)$$

where z is measured upwards from the still water level. The average fluid acceleration, $\dot{\bar{u}}$, is then:-

$$\dot{\bar{u}} = \frac{1}{V} \int_V \dot{u} dr = \frac{1}{V} \int_{-d_t}^{o} \int_{-r}^{r} 2(r^2-x^2)^{\frac{1}{2}} \dot{u} dx dz$$

$$= \frac{2a\omega^2}{Vk} \left[1 - \frac{\sinh(d-d_t)}{\sinh(kd)}\right] \int_{-r}^{r} (r^2-x^2)^{\frac{1}{2}} \cos(kx-\omega t) dx \qquad (4.18)$$

where d_t is the draft of the buoy. The integral in equation (4.18) can be re-written as follows:-

$$\int_{-r}^{r} (r^2-x^2)^{\frac{1}{2}}\cos(kx-\omega t)\,dx = \int_{-r}^{r}(r^2-x^2)^{\frac{1}{2}}\cos(kx)\cos(\omega t)dx$$

$$= r^2\cos(\omega t)\int_{o}^{\pi} \sin^2\theta\cos(kr\cos\theta)d\theta$$

$$= (\frac{r}{k})\cos(\omega t)\int_{o}^{\pi} \cos\theta\sin(kr\cos\theta)d\theta \qquad (4.19)$$

having put $x = r\cos\theta$, and integrated by parts. By expanding $\sin(kr\cos\theta)$ in series form it can be shown that:-

$$\int_{o}^{\pi} \cos\theta\sin(kr\cos\theta)d\theta = \pi J_1(kr) \qquad (4.20)$$

where $J_1(kr)$ is the Bessel function of the first kind of order one. The inertia force can then be written as:-

$$\frac{F_1}{\rho V(1+C_{a_1})} = \frac{2a\omega^2}{k^2 r d_t} J_1(kr)\left[1 - \frac{\sinh k(d-d_t)}{\sinh(kd)}\right]\cos(\omega t) \qquad (4.21)$$

4.5.2 Heave

The inertia force in heave in regular waves is written as:-

$$F_3 = \rho V\left[1 + C_{a_3}\right]\dot{\bar{v}} + F_{3_p} \qquad (4.22)$$

where C_{a_3} is a frequency dependent added mass coefficient, being equal to the heave added mass divided by the mass of displaced fluid, $\dot{\bar{v}}$ is the average acceleration of the fluid which would occupy the region taken up by the buoy, were the buoy not present and F_{3p} is a correction term to allow for the change in buoyancy caused by the wave profile. Writing:-

$$\dot{v} = -a\omega^2 \frac{\sinh k(z+d)}{\sinh(kd)} \sin(\omega t-kx) \qquad (4.23)$$

it can be shown by an argument similar to that used in the above section, that:-

$$\frac{F_3}{\rho V(1+C_{a_3})} = (\frac{2a\omega^2}{k^2 r d_t})J_1(kr)\left[\frac{\cosh k(d-d_t)-\cosh(kd)}{\sinh(kd)}\right]\sin(\omega t)+F_{3p}/\rho V(1+C_{a_3}) \qquad (4.24)$$

The upthrust due to the wave profile $\eta = a\sin(\omega t-kx)$, will be:-

$$F_{3p} = \int_{-r}^{r}\int_{o}^{\eta} 2g\rho(r^2-x^2)^{\frac{1}{2}}dzdx$$

$$= 2\rho g\int_{-r}^{r} a(r^2-x^2)^{\frac{1}{2}}\sin(\omega t-kx)dx$$

$$= \frac{2\rho a\omega^2}{k^2}\pi r J_1(kr)\sin(\omega t) \qquad (4.25)$$

4.5.3 Roll and Pitch

This section will consider the inertia moment induced in pitch by a regular wave propagating along the x-axis. For different directions of wave propagation, the total moment will have the same form as the derived result, which can then be resolved into a roll and pitch moment. The dynamic subsurface pressure, p, acting on the base of the buoy will produce a pitch moment which is given by:-

$$M = -\int_s pxds = -\int_{-r}^{r} 2px(r^2-x^2)^{\frac{1}{2}}dx \qquad (4.26)$$

where:-

$$p = \rho ag\left(\frac{\cosh\, k(d-d_t)}{\cosh(kd)}\right)\sin(\omega t-kx) \qquad (4.27)$$

Equation (4.26) then involves the integral:-

$$\int_{-r}^{r} x(r^2-x^2)^{\frac{1}{2}}\sin(\omega t-kx)dx = -\int_{-r}^{r} x(r^2-x^2)^{\frac{1}{2}}\sin(kx)\cos\omega t dx \qquad (4.28)$$

Putting $x = r\cos\theta$, this integral becomes:-

$$-\int_{-r}^{r} x(r^2-x^2)^{\frac{1}{2}}\sin(kx)dx = -r^3\int_{o}^{\pi}\cos\theta\sin^2\theta\sin(kr\cos\theta)d\theta$$

$$= \frac{r^2}{k}\int_{o}^{\pi}(\cos^2\theta-\sin^2\theta)\cos(kr\cos\theta)d\theta$$

$$= \frac{r^2}{k}\int_{o}^{\pi}\cos(kr\cos\theta)d\theta - \frac{2r^2}{k}\int_{o}^{\pi}\sin^2\theta\cos(kr\cos\theta)d\theta$$

$$= \frac{r^2}{k}\{\pi J_o(kr)-(\frac{2\pi}{kr})J_1(kr)\} \qquad (4.29)$$

where integration by parts and series expansions have been used.

Using:-

$$J_0(x) = J_1(x)\left[\frac{2}{x} - \frac{x}{4}\right] - \frac{x}{4} J_3(x) \qquad (4.30)$$

the moment produced by the pressure on the base becomes:-

$$M = \tfrac{1}{2}\rho a g \pi r^3 \frac{\cosh k(d-d_t)}{\cosh(kd)} \left[J_1(kr) + J_3(kr)\right] \cos(\omega t) \qquad (4.31)$$

The horizontal forces acting in surge will also produce a moment in pitch, which will be:-

$$M = (z_a - z_g)F_1$$

where z_g and z_a are the distances above the still water level of the centre of gravity of the buoy and the point of application of the horizontal force, F_1, (both negative). z_a can be found from:-

$$\int_{-d_t}^{o} p(z - z_a)dz = 0 \qquad (4.33)$$

Substituting (4.27) leads to:-

$$z_a = \frac{\cosh(kd) - \cosh k(d-d_t) - kd_t \sinh k(d-d_t)}{k\left[\sinh k(d-d_t) - \sinh(kd)\right]} \qquad (4.34)$$

5.0 THE THEORY OF SHIP MOTIONS

5.1 Introduction

5.1.1 The Hydrodynamic Problem

Ship motions can be of two forms - firstly the self-imposed manoeuvring motions in the horizontal plane, and secondly the oscillatory motions in all degrees of freedom caused by the action of wave forces. It has been shown by Gerritsma and Beukelman (ref. 51) that these two types of motion are not independent, in that the manoeuvring velocities can have a large effect upon the oscillatory motions. Manoeuvring has been discussed at length by Newman (ref.13) and Stoker (ref. 44) and will not be considered here as the concern is with moored vessels. The response of a ship to ocean waves is in reality a highly complex non-linear problem. Waves may break over the vessel, or conversely the bow may become clear of the water, causing a slamming effect when it is submerged. In addition to this, viscous effects may be present in the form of either viscous drag or vortex shedding, both of which are very difficult to model mathematically. The ocean waves themselves will be random and multi-directional and may not conform to the properties predicted by linear wave theory (Appendix B). Also, as discussed in Chapter 6, the wave forces imposed upon the vessel occur not only at wave frequency, but also at lower frequencies, due to second order effects. This chapter will consider the motions induced by those forces acting at wave frequency, i.e. the 'first order' motions.

Faced with the above problem, a full mathematical solution is clearly impossible and several idealisations must be made. Usually, viscous effects are neglected and the fluid is considered to be incompressible and irrotational so that a velocity potential ϕ exists. Next, it is usually assumed that the problem is linear, i.e. linear wave theory is used, and it is assumed that the amplitude of a disturbance in the fluid caused by vessel motion is linearly proportional to the amplitude of the motion. The wave and vessel motion amplitudes are considered to be small quantities such that squared and higher powers can be neglected. Effects such as slamming are not considered. The problem is then solved for a regular wave, and the response for a random seastate is taken to be a linear superposition of regular wave responses, amenable to solution by spectral analysis

techniques. The complete velocity potential when the incident sea-state consists of one regular wave of frequency ω is written as:-

$$\phi = \mu e^{-i\omega t} \tag{5.1}$$

$$\mu = -i\omega \sum_{0}^{7} \psi_j \zeta_j \qquad j = 0....7 \tag{5.2}$$

where ζ_1 to ζ_6 are the amplitudes of motion in the six degrees of freedom of the vessel (see Figure 5.1), ζ_0 is the amplitude of the incident wave, and ζ_7 is an amplitude associated with the diffracted wave. For j = 1 to 6, $-i\omega\psi_j$ is the amplitude of the velocity potential caused by a motion of frequency ω and unit amplitude in the j'th degree of freedom. $-i\omega\psi_0$ and $-i\omega\psi_7$ are the velocity potentials associated with the incident and diffracted waves respectively. Van Oortmerssen (ref 45) has shown that the linear equations of motion of the vessel can then be written in the form:-

$$\sum_{j=1}^{6} \{-\omega^2(M_{kj}+a_{kj}) - i\omega b_{kj} + c_{kj}\}\zeta_j = (T_{ko}-T_{ok})\zeta_0, k=1...6 \tag{5.3}$$

where:-

$$T_{kj} = -\rho\omega^2 \int_s \psi_j n_k ds \qquad k,j = 0...7 \tag{5.4}$$

$$a_{kj} = \frac{1}{\omega^2} \mathrm{Re}\{T_{kj}\} \quad ; \quad b_{kj} = \frac{1}{i\omega} \mathrm{Im}\{T_{kj}\} \quad k,j=1..6 \tag{5.5}$$

The integral in equation (5.4) is over the submerged surface of the vessel, and n_k represents the normal component in the k'th direction. Physically, $T_{ko}\zeta_o$ and $-T_{ok}\zeta_o$ are the forces (k=1,2,3) and moments (k=4,5,6) exerted by the pressure fields associated with the incident and diffracted waves. M_{kj} is the structural mass matrix of the vessel and c_{kj} is the linear stiffness matrix due to both hydrostatic effects and mooring lines. a_{kj} and b_{kj} are the added mass and damping tensors, which can be proved to be symmetric (see Newman, ref. 13). If the potentials ψ_j can be found, then the complex motion amplitudes ζ_j can be found from equation (5.3) by a matrix inversion. The problem of finding the ψ's is discussed in the next section.

Vinge (ref. 46) has developed an alternative approach for the two dimensional rolling motions of ships in beam waves. This involves a numerical timestep integration procedure, which is able to

incorporate breaking waves and the shipping of water onto the deck. The two-dimensional nature of this solution limits its usefulness in practical situations, although it does give an insight into some of the non-linear mechanisms involved.

5.1.2 Methods of Solution

It can be shown from Green's Theorem (see Lamb, ref. 47) that the velocity potential inside a fluid region can be represented by a distribution of source like functions over the surface of the region. In mathematical terms:-

$$\phi(x,y,z) = \frac{1}{4\pi}\int_s f(\alpha,\beta,\gamma)G(x,y,z;\alpha,\beta,\gamma)ds \qquad (5.6)$$

where $G(x,y,z:\alpha,\beta,\gamma)$ is the potential at (x,y,z) due to a source like function at (α,β,γ) and $f(\alpha,\beta,\gamma)$ is a measure of the strength of this function. The integral is taken over the boundary surface, s. For ship motion problems, it can be shown that if G is chosen so as to satisfy the free surface and sea-bed boundary conditions, then s reduces to the submerged surface of the ship. Such an expression for G has been given by Wehausen and Laitone (ref. 48), for both the three-dimensional and two-dimensional case. Each of the potentials ψ_j (j=1...6) contained in equation (5.2) can then be written as:-

$$\psi_j(x,y,z) = \frac{1}{4\pi}\int_s f_j(\alpha,\beta,\gamma)G(x,y,z:\alpha,\beta,\gamma)ds \qquad (5.7)$$

where the functions $f_j(\alpha,\beta,\gamma)$ are as yet unknown. The boundary condition that there is zero flow through the ship hull can be expressed as:-

$$m_j(x,y,z) = \frac{\partial\psi_j(x,y,z)}{\partial n} \quad \text{on s} \qquad (5.8)$$

where $m_j(x,y,z)$ is the normal displacement of the ship hull at (x,y,z) due to a unit displacement in the j'th degree of freedom. Applying (5.7) yields:-

$$m_j(x,y,z) = -\tfrac{1}{2}f_j(x,y,z) + \frac{1}{4\pi}\int_s f_j(\alpha,\beta,\gamma)\frac{\partial G}{\partial n}(x,y,z:\alpha,\beta,\gamma)ds \text{ on s} \qquad (5.9)$$

where the fact that $\frac{\partial G}{\partial n}$ is singular at the point $(x,y,z) = (\alpha,\beta,\gamma)$ has lead to the first term on the right hand side (see Newman, ref. 13) Equation (5.9) forms the basis of the diffraction packages, such as NMIWAVE, currently in use in the offshore industry. The surface s is divided into a finite number of flat plates (see Figure 5.2) and equation (5.9) recast in matrix form. A matrix inversion then yields the value of $f_j(x,y,z)$ at the centre of each of these plates, which can then be substituted into equation (5.7) to yield the velocity potentials. Such packages tend to be expensive to use due to the large number of plate elements required (typically 200) and the nature of $G(\alpha,\beta,\gamma:x,y,z)$, which is in the form of an infinite series of which a large number of terms must be considered. Due to the way in which the problem is formulated, the equations model not only the fluid surrounding the vessel, but also a fictitious fluid region inside the vessel. Problems have been reported (see Taylor, ref. 49) where the incident wave frequency has corresponded to a resonant frequency of this interior region, and caused a breakdown of the numerical calculation procedure.

One alternative to the above fully three-dimensional approach is 'strip theory', in which the vessel is divided into a number of strips, flow about each of which is considered to be two-dimensional and independent of the flow about any other, as illustrated in Figure 5.3. This method can use either a two-dimensional form of the above equations or draw upon the significant amount of published data which is now available. This method was first applied to the heaving and pitching of a ship in head seas by Korvin-Kroukovsky and Jacobs (ref. 50) and has been much refined since. Gerritsma and Beukelman (ref. 51), Vughts (ref. 52) and Salvensen et al (ref. 53) have all presented strip theories for a ship underway in head seas, and good agreement with model test results has been found. Sectional properties are used to build up the complete added mass and damping matrices for the vessel, as will be discussed in section (5.2).

Migliore and Palo (ref. 54) have compared strip theory and three-dimensional diffraction theory results for various types of barge in head seas. They concluded that strip theory could be used with confidence when the length to breadth ratio was greater than 8.0, and the length to draft ratio was greater than 10.0. For a typical VLCC (Very Large Crude Carrier) of the type used at offshore

mooring terminals, these ratios are of the order 7.0 and 16.0 respectively. This would suggest that the use of strip theory on this type of vessel should yield reasonably accurate results for head seas. These results will be less accurate for oblique seas, due to the greater three-dimensional diffraction effects occurring in the horizontal plane. Oblique seas at large angles of incidence are not expected in the case of an offshore mooring terminal, since the system is designed to weathervane to face the worst combination of wind, waves and current.

Although the diffraction method yields exact results within the limits of potential theory, the presence of wind and current is not accounted for. It is known that there is an interaction effect between waves and current which is not as yet fully understood, but which may cause a significant difference between diffraction theory results and the actual motions of the vessel. In view of the many problems which still exist, it was decided to use the simpler and less expensive (in terms of computer time) strip theory for the analysis of the SBS system detailed in Chapter 8. This method is outlined below.

5.2 Strip Theory

5.2.1 The Added Mass Tensor

The added mass force acting on the vessel in the i'th direction can be written as:-

$$F_i = \int \{ - \frac{d}{dt} (\sum_j A'_{ij} q_j) \, d\xi \qquad (5.10)$$

where ξ is a dummy variable taken along the length of the ship, q_j is the velocity of the ship in the j'th direction and A'_{ij} is the added mass per unit length at ξ. In strip theory, coupling of the longitudinal (surge, heave and pitch) and transverse (sway, roll and yaw) degrees of freedom is neglected, making the relevant terms of A'_{ij} zero. The coefficients A'_{ij} can be found by using a two-dimensional form of the equations given in section 5.1.2, or by referring to published data. The latter method is discussed below and a summary of the terms, noting that A'_{ij} is symmetric, is given in Figure 5.7.

5.2.1.1 Surge

The added mass in surge is small, being of the order of 5% of the displaced mass of fluid, due to the streamlining of the vessel. Sommet (ref. 55) has given the following expression for a vertically sided prismatic hull:

$$A_{11} = \frac{2}{\pi}\gamma\{\frac{2}{\pi^2}\frac{h}{(L-1)}(1 - \frac{2h}{\pi^2 L})\frac{\sin^2\pi\theta}{\theta} + \theta G(\frac{1}{L})\}\nabla \qquad (5.11)$$

where A_{11} is the total surge added mass, θ is the draft to water depth ratio, h is the water depth, L is the vessel length, γ is the angle the bow makes to the centreline, ∇ is the displaced mass of water and $G(\frac{1}{L})$ is a function plotted by Sommet, and reproduced by Muga and Wilson (ref. 34). Note that this result is independent of frequency, whereas three-dimensional diffraction theory results given by Van Oortmerssen (ref. 45) for a 200,000 DWT tanker, show a slight frequency dependence. Added mass data for VLCC's has also been given by Wichers and Sluijs (ref. 56).

The fact that the surge added mass force will tend to act at the centre of buoyancy, whereas the coordinate system (Figure 5.1) has its origin at the centre of gravity, will introduce a surge-pitch coupling term. This will be $A_{51} = -A_{11}\,BG$, where BG is the distance the centre of buoyancy lies below the centre of gravity.

5.2.1.2 Sway

The expression generally used for the sway added mass per unit length is:-

$$A'_{22} = \rho S k_y k'_4 \qquad (5.12)$$

where $\rho S k_y$ is the added mass for zero frequency and k'_4 is a frequency correction factor. Muga and Wilson (ref. 34) state that:-

$$\rho S k_y = \tfrac{1}{2} C'_z \pi d_t^2 \qquad (5.13)$$

where d_t is the draft of the section and C'_z is a factor given in graphical form by Prohaska (ref. 57) and shown in Figure 5.5. Kaplan and Ulc (ref. 58) have given an approximate expression for the frequency correction factor as:-

$$k'_4 = 1 - \frac{2}{\pi}\left(\frac{\omega^2 d_t}{g}\right) \qquad (5.14)$$

Figure 5.4 shows a typical strip at position ξ, from which it can be seen that there will be a sway-yaw coupling term given by $A'_{62} = \xi A'_{22}$. Also, the roll-sway coupling can be approximated to $A'_{42} = BGA'_{22}$, which will produce a roll-yaw coupling of $A'_{46} = \xi A'_{42}$.

5.2.1.3 Heave

The heave added mass can be calculated from:-

$$A'_{33} = C\,\frac{\pi\rho B^2}{8} \qquad (5.15)$$

where B is the beam of the vessel and C is a frequency dependent coefficient given by Grim (ref. 59). Figure 5.6 shows values of C for a range of section coefficients (β) and beam to draft ratios. From Figure 5.4 it can be seen that there will be a heave-pitch coupling term given by $A'_{53} = \xi A'_{33}$.

5.2.1.4 Roll

The added mass in roll is probably the most difficult to estimate, due to it's sensitivity upon the shape of the section. One possible expression, based upon the sway added mass coefficient, is:-

$$A'_{44} = BG^2 A'_{22} \qquad (5.16)$$

It can be seen, however, that this formula will be inadequate for many sectional shapes - a circular section with the CoG at its centre will have no roll added mass, whereas (5.16) may predict quite a high value. Bhattacharyya (ref. 60) has offered two alternative approaches. In the first, the structural moment of inertia per unit length of the section is written:-

$$M'_{44} = \nabla k_{xx}^2 \qquad (5.17)$$

where ∇ is the structural mass per unit length and k_{xx} is the radius of gyration in roll. The added moment of inertia per unit length is then written as:-

$$A'_{44} = \nabla' k_{xx}^2 \qquad (5.18)$$

where, typically, ∇' is of the order of 20% of ∇. In the second approach, the total roll inertia per unit length is written as:-

$$M'_{44} + A'_{44} = \nabla k''^{2}_{xx} \qquad (5.19)$$

where k''_{xx} is a modified radius of gyration. Usually k''_{xx} lies between 0.33 and 0.45 times the breadth of the section. These formulae were compared for a 135,000 DWT tanker having a mass of 1.549×10^8kg, a structural roll moment of inertia of 4.143×10^{10}kgm^2 and a beam of 43m. Equation (5.18) with $\nabla' = 0.2\nabla$ gave a total roll moment of inertia of 4.97×10^{10}kgm^2, whereas (5.19) gave 3.119×10^{10}kgm^2 and 5.799×10^{10}kgm^2 (an average of 4.46×10^{10}kgm^2) for $k''_{xx} = 0.33B$ and 0.45B respectively. Equation (5.16) gave 4.35×10^{10}kgm^2 for low frequency oscillations and 4.16×10^{10}kgm^2 for high frequency oscillations. As these results are all of similar magnitude, it was decided to use the simplest method, equation (5.18), in the analysis contained in Chapter 8.

5.2.1.5 Pitch

The added mass per unit length in pitch can, with reference to Figure 5.4, be written in terms of the heave added mass as:-

$$A'_{55} = \xi^2 A'_{33} \qquad (5.20)$$

where A'_{33} is given by equation (5.15)

5.2.1.6 Yaw

The yaw added mass can be written in terms of the sway added mass as:-

$$A'_{66} = \xi^2 A'_{22} \qquad (5.21)$$

where A'_{22} is given by equation (5.12).

5.2.2 The Damping Tensor

The potential damping force due to wave generation acting in the i'th direction can be written as:-

$$F_i = \int\{-\sum_j C_{ij} N'_{ij} q_j\}d\xi \qquad (5.22)$$

where ξ is a dummy variable taken along the length of the ship, q_j is the velocity of the ship in the j'th direction, N'_{ij} is the two-dimensional damping coefficient per unit length and C_{ij} is a correction factor for three-dimensional effects. These coefficients can be obtained from published data as explained below, and summarised in Figure 5.12.

5.2.2.1 Surge

Muga and Wilson (ref. 34) state that the potential damping in surge can be written as:-

$$C_{11} N'_{11} = f(\omega) C_{33} N'_{33} \qquad (5.23)$$

where C_{33} and N'_{33} are heave coefficients discussed in Section 5.2.2.3. The frequency dependent function $f(\omega)$ has been quoted as being in the order of 0.1 by Newman (ref. 61). Viscous effects are important when considering surge damping, and are discussed in Sections 6.3.1 and 6.3.2.

5.2.2.2 Sway

The damping coefficient in sway can be written as:-

$$N'_{22} = \frac{\rho\omega^5}{16g^2} B^4 d_y^2 \qquad (5.24)$$

where dy is a coefficient dependent upon the section properties, shown in Figure 5.8 (see Vossers, ref. 62). The three-dimensional coefficient C_{22} has been plotted by Kaplan and Hu (ref. 63) for a spheroid, which may overestimate the effect for a slab sided vessel such as a VLCC. From Figure 5.4 it can be seen that there is a sway-yaw coupling term given by $N'_{42} = \xi N'_{22}$ and a sway-roll coupling term approximated by $N'_{42} = BGN'_{22}$. This will produce a roll-yaw coupling term of $N'_{64} = \xi N'_{42}$. Usually it is considered that $C_{42} = C_{46} = C_{22}$ and $C_{66} = 1$ (see Muga and Wilson, ref. 34)

5.2.2.3 Heave

The heave damping coefficient is written as:-

$$N'_{33} = \frac{\rho g^2}{\omega^3} \bar{A}_z^2 \qquad (5.25)$$

where $\bar{A}_z$ is the ratio of the amplitude of the heave generated wave to the amplitude of the heaving oscillations. A proof of this formula has been given by McCormick (ref. 64). $\bar{A}_z$ has been plotted by Grim (ref. 59) for a variety of section properties and is shown in Figure 5.9. Havelock (ref. 65) has given results for C_{33} although Korvin-Kroukovsky (ref. 50)has stated that a value of $C_{33} = 1$ may be advisable. From Figure 5.4 it can be seen that there will be a heave-pitch coupling term given by $N'_{53} = \xi N'_{33}$. Muga and Wilson (ref. 34) state that $C_{53} = 1$.

5.2.2.4 Roll

Roll damping is highly dependent upon viscous effects and hence it cannot be estimated accurately by potential theory, particularly if bilge keel dampers are fitted. Reference 60 gives the roll damping moment as a combination of linear and quadratic terms:-

$$M_r = A\dot{\phi} + B\dot{\phi}|\dot{\phi}| \qquad (5.26)$$

where A and B are constants, which can be found from model or full scale tests, and $\dot{\phi}$ is the roll velocity. The model is given an initial displacement and an extinction curve, such as that shown in Figure 5.10. is plotted. New constants k_1 and k_2 are then defined as:-

$$d\phi = k_1\phi + k_2\phi^2 \qquad (5.27)$$

where $d\phi$ is the loss in amplitude over a half cycle and ϕ is the amplitude at the beginning of the cycle. It can be shown (see Bhattacharyya, ref. 60) that:-

$$A = k_1 2\overline{GM}\, Mg/(\pi\omega_n) \quad ; \quad B = k_2 3\overline{GM}\, Mg/(4\omega_n{}^2) \qquad (5.28)$$

where $\overline{GM}$ is the roll metacentric height, M is the mass of the ship and ω_n is the natural frequency in roll. k_1 and k_2 are given in Figure 5.10 for various types of ship, with and without bilge keels, after ref. 66. The equivalent damping ratio, β, can be defined from equation (5.26) as:-

$$\beta = \frac{1}{2\omega_n(I+I_a)}\left[A+B|\dot{\phi}|\right] \simeq \frac{k_1}{\pi} + \frac{3k_2}{8\omega_n}|\dot{\phi}| \qquad (5.29)$$

which is time dependent due to the non-linear nature of this equation. $(I+I_a)$ is the total roll moment of inertia of the ship. In a random sea state, the equivalent linearisation method of section 2.3.1 can be applied to yield:-

$$M_r = \left[A + \sqrt{\frac{8}{\pi}}\,\sigma_{\dot{\phi}}B\right]\dot{\phi} \qquad (5.30)$$

where $\sigma_{\dot{\phi}}$ is the rms value of the roll velocity. This then gives:-

$$\beta = \frac{k_1}{\pi} + \frac{3}{8\omega_n}\sqrt{\frac{8}{\pi}}\,\sigma_{\dot{\phi}}k_2 = \beta_L + \beta_{N.L}, \text{ say} \qquad (5.31)$$

If the maximum roll amplitude is around 20^o and the mean frequency is about 0.36 rad/sec, then typically $\sigma_{\dot{\phi}} \simeq 0.126$ rad/sec (0.25 of the maximum, due to the results of Longuet-Higgins, ref. 28). Taking values from Figure 5.10 for the Greyhound then gives $\beta_L = 0.014$, $\beta_{N.L} = 0.000334$ for no bilge keels and $\beta_L = 0.0111$ and $\beta_{N.L} = 0.005$ for bilge keels, which shows that the damping in roll can be very small. Other values, given by ref.66, are shown in Figure 5.11, from which it can be seen that forward speed (and therefore current) can cause a considerable increase in roll damping.

5.2.2.5 Pitch

The damping coefficient in pitch can be expressed as:-

$$N'_{55} = \xi^2 N'_{33} \qquad (5.32)$$

where N'_{33} is given by equation (5.25). Havelock (ref. 65) has plotted C_{55}, although a value of 1 may suffice.

5.2.2.6 Yaw

The yaw damping coefficient may be written as:-

$$N'_{66} = \xi^2 N'_{22} \tag{5.33}$$

where N'_{22} is given by equation (5.24). Hsu and Kaplan (ref. 63) have plotted the three-dimensional correction factor C_{66} for a spheroid, although a value of 1 may be more applicable to a VLCC.

5.2.3 Hydrostatic Stiffness

Buoyancy effects produce hydrostatic stiffness terms in heave, pitch and roll, which are, respectively:-

$$F_3 = \rho g A \gamma + C_{35}\theta \tag{5.34}$$

$$F_5 = \overline{GM}_p Mg\theta + C_{35}\gamma \tag{5.35}$$

$$F_4 = \overline{GM}_r Mg\phi \tag{5.36}$$

where γ, θ and ϕ are the displacements, A is the waterplane area of the ship, M is the mass and $\overline{GM}_r$ and $\overline{GM}_p$ are the roll and pitch metacentric heights (see reference 66). C_{35} is a coupling term between heave and pitch, given by:-

$$C_{35} = \rho g \int \xi B d\xi \tag{5.37}$$

where B is the beam at ξ.

5.2.4 Linear Wave Forces

Within strip theory there are three possible methods of calculating the linear wave forces acting on a ship. The first two rely on the solution of the two-dimensional form of the equations given in 5.1.2. In the first of these, the hydrodynamic pressure due to each potential (diffracted, incident and motion induced) is integrated over the submerged hull. In the second, the two-dimensional Haskind relation (see Newman, ref. 67) is utilised, obviating the need to calculate the diffracted potential. The third method is less accurate but involves far less computer time, since it requires only the incident wave potential and the added mass and damping coefficients,

rather than a complete solution for the velocity potential. The wave forces are considered to be composed of inertia forces, damping forces and wave profile effects. The general method of calculating these forces is given below, and detailed expressions are given in Appendix D.

5.2.4.1 Inertia Forces

The inertia forces per unit length acting in surge, sway and heave at a position ξ along the ship are each written in the form:-

$$F_i'(t) = \left[\rho B d_t \beta + A_{ii}\right] \bar{\ddot{q}}_i(\xi,t) \qquad i = 1,2,3 \qquad (5.38)$$

where B, d_t and β are the beam, draft and section coefficient at ξ. $\bar{\ddot{q}}_i(\xi,t)$ is the average acceleration, in the i'th direction, of the fluid which would occupy the region $x = \xi$ to $\xi+d\xi$ were the vessel not present. This can be found from:-

$$\bar{\ddot{q}}_i(\xi,t) = \frac{1}{Bd_t} \int_{-B/2}^{B/2} \int_{-d_t}^{0} \ddot{q}_i(\xi,t,y,z)\,dy\,dz \qquad (5.39)$$

where $\ddot{q}_i$ is the fluid acceleration due to the incident wave. Equation (5.38) is similar in form to the inertia force appearing in Morison's equation (see Appendix C) being due to the Froude-Krylov Force plus an additional term due to diffraction. The total inertia forces in surge, sway and heave are then:-

$$F_i(t) = \int F_i'(t)\,d\xi \qquad i = 1,2,3 \qquad (5.40)$$

and the roll, pitch and yaw moments can be written as:-

$$F_4(t) = F_2(t)BG \qquad (5.41)$$

$$F_5(t) = -\int \xi F_3'(t)\,d\xi - F_1(t)BG \qquad (5.42)$$

$$F_6(t) = \int \xi F_2'(t)\,d\xi \qquad (5.43)$$

where BG is the distance the centre of buoyancy lies below the centre of gravity.

5.2.4.2 Damping Forces

These forces modify the potential damping terms to allow for the fact that the ship is not oscillating in still water. The force per unit length, in the i'th direction, at ξ is written as:-

$$F_i'(t) = C_{ii}N_{ii}'\bar{\dot{q}}_i(\xi,t) \qquad i = 1,2,3 \qquad (5.44)$$

where $\bar{\dot{q}}_i(\xi,t)$ is the velocity equivalent of $\bar{\ddot{q}}_i(\xi,t)$ and is given by:-

$$\bar{\dot{q}}_i(\xi,t) = \frac{1}{Bd_t}\iint \dot{q}_i(\xi,t,y,z)\,dydz \qquad (5.45)$$

The total forces in surge, sway and heave, and the pitch and yaw moments, then have the same form as equations (5.40), (5.42) and (5.43). As the potential damping in roll is small, $F_4(t)$ can be taken to be zero.

5.2.4.3 Wave Profile Effects

The force acting in heave due to the wave profile can be written:-

$$F_3(t) = \rho g A\bar{\eta}(t) \qquad (5.46)$$

where $\bar{\eta}(t)$ is the average surface elevation over the waterplane area, A. This can be found from:-

$$\bar{\eta}(t) = \frac{1}{LB}\int_{-L/2}^{L/2}\int_{-B/2}^{B/2}\eta(t,\xi,y)\,d\xi dy \qquad (5.47)$$

where η is the profile or amplitude of the incident wave. Similarly, the moment induced in pitch is:-

$$F_5(t) = \rho g A\bar{m}(t) \qquad (5.48)$$

$$\bar{m}(t) = \frac{1}{LB}\int_{-L/2}^{L/2}\int_{-B/2}^{B/2}\xi\eta(t,\xi,y)\,d\xi dy \qquad (5.49)$$

These terms can be thought of as being correction terms to the inertia forces - the tanker is not subject to the same forces as the displaced fluid, since it does not have the pressure of the wave profile acting on it. Thus the pressure of the wave profile is subtracted from (i.e.

the upthrust added to) the inertia forces. The wave slope will produce a moment in roll, due to hydrostatic effects, given by:-

$$F_4(t) = \overline{GM}_r \, Mg \, \bar{\eta}_y(t) \tag{5.50}$$

$$\bar{\eta}_y(t) = \frac{1}{LB} \int_{-L/2}^{L/2} \int_{-B/2}^{B/2} \eta_y(t,\xi,y) d\xi dy \tag{5.51}$$

where η_y is the slope of the incident wave in the y direction.

5.3 Viscous Effects

5.3.1 Damping and Stiffness Terms due to Current

Empirical formulae for the current forces in surge, sway and yaw acting on a stationary VLCC have been given by the Oil Companies International Marine Forum (ref. 68). These equations are of the form:-

$$F_i = C_i V_c^2 f_i(\theta) \qquad i = 1,2,6 \tag{5.52}$$

where C_i is a constant coefficient, V_c is the current velocity and $f(\theta)$ is a function of the incidence of the current to the bow of the vessel. Equation (5.52) can be modified to allow for the vessel having surge and sway velocities, u and v and a yaw displacement ψ (see Figure 5.13) to give:-

$$\begin{aligned} F_i(u,v,\psi) &= C_i\{(V_c\cos\theta+u)^2 + (V_c\sin\theta-v)^2\} f_i(\phi) \\ &= C_i g(u,v) f_i(\phi), \text{ say} \end{aligned} \tag{5.53}$$

$$\phi = \tan^{-1}\{(V_c\sin\theta-v)/(V_c\cos\theta+u)\}+\psi \tag{5.54}$$

If u, v and ψ are small perturbations from the mean position of the vessel, then a McClauren's expansion gives:-

$$\begin{aligned} F_i(u,v,\psi) = F_i\Big|_o + C_i\{ & u\left[\frac{\partial g}{\partial u} f_i(\phi) + g\frac{\partial \phi}{\partial u}\frac{\partial f_i}{\partial \phi}\right]\Big|_o + v\left[\frac{\partial g}{\partial v} f_i(\phi) + g\frac{\partial \phi}{\partial v}\frac{\partial f_i}{\partial \phi}\right]\Big|_o \\ & + \psi\left[g\frac{\partial \phi}{\partial \psi}\frac{\partial f_i}{\partial \phi}\right]\Big|_o \} \end{aligned} \tag{5.55}$$

where $\Big|_o$ represents evaluation at $u=v=\psi=0$. It can be shown that:-

$$\left.\frac{\partial\phi}{\partial u}\right|_o = \frac{-\sin\theta}{V_c} \; ; \; \left.\frac{\partial\phi}{\partial v}\right|_o = \frac{-\cos\theta}{V_c} \; ; \; \left.\frac{\partial\phi}{\partial\psi}\right|_o = 1 \qquad (5.56)$$

$$\left.\frac{\partial g}{\partial u}\right|_o = 2V_c\cos\theta \; ; \; \left.\frac{\partial g}{\partial v}\right|_o = -2V_c\sin\theta \qquad (5.57)$$

Equation (5.55) then becomes:-

$$F_i(u,v,\psi) = F_i|_o + C_i V_c\{u\left[2\cos\theta\, f_i(\theta) - \sin\theta\left.\frac{\partial f_i}{\partial\phi}\right|_o\right] + v\left[-2\sin\theta - f_i(\theta)\cos\theta\left.\frac{\partial f_i}{\partial\phi}\right|_o\right] + \psi\left[V_c\left.\frac{\partial f_i}{\partial\phi}\right|_o\right]\} \qquad (5.58)$$

The first term in this equation represents the mean force, the second and third terms represent damping forces, and the fourth term is a restoring force. These terms can be added to the damping and stiffness matrices given by strip theory. Note that the above analysis does not predict any damping in yaw, a fact which is discussed in detail in Chapter 7.

5.3.2 Non-Linear Surge Damping in Waves

Wichers and Sluijs (ref. 56) have stated that the surge damping force on a VLCC in regular head waves can be written as:-

$$F_1 = \left[B_o + B^2(\omega)\eta^2\right]\dot{x} = B_x\dot{x} \qquad (5.59)$$

where $\dot{x}$ is the surge velocity, B_o is the still water damping coefficient, including both viscous and potential effects, η is the incident wave amplitude and $B^2(\omega)$ is a function of frequency which depends on the dimensions of the vessel. Wichers and Sluijs (ref. 56) have plotted this function for a 200,000 DWT tanker, and a curve which fits their results is:-

$$B^2(\omega) = (52\omega - 39\omega^2 - 12) \times 10^4 \text{ tonne-sec/m} \qquad (5.60)$$

for $0.3 < \omega < 1.0$ and zero elsewhere. Langley and Kirk (ref. 11) linearised equation (5.59) in a random head sea by replacing the non-linear damping coefficient with its r.m.s. value, which was found to be:-

$$\sigma(B_x) = \{\left[B_o + 2.\int_o^\infty B^2(\omega) S_\eta(\omega) d\omega\right]^2 + 8 \int_o^\infty \int_o^\infty B^4(\omega + \tfrac{1}{2}\omega_k) S_\eta(\omega) S_\eta(\omega+\omega_k) d\omega d\omega_k\}^{\frac{1}{2}} \quad (5.61)$$

where $S_\eta(\omega)$ is the wave spectrum. This value can be used in place of that given in section 5.2.2.1. The value used for the surge damping coefficient should be as realistic as possible, in view of the fact that slow drift forces (see Chapter 6) may induce resonance in surge.

6.0 SLOW DRIFT MOTIONS OF MOORED OFFSHORE STRUCTURES

6.1 Introduction

As mentioned in section 1.2, large amplitude low frequency motions of single point mooring terminals can be caused by a number of different mechanisms. One of these is the 'slow drift' phenomena, in which second order effects produce forces which occur at all frequencies ranging from zero to the bandwidth of the incident wave spectrum. Although these forces are small, they can occur at the natural frequencies of the horizontal degrees of freedom (surge, sway and yaw) of a moored vessel, and thus induce resonance. Damping in these degrees of freedom, especially surge, can be very low, and thus large amplitudes of response can be induced. An indication of the magnitude of response which can be expected has been given by Bowers (ref. 24), who performed model tests to simulate the slow surge motions of a tanker moored in irregular head seas. It was found that the r.m.s. response could be written as $\sigma = (H_s/3.72)^2$ where H_s is the significant wave height, a maximum of H_s = 3m being used in the model tests. Verhagen and van Sluijs (ref. 69) performed model tests relating to a tanker in beam seas, and shows that the r.m.s. sway response was given by $\sigma = 1.2(H_s^2/T_z)$ where T_z represents the average period of the incident seastate. The maximum significant wave height considered in these tests was 4.72m. Although both these results are of limited validity, they indicate that r.m.s. response values of greater than 10m may be expected in severe seastates (say H_s > 10m), a fact which has been verified by other researchers (see for example Wichers and van Sluijs, ref. 56).

Slow drift forces have been the subject of much research over the last ten years, and their causes are now thought to be well understood. The forces fall into two categories - firstly those which are proportional to the product of two first order quantities and are caused by non-linear effects, and secondly those which are due to the presence of a second order velocity potential $\phi^{(2)}$ (often called 'set-down' effects see Stoker, ref. 44).In a random sea this second order potential is due to the 'beating' effect which occurs between first order components of slightly differing frequencies. It is found that in regular waves, where the slow drift forces have a constant value, the potential $\phi^{(2)}$ produces no net forces in either surge, sway or yaw.

Two approximate methods exist for calculating the mean forces exerted on a body in regular waves. The first is due to Owen and Lightfoot (ref. 70) and is an extension of an earlier result derived by Havelock (ref. 71). The incident wave is assumed to be of such a high frequency that total reflection is achieved, and body motions are negligible. The mean forces acting in surge, sway and yaw can then be found in terms of an integral around the waterline of the body, which can be of arbitrary shape. This method is discussed in more detail in section 6.3, and can be regarded as an asymptotic solution as the frequency of the incident wave tends to infinity. The second approximate method is due to Newman (ref. 72) and is based upon slender body theory. This assumes that the vessel length and the incident wave length are of the same order, and that both are much greater than the vessel beam and draft. This method is only valid for low frequency waves whose angle of incidence to the bow is not too great - in fact in beam seas no mean force is predicted in sway, since the beam is assumed to be so small that no diffraction occurs, and the vessel is completely surface following. Diffraction programs such as NMIWAVE (ref. 73), and NV459 (ref. 74) have now been developed which are capable of providing numerical solutions for the velocity potential produced when a body floats in regular waves. Using the theory of Lamb (ref. 47), the velocity potential is expressed as a source distribution over the submerged surface of the body. Given this potential, one of two methods can be used to calculate the steady drift forces. The first has been described by Pinkster (ref. 75) and Faltinsen and Loken (ref. 76), and involves the integration of second order terms over the surface of the body, as discussed in section 6.2.1. The second is due to Newman (ref. 72), and considers the conservation of momentum over a control surface far from the body; this is discussed in section 6.2.2.

Three methods are currently in use to calculate the slow drift forces occurring in irregular seas. In the first of these, set-down effects are ignored and an approximation due to Newman (ref. 77) is utilised. This approximation states that the slow drift forces in irregular seas can be predicted from the mean forces exerted by regular waves. Although this method can sometimes be inaccurate, it is easy to apply and requires knowledge of the 'reflection coefficient'

only (the plot of non-dimensionalised mean force in regular waves against frequency). This method is referred to as the Newman/Pinkster method in reference 78 . The sensitivity of the results yielded by this method to the shape of the wave spectrum and the reflection coefficient is discussed in section 6.5. The second method is due to Bowers (ref. 24), and is applicable to a vessel moored in head seas. The second order potential of the incident waves, which is assumed to be unchanged by the presence of the vessel, is used to calculate the second order pressure, which is then integrated over the submerged surface of the vessel. The second order force due to the finite wave height of the incident waves is also considered, although terms due to the velocity squared term in Bernoulli's equation and vessel motions are ignored. This method neglects diffraction and radiation effects, and thus it cannot account for the mean force which is exerted by an irregular sea. The third method (see Pinkster, ref. 75) uses second order transfer functions to describe those terms which are due to the product of two first order terms, this treatment being exact. The forces due to the second order potential are calculated using either the Bowers method (ref. 24) or a method due to Pinkster (ref. 75). No exact solution for the second order potential terms has yet been found - Lighthill (ref. 79) was able to express this potential in terms of the first order potential in a way which involved an integral over the whole sea surface, but computational difficulties have prevented the use of this method.

In all the literature which has been published to date, the incident irregular seastate has been considered to be uni-directional. Reference 78 states that the third method described above is capable of dealing with directional spectra, but it's use for this purpose is limited by the amount of computer time required - second order transfer functions would need to be found between each pair of waves for all frequencies and directions. In practise a vessel moored off-shore is subjected to multi-directional seastates which may contain non-linear and breaking waves, in addition to which there may also be a current. It should therefore be noted that although the mathematical models described above are theoretically and computationally advanced, they still fall far short of providing a full solution to the second order problem, and much work is still to be done in this area.

Very little is yet known about the statistical properties of the slow drift phenomena, although knowledge of these properties is essential if maximum values of response are to be estimated from the r.m.s. values yielded by either frequency or time domain programs (see Chapter 2). Roberts (ref. 26) showed that if the slow drift force is calculated using the 'reflection coefficient' method and the reflection coefficient is assumed to be constant over frequency, then the surface profile of the drift force has an exponential distribution. He then used the Fokker-Planck equation (ref. 27) to examine the statistics of the response, but in so doing approximated the slow drift force to Gaussian. This type of approximation can lead to large errors when used in time domain programs, as pointed out by Kaplan (ref. 23) in his comment on a paper by Oppenheim and Wilson (ref. 21). New work by the author on the statistics of slow drift forces is included in section 6.4.3 of this thesis.

6.2 Second Order Forces on a Floating Body

6.2.1 Body Surface Method

As mentioned in section 6.1, there are two methods of calculating the second order forces acting on a floating body, the first of which involves integration of pressure terms over the body surface. This method will be discussed in this section. Bernoulli's equation for the pressure in an ideal fluid is:-

$$p = -\rho g y - \rho \phi_t - \tfrac{1}{2}\rho(\nabla\phi.\nabla\phi) \qquad (6.1)$$

where ϕ is the velocity potential. Consider now a floating body performing simple harmonic motion in all six degrees of freedom about some mean position, and let (X,Y,Z) be a fixed axis system centred at the mean position of the C.G. Let (d_1,d_2,d_3) and $(\theta_1,\theta_2,\theta_3)$ be the linear and angular displacements of the body. Suppose the point $\underset{\sim}{q}$ lies on the submerged surface of the body, and has coordinates $\underset{\sim}{q}_o = (x_o,y_o,z_o)$ when the body is in the equilibrium position (see Figure 6.1). The instantaneous position of this point will then be given by the vector

$$\underset{\sim}{q} = \underset{\sim}{q}_o + (d_1,d_2,d_3) + (\theta_1,\theta_2,\theta_3) \times \underset{\sim}{q}_o = \underset{\sim}{q}_o + \Delta\underset{\sim}{q} \qquad (6.2)$$

where x denotes a vector or cross product.

In linear theory the pressure is evaluated at $\underset{\sim}{q}_o$ and the velocity squared terms are neglected. Now using the Taylor series expansion:-

$$\phi(\underset{\sim}{q}_o + \Delta\underset{\sim}{q}) = \phi(\underset{\sim}{q}_o) + \Delta\underset{\sim}{q}.\nabla\phi(\underset{\sim}{q}_o) \qquad (6.3)$$

equation (6.1) can be expanded to second order:-

$$p = -\rho gy - \rho\phi_t^{(1)}\big|_m - \rho\phi_t^{(2)}\big|_m - \rho\Delta\underset{\sim}{q}.\nabla\phi_t^{(1)}\big|_m - \tfrac{1}{2}\rho\left[\nabla\phi^{(1)}.\nabla\phi^{(1)}\right]\big|_m \qquad (6.4)$$

where $|_m$ represents evaluation at the mean position (x_o, y_o, z_o), $\phi^{(1)}$ is the first order potential given by linear wave theory and $\phi^{(2)}$ is the second order potential (see Stoker, ref 44). The pressure, as given by (6.4), then produces the following components of second order force on the body:-

a) In the region of the still water level, there is a second order force produced by integrating the first order terms in (6.4) over the region between the wave elevation and the displaced water line position. Suppose a point on the water line moves up by a distance d to the instantaneous position (see Figure 6.2). Then:-

$$F_i^{(2)} = -\int_c \int_d^{\eta} \rho n_i \, dy \, d\ell \quad ; \quad i = 1,2,3 \qquad (6.5)$$

where n_i is the component of the unit normal to $d\ell$ in the i'th direction, and c is the water line. Using equation (6.4) and the fact that linear wave theory gives $\phi_t^{(1)} = -g\eta$, then,

$$F_i^{(2)} = \int_c \int_d^{\eta} (\rho gy - \rho g\eta) n_i \, dy \, d\ell = \int_c \rho g\left[\tfrac{1}{2}y^2 - y\eta\right]_d^{\eta} n_i \, d\ell$$

$$= \int_c \tfrac{1}{2}\rho g(\eta - d)^2 n_i \, d\ell \qquad (6.6)$$

This is usually called the relative wave height contribution. d can be found as the z component of $\Delta\underset{\sim}{q}$.

b) The velocity squared terms can be integrated over the mean position of the submerged surface (S_o, say) to produce:-

$$F_i^{(2)} = \iint_{S_o} \tfrac{1}{2}\rho\left[\nabla\phi^{(1)}.\nabla\phi^{(1)}\right] n_i \, ds \quad ; \quad i = 1,2,3 \qquad (6.7)$$

c) The pressure gradient term can be integrated over S_o:-

$$F_i^{(2)} = \iint_{S_o} \rho \Delta \underset{\sim}{q} . \nabla \phi_t^{(1)} n_i ds \quad ; \quad i = 1,2,3 \tag{6.8}$$

d) Since the pressure acts normally to the surface of the body, the line of action of each of the first order hydrodynamic forces acting on the body will rotate with the body. If these forces are (F_1,F_2,F_3) then the rotation produces a second order force:-

$$(F_1^{(2)},F_2^{(2)},F_3^{(2)}) = (\theta_1,\theta_2,\theta_3) \times (F_1,F_2,F_3) \tag{6.9}$$

However, from the equations of motion:-

$$m(\ddot{d}_1,\ddot{d}_2,\ddot{d}_3) = (F_1,F_2,F_3) \tag{6.10}$$

where m is the structural mass, the second order force can be written as:-

$$(F_1^{(2)},F_2^{(2)},F_3^{(2)}) = m(\theta_1,\theta_2,\theta_3) \times (\ddot{d}_1,\ddot{d}_2,\ddot{d}_3) \tag{6.11}$$

e) The pressure due to the second order potential can be integrated over S_o to yield:-

$$F_i^{(2)} = \iint_{S_o} \rho \phi_t^{(2)} n_i ds \quad ; \quad i = 1,2,3 \tag{6.12}$$

The second order moments can be found by replacing n_i in the above equations with the appropriate component of $\underset{\sim}{q}_o \times \underset{\sim}{n}$, where $\underset{\sim}{n}$ is the unit normal vector (n_1,n_2,n_3). It is usually found (see for example reference 75) that (a) and (b) are opposite in sign, and together produce the greatest individual contributions to the second order force, which are to a large extent self cancelling.

6.2.2 The Momentum Method

Newman (ref. 72) has shown that the mean drift forces acting on a floating body can be found by considering the conservation of momentum of the fluid. In reference (13) it is shown that the hydro-

dynamic forces acting on a body submerged in an infinite fluid region can be written as:-

$$\underset{\sim}{F} = -\rho\frac{d}{dt}\int_{S_B} \phi\underset{\sim}{n}ds - \rho\int_{S_C}\left[\frac{\partial\phi}{\partial n}\nabla\phi - \underset{\sim}{n}\tfrac{1}{2}\nabla\phi.\nabla\phi\right]ds \qquad (6.13)$$

where S_B is the body surface, S_C is some fixed control surface and ϕ is the velocity potential. The normals $\underset{\sim}{n}$ are taken to point out of the surfaces (see Figure 6.3). Equation (6.13) can be applied to a body floating in a fluid of finite depth by including the free surface and the lower boundary into the control surface S_C. Using the divergence theorem and the fact that S_C is fixed, it can be shown that:-

$$\rho\ \frac{d}{dt}\int_v \nabla\phi d\tau = \rho\frac{d}{dt}\int_{S_B}\phi\underset{\sim}{n}ds - \rho\int_{S_C}\frac{\partial\phi}{\partial t}\underset{\sim}{n}\ ds \qquad (6.14)$$

where v is the volume enclosed between the body surface and the control surface. If S_C contains a sufficiently large volume for the conservation of momentum to be applied then:-

$$\rho\frac{d}{dt}\int_v \nabla\phi d\tau = 0 \qquad (6.15)$$

which, together with equations (6.13) and (6.14) leads to:-

$$\underset{\sim}{F} = \rho\int_{S_C}\{\frac{\partial\phi}{\partial t}\underset{\sim}{n} + \tfrac{1}{2}\nabla\phi.\nabla\phi\underset{\sim}{n} - \frac{\partial\phi}{\partial n}\nabla\phi\}\,ds \qquad (6.16)$$

Applying Bernoulli's equation leads to the following expression for the mean forces:-

$$\underset{\sim}{\bar{F}} = <-\int_{S_C}\{p\underset{\sim}{n} + \rho\frac{\partial\phi}{\partial n}\nabla\phi\}\,ds> \qquad (6.17)$$

Similarly, by use of the expression for the hydrodynamic moment acting on a body which is given in reference 13 , and applying conservation of angular momentum, it can be shown that the mean moment is given by:-

$$\underset{\sim}{\bar{M}} = <-\int_{S_C}\{p(\underset{\sim}{r}x\underset{\sim}{n}) + \rho(\underset{\sim}{r}\ x\ \frac{\partial\phi}{\partial n}\nabla\phi)\}ds> \qquad (6.18)$$

When considering the forces and moments acting in the horizontal plane (surge, sway and yaw), there is no contribution from the integrals over the free surface or the lower boundary. Faltinsen and Michelsen

(ref. 74) considered the remaining portion of S_C to be a vertical cylinder of radius r, extending from the lower boundary to the wave profile, so that (see Figure 6.4):-

$$\underset{\sim}{n} = (\cos\theta, \sin\theta, 0) \quad ; \quad \underset{\sim}{r} = (r\cos\theta, r\sin\theta, Z) \tag{6.19}$$

$$\nabla\phi = (V_r\cos\theta - V_\theta\sin\theta, V_\theta\cos\theta + V_r\sin\theta, V_Z)$$

where V_r and V_θ are the radial and transverse components of fluid velocity respectively. The final expressions for the mean forces and moments in surge, sway and yaw are then:-

$$\bar{F}_1 = \left\langle -\int_{S_C} \{p\cos\theta + \rho V_r[V_r\cos\theta - V_\theta\sin\theta]\} r\,d\theta\,dZ \right\rangle \tag{6.20}$$

$$\bar{F}_2 = \left\langle -\int_{S_C} \{p\sin\theta + \rho V_r[V_\theta\cos\theta + V_r\sin\theta]\} r\,d\theta\,dZ \right\rangle \tag{6.21}$$

$$\bar{M}_3 = \left\langle -\int_{S_C} \rho V_r V_\theta r^2\,d\theta\,dZ \right\rangle \tag{6.22}$$

A form of these equations, suitable for use with diffraction programs, in which the fluid pressures and velocities are assumed to be due to a source distribution over the body surface has been given in reference 78. This reference has compared results obtained for the mean force in regular waves using this method, with results obtained using the method outlined in section 6.2.1., and excellent agreement has been found.

6.3 Second Order Forces in Regular Waves

In regular waves of frequency ω, the first order potential and body motions can be written in the form:-

$$\phi^{(1)} = a\phi^{(1)}(i\omega)e^{i\omega t}; \quad \underset{\sim}{d} = a\underset{\sim}{d}(i\omega)e^{i\omega t}; \quad \underset{\sim}{\theta} = a\underset{\sim}{\theta}(i\omega)e^{i\omega t} \tag{6.23}$$

where a is the wave amplitude and real parts are assumed. A typical second order term, being the product of two first order terms, will then be of the form:

$$F_i^{(2)} = \mathrm{Re}\{aAe^{i\omega t}\}\mathrm{Re}\{aBe^{i\omega t}\} = \tfrac{1}{2}\mathrm{Re}\{a^2AB\ e^{2i\omega t} + a^2AB^*\} \tag{6.24}$$

i.e. in regular waves the second order effects produce a mean force and a force having twice the wave frequency, both of these forces being proportional to the wave amplitude squared. The plot of mean force against frequency, when non-dimensionalised, is usually called the reflection coefficient, $R^2(\omega)$. A number of surge reflection coefficients are shown in Figure 6.5. As the frequency tends to infinity the drift force approaches a constant value, and the situation can be idealised as shown in Figure 6.6. It is assumed that body motions tend to zero and that there is total reflection from the front of the body producing a shadow region to the rear. Also, since for large frequencies the wave motions decay rapidly with depth, the body is assumed to be slab sided with infinite draft. Owen and Lightfoot (ref. 70) have shown that terms (a) and (b) of section 6.2.1 produce a mean drift force given by:-

$$F_i = \tfrac{1}{2}\rho g a^2 \int_L \sin^2(\theta+\mu) n_i \, d\ell \qquad (6.25)$$

where a is the wave amplitude, θ the angle of the unit tangent to the x-axis, μ the angle of the incident waves to the x-axis and L the waterline curve, excluding the shadow region, n_1 and n_2 are the x and y components of the inwards pointing normal to the waterline, and n_6 (for yaw) is given by xn_2-yn_1. For a rectangular barge of length L and beam B, equation (6.25) yields $F_1 = \tfrac{1}{2}\rho g B a^2 \cos^2\mu$ and $F_2 = \tfrac{1}{2}\rho g L a^2 \sin^2\mu$. For a cylinder of radius r it can be shown that $F_1 = A\cos\mu$ and $F_2 = A\sin\mu$ where $A = \tfrac{2}{3}\rho g a^2 r$.

Newman (ref. 72) has developed an approximate method of calculating the mean drift forces exerted by low frequency incident waves, this approach being based upon slender body theory.

6.4 Second Order Forces in Irregular Waves

6.4.1 General Theory

The first order potential and body motions in irregular waves, will each have the form:-

$$\sum_n a_n \left[f_n \cos(\omega_n t - k_n x - \varepsilon_n) + g_n \sin(\omega_n t - k_n x - \varepsilon_n) \right] \qquad (6.26)$$

where a_n, ω_n, k_n and ε_n are the amplitude, frequency, wavenumber and phase angle of the n'th wave component; f_n and g_n are transfer functions.

Second order forces will involve the product of terms having the form of (6.26), from which it can be shown that a low frequency force will be produced in the form:-

$$\tilde{F}^{(2)} = \sum_n \sum_m a_n a_m \{T^c_{nm} \cos\theta_{nm} + T^s_{nm} \sin\theta_{nm}\}$$

$$\theta_{nm} = (\omega_n - \omega_m)t - (\varepsilon_n - \varepsilon_m) \qquad (6.27)$$

where T^c_{nm} and T^s_{nm} are second order transfer functions with $T^c_{nm} = T^c_{mn}$ and $T^s_{nm} = -T^s_{mn}$, and where x has been set to zero for convenience. The mean second order force given by (6.27) is:-

$$\bar{F}^{(2)} = \sum_n a_n^2 T^c_{nn} \qquad (6.28)$$

i.e. the total mean force is the sum of the mean forces produced by each regular wave component. It then follows that T^c_{nn} is proportional to the reflection coefficient of the previous section. Newman (ref. 77) postulated that the following approximations may be valid:-

$$T^c_{nm} = T^c_{nn} \quad ; \quad T^s_{nm} = 0 \qquad (6.29)$$

which has been verified for an infinitely long cylinder in beam seas by Faltinsen and Loken (ref. 76). Figure 6.7 shows some of the results they obtained. It should be noted that $T^c_{nm} \simeq T^c_{nn}$ only appears to be valid for those terms which have ω_n close to ω_m - these terms, however, are the ones which are likely to dominate the response of the vessel, since they will occur at or near to the natural frequencies of the horizontal degrees of freedom. Figure 6.8 shows T^c_{nm} for a tanker moored in head seas, as given by Pinkster (ref. 75). Although the off-diagonal terms appear to be substantially different from the diagonal terms, it can be seen that the difference between the frequency components is quite high, being 0.1 rad/s. If the Newman approximation is accepted then it follows that knowledge of the mean drift force in regular waves is sufficient to predict the slow motions produced by irregular seas. In neglecting T^s_{nm}, the terms due to the second order potential $\phi^{(2)}$ have been omitted. An approximate method

of including the effect of $\phi^{(2)}$ has been given by Pinkster and Hooft (ref. 80). This method is based on a result given by Bowers (ref. 24) who has shown that for undisturbed waves with:-

$$\phi^{(1)} = \sum_n \frac{a_n g \cosh k_n(y+d)}{\omega_n \cosh(k_n d)} \cos(k_n x + \omega_n t + \varepsilon_n) \qquad (6.30)$$

the second order potential is given by:-

$$\phi^{(2)} = \sum\sum_{nm} a_n a_m A_{nm} \frac{\cosh[(k_n-k_m)(y+d)]}{\cosh(k_n-k_m)d} \cos[(k_n-k_m)x+(\omega_n-\omega_m)t+(\varepsilon_n-\varepsilon_m)] \qquad (6.31)$$

where A_{nm} is given in reference 24. This suggests the following method of estimating the second order force $F^{(2)}$, due to $\phi^{(2)}$, when the first order force, $F^{(1)}$, is known:-

$$F_n^{(1)} \rightarrow \text{replace} \begin{Bmatrix} k_n \\ \omega_n \\ \varepsilon_n \end{Bmatrix} \text{with} \begin{Bmatrix} k_n-k_m \\ \omega_n-\omega_m \\ \varepsilon_n-\varepsilon_m \end{Bmatrix} \rightarrow \text{replace } a_n \text{ with } a_n a_m$$

$$\rightarrow \text{multiply by } f_{nm} \rightarrow F_{nm}^{(2)}$$

where $f_{nm} = A_{nm}(\omega_n-\omega_m)/g$. Pinkster (ref. 75) has compared results for T_{nm}^s given by the above method with exact results (obtainable in 2-D) given by Faltinsen and Loken (ref. 76) and good agreement has been found when ω_n and ω_m are not too widely separated. One method of gauging the importance of $\phi^{(2)}$ is to compare results for the mean force on a body measured in regular waves with those measured in regular wave groups, since $\phi^{(2)}$ only contributes when more than one wave is present. Figure 6.9 has been taken from reference 75 and concerns a semi-submersible in head seas. It would appear that $\phi^{(2)}$ has most effect on low frequency wave groups.

Bowers (ref. 24) has presented an alternative approach to calculating the slowly varying forces on a vessel in irregular head seas. The undisturbed second order pressure, which can be found from equation (6.31), is integrated over the submerged section of the vessel, whose motions are neglected. An additional second order force due to the finite first order wave height is also included.

Reference 78 gives a comparison between the various methods of calculating the slow drift force. In the slow drift analysis contained in Chapter 8, the Newman approximation is used. It is thought that the simplicity of this method more than compensates for the errors it may involve, especially in view of the problems which still exist in the calculation of second order effects, which are discussed in section 6.1.

6.4.2 The Spectrum of Second Order Force and Response

Given the slow drift force in the form of equation (6.27), Pinkster (ref. 75) has stated that it's spectrum can be written:-

$$S_F(\omega_k) = 8 \int_o^\infty S\eta(\omega+\omega_k) S\eta(\omega) [F(\omega+\omega_k,\omega)]^2 d\omega \qquad (6.32)$$

where:-

$$F(\omega_n,\omega_m) = [(T^c_{nm})^2 + (T^s_{nm})^2]^{\frac{1}{2}} \qquad (6.33)$$

and $S\eta(\omega)$ is the wave amplitude spectrum. In reference 25 , Pinkster applied the Newman approximation to a barge moored in head seas, and obtained the result:-

$$S_F(\omega_k) = 2(\rho g B)^2 \int_o^\infty S\eta(\omega+\omega_k) S\eta(\omega) R^4(\omega+\tfrac{1}{2}\omega_k) d\omega \qquad (6.34)$$

where $R^2(\omega)$ is the non-dimensional reflection coefficient and B is the beam of the barge. It can be seen that the form of (6.32) is slightly different to that of (6.34) - in the former the second order transfer function is a function of $\omega + \omega_k$, whereas in the latter it is a function of $\omega + \frac{1}{2}\omega_k$. The reason for this is that equations (6.32) and (6.34) are not exact, but rather are based upon the spectrum of the square of the wave amplitude (see Rice, ref. 81), modified to accommodate the second order transfer functions.

The Bowers method of calculating the slow drift forces on a vessel moored in head seas (see ref. 24) leads to the following expression for the drift force spectrum:-

$$S_F(\omega_k) = 2(\rho g B)^2 \left[1 - \frac{d_t}{d}\right]^2 \int_o^\infty S\eta(\omega) S\eta(\omega+\omega_k) \sin^2\{\tfrac{1}{2}L[k(\omega)-k(\omega+\omega_k)]\} d\omega \qquad (6.35)$$

where $k(\omega)$ represents the wavenumber of a wave of frequency ω (see Appendix B).

The spectrum of the second order response (for linear systems) can be obtained by multiplying the force spectrum by the modulus squared of the response transfer function. For non-linear systems the equations must first be linearised, as discussed in Chapter 2.

6.4.3 The Statistics of the Second Order Force and Response

6.4.3.1 The Wave Envelope a(t)

In order to discuss the statistics of the slow drift force, it is first necessary to introduce the concept of the wave envelope a(t). This corresponds to the slow variation in wave amplitude which occurs in a random sea, as shown in Figure 6.10. The surface profile can be written as follows:-

$$\eta(t) = \sum_n a_n \cos(\omega_n t + \varepsilon_n) = \sum_n a_n \cos\left[(\omega_n - \omega_r)t + \omega_r t + \varepsilon_n\right] \tag{6.36}$$

where ω_r is some fixed central frequency - corresponding to the spectral peak, say. By rearranging equation (6.36) it is possible to write

$$\eta(t) = a(t)\cos\left[\omega_r t + \theta(t)\right] \tag{6.37}$$

where $a(t) = \left[A^2+B^2\right]^{\frac{1}{2}}$; $\theta(t) = \tan^{-1}\left(\frac{B}{A}\right)$

$$A = \sum_n a_n \cos\left[(\omega_n-\omega_r)t+\varepsilon_n\right]; \quad B = \sum_n a_n \sin\left[(\omega_n-\omega_r)t+\varepsilon_n\right]$$

Equation (6.37) then represents the seastate as a single wave with time varying amplitude and frequency. The square of the envelope, $a^2(t)$, has the following form:-

$$\begin{aligned} a^2(t) &= \sum_{nm}\sum a_n a_m \{\cos\left[(\omega_n-\omega_r)t+\varepsilon_n\right]\cos\left[(\omega_m-\omega_r)t+\varepsilon_m\right] \\ &\quad + \sin\left[(\omega_n-\omega_r)t+\varepsilon_n\right]\sin\left[(\omega_m-\omega_r)t+\varepsilon_m\right]\} \\ &= \sum_{nm}\sum a_n a_m \cos\left[(\omega_n-\omega_m)t + \varepsilon_n - \varepsilon_m\right] \end{aligned} \tag{6.38}$$

Comparing this to equation (6.27), applying the Newman approximation and assuming that the reflection coefficient is constant over frequency

leads to:-

$$F(t) = C\, a^2(t) \tag{6.39}$$

where F(t) is the slow drift force and C is a constant. Although the assumption of a constant reflection coefficient is unlikely to be true, the errors involved should be fairly small providing the incident seastate is narrow banded. This approach has been used by Roberts (ref. 26).

The terms A and B, and thus $\dot{A}$ and $\dot{B}$, are Gaussian, which means that the jpdf (joint probability density function) of these terms can be written (see Lin, ref. 27):-

$$p(A,\dot{A},B,\dot{B}) = \frac{1}{4\pi^2\sigma_\eta{}^2\sigma_{\dot{\eta}}{}^2} \exp\{-\tfrac{1}{2}[(\frac{A}{\sigma_\eta})^2 + (\frac{\dot{A}}{\sigma_{\dot{\eta}}})^2 + (\frac{B}{\sigma_\eta})^2 + (\frac{\dot{B}}{\sigma_{\dot{\eta}}})^2]\} \tag{6.40}$$

where σ_η and $\sigma_{\dot{\eta}}$ represent the r.m.s. displacement and vertical velocity of the surface profile. The jpdf of a(t) and θ(t) and their time derivatives can be found from the following transformation law:-

$$p(a,\dot{a},\theta,\dot{\theta}) = |J|\, p(A,\dot{A},B,\dot{B}) \tag{6.41}$$

where |J| is the Jacobian:-

$$|J| = \begin{vmatrix} \frac{\partial A}{\partial a} & \frac{\partial A}{\partial \dot{a}} & \frac{\partial A}{\partial \theta} & \frac{\partial A}{\partial \dot{\theta}} \\ \frac{\partial \dot{A}}{\partial a} & \frac{\partial \dot{A}}{\partial \dot{a}} & \frac{\partial \dot{A}}{\partial \theta} & \frac{\partial \dot{A}}{\partial \dot{\theta}} \\ \frac{\partial B}{\partial a} & \frac{\partial B}{\partial \dot{a}} & \frac{\partial B}{\partial \theta} & \frac{\partial B}{\partial \dot{\theta}} \\ \frac{\partial \dot{B}}{\partial a} & \frac{\partial \dot{B}}{\partial \dot{a}} & \frac{\partial \dot{B}}{\partial \theta} & \frac{\partial \dot{B}}{\partial \dot{\theta}} \end{vmatrix} \tag{6.42}$$

From equation (6.37), the following relations hold:-

$$A = a\cos\theta \quad ; \quad B = a\sin\theta$$

$$\dot{A} = \dot{a}\cos\theta - a\dot{\theta}\sin\theta \quad ; \quad \dot{B} = \dot{a}\sin\theta + a\dot{\theta}\cos\theta$$

from which it can be shown that $|J| = a^2$. It then follows from equation

(6.41) that:-

$$p(a,\dot{a},\theta,\dot{\theta}) = \frac{a^2}{4\pi^2\sigma_\eta^{\,2}\,\sigma_{\dot{\eta}}^{\,2}} \exp\{-\tfrac{1}{2}\left[\left(\frac{a}{\sigma_\eta}\right)^2 + \frac{\dot{a}^2+a^2\dot{\theta}^2}{\sigma_{\dot{\eta}}^{\,2}}\right]\} \qquad (6.43)$$

which agrees with a result obtained by Tikhonov (ref. 82). The jpdf of a and $\dot{a}$ can be found from (6.43) as follows:-

$$p(a,\dot{a}) = \int_{-\infty}^{\infty}\int_{0}^{2\pi} p(a,\dot{a},\theta,\dot{\theta})\,d\dot{\theta}\,d\theta$$

$$= \frac{a}{\sqrt{2\pi}\sigma_\eta^{\,2}\,\sigma_{\dot{\eta}}} \exp\{-\tfrac{1}{2}\left[\left(\frac{a}{\sigma_\eta}\right)^2 + \left(\frac{\dot{a}}{\sigma_{\dot{\eta}}}\right)^2\right]\} \qquad (6.44)$$

Further integration over $\dot{a}$ shows that the p.d.f. of the envelope itself is Rayleigh. The above analysis has assumed that the incident seastate is narrow banded. If this is not the case, then the more general analysis of Longuet-Higgins (ref. 28) must be used.

6.4.3.2 <u>The Slow Drift Force Distribution</u>

From equations (6.39) and (6.44) it can be shown that the mean, variance and r.m.s. values of the slow drift force are given by:-

$$\bar{F} = 2C\sigma_\eta^{\,2} \quad ; \quad \langle F^2 \rangle = 8C^2\sigma_\eta^{\,2} \quad ; \quad \sigma_F^{\,2} = 4C^2\sigma_\eta^{\,4} \qquad (6.45)$$

It can also be seen from equation (6.39) that the drift force can never change sign, since $a^2(t)$ is always positive. The jpdf of the drift force and its time derivative can be found from:-

$$p(F,\dot{F}) = \begin{vmatrix} \frac{\partial a}{\partial F} & \frac{\partial a}{\partial \dot{F}} \\ \frac{\partial \dot{a}}{\partial F} & \frac{\partial \dot{a}}{\partial \dot{F}} \end{vmatrix} p(a,\dot{a}) \qquad (6.46)$$

which, together with equations (6.39) and (6.44), leads to:-

$$p(F,\dot{F}) = \left[4C^{\frac{3}{2}}\sqrt{2\pi}\,\sigma_\eta^{\,2}\,\sigma_{\dot{\eta}}\,F^{\frac{1}{2}}\right]^{-1} \exp\{-\tfrac{1}{2}\left[\frac{F}{C\sigma_\eta^{\,2}} + \frac{\dot{F}^2}{4CF\sigma_{\dot{\eta}}^{\,2}}\right]\} \qquad (6.47)$$

Integration over $\dot{F}$ yields an exponential distribution for the drift force profile:-

$$p(F) = \frac{1}{2C\sigma_\eta^2} e^{-F/2C\sigma_\eta^2} \tag{6.48}$$

6.4.3.3 Slow Drift Peak Distribution

Lin (ref. 27) has shown that the p.d.f. of the positive maxima of a narrow banded process, with j.p.d.f. $p(x,\dot{x})$, is given by:-

$$p_x(m) = -\frac{1}{\lambda} \frac{d}{dm} \int_0^\infty \dot{x} p(m,\dot{x}) d\dot{x} \tag{6.49}$$

where λ is the mean frequency of zero crossings with positive slope, and is given by:-

$$\lambda = \int_0^\infty \dot{x} p(0,\dot{x}) d\dot{x} \tag{6.50}$$

Although the slow drift forces are not narrow banded, only those forces which act near to the natural frequencies of a moored vessel are important when considering the response, since the damping present tends to be low. The following analysis will concern these forces only, and the narrow banded assumption will be employed. The slow drift force can be adjusted to zero mean by putting $G(t) = F(t) - \bar{F}$. $G(t)$ then represents the slowly varying part of the slow drift force, and equation (6.48) implies:-

$$p(G,\dot{G}) = \left[4C^{\frac{1}{2}}\sqrt{2\pi}\sigma_\eta^2 \sigma_{\dot{\eta}} (G+\bar{F})^{\frac{1}{2}}\right]^{-1} \exp\left\{-\tfrac{1}{2}\left[\frac{G+\bar{F}}{C\sigma_\eta^2} + \frac{\dot{G}^2}{4C\sigma_{\dot{\eta}}^2 (G+\bar{F})}\right]\right. \tag{6.51}$$

Using equations (6.48) and (6.50) it can be shown that:-

$$p_G(m) = -\frac{1}{\bar{F}^{\frac{1}{2}}} \frac{d}{dm} \left\{(m+\bar{F})^{\frac{1}{2}} \exp(-\frac{m}{\bar{F}})\right\} \tag{6.52}$$

Letting v be a random variable representing the ratio of the maxima of G to the r.m.s. value of G (i.e. $v = m/\sigma_F$), and using equation (6.45), the above equation can be written:-

$$p_G(v) = -\frac{d}{dv} \left\{(1+v)^{\frac{1}{2}} e^{-v}\right\} \tag{6.53}$$

6.4.3.4 Statistics of a Group of N Maxima

Given one maxima, let the probability that it exceeds a ratio v be written as P(v). From probability theory:-

$$p_G(v) = \frac{d}{dv}\left[1-P(v)\right] = -\frac{d}{dv}\left[P(v)\right] \qquad (6.54)$$

Equation (6.53) then implies that:-

$$P(v) = (1+v)^{\frac{1}{2}}\, e^{-v} \qquad (6.55)$$

Consider now a group of N maxima. The probability that at least one of the N maxima has a ratio greater than v is equivalent to one minus the probability that no maximum has a ratio greater than this value, i.e., the probability that at least one maximum has a ratio greater than $v = 1 - \left[1 - P(v)\right]^N$

$$= 1 - e^{-NP(v)} \text{ for large N} \qquad (6.56)$$

If the function $Q_N(v)$ is introduced such that:

$$1 - Q_N(v) = 1 - e^{-NP(v)} \rightarrow Q_N(v) = e^{-NP(v)} \qquad (6.57)$$

then physically, $Q_N(v)$ is the probability that the largest maximum in N waves has a ratio less than or equal to v, i.e. $Q_N(v)$ is the probability function for the largest maximum in N waves. The modal value of the largest maximum in a group of N waves, for a large sample of groups, is then given by the solution to:-

$$Q_N''(v) = 0 \qquad (6.58)$$

which can be found numerically, given equations (6.55) and (6.57). The mean value of the largest maxima in N waves will be

$$\bar{v} = \int_0^\infty v Q_N'(v)\,dv \qquad (6.59)$$

Numerical results for various values of N are shown in Figure 6.11. A comparison to time domain results, found using equations (6.38) and (6.39) is given in section 6.4.3.7.

6.4.3.5. Statistics of the Slow Drift Minima

The minima of the slow drift force are most easily discussed by considering a function P such that P = -G. The joint probability density function of P is then given by (see equation 6.51):-

$$p(P,\dot{P}) = \left[4C^{\frac{1}{2}}\sqrt{2\pi}\,\sigma_\eta^{2}\,\sigma_{\dot{\eta}}(\bar{F}-P)^{\frac{1}{2}}\right]^{-1}\exp\left\{-\frac{1}{2}\left[\frac{\bar{F}-P}{C\sigma_\eta^{2}}+\frac{\dot{P}^2}{4C\sigma_{\dot{\eta}}^{2}(\bar{F}-P)}\right]\right\} \qquad (6.60)$$

and the maxima of P correspond to the minima of G. Lin (ref. 27) has shown that for a random process x, with jpdf $p(x,\dot{x})$, the mean frequency of crossing a level 'a' with positive slope is:-

$$\bar{V}_a^{+} = \int_0^{\infty}\dot{x}p(a,\dot{x})d\dot{x} \qquad (6.61)$$

For the function P it can be shown that:-

$$\bar{V}_a^{+} \alpha (\bar{F}-a)^{\frac{1}{2}}\exp(a/\bar{F}) \qquad (6.62)$$

where, from the definition of P, P cannot exceed $\bar{F}$. For most random processes, it would be expected that the frequency of crossing a level 'a' would decrease monotonically as the value of 'a' increases. This is not true of P, however. $\bar{V}_a^{+}$ increases with 'a' until a maximum is reached at $a = 0.5\bar{F}$, after which it decreases steadily to zero at $a = \bar{F}$. This means that there are some positive levels of P which are crossed more frequently than lower positive levels - a fact which can only be true if the positive side of P is by nature broad banded, and contains a substantial number of positive minima. From the definition of P, this implies that the negative side of the slowly varying drift force cannot be considered to be narrow banded, and thus the analysis of sections 6.4.3.3. and 6.4.3.4. is not applicable to the slow drift minima. As an aside, the mean frequency of crossing a level 'a' with positive slope, for the positive side of the slow drift force, is given by:-

$$\bar{V}_a^{+} \alpha (a+\bar{F})^{\frac{1}{2}}\exp(-a/\bar{F}) \qquad (6.63)$$

which is monotonically decreasing with a. This justifies the use of the narrow banded assumption for the slow drift maxima. Figure 6.12

shows a typical time history of slow drift force and illustrates the above points - it can be seen that whereas there are relatively few positive maxima, the number of negative maxima is substantial. It can be shown from equation (6.60) that the probability of the random process P exceeding a level 'a' is:-

$$P(\geq a) = 1 - \exp\{\frac{a}{\bar{F}} - 1\} \qquad (6.64)$$

which is approximately 10% when $a = 0.9\bar{F}$. This suggests that the process P will frequently reach a maximum value close to $\bar{F}$. Thus, although it is very difficult to discuss the statistics of the slow drift minima in detail, it seems reasonable to assume that a value of $-\bar{F}$ will be reached in any group of N maxima.

6.4.3.6 Statistics of the Slow Drift Response

It is likely that the equations of motion of the horizontal degrees of freedom of a moored vessel will contain non-linearities in both the damping and stiffness terms, possibly of the type shown in equation (2.27) and discussed in section 2.4. Although the r.m.s. response in these degrees of freedom can be predicted quite accurately by linearisation procedures (see Chapter 2), the statistics of the response are much more difficult to determine - especially if the exciting force is non-Gaussian, as is the case with slow drift forces. Roberts (ref. 26) examined the statistics of the slow drift response of a non-linear system using the Fokker-Planck equation, but use of this method involved the assumption that the slow drift force was Gaussian white noise. No attempt is made here to analyse the statistics of the slow drift response - except to state that if the system is linear, then the response properties might be expected to be somewhere between those of a Gaussian process and those predicted above for the slow drift force. The next section contains numerical results for the r.m.s. and maximum values of the slow drift response of a linear system obtained by time domain analysis.

6.4.3.7 Numerical Calculations and Results

The time history of the slow drift force in an irregular sea is given by equation (6.27). If the Newman approximation (ref. 77)

and equation (6.29)) is applied, and the reflection coefficient assumed to be constant with frequency then this equation can be re-written as:-

$$F(t) = C \sum_n \sum_m a_n a_m \cos[(\omega_n - \omega_m)t + \varepsilon_n - \varepsilon_m] \qquad (6.65)$$

where C is a constant. This is then in the same form as equations (6.39) and (6.38) and is amenable to the statistical analysis of the above sections. If this force acts on a linear system such that:-

$$\ddot{x} + 2\beta\omega\dot{x} + \omega^2 x = F(t) \qquad (6.66)$$

then the time history of the response can be found from:-

$$x(t) = C \sum_n \sum_m a_n a_m \{f_{nm}\cos[(\omega_n - \omega_m)t + \varepsilon_n - \varepsilon_m] + g_{nm}\sin[(\omega_n - \omega_m)t + \varepsilon_n - \varepsilon_m]\} \qquad (6.67)$$

where:-

$$f_{nm} = [\omega^2 - (\omega_n - \omega_m)^2]/h_{nm} \; ; \; g_{nm} = 2\beta\omega(\omega_n - \omega_m)/h_{nm}$$

$$h_{nm} = [\omega^2 - (\omega_n - \omega_m)^2]^2 + [2\beta\omega(\omega_n - \omega_m)]^2$$

Equations (6.65) and 6.67) were programed onto a digital computer to obtain time histories of the slow drift force and response. The phase angles, ε_n, were chosen at random in such a way as to have a rectangular distribution between 0 and 2π. The wave amplitudes a_n and frequencies ω_n, were obtained by dividing the incident wave spectrum into strips (in practise twenty were used), as discussed in section 2.3.2.3. Equal area strips were taken so as to obtain a variation in the frequency interval between adjacent strips, since the use of equal frequency intervals leads to the time histories being repeated after a time T = (2π/frequency interval) seconds. A JONSWAP wave spectrum having a significant wave height of 15m and an average period of 14 seconds was used, and in order to reduce computing time this spectrum was considered to be present in the region ω = 0.3045 to 0.3645 rad/sec only. The linear system was taken to have a natural frequency ω = 0.02 rad/s and a damping ratio β = 0.1, so as to be typical of a moored offshore vessel. The computer program was written such that

time histories of the slow drift force (adjusted to zero mean) and response were produced until the force had undergone a specified number of zero crossings with positive slope (corresponding to N in equation (6.56)), and the maximum values of force and response occurring within this time were noted. In practise values for N of 15, 30 and 45 were considered, and the program was run 30 times for each case. The mean values of the ratio (maximum value of slow drift force after N zero crossings/r.m.s. value) obtained from these results are compared with those predicted by equation (6.59) in Figure (6.13). This Figure also shows the modal value of this ratio which is predicted by equation (6.58). Figure 6.14 shows the number of maximum values occurring in certain ranges for each of the three sets of thirty results.

It can be seen that there is reasonable agreement between the mean values obtained from the statistical theory and the time domain analysis, the maximum disagreement being of the order of 11%. The differences may be due to the errors involved in the assumption that the slow drift force is narrow banded (section 6.4.3.3), or the fact that a relatively small number (thirty) of time domain runs were taken, in order to limit the computer costs. Were the slow drift force assumed to be Gaussian then the theory of Longeut-Higgins (ref.28 , or see Kirk, ref. 22) would yield mean values of 2.58, 2.83 and 2.97 for the ratio of the maximum value to the r.m.s. value when N = 15, 30 and 45 respectively, which are considerably different from the results shown in Figure 6.13. The minimum value of the slow drift force is likely to be approximately minus one times the r.m.s. value, irrespective of the value of N, as shown in section 6.4.3.5. The average ratios of the maximum span (maximum to minimum) of the slow drift force to the r.m.s. value, as given by the statistical theory of the previous sections, will then be 5.08, 5.85 and 6.29 for N = 15, 30 and 45. These values are surprisingly close to the values of 5.16, 5.66 and 5.94 which would be predicted by the Gaussian assumption. This is not so for larger values of N however. When N = 1000, the Gaussian assumption predicts an average ratio of 7.74, whereas equation (6.59) yields 9.01.

A comparison between Figures 6.13 and 6.14 shows that it is only in the case N = 45 that the modal value predicted by equation (6.58)

lies within the region containing the most number of time domain results. The discrepancies when N = 15 and 30 may be due to the small number of time domain results which were obtained, together with the theoretical inaccuracies caused by the narrow banded assumption of section 6.4.3.3.

The above results would indicate that the statistical theory of sections 6.4.3.1 to 6.4.3.5. provides a reasonable description of the statistics of the slow drift force as given by equation (6.65). It should be noted, however, that this equation differs from the true slow drift force in that the Newman approximation has been applied and a constant reflection coefficient has been assumed. Although it is known that in many cases the application of the Newman approximation does not lead to large errors, the effect of the assumption of a constant reflection coefficient is less certain. Roberts (ref. 26) has stated that this assumption may be valid when the incident seastate is narrow banded. When this is not the case, the errors involved may be significant, and the statistics of the slow drift force become much more difficult, if not impossible, to analyse. The above analysis may then give only a qualitative idea of the statistical properties of the slow drift force, but even so the results obtained are a considerable improvement on those of more sweeping approximations, such as the assumptions of a Gaussian slow drift force. Much further research will be required before it can be said that the statistics of the slow drift force are completely understood.

For each of the program runs mentioned above, a time history of the response of the linear system was obtained. The maximum response and the number of zero crossings with positive slope for each of these runs was noted. A large variability was found in the response - for example a run with 25 crossings may have a ratio of maximum to r.m.s. of 4.11, whereas for a run with 28 zero crossings this value may only be 2.83. Typical values of this ratio, after averaging, were 3.38, 3.55 and 3.74 for 28, 54 and 85 crossings. This compares with vaLues of 2.81, 3.03 and 3.17 which would be given by a Gaussian response and 4.77, 5.49 and 5.98 which would be predicted by equation (6.59). It can be seen that the time domain results lie somewhere between these two sets of values, being around 20% higher than the former and 30-40% lower than the latter, which would suggest that the linear system tends to filter the forcing function to produce

a signal whose statistical properties are more Gaussian. It can also be seen that caution is required when estimating the maximum expected slow drift response from an r.m.s. value given by a frequency domain analysis, since a simple Gaussian assumption may lead to a significant underestimate. Further analysis of the statistical properties of the slow drift response was considered to be beyond the scope of the present work, although this remains a pressing problem in the field of offshore dynamics.

6.5 Sensitivity of the Slow Drift Force and Response to Wave Spectrum and Reflection Coefficient

For any given seastate with specified significant wave height and average period, a number of different theoretical spectra may be used to represent the distribution of energy over the frequency range (see Appendix A). Although measurements performed at the site under consideration will often indicate the most suitable choice of spectrum, it may be that in certain cases no one type of theoretical spectrum will give a sufficiently accurate representation of the seastate. In these circumstances a random dynamic analysis may be performed using several different types of wave spectrum and a comparison made between the results obtained. This section investigates the sensitivity of the slow drift force and response to the type of theoretical spectrum which is used by considering the slow motions of a tanker moored by a non-linear bow hawser in a head sea, which is represented by either a JONSWAP, Pierson-Moskowitz or I.S.S.C. wave spectrum. The Newman approximation is applied and the effect of changing the shape of the reflection coefficient is also investigated by considering the three reflection coefficients shown in Figure 6.15.

The equation of motion of the tanker system in surge is written as (neglecting quadratic damping):-

$$(M + Ma)\ddot{x} + B_x\dot{x} + k_1 x + k_3 x^3 = F_s(t) \qquad (6.68)$$

where M and Ma are the mass and added mass of the vessel, B_x is a linear damping coefficient, k_1 and k_3 are mooring stiffness coefficients about the zero offset position and $F_s(t)$ is the slow drift force. The spectrum and mean value of this force have been given by

Pinkster (ref. 25) as:-

$$S_F(\omega_k) = 2(\rho g B)^2 \int_0^\infty S_\eta(\omega) S_\eta(\omega+\omega_k) R^4(\omega+\tfrac{1}{2}\omega_k)\, d\omega \qquad (6.69)$$

$$\bar{F}_S = \rho g B \int_0^\infty R^2(\omega) S_\eta(\omega)\, d\omega \qquad (6.70)$$

where B is the beam of the vessel. The mean force given by equation (6.70) is applied to equation (6.68) to obtain a static offset position. The stiffness properties about this offset position are no longer the same as those given by equation (6.68) and this equation is modified to:-

$$(M + Ma)\ddot{x} + B_x\dot{x} + k_1'x + k_2x^2 + k_3x^3 = F_S(t) \qquad (6.71)$$

where:-

$$k_1' = k_1 + 3k_3x_0^2 \quad ; \quad k_2 = 3k_3x_0 \qquad (6.72)$$

and x_0 is the static offset. In order to solve equation (6.71) in the frequency domain, the stiffness term is linearised by the equivalent linearisation method (see section 2.3.1) to yield:-

$$(M + Ma)\ddot{x} + B_x\dot{x} + (k_1' + \frac{4}{\sqrt{2\pi}} k_2\sigma_x + 3k_3\sigma_x^2)x = F_S(t) \qquad (6.73)$$

where σ_x^2 is the mean squared value of response, necessitating an iterative solution. This method of linearisation involves the assumption that the response is Gaussian, which, as shown in Sections 6.4.3.6 and 6.4.3.7, will not be the case. The absence of more detailed information about the statistical nature of the response means, however, that any errors introduced by this assumptions cannot be avoided.

Figures 6.16 to 6.18 show the spectrum of the slow drift force for three different reflection coefficients, R1, R2 and R3, when the significant wave height is 15m, 7.5m and 4m. R1 is the reflection coefficient given by Remery and Hermans (ref. 83) for a barge in head seas, and R2 and R3 are modified forms of this coefficient (see Figure 6.15) - R2 does not approach the asymptotic value at high

frequencies, whereas R3 does not include the low frequency values. For the 15m significant wave height seastate (Figure 6.16) it can be seen that the spectra given by R1 and R2 are in reasonable agreement, both being considerably greater than that given by R3. This is because the peak of the incident wave spectrum occurs at the relatively low frequency of 0.346 rad/sec, and thus the spectrum of slow drift force is dependent upon the low frequency region of the reflection coefficient where R1 and R2 are in agreement. Figure 6.22 shows that, as would be expected, the mean slow drift force given by R3 is less than that given by R2 which, in turn, is less than that given by R1. It is interesting to note, however, that the r.m.s. response predicted by R2 is slightly greater than that predicted by R1, although the slow drift force is less. This can be explained by referring to the linearised stiffness - the lower mean force predicted by R2 leads to a lower value of linearised stiffness, which acts to produce a greater value of response (c.f. the response of a linear system to white noise excitation is inversely proportional to the square root of the stiffness, the slow drift force being comparable to white noise for lightly damped systems). Figure 6.17 shows similar results for H_s = 7.5m. The values for the force and response are slightly greater than in the H_s = 15m case due to the fact that the peak of the spectrum (ω = 0.534 rad/sec) lies in a region where the values of the reflection coefficient are greater. Figure 6.18 shows results for H_s = 4m. Closer agreement is found between R3 and R1 since the spectrum of the slow drift force depends largely upon the asymptotic value of the reflection coefficient due to the high frequency (0.666 rad/sec) of the peak of the incident spectrum. R2 greatly underestimates the force spectrum at higher separation frequencies. These results would tend to indicate that the slow drift force and response are sensitive to the values of the reflection coefficient which occur at frequencies near to the spectral peak.

Figures 6.19 to 6.21 show results for the spectrum of the slow drift force as given by the JONSWAP, Pierson-Moskowitz and ISSC wave spectra, for three significant wave heights. The corresponding values of linearised stiffness, mean force and r.m.s. response are shown in Figure 6.22. It can be seen that, apart from the agreement between the ISSC and Pierson-Moskowitz spectra when H_s = 4m, there is

a considerable discrepancy in all cases. The ISSC spectrum gives results which are consistently higher than those of the Pierson-Moskowitz spectrum and which also exceed those given by the JONSWAP spectrum for H_S = 15m, although they are less than these for the lower seastates. This would indicate that care should be taken when choosing the wave spectrum to be used in a slow drift analysis. If the theoretical spectrum chosen differs in type from that occurring at the actual location then considerable errors in the slow drift force and response could be incurred. Also, the type of spectrum which yields the maximum response would appear to depend upon the significant wave height considered, and thus it is not possible to recommend a spectral type which will give conservative answers in all cases.

7.0 UNSTABLE MOTIONS OF A SPM/SBS SYSTEM

7.1 Introduction

As discussed in section 1.2.3, single point mooring systems can undergo low frequency large amplitude limit cycle oscillations due to the action of wind and current alone. These oscillations are generally referred to as 'fishtailing motions', and a descriptive explanation of their cause has been given in the above mentioned section. Wichers (ref. 17) has developed a mathematical model for this phenomenon, involving timestep integration and the use of semi-empirical formulae to represent the viscous forces acting on the tanker. Wicher's model refers to a SPM system, in which the motions of the buoy are neglected. The present chapter extends this model to deal with a SBS system, buoy motions being included, in order to investigate whether instabilities are possible in this type of system. It was found that these occur only in cases where, in the mean position, the current lies at a large angle of incidence to the vessel (of the order of 40^{o} or more). These instabilities are different in nature to 'fishtailing motions', which do not occur, due mainly to the lack of freedom afforded by the mooring system - there is no equivalent to the 'initial length' of the hawser of the SPM system. These points are discussed in more detail in section 7.7. The model is also modified to include the effect of mean drift forces and moments (see 6.4), and used to calculate the static offset of stable systems, when subject to wind, wave and current forces. Also included in the chapter is a literature survey of the methods available for calculating the viscous forces on a moving VLCC.

7.2 Wind and Current Forces on Stationary VLCC's

Comprehensive data for the calculation of wind and current forces on stationary VLCC's (Very Large Crude Carriers) has been published by the Oil Companies International Marine Forum (OCIMF, ref. 68). Empirical formulae for these forces are quoted as:-

$$\text{Wind:}\quad F_{xw} = C_{xw}(\theta)BV_w^2A_T \qquad \text{Current:}\quad F_{xc} = C_{xc}(\theta)AV_c^2TL_{BP}$$

$$F_{yw} = C_{yw}(\theta)BV_w^2A_L \qquad F_{yc} = C_{yc}(\theta)AV_c^2TL_{BP}$$

$$M_{xyw} = C_{xyw}(\theta)BV_w^2A_LL_{BP} \qquad M_{xyc} = C_{xyc}(\theta)AV_c^2TL_{BP}^2 \qquad (7.1)$$

where the sign convention and notation are as follows:-

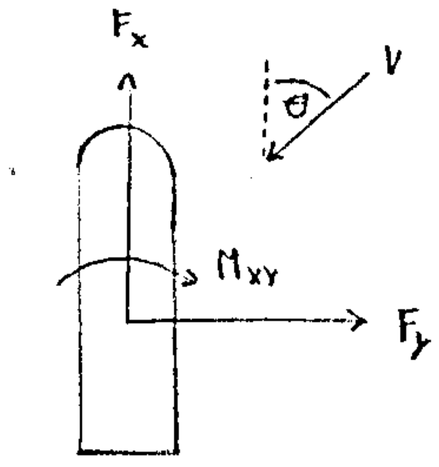

A = Water density /(1.973)

B = Air density /(1.973)

T = Draft of vessel

L_{BP} = Length between perpendiculars

A_T = Transverse wind area

A_L = Broadside wind area

and all quantities are to be measured in S.I.units. In the OCIMF data, the coefficients (θ) are plotted for a variety of water depth/ draft ratios for vessels with both U-shaped and conventional bow configurations. Typical curves, to give an indication of their shape are shown in Figure 7.1. $C_y(\theta)$ and $C_{xy}(\theta)$ are odd functions, whereas $C_x(\theta)$ is even. As an alternative to the OCIMF data, Remery and van Oortmerssen (ref. 84) have expressed the above curves in terms of Fourier coefficients such that:-

$$C_{xyc}(\theta) = \sum_{n=1}^{5} b_n \sin(n\theta), \text{ etc} \qquad (7.2)$$

the terms b_n being found from experiment.

7.3 Viscous Forces on a Moving VLCC

7.3.1 General Methods of Calculation

In practise, it is of more interest to calculate the viscous forces on a moving VLCC than to calculate the current forces on a stationary vessel. Consider a vessel moving in a current, as shown in Figure 7.2. The magnitude of the relative velocity between the vessel and the fluid is:-

$$V_r = \{(U + V_c\cos\theta)^2 + (V + V_c\sin\theta)^2\}^{\frac{1}{2}} \qquad (7.3)$$

and the relative heading of this velocity is:-

$$\theta_r = \tan^{-1}\{(V_c\sin\theta + V)/(V_c\cos\theta + U)\} \qquad (7.4)$$

An obvious method of calculating the viscous forces acting on the

vessel is to modify the set of equations (7.1) by replacing V_c with V_r and θ with θ_r. Although this method accommodates any surge or sway velocity the vessel might have, it does not take the yaw velocity into account. Various researchers have employed different methods to include this effect, as discussed in sections 7.3.2 to 7.3.5 below. All of these methods are semi-empirical due to the complex nature of viscous flow, and their validity rests on comparisons with model tests.

7.3.2 The Method of Molin and Bureau

Molin and Bureau (ref. 19) have given the viscous forces in surge, sway and yaw as:-

$$F_{xc} = C_{xc}(\theta_r)AV_r^2 TL_{BP} \tag{7.5}$$

$$F_{yc} = C_{yc}(\theta_r)AV_r^2 TL_{BP}+C_{yc}(90^o)A\int_L T(x)\{v(x,\dot{\psi})V(x,\dot{\psi}) -v(x,0)V(x,0)\}dx \tag{7.6}$$

$$M_{xyc} = C_{xyc}(\theta_r)AV_r^2 TL_{BP}+C_{yc}(90^o)A\int_L T(x)x\{v(x,\dot{\psi})V(x,\dot{\psi}) -v(x,0)V(x,0)\}dx \tag{7.7}$$

where the integral is along the length of the vessel (dummy variable x). V is the total relative velocity at position x on the vessel, v is the relative velocity in sway at this point and T is the draft. The first terms in these expressions correspond to the modified OCIMF formulae, the additional terms in (7.6) and (7.7) vanishing when $\dot{\psi} = 0$ and being based upon model test results.

7.3.3 The Method of Ratcliffe and Clarke

Ratcliffe and Clarke (ref. 18) define the drag force on an element dx as:-

$$dY = \tfrac{1}{2}\rho T(x)C_D(x)V|V|dx \tag{7.8}$$

where T(x) is the vessel draft at x, $C_D(x)$ is the drag coefficient at this point, ρ is the fluid density and V is the relative velocity in sway. The viscous forces are then given as:-

$$F_{xc} = C_{xc}(\theta_r)AV_r^2 TL_{BP} \quad (7.9)$$

$$F_{yc} = \int_L dY \quad (7.10)$$

$$M_{xyc} = C_{xyc}(\theta_r)AV_r^2 TL_{BP} + \int_L xdY \quad (7.11)$$

F_{xc} is equivalent to the modified OCIMF result. The first term in M_{xyc} is included to account for the non-viscous 'Munk Moment' which acts on a moving vessel (an effect first noted on airships, see ref. 13).

7.3.4 The Method of Faltinsen et al

Faltinsen et al (ref. 85) give the viscous forces as:-

$$F_{xc} = C_{xc}(\theta_r)AV_r^2 TL_{BP} \quad (7.12)$$

$$F_{yc} = \tfrac{1}{2}\rho \int_L C_D(x)T(x)V|V|\,dx \quad (7.13)$$

- large angles of incidence

$$= \text{Lifting Theory}$$

- small angles of incidence

$$M_{xyc} = \text{Munk Moment} + \tfrac{1}{2}\rho\int_L xC_D(x)T(x)V|V|\,dx \quad (7.14)$$

- large angles of incidence

$$= \text{Munk Moment} + \text{Lifting Theory}$$

- small angles of incidence

where V is the relative sway velocity at position x. Again, F_{xc} is the modified OCIMF result. The lifting theory referred to is the same as that used for aerofoil sections.

7.3.5 The Method of Wichers

Wichers (ref. 17) modifies the OCIMF results to allow for the effect of yaw velocity as follows:-

$$F_{xc} = C_{xc}(\theta_r)AV_r^2 TL_{BP} \quad (7.15)$$

$$F_{yc} = C_{yc}(\theta_r)AV_r^2 TL_{BP} + \int_L dF \quad (7.16)$$

$$M_{xyc} = C_{xyc}(\theta_r)AV_r^2 TL_{BP}^2 + \int_L xdF \quad (7.17)$$

where:-

$$dF = \tfrac{1}{2}AT\ a(x)\{(v-x\dot{\psi})|v-x\dot{\psi}|-v|v|\}dx \qquad (7.18)$$

and v is the relative sway velocity. Since the function a(x), (corresponding to a drag coefficient) is unknown, Wichers applies the following technique:-

$$F_{yc} = C_{yc}(\theta_r)AV_r^2\ TL_{BP}+E\int_L AT\{(v-x\dot{\psi})|v-x\dot{\psi}|-v|v|\}dx \qquad (7.19)$$

$$M_{xyc} = C_{xyc}(\theta_r)AV_r^2\ TL_{BP}^2+C\int_L ATx(v-x\dot{\psi})|v-x\dot{\psi}|dx \qquad (7.20)$$

and chooses the coefficients E and C to match model test results. Good agreement is found for E = 0 and C = $5C_{yc}(90^o)$. This method is used in the analysis of section 7.4. Wichers also quotes the following results for the wind forces on a moving vessel:-

$$F_{xw} = C_{xw}(\theta_r)BV_{rw}^2\ A_T \qquad (7.21)$$

$$F_{yw} = C_{yw}(\theta_r)BV_{rw}^2A_L+C_{yw}(90^o)\int_L B(A_L/L)\{(v-x\dot{\psi})|v-x\dot{\psi}|-v|v|\}dx \qquad (7.22)$$

$$M_{xyw} = C_{xyw}(\theta_r)BV_{rw}^2A_LL_{BP}+C_{yw}(90^o)\int_L B(A_L/L)x(v-x\dot{\psi})|v-x\dot{\psi}|dx \qquad (7.23)$$

where v is the relative wind velocity in sway and V_{rw} is the total relative wind velocity.

7.4 Equations of Lateral Motion of a SBS/SPM System.

The equations of (yaw, sway, surge) motion of an SBS system are derived below, and then modified to reproduce Wichers model for an SPM with a fixed buoy. Three coordinate systems are consdiered, and as shown in Figure 7.3 these are:-

X,Y,Z	Reference axes, fixed in space
x_1,y_1,z_1	Axes moving with the VLCC, with the origin at the CoG
x_2,y_2,z_2	Stationary axes, coinciding with (x_1,y_1,z_1) at the moment of time under consideration, and with respect to which the equations of motion will be formulated.

Consider a point on the tanker having coordinates (ℓ_1,ℓ_2,ℓ_3) wrt the tanker fixed axes (x_1,y_1,z_1). The velocity and acceleration of this point relative to the fixed system (x_2,y_2,z_2) are required, given that the tanker has surge, sway and yaw velocities $\dot{x}$, $\dot{y}$ and $\dot{\psi}$. If the tanker were not rotating then the required velocity would be simply $(\dot{x},\dot{y},0)$. However, to allow for rotation we must use the following result:-

$$\frac{d}{dt_f}(\underset{\sim}{G}) = \frac{d}{dt_r}(\underset{\sim}{G}) + \underset{\sim}{\omega} \times \underset{\sim}{G} \qquad (7.24)$$

where $\frac{d}{dt_f}(\underset{\sim}{G})$ = Derivative of $\underset{\sim}{G}$ as seen by an observer in a fixed frame.

$\frac{d}{dt_r}(\underset{\sim}{G})$ = Derivative of $\underset{\sim}{G}$ as seen by an observer in a rotating frame, coinciding with the fixed frame at the time of observation.

and $\underset{\sim}{\omega}$ is the angular velocity vector of the rotating frame. The velocity in the fixed frame is then:-

$$(\dot{x},\dot{y},0) + (0,0,\dot{\psi}) \times (\ell_1,\ell_2,\ell_3) = (\dot{x}-\ell_2\dot{\psi},\dot{y}+\ell_1\dot{\psi},0) = \underset{\sim}{v}, \text{say} \qquad (7.25)$$

The acceleration in (x_2,y_2,z_2) is then:-

$$\dot{\underset{\sim}{v}} + (0,0,\dot{\psi})\times\underset{\sim}{v} = [\ddot{x}-\ell_2\ddot{\psi}-\dot{\psi}(\dot{y}+\ell_1\dot{\psi}),\ddot{y}+\ell_1\ddot{\psi}+\dot{\psi}(\dot{x}-\ell_2\dot{\psi}),0] \qquad (7.26)$$

Consider now an SBS system (see section 1.4.1) with the yoke C.G. at $(\ell_1,0,\ell_3)$ and the buoy C.G. at $(\ell_2,0,\ell_4)$, both with respect to the tanker axes (x_1,y_1,z_1). The velocities and accelerations, w.r.t. (x_2,y_2,z_2) are shown in Figure 7.4. Assuming that the system has the following masses and moments of inertia:-

Tanker: Structural mass = M_T, Surge added mass = M_{TA1}, Sway added mass = M_{TA2}
Structural M of I = I_T, Added M of I = M_{66}.

Yoke: Structural mass = M_Y, Structural M of I about tanker C.G. = I_{YG}

Buoy: Structural mass = M_B, Added mass in surge or sway = M_{BA},
Structural M of I about tanker C.G. = I_{BG}

then the inertia relief forces can be summarised as follows:-

$$\text{Surge, structural} = M_T(\ddot{x}-y\dot{\psi})+M_Y[\ddot{x}-\dot{\psi}(\dot{y}+\ell_1\dot{\psi})]+M_B[\ddot{x}-\dot{\psi}(\dot{y}+\ell_2\dot{\psi})] \qquad (7.27)$$

$$\text{Surge, added} = (M_{TAI} + M_{BA})\ddot{x} \qquad (7.28)$$

$$\text{Sway, structural} = M_T(\ddot{y}+\dot{x}\dot{\psi})+M_Y(\ddot{y}+\ell_1\ddot{\psi}+\dot{x}\dot{\psi})+M_B(\ddot{y}+\ell_2\ddot{\psi}+\dot{x}\dot{\psi}) \qquad (7.29)$$

$$\text{Sway, added} = M_{TA2}\ddot{y} + M_{BA}(\ddot{y}+\ell_2\ddot{\psi}) \qquad (7.30)$$

$$\text{Yaw, structural} = I_T\ddot{\psi}+I_{YG}\ddot{\psi}+I_{BG}\ddot{\psi}+\ell_1 M_Y(\ddot{y}+\dot{x}\dot{\psi})+\ell_2 M_B(\ddot{y}+\dot{x}\dot{\psi}) \qquad (7.31)$$

$$\text{Yaw, added} = M_{66}\ddot{\psi}+M_{BA}\ell_2(\ddot{y}+\ell_2\ddot{\psi}) \qquad (7.32)$$

Following Wichers (ref. 17) added mass effects have been considered on the linear terms only. The current and wind forces acting on the system are summarised in Figure 7.5 and detailed expressions for these are given in Appendix E. In order to evaluate the mooring force, it is first necessary to calculate the position of the mooring buoy with respect to the reference axes (X,Y,Z). If the C.G. of the tanker has coordinates X_o and Y_o at t = 0, with respect to these axes, then the coordinates at a general time are:-

$$X_G(t) = X_o + \int_o^t (\dot{y}\sin\psi-\dot{x}\cos\psi)dt \qquad (7.33)$$

$$Y_G(t) = Y_o - \int_o^t (\dot{y}\cos\psi+\dot{x}\sin\psi)dt \qquad (7.34)$$

and the coordinates of the buoy can be written as:-

$$X_B(t) = X_G(t) - \ell_2\cos\psi \qquad (7.35)$$

$$Y_B(t) = Y_G(t) - \ell_2\sin\psi \qquad (7.36)$$

Assuming that in the absence of wind and current, the buoy has $X_B=Y_B=0$, the mooring forces can now be calculated. The horizontal excursion, e, of the moorings is $e^2=X_B{}^2+Y_B{}^2$. The restoring force acting towards the

origin will be some non-linear function of this, F(e) say. Referring to Figure 7.6 it can be seen that:-

$$F_1 = F(e)\, X_B/e \quad ; \quad F_2 = F(e)\, Y_B/e \qquad (7.37)$$

and thus the longitudinal and lateral components of the buoy reaction on the tanker are given by:-

$$F_m^{(1)} = F_1 \cos\psi + F_2 \sin\psi \quad ; \quad F_m^{(2)} = F_2 \cos\psi - F_1 \sin\psi \qquad (7.38)$$

In addition to the forces listed above, the tanker also experiences potential damping forces in surge, sway and yaw given by $b_{11}\dot{x}$, $b_{22}\dot{y}$ and $b_{66}\dot{\psi}$. In practise added mass and damping coefficients are frequency dependent, but for a time domain analysis constant values must be used. It is found that the coefficients obtained by diffraction programs, tend to assume constant values for low frequencies, these low frequency limits being used for the above analysis. An alternative treatment of the added mass and damping forces is given in section 7.5. The complete equations of lateral motion of the system can now be written:-

$$\begin{aligned} C_1\ddot{x} + b_{11}\dot{x} - C_2\dot{y}\dot{\psi} - C_3\dot{\psi}^2 &= F_c^{(1)} + F_w^{(1)} + F_{CB}^{(1)} + F_m^{(1)} + F_p^{(1)} \\ C_6\ddot{y} + b_{22}\dot{y} + C_2\dot{x}\dot{\psi} + C_4\ddot{\psi} &= F_c^{(2)} + F_w^{(2)} + F_{CB}^{(2)} + F_m^{(2)} \qquad (7.39) \\ C_5\ddot{\psi} + C_3\dot{x}\dot{\psi} + C_4\ddot{y} + b_{66}\dot{\psi} &= F_c^{(3)} + F_w^{(3)} + \ell_2 (F_{CB}^{(2)} + F_m^{(2)}) \end{aligned}$$

where the constants C_1 to C_6 are given in Appendix E. To modify the above equations for a tanker moored via a bow hawser to a fixed point, the yoke and buoy masses, added masses and inertias are placed equal to zero, and ℓ_2 is replaced by ℓ_1. Also, the mooring forces are modified to allow for the initial hawser length ℓ_o, so that F(e) is replaced with $F(e-\ell_o)$

7.5 Modification of the Added Mass and Potential Damping Terms

In the frequency domain, the added mass and damping force acting in the j'th direction on a body undergoing simple harmonic motion of

frequency ω is written:-

$$F_{jj}(\omega) = m_{jj}(\omega)\ddot{x}_j + b_{jj}(\omega)\dot{x}_j \qquad (7.40)$$

In the time domain, where the motion may not be SHM, the above representation is inadequate. Cummins (ref. 86) has suggested the introduction of a frequency independent added mass coefficient m'_{jj}, and a retardation function $k_{jj}(t)$ so that:-

$$m_{jj}(\omega)\ddot{x}_j + b_{jj}(\omega)\dot{x}_j = m'_{jj}\ddot{x}_j - \int_{-\infty}^{t} k_{jj}(t-\tau)\dot{x}_j(\tau)d\tau \qquad (7.41)$$

In the case of SHM with $x_j = x'_j e^{i\omega t}$ the above equation becomes:-

$$-\omega^2 m_{jj}(\omega)+i\omega b_{jj}(\omega) = -\omega^2 m'_{jj} - \int_0^{\infty} i\omega k_{jj}(t-\tau)e^{i\omega(\tau-t)}d\tau$$

$$= -\omega^2 m'_{jj} + \int_0^{\infty} i\omega k_{jj}(t)e^{i\omega t}dt \qquad (7.42)$$

Equating real and imaginary parts gives:-

$$m_{jj}(\omega) = m'_{jj} - \frac{1}{\omega}\int_0^{\infty} k_{jj}(t)\sin(\omega t)dt \qquad (7.43)$$

$$b_{jj}(\omega) = \int_0^{\infty} k_{jj}(t)\cos(\omega t)dt \qquad (7.44)$$

Given $m_{jj}(\omega)$ and $b_{jj}(\omega)$, then $k_{jj}(t)$ and m'_{jj} can be found by firstly applying the inverse Fourier transform to (7.44):-

$$k_{jj}(t) = \frac{2}{\pi}\int_0^{\infty} b_{jj}(\omega)\cos(\omega t)d\omega \qquad (7.45)$$

and then using the result in:-

$$m'_{jj} = m_{jj}(\omega) + \frac{1}{\omega}\int_0^{\infty} k_{jj}(t)\sin(\omega t)dt \qquad (7.46)$$

The RHS of this expression should have the same value for all values of ω. In particular, as $\omega \to 0$:-

$$m'_{jj} = m_{jj}(0) + \int_0^{\infty} k_{jj}(t)tdt \qquad (7.47)$$

A typical plot of $k_{jj}(t)$ is shown in Figure 7.7. Use of m'_{jj} and $k_{jj}(t)$ rather than $m_{jj}(\omega)$ and $b_{jj}(\omega)$ yields more accurate results when discontinuities such as snatch loads occur (see Wichers, ref. 17). For the SBS system, where snatch loads are not a problem, it is considered that equation (7.40), evaluated as $\omega \to 0$, should yield sufficiently accurate results.

7.6 Time Domain Solution

The equations of motion (7.39) are highly non-linear, and thus a time domain solution is required. Wichers (ref. 17) obtained results for a SPM system using a fourth order Runge-Kutta method with $\Delta t = 0.55$. In the present work, a Newmark-Beta method with $\Delta t = 30s$ and $\beta = 1/6$ was used. The results given by this method for a 130,000 DWT VLCC, moored in a 1.03m/s current to a fixed point via a 45m bow hawser, were checked against the corresponding results given by Wichers (Figure 26, ref. 17), and exact agreement was found. These results are shown in Figure 7.8. Having checked the integration routine, results were obtained for a SBS system, moored in a variety of wind and current combinations.

7.7 SBS System Results

The stability of the SBS system was investigated for current velocities of 1.4 and 0.6m/s. For each of these velocities, a 30m/s wind at an angle of incidence of 0^o, 30^o, 60^o and 90^o to the current direction was considered, as well as the zero wind case. The dimensions of the SBS system are given in Chapter 9. In most cases the system was found to be stable and produce traces similar to those shown in Figures 7.9 and 7.10. Unstable motions were found, however, for the 0.6m/s current when the wind had angles of incidence of 60^o and 90^o. Plots of the limit cycles obtained are shown in Figures 7.11 and 7.12, from which it can be seen that these are different in nature to fishtailing motions, in that the yaw angle remains constant. In both these cases the equilibrium angle of incidence of the current is high -45.8^o and 68.7^o respectively. From Figure 7.13, which shows the longitudinal current coefficient C_{xc}, it can be seen that at these angles the surge force produced by the current acts into the current direction, rather than the reverse, due to lifting effects. This introduces the possibility of negative damping in surge, which may be the cause of the instability.

In section 5.3.1 the damping coefficient in surge, due to current at an incidence of θ, was found to be proportional to:-

$$\sin\theta \frac{\partial C_{xc}(\theta)}{\partial \theta} - 2\cos\theta \, C_{xc}(\theta)$$

Using the curve given in Figure 7.13, it can be shown that this coefficient is negative for $39^o<\theta<69^o$ and $90^o<\theta<129^o$. For all cases when the system was found to be stable, the equilibrium angles of current incidence lay outside these ranges, which suggests that surge effects are, in fact, producing the instabilities. The amplitudes of the limit cycles (see Figures 7.11 and 7.12) are of the same order as the motions which would be produced by second order slow drift forces (see section 6.4), and would be indistinguishable from these in either model tests or the actual system. It must be noted that it is unlikely in practise for the environmental conditions to be such that the SBS system will adopt such large angles of incidence to the current direction as those given here, although it may be that for vessels having a different form of C_{xc}, this type of instability can occur at lower angles of incidence.

Wichers (ref. 17) has shown that the freedom afforded by the initial hawser length is the major cause of fishtailing in SPM systems. The fact that this has no parallel in the SBS system probably accounts for the lack of this type of motion in this system.

The model developed in this chapter takes no account of wave effects, such as the wave damping discussed in section 5.3.2, and no interaction between slow drift and unstable motions has been considered, and thus the results are qualitative only. To include these effects would greatly increase the computing costs, and produce results which would be difficult to interpret physically. Also, the study of slow drift forces in the time domain is not well understood at the present time due to difficulties in determining the phase between the forces in the various directions (see section 8.3.2), and thus the extent to which these forces can be realistically modelled is questionable.

7.8 Inclusion of the Mean Drift Forces

As stated in section 6.4, a vessel moored in irregular seas will experience mean forces acting in surge, sway and yaw due to

second order effects. These can be written as (see Figure 7.14):-

$$\bar{F}_1 = -\rho g B \int_0^\infty R_1^2(\omega,\theta) S_\eta(\omega) d\omega \quad (7.48)$$

$$\bar{F}_2 = \rho g L \int_0^\infty R_2^2(\omega,\theta) S_\eta(\omega) d\omega \quad (7.49)$$

$$\bar{F}_3 = 2\rho g L^2 \int_0^\infty R_3^2(\omega,\theta) S_\eta(\omega) d\omega \quad (7.50)$$

where $R_1^2(\omega,\theta)$ is a reflection coefficient, θ is the angle of incidence of the seastate and $S_\eta(\omega)$ is the wave spectrum. B and L are the beam and length of the vessel respectively. Oppenheim and Wilson (ref. 21) have given the following approximate formulae for the dependence of the reflection coefficients upon the angle of incidence:-

$$R_1^2(\omega,\theta) = R_1^2(\omega,0^o)\cos^3\theta + (L/B)R_2^2(\omega,90^o)\sin^2\theta\cos\theta \quad (7.51)$$

$$R_2^2(\omega,\theta) = (B/L)R_1^2(\omega,0^o)\cos^2\theta\sin\theta + R_2^2(\omega,90^o)\sin^3\theta \quad (7.52)$$

$$R_3^2(\omega,\theta) = R_3^2(\omega,45^o)\sin(2\theta)|\sin(2\theta)| \quad (7.53)$$

The coefficients $R_1^2(\omega,0^o)$, $R_2^2(\omega,90^o)$ and $R_3^2(\omega,45^o)$ have been given by Faltinsen et al (ref. 85) and are plotted in Figure 7.15. If the direction of wave propagation lies at an angle θ_{wv} to the current direction (equivalent to θ_w for the wind, see Figure 7.3) then the angle θ in the above equations will be given by:-

$$\theta = \theta_{wv} + \psi \quad (7.54)$$

The mean drift forces can then be included into the model by adding $\bar{F}_1$, $\bar{F}_2$ and $\bar{F}_3$ to the right hand side of equation (7.39). Figures 7.16 and 7.17 show results for the same wind and current conditions as were used for Figures 7.9 and 7.10, but with the addition of a sea-state with significant wave height of 7.5m, lying at 30^o to the current direction. The static position yielded by this model can be incorporated into the dynamic analysis given in Chapter 8.

8.0 RANDOM DYNAMIC ANALYSIS OF A SBS SYSTEM

8.1 Introduction

Chapters 2 to 7 are each concerned with a particular aspect of the dynamic analysis of offshore mooring terminals. The results and conclusions of these six chapters will now be used in the analysis of a Single Buoy Storage (SBS) system. This system, which has been described in Section 1.4.1., comprises a tanker linked to a catenary moored buoy via a rigid yoke. It is assumed that the system is subjected to non-colinear wind, wave and current forces and that the wave spectrum itself may be multi-directional, facts which imply that a fully three-dimensional analysis of the system is required. A vector approach is used to formulate the equations of motion, which are non-linear due to the action of the catenary mooring lines and the drag forces on the buoy. As it was found in Chapter 2 that perhaps the best method of analysing a system subjected to non white-noise random excitation, is to use the equivalent linearisation method followed by a spectral analysis, this method is selected and yields the r.m.s. values of the quantities of interest, from which maximum expected values are estimated, due consideration being given to the results of Section 6.4.3 which concern the statistics of the slow drift response. The linearisation procedure for the catenary mooring and drag force terms have been outlined in Sections 3.5 and 4.3 respectively. The first order wave forces acting on the tanker and the buoy, together with their mass, added mass, damping and stiffness matrices, which are all required for the equations of motion, are found using the analysis of Chapters 4 and 5. Also required are the second order wave forces acting on the tanker in surge, sway and yaw, which are found using the Newman approximation (see Chapter 6) and reflection coefficients given by Faltinsen et al (ref. 85). The solution to the linearised equations of motion is an iterative one since the coefficients introduced by the linearisation procedure are dependent upon both the first and second order response of the system.

The analysis of Chapter 7 is used to investigate the stability of the system when subjected to wind, current and mean drift forces alone. For those systems which are stable, this analysis yields the static offset position about which the first and second order

oscilliatory motions are assumed to occur. For unstable systems (which are unlikely) lack of information about the interaction effects between fishtailing and slow drift motions precludes the use of a frequency domain analysis. Such a system could be studied in the time domain, but this is considered to be beyond the scope of the present work due to the large computing costs which would be incurred.

8.2 Formulation of the Equations of Motion

8.2.1 Coordinate Systems, Transformations and Constraints

The following five coordinate systems will be used in the derivation of the equations of motion of the SBS system (see Figure 8.1).

z - A reference system fixed in space with origin lying on the still water level, one of whose axes is parallel to the direction of wave propagation

x - A coordinate system with origin at the static equilibrium position of the tanker C.G. and whose axes are parallel to the static position of the principal axes of the tanker.

y - A coordinate system similar to x, but related to the instantaneous position of the tanker.

q - A coordinate system with origin at the static equilibrium position of the buoy C.G. and one of whose axes (q_3) lies along the static position of the axis of symmetry of the buoy which is parallel to it's sides. The other two axes are defined such that their horizontal projections are parallel to the horizontal projections of x_1 and x_2 (see Figure 8.1).

p - A coordinate system similar to q, but defined with respect to the instantaneous position of the tanker and buoy.

In the absence of wind, waves and current it is assumed that the centre of the buoy would lie over the origin of the z reference frame. When the environmental forces are present, the static offset position of the tanker is defined by surge, sway and heave displacement of (e_1, e_2, e_3) and a yaw displacement of e_6. The buoy position is defined by translational displacements (f_1, f_2, f_3) and a rotation

f_5, representing the angle that the q_3 axis subtends to the vertical. The sign convention used for these displacements is shown in Figure 8.1. When the analysis of Chapter 7 is used to find the static offset position of the system, the displacements e_3 and f_3 are neglected on the assumption that they will be small in practice. This is necessary due to the fact that the analysis of this chapter is two-dimensional, dealing with displacements in the horizontal plane only. f_5 is then dictated by the geometry of the yoke system. If $(\underset{\sim}{P})_i$ is used to represent the coordinates of a point $\underset{\sim}{P}$ with respect to the i coordinate system, where i represents any of the five systems defined above, then the transformations between the x, q and z frames can be written as:-

$$x \rightarrow z : \quad (\underset{\sim}{P})_z = A(\underset{\sim}{P})_x - \underset{\sim}{e} \tag{8.1}$$

$$q \rightarrow z : \quad (\underset{\sim}{P})_z = AD(\underset{\sim}{P})_q - \underset{\sim}{f} \tag{8.2}$$

$$q \rightarrow x : \quad (\underset{\sim}{P})_x = D(\underset{\sim}{P})_q + A^{-1}(\underset{\sim}{e} - \underset{\sim}{f}) \tag{8.3}$$

where

$$A = \begin{bmatrix} \cos e_6 & -\sin e_6 & 0 \\ \sin e_6 & \cos e_6 & 0 \\ 0 & 0 & 1 \end{bmatrix} \qquad D = \begin{bmatrix} \cos f_5 & 0 & \sin f_5 \\ 0 & 1 & 0 \\ -\sin f_5 & 0 & \cos f_5 \end{bmatrix} \tag{8.4}$$

and $\underset{\sim}{e} = (e_1, e_2, e_3)^T$, $\underset{\sim}{f} = (f_1, f_2, f_3)^T$. The oscillatory translation displacements of the tanker from the equilibrium position are now defined as $\underset{\sim}{d} = (d_1, d_2, d_3)^T$ and the rotations in roll, pitch and yaw as θ_1, θ_2 and θ_3. The corresponding translational displacements of the buoy are written as $\underset{\sim}{b} = (b_1, b_2, b_3)^T$ and the rotations as ψ_1, ψ_2 and ψ_3. If these displacements are assumed to be small, such that second order products can be neglected, then the following transformations can be derived:

$$x \rightarrow y : \quad (\underset{\sim}{P})_y = B[(\underset{\sim}{P})_x - \underset{\sim}{d}] \tag{8.5}$$

$$y \rightarrow z : \quad (\underset{\sim}{P})_z = AB^{-1}(\underset{\sim}{P})_y + A\underset{\sim}{d} - \underset{\sim}{e} \tag{8.6}$$

$$q \rightarrow p : \quad (\underset{\sim}{P})_p = C[(\underset{\sim}{P})_q - \underset{\sim}{b}] \tag{8.7}$$

$$p \to z : \quad (\underset{\sim}{P})_z = ADC^{-1}(\underset{\sim}{P})_p + AD\underset{\sim}{b} - \underset{\sim}{f} \tag{8.8}$$

$$p \to x : \quad (\underset{\sim}{P})_x = D\{C^{-1}(\underset{\sim}{P})_p + \underset{\sim}{b}\} + A^{-1}(\underset{\sim}{e} - \underset{\sim}{f}) \tag{8.9}$$

$$y \to q : \quad (\underset{\sim}{P})_q = D^{-1}\{B^{-1}(\underset{\sim}{P})_y + \underset{\sim}{d} + A^{-1}(\underset{\sim}{f} - \underset{\sim}{e})\} \tag{8.10}$$

where

$$B = \begin{bmatrix} 1 & \theta_3 & -\theta_2 \\ -\theta_3 & 1 & \theta_1 \\ \theta_2 & -\theta_1 & 1 \end{bmatrix} \quad ; \quad C = \begin{bmatrix} 1 & \psi_3 & -\psi_2 \\ -\psi_3 & 1 & \psi_1 \\ \psi_2 & -\psi_1 & 1 \end{bmatrix} \tag{8.11}$$

and to first order $B^{-1} \simeq B^T$, $C^{-1} = C^T$. The following vectors are introduced to represent the coordinates of various points on the system, as shown in Figure 8.2:-

$\underset{\sim}{m}$ = the point where the yoke attaches to the top of the buoy

$\underset{\sim}{t}$ = the point midway between the two pivots which attach the yoke to the tanker

$\underset{\sim}{p}$ = the left hand tanker pivot

$\underset{\sim}{s}$ = the right hand tanker pivot

In the following analysis the axis system to which these points are referred is written as a subscript such that, for example $\underset{\sim}{s}_p$ would represent the coordinates of the right hand tanker pivot with respect to the p coordinate system, and would be written $\underset{\sim}{s}_p = (s_{1p}, s_{2p}, s_{3p})$. The numerical values of $\underset{\sim}{t}_y$, $\underset{\sim}{s}_y$, $\underset{\sim}{p}_y$ and $\underset{\sim}{m}_p$ are then known from the geometry of the tanker and the buoy. So far, twelve degrees of freedom have been considered - six for the tanker and six for the buoy. This number can be reduced by applying the following constraints:-

(i) The yoke is in extensible, which means that the distance between the points $\underset{\sim}{m}$ and $\underset{\sim}{t}$ is constant and equal to the length of the yoke axis of symmetry, ℓ_m say. This constraint can be written in vector form as:-

$$|\underset{\sim}{m}_p - \underset{\sim}{t}_p| = \ell_m \tag{8.12}$$

Using equations (8.10) and (8.7) to represent $\underset{\sim}{t}_p$ in terms of the known quantity $\underset{\sim}{t}_y$, this becomes an equation between the twelve degrees of freedom of the system.

(ii) The yoke subtends a constant angle in the vertical plane to the top surface of the buoy, since the pivot between these two allows rotational freedom about the p_3 axis only. Referring to Figure 8.3 this constraint can be written as:-

$$\overset{\frown}{(\underset{\sim}{t}_p - \underset{\sim}{m}_p)}.(0,0,1) \quad = \quad \cos\alpha \qquad (8.13)$$

where $\underset{\sim}{v}$ represents a unit vector in the direction of $\underset{\sim}{v}$. Again, $\underset{\sim}{t}_p$ can be written in terms of the known quantity $\underset{\sim}{t}_y$ to obtain an equation between the twelve degrees of freedom.

(iii) The hinges at the tanker allow no rotational freedom about the y_3 axis, and thus the horizontal projection of the centreline of the yoke must always lie along the y_1 axis. This can be expressed as:-

$$(\underset{\sim}{t}_y - \underset{\sim}{m}_y).(0,1,0) \quad = \quad 0 \qquad (8.14)$$

Using equations (8.7) and (8.10), $\underset{\sim}{m}_y$ can be written in terms of the known quantity $\underset{\sim}{m}_p$ to produce an equation involving twelve degrees of freedom.

(iv) The hinges which connect the yoke to the tanker and the buoy are such that there can be no relative roll motion between the buoy and the tanker. This can be expressed in vectorial form as:-

$$(\underset{\sim}{s}_p - \underset{\sim}{p}_p).(0,0,1) \quad = \quad 0 \qquad (8.15)$$

where equations (8.7) and (8.10) can be used to express $\underset{\sim}{s}_p$ and $\underset{\sim}{p}_p$ in terms of the known quantities $\underset{\sim}{s}_y$ and $\underset{\sim}{p}_y$.

The above four constraints can be expanded to first order and used to eliminate four of the original twelve degrees of freedom. In practice the buoy motions of surge, sway,heave and roll were eliminated, linear expressions being found for these in terms of the remaining eight degrees of freedom (see Appendix G).

In the derivation of the equations of motion it will be necessary to satisfy dynamic equilibrium for the yoke system. The simplest way to do this is to consider the yoke as a disconnected body having six degrees of freedom and dynamic reactions applied at the hinge points. In order to incorporate the six equations obtained

from this procedure into the equations of motion of the complete system, it will be necessary to express the yoke degrees of freedom in terms of those of the buoy and the tanker. The method of doing this is now outlined.

Let the coordinate system n have its origin at the static offset position of the yoke C.G. with the n_1 axis lying along the yoke axis of symmetry, pointing towards the buoy, and the n_2 axis parallel to x_2 (see Figure 8.4). Also, let the axis system m be defined similarly, but with respect to the instantaneous position of the system. If the dynamic translational displacements of the yoke are written as $\underset{\sim}{j} = (j_1, j_2, j_3)^T$ and the dynamic rotational displacements about n as ϕ_1, ϕ_2 and ϕ_3, the the following transformation applies:-

$$n \rightarrow m : \quad (\underset{\sim}{P})_m = F\{(\underset{\sim}{P})_n - \underset{\sim}{j}\}; \quad F = \begin{pmatrix} 1 & \phi_3 & -\phi_2 \\ -\phi_3 & 1 & \phi_1 \\ \phi_2 & -\phi_1 & 1 \end{pmatrix} \tag{8.16}$$

The transformation between the x and the n axis systems will now be found. If $\underset{\sim}{c}$ represents the centre of gravity of the yoke system then it follows that:-

$$\underset{\sim}{c}_x = \underset{\sim}{t}_x + \ell_g(\widehat{\underset{\sim}{m}_x - \underset{\sim}{t}_x}) \tag{8.17}$$

where ℓ_g is the distance along the yoke axis of symmetry between the yoke centre of gravity and the hinges at the tanker. If the system is now considered to lie at the equilibrium position such that $\underset{\sim}{t}_x = \underset{\sim}{t}_y$, $\underset{\sim}{m}_p = \underset{\sim}{m}_q$ and the dynamic displacements at zero, then by use of equation (8.9), it can be shown that:-

$$\underset{\sim}{c}_x = \underset{\sim}{t}_y + \ell_g(\widehat{D\underset{\sim}{m}_p - A^{-1}\underset{\sim}{f} + A^{-1}\underset{\sim}{e} - \underset{\sim}{t}_y}) = \underset{\sim}{u} \text{ say} \tag{8.18}$$

where $\underset{\sim}{u}$ is now considered to be a known constant vector $(u_1, u_2, u_3)^T$. Now let $\underset{\sim}{n}_{x1}, \underset{\sim}{n}_{x2}$ and $\underset{\sim}{n}_{x3}$ be unit vectors in the directions of the three n axes, when expressed in x coordinates. It can be seen that:-

$$\begin{aligned} \underset{\sim}{n}_{x1} &= (\widehat{\underset{\sim}{m}_x - \underset{\sim}{t}_x}) = (\widehat{D\underset{\sim}{m}_p - A^{-1}\underset{\sim}{f} + A^{-1}\underset{\sim}{e} - \underset{\sim}{t}_y}) \\ &= (\gamma, 0, \delta)^T \text{ say} \end{aligned} \tag{8.19}$$

$$\underset{\sim}{n}_{x2} = \underset{\sim}{x}_2 = (0,1,0)^T \tag{8.20}$$

when the system is in the equilibrium position. δ and γ are then known constants. Orthogonality then implies that $\underset{\sim}{n}_{x3} = (-\delta,0,\gamma)^T$. These expressions for the n axes in terms of the x coordinate system, together with equation (8.18) lead to the following transformation law:-

$$n \rightarrow x : \quad (\underset{\sim}{P})_x = E(\underset{\sim}{P})_n + \underset{\sim}{u} \quad : \quad E = \begin{pmatrix} \gamma & 0 & -\delta \\ 0 & 1 & 0 \\ \delta & 0 & \gamma \end{pmatrix} \tag{8.21}$$

Relationships between the yoke and tanker displacements can be found by noting that the instantaneous positions of the points $\underset{\sim}{s}$ and $\underset{\sim}{p}$ must be the same when defined in terms of the yoke displacements as when defined in terms of the tanker displacements i.e. if $\underset{\sim}{s}_y$ and $\underset{\sim}{p}_y$ are transformed into m coordinates, then $\underset{\sim}{s}_m$ and $\underset{\sim}{p}_m$ should be obtained, which are known from the geometry of the yoke. Thus:-

$$\underset{\sim}{s}_m = F\{E^{-1}B^{-1}\underset{\sim}{s}_y + E^{-1}\underset{\sim}{d} - E^{-1}\underset{\sim}{u} - \underset{\sim}{j}\} \tag{8.22}$$

$$\underset{\sim}{p}_m = F\{E^{-1}B^{-1}\underset{\sim}{p}_y + E^{-1}\underset{\sim}{d} - E^{-1}\underset{\sim}{u} - \underset{\sim}{j}\} \tag{8.23}$$

In practise, the above two vector equations yield five independent equations for the six yoke degrees of freedom. The final equation is obtained by noting that due to the nature of the hinge between the buoy and the yoke, ϕ_2 must equal ψ_2. Each yoke displacement can then be expressed as a linear combination of the tanker and buoy displacements (see Appendix G).

8.2.2 Equations of Motion in Vector Form

Figure 8.5 shows the reactions and bending moments imposed upon the buoy by the pivot connection to the yoke system. In p coordinates these reactions and moments are written as $\underset{\sim}{R}_p = (R_{1p},R_{2p},R_{3p})^T$ and $\underset{\sim}{M}_p = (M_{1p},M_{2p},M_{3p})^T$. Transforming to the buoy equilibrium coordinates, q, gives $\underset{\sim}{R}_q = C^{-1}\underset{\sim}{R}_p$ and $\underset{\sim}{M}_q = C^{-1}\underset{\sim}{M}_p$. If the reactions and bending moments are considered to be first order dynamic quantities then

reference to the definition of C, equation (8.11), show that to first order the transformation is simply $\underset{\sim}{R}_q = \underset{\sim}{R}_p$ and $\underset{\sim}{M}_q = \underset{\sim}{M}_p$. The buoy equation of motion in q coordinates is then written as:-

$$(M_B + M_{BA})\ddot{\underset{\sim}{G}} + D_B\dot{\underset{\sim}{G}} + \underset{\sim}{K}_c + K_h\underset{\sim}{G} - (\underset{\sim}{R}_q, \underset{\sim}{M}_q + (\underset{\sim}{m}_q - \underset{\sim}{b}) \times \underset{\sim}{R}_q)^T = \underset{\sim}{F}_B \tag{8.24}$$

where $\underset{\sim}{G}$ is the vector of buoy displacements $(b_1, b_2, b_3, \psi_1, \psi_2, \psi_3)^T$ M, M_{BA}, D_B and K_h are the mass, added mass, damping and hydrostatic stiffness matrices of the buoy, which are given in Chapter 4. The matrix D_B contains terms which depend upon the r.m.s. buoy displacements, introduced by the linearisation of the drag force acting on the buoy. $\underset{\sim}{K}_C$ is a restoring force vector due to the action of the catenary mooring lines, which contains terms that are non-linear in the buoy displacements (see Chapter 3). This vector is considered to have non-linearities in the horizontal plane only, and these are linearised using the method outlined in Section 3.5. $\underset{\sim}{F}_B$ is the wave force vector which acts on the buoy and which can be found from the analysis of Chapter 4. The notation used for the last term on the left hand side of equation (8.24) is such that if $\underset{\sim}{a} = (a_1, a_2, a_3)^T$ and $\underset{\sim}{b} = (b_1, b_2, b_3)^T$ then the vector $(\underset{\sim}{a}, \underset{\sim}{b})^T$ represents $(a_1, a_2, a_3, b_1, b_2, b_3)^T$. To first order this term can be written as:-

$$(\underset{\sim}{R}_q, \underset{\sim}{M}_q + (\underset{\sim}{m}_q - \underset{\sim}{b}) \times \underset{\sim}{R}_q)^T = (\underset{\sim}{R}_p, \underset{\sim}{M}_p + \underset{\sim}{m}_p \times \underset{\sim}{R}_p)^T = A_1 \underset{\sim}{\bar{R}}_1 \tag{8.25}$$

where $\underset{\sim}{\bar{R}}_1 = (R_{1p}, R_{2p}, R_{3p}, M_{1p}, M_{2p}, 0)^T$ and A_1 is some constant 6 x 6 matrix (see Appendix G). Equation (8.24) can then be solved to give the reactions and bending moments in terms of the wave forces and buoy displacements:-

$$\underset{\sim}{\bar{R}}_1 = A_1^{-1}\left[(M_B + M_{BA})\ddot{\underset{\sim}{G}} + D_B\dot{\underset{\sim}{G}} + \underset{\sim}{K}_c + K_h\underset{\sim}{G} - \underset{\sim}{F}_B\right] \tag{8.26}$$

The reactions acting on the tanker are shown in Figure 8.6. Those at $\underset{\sim}{s}$ and $\underset{\sim}{p}$ due to the action of the yoke hinges are written in y coordinates as $\underset{\sim}{S}_y = (S_{1y}, 0, S_{3y})^T$ and $\underset{\sim}{P}_y = (P_{1y}, 0, P_{3y})^T$. The yoke also transmits a total transverse reaction given in y coordinates by $\underset{\sim}{T}_y = (0, P_{2y}, 0)^T$. Equations (8.5) and (8.21) imply that the reactions transmitted to the yoke at the tanker hinges can be written in n

coordinates as $\underset{\sim}{S}_n = -E^{-1}B^{-1}\underset{\sim}{S}_y$, $\underset{\sim}{P}_n = -E^{-1}B^{-1}\underset{\sim}{P}_y$ and $\underset{\sim}{T}_n = -E^{-1}B^{-1}\underset{\sim}{T}_y$. The negative signs are introduced due to the fact that the reactions at the yoke are equal and opposite to those at the tanker. If the reactions are considered to be first order dynamic quantities then to first order these transformations become $\underset{\sim}{S}_n = -E^{-1}\underset{\sim}{S}_y$, $\underset{\sim}{P}_n = -E^{-1}\underset{\sim}{P}_y$ and $\underset{\sim}{T}_n = -E^{-1}\underset{\sim}{T}_y$. Similarly, equations (8.3) and (8.21) imply that the reactions and bending moments transmitted to the yoke at the point of attachment of the buoy can be written in n coordinates as $\underset{\sim}{R}_n = -E^{-1}D\underset{\sim}{R}_q$ and $\underset{\sim}{M}_n = -E^{-1}D\underset{\sim}{M}_q$. The equations of motion of the yoke can then be written to first order as:-

$$M_y\ddot{\underset{\sim}{j}} - (\underset{\sim}{S}_n + \underset{\sim}{P}_n + \underset{\sim}{T}_n + \underset{\sim}{R}_n, \underset{\sim}{M}_n + \underset{\sim}{s}_m \times \underset{\sim}{S}_n + \underset{\sim}{p}_m \times \underset{\sim}{P}_n + \underset{\sim}{t}_m \times \underset{\sim}{T}_n + \underset{\sim}{m}_m \times \underset{\sim}{R}_n) = 0 \tag{8.27}$$

where $\underset{\sim}{s}_m$, $\underset{\sim}{p}_m$, $\underset{\sim}{t}_m$ and $\underset{\sim}{m}_m$ are all known from the geometry of the yoke structure. The above equation can be re-written as:-

$$\underset{\sim}{\bar{R}}_2 = A_2^{-1}\{M_y\ddot{\underset{\sim}{j}} - (\underset{\sim}{R}_n, \underset{\sim}{M}_n + \underset{\sim}{m}_m \times \underset{\sim}{R}_n)\} \tag{8.28}$$

where $\underset{\sim}{\bar{R}}_2 = (S_{1y}, S_{3y}, P_{1y}, P_{2y}, P_{3y}, 0)^T$ and A_2 is some 6 x 6 matrix (see Appendix G). It was shown in the previous section that $\underset{\sim}{j}$ can be expressed in terms of the degrees of freedom of the tanker and the buoy (see Appendix G) while equation (8.26) implies that $\underset{\sim}{M}_n$ and $\underset{\sim}{R}_n$ can be expressed in terms of these degrees of freedom and the wave forces acting on the buoy. Equation 8.28 is then an equation expressing the reactions at the tanker in terms of these quantities.

To first order the reactions at the tanker can be written in x coordinates as $\underset{\sim}{P}_x = \underset{\sim}{P}_y$, $\underset{\sim}{S}_x = \underset{\sim}{S}_y$ and $\underset{\sim}{T}_x = \underset{\sim}{T}_y$. The tanker equations of motion are then:-

$$(M_T+M_{TA})\ddot{\underset{\sim}{D}} + D_T\dot{\underset{\sim}{D}} + K_T\underset{\sim}{D} - (\underset{\sim}{S}_y+\underset{\sim}{P}_y+\underset{\sim}{T}_y, \underset{\sim}{s}_y x \underset{\sim}{S}_y + \underset{\sim}{p}_y x \underset{\sim}{P}_y + \underset{\sim}{t}_y x \underset{\sim}{T}_y) = \underset{\sim}{F}_{Td} \tag{8.29}$$

where $\underset{\sim}{D}$ is the vector of tanker displacements $(d_1, d_2, d_3, \theta_1, \theta_2, \theta_3)^T$. M_T, M_{TA}, D_T and K_T are the mass, added mass, damping and hydrostatic stiffness matrices for the tanker, which have been given in Chapter 5. $\underset{\sim}{F}_{Td}$ is a vector containing both the first and second order wave forces acting on the tanker, expressions for which have been given in Chapters 5 and 6 respectively. Using equation (8.28), the last term on the left hand side of equation (8.29) can be written in terms of the displace-

ments of the tanker and the buoy and the wave forces acting on the buoy. If the geometrical constraints, equations (8.12) to (8.15), are then used to express the buoy motions of surge, sway, heave and roll in terms of the remaining degrees of freedom, equation (8.29) may, after some manipulation, be written in the form:-

$$\underset{\sim}{M}\ddot{\underset{\sim}{Q}} + \underset{\sim}{D}\dot{\underset{\sim}{Q}} + \underset{\sim}{K}\underset{\sim}{Q} = \underset{\sim}{F}_T + A_3\underset{\sim}{F}_B \qquad (8.30)$$

where $\underset{\sim}{Q} = (d_1, d_2, d_3, \theta_1, \theta_2, \theta_3, \psi_2, \psi_3)^T$ - the displacement vector containing the 8 independent degrees of freedom

M = An 8x8 mass matrix containing structural mass contributions from the whole system and frequency dependent added mass contributions from the tanker and buoy (see sections 5.2.1 and 4.2).

D = An 8x8 damping matrix containing frequency dependent terms due to the potential damping of the buoy and the tanker (see sections 4.2 and 5.2.2), constant terms due to the current and wave damping forces acting on the tanker (sections 5.3.1 and 5.3.2),and terms which are due to the linearisation of the drag forces acting on the buoy and which are dependent upon the r.m.s. displacements of the system (section 4.3).

K = An 8x8 stiffness matrix which contains terms due to the hydrostatic stiffness of the tanker and buoy (sections 4.4 and 5.2.3) and terms due to the linearised catenary moorings some of which are dependent upon the transfer functions of the displacements of the system.

$\underset{\sim}{F}_T$= An 8x1 force vector whose first six entries are the first and second order wave forces acting on the tanker, as given by sections 5.2.4 and 6.4. The last two entries are zero.

A_3= A transformation matrix which depends upon the geometry of the system and is found by rearranging equation (8.29) into the form of equation (8.30) and collecting to the RHS all the terms which depend upon the wave forces acting on the buoy (see Appendix G).

$\underset{\sim}{F}_B$= An 8x1 force vector whose first six entries represent the wave forces acting on the buoy as given by the sections 4.3 and 4.5, and whose last two entries are zero. This vector contains some terms which are due to the linearised drag force and thus depend upon the r.m.s. displacements of the system.

Details of M, D, K and A_3 are given in Appendix G. Equation (8.30) represents the final form of the equations of motion of the system.

8.3 Solution of the Equations of Motion in the Frequency Domain

8.3.1 Characteristics of Response

The response of the system is assumed to be a linear sum of the response at wave frequency (0.1~1.0 rads/sec) caused by the first order wave forces, and the response at around the natural frequencies of the lateral degrees of freedom of the tanker (~0.02 rads/sec) induced by the second order or slow drift forces. Representing these two types of response by $\underset{\sim}{Q}_d$ and $\underset{\sim}{Q}_s$, equation (8.30) can be written in the form:-

$$M(\ddot{\underset{\sim}{Q}}_d + \ddot{\underset{\sim}{Q}}_s) + D(\dot{\underset{\sim}{Q}}_d + \dot{\underset{\sim}{Q}}_s) + K(\underset{\sim}{Q}_d + \underset{\sim}{Q}_s) = \underset{\sim}{F}_d + \underset{\sim}{F}_s \qquad (8.31)$$

where $\underset{\sim}{F}_d$ is a vector containing terms due to the first order wave forces acting on the system, and $\underset{\sim}{F}_s$ is the vector of slow drift forces acting on the tanker. The fact that the two types of response occur at widely differing frequencies suggests that they can be treated separately, and that equation (8.31) can be broken down into two equations as follows:-

$$M\ddot{\underset{\sim}{Q}}_d + D\dot{\underset{\sim}{Q}}_d + K\underset{\sim}{Q}_d = \underset{\sim}{F}_d \qquad (8.32)$$

$$M\ddot{\underset{\sim}{Q}}_s + D\dot{\underset{\sim}{Q}}_s + K\underset{\sim}{Q}_s = \underset{\sim}{F}_s \qquad (8.33)$$

The solution of these two equations is treated separately in sections 8.3.2 and 8.3.3, and the coupling between them via the constants of linearisation is discussed in section 8.3.4.

8.3.2 First Order Response

In order to solve for the first order response in the frequency domain, it is assumed that the force and response in regular waves are simple harmonic, and can be written in complex form as:-

$$\underset{\sim}{Q}_d = a\,\bar{\underset{\sim}{Q}}_d(i\omega,i\theta)e^{i\omega t} \quad ; \quad \underset{\sim}{F}_d = a\,\bar{\underset{\sim}{F}}_d(i\omega,i\theta)e^{i\omega t} \qquad (8.34)$$

where real parts are assumed. a, ω and θ represent the amplitude, frequency and angle of incidence to the x_1 axis of the incident waves. The functions $\bar{\underset{\sim}{Q}}_d(i\omega,i\theta)$ and $\bar{\underset{\sim}{F}}_d(i\omega,i\theta)$ are complex transfer functions, the latter of which can be found by applying the analysis of sections 4.3, 4.5, 5.2.4 and Appendix D to the first order wave forces appearing on the right hand side of equation (8.30). Substituting (8.34) into (8.32) gives the solution for the response transfer functions as:

$$\bar{\underset{\sim}{Q}}_d(i\omega,i\theta) = \left[-\omega^2 M + i\omega D + K\right]^{-1}\bar{\underset{\sim}{F}}_d(i\omega,i\theta) \qquad (8.35)$$

If it is assumed that the incident random seastate is multi-directional then the application of standard spectral techniques (see for example, ref. 27) gives the mean squared value of response as:-

$$\sigma^2_{Q_d} = \int_0^{\infty}\int_{-\pi}^{\pi} \left|\bar{\underset{\sim}{Q}}_d(i\omega,i\theta)\right|^2 S_\eta(\omega)S(\theta)\,d\omega\,d\theta \qquad (8.36)$$

where $|\underset{\sim}{Q}_d|$ represents the modulas of each complex number in the vector, rather than the magnitude of the vector. $S_\eta(\omega)$ is the wave spectrum (see Appendix A) and $S(\theta)$ is a spreading function such that $\int_{-\pi}^{\pi} S(\theta) = 1$. Battjes (ref. 87) states that a general expression for $S(\theta)$ is:-

$$S(\theta) = A(n)\cos^n(\theta - \theta_o) \quad \text{for } |\theta-\theta_o| \leq \frac{\pi}{2} \qquad (8.37)$$

$$= 0 \quad \text{elsewhere}$$

where, in this case, θ_o is the angle subtended between the mean direction of the wave propagation and the x_1 axis. A(n) is a normalisation constant such that A(1) = 1, A(2) = $2/\pi$ and A(n+2) = (n+1)/(n+2)A(n). Reference (87) states that the parameter n generally varies with frequency, but that a constant value of n = 2 is often used for wind driven waves, a procedure which was adopted

for the present work. When the seastate is unidirectional at an angle θ_o to the x_1 axis, then $S(\theta)$ becomes the Dirac delta function $\delta(\theta-\theta_o)$, leading to:-

$$\underset{\sim}{\sigma}^2_{Q_d} = \int_0^\infty |\underset{\sim}{\bar{Q}}_d(i\omega, i\theta_o)|^2 S_\eta(\omega) d\omega \qquad (8.38)$$

Due to the linearisation procedures employed, equations (8.36) and (8.38) do not represent closed form solutions, since the matrices D and K appearing in equation (8.35) depend upon the first and second order response of the system. The iterative solution technique required is outlined in Section 8.3.4.

8.3.3 Second Order Response

The second order forces cover a frequency range from 0rad/sec up to the bandwidth of the incident wave spectrum and are, by nature, much smaller than the first order wave forces. This implies that they will only cause a significant response in those degrees of freedom which are lightly damped and whose natural frequencies lie below the incident wave spectrum - in practise the surge, sway and yaw motions of the tanker. For this reason the second order response in the other degrees of freedom is neglected and equation (8.33) is reduced to three equations:-

$$M'\ddot{\underset{\sim}{Q}}_{rs} + D'\dot{\underset{\sim}{Q}}_{rs} + K'\underset{\sim}{Q}_{rs} = \underset{\sim}{F}_{rs} \qquad (8.39)$$

where $\underset{\sim}{F}_{rs} = (F_{1s}, F_{2s}, F_{6s})$ and $\underset{\sim}{Q}_{rs} = (d_{1s}, d_{2s}, \theta_{3s})$ represent the slow dirft force and response in surge, sway and yaw. M', D' and K' are 3 x 3 matrices, being reduced forms of M, D and K, neglecting coupling between d_{1s}, d_{2s}, θ_{3s} and the other degrees of freedom. As discussed in section 6.4.1, it is theoretically possible to predict the slow drift force when the seastate is multidirectional by using source-sink theory to find the first order potentials. Such an approach requires a vast amount of computer time however, and will not be used here. Rather, the slow drift response will only be considered when the incident seastate is unidirectional, and the Newman approximation (see section 6.4.1) will be applied to the slow

drift force. It is assumed that in a regular wave group, consisting of two waves having frequencies ω and $\omega + \omega_k$ and amplitudes A_1 and A_2, $\underset{\sim}{F}_{rs}$ can be written as:-

$$\underset{\sim}{F}_{rs} = \begin{bmatrix} F_1(\omega+\tfrac{1}{2}\omega_k)\ \phi_1(i\omega, i\omega_k) \\ F_2(\omega+\tfrac{1}{2}\omega_k)\ \phi_2(i\omega, i\omega_k) \\ F_6(\omega+\tfrac{1}{2}\omega_k)\ \phi_6(i\omega, i\omega_k) \end{bmatrix} A_1 A_2 e^{i\omega_k t} \qquad (8.40)$$

where $\phi_i(i\omega, i\omega_k)$ is a function which governs the phase of a response only, so that $|\phi_i(i\omega, i\omega_k)| = 1$. $F_1(\omega)$, $F_2(\omega)$ and $F_6(\omega)$ are defined such that the mean force vector in a regular wave of frequency ω and amplitude A is:-

$$\underset{\sim}{\bar{F}}_{rs} = A^2 \left[F_1(\omega),\ F_2(\omega),\ F_6(\omega)\right]^T \qquad (8.41)$$

from which it can be seen that $F_i(\omega)$ is a dimensional form of reflection coefficient (see section 6.3). The slow drift response to this regular wave group will occur at the difference frequency ω_k, and can be shown from equation (8.39) to be:-

$$\underset{\sim}{Q}_{rs} = \left[-\omega_k^2 M' + i\omega_k D' + K'\right]^{-1} \underset{\sim}{F}_{rs} = A_1 A_2\ \underset{\sim}{T}(i\omega, i\omega_k) e^{i\omega_k t}, \text{say} \qquad (8.42)$$

Pinkster (ref. 75) has shown that the spectrum of slow drift response in a random sea will then be given by:-

$$\underset{\sim}{S}_Q(\omega_k) = 8\int_0^\infty \left|\underset{\sim}{T}(i\omega, i\omega_k)\right|^2 S_\eta(\omega) S_\eta(\omega+\omega_k)\, d\omega$$

$$\sigma_Q^2 = \int_0^\infty \underset{\sim}{S}_Q(\omega_k)\, d\omega_k \qquad (8.43)$$

where $\left|\underset{\sim}{T}(i\omega, i\omega_k)\right|^2$ indicates that the modulus squared of each entry in the vector is required.

The functions $F_i(\omega)$ appearing in equation (8.40) are dependent upon the angle of incidence of the direction of wave propagation to the longitudinal axis of the tanker, θ say. Oppenheim and Wilson (ref. 21) have quoted the following approximate formulae for this dependence:-

$$F_1(\omega,\theta) = F_1(\omega,0^0)\cos^3\theta + F_2(\omega,90^0)\sin^2\theta\cos\theta \qquad (8.44)$$

$$F_2(\omega,\theta) = F_2(\omega,0^0)\cos^2\theta\sin\theta + F_2(\omega,90^0)\sin^3\theta \qquad (8.45)$$

$$F_6(\omega,\theta) = F_6(\omega,45^0)\sin(2\theta)|\sin(2\theta)| \qquad (8.46)$$

where $F_i(\omega,\theta)$ represents the function $F_i(\omega)$ evaluated at θ. The functions appearing on the right hand side of these expressions must be found from either source-sink numerical methods or model tests. For the present work, the published results of Faltinsen et al (ref 85) were used, which concern a 130,000 DWT tanker loaded to both full and half draft. This reference has used source sink methods to produce plots of $F_1(\omega)$, $F_2(\omega)$ and $F_6(\omega)$ against θ for seven frequency values.

In applying the Newman approximation (see section 6.4.1) it has been assumed that each of the slow drift forces is in phase with the low frequency component of the square of the surface elevation, and thus that the phase functions ϕ_i of equation (8.40) are all unity. In order to examine the sensitivity of the response to this assumption, several different values of the functions ϕ_i were used, and the results obtained are noted in Chapter 9.

Equation (8.43) does not represent a closed solution for the slow drift response, since some of the terms in the matrices D' and K' are dependent upon both the first and second order response of the system, due to linearisation. The iterative solution method which is required is discussed in the next section.

8.3.4 Iterative Solution Method

The drag forces acting on the buoy are linearised using the method outlined in section 4.3 and Appendix F, after having expressed the buoy degrees of freedom of surge, sway and roll (i.e. b_1, b_2 and ψ_1) in terms of the tanker degrees of freedom via the constraints given in section 8.2.1. The linearised coefficients given by this method contain terms which depend upon the r.m.s. values of the relative velocities in surge and sway between the buoy and the fluid, evaluated at a number of depths below the mean water level. These relative velocities, which can be expressed in terms of the fluid motions and the system displacements $\underset{\sim}{Q}$, will have both a first and second order component, the latter being due to the slow drift response

of the tanker in surge, sway and yaw. If the transfer functions $\bar{\underset{\sim}{Q}}_d$ and $\underset{\sim}{T}$ are known from equations (8.35) and (8.42) then the transfer functions for these two components can be found, and hence their r.m.s. values. The total r.m.s. value is then found by assuming statistical independence between the two components, such that:-

$$\sigma_T^2 = \sigma_1^2 + \sigma_2^2 \qquad (8.47)$$

where σ_T, σ_1 and σ_2 are the r.m.s. total, first order and second order responses, respectively.

The restoring forces which act in the horizontal plane are linearised by the method given in section 3.5, the horizontal displacements of the buoy being expressed in terms of the system displacements $\underset{\sim}{Q}$ via the constraints of section 8.2.1. The constants of linearisation are dependent upon the transfer functions of the horizontal displacements, which can be found if $\bar{\underset{\sim}{Q}}_d$ and $\underset{\sim}{T}$ are known.

It can be seen that for both the catenary moorings and the drag force acting on the buoy the constants of linearisation are dependent upon the response of the system. This leads to an iterative solution technique in which initial values of the constants of linearisation are estimated to produce the matrices D, K, D' and K'. Equations (8.35) and (8.43) then give the system response, from which new values of these constants can be calculated. These can then be inserted into the relevant matrices and the system response re-calculated. This will then yield further values for these constants. This process is repeated until satisfactory convergence is achieved.

8.4 Calculation of the Yoke Reactions

8.4.1 Reactions at the Tanker

By rearranging the last term on the left hand side, equation (8.29) can be written in the form:-

$$A_4 \bar{\underset{\sim}{R}}_2 = (M_T + M_{TA})\ddot{\underset{\sim}{D}} + D_T\dot{\underset{\sim}{D}} + K_T\underset{\sim}{D} - \underset{\sim}{F}_{Td} \qquad (8.48)$$

where $\bar{\underset{\sim}{R}}_2 = (S_{1y}, S_{3y}, P_{1y}, P_{2y}, P_{3y}, 0)$ and A_4 is a 6x6 matrix whose entries are determined by the coordinates of the points $\underset{\sim}{s}_y$, $\underset{\sim}{p}_y$ and $\underset{\sim}{t}_y$,

which are known from the dimensions of the tanker. This matrix is given in Appendix G. The displacement vector of the tanker, $\underset{\sim}{D}$, can be considered to be the sum of a first order term, $\underset{\sim}{D}_d$, and a second order term, $\underset{\sim}{D}_s$, both of which are determined once equation (8.30) has been solved for the displacement vector of the whole system, $\underset{\sim}{Q}$, by the method outlined in section 8.3. The transfer functions for the first order tanker displacements, $\underset{\sim}{\bar{D}}_d(i\omega,i\theta)$ say, can be found from equation (8.35), and substitution into (8.48) then yields the transfer functions for the first order tanker reactions:-

$$\underset{\sim}{\bar{R}}_{2d}(i\omega,i\theta) = A_4^{-1}\left[-\omega^2(M_T+M_{TA})+i\omega D_T+K_T\right]\underset{\sim}{\bar{D}}_d(i\omega,i\theta)-A_4^{-1}\underset{\sim}{\bar{F}}_{Td}(i\omega,i\theta) \tag{8.49}$$

where $\underset{\sim}{\bar{F}}_{Td}(i\omega,i\theta)$ is a vector containing the transfer functions of the wave forces on the tanker. The r.m.s. values of these reactions are then given by:-

$$\underset{\sim}{\sigma}^2_{R2d} = \int_0^\infty\int_{-\pi}^{\pi}\left|\underset{\sim}{\bar{R}}_{2d}(i\omega,i\theta)\right|^2 S_\eta(\omega)S(\theta)\,d\omega\,d\theta \tag{8.50}$$

In section 8.3.3 it was assumed that slow drift response occurs in surge, sway and yaw only and the second order displacement vector was written as $\underset{\sim}{Q}_{rs} = (d_{1s},d_{2s},\theta_{3s})$. Applying this to equation (8.48) and considering reactions which lie in the horizontal plane only leads to:-

$$A_4'\underset{\sim}{\bar{R}}_{2s} = (M_T'+M_{TA}')\ddot{\underset{\sim}{Q}}_{rs} + D_T'\dot{\underset{\sim}{Q}}_{rs} + K_T'\underset{\sim}{Q}_{rs} - \underset{\sim}{F}_{rs} \tag{8.51}$$

where $\bar{R}_{2s} = (S_{1ys},P_{1ys},P_{2ys})$ and the prime on the matrices indicates that they have been reduced to 3x3, neglecting the coupling terms to any of the other degrees of freedom or reactions. $\underset{\sim}{F}_{rs}$ is the slow drift vector, introduced in section 8.3.3. Using equation (8.42) it can be shown that the spectra of the second order reactions are given by:

$$\begin{aligned}\underset{\sim}{S}_{R2s}(\omega_k) &= 8\int_0^\infty\left|\underset{\sim}{X}(i\omega,i\omega_k)\right|^2 S_\eta(\omega)S_\eta(\omega+\omega_k)\,d\omega\\ \underset{\sim}{\sigma}^2_{R2s} &= \int_0^\infty \underset{\sim}{S}_{R2s}(\omega_k)\,d\omega_k\end{aligned} \tag{8.52}$$

where:-

$$\underset{\sim}{X}(i\omega, i\omega_k) = [A_4']^{-1}\{-\omega_k^2(M_T'+M_{TA}')+i\omega_k D_T'+K_T'\}\underset{\sim}{T}(i\omega, i\omega_k)$$

$$-[A_4']^{-1}(F_1\phi_1, F_2\phi_2, F_6\phi_6)^T \qquad (8.53)$$

For those reactions which have both a first order and a second order component, the total r.m.s. value can be found by assuming statistical independence and applying an equation of the type (8.47).

8.4.2 Reactions and Bending Moments at the Buoy

Using the constraints of section 8.2.1 it is possible to express the buoy displacements in terms of those of the whole system as follows:-

$$\underset{\sim}{G} = A_c\underset{\sim}{Q} \qquad (8.54)$$

where A_c is a 6x8 matrix whose entries are determined by the geometry of the system (see Appendix G). Equation (8.26) can then be written in the form:-

$$\underset{\sim}{\bar{R}}_1 = A_1^{-1}[(M_B+M_{BA})A_c\ddot{\underset{\sim}{Q}} + D_B A_c\dot{\underset{\sim}{Q}} + (K_L+K_h)A_c\underset{\sim}{Q} - \underset{\sim}{F}_B] \qquad (8.55)$$

where the catenary force vector $\underset{\sim}{K}_c$ has been replaced with $K_L\underset{\sim}{G}$, K_L being the linearised stiffness matrix. The transfer functions for the first order buoy reactions and moments are then:-

$$\underset{\sim}{\bar{R}}_{1d}(i\omega, i\theta) = A_1^{-1}[-\omega^2(M_B+M_{BA})+i\omega D_B+K_L+K_h]A_c\underset{\sim}{\bar{Q}}_d(i\omega, i\theta) - A_1^{-1}\underset{\sim}{\bar{F}}_B(i\omega, i\theta) \qquad (8.56)$$

where $\underset{\sim}{\bar{Q}}_d(i\omega, i\theta)$ is given by equation (8.35) and $\underset{\sim}{\bar{F}}_B(i\omega, i\theta)$ is a vector containing the transfer functions of the wave forces acting on the buoy. The r.m.s. values of these reactions are:-

$$\underset{\sim}{\sigma}^2_{R_1 d} = \int_0^{\infty}\int_{-\pi}^{\pi} |\underset{\sim}{\bar{R}}_{1d}(i\omega, i\theta)|^2 S_\eta(\omega)S(\theta)d\omega d\theta \qquad (8.57)$$

Similarly, the transfer functions for the second order reactions can

be found from equations (8.55) and (8.42) to be:-

$$\underset{\sim}{Y}(i\omega, i\omega_k) = A_1^{-1}\left[-\omega_k^2(M_B+M_{BA})+i\omega_k D_B+K_L+K_h\right]A_c M_E \underset{\sim}{T}(i\omega, i\omega_k) \quad (8.58)$$

where M_E is a matrix which when multiplied into $\underset{\sim}{Q}_{rs}$ produces $(d_{1s}, d_{2s}, 0, 0, 0, \theta_{3s}, 0, 0)^T$ i.e. the full $\underset{\sim}{Q}$ vector for slow drift motions (see Appendix G). The spectra of second order reactions are then:-

$$\begin{aligned} \underset{\sim}{S}_{R1s}(\omega_k) &= 8\int_0^\infty |\underset{\sim}{Y}(i\omega, i\omega_k)|^2 S_\eta(\omega) S_\eta(\omega+\omega_k)\, d\omega \\ \underset{\sim}{\sigma}^2_{R1s} &= \int_0^\infty \underset{\sim}{S}_{R1s}(\omega_k)\, d\omega_k \end{aligned} \quad (8.59)$$

The total r.m.s. values of those reactions and moments which have both a first order and second order contribution are found, as in the above section, by assuming statistical independence.

9.0 RESULTS OF THE RANDOM DYNAMIC ANALYSIS OF AN SBS SYSTEM

9.1 Introduction

In order to perform the analysis given in the previous chapter it is necessary to use a digital computer. In the present study, the VAX 780 computer of the Cranfield Computer Centre was used. Although this machine is a mini-computer, it's use of the virtual memory system affords it mainframe capacity, and thus the solution of a problem of the present magnitude lies well within it's capacity. The equations given in the previous chapter were coded into FORTRAN, use being made of the NAG Library subroutine FO4ADF for the complex matrix inversion contained in equation (8.35). The integrations appearing in equations of the type (8.38) were performed using the trapezium rule, forty frequency intervals between 0.2 and 1.6 rad/sec being considered for the incident wave spectrum. The slow drift force spectrum was assumed to extend from 0.0 to 1.0 rad/sec and again, forty frequency intervals were used. Thirty of these were concentrated in the region 0 to $2\omega_{np}$ where ω_{np} is the highest natural frequency for the three lateral degrees of freedom (surge, sway and yaw). This was done in view of the fact that the transfer functions of these three degrees of freedom are highly peaked at the natural frequencies, and thus a fine frequency mesh is required in these regions. In calculating the added mass and damping coefficients for the tanker heave and pitch, the vessel was divided into three sections and the coefficients for each were found from Grim's Data Sheets (ref.66). The drag forces acting on the buoy were linearised by dividing the submerged section into four strips, a linearised coefficient in both surge and sway then being found for each strip, as discussed in Appendix F. In those cases where a directional seastate was considered, the first order response alone was calculated, for reasons stated in section 6. 1. For a unidirectional seastate, both first and second order responses were calculated, coupling between the two caused by the non-linear catenary moorings and the drag forces on the buoy being taken into account, as discussed in the previous chapter.

The above procedure was used to calculate the dynamic response of a number of SBS systems. In all, five different types of tanker were considered, the details of which are shown in Figure 9.1. The three different mooring configurations described in Figures 9.2, 9.3

and 9.4 were also considered. The results obtained are presented in the following sections, in which the effect upon the response of changes in the method of analysis, the dimensions of the system and the environmental conditions are discussed.

In all of the following sections the approach has been to assume the angles of incidence of the waves and current to which the system is subjected, rather than to perform a complete static analysis. The advantage of this approach is that it allows the investigation of the effect of varying certain parameters upon the first and second order response of the system to be carried out without introducing any confusion as to whether changes in the response are due to changes in the static equilibrium position rather than a direct result of a change in the parameters. No calculations concerning the mean drift forces acting on the vessel have been performed, as these have been well documented in reference (88), which gives the mean drift force in the i'th direction in a random seastate of significant wave height H_s (JONSWAP spectrum) as:-

$$\bar{F}_i = \left(\frac{\rho g L^n}{8}\right) Q_i^2 H_s^2 \qquad (9.1)$$

where n is 1 for surge and sway and 2 for the yaw moment. The functions Q_i are plotted as functions of T_2, the mean zero crossing period of the incident seastate. These results are reproduced in Figures 9.5 and 9.6, where it should be noted that the yaw moment acts so as to force the vessel into a position parallel to the wave crests.

If the purpose of this chapter had been to determine the response of the SBS system to a particular set of environmental conditions (as would be the case in the design of a system for a particular location), rather than to examine the response properties of the system in general, then the approach would be first to use the analysis of Chapter 7 to determine the stability of the system. If the system is stable then this analysis would yield the static equilibrium position, about which the dynamic response would be assumed to occur. This response would then be calculated using the analysis of Chapter 8, suitable terms being introduced to allow for the stiffness properties produced by the current and mean drift forces (see sections 5.3.1 and 9.6.2). If the system is not stable (which is

unlikely for an SBS system) then the approach would be to include the slowly varying drift forces into the time domain analysis of Chapter 7 to yield a time history of the slowly varying motions of the system. The first order response would then be superimposed on these motions, a particular point in the time history of the slow response being considered as the static equilibrium position for the calculation of the first order response. This would tend to be very expensive due to the large computer times required to simulate the slowly varying drift forces.

9.2 Natural Frequencies of the System

From equation (8.30), the equations of free, small amplitude, undamped vibrations of the system can be written as:-

$$M\ddot{\underset{\sim}{Q}} + K\underset{\sim}{Q} = \underset{\sim}{0} \qquad (9.2)$$

where M and K are the mass and stiffness matrices (see section 8.2.2) and $\underset{\sim}{Q}$ is the displacement vector. For simple harmonic motion, equation (9.2) assumes the well known form of an eigen problem, the solution of which yields the natural frequencies and mode shapes of the system, i.e.

$$\left[-\omega_n^2 M + K\right] \underset{\sim}{Q}_n = \underset{\sim}{0} \qquad (9.3)$$

where ω_n and $\underset{\sim}{Q}_n$ are the n'th natural frequency and mode shape. This equation is slightly different from the usual eigen problem in that the added mass terms in M are frequency dependent. For the present free vibration analysis a constant mass matrix was used, the frequency dependent terms being evaluated at 0.36 rad/sec, the peak frequency of a 100 year North Sea design storm. The NAG subroutine F02BJF was used to solve equation (9.3) for a number of SBS systems in three different circumstances. Firstly, the natural frequencies for small amplitude motions in still water were found, the stiffness matrix involving both the hydrostatic stiffness terms and the coefficients of the linear terms in the restoring forces due to the catenary moorings (see section 3.2.3). Secondly, the natural frequencies in the presence of a 1m/s current were found, the stiffness matrix having additional terms due to the current (see section 5.3.1). Lastly, the

natural frequencies were calculated using the linearised catenary stiffness of section 3.5. The linearisation considered both the direct and slow drift motions caused by a JONSWAP spectrum of significant wave height 15m directed towards the vessel at 15^{o} off the bow. This case also considered a 1 m/s current directed onto the bow of the vessel.

Seven degrees of freedom were considered in this analysis - the surge, sway, heave, roll, pitch and yaw motions of the vessel and the pitch motion of the buoy (which involves the rotation of the yoke structure about the tanker hinges). The yaw motion of the buoy was neglected, as it is uncoupled from the other degrees of freedom and experiences no exciting force when the system is subjected to a general seastate.

Figure 9.7 shows results for a 130,000 DWT tanker at both full and half draft, as well as for a 200,000 DWT tanker at full draft, the mooring system considered being that detailed in Figure 9.3. Figure 9.8 shows results for the 130,000 DWT tanker at half draft for three loading conditions - those where the centre of gravity is forward of midships, midships and aft of midships. Finally, Figure 9.9 shows results for the 130,000 DWT tanker at full draft for three different mooring configurations, being those detailed in Figures 9.2, 9.3 and 9.4

When the system is in still water the tanker is able to weathervane about the buoy without disturbing the mooring system or altering its submerged volume, and thus there is no stiffness to oppose this motion. This 'mode' therefore has a natural frequency of zero (and thus an infinite natural period), as shown in Figures 9.7, 9.8 and 9.9. The other modes in the horizontal plane are the 'surge only' mode and a coupled 'yaw-sway' mode in which the yaw and sway motions are in phase. In the vertical plane, the heave and pitch of the tanker are coupled, which leads to two modes - one in which the motions are in phase and one in which they are out of phase. The final two modes are those of tanker roll and buoy pitch, the coupling between these and the other degrees of freedom being very slight. When a current is present, additional stiffness terms k_{16} ,k_{26} and k_{66} are introduced, as shown in section 5.3.1, and the system has three non-zero natural frequencies for motions in the horizontal plane. The

first of these, surge, is not affected by the presence of current. The natural frequency of the second, in which the yaw and sway motions are in phase, is slightly reduced due to the fact that the current stiffness terms k_{26} and k_{66} tend to be negative. The third mode in the horizontal plane is that in which the yaw and sway motions are out of phase, the restoring forces being supplied mainly by the current. This mode has a very low natural frequency, a typical natural period being in the order of 40 minutes.

Figure 9.7 shows the effect of vessel size on the natural frequencies of the system. It can be seen that the roll natural frequency of each vessel lies well within the range of the incident wave frequencies (0.2 - 1.6 rad/sec), which is of particular concern since the roll damping is light. The problem of large amplitude resonant motions does not occur however, due to the fact that in a single point mooring system the vessel is free to weathervane to face the incoming waves, thus minimizing the roll exciting moments. Figure 9.11.4 shows the roll transfer function for a fully loaded 130,000 DWT tanker in a seastate incident of 15^{o} off the bow. It can be seen from this Figure that the roll response per unit wave height is very small for frequencies which are close to the natural frequency (0.468 rad/sec). Figure 9.15.4 shows how this response increases rapidly with the angle of incidence of the seastate to the bow of the vessel. The natural frequencies of the two heave and pitch modes also lie within the range of the incident wave frequencies, although in this case resonance is not a problem due to the large amount of potential damping which is present. As would be expected, the natural frequencies of the horizontal plane modes decrease slightly as the displacement of the vessel increases due to the extra fluid added mass.

Figure 9.8 shows the effect of the tanker loading condition on the natural frequencies of a SBS system in which the vessel is a 130,000 DWT tanker at half draft. Three cases are considered - those where the centre of gravity of the vessel is midships, 60m fore of midships and 60m aft of midships. It can be seen that as the centre of gravity moves aft, the natural frequency of the yaw-sway in phase mode increases, whereas that of the yaw-sway out of phase mode decreases. The reverse is true of the heave-pitch modes. The percentage changes are greatest for the yaw-sway out of phase mode, where a

58% increase in the natural frequency is caused by moving the centre of gravity from 60m aft of midships to 60m fore of midships. The effect of these changes upon the response of the system is discussed in section 9.5.2.

Figure 9.9 shows the effect of the mooring configuration on the natural frequencies of a SBS system in which the vessel is a 130,000 DWT fully loaded tanker. The three mooring configurations considered are shown in Figures 9.2, 9.3 and 9.4. It can be seen that the mooring configuration does not affect the natural frequencies of the roll, heave or pitch motions of the tanker and causes only a slight change in that of the buoy pitch motion. The latter is due to the fact that the vertical plane restoring forces caused by the catenary lines are much smaller then the hydrostatic restoring forces caused by the buoy. In the presence of current, but without using the linearised stiffness coefficients, the surge and yaw-sway in phase natural frequencies are approximately proportional to the square root of the horizontal plane linear stiffness of the mooring configuration. The yaw-sway out of phase natural frequency does not change substantially with the mooring configuration, as the stiffness in this mode is due mainly to the current. Use of the linearised stiffness coefficients has most effect for the configuration shown in Figure 9.2, for which the ratio of the cubic horizontal stiffness coefficient to the linear horizontal stiffness coefficient is greatest and here 155% and 97% changes in the surge and yaw-sway in phase natural frequencies are found, the r.m.s. surge displacement being 21.23m. It should be noticed that this displacement, and thus the results quoted above, is fairly sensitive to the surge damping which is assumed to act on the tanker (see section 9.4.8). Figure 9.10 shows results for the amplitude dependent surge natural frequency of this configuration, as given by the analysis of section 3.4, which is based on the Duffing Equation. As would be expected, the result for zero amplitude vibrations corresponds to the unlinearised result of Figure 9.9. The natural frequency given by the linearised catenary stiffness is approximately equal to that of free vibrations of amplitude 44m. The fact that this amplitude is less than the maximum amplitude which would be predicted by four times the r.m.s. displacement is to be expected, since the majority of cycles in the random response will have an amplitude much less than this value.

9.3 Transfer Functions and Slow Drift Response Spectra

9.3.1 First Order Transfer Functions

Figures 9.11 to 9.14 show the moduli squared of the complex transfer functions of the first order motions and yoke reactions of four different SBS systems, each of which has the mooring configuration shown in Figure 9.3. Figure 9.11 is a case in which the vessel is a 130,000 DWT tanker loaded to full draft. Figures 9.12 and 9.13 both concern a 130,000 DWT tanker loaded to half draft, the ballasting arrangement of the former being such that the centre of gravity is midships, and the latter is such that the centre of gravity is 60m fore of midships. Figure 9.14 concerns a 200,000 DWT tanker, loaded to full draft. The phase diagrams shown in these figures refer to the phase angle δ by which the responses lead the wave surface elevation at the centre of the tanker, i.e. if the surface elevation of the centre of the tanker can be written as:-

$$\eta = \mathrm{Re}\{\eta(i\omega)e^{i\omega t}\} = \mathrm{Re}\{|\eta(i\omega)|e^{i(\omega t+\gamma)}\}$$

then the response can be written as:-

$$x = \mathrm{Re}\{x(i\omega)e^{i\omega t}\} = \mathrm{Re}\{|x(i\omega)|e^{i(\omega t+\gamma+\delta)}\}$$

The fluid potential w.r.t. the equilibrium axes of the tanker is taken to be:

$$\phi = \frac{ag}{\omega}\left(\frac{\cosh\, k(d+z)}{\cosh\, kd}\right) e^{ik(x\cos\theta - y\sin\theta)} e^{i\omega t}$$

where θ is the angle of incidence of the waves to the bow of the tanker, which in this case is considered to be 15^{o}. This leads to a wave surface elevation of the centre of the tanker of $-iae^{i\omega t}$.

Figure 9.15 shows the effect of the angle of incidence of the seastate upon the transfer functions of the first system, - that in which the vessel is a fully loaded 130,000 DWT tanker. The transfer functions of the various items are considered in turn below. A detailed comparison between the response characteristics of the different vessels is given in sections 9.5.1 and 9.5.2.

9.3.1.1.Surge

The surge transfer functions of each of the four systems have similar characteristics. In each case the transfer function is largest for low frequency waves. This is to be expected as the low natural frequency in surge leads to an inertia dominated response, in which the vessel motion tends to follow the surge motions of the fluid, which are greatest for the low frequency long waves. This is confirmed by the fact that the surge motion leads the surface elevation by a phase angle of $\pi/2$ rads at these frequencies, and is thus in phase with the fluid motion. For a rectangular flat ended vessel the surge response will be zero for those waves in which the pressure forces acting over the bow and stern are equal and opposite. Neglecting diffraction, this occurs when the wavelength is equal to the length of the vessel, or $\sin(\frac{1}{2}kL\cos\theta) = 0$ (see Appendix D), which for $\theta = 15^{o}$ and L = 300m leads to a first value of frequency of $\omega = 0.48$ rad/sec. For the 130,000 DWT vessel, the transfer function has a zero at $\omega = 0.55$ rad/sec, the discrepancy being due to the taper of the vessel and the fact that the surge forces acting on the buoy are transmitted to the tanker via the rigid yoke structure.

9.3.1.2.Sway

As would be expected, the transfer functions of the inertia dominated sway response are similar in shape to those of the surge response. The sway response lags behind the surface elevation by a phase angle of $\pi/2$ rads for the low frequency waves, and is therefore in phase with the sway motions of the fluid at these frequencies. It is shown in Appendix D that the sway response of a rectangular vessel is zero when $\sin(\frac{1}{2}kL\cos\theta) = 0$, which corresponds to the point of zero surge response. This explains why both the surge and sway transfer functions have zeros at near to $\omega = 0.55$ rad/sec.

9.3.1.3.Heave

The heave exciting force has two main components, (1) the inertia force caused by the vertical acceleration of the fluid and (2) the changing buoyancy force caused by the wave profile. The buoyancy force tends to dominate and for low frequency waves the vessel responds in phase with the wave surface elevation at the centre of the vessel. For a rectangular vessel, both of these forces have zero's at the same points as the surge and sway forces, and thus the

heave transfer function has a zero somewhere between ω = 0.48 rad/sec and ω = 0.55 rad/sec. The second and third zero's of the function $\sin(\frac{1}{2}kL\cos\theta)$ are also visible in the heave transfer function, at slightly higher frequencies.

9.3.1.4.Roll

The exciting moment in roll comprises (1) an inertia moment caused by the inertia forces acting in sway on the tanker and the buoy, and (2) a buoyancy moment produced by the wave slope, these moments being 180^{o} out of phase. For the full draft vessels (Figures 9.11 and 9.14) the moments produced by the sway inertia forces are relatively small, and the wave slope term dominates. Since the wave slope per unit waveheight is greater for high freqneucy, short wavelength waves, the roll transfer functions are greater for these frequencies. For a rectangular vessel of length L and beam B the roll moment due to the wave slope is zero when either $\sin(\frac{1}{2}kB\sin\theta) = 0$ or $\sin(\frac{1}{2}kL\cos\theta) = 0$, as is shown in Appendix D. At high frequencies the frequencies at which these functions are zero are closely spaced, which produces the peaky appearance of the transfer functions shown in Figures 9.11.4 and 9.14.4. For the half draft vessels (Figures 9.12 and 9.13) the contribution of the moment due to the inertia forces acting in sway is greater, one reason being that the moment arm of the sway forces acting on the buoy increases as the vessel lifts out of the water. This tends to decrease the total moment acting in roll, which is reflected in the fact that the roll transfer functions for the half draft vessels are less than those of the full draft vessels. Again, the roll response tends to be larger for the higher frequencies, and the transfer functions have a peaky appearance.

9.3.1.5.Pitch

The exciting moments in pitch are (1) an inertia moment due to the vertical acceleration of the fluid,and (2) a buoyancy moment caused by the wave profile. For low frequency waves the latter dominates and the vessel pitch motions tend to follow the slope of the surface elevation, thus lagging behind the surface elevation at the centre of the vessel by a phase angle of $\pi/2$ rads. The pitch response is greatest for the low frequency, long waves where the wave slope is fairly constant over the length of the vessel, and exhibits zero's close to those of the heave response (see Appendix D).

9.3.1.6.Yaw

Yaw motions are inertia dominated due to the low natural frequencies of the lateral modes of response and are caused by the moments produced by the inertia forces acting in sway. The phase of the yaw moment is dependent upon the shape of the waterplane area of the vessel and the position of the centre of gravity. For a rectangular vessel with the centre of gravity amidships, the yaw response in low frequency waves is in phase with the surface elevation at the centre of the vessel. The zero's in the yaw transfer functions are near to those of the pitch transfer functions.

9.3.1.7.Buoy Pitch

The pitch motions of the buoy involve the rotation of the yoke structure about the tanker hinges and are therefore dependent upon the relative vertical motion between these hinges and the buoy. For very low frequency waves, buoyancy effects will tend to make the whole system heave in phase with the surface elevation, in which case there will be no pitching of the buoy. This is reflected in the low values of the buoy pitch transfer function for $\omega \simeq 0.2$ rad/sec. The pitching motions of the tanker will tend to increase the relative vertical motion between the buoy and the tanker hinges, which leads to peaks in the buoy pitch transfer function of frequencies which correspond to those in the tanker pitch transfer function. For high frequency waves the heave and pitch motions of the tanker and the heave motions of the buoy are small, and thus the buoy pitch transfer function has low values at these frequencies.

9.3.1.8.Horizontal Plane Tanker Reactions P1,S1 and P2.

The first order reactions in the yoke structure are caused mainly by the net forces which act on the buoy. If the motions of the system are such that the buoy is allowed to move with the surrounding fluid, then the yoke reactions will be small. On the other hand, if the vessel motions cause the buoy response to be opposed to the fluid motion then large reactions will be produced. For low frequency waves the whole system tends to follow the wave motion and thus the transfer functions of the reactions which act on the tanker in the horizontal plane (P1,S1 and P2) are small at these frequencies. If the vessel moves in the positive surge direction then equal reactions P1 and S1 are produced, both of which are negative. If the vessel moves in sway then equal and opposite reactions

P1 and S1 are produced, P1 being positive. The fact that the surge and sway motions of the vessel are 180° out of phase for the wave direction considered means that these effects tend to add for P1 and subtract for S1, which explains why the transfer function of P1 is greater than that of S1. As there are many factors which contribute to the reactions P1, P2 and S1 it is difficult to give a simple explanation for the shape of their transfer functions. The waves in which the vessel motions are liable to move the buoy in opposition to the fluid have short wavelengths and high frequencies, where, for example, sway inertia forces may cancel over the large submerged surface of the tanker and yet be large on the buoy. At these high frequencies the wavelength changes rapidly with the frequency and thus frequencies which are relatively close may produce widely differing reactions. This may explain the high, narrow peaks which appear in the high frequency range of the transfer functions in Figures 9.11.8 and 9.11.10. Also, the reactions will be largely due to inertia forces which increase with the square of wave frequency.

9.3.1.9.Vertical Plane Tanker Reactions P3 and S3.

For the incident wave direction which has been considered, the transfer function of the tanker reaction P3 is slightly greater than that on the opposite side of the vessel, S3. Both of these transfer functions are peaky in appearance and are of considerable magnitude over a wide range of frequencies. The lowest frequency peak occurs at a frequency close to where the sway response is zero, and corresponds to a wave in which the sway inertia forces acting on the buoy are balanced by the yoke reactions rather than by inertia relief. It is difficult to explain the nature of these reactions in simple terms since they contain contributions from all vessel motions except surge.

9.3.1.10.Buoy Reactions R1, R2 and R3.

The transfer function of the buoy reaction R1 is similar in form to that of the tanker reactions P1 and S1, except that it is smaller for high frequencies. This suggests that sway effects, which do not contribute to R1, are responsible for the high narrow peaks which occur in the transfer functions of P1 and S1 at high frequencies. The transfer function of R2 is similar in shape to that of P2, although slightly smaller in magnitude. The difference between these two reactions is accounted for by the sway inertia relief of the yoke

structure. The transfer function of R3 peaks at almost the same frequency as that of R1 and is similar in shape.

9.3.1.11.Buoy Moments M1 and M2

As might be expected, the transfer function of the moment M1 is similar in shape to that of the roll response of the tanker. Also, the transfer function of the moment M2, which in part balances the moment produced on the buoy by the reaction R1 is similar in shape to that of this reaction.

9.3.2 Second Order Response Spectra

It was shown in section 8.3.3 that the transfer functions of the second order response to a regular wave group are functions of both ω_k, the separation frequency of the group, and ω, the mean frequency of the group. Any plot of these functions would therefore need to be of a three dimensional nature as opposed to the more usual transfer function plot of response against 'frequency'. Rather than present such plots in this section, the spectra of the second order responses are shown, these being functions of the separation frequency ω_k only. Figures 9.16 to 9.25 show the spectra of the second order motions and yoke reactions of a SBS system which is subjected to a unidirectional random seastate with H_s = 15m, directed at 15° to the bow of the vessel, together with a colinear 1 m/s current. The system considered consists of a 130,000 DWT tanker loaded to full draft and moored via the arrangement shown in Figure 9.3.

Figure 9.16 shows the spectrum of the surge response, the peak of which occurs at the surge natural frequency, ω_k = 0.026 rad/sec. Although the second order exciting forces are broad banded, the low level of damping present in surge (see section 9.4.8) leads to a very narrow banded response. The spectra of the yoke reactions P1, S1 and R1, and the bending moment M2 closely resemble the surge spectrum, being due to the restoring forces induced in the mooring system by the surge displacement.

Figures 9.17 and 9.18 show the spectra of the sway and yaw responses, these being greatest for very low values of ω_k. This is because the slow drift response in sway and yaw tends to occur in the out-of-plane mode whose natural frequency is very low, being 0.0041 rad/sec. A small secondary peak can be seen in the yaw spectrum at the natural frequency of the in-phase mode, ω_k = 0.04 rad/sec.

The spectra of the yoke reactions P2 and R2, and the moment M1 are all similar in appearance, showing peaks at both the surge natural frequency and the yaw-sway in phase natural frequency, these being the modes which produce displacements in the buoy position and hence restoring forces in the catenary moorings. The peaks at the surge natural frequency are mainly due to the increase in the linearised stiffness term k_{yy} caused by the increased surge response.

The spectra of the slow drift forces themselves are not shown in this chapter since these have the usual broad banded appearance. Examples of the slow drift force spectra are given in Chapter 6.

9.4 Investigations concerning the Methods of Analysis

9.4.1. Comparison between 3-D and 2-D Analysis

It has been common in the past for offshore mooring terminals such as the SBS system to be analysed in two dimensions only and it is assumed that the forces due to wind, current and waves are all colinear, causing the system to weathervane until the longitudinal axis of the vessel is in line with the resultant of these forces. Motions of the vessel are then considered to take place in the vertical plane only (i.e. surge, heave and pitch). Examples of this type of approach can be found in references (10) and (11). The effect of this approximation is examined here by considering the response of a SBS system to a head sea. Two cases are considered - first the sea-state is taken to be unidirectional and secondly a cosine squared spreading function (ref.87) is used. In the latter case, five angular components are used to evaluate the numerical integrations involved in equations of the type 8.36, the validity of which is shown in the next section. In both cases a current of 1 m/s is used in-line with the principal direction of wave propagation and a JONSWAP wave spectrum with H_s = 15m. The vessel considered is a 130,000 DWT VLCC at full draft, details of which are given in Figure 9.1. Details of the yoke, buoy and mooring system are given in Figure 9.3.

The comparison is made in the top two entries of Figure 9.27, the key to which is given in Figure 9.26. As would be expected the two dimensional approach predicts no out of plane motions, and thus the vessel motions of yaw, sway and roll, together with the tanker reaction P2 and the buoy reactions R2 and M1 are zero. The three dimensional seastate, however, produces considerable out of plane

motions, which lead to increases of 75% and 70% in the horizontal and vertical reactions at the tanker. Also, the reactions which were previously zero assume fairly large values - for example P2 has an r.m.s. value of 103.4 tonnes.

It can be seen from these results that the 2-D approximation can lead to a considerable underestimation of the forces which are likely to occur within the system - errors as large as 75% being possible when the true seastate has a cosine squared spreading function. Thus a two dimensional approach should be used with care - and unless it can be shown that the location at which the terminal is to be situated actually experiences unidirectional seas, either a three dimensional analysis or large factors of safety should be used.

9.4.2 Effect of the Spreading Function

The use of a spreading function in the description of the incident seastate greatly increases the amount of computer time needed to solve an offshore dynamics problem. This is because transfer functions for the items of interest must not only be calculated for each frequency but for each possible combination of frequency and angle of incidence. It is useful therefore to examine whether the use of a spreading function is always necessary. For example, in a problem which is already three dimensional due to non-colinear waves and current, the assumption of a unidirectional sea-state may yield sufficiently accurate results. It is also useful to determine the least number of angular components which are required to perform integrals of the type 8.36 accurately, since computer time increases with the number of components considered.

The second and third entries in Figure 9.27 show results for the system described in the previous section and correspond to the use of five and ten angular components respectively. It can be seen that the differences between these two sets of results are very small, which would imply that sufficient accuracy can be obtained by using five angular components only. It was also found that the use of fewer components than this causes a significant reduction in the response in the horizontal plane. Thus five angular components were used for all the cases below in which a directional sea is considered.

Figure 9.28 concerns a SBS system in which the wind, current and mean drift forces have combined to align the vessel at 15^{o} to the

direction of the incident waves. It can be seen from this Figure that the use of a spreading function causes a large increase in the out of plane response - sway, roll and yaw increase by 192%, 400% and 73% respectively. Most of the reactions at the buoy and the tanker are also increased, the most significant being a 278% increase in S1. Figure 9.29 shows results for the case where the vessel is aligned at 45^{o} to the direction of the incident waves. Although this is unlikely to occur in practise with a system which is free to weather-vane, such a case may be possible when more rigid types of moorings are used. The effect of the spreading function is less pronounced than in the 0^{o} or 15^{o} incidence cases, although there is a large (116%) increase in roll. The yaw motion is decreased since those wave components which lie at a high angle of incidence to the vessel produce little yaw. (c.f. for a symmetric vessel in beam seas the yaw is zero). This causes a reduction in many of the reactions.

From these results it can be concluded that the use of a spreading function in the dynamic analysis of offshore mooring terminals causes a significant change in the calculated response, the forces within the system tending to be increased. This is mainly due to the large degree of directional dependence displayed by the response of the moored vessel, it's longitudinal and transverse dimensions differing greatly. For more radially symmetric offshore structures such as the articulated tower (ref.89) or the tension leg platform (ref.90) it is possible that the effect of the spreading function is not so marked, and its use not so important. Results for various sizes of structures are given in ref.(87).

9.4.3. Effect of the Spectral Type

Figure 9.31 shows results for the first order response of a SBS system subjected to a directional head sea with H_s = 15m, and a current of 1 m/s parallel to the vessel. The dimensions of the system are as shown in Figures 9.1 and 9.3, a 130,000 DWT tanker at full draft being considered. Three sets of results are shown, corresponding to the JONSWAP, Pierson-Moskowitz and ISSC formulation of the incident wave spectrum (see ref.91, Appendix A and Figure 9.30).

It can be seen that these three spectra produce fairly consistent results, the maximum discrepancies being in the region of 20%. These discrepancies are to be expected as there is a significant

difference in the distribution of wave energy with frequency as given by the different spectra, and the transfer functions of the system vary considerably with frequency (see Figure 9.11). It should be noted that these results are specific to the system considered and cannot be generalised to other types of offshore structure - for example the response of a structure in which the natural frequency of a very lightly damped mode lies within the frequency range of the incident waves will be highly sensitive to the value of the wave spectrum at this frequency. For the present system it can be noted that the use of a wave spectrum which does not accurately represent the actual environmental conditions at a given location may lead to errors in the first order response which are likely to be around 20%.

Figure 9.32 shows results for the second order response of the above system when subjected to a unidirectional seastate at an angle of incidence of 15^{o} to the bow. The differences in the values of response predicted by the various spectra are greater in this case than for the first order response, the maximum difference being about 30%. This is due to the fact that the spectral form can have a significant effect on the shape of the slow drift force spectrum, as discussed in section 6.5. It is therefore of considerable importance for the theoretical wave spectrum to match the actual environmental conditions as closely as possible in order to avoid large errors in the predicted second order response.

It is known that the wave rider buoys which are used to collect data from which empirical wave spectra are derived, are insensitive to wave periods greater than 20s ($\omega < 0.3$ rad/sec). However, many of the empirical formulations, for example the JONSWAP wave spectrum predict that there will be wave energy between the periods of 20s and 30s ($0.2 < \omega < 0.3$ rad/sec) in severe storm conditions ($H_s > 15$m). In order to assess the contribution of this region of the spectrum to the response of the SBS system the results of two computer runs for an $H_s = 15$m JONSWAP wave spectrum were compared. In the first of these the wave spectrum was assumed to extend from 0.2 to 1.0 rad/sec and 40 frequency components were taken, whereas in the second 35 frequency components were taken between 0.3 and 1.0 rad/sec. Differences of around 5% were found for the first order surge and sway

response of the vessel, the agreement between the remaining first order terms and all the second order terms being much closer. The differences in surge and sway are due to the fact that the low frequency components of the spectrum decay vary gradually with depth and thus produce considerable lateral forces over the draft of the vessel, even though their amplitude may be very small. This point is reflected in the transfer functions of surge and sway (see Figure 9.11) which have high values for low frequencies. This effect would be expected to be more pronounced for a structure such as an articulated tower, where the slow decay of the low frequency portion of the spectrum will lead to large moments about the sea bed pivot. For the present system any errors in the response caused by errors in the measurement of the low frequency end of the spectrum would be expected to be small.

9.4.4 Effect of Approximations concerning Directional Dependence of Reflection Coefficients

As stated in section 6.4.1, Newman (ref.77) has shown that the second order forces acting on a vessel moored in irregular seas can be expressed approximately in terms of the mean forces exerted by regular waves. This approximation has been utilised in the calculation of the slow drift response of the SBS system, which is detailed in section 8.3.3. The mean drift forces are dependent upon both the angle of incidence and the frequency of the regular waves and are usually calculated using source-sink computer programs (for example, see ref.78). As the computing time required to calculate the mean forces exerted by every possible combination of angle of incidence and frequency is very large, approximations are sought which will reduce this computing time. Oppenheim and Wilson (ref.21) have quoted the following approximate formulae for the dependence of the mean forces upon the angle of incidence of the regular waves:-

$$F_1(\omega,\theta) = F_1(\omega,0^o)\cos^3\theta + F_2(\omega,90^o)\sin^2\theta\cos\theta \qquad (9.4)$$

$$F_2(\omega,\theta) = F_1(\omega,0^o)\cos^2\theta\sin\theta + F_2(\omega,90^o)\sin^3\theta \qquad (9.5)$$

$$F_6(\omega,\theta) = F_6(\omega,45^o)\sin2\theta|\sin2\theta| \qquad (9.6)$$

where $F_1(\omega,\theta)$, $F_2(\omega,\theta)$ and $F_6(\omega,\theta)$ are the mean forces exerted in surge, sway and yaw by a wave of frequency ω and incidence θ to the

bow of the vessel. The purpose of the present section is to examine the validity of this approximation with regard to the slow drift response of the SBS system. Results using the above formulae are compared with those obtained using the exact values of $F_i(\omega,\theta)$ which have been given by Faltinsen et al (ref.85) for a fully loaded 130,000 DWT tanker.

Figure 9.33 compares the values of $F_i(\omega,\theta)$ given by the Oppenheim and Wilson approximation (ref.21) with the exact values computed by Faltinsen et al (ref.85), for the case ω = 0.562 rad/sec. It can be seen that although the curves have similar shape, large differences can be found in certain regions. It was found that much greater discrepancies exist at other frequencies, a fact which is displayed in Figures 9.34 and 9.35. These figures show plots of $F_i(\omega,\theta)$ against ω for $\theta = 15^o$ and 45^o respectively. Using the analysis of section 8.3.3 the mean forces were used to predict the second order responses of the SBS system, which are shown in Figure 9.36. As would be expected the large discrepancies in the mean forces lead to large differences in the r.m.s. second order displacements. For example, the Oppenheim and Wilson approximation (ref.21) predicts an r.m.s. sway displacement of 8.9m in a 15^o sea, whereas the Faltinsen et al results (ref.85) lead to an r.m.s. displacement of 66.24m. Similar errors can be found in the yaw response and in the yoke reactions. It should be noted that ref (85) gives no results for the mean forces exerted by waves with frequency less than 0.461 rad/sec. In order to extend the curves shown in Figures 9.34 and 9.35 to low frequency waves, a tangent to the curve at 0.461 rad/sec has been drawn to the frequency axis, or for those cases where this would intersect at a negative frequency a straight line to the origin has been used. This will probably lead to an overestimate of the mean forces occurring at low frequencies and thus the results quoted above are likely to be considerably greater than those obtained in practise. Although the discrepancies between the results obtained by the two methods are reduced in a 45^o incident sea the differences are still large - for example the surge response predicted by the Oppenheim and Wilson approximation (ref.21) is 1.6 times that predicted by the Faltinsen et al (ref.85) results.

Although the Oppenheim and Wilson approximation (ref.21) is attractive in that it requires the mean slow drift forces to be

computed in regular waves of incidence 0^o, 45^o and 90^o only, the above results would indicate that its use is to be avoided if at all possible as it can lead to wildly inaccurate results. It would appear that the second order phenomena which lead to the production of mean forces in regular waves are of too complex a nature for their angular dependence to be described in any simple way, and that ideally source-sink results should be obtained for each angle of incidence under consideration.

9.4.5 Effect of Phase Differences between Slow Drift Forces

As noted in section 8.3.3, in applying the Newman approximation (ref.77) to the slow drift forces acting in irregular seas it has been assumed that each of these forces is in phase with the low frequency component of the square of the wave surface elevation. This section investigates the effect of this assumption on the slow drift response of the SBS system. Figure 9.37 shows results for the second order response in an irregular sea with H_s = 15m and V_c = 1 m/s, both at an angle of incidence of 15^o to the bow. Four cases are considered - those of all the forces being in phase and of each force being 180^o out of phase with the other two forces. It can be seen that for those cases where the yaw and sway forces are out of phase with each other, the yaw and sway responses of the vessel are more than twice those of the other two cases. This is due to the fact that the mode of the slow drift response of the system is such that the vessel tends to rotate about the buoy, i.e. the yaw and sway are out of phase. Thus a greater response is produced when the exciting forces in these degrees of freedom are out of phase. It was found that although the yaw and sway responses are increased, the lateral displacement of the buoy is decreased, which produces a reduction in several of the yoke reactions. The case where the surge force is out of phase is equivalent to the system being subjected to irregular waves at an incidence of -15^o and a steady current at an incidence of 15^o, all the forces being in phase. Any change in the response of the system caused by the change in the phase of the surge force, other than the interchanging of the reactions S1 and P1, will therefore be due to the damping and stiffness terms produced by the current (see section 5.3.1).

It can be concluded that the slow drift response of the system is greatly increased if, contrary to the assumptions which lie behind the Newman approximation (ref.77), the slow drift forces in sway and

yaw are 180° out of phase. As no alternative information is available at the present time, it will be assumed here that the Newman approximation is correct in its prediction of the phases between the slow drift forces, although it is noted that this is an area for further research.

9.4.6 Effect of Viscous Roll Damping

In section 5.2.2.4 it was stated that roll damping is primarily viscous and nonlinear in nature. Difficulty arises in trying to estimate an accurate value for the roll damping coefficient since it tends to be sensitive to the shape of the vessel hull, current velocity and direction. In addition the non-linear nature of the roll damping necessitates the use of a linearisation technique to derive an equivalent linear damping coefficient, since the roll damping depends upon the roll motions of the vessel.

In view of the above difficulties it is unlikely that the roll damping coefficient which is used in the analysis of the previous chapter will be reliable. The purpose of the present section is to examine the effect of uncertainty in the damping coefficient on the first order response of the SBS system. Figure 9.38 shows results for the first order response of the SBS to directional head seas of H_s = 15m and V_c = 1 m/s, parallel to the bow. Results are shown for three values of the non-dimensional damping coefficient β_{VIS} which represents the damping due to viscosity alone, being additional to the damping due to potential effects and the drag forces acting on the buoy. It can be seen that changing the value of β_{VIS} from 0.0 to 0.05 produces a 73% decrease in the roll response of the vessel. The only other significant changes are an 11% decrease in P3 and S3 and a 35% decrease in M1. Increasing the coefficient from 0.05 to 0.1 produces an 18% decrease in roll but has no significant effect on either the reactions at the buoy or at the tanker.

In practise, it is likely that β_{VIS} will lie somewhere between 0.05 and 0.1. It can thus be concluded that inaccuracies in this coefficient may produce significant errors in the roll response of the vessel, but will not significantly effect the reactions at the buoy and the tanker. The results for the roll response of the vessel are therefore to be viewed with caution.

9.4.7 Effect of Coupling between First and Second Order Responses

In Chapter 8, the first and second order responses of the SBS system were shown to be coupled due to the non-linear catenary moorings and the drag forces acting on the buoy. Figures 9.39 and 9.40 illustrate the effect of this coupling on the response of a SBS system with a 130,000 DWT tanker at full draft, moored in the configuration of Figure 9.3. The environmental conditions considered are a H_s = 15m unidirectional seastate and a colinear 1 m/s current, incident at 15^o to the bow of the vessel.

Figure 9.39 shows that the greatest differences between the coupled and uncoupled first order responses occur in the tanker reaction S1 (8.9%) and the buoy moments M1 and M2 (7.5% and 4.2%). These differences are due to the fact that the linearised horizontal stiffness coefficients of the catenary mooring system are greater for the coupled response since the large second order displacements are included in the linearisation. The overall effect of coupling on the first order response is small since the motions tend to be inertia dominated and thus independent of the mooring system (see section 9.5.3) and the drag forces acting on the buoy.

Figure 9.40 indicates that the effect of coupling on the second order motions of the system is greatest in surge, with a decrease of 5.5% from the uncoupled case. This leads to reductions of about 10% in R1, P1 and S1, and a larger reduction of 39% in M2, caused by a combination of the reduction in R1 and the reduced moment due to the catenary coupling term k_{51}. These effects are mainly due to the fact that the r.m.s. relative velocities between the fluid and the buoy are reduced when first order motions are omitted, which leads to a reduction in the magnitude of the linearised damping forces caused by the drag forces acting on the buoy (see section 4.3). The r.m.s. relative velocities in surge and sway are 1.85 m/s and 0.69 m/s in the coupled case and 0.48 m/s and 0.15 m/s in the uncoupled case. These lead to values of the linearised coefficients 'a' (see section 4.3 and Appendix F) of 3.30 and 1.12 for surge and sway in the coupled case and 1.36 and 0.361 for the uncoupled case. The reduction in the buoy damping forces has most effect on surge motions, since the response in sway and yaw is such that the vessel rotates about the buoy with small lateral displacement.

It can be concluded that for the particular system under investigation it is necessary to include coupling between first and second order responses, the effect being greatest for the second order response. For other types of mooring system this coupling may have a more significant effect on second order motions - for example the SALS system (see section 1.4.5) uses a yoke structure which has a 40m long, 10m diameter buoyancy chamber, parallel to the beam of the vessel. In ref.(11) the damping forces acting on this chamber were found to have a considerable effect on the second order surge response and thus the response will be sensitive to the derived linearised damping coefficients.

9.4.8 Effect of the Choice of the Surge Damping Coefficient on Second Order Response

Surge damping acting on the tanker at low frequencies consists of wave potential damping, viscous damping due to current (see section 5.3.1) and additional viscous damping caused by the presence of waves (see section 5.3.2). A realistic estimation of the magnitude of these damping terms is difficult due to the complexity of the mechanisms involved. Thus the calculation of the damping due to current is based on an empirical formulation of the viscous forces acting on a moving VLCC, and wave damping is calculated using experimental results obtained by Wichers and Sluijs (ref.56). The accuracy of the latter is especially suspect in a severe seastate, since the largest wave height considered in the model tests of reference (56) was 6m. Because the slow drift response of the SBS is a resonant phenomena, the assumed value of the surge damping coefficient will be of considerable importance, and its value for an SBS with V_c = 1 m/s and a random seastate of H_s = 15m, incident at 0^o and 15^o to the bow of the vessel respectively, is shown below:-

Linearised damping due to drag forces on buoy	=	1.88×10^5
Potential damping	=	1.16×10^5
Current damping	=	3.28×10^5
Wave damping	=	9.58×10^5
Total damping coefficient	=	1.59×10^6 N/m/s

Clearly the greatest contribution is from wave damping, which is perhaps the most difficult to determine accurately in a random sea-

state. To investigate the effect of inaccuracies occurring in this term, the second order response of the system was calculated using three values for the surge damping coefficient, the results being shown in Figure 9.43. The damping was first considered to be due to the drag forces on the buoy and potential damping only, secondly the current damping was included, and finally the wave damping was also included. The results shown in Figure 9.43 are explained in terms of a simple model of the surge response of the system which is developed below.

Since the damping in surge is small and the second order force is broad banded it is reasonable to approximate the latter by white noise of spectral density S_o say. The mean square response of a linear system to white noise takes the form of the well known result:-

$$\sigma_x^2 = \frac{\pi S_o}{2Bk} \qquad (9.7)$$

where B = damping coefficient and k = stiffness. The surge response of the SBS system is not governed by an equation as simple as (9.7) however, since the catenary moorings and the buoy drag forces are non-linear. The linearised drag force depends on the r.m.s. relative velocity between the fluid and the buoy, which is determined mainly by the first order response. For this reason the non-linear nature of the drag forces will be neglected when considering the second order response. To use spectral analysis, the catenary mooring forces have been linearised by the method given in section 3.5. If the coupling between surge and the other degrees of freedom is neglected, then the linearised stiffness has the form:-

$$k = k_1 + 3k_3\sigma_x^2 \qquad (9.8)$$

where k_1 and k_3 are the linear and cubic coefficients of the true restoring force. Substituting into (9.7) and solving for σ_x^2 leads to:-

$$\sigma_x^2 = \tfrac{1}{2}\{-a + \sqrt{a^2 + 4b}\} \qquad (9.9)$$

where:-

$$a = (k_1/3k_3) \quad ; \quad b = (\pi S_o/6k_3B) \tag{9.10}$$

The accuracy of equation (9.9) is investigated by referring to Figure 9.43. Firstly, the second result in Figure 9.43 is used to calculate S_o, then equation (9.9) is used to predict results corresponding to the first and third entries in the figure. The value of S_o is $1.2 \times 10^{13} N^2$-sec, giving σ_x = 20.46m and 11.69m compared to σ_x=19.16m and 12.46m shown in Figure 9.43. From this it can be concluded that equation (9.9) is probably accurate to within 10%. This equation was used to construct Figure 9.41 which shows the variation in the r.m.s. second order surge displacement with the surge damping coefficient. It can be seen that the response is fairly insensitive when the damping is large, but changes rapidly for values of B below 4×10^5N/m/s ($\beta \simeq 0.5$). The values of the equivalent damping ratio, β, shown in Figure 9.43 are approximate since no account has been taken of the change in the surge natural frequency caused by the changing linearised stiffness. Figure 9.43 also shows the results for a linear system whose stiffness corresponds to the linearised stiffness obtained when $B = 8 \times 10^5$ N/m/s, and shows that the effect of the non-linear mooring lines is to make the response less sensitive to the damping coefficient than in the case of a linear system. The r.m.s. mooring restoring force can be written as:-

$$\sigma_F = k\sigma_x = k_1\sigma_x + 3k_3\sigma_x^3 \tag{9.11}$$

Using the values of σ_x in Figure 9.43 leads to values of $\sigma_F = 2.57 \times 10^6$N, 1.81×10^6N and 9.69×10^5N which agree well with the values of R1 given in this figure. The cubic term in equation (9.11) implies that the r.m.s. restoring force, and thus the r.m.s yoke reactions which are dependent upon this force, will be much more sensitive to the value of the surge damping coefficient than the surge response, a fact which is illustrated in Figure 9.42. Also shown is the r.m.s. restoring force for a linear system which has less dependence upon the damping coefficient.

It can be concluded that since the second order motions of the SBS are resonant, the slow drift surge response and associated yoke reactions are sensitive to the assumed value of the surge

damping coefficient. The effect of the mooring non-linearity is to increase the dependence of the yoke reactions upon this coefficient and to decrease that of the surge displacement. Typically the surge damping coefficient will lie between (1) 4 x 10^5N/m/s and (2) 1.6 x 10^6N/m/s, use of (1) leading to a surge displacement and a yoke reaction R1 which are respectively 54% and 161% larger than those given by (2). It is apparent that the determination of the low frequency surge damping coefficients for VLCC's requires more research - in particular the model tests performed by Wichers and Sluijs (ref.56) on wave damping coefficients need to be extended to cover a wider range of vessels and greater wave heights.

The surge damping coefficient which has been used in this chapter is conservative, the wave damping term having been neglected.

9.5 Investigations of Changes in the Dimensions of the System

9.5.1. Effect of Tanker Size

The effect of the tanker size and draft on the natural frequencies of the SBS has been discussed in section 9.2. This section investigates the effect of these dimensions on first and second order response. Three cases are considered - a 130,000 DWT tanker at full draft and half draft and a 200,000 DWT tanker at full draft, the dimensions of which are shown in Figure 9.1. For both full draft vessels the junction of the yoke structure to the tanker lies at 10m above MWL. This means that any difference in the yoke reactions will be due to the tanker size rather than the mooring configuration. The r.m.s. first order responses are shown in Figure 9.44, the environmental conditions being a current of 1 m/s directed onto the bow of the vessel and a directional head sea of H_s = 15m. Figure 9.45 shows the r.m.s. second order responses for a unidirectional seastate of H_s = 15m directed at 15^o to the bow of the vessel, together with a colinear current of 1 m/s.

It can be seen from Figure 9.44 that apart from roll and buoy pitch, the first order displacements of the system are all less for the 200,000 DWT tanker than for the fully loaded 130,000 DWT tanker, this being due mainly to it's larger inertia. The roll is greater for the larger vessel since the roll natural frequency (0.36rad/sec) lies close to the peak frequency of the incident wave spectrum

(0.364 rad/sec), and the buoy pitch is greater due to the reduction in the heave and pitch motions of the vessel and hence the increase in the relative vertical motions between the yoke connection point and the buoy. The smaller response of the larger vessel leads to an increase in all the reactions and moments other than M1 and R3 which are governed mainly by the roll and buoy pitch. These increases are to be expected as it is a general rule that the less compliant an inertia dominated structure is, the greater the internal loads it must withstand. The lateral degrees of freedom of the system (surge, sway and yaw) have natural frequencies much lower than the frequencies of the first order exciting forces and are therefore inertia dominated. Also Figure 9.44 shows that, with the exception of yaw and buoy pitch, the r.m.s. displacements of the 130,000 DWT tanker are greater for the half draft condition than for the full draft condition. Heave and pitch are larger due to the fact that at half draft the keel of the vessel is closer to the still water level and thus experiences greater dynamic subsurface pressures, as well as the fact that the vessel is lighter. The reduced draft and displacement also account for the increase in surge, sway and roll, the latter increasing despite a shift in the roll natural frequency away from the spectral peak (see section 9.2). The buoy pitch is decreased due to the decrease in the relative vertical motion between the buoy and the tanker pivots. The slight reduction in yaw is due to the different shape of the waterplane areas at half and full draft. At half draft the pivots between the tanker and the yoke are 18m above the M.W.L. and 10m at full draft. This causes an increase in the vertical distance between the reactions R2 and S2 and thus an increase in the yoke rolling moment. This increase is balanced by an increase in the reactions P3 and S3 and the moment M1. Most of the other yoke reactions are reduced due to the increased compliancy of the system, although R1 is increased due to the greater static tilt of the buoy.

Figure 9.45 shows that the slow drift motions of the 130,000 DWT tanker are much greater at full draft than half draft. Since this motion is resonant, the larger response produces greater yoke reactions - with the exception of R3, which is greater at half draft due to the greater static tilt of the buoy. The moments M1 and M2 are less for the full draft case due to the fact that the large

lateral displacements of the buoy produce moments via the catenary coupling terms k_{42} and k_{51} which tend to balance those produced by R1 and R2. The reflection coefficients used in the calculation of the second order response of the 130,000 DWT vessel at both full and half draft were the exact values given by Faltinsen et al (ref.85). For the 200,000 DWT vessel no published information was available and so the Faltinsen et al (ref.85) coefficients for the full draft 130,000 DWT tanker were used, which led to the results shown in Figure 9.45. It can be seen that the predicted displacements and reactions are in general less than those of the smaller vessel. This is probably due to the fact that in using the Faltinsen et al (ref.85) coefficients, no account has been taken of the greater draft and flatter bow configuration of the larger vessel. McLeod and Smulders (ref.2) state that in general the second order response increases with the vessel displacement, which would suggest that the response of the 200,000 DWT vessel would be greater if the exact reflection coefficients were used.

In general an increase in vessel size causes a decrease in first order response and an increase in second order response, with an increase in both the first and second order yoke reactions. In selecting the optimum tanker size for a particular location, several factors should be considered, (1) the slow drift motions of the system must not be so great as to cause damage to the mooring system or riser, (2) the maximum expected yoke reactions and moments must be within the design capacity of the yoke structure, (3) the first order accelerations must not adversely effect the operation of processing equipment, or, in design storm conditions, cause damage to the internal fittings of the tanker. Factors (1) and (2) would suggest the use of a small vessel, whereas the third would would lead to a large vessel. The actual choice of tanker size will depend upon the environmental conditions at the proposed location and the sensitivity of the processing equipment to dynamic system motions.

9.5.2 Effect of the Tanker Loading Condition

It was shown in the previous section that the response and yoke reactions of an SBS are in general greater with the tanker at half draft than when fully loaded. The half draft condition corresponds to the ballasting when the vessel has offloaded oil to a shuttle tanker.

This section investigates three ballast configurations for a 130,000 DWT tanker at half draft - where the centre of gravity,G, of the tanker is 60m fore of midships, midships and 60m aft of midships (see Figure 9.1 for details). The first and second order responses are shown in Figures 9.46 and 9.47, the conditions being the same as in the previous section.

Figure 9.46 shows the first order pivot reactions increase considerably with the distance of the centre of gravity from the bow of the vessel. This is due to the fact that the vessel will tend to yaw and pitch about G and thus the further forward the location of G the less will be the motions of the bow produced by these rotations. Since yaw and sway are out of phase (see Figure 9.11) the reduced yaw motion at the bow means that the buoy will follow the sway motion of the fluid more closely and thus will impose less sway forces on the yoke. This causes a reduction in R2 and a corresponding reduction in M1 and all the reactions at the tanker. These reductions occur in spite of a slight increase in the magntidues of the vessel yaw and sway motions. Moving G 60m forward of midships causes a 22%, 9% and 20% decrease in the vertical, longitudinal and transverse reactions at the tanker, respectively, together with a 9% decrease in the transverse reaction at the buoy.

Figure 9.47 shows that the location of G has much less effect on the second order response than the first order response, because the second order response is resonant rather than inertia dominated and thus less dependent on the form of the mass of the tanker.

From the above results it can be concluded that the first order yoke reactions and moments can be considerably reduced by ballasting the tanker so that G lies forward of midships. Such ballasting would be advisable in practise wherever possible.

9.5.3 Effect of the Mooring Configuration

To investigate the effect of the mooring configuration on the dynamic response, the three mooring configurations shown in Figures 9.2, 9.3 and 9.4 were considered. Each one uses six catenary anchor legs of 147mm (6") diameter stud link chain, which has a weight in air of 4797 N/m and in seawater of 4150 N/m. The configurations were arrived at using the design method of section 3.3, which requires that the water depth, d, the length of each anchor chain, the maximum

static horizontal force on the system and the maximum horizontal static excursion be specified. The length of each chain was taken as 4d and the maximum allowable horizontal static excursion was taken as 0.2, 0.3 and 0.4 times d for the three configurations. Rather than selecting the maximum static horizontal force on the system the chain weight described above was specified. It was then found that the three configurations could resist horizontal forces of 335, 312 and 286 tonnes respectively at the maximum excursion. The design condition for the maximum horizontal force was taken to be colinear wind and current with velocities of 45 m/s and and 1.6 m/s respectively (North Sea conditions). Considering a 130,000 DWT tanker at full draft it was found from ref.(68) that this produces a static force of 190 tonnes. Allowing an extra 80 tonnes say for the mean drift forces brings the total to 270 tonnes, which is within the capacity of each mooring configuration. The horizontal 'stiffness' properties of each configuration were represented by linear and cubic 'stiffness' terms as discussed in section 3.2.3.

Figure 9.49 shows the first order response of the system, the environmental conditions considered being a directional head sea of H_s = 15m and V_c = 1 m/s directed at the bow. It is seen that the mooring configuration has little effect on the first order response for surge, sway and yaw because the motions are inertia dominated and almost independent of stiffness. The tanker heave and pitch motions are virtually uncoupled from the mooring system and thus independent of the mooring configuration, while the heave restoring forces on the buoy due to buoyancy (252 tonnes/m) is much greater than that due to even the stiffest mooring system (8.9 tonnes/m). This means that buoy pitch (which involves the rotation of the yoke about the tanker hinges) is almost unaffected by the mooring lines. The roll motion increases slightly with the stiffness of the mooring due to the fact that the roll natural frequency moves towards the peak frequency of the wave spectrum (see section 9.2). This in turn, causes a slight increase in R2 and M1.

Figure 9.50 shows the second order response for a unidirectional seastate of H_s = 15m and V_c = 1 m/s, both directed at 15^o to the bow of the vessel. Figure 9.48 gives values for the linearised horizontal stiffness of the mooring systems, the linearisation method used being

given in section 3.5. It can be seen that these stiffnesses are in the ratio 2.69:1.55:1. From Figure 9.48 it can be shown that the inverse square of the surge responses are in the ratio 3.04:1.58:1. These results are in accord with the fact that the slow drift response is resonant, being proportional to the inverse of the natural frequency and thus inversely proportional to the square root of the stiffness. The effect of the mooring configuration on sway and yaw response is much less due to the fact that the vessel tends to respond in these degrees of freedom so that the tanker rotates around the buoy, thus causing the lateral displacements of the buoy to be small. It can be seen that all the tanker reactions, together with the buoy reactions and moments, increase with the stiffness properties of the mooring.

It can be concluded that the mooring configuration has considerable effect on the second order response. This effect is greatest in surge, the r.m.s. displacement being inversely proportional to $\sqrt{k_x}$ the horizontal stiffness of the moorings. Increasing the mooring stiffness also increases the second order yoke reactions and moments. It was shown in section 9.4 that the second order response increases with vessel size. The present section shows that the second order buoy lateral displacements can be kept within required limits if the stiffness of the mooring system is increased with the vessel size. This, however, can only be achieved up to a certain point, beyond which the mooring system needed to provide the required stiffness properties may be impractical or lead to failure of the mooring lines or anchor pulling.

9.5.4 Comparison with First Order Response of Unrestrained Tanker

Chapter 6 showed that the mean second order forces acting on a body in regular waves are dependent on the first order motions of the body. These forces, when non-dimensionalised, are called the 'Reflection Coefficients' and, with the Newman approximation (ref.77), they are used to calculate the slowly varying forces in irregular waves. In the present work, the reflection coefficients given by Faltinsen et al (ref.85) for an unrestrained 130,000 DWT tanker have been used to calculate the second order response of a SBS, no account being taken of the fact that the mooring system may effect the first order response of the vessel and hence it's reflection coefficients.

The purpose of the present section is to examine the effect of the mooring system on the first order vessel response, to decide if the use of reflection coefficients which refer to an unrestrained vessel is valid.

Figure 9.51 compares the first order response of an unrestrained 130,000 DWT fully loaded tanker with that of the same vessel moored via the configuration shown in Figure 9.3. In order to make the result as general as possible, a spreading sea of H_s = 15m is used, the principle direction of propagation being directed onto the bow of the vessel. The greatest differences in the response occur in roll, surge and yaw, and are 3.8%, 2.3% and 2% respectively, the differences in the remaining three degrees of freedom all being less than 1%. The accuracy of the computed roll response is subject to the limitations stated in section 9.4, which makes the accuracy of the above result for the difference in roll questionable. Since the mooring system does not significantly effect the first order response, the use of reflection coefficients which refer to an unrestrained vessel appears to be valid. This may not be the case for mooring systems which moor the vessel more rigidly than the present system - for example it might be expected that the vertical wave forces acting on the large buoyancy chamber of the SALS system (see section 1.4.5) could cause a significant change in the heave and pitch response of the vessel, necessitating the use of a diffraction program (for example, ref.78) to calculate the reflection coefficients of the system as a whole. Such a program would need to incorporate non-linear drag forces on the buoyancy chamber, which would have to be linearised.

9.6 Investigations of Changes in Environmental Conditions

9.6.1 Effect of Significant Wave Height, H_s

Figures 9.55 to 9.69 plot the effect of H_s on the response and yoke reactions of a SBS system with a 130,000 DWT tanker at full draft moored as shown in Figure 9.3. A unidirectional single parameter JONSWAP wave spectrum was used (see Appendix A), the relationship between the H_s and the frequency of the spectral peak being, $\omega_p = 1.416 H_s^{-\frac{1}{2}}$, i.e. as H_s increases the energy in the seastate occurs at lower frequencies, as shown in Figure 9.55. The seastate

was taken to be colinear with a current of 1 m/s incident at an angle of 15^{o} and the first and second order responses were found by the analysis of chapter 8.

Figure 9.56 shows plots of the r.m.s. first order translational displacements against H_s. It can be seen that the increase in these displacements with H_s is greater than would be predicted by a linear relationship, i.e. the slopes of the curves increases with H_s rather than remain constant. This is due to the fact that the transfer functions of surge, sway and heave are largest for low frequency waves (see Figure 9.11), and thus an increase in H_s increases the displacements not only because of the increased wave height, but also because of the lower frequency of the energy in the wave spectrum. The increase in the heave displacement curve at about H_s = 6m corresponds to the region where the frequency of the spectral peak is close to the frequency of the peak in the heave transfer function which occurs at ω = 0.6 rad/sec. For H_s = 15m, the assumption that the maximum expected value is five times the r.m.s. value (see Chapter 2) leads to maximum first order surge, sway and heave displacements of 9.5m, 2.65m and 8.98m respectively. Figure 9.57 plots the r.m.s. first order translational accelerations of the system against H_s. The slopes of these curves are not as great as those of the displacement curves due to the fact that although the amplitude of response increases with H_s, the frequency of vibration decreases, thus limiting the magnitude of the accelerations. It can be seen that the rise in the heave displacement curve at H_s = 6m produces a corresponding rise in the heave acceleration curve. The maximum translational accelerations of the system occur at H_s = 16m and taking five times the r.m.s. yields 1.13, 0.33 and 1.25 m/s/s for surge, sway and heave respectively.

Figure 9.58 shows the r.m.s. first order rotational displacements against H_s. The fact that the roll displacement increases very gradually with H_s can be explained by considering the roll transfer function (see Figure 9.11). At the angle of incidence of 15^{o} considered, the roll transfer function has large values only for $\omega > 0.9$ rad/sec. Increasing H_s has the effect of moving the energy in the wave spectrum away from these frequencies, which will tend to reduce the increase in the roll response caused by the greater energy

in the wave spectrum. The increase in the yaw and pitch responses with H_S are similar to those which occur in sway and heave. Note that the pitch curve has a decreasing slope for values of H_S greater than 10m due to the fact that beyond this point the peak in the incident wave spectrum moves away from the largest peak in the pitch transfer function (see Figure 9.11.5). This is also the case for the buoy pitch response (see Figure 9.11.6). The maximum expected rotational responses can be estimated by taking five times the r.m.s. values at H_S = 16m, which yields 1.45°, 9.73°, 2.48° and 33.95° respectively for the roll, pitch and yaw of the tanker and the pitch of the buoy. The low values of roll and yaw are due to the incident seastate being at 15° to the bow of the vessel and is close to a head sea. The maximum roll predicted by a multidirectional sea, rather than a unidirectional sea, at the same angle of incidence is 6.3° (see Figure 9.28). The accuracy of the predicted roll response is subject to the limitations given in section 9.4.6. It was found that the pitching of the buoy (which involves the rotation of the yoke about the tanker hinges) leads to a maximum buoy heave displacement of around 15m, which implies that the buoy is almost surface following. McLeod and Smulders (ref.2) state that tanker mounted processing equipment used in the Garoupa Field in S.E.Asia is designed to be operational for roll and pitch responses of up to 11° and 3° respectively. This equipment was installed in a 54,000 DWT tanker moored by a yoke-tower arrangement (see section 1.4.4) in 1979. If used in the present SBS system, this equipment would be rendered inoperable due to pitch response for seastates with H_S > 8m. This arrangement would however be acceptable for S.E.Asia, where the 100-year storm condition corresponds to a H_S = 6m, but it's use would not be feasible for the North Sea where an H_S > 15m is possible. To allow a greater severity of seastate, either more effective processing equipment could be installed, or the pitch response could be reduced by using a larger tanker (see section 9.5.1). The yoke-tower system installed in the North Sea Fulmar Field in 1980 moors a 210,000 DWT tanker but the details of it's processing equipment are not readily available.

Figure 9.59 plots the r.m.s. first order rotational accelerations of the system against H_S. It can be seen that the maximum accelerations occur when H_S = 16m, although the roll acceleration has a secondary peak

at H_s = 10m. The largest of the maximum expected values of the tanker rotational accelerations is that in pitch, which is 0.0256 rad/s/s. This would lead to a vertical acceleration of 2.9 m/s/s at the bow of the vessel, which is about twice that due to heave. The maximum expected rotational acceleration for the buoy pitch is 0.122 rad/s/s, and it was found that the maximum expected vertical acceleration of the buoy is around 2 m/s/s.

Figure 9.60 gives the r.m.s. first order horizontal plane reactions at the tanker against H_s. It can be seen that the longitudinal reaction P1, which lies on the side of the vessel which faces the incident waves, is much greater than the longitudinal reaction S1. This can be explained as follows - a positive surge motion of the vessel causes reactions P1 and S1 which are equal in magnitude and are both negative. A positive sway motion causes reactions P1 and S1 which are equal in magnitude and opposite in sign, P1 being positive. Referring to the surge and sway transfer functions (Figures 9.11.1 and 9.11.2) shows that these motions tend to be 180° out of phase. This causes the surge and sway effects to add for the reaction P1 and to subtract for the reaction S1, causing P1 to be the greater. The maximum expected values of P1, S1 and P2 at H_s = 16m are 889 tonnes, 200 tonnes and 301 tonnes respectively. Note that the magnitude of P2 is considerable despite the low values of response in yaw and sway.

Figure 9.61 gives the r.m.s. first order vertical reactions P3 and S3 against H_s. Sway, pitch, heave, yaw and roll effects combine to make P3 slightly greater than S3. There is a slight rise in the two curves near H_s = 6m, which corresponds to that in the heave displacement curve (see Figure 9.56). The maximum expected values of S3 and P3 are 82 tonnes and 86 tonnes respectively.

Figure 9.62 gives the r.m.s. first order buoy reactions against H_s, the maximum values of which occur when H_s = 16m and using 5σ yields 949, 258 and 161 tonnes for R1, R2 and R3.

Figure 9.63 shows the moments M1 and M2 which must be carried by the link which connects the yoke to the buoy, the maximum expected values being 1039 tonne-m and 3197 tonne-m.

Figures 9.64 and 9.65 plot the linearised horizontal plane stiffnesses of the catenary moorings against H_s. For the particular

system considered it can be seen that although the off-diagonal terms k_{xy} and k_{yx} increase rapidly with H_s they are always much smaller than the diagonal terms k_{xx} and k_{yy}. This was also found to be the case for the mooring configurations shown in Figures 9.2 and 9.4 which suggests that these terms can be neglected thus simplifying the linearisation method of section 3.5. In section 3.2.3. the horizontal mooring restoring force was taken as a cubic in displacement x such that:-

$$F = k_1 x + k_3 x^3 \qquad (9.12)$$

Using a ratio $k_1/k_3 = 407$, it was found that at H_s = 16m the linearised diagonal stiffness terms k_{xx} and k_{yy} were 218% and 85% greater than k_1. This increase would be expected to be greater for more non-linear mooring systems in which this ratio is less - for example increases of 546% and 227% were found for the system shown in Figure 9.2, where $k_1/k_3 = 258$.

In regular waves the mean drift forces are proportional to H^2 which suggests that in a random sea the r.m.s. second order motions will be proportional to H_s^2. However Figure 9.66 shows that this is not the case, the increase in the response with H_s being much less than expected. This is due to two factors - (1) the equivalent stiffness of the non-linear moorings increases with H_s, which following the results of section 9.5.3 will tend to limit the response, (2) the higher seastates tend to contain waves of a lower frequency for which the reflection coefficients (Figure 9.34) have lower values. The maximum r.m.s. responses occur at H_s = 16m and are 16.94m and 8.97m for surge and sway and 3.3° for yaw. As stated in section 6.4.3, it is difficult to accurately predict the maximum expected displacements from the r.m.s. values, due to the complex statistical nature of the slow drift response. The slow drift motions tend to occur at the natural frequencies of the systems horizontal motions which are 0.02638, 0.04012 and 0.004092 rad/sec, and suggest that in a 12hr storm there will be 280 or less cycles of slow drift response. Were this response Gaussian and narrow banded, then the results of Longuet-Higgins (see ref.28 and section 2.2.2) for the modal value of the maximum would predict a value of 3.35σ. As it was shown in section 6.4.3.7. that this is likely to be an underestimate, a value of 4σ will be used. This leads to maximum second order displacements of 67.76m and 35.88m

in surge and sway and 12^{o} in yaw. Although these displacements at first sight appear to be large, they are not much greater than the beam of the vessel (47.2m).

Figure 9.67 plots the r.m.s. second order tanker reactions S1, P1 and P2 against H_s. Maximum values occur at H_s = 16m and taking 4σ yields 486, 352 and 106 tonnes, which are comparable to the first order reactions. Figure 9.68 shows the r.m.s. second order reactions at the buoy, the maximum expected values being 778 and 108 tonnes for R1 and R2, which again are comparable to the first order values.

Figure 9.69 gives the r.m.s. second order buoy moments against H_s. The maximum value of M2, using 4σ, is 776.4 tonne-m at H_s = 6m. The reason for the maximum occurring at this H_s rather than at H_s=16m, is that an increase in the surge response effects M2 in two ways. Firstly a larger moment is produced by the k_{51} catenary stiffness coupling term, and secondly the moment due to R1 increases. These two effects are opposite in sign and they do not combine to produce the largest value of M2 at the largest value of H_s. Similarly the maximum value of M1 occurs at H_s = 14m and is 302.32 tonne-m.

If it is assumed that the first and second order motions and reactions are statistically independent then the total r.m.s. values of these items can be found from:-

$$\sigma_T^2 = \sigma_F^2 + \sigma_S^2 \qquad (9.13)$$

where σ_T = total r.m.s. motion or reaction.
σ_F = first order r.m.s. motion or reaction
σ_S = second order r.m.s. motion or reaction.

The maximum expected values of all items at H_s = 16m, being taken as five times the total r.m.s. values, are shown in Figure 9.70.

It can be shown from elementary beam theory that the minimum radius, r, of a solid steel rod which will support a bending moment M without yielding is:-

$$r = \left[\frac{4M}{\pi\sigma} \right]^{\frac{1}{3}} \qquad (9.14)$$

where σ is the yield stress of the steel. From Figure 9.70 it can be seen that if M1 and M2 both achieve their maximum expected values at the same time then the maximum resultant bending moment at the buoy will be 3412 tonne-m. If σ = 355 N/mm^2 then equation (9.14) implies

that a solid steel rod of radius 0.496m is required to support this moment. Such a rod would weigh about 6 tonnes/m and could easily support R1 and R2 in shear and R3 in compression. These calculations indicate that it would be possible to design a link between the yoke and the buoy whose dimensions are compatible with those of the rest of the system and which is capable of withstanding the applied dynamic loads. In practice the link will be a hollow tubular structure through which all transfer pipes will run. Details of the structural design of the SBS system which have been installed to date have not been found in the published literature. Were P1, P3, S1 and S3 to achieve their maximum values simultaneously then the resultant reactions acting on the tanker hinges would be 995 tonnes on the port side and 645 tonnes on the starboard side. A solid steel rod of radius 10cm is required to support the port reaction in shear, which indicates that it would be possible to design hinges compatible in size with the rest of the structure and which are capable of withstanding the applied dynamic loads.

9.6.2 Effect of Current

As stated in section 9.1 no detailed static analysis of the system has been performed in this chapter, and thus the effect of the current on the static equilibrium position has not been studied. In practice this equilibrium position is due to a combination of current, wind and mean drift forces. In section 5.3.1 it was shown that the current forces produce damping and stiffness terms, which have been included in the present dynamic analysis. Similar terms, although of smaller magnitude, will be produced by the wind forces and the mean drift forces will produce additional stiffness terms. In fact, the restoring forces due to wind, current and mean drift are the only stiffness terms which exist in the mode of response where the tanker rotates about the buoy (weathervanes). Without these terms the equation of slow drift motion of this mode would have the form:-

$$M_G\ddot{\phi} + B_G\dot{\phi} = F_s \qquad (9.15)$$

where M_G and B_G are the generalised mass and damping , ϕ is the modal response amplitude and F_s is the generalised slow drift force in this mode. Solution in the frequency domain would then yield a transfer function for ϕ in the form:-

$$H_{\phi}(i\omega_k) = \left[-\omega_k^2 M_G + i\omega_k B_G\right]^{-1} \tag{9.16}$$

Approximating the generalised slow drift force to white noise of spectral density S_o gives the mean squared response as:-

$$\sigma_{\phi}^2 = \int_0^{\infty} S_o \left| H(i\omega_k) \right|^2 d\omega_k \tag{9.17}$$

which, in theory, is infinite. The stiffness terms caused by current, wind and mean drift forces therefore have a crucial effect on the slow drift response in this mode. In all of the results presented in this chapter, the stiffness terms due to current have been included, but those due to the mean drift force have been neglected. These terms can be calculated by firstly considering the mean drift moment acting in this mode, which will be:-

$$\bar{F} = \bar{F}_6 - \ell \bar{F}_2 \tag{9.18}$$

where $\bar{F}_2$ and $\bar{F}_6$ are the mean drift force and moment acting on the vessel in sway and yaw, and ℓ is the horizontal distance between the centres of gravity of the tanker and the buoy. $\bar{F}_2$ and $\bar{F}_6$ can be calculated in terms of the reflection coefficients $F_2(\omega,\theta)$ and $F_6(\omega,\theta)$ of section 8.3.3. as:-

$$\bar{F}_2 = \int_0^{\infty} F_2(\omega,\theta) S_{\eta}(\omega) d\omega \; ; \; \bar{F}_6 = \int_0^{\infty} F_6(\omega,\theta) S_{\eta}(\omega) d\omega \tag{9.19}$$

where θ is the incidence of the waves to the static equilibrium position of the vessel. The stiffness in this mode can be written as:-

$$k = -\frac{\partial}{\partial\theta}\left\{ \int_0^{\infty} F_6(\omega,\theta) S_{\eta}(\omega) d\omega - \ell \int_0^{\infty} F_2(\omega,\theta) S_{\eta}(\omega) d\omega \right\} \tag{9.20}$$

In general this expression will have to be evaluated numerically. If the Oppenheim and Wilson approximation is applied to $F_i(\omega,\theta)$ (see ref.21, and section 9.4.4) then the following result is obtained:-

$$k = \ell \bar{F}_1' (\cos^3\theta - 2\cos\theta\sin^2\theta) + \ell \bar{F}_2' (3\sin^2\theta\cos\theta) - \bar{F}_6' (4\sin 2\theta \cos 2\theta) \tag{9.21}$$

where $\bar{F}_1'$, $\bar{F}_2'$ and $\bar{F}_6'$ are the mean drift forces in surge, sway and yaw evaluated for $\theta = 0^o$, 90^o and 45^o respectively, which can be found from the results given in reference (88) (see equation(9.1) and Figures 9.5 and 9.6). Applying the above formula to a SBS system with a fully loaded 130,000 DWT tanker yields $k = 2.88 \times 10^7$N-m/rad when a seastate with H_s = 15m is incident at 15^o to the bow of the vessel. The stiffness in this mode due to a 1 m/s current at the same angle of incidence can be found from the analysis of section 5.3.1 to be 1.43×10^8N-m/rad. For a 1 m/s current incident on to the bow of the vessel this value becomes 6.47×10^7N-m/rad. The fact that the stiffness terms due to the mean drift forces have been neglected in this chapter would therefore not be expected to lead to large errors in the results,as the greater stiffness terms due to current have been included. When zero current is to be considered, however, as is the case in the present section, it is vital that the mean drift stiffness terms are included, in order to avoid the theoretical result of an infinite slow drift response.

Figures 9.52 and 9.53 compare the first and second order response of a SBS system with and without the presence of current. The incident seastate is considered to be unidirectional with H_s = 15m, incident at 15^o to the bow of the vessel on the starboard side. The current, when included, is taken to be of velocity 1 m/s, incident at 15^o to the bow of the vessel on the port side. The stiffness terms due to the mean drift forces are included in both cases.

From Figure 9.53 it can be seen that without the damping and stiffness terms which are provided by the current, the slow drift response is increased by factors of 15%, 287% and 246% in surge, sway and yaw respectively. Also it is found that the r.m.s. second order sway displacement of the buoy increases from 4.6m to 6m. The linearised damping coefficients which arise from the non-linear drag forces acting on the buoy depend upon and increase with both the r.m.s, relative fluid velocity past the buoy and the current velocity (see section 4.3 and Appendix C). The surge damping coefficients are 10% larger when the current is present, although the sway damping coefficients remain approximately constant, the increase in the current velocity being balanced by a decrease in the r.m.s. second order sway velocity of the buoy. The increases in the second order surge and sway responses of

the buoy in the absence of current produce increases in the second order yoke reactions which are proportionally larger due to the non-linear nature of the catenary mooring lines.

The damping and stiffness terms due to current act in those degrees of freedom of the tanker whose first order motions are all inertia dominated, and thus have little effect upon the first order response of the system, as can be seen from Figure 9.52. The first order yoke reactions tend to be slightly greater when current is present due to a combination of the increased linearised drag forces acting on the buoy and the decreased linearised stiffness coefficients caused by the smaller second order motions.

It can be concluded that although current has little effect on the first order response of the system it can be a major factor in determining the second order response. The current velocity used here (1 m/s) is considered to be typical of North Sea conditions - for example in the Thistle Field a current velocity of 0.76 m/s is estimated to be exceeded less than 1% of the time and the current velocity with a 100 year period is 1.31 m/s. In section 5.3.1 it was shown that the damping terms due to current are directly proportional to the current velocity, whereas the stiffness terms are proportional to the current velocity squared. This would suggest that the second order response will not only be sensitive to the presence of current, but also to its magnitude.

9.6.3 Effect of Angle of Incidence of Seastate on Second Order Response

In all the results concerning the second order response of the SBS system in this chapter, the seastate has been considered to be incident at 15^{o} to the bow of the vessel. Results for other angles of incidence (with H_s = 15m) are shown in Figure 9.54, the vessel being a 130,000 DWT tanker at full draft and a 1 m/s current incident onto the bow of the vessel being included. In determining the reflection coefficients for use in the slow drift force calculation, the Oppenheim and Wilson approximation (ref.21) has been used. This means that the numerical accuracy of the results shown in Figure 9.54 is subject to the limitations noted in section 9.4.4, although the general trends shown in this figure are thought to be reliable.

Thus the surge response of the system is not much effected by a change in the angle of incidence from 5^{o} to 20^{o}, the reduction in the

r.m.s. response being only in the region of 3%. This leads to similar reductions in the reactions R1 and R3 and the buoy moment M2. The sway and yaw response, however, undergo significant increases of 139% and 143% as the angle of incidence changes from 5^{o} to 20^{o}. The percentage increases induced in the yoke reactions R2, M1 and P2 are greater than this, since these tend to depend on the r.m.s. lateral displacements of the buoy and the linearised catenary stiffnesses. The r.m.s. lateral buoy displacement increases from 1m to 6.2m whilst the k_{yy} stiffness term increases from 6.2 tonnes/m to 7.1 tonnes/m, effects which combine to produce increases of as much as 670% in some of the yoke reactions.

It can be concluded that the second order surge response of the system is not sensitive to the angle of incidence of the seastate, whereas the sway and yaw responses, together with their associated reactions, are highly sensitive. This implies that in determining the design loads in a SBS system, it is crucial that the static offset position be accurately determined, or at least that the angle of incidence of the seastate is not underestimated.

10. CONCLUSIONS AND RECOMMENDATIONS

Various aspects of the dynamic analysis of offshore mooring terminals have been considered in turn, and then applied to a Single Buoy Storage (SBS) system. The results fall into four categories which concern (1) the various methods of analysis, (2) the unstable motions of the system, (3) the first order response, and (4) the second order forces and responses. The general conclusions which can be drawn from this work, together with recommendations for further work are listed below.

10.1 Methods of Analysis

(a) The Equivalent Linearisation Method, Time Domain Analysis and Caughey's Equivalent Non-Linear Differential Equation Method all yield similar results for the r.m.s.displacement and velocity of a non-linear single degree of freedom system of the type discussed in section 2.4, when the excitation is Gaussian white noise. The application of the Caughey Method to more general systems is limited, as it is derived from the Fokker-Planck equation, whose solution demands that the excitation be of this type. This is not true of the Equivalent Linearisation Method, which is applicable to multi-degree of freedom non-linear systems subjected to any type of excitation, although the statistics of the response must be assumed when calculating the linearised coefficients. In view of the results of section 2.4.5 it is thought that this method will yield reliable r.m.s. values when applied to the dynamic analysis of offshore mooring terminals. Maximum values can then be determined by assuming a Gaussian response. For those cases where the response is likely to be highly non-Gaussian, time domain analysis should be used.

(b) A two dimensional analysis of a yoke model vessel can lead to a severe under-estimation of the yoke reactions for those cases where the environmental conditions do not consist of a unidirectional head sea with colinear wind and current and thus a three dimensional model should be used.

(c) The use of a spreading function in the definition of the incident seastate can lead to substantial increases in the first order yoke reactions of a SBS system, even in those cases where the problem is

already three dimensional due to oblique seas. This is due to the high degree of directional dependence displayed by the response of the moored tanker, and the effect is likely to be less marked for more radially symmetric offshore structures.

(d) Coupling the first and second order responses of a SBS system via the non-linear mooring and drag forces has a significant effect on the second order response, which is greater in the uncoupled case due to a decrease in the linearised buoy damping coefficients.

10.2 Unstable Motions of the SBS System

(a) The SBS system is found to be dynamically stable in all combinations of wind and current which are likely to occur in practice. The vessel does not undergo the 'fishtailing' motions as for a tanker moored by a bow hawser since the freedom afforded by the hawser is not present, and the mooring buoy provides additional damping.

(b) Unstable motions can be induced when the bearing between the wind and current is in the region of 50^{o}-90^{o}, which is unrealistically high. These motions differ from 'fishtailing' in that the vessel undergoes surge and sway only. This effect is due to the complicated lift forces which act on a vessel at high angles of incidence.

10.3 First Order SBS Response

(a) The first order motions of the system tend to decrease as the vessel size increases. This decrease in the response is accompanied by an increase in the yoke pivot reactions, which is to be expected as it is a general rule that the less compliant a system, the greater the internal loads it must withstand.

(b) The first order yoke reactions can be reduced by ballasting the vessel such that the C.G. is moved towards the yoke pivots, as the vessel tends to rotate about this point. The same effect can be obtained by attaching the yoke to the stern of the vessel, as in many cases the tanker C.G. lies aft of midships.

(c) The attachment of the yoke to the tanker has little effect on it's r.m.s. first order motions, and thus it is thought that the 'reflection coefficients' of an unrestrained tanker are applicable to a yoke moored vessel.

10.4 Second Order Force and Response

(a) It was shown in section 6.5 that the spectrum of the second order force is sensitive to the value of the reflection coefficient at the peak frequency of the wave spectrum. As reflection coefficients tend to vary considerably with frequency, this means that the force spectrum for a given system will be sensitive to the wave spectrum selected. The wave spectrum for a given location should therefore be determined as accurately as possible.

(b) The statistics of the slow drift force are far from Gaussian - the approximate analysis of section 6.4 showed that for 3000 force maxima the greatest and least values which might be expected are 9.8 and -1 times the r.m.s. value respectively, which compare with values of ±4 for a Gaussian force. The fact that the system is lightly damped leads to a response which although statistically complex is nearly Gaussian.

(c) The mode of the second order response in sway and yaw tends to be such that the vessel rotates about the buoy. The magnitude of this response is highly sensitive to the stiffness terms which are provided by the current and mean drift forces, and thus an accurate determination of these terms is essential. This response is also found to be sensitive to the angle of incidence of the seastate to the bow of the vessel.

(d) The second order surge response is sensitive to the value of the surge damping coefficient. As this coefficient is very difficult to determine accurately, results for surge motion should be viewed with caution.

(e) Results obtained using approximate formulae for the angular dependence of the reflection coefficients differ widely from those

obtained using the 'correct' coefficients. It is therefore advisable that the use of these approximate formulae is avoided wherever possible.

(f) The second order response increases with the displacement of the vessel, but is not as sensitive to the C.G. position as is the first order response.

(g) An increase in the stiffness of the mooring system leads to a reduction in the second order motions and an increase in the second order pivot reactions.

(h) In view of the many uncertainties which are present in the calculation of the second order response, it is not thought that this response can, as yet, be predicted with confidence. Care should be taken that the complexity of the mathematical models which are currently available does not lead to over confidence, as even the best of these models are based on rather sweeping assumptions. For example, diffraction programs currently in use assume potential flow and linear wave theory and neglect such effects as current interaction, breaking waves and viscous drag.

10.5 Recommendations for Further Work

(a) There is a need for a further investigation of the statistics of the slow drift force and response, as at the present time it is not possible to estimate the maximum expected response from the r.m.s. values. This work would probably need to be done in the time domain, the probability density functions of force and response being calculated numerically.

(b) The effect of the directionality of the incident seastate on the second order response has yet to be investigated. Molin and Fauveau (ref.93) have recently shown that this has a marked effect on the 'set-down' or second order potential contribution to the slow drift force, and it would be interesting to see whether this is also true of the other components.

(c) The experiments of Wichers and Sluijs (ref.56) concerning the surge damping of a ship in waves need to be extended to deal with a wider range of vessels and greater wave heights. At present the low frequency surge damping coefficient, to which the slow drift response is sensitive, cannot be determined accurately.

(d) In section 3.2.2 the stiffness curves of the catenary mooring lines were approximated by cubics. It is possible that, considering the large values obtained for the second order response in surge, the use of a higher order polynomial would be more appropriate. The linearisation method of section 3.5. could be extended to deal with a general polynomial and the effect on the second order response investigated.

(e) The dynamic response of the mooring lines, subjected to both low frequency and high frequency displacements of the upper end, has not been considered in this thesis, and is an area for further work.

REFERENCES

1. SMULDERS,L.H. REMERY,G.F. "The Mooring of a Tanker to a Single Point by a Rigid Yoke",1979 Offshore Technology Conference, Houston,Texas. Paper No.OTC 3567

2. McLEOD,W.R. SMULDERS,L.H. "An Analysis of Tanker-Based Floating Production Systems for Small Offshore Fields" EUROPEC,London 1980. Paper No.EUR 269.

3. FLORY,J.F. et al "Guidelines for Deep Water Port Single Point Mooring Design". US Department of Transport Report No.CG-D-49-77, September 1977

4. ALAGHEBAND-OSKOUI,S. "A Study of Anchoring Methods for Offshore Structures". 1982 MSc Thesis, Cranfield Institute of Technology.

5. STEWART,W.P. "The Dynamic Analysis of a Single Buoy Mooring System" 1975 MSc.Thesis, Cranfield Institute of Technology.

6. KIRK,C.L. JAIN,R.K. "Response of Articulated Towers to Waves and Currents" 1977 Offshore Technology Conference, Houston,Texas. Paper No.OTC 2798.

7. KYRIKARDES,A. "Random Dynamic Analysis of a Tanker-Tower System". 1982 MSc Thesis, Cranfield Institute of Technology.

8. SAGOT,A. HEIJST,W.J.V. "The Advantages of the Single Buoy Storage System". 1973 Offshore Technology Conference, Houston,Texas. Paper No. OTC 1918.

9. MERKERT,G. "Offshore Wells Coupled to Storage and Treatment vessel". The Surveyor,August 1981

10. CHAKRABARTI,S.K. COTTER,D.C. "Analysis of a Tower-Tanker System" 1978 Offshore Technology Conference, Houston,Texas. Paper No.OTC 3202

11. LANGLEY,R.S. KIRK,C.L. "Random Dynamic Analysis of an Offshore Single Anchor Leg Storage System" Applied Ocean Research, Vol.4,No.4,October 1982.

12. PORANSKI et al "The First Yoke Mooring for a VLCC in the Open Ocean" 1979 Offshore Technology Conference, Houston, Texas, Paper No.3564

13. NEWMAN,J.N. "Marine Hydrodynamics" MIT Press, 1977

14. PINKSTER,J.A.
REMERY,G.F.M.
"The Role of Model Tests in the Design of Single Point Mooring Terminals".
1975 Offshore Technology Conference, Houston,Texas. Paper No. OTC 2212

15. OWEN,D.G.
LINFOOT,B.T.
"The Development of Mathematical Models of Single Point Mooring Installations"
1976 Offshore Technology Conference, Houston,Texas. Paper No.OTC 2490

16. LOKEN,A.E.
OLSEN,O.A.
"The Influence of Slowly Varying Wave Forces on Mooring Systems".
1979 Offshore Technology Conference, Houston,Texas. Paper No. OTC 3626.

17. WICHERS,J.E.W.
"Slowly Oscillating Mooring Forces in Single Point Mooring Systems"
BOSS'79, Imperial College, London
Paper No.27.

18. RATCLIFFE,A.T.
CLARK,D.
"Development of a Comprehensive Simulation Model of a Single Point Mooring System".
Royal Institute of Naval Architects, Spring Meetings 1980. Paper No.9.

19. MOLIN,B.
BUREAU,G.
"A Simulation Model for the Dynamic Behaviour of Tankers Moored to Single Point Moorings".
Int.Symposium on Ocean Engineering Ship Handling, Sweden, 1980. Paper No.4.

20. SØRHEIM,H.
"Analysis of Motion in Single Point Mooring Systems"
Norwegian Maritime Research. No.1, 1981.

21. OPPENHEIM,B.W.
WILSON,P.A.
"Low Frequency Dynamics of Moored Vessels"
Marine Technology, Vol.19,No.1,pp 1-22.

22. KIRK,C.L.
"Random Vibration and Stochastic Processes"
MSc Course Lecture Notes, Cranfield Institute of Technology.

23. KAPLAN,P.
"Comment on Oppenheim and Wilson: Continuous Digital Simulation of the Second-Order Slowly Varying Wave Drift Force".
Journal of Ship Research,Vol.26,No.1
March 1982, pp 36-37.

24. BOWERS,E.C.
"Long Period Oscillations of Moored Ships Subject to Short Wave Seas".
Royal Institute of Naval Architects.
Paper No. W4, 1975.

25. PINKSTER,J.A.
"Low Frequency Phenomena Associated with Vessels Moored at Sea".
Society of Petroleum Engineers.
Paper No.4837, 1975.

26. ROBERTS,J.B. "Nonlinear Analysis of Slow Drift Oscillations of Moored Vessels in Random Seas". Journal of Ship Research,Vol.25, No.2,June 1981,pp 130-140.

27. LIN,Y.K. "Probabilistic Theory of Structural Dynamics" McGraw-Hill Book Company, 1967.

28. CARTWRIGHT,D.E. LONGUET-HIGGINS,M.S. "The Statistical Distribution of the Maxima of a Random Function". Proc.of the Royal Society of London Series A 1956.

29. KIRK,C.L. "Application of the Fokker-Planck Equation to Random Vibration of Non-Linear Systems" Cranfield Report Aero No.20, 1974, Cranfield Institute of Technology.

30. BERTEAUX,H.O. "Buoy Engineering" John Wiley and Sons, 1976.

31. NIEDZWECKI,J.M. CASARELLA,M.J. "On the Design of Mooring Lines for Deep Water Applications" Transactions of the American Society of Mechanical Engineers, 1976. Paper No. 75-WA/OcE-1

32. ANSARI,K.A. "How to Design a Multi-Component Mooring System" Ocean Industry,March 1979, pp 60-67

33. JAIN,R.K. "A Simple Method of Calculating the Equivalent Stiffness in Mooring Cables" Applied Ocean Research Vol.2,No.3,1980.

34. MUGA,B.J. WILSON,J.F. "Dynamic Analysis of Ocean Structures" Plenum Press, 1970.

35. STOKER,J.J. "Non-Linear Vibrations" Interscience Publishers Inc,1950.

36. SHARPKAYA,T. "In-Line and Transverse Forces on Cylinders in Oscillating Flow at High Reynolds' Numbers". 1976 Offshore Technology Conference,Houston, Texas. Paper No. OTC 2533.

37. BEARMAN,P.W. "Flow Induced Oscillations of Marine Structures" Notes for Short Course on Fluid Loading and Dynamics of Offshore Structures held at Imperial College,London,Sept.14-16 1981.

38. REMERY,G.F.M. KOKEEL,R. "On the Wave Induced Motions of Mooring Buoys" 1976 Offshore Technology Conference, Houston, Texas. Paper No. OTC 2468.

39. SABUNCU,T. CALISAL,S. "Hydrodynamic Coefficients for Vertical Circular Cylinders at Finite Depth". Ocean Engineering,Vol.8,pp 25-63,1981.

40. GARRISON,C.J. "Numerical Methods in Offshore Engineering" pp.87-140. Ed.Zienkiewicz,Lewis and Stagg. J.Wiley, 1978.

41. CARSON,R.N. "On the Capsize Performance of a Discus Buoy in Deep Sea Breakers". Ocean Engineering,Vol.9,pp 501-514,1982.

42. GARRET,C.J. "Wave Forces on a Circular Dock" Journal of Fluid Mechanics,Vol.46, pp 129-139, 1971.

43. WU,S.C. TUNG,C.C. "Random Response of Offshore Structures to Wave and Current Forces". Dept.of Civil Engineering,North Carolina State University. Sea Grant Publication, UNC-SG-75-22, Sept.1975.

44. STOKER,J.J. "Water Waves" Interscience Publishers, 1957.

45. VAN OORTMERSSEN,G. "The Motions of a Moored Ship in Waves" Publication No.S10 of the Netherlands Ship Model Basin, 1981.

46. VINGE,T. BREVIG,P. "Nonlinear Ship Motions" SIS Report,Norwegian Hydrohynamic Laboratories, 1980.

47. LAMB,H. "Hydrodynamics" 6th ed.Cambridge University Press.

48. WEHAUSEN,J.V. LAITONE,E.V. "Handbuch der Physik" Vol.9,Springer Verlag,Berlin 1960.

49. EATOCK TAYLOR,R. "Flow Past Large Bodies - Numerical Methods" Notes for Short Course on Fluid Loading and Dynamics of Offshore Structures held at Imperial College,London,Sept.14-16,1981.

50. KROVIN-KROUKOVSKY,B.V JACOBS,W.R. "Pitching and Heaving Motions of a Ship in Regular Waves". Transactions of the Society of Naval Architects and Marine Engineers, Vol.65,pp 590-632,1957.

51. GERRITSMA,J. BEUKELMAN,W. "Analysis of the Modified Strip Theory for the Calculation of Ship Motions and Wave Bending Moments". International Shipbuilding Prog.,Vol.14, pp 319-337,1967.

52. VUGHTS,J.H. "The Hydrodynamic Forces and Ship Motions in Oblique Waves". Netherlands Ship Research Centre, Report No.150S,1971.

53. SALVENSEN,N.
TUCK,E.O.
FALTINSEN,O. "Ship Motions and Sea Loads"
Transactions of the Society of Naval Architects and Marine Engineers.
Vol.78,pp 250-287,1970.

54. MIGLIORE,M.J.
PALO,P. "Analysis of Barge Motion using Strip and Three Dimensional Source Theories"
1979 Offshore Technology Conference,
Houston,Texas, Paper No.OTC 3558.

55. SOMMET,J. "The Added Mass of a Ship Oscillating with Longitudinal Motion".
Sogreah,Crenoble, France.

56. WICHERS,J.E.W.
SLUIJS,M.F. "The Influence of Waves on the Low Frequency Hydrodynamic Coefficients of Moored Vessels"
1979 Offshore Technology Conference,
Houston,Texas, Paper No.OTC 1500.

57. PROHASKA,C.W. "The Vertical Vibration of Ships"
The Shipbuilder and Marine Engine-builder,
Oct-Nov.1947, pp 542-546,593-599.

58. KAPLAN,P.
ULC,S. "A Dimensional Method for Calculating Lateral Bending Moments on Ships in Oblique Waves". Technical Research Group Inc.
Report TRG-147-SR-1, November 1961.

59. JACOBS,W.R.
DALZELL,J. "Guide to Computational Procedure for Analytical Evaluation of Ship Bending-Moments in Regular Waves".
Davidson Laboratory Report 791
October 1960.

60. BHATTACHARYYA,R. "Dynamics of Marine Vehicles"
John Wiley, 1978.

61. NEWMAN,J.N. "The Damping of an Oscillating Ellipsoid near a Free Surface". Journal of Ship Research, Vol.5,no.3 pp 44-59,1962.

62. VOSSERS,G. "Fundamentals of the Behavious of Ships in Waves". International Shipbuilding Progress, 1960.

63. HU,P.N.
KAPLAN,P. "On the Lateral Damping Coefficients of Submerged Slender Bodies of Revolution"
Stevens Institute of Technology,
Davidson Laboratory Report No.830.
Feb.1962.

64. McCORMICK,M.E. "Ocean Engineering Wave Mechanics" John Wiley and Sons, pp 123-127

65. HAVELOCK,J.H. "The Damping of Heave and Pitch: A Comparison of Two-Dimensional and Three-Dimensional Calculations". Transactions, The Institution of Naval Architects,Vol.98,no.4,pp 464-468, Oct.1956.

66. SNAME "Principles of Naval Architecture" Society of Naval and Marine Engineers.

67. NEWMAN,J.N. "Interaction of Waves with Two-Dimensional Obstacles : a Relation between the Radiation and Scattering Problems", Journal of Fluid Mechanics,Vol.71,part 2, pp 273-282, 1975.

68. OCIMF "Prediction of Wind and Current Loads on VLCC's" Oil Companies International Marine Forum.

69. VERHAGEN,J.H.G. VAN SLUIJS,M.F. "The Low Frequency Drifting Force on a Floating Body in Waves". International Ship Building Progress,No.188,1970.

70. OWEN,D.G. LIGHTFOOT,B.T. "Theoretical Ship Technology Research Symposium".San Francisco, 1977.pp 315-324. SNAME

71. HAVELOCK,T.H. "The Pressure of Water Waves on a Fixed Obstacle". Proc.Roy.Soc.London,Vol.A175, pp 409-421, (1940).

72. NEWMAN,J.N. "The Drift Force and Moment on Ships in Waves" Journal of Ship Research,1967. Vol.11,pp 51-60.

73. STANDING,R.G. DACUNHA,N.M.C. MATTEN,R.B. "Mean Drift Forces : Theory and Experiment" National Maritime Institute, Report No.NMI R124,December 1981.

74. FALTINSEN,O.M. MICHELSEN,F.C. "Motions of Large Structures in Waves at Zero Froude Number" Proc.Int.Symp.of the Dynamics of Marine Vehicles and Structures in Waves, University College London,1974.

75. PINKSTER,J.A. "Low Frequency Second Order Wave Exciting Forces on Floating Structures" Publication No.650 of the Netherlands Ship Model Basin, 1980.

76. FALTINSEN,O.M. LOKEN,A.E. "Slow Drift Oscillations of a Ship in Irregular Waves" Applied Ocean Research, Vol.1,No.1,pp 21-31, (1979).

77. NEWMAN,J.N. "Second Order,Slowly-Varying Forces on Vessels in Irregular Waves" Proc.Int.Symp. of the Dynamics of Marine Vehicles and Structures in Waves, University College, London, 1974.

78. STANDING,R.G.
DACUNHA,N.M.C.
MATTEN,R.B. "Slowly Varying Second Order Wave Forces : Theory and Experiment". National Maritime Institute, Report NMI R138,October 1981.

79. LIGHTHILL,M.J. "Waves and Wave Loading" BOSS'79,Imperial College London,pp 1-40.

80. PINKSTER,J.A.
HOOFT,J.P. "Low Frequency Drifting Forces on Moored Structures in Waves" Publication No.600 of the Netherlands Ship Model Basin, 1978.

81. RICE,S.O. "Mathematical Analysis of Random Noise" Included in "Selected Papers on Noise and Stochastic Processes" Ed.N.Wax,Dover, New,York,1954.

82. TIKHONOV,V.I.
KUZNETSOV,P.I. "Non-Linear Transformations of Stochastic Processes". Oxford,Pergamon Press,1965 pp 137-142.

83. REMERY,G.F.M.
HERMANS,A.J. "The Slow Drift Oscillations of a Moored Object in Random Seas". 1971 Offshore Technology Conference,Houston,Texas Paper No.OTC 1500.

84. REMERY,G.F.M.
VAN OORTMERSSEN,G. "The Mean Wave, Wind and Current Forces on Offshore Structures and their Role in the Design of Mooring Systems". 1973 Offshore Technology Conference,Houston, Texas. Paper No.OTC 1741.

85. FALTINSEN,O.M.
KJAERLAND,O.
LIAPIS,N.
WALDERHAUG,H. "Hydrodynamic Analysis of Tankers at Single Point Mooring Systems". BOSS'79,Imperial College London. Paper No.59.

86. CUMMINS,W.E. "The Impulse Response Function and Ship Motions" Department of the Navy,David Taylor Model Basin,Washington,Report 1661,Oct.1962.

87. BATTJES,J.A. "Effects of Short-Crestedness on Wave Loads on Long Structures". Applied Ocean Research Vol.4,No.3,July 1982.

88. FALTINSEN,O.M. "Sea Loads and Motions of Marine Structures" Norwegian Institute of Technology Lecture Notes, 1979.

89. KIRK,C.L.
BOSE,P.
"Dynamic Response of Articulated Platforms in Random Seas". International Conference on Flow Induced Vibration in Engineering, Reading, England, Sept.14-16,1982.

90. KIRK,C.L.
ETOK,E.U.
"Dynamic Response of a Tethered Production Platform in a Random Seastate"
BOSS'79, Imperial College London.
Paper No.57.

91. SPIDSOE,N.
SIGBJORNSSON,R.
"On the Reliability of Standard Wave Spectra in Structural Response Analysis"
Engineering Structures,Vol.2,pp 123-135.
April 1980.

92. HOGBEN,N.
STANDING,R.G.
"Experience in Computing Wave Loads on Large Bodies" 1975 Offshore Technology Conference,Houston,Texas.Paper No.OTC 2189.

93. MOLIN,B.
FAUVEAU,V.
"Effect of Wave-Directionality on Second Order Loads Induced by Set Down"
To be published in Applied Ocean Research.

APPENDIX A - WAVE SPECTRA

The surface elevation $\eta(t)$ at any particular sea location will have a random time history. Since linear wave theory is well understood, it is useful to consider $\eta(t)$ as being the sum of a number of linear wave components. A measure of how dominant a wave of a particular frequency is in the seastate is the 'power spectral density' at this frequency, and the graph of power spectral density against frequency is called the wave spectrum. Given the time history of the seastate it is theoretically possible to find the wave spectrum via the following equation:-

$$S_{\eta\eta}(\omega) = (\frac{2}{\pi})\int_0^\infty R_{\eta\eta}(\tau)\cos(\omega-\tau)\,d\omega \qquad (A.1)$$

where $R_{\eta\eta}(\tau)$ is the auto-correlation function given by:-

$$R_{\eta\eta}(\tau) = \lim_{T\to\infty} \int_{-T}^{T} \eta(t)\eta(t+\tau)dt/2T \qquad (A.2)$$

Since $\eta(t)$ will depend on the location considered and the weather conditions, it can be seen that a spectrum found by the above method will only be valid for one seastate in one location. Much research has been carried out to find wave spectra which can be used generally, and a summary and comparison of the wave spectra which are available today is given by Spidsoe and Sigbjornsson (ref.91). The wave spectra which are most frequently used are as follows:-

a) The ISSC wave spectrum. This is defined as:-

$$S_{\eta\eta}(\omega) = A\omega^{-5} \exp\{-B\omega^{-4}\} \qquad (A.3)$$

where: $A = 173H_s^2/T^4$ (A.4)

$$B = 691/T^4 \qquad (A.5)$$

H_s is the significant wave height and T is the average wave period. This spectrum is valid for deep water and fully developed seas.

b) The JONSWAP (Joint North Sea Wave Project) spectrum. This is given by:-

$$S_{\eta\eta}(\omega) = \alpha g^2\omega^{-5} \exp\left[-\beta(\frac{\omega}{\omega_m})^{-4}\right]\gamma^{\exp\left[-(\omega-\omega_m)^2/2\sigma^2\omega_m^2\right]} \qquad (A.6)$$

This spectrum applies to limited fetch areas and homogeneous wind fields and is thought to apply generally to the North Sea. The parameters α, ω_m and γ depend upon the significant wave height and the expected zero crossing period. Figure (A.1) shows values of these parameters which are to be used. The following values of σ and β were found from measurements taken on the Norwegian continental shelf:-

$$\sigma = 0.07; \quad \omega < \omega_m \tag{A.7}$$

$$\sigma = 0.09 \quad \omega > \omega_m \tag{A.8}$$

$$\beta = 1.25 \tag{A.9}$$

For $H_s < 2m$ it is recommended that the Pierson-Moskowitz spectrum should be used. A one parameter form of the JONSWAP spectrum, depending on H_s only, also exists. The value of α is fixed at 0.0081 and ω_m is found from $\omega_m = 1.416\ H_s^{-\frac{1}{2}}$.

c) The Pierson-Moskowitz spectrum. This is the same as the JONSWAP spectrum except:-

$$\gamma = 1.0 \tag{A.10}$$

$$\alpha = 1.2887(H_s/T_z^{\,2})^2 \tag{A.11}$$

$$\omega_m = 8.8445/T_z \tag{A.12}$$

and is applicable to broad fetch areas and lower seastates.

APPENDIX B - LINEAR WAVE THEORY

Consider the fluid region shown in Figure B.1. If the fluid is considered to be both incompressible and irrotational, then it's motion can be completely defined by a velocity potential $\phi(x,y,z,t)$, which must satisfy the following conditions:-

a) Laplace's equation. This arises from the basic assumption that the flow is irrotational and incompressible, and states that within the fluid region

$$\nabla^2\phi = 0 \qquad \text{(B.1)}$$

b) The boundary condition on the sea-bed. This states that there is no flow through the sea-bed, or

$$\frac{\partial\phi}{\partial n} = 0 \qquad \text{(B.2)}$$

on $y = -h(x,z)$

c) Bernoulli's equation. This arises from the equation of motion of the fluid, and states

$$g\eta + \phi_t + \tfrac{1}{2}(\phi_x^2 + \phi_y^2 + \phi_z^2) = 0 \qquad \text{(B.3)}$$

on $y = \eta(x,z,t)$

d) The kinematic free surface condition. This arises from the assumption that any particle which is once on the free surface remains on it, and states

$$\phi_x\eta_x - \phi_y + \phi_z\eta_z + \eta_t = 0 \qquad \text{(B.4)}$$

on $y = \eta(x,z,t)$.

Clearly, the task of finding the functions ϕ and η which satisfy the above four conditions is an extremely difficult one, and at the present time this problem has only been solved approximately. The method of solution which gives rise to linear wave theory is the so-called perturbation method, which has been discussed at length by Stoker (ref.44). In this method it is assumed that the velocity of the water particles, the free surface elevation and their derivatives are small quantities, and that ϕ and η can be expressed in terms of some

parameter ε as follows

$$\phi = \varepsilon\phi^{(1)} + \varepsilon^2\phi^{(2)} + \varepsilon^3\phi^{(3)} + \ldots \quad (B.5)$$

$$\eta = \eta^{(0)} + \varepsilon\eta^{(1)} + \varepsilon^2\eta^{(2)} + \ldots \quad (B.6)$$

where:

$\phi^{(k)}$ = kth order solution for ϕ, which satisfies B.1 and B.2.

$\eta^{(k)}$ = kth order solution for η.

The solution then proceeds by inserting equations B.5 and B.6 into equation B.3 and expanding in terms of ε. Equating powers of ε leads to an infinite number of equations which must be satisfied on $y = \eta^{(0)}$ the first three of which are:

$$\eta^{(0)} = 0 \quad (B.7)$$

$$g\eta^{(1)} + \phi_t^{(1)} = 0 \quad (B.8)$$

$$g\eta^{(2)} + \phi_t^{(2)} + \tfrac{1}{2}\{[\phi_x^{(1)}]^2 + [\phi_y^{(1)}]^2 + [\phi_z^{(1)}]^2\} + \eta^{(1)}\phi_{ty}^{(1)} = 0 \quad (B.9)$$

From equation B.7 it can be seen that B.8 and B.9 are to be satisfied on $y = 0$. Similarly, insertion of B.5 and B.6 into B.4 produces another series of equations to be satisfied on $y = 0$, the first two of which are:-

$$\eta_t^{(1)} = \phi_y^{(1)} \quad (B.10)$$

$$\eta_t^{(2)} = \phi_y^{(2)} - \phi_x^{(1)}\eta_x^{(1)} - \phi_z^{(1)}\eta_z^{(1)} + \phi_{yy}^{(1)}\eta^{(1)} \quad (B.11)$$

Linear wave theory abandons the series for ϕ (equation B.5) after the first term, and also assumes that the fluid motion is two-dimensional. This means that a velocity potential ϕ is now sought which satisfies equations B.1, B.2, B.8 and B.10 and is independent of z. It can be shown that for a uniform fluid depth d, the required velocity potential is:-

$$\phi = \frac{ag\cosh k(y+d)}{\omega\cosh(kd)}\sin(kx - \omega t) \quad (B.12)$$

where:-

a = Wave amplitude

ω = Wave frequency (radians per second)

k = Wavenumber = $2\pi/(\text{wavelength})$

This leads to the following results:-

$$u = \phi_x = a\omega \frac{\cosh k(d+y)}{\cosh(kd)} \cos(kx - \omega t) \qquad (B.13)$$

$$v = \phi_y = a\omega \frac{\sinh k(d+y)}{\sinh(kd)} \sin(kx - \omega t) \qquad (B.14)$$

$$\dot{u} = a\omega^2 \frac{\cosh k(d+y)}{\sinh(kd)} \sin(kx - \omega t) \qquad (B.15)$$

$$\dot{v} = -a\omega^2 \frac{\sinh k(d+y)}{\sinh(kd)} \cos(kx - \omega t) \qquad (B.16)$$

$$p = -\rho\phi_t = \rho g a \frac{\cosh k(d+y)}{\cosh(kd)} \cos(kx - \omega t) \qquad (B.17)$$

$$\eta = a\cos(kx - \omega t) \qquad (B.18)$$

It can be seen from the above derivation that linear wave theory is not the complete answer to the problem, but only the first approximation. However, it has been shown by Hogben and Standing (ref.92) that in most cases linear wave theory is adequate for calculating wave forces.

APPENDIX C - MORISON'S EQUATION AND THE LINEARISATION OF DRAG FORCE

C.1. Morisons Equation

Two different methods of analysis are presently available for the calculation of fluid-structure interactions. The first of these is diffraction (or potential flow) theory, and the second is a semi-empirical approach based on Morison's equation. Diffraction theory seeks to represent the flow around the body by a distribution of sources and sinks over the body surface. The fluid is considered to be irrotational, incompressible and inviscid, and the required source/sink distribution is found by a numerical solution using Green's functions. This approach is discussed by Newman (ref.13).

Diffraction theory cannot accommodate viscous effects, whereas the second method of approach, Morisons equation, can. It can be shown that for waves of amplitude 'a' the ratio of viscous forces to inertial forces is proportional to a/ℓ, where ℓ is some typical length for the structure. When the inertial forces are dominant, empirical evidence suggests that the inertial force per unit length acting on a fixed cylindrical body can be written as:-

$$F_I = \tfrac{1}{4}\pi\rho D^2 C_m \dot{u} \qquad (C.1)$$

where D is the diameter of the body, ρ is the fluid density, $\dot{u}$ is the fluid acceleration normal to the body and C_m is the inertial coefficient. Similarly, when the viscous forces are dominant the drag force per unit length on such a body can be written as:-

$$F_D = \tfrac{1}{2}\rho C_D D|u_r|u_r \qquad (C.2)$$

where C_D is a drag coefficient and u_r is the velocity of the fluid perpendicular to the body. Morison's equation states that when neither viscous or inertial forces are dominant, the total force per unit length can be found from the sum of C.1 and C.2, i.e.

$$F_T = \tfrac{1}{4}\pi\rho D^2 C_m \dot{u} + \tfrac{1}{2}\rho C_D D|u_r|u_r \qquad (C.3)$$

It can be seen that C.3. has an inbuilt contradiction, since C.1 is only valid when $a \ll \ell$ and C.2 is only valid when $a \gg \ell$, and so the

justification of Morison's equation is strictly pragmatic and must rest with experimental confirmation. If the body is no longer fixed, then C.3 is modified and becomes:-

$$F_T = \tfrac{1}{4}\pi\rho D^2 C_m \dot{u} - \tfrac{1}{4}\pi\rho D^2 C_a \ddot{z} + \tfrac{1}{2}\rho C_D D|u_r|u_r \qquad (C.4)$$

where $\ddot{z}$ is the structural acceleration (in the same directions as $\dot{u}$), C_a is given by $(C_m - 1)$ and u_r now contains a correction involving $\dot{z}$. When considering a problem in dynamics, it is usual to take the second term in C.4 over to the left hand side of the equation.

The ranges of validity of Morison's equation and diffraction theory are illustrated in Figure (C.1).

C.2 Linearisation of the Drag Force

The drag force shown in equation C.2 is non-linear, and must be linearised if a frequency domain analysis is to be performed. In the presence of current, the drag force becomes:-

$$F_D = \tfrac{1}{2}\rho C_D D(v+v_c)|v+v_c| \qquad (C.5)$$

where v is the relative oscillatory velocity between the structure and the fluid and v_c is the current velocity. Tung and Wu (ref.43) have linearised equation C.5 using the equivalent linearisation technique (see section 2.3.1). The drag force is written in terms of a linear term plus an error term, as follows:-

$$F_D = \tfrac{1}{2}\rho C_D D(av+b) + \varepsilon \qquad (C.6)$$

$$\varepsilon = \tfrac{1}{2}\rho C_D D(v+v_c)|v+v_c| - \tfrac{1}{2}\rho C_D D(av+b) \qquad (C.7)$$

Values of the coefficients a and b are then found such that ε is minimised in the mean squared sense. Tung and Wu (ref.43) have shown that if v is assumed to be Gaussian, then the required values of a and b are:-

$$a = \sqrt{\frac{8}{\pi}}\{\sigma_v \exp[-\tfrac{1}{2}(v_c/\sigma_v)^2] + \sqrt{2\pi}\, v_c\, \mathrm{erf}(v_c/\sigma_v)\} \qquad (C.8)$$

$$b = \sqrt{\frac{2}{\pi}} \{v_c\sigma_v \exp[-\tfrac{1}{2}(v_c/\sigma_v)^2] + \sqrt{2\pi}(\sigma_v^2 + v_c^2)\,\mathrm{erf}(v_c/\sigma_v)\} \tag{C.9}$$

where:-

$$\mathrm{erf}(x) = \frac{1}{\sqrt{2\pi}} \int_0^x e^{-\frac{1}{2}y^2} dy \tag{C.10}$$

when $v_c = 0$ this result is known as Borgman's approximation.

APPENDIX D - LINEAR WAVE FORCES ON A VLCC

D.1 Introduction

The strip theory method of calculating the linear wave forces acting on a ship has been discussed in general terms in section 5.2.4. This Appendix gives detailed expressions for the wave forces acting on one strip having constant sectional properties (beam B_s, draft T_s and section coefficient β_s) and extending from x = a to x = b, as shown in Figure D.1. The direction of propagation of the incident wave is taken to lie at a general angle θ to the x-axis and to have a complex velocity potential (see Appendix B) of:-

$$\phi = \frac{ag}{\omega} \frac{\cosh k(z+d)}{\cosh(kd)} e^{ik(x\cos\theta - y\sin\theta)} e^{i\omega t} \qquad (D.1)$$

The various components of the linear wave forces are discussed in the following sections, in which added mass coefficients are defined as:-

$$C_{ii} = \frac{L_s A'_{ii}}{L_s B_s T_s \beta_s} \qquad (D.2)$$

D.2 Inertia Forces and Forces due to the Wave Profile

D.2.1. Surge

Equation (5.38) gives the inertia force acting in surge as:-

$$F_1(t) = L_s\left[\rho B_s T_s \beta_s + A'_{11}\right]\bar{\ddot{q}}_1 \qquad (D.3)$$

where, in this instance:-

$$\bar{\ddot{q}}_1 = \frac{1}{L_s B_s T_s} \int_{-0.5B_s}^{0.5B_s} \int_{a}^{b} \int_{-T_s}^{0} \dot{\phi}_x \, dy\,dx\,dz \qquad (D.4)$$

Using equation (D.1) it can be shown that:-

$$F_1(t) = \frac{2i\rho a\omega^2 g_s^s \beta_s (1+C_{11})}{k^3 \sin\theta} \left[e^{ikb\cos\theta} - e^{ika\cos\theta}\right] \sin(\tfrac{1}{2}kB_s\sin\theta) e^{i\omega t} \qquad (D.5)$$

where

$$g_s^s = 1 - \frac{\sinh k(d-T_s)}{\sinh(kd)} \qquad (D.6)$$

Equation (D.6) is not valid for the case θ=0, since the denominator

becomes zero, and a modified equation must be used:-

$$F_1(t) = \frac{i\rho a\omega^2 g_s^s \beta_s B_s (1+C_{11})}{k^2} \left[e^{ikb} - e^{ika}\right] e^{i\omega t} \qquad (D.7)$$

D.2.2 Sway

The inertia force acting in sway is:-

$$F_2(t) = L_s \left[\rho B_s T_s \beta_s + A'_{22}\right] \ddot{\bar{q}}_2 \qquad (D.8)$$

where:-

$$\ddot{\bar{q}}_2 = \frac{1}{L_s B_s T_s} \int_{-0.5B_s}^{0.5B_s} \int_a^b \int_{-T_s}^{\theta} \dot{\phi}_y \, dy dx dz \qquad (D.9)$$

Using equation (D.1) it can be shown that:-

$$F_2(t) = \frac{-2i\rho a\omega^2 g_s^s \beta_s (1+C_{22})}{k^3 \cos\theta} \left[e^{ikb\cos\theta} - e^{ika\cos\theta}\right] \sin(\tfrac{1}{2}kB_s \sin\theta) e^{i\omega t} \qquad (D.10)$$

for the case $\theta \neq 90^o$, and that when $\theta = 90^o$:-

$$F_2(t) = \frac{2\rho a\omega^2 g_s^s L_s \beta_s (1+C_{22})}{k^2} \sin(\tfrac{1}{2}kB_s) e^{i\omega t} \qquad (D.11)$$

D.2.3 Heave

The inertia force in heave is:-

$$F_3(t) = L_s \left[\rho B_s T_s \beta_s + A'_{33}\right] \ddot{\bar{q}}_3 \qquad (D.12)$$

where $\ddot{\bar{q}}_3 = \frac{1}{L_s B_s T_s} \int_{-0.5B_s}^{0.5B_s} \int_a^b \int_{-T_s}^{0} \dot{\phi}_z \, dy dx dz \qquad (D.13)$

Using equation (D.1) it can be shown that:-

$$F_3(t) = \frac{2\rho a\omega^2 \beta_s g_s^s (1+C_{33})}{k^3 \cos\theta \sin\theta} \left[e^{ikb\cos\theta} - e^{ika\cos\theta}\right] \sin(\tfrac{1}{2}kB_s \sin\theta) e^{i\omega t} \qquad (D.14)$$

where:-

$$g_c^s = \left[\cosh(kd) - \cosh k(d-T_s)\right] / \sinh(kd) \qquad (D.15)$$

Equation (D.14) is not valid for $\theta=0^o$ or $\theta=90^o$. For head seas ($\theta=0^o$) the heave force becomes:-

$$F_3(t) = \frac{\rho a \omega^2 \beta_s B_s g_c^s (1+C_{33})}{k^2} \left[e^{ikb} - e^{ika}\right] e^{i\omega t} \qquad (D.16)$$

and for beam seas ($\theta=90^o$) this force is:-

$$F_3(t) = \frac{2i\rho a \omega^2 \beta_s L_s g_c^s (1+C_{33})}{k^2} .\sin(\tfrac{1}{2}kB_s) e^{i\omega t} \qquad (D.17)$$

The wave profile produces an additional force in heave (see equation 5.46) of:-

$$F_{3p}(t) = \rho g L_s B_s \bar{\eta}(t) \qquad (D.18)$$

where

$$\bar{\eta} = \frac{1}{L_s B_s} \int_{-0.5B_s}^{0.5B_s} \int_a^b \left[- \frac{1}{g} \dot{\phi}(z=0)\right] dydx \qquad (D.19)$$

From (D.1) it can be shown that:-

$$F_{3p}(t) = \frac{-2\rho a g}{k^2 \sin\theta \cos\theta} \left[e^{ikbcos\theta} - e^{ikacos\theta}\right] \sin(\tfrac{1}{2}kB_s \sin\theta) e^{i\omega t} \qquad (D.20)$$

Again, this equation is not valid for the cases $\theta=0^o$ and $\theta=90^o$, where modifications must be made to produce equations similar in form to (D.16) and (D.17).

D.2.4 Roll

The inertia moment in roll is given by $F_2(t)BG$, where $F_2(t)$ is given by equations (D.10) and (D.11) and BG is the distance of the centre of buoyancy below the centre of gravity. The rolling moment produced by the wave profile (see 5.50) is:-

$$F_{4P}(t) = \overline{GM}_r \, Mg \, \frac{1}{L_s B_s} \int_{-0.5B_s}^{0.5B_s} \int_a^b \left[- \frac{1}{g} \dot{\phi}_y(z=0)\right] dydx \qquad (D.21)$$

where $\overline{GM}_r$ is the roll metacentric height. From equation (D.1):-

$$F_{4p}(t) = \frac{T_s \rho g \overline{GM}_r 2ia}{k\cos\theta} \left[e^{ikbcos\theta} - e^{ikacos\theta}\right] \sin(\tfrac{1}{2}kB_s \sin\theta) e^{i\omega t} \qquad (D.22)$$

when $\theta = 90^o$, this equation becomes:-

$$F_{4p}(t) = -2T_s \rho g a \overline{GM}_r L_s \sin(\tfrac{1}{2}kB_s) e^{i\omega t} \qquad (D.23)$$

D.2.5 Pitch

The inertia moment in pitch (see equation 5.42) is:-

$$F_5(t) = -L_s\left[\rho B_s T_s \beta_s + A_{33}'\right]\left[\overline{\ddot{xq}_3}\right] - F_1(t)BG \qquad (D.24)$$

where:-

$$\left[\overline{\ddot{xq}_3}\right] = \frac{1}{L_s B_s T_s}\int_{-0.5B_s}^{0.5B_s}\int_{a}^{b}\int_{-T_s}^{o} \dot{x\phi}_z \, dydxdz \qquad (D.25)$$

Equation (D.1) then yields:-

$$F_5(t) = \frac{-2\rho a\omega^2 \beta_s g_c^s (1+C_{33})}{k^3 \cos\theta \sin\theta}\left\{e^{ikb\cos\theta}\left[b+\frac{i}{k\cos\theta}\right] - e^{ika\cos\theta}\left[a+\frac{i}{k\cos\theta}\right]\right\}$$

$$\sin(\tfrac{1}{2}kB_s\sin\theta)e^{i\omega t} - F_1(t)BG \qquad (D.26)$$

which is valid for all cases except $\theta=0^o$ and $\theta=90^o$. For head seas ($\theta=0^o$) this equation becomes:-

$$F_5(t) = \frac{-\rho a\omega^2 \beta_s B_s g_c^s (1+C_{33})}{k^2}\left\{e^{ikb}\left[b+\frac{i}{k}\right] - e^{ika}\left[a+\frac{i}{k}\right]\right\}e^{i\omega t} - F_1(t)BG \qquad (D.27)$$

and for beam seas ($\theta=90^o$) this equation is:-

$$F_5(t) = \frac{-i\rho a\omega^2 \beta_s g_c^s (1+C_{33})}{k^2}(b^2-a^2)\sin(\tfrac{1}{2}kB_s)e^{i\omega t} - F_1(t)BG \qquad (D.28)$$

The pitch moment due to the wave profile can be shown to be:-

$$F_{5p}(t) = \frac{2a\rho g}{k^2 \sin\theta\cos\theta}\left\{e^{ikb\cos\theta}\left[b+\frac{i}{k\cos\theta}\right] - e^{ika\cos\theta}\left[a+\frac{i}{k\cos\theta}\right]\right\}\sin(\tfrac{1}{2}kB_s\sin\theta)e^{i\omega t} \qquad (D.29)$$

which must be modified for the cases $\theta=0^o$ and $\theta=90^o$ to produce equations similar in form to (D.27) and (D.28).

D.2.6 Yaw

The inertia moment in yaw can be written (see equation 5.43):-

$$F_6(t) = L_s\left[\rho B_s T_s \beta_s + A_{22}'\right]\left[\overline{\ddot{xq}_2}\right] \qquad (D.30)$$

where:-

$$\overline{[\ddot{x}q_2]} = \frac{1}{L_s B_s T_s} \int_{-0.5B_s}^{0.5B_s} \int_{a}^{b} \int_{-T_s}^{0} x\dot{\phi}_y \, dydxdz \qquad (D.31)$$

Using (D.1) it can be shown that

$$F_6(t) = \frac{-2ia\omega^2\rho\beta_s g_s^s(1+C_{22})}{k^3\cos\theta} \{e^{ikbcos\theta}[b+\frac{i}{kcos\theta}]-e^{ikacos\theta}[a+\frac{i}{kcos\theta}]\}$$

$$\sin(\tfrac{1}{2}kB_s\sin\theta)e^{i\omega t} \qquad (D.32)$$

for all cases except $\theta=90^o$, when

$$F_6(t) = \frac{\rho a\omega^2\beta_s g_s^s(1+C_{22})}{k^2}(b^2-a^2)\sin(\tfrac{1}{2}kB_s)e^{i\omega t} \qquad (D.33)$$

D.3 Damping Forces

The damping forces and moments can be obtained by multiplying those terms in the inertia forces involving added mass coefficients, by the factor:-

$$\frac{N'_{ii}L_s}{\rho\beta_s L_s T_s B_s(1+C_{ii})i\omega}$$

where N'_{ii} is the damping coefficient per unit length, including the correction factor for three dimensional effects. This converts acceleration terms to velocity terms and replaces the mass plus added mass with the damping coefficient. This then leads to the following damping forces:-

$$F_{d1}(t) = \frac{2a\omega g_s^s N'_{11}}{T_s B_s k^3\sin\theta}[e^{ikbcos\theta}-e^{ikacos\theta}]\sin(\tfrac{1}{2}kB_s\sin\theta)e^{i\omega t} \qquad (D.34)$$

$$F_{d2}(t) = \frac{-2a\omega g_s^s N'_{22}}{T_s B_s k^3\cos\theta}[e^{ikbcos\theta}-e^{ikacos\theta}]\sin(\tfrac{1}{2}kB_s\sin\theta)e^{i\omega t} \qquad (D.35)$$

$$F_{d3}(t) = \frac{-2ia\omega g_c^s N'_{33}}{T_s B_s k^3\cos\theta\sin\theta}[e^{ikbcos\theta}-e^{ikacos\theta}]\sin(\tfrac{1}{2}kB_s\sin\theta)e^{i\omega t} \qquad (D.36)$$

$$F_{d5}(t) = \frac{2ia\omega g_c^s N'_{33}}{T_s B_s k^3 \cos\theta \sin\theta}\{e^{ikbcos\theta}\left[b+\frac{i}{kcos\theta}\right]-e^{ikacos\theta}\left[a+\frac{i}{kcos\theta}\right]\}$$

$$\sin(\tfrac{1}{2}kB_s\sin\theta) + F_{d1}(t)BG \qquad (D.37)$$

$$F_{d6}(t) = \frac{-2a\omega g_s^s N'_{22}}{k^3\cos\theta\ T_s B_s}\{e^{ikbcos\theta}\left[b+\frac{i}{kcos\theta}\right]-e^{ikacos\theta}\left[a+\frac{i}{kcos\theta}\right]\}\sin(\tfrac{1}{2}kB_s\sin\theta)$$

(D.38)

$F_{d4}(t)$ does not appear since roll damping is mainly viscous. Appropriate modifications must be made to the above when $\theta=0^o$ or $\theta=90^o$.

APPENDIX E - WIND AND CURRENT FORCES ON A SBS SYSTEM

Detailed expressions for the wind and current forces acting on an SBS system, discussed in Chapter 7 and shown in Figure 7.5, are as follows:-

$$F_C^1 = C_{xc}(\theta)AV_r^2TL_{BP} \tag{E.1}$$

$$F_C^2 = C_{yc}(\theta)AV_r^2TL_{BP} \tag{E.2}$$

$$F_C^3 = C_{xyc}(\theta)AV_r^2\,TL_{BP}^2+5C_{yc}(90^0)\int_L ATx(V_c\sin\psi-\dot{y}-x\dot{\psi})\,|V_c\sin\psi-\dot{y}-x\dot{\psi}|\,dx \tag{E.3}$$

$$V_r^2 = (\dot{x} + V_c\cos\psi)^2 + (\dot{y} - V_c\sin\psi)^2 \tag{E.4}$$

$$\theta = \tan^{-1}\{(\dot{y} - V_c\sin\psi)/(\dot{x} + V_c\cos\psi)\} \tag{E.5}$$

$$F_{CB}^1 = -F\cos\phi \tag{E.6}$$

$$F_{CB}^2 = -F\sin\phi \tag{E.7}$$

$$F = \tfrac{1}{2}\rho C_D D d_t V_{r2}^2 \tag{E.8}$$

$$V_{r_2}^2 = (V_c\cos\psi + \dot{x})^2 + (\dot{y} + \ell_2\dot{\psi} - V_c\sin\psi)^2 \tag{E.9}$$

$$\phi = \tan^{-1}\{(\dot{y} + \ell_2\dot{\psi} - V_c\sin\psi)/(V_c\cos\psi + \dot{x})\} \tag{E.10}$$

$$F_W^1 = C_{xw}(\alpha)BV_{rw}^2\,A_T \tag{E.11}$$

$$F_W^2 = C_{yw}(\alpha)B\,V_{rw}^2\,A_L + C_{yw}(90^0)\int_L B(A_L/L)\{V_1|V_1| - V_2|V_2|\}dx \tag{E.12}$$

$$F_W^3 = C_{xyw}(\alpha)B\,V_{rw}^2A_LL_{BP} + C_{yw}(90^0)\int_L B(A_L/L)xV_1|V_1|\,dx \tag{E.13}$$

$$V_1 = V_w\sin(\theta_w + \psi) - \dot{y} - x\dot{\psi} \tag{E.14}$$

$$V_2 = V_w\sin(\theta_w + \psi) - \dot{y} \tag{E.15}$$

$$V_{rw}^2 = (\dot{x} + V_w\cos[\theta_w + \psi])^2 + (\dot{y} - V_w\sin[\theta_w + \psi])^2 \tag{E.16}$$

$$\alpha = \tan^{-1}\{(\dot{y} - V_w\sin[\theta_w + \psi])/(\dot{x} + V_w\cos[\theta_w + \psi])\} \qquad (E.17)$$

where C_D, D and d_t are the drag coefficient, diameter and draft of the buoy, and the remaining notation is as in Chapter 7.

The coefficients given in (7.39), the equations of motion of the system, are:-

$$C_1 = M_T + M_Y + M_B + M_{TAI} + M_{BA} \qquad (E.18)$$

$$C_2 = M_T + M_Y + M_B \qquad (E.19)$$

$$C_3 = M_Y\ell_1 + M_B\ell_2 \qquad (E.20)$$

$$C_4 = \ell_1 M_Y + \ell_2 M_B + \ell_2 M_{BA} \qquad (E.21)$$

$$C_5 = I_T + I_{YG} + I_{BG} + M_{66} + M_{BA}\ell_2^2 \qquad (E.22)$$

$$C_6 = M_T + M_Y + M_B + M_{TA2} + M_{BA} \qquad (E.23)$$

APPENDIX F - LINEARISED FORCES ON A MOORING BUOY

Detailed expressions for the terms on the RHS of equation (4.12) are given below, the notation used being the same as that of Chapter 4:-

$$B_{11} = \tfrac{1}{2}\rho C_D D \int_{-d_t}^{S} a_x(z)dz \quad ; \quad B_{15} = \tfrac{1}{2}\rho C_D D \int_{-d_t}^{S} z\, a_x(z)dz \qquad (F.1)$$

$$B_{22} = \tfrac{1}{2}\rho C_D D \int_{-d_t}^{S} a_y(z)dz \quad ; \quad B_{24} = -\tfrac{1}{2}\rho C_D D \int_{-d_t}^{S} z\, a_y(z)dz \qquad (F.2)$$

$$B_{44} = \tfrac{1}{2}\rho C_D D \int_{-d_t}^{S} z\, a_y(dz) \quad ; \quad B_{55} = \tfrac{1}{2}\rho C_D D \int_{-d_t}^{S} z\, a_x(z)dz \qquad (F.3)$$

$$F_{d1} = -\tfrac{1}{2}\rho C_D D \int_{-d_t}^{S} a_x(z)u(z)\cos\theta dz \; ; \; F_{c1} = \tfrac{1}{2}\rho C_D D \int_{-d_t}^{S} b_x(z)dz \qquad (F.4)$$

$$F_{d2} = \tfrac{1}{2}\rho C_D D \int_{-d_t}^{S} a_y(z)u(z)\sin\theta dz \; ; \; F_{c2} = \tfrac{1}{2}\rho C_D D \int_{-d_t}^{S} b_y(z)dz \qquad (F.5)$$

$$M_{d1} = \tfrac{1}{2}\rho C_D D \int_{-d_t}^{S} z a_y(z)u(z)\sin\theta dz \; ; \; M_{c1} = -\tfrac{1}{2}\rho C_D D \int_{-d_t}^{S} z b_y(z)dz \qquad (F.6)$$

$$M_{d2} = -\tfrac{1}{2}\rho C_D D \int_{-d_t}^{S} z a_x(z)u(z)\cos\theta dz \; ; \; M_{c2} = \tfrac{1}{2}\rho C_D D \int_{-d_t}^{S} z b_x(z)dz \qquad (F.7)$$

The coefficients $a_x(z)$, $b_x(z)$, $a_y(z)$ and $b_y(z)$ are due to Tung and Wu (ref.43) and are given in Appendix C. The above integrals can be calculated numerically using the trapezium rule, i.e. the buoy is divided into a discrete number of strips, over each of which the integrands are considered to be constant. The integral signs in the above are then replaced with summation signs.

APPENDIX G - EQUATIONS OF MOTION OF A SBS SYSTEM

G.1 Introduction

The dynamic analysis of a SBS (Single Buoy Storage) system has been discussed in Chapter 8, in which the equations of motion of the system are formulated vectorially and are finally expressed in matrix form, few details being given. The present Appendix contains detailed expressions for these equations, together with a number of matrices which are required for their formulation. The notation which is used to define the dimensions of the system is shown in Figure G.1.

G.2 Constraints

In section 8.2.1 a number of geometrical constraints are introduced and it is stated that these constraints can be used to express the buoy degrees of freedom of surge, sway, heave and roll in terms of the degrees of freedom of the tanker. This fact is utilised in section 8.4.2, where it is stated (equation 8.54) that:-

$$\underset{\sim}{G} = A_C \underset{\sim}{Q} \qquad (G.1)$$

where $\underset{\sim}{G}$ is the vector of buoy displacements and $\underset{\sim}{Q}$ is the vector of displacements for the full eight degree of freedom system. It can be shown that equations (8.12) to (8.15) yield the following form of A_C:-

$$A_C = \begin{bmatrix} C_1 & 0 & -C_2 & 0 & C_3 & 0 & C_4 & 0 \\ 0 & 1 & 0 & C_5 & 0 & C_6 & 0 & 0 \\ C_2 & 0 & C_1 & 0 & C_7 & 0 & C_8 & 0 \\ 0 & 0 & 0 & C_1 & 0 & -C_2 & 0 & 0 \\ 0 & 0 & 0 & 0 & 0 & 0 & 1 & 0 \\ 0 & 0 & 0 & 0 & 0 & 0 & 0 & 1 \end{bmatrix} \qquad (G.2)$$

where:-

$C_1 = \cos f_5$ $\quad C_2 = \sin f_5$ $\quad C_3 = s_1 \sin f_5 + s_3 \cos f_5$

$C_4 = -(\ell_m \cos\alpha + m_3)$ $\quad C_5 = f_3 - e_3$ $\quad C_6 = (e_1 - f_1)\cos e_6 + (e_2 - f_2)\sin e_6$

$C_7 = s_3 \sin f_s - s_1 \cos f_5$ $\quad C_8 = -\ell_m \sin\alpha$

Section 8.2.1 also states that equations (8.22) and (8.23) can be used to express the yoke degrees of freedom $\underset{\sim}{j}$ in terms of the system

displacements $\underset{\sim}{Q}$. If this fact is expressed in the form:-

$$\underset{\sim}{j} = A_D \underset{\sim}{Q} \tag{G.3}$$

then it can be shown that:-

$$A_D = \begin{bmatrix} \gamma & 0 & \delta & 0 & C_9 & 0 & 0 & 0 \\ 0 & 1 & 0 & C_{10} & 0 & C_{11} & 0 & 0 \\ -\delta & 0 & \gamma & 0 & C_{12} & 0 & -\ell_g & 0 \\ 0 & 0 & 0 & \gamma & 0 & \delta & 0 & 0 \\ 0 & 0 & 0 & 0 & 0 & 0 & 1 & 0 \\ 0 & 0 & 0 & -\delta & 0 & \gamma & 0 & 0 \end{bmatrix} \tag{G.4}$$

where:-

$$C_9 = \gamma s_3 - \delta s_1 \qquad C_{10} = -(\delta \ell_g + s_3) \qquad C_{11} = \gamma \ell_g + s_1$$
$$C_{12} = -(\gamma s_1 + \delta s_3)$$

γ and δ in the above can be found from equation (8.19) to be:-

$$\gamma = a(a^2 + b^2)^{-\frac{1}{2}} \qquad \delta = b(a^2 + b^2)^{-\frac{1}{2}} \tag{G.5}$$

where:-

$$a = m_3 \sin f_5 + (e_1 - f_1)\cos e_6 + (e_2 - f_2)\sin e_6 - t_1$$
$$b = m_3 \cos f_5 + e_3 - f_3 - t_3$$

G.3 The Matrices A_1, A_2, A_3 and M_E

Equation (8.26) introduces the matrix A_1 in order to express the buoy reactions in terms of the wave forces acting on the buoy and the buoy degrees of freedom. It can be shown that:-

$$A_1 = I + A_1' \tag{G.6}$$

where I is the 6 x 6 identity matrix and A_1' is a 6 x 6 matrix with all entries zero except $A_1'(4,2) = -m_3$ and $A_1'(5,1) = m_3$.

Similarly, the matrix A_2 is introduced in equation (8.28) in order to express the reactions at the tanker in terms of the yoke degrees of freedom and the reactions at the buoy. It can be shown that this matrix can be written as:-

$$A_2 = \begin{bmatrix} \gamma & \delta & \gamma & 0 & \delta & 0 \\ 0 & 0 & 0 & 1 & 0 & 0 \\ -\delta & \gamma & -\delta & 0 & \gamma & 0 \\ s_2\delta & -s_2\gamma & -s_2\delta & 0 & \gamma s_2 & 0 \\ -\delta\ell_g & \gamma\ell_g & -\delta\ell_g & 0 & \gamma\ell_g & 1 \\ s_2\gamma & s_2\delta & -s_2\gamma & -\ell_g & -s_2\delta & 0 \end{bmatrix} \qquad (G.7)$$

By expanding the last term on the LHS of equation (8.29) it can be shown that the matrix A_3 which appears in equation (8.30) is an 8 x 8 matrix which can be found by transposing A_c and adding two columns of zeros to the right hand side.

The matrix M_E which appears in equation (8.58) is given by:-

$$M_E = \begin{bmatrix} 1 & 0 & 0 & 0 & 0 & 0 & 0 & 0 \\ 0 & 1 & 0 & 0 & 0 & 0 & 0 & 0 \\ 0 & 0 & 0 & 0 & 0 & 1 & 0 & 0 \end{bmatrix}^T \qquad (G.8)$$

The matrix A_4 which appears in equation (8.48) can be shown to be:-

$$A_4 = \begin{bmatrix} 1 & 0 & 1 & 0 & 0 & 0 \\ 0 & 0 & 0 & 1 & 0 & 0 \\ 0 & 1 & 0 & 0 & 1 & 0 \\ 0 & -s_2 & 0 & -s_3 & s_2 & 0 \\ s_3 & -s_1 & s_3 & 0 & -s_1 & 0 \\ s_2 & 0 & -s_2 & s_1 & 0 & 1 \end{bmatrix} \qquad (G.9)$$

G.4. The Equations of Motion

It can be shown from the analysis of Chapter 8 that the equations of motion of the system can be written in the final form:-

$$[M+M_{TA}-M_1]\ddot{\underset{\sim}{Q}} + [D_S+D_C-M_2]\dot{\underset{\sim}{Q}} + [k_h+k_c-M_4]\underset{\sim}{Q} = \underset{\sim}{F_T} + [A_3]\underset{\sim}{F_B} \qquad (G.10)$$

where:-

M = Mass matrix for the tanker

M_{TA} = Frequency dependent added mass matrix for the tanker, as given in section 5.2.1.

D_S = Frequency dependent potential damping matrix for the tanker, as given in section 5.2.2.

D_C = Damping matrix for the tanker which is caused by current effects, as discussed in section 5.3.1.

k_h = Hydrostatic stiffness matrix for the tanker, as given in section 5.2.3.

k_c = Stiffness matrix for the tanker which is caused by current effects, as discussed in section 5.3.1.

The above matrices are expanded from 6 x 6 to 8 x 8 by the addition of two rows and two columns of zeros. The vectors $\underset{\sim}{F}_T$ and $\underset{\sim}{F}_B$ in the above equation are those which appear on the right hand side of equation (8.30) and which are described in section 8.2.2. The matrix M_4 has the form:-

$$M_4 = M_3 - [A_C]^T[S][A_C] \qquad (G.11)$$

where $|S|$ is the linearised 6 x 6 stiffness matrix for the buoy (see section 3.5) and A_C is given in equation (G.2). The matrices M_1, M_2 and M_3 are symmetric and can be written as follows:-

$$M_1 = \begin{bmatrix} C_{13} & 0 & C_{14} & 0 & C_{15} & 0 & C_{16} & 0 \\ & C_{17} & 0 & C_{18} & 0 & C_{19} & 0 & 0 \\ & & C_{20} & 0 & C_{21} & 0 & C_{22} & 0 \\ & & & C_{23} & 0 & C_{24} & 0 & 0 \\ & & & & C_{25} & 0 & C_{26} & 0 \\ & & & & & C_{27} & 0 & 0 \\ & & & & & & C_{28} & 0 \\ & & & & & & & C_{29} \end{bmatrix} \qquad (G.12)$$

$$M_2 = \begin{bmatrix} C_{30} & 0 & C_{31} & 0 & C_{32} & 0 & C_{33} & 0 \\ & C_{34} & 0 & C_{35} & 0 & C_{36} & 0 & 0 \\ & & C_{37} & 0 & C_{38} & 0 & C_{39} & 0 \\ & & & C_{40} & 0 & C_{41} & 0 & 0 \\ & & & & C_{42} & 0 & C_{43} & 0 \\ & & & & & C_{44} & 0 & 0 \\ & & & & & & C_{45} & 0 \\ & & & & & & & 0 \end{bmatrix} \qquad (G.13)$$

$$M = \begin{bmatrix} 0 & 0 & 0 & 0 & 0 & 0 & 0 & 0 \\ & 0 & 0 & 0 & 0 & 0 & 0 & 0 \\ & & C_{46} & 0 & C_{47} & 0 & C_{48} & 0 \\ & & & C_{49} & 0 & C_{50} & 0 & 0 \\ & & & & C_{51} & 0 & C_{52} & 0 \\ & & & & & C_{53} & 0 & 0 \\ & & & & & & C_{54} & 0 \\ & & & & & & & 0 \end{bmatrix} \qquad (G.14)$$

where:-

$C_{13} = -M_y - M - M_{11} C_1^2 - M_{33} C_2^2 - 2M_{13} C_1 C_2$

$C_{14} = C_1 C_2 (M_{11} + M_{33}) + M_{13} (C_2^2 - C_1^2)$

$C_{15} = -(M+M_y) s_3 - M_{13} 2 s_3 C_1 C_2 - M_{11} C_1 C_3 - M_{33} C_2 C_7$

$C_{16} = -\delta M_y \ell g - M(C_4 C_1 + C_2 C_8) - M_{13} (C_1 C_8 + C_4 C_2) - M_{11} C_1 C_4 - M_{33} C_2 C_8 - m_{15} C_1$

$C_{17} = -(M_y + M + M_{11})$

$C_{18} = M_y (\delta \ell g + s_3) - (f_3 - e_3)(M + m_{11}) - m_{15} C_1$

$C_{19} = -M_y (\gamma \ell g + s_1) - (M + m_{11}) C_6 + m_{15} C_2$

$C_{20} = -M_y - M - M_{11} C_2^2 - M_{33} C_1^2 + 2M_{13} C_1 C_2$

$C_{21} = s_1 (M_y + M) + M_{11} C_3 C_2 - M_{33} C_7 C_1 + M_{13} [s_3 (C_2^2 - C_1^2) - 2 s_1 C_1 C_2]$

$C_{22} = M(C_4 C_2 - C_8 C_1) + \gamma M_y \ell g + m_{15} C_2 + m_{11} C_4 C_2 - m_{33} C_8 C_1 + M_{13} (C_8 C_2 - C_4 C_1)$

$C_{23} = -\gamma^2 I_{y1} - \delta^2 I_{y3} + (M + m_{11})(s_3 + \delta \ell_m - m_3 C_1) - m_{15} C_1 (m_3 C_1 + C_5 - s_3 - \delta \ell_m)$
$- (I_R + m_{44}) C_1^2 - M_y (s_3 + \delta \ell g)^2$

$C_{24} = \delta\gamma (I_{y3} - I_{y1}) + M_y (\delta\gamma \ell g^2 + \delta \ell g s_1 + \gamma \ell g s_3 + s_3 s_1) - (M + m_{11}) C_6 (C_1 m_3 - \delta \ell_m - s_3)$
$+ m_{15} C_2 (m_3 C_1 - \delta \ell_m - s_3) - m_{15} C_6 C_1 + (I_R + m_{44}) C_1 C_2$

$C_{25} = -M_y (s_1^2 + s_3^2) - M(s_1^2 + s_3^2) - M_{33} C_7^2 - M_{11} C_3^2 - 2M_{13} C_7 C_3$

$C_{26} = -M_y \ell g (\delta s_3 + \gamma s_1) - M(C_4 C_3 + C_8 C_7) - m_{11} C_4 C_3 - m_{33} C_8 C_7 - M_{13} (C_8 C_3 + C_7 C_4) - m_{15} C_3$

$C_{27} = (M + m_{11})(m_3 C_2 - \gamma \ell_m - s_1) + m_{15} C_2 (C_6 + \gamma \ell_m + s_1 - m_3 C_2) - (I_R + m_{44}) C_2^2$
$- \delta^2 I_{y1} - \gamma^2 I_{y3} - M_y (\gamma \ell g + s_1)^2$

$C_{28} = m_3 (M + m_{11}) C_4 + m_3 m_{15} - m_{15} C_4 - (I_R + m_{44}) + m_3 M_{13} C_8$
$- (\gamma C_2 + \delta C_1) [(M + M_{11}) C_4 + m_{15} + C_8 M_{13}] \ell_m + (\gamma C_1 - \delta C_2) [(M + M_{33}) C_8 + C_4 M_{13}] \ell_m$
$- I_{y2} - M_y \ell g^2$

$$C_{29} = -I_y$$

$$C_{30} = -\beta_{33} C_2^2 - \beta_{11} C_1^2$$

$$C_{31} = (\beta_{11} - \beta_{33}) C_1 C_2$$

$$C_{32} = -\beta_{11} C_3 C_1 - \beta_{33} C_7 C_2$$

$$C_{33} = -\beta_{33} C_8 C_2 - \beta_{11} C_4 C_1 - \beta_{15} C_1$$

$$C_{34} = -\beta_{22}$$

$$C_{35} = \beta_{22} (e_3 - f_3) - \beta_{24} C_1$$

$$C_{36} = -\beta_{22} (s_1 + \gamma \ell_m - m_3 C_2) + \beta_{24} C_2$$

$$C_{37} = -\beta_{11} C_2^2 - \beta_{33} C_1^2$$

$$C_{38} = \beta_{11} C_2 C_3 - \beta_{33} C_2 C_7$$

$$C_{39} = \beta_{11} C_4 C_2 + \beta_{15} C_2 - \beta_{33} C_8 C_1$$

$$C_{40} = \beta_{22} C_5 (s_3 + \delta \ell_m - m_3 C_1) + \beta_{24} C_1 (s_3 + \delta \ell_m - m_3 C_1 - C_5) - \beta_{44} C_1^2$$

$$C_{41} = \beta_{44} C_1 C_2 + \beta_{22} [(s_1 + \gamma \ell_m - m_3 C_2)(-m_3 C_1 + \delta \ell_m + s_3)]$$
$$- \beta_{24} [(s_1 + \gamma \ell_m - 2m_3 C_2) C_1 + (\delta \ell_m + s_3) C_2]$$

$$C_{42} = -\beta_{11} C_3^2 - \beta_{33} C_7^2$$

$$C_{43} = -(\beta_{11} C_4 + \beta_{15}) C_3 - \beta_{33} C_9 C_7$$

$$C_{44} = \beta_{24} C_2 (\gamma \ell_m + s_1 + C_6 - m_3 C_2) + \beta_{22} C_6 (m_3 C_2 - s_1 - \gamma \ell_m) - \beta_{44} C_2^2$$

$$C_{45} = \beta_{11} C_4 (m_3 - \ell_m \gamma C_2 - \ell_m \delta C_1) + \beta_{15} (m_3 - C_4 - \ell_m \gamma C_2 - \ell_m \delta C_1) - \beta_{55} + (\gamma C_1 - \delta C_2) \ell_m \beta_{33} C_8$$

$$C_{46} = -k_1$$

$$C_{47} = t_1 k_1$$

$$C_{48} = k_1 (\ell_m \sin\alpha C_1 - \ell_m \cos\alpha C_2 - m_3 C_2)$$

$$C_{49} = -k_2 C_1^2$$

$$C_{50} = k_2 C_1 C_2$$

$$C_{51} = -s_1 t_1 k_1$$

$$C_{52} = -s_1 k_1 (\ell_m \sin\alpha C_1 - \ell_m \cos\alpha C_2 - m_3 C_2)$$

$$C_{53} = -k_2 C_2^2$$

$$C_{54} = k_1 \ell_m \gamma [C_8 C_1 - C_4 C_2]$$

found from the method outlined in section 8.3.4. The mass of the yoke and its moments of inertia in roll, pitch and yaw have been represented by M_y, I_{y1}, I_{y2} and I_{y3}.

and the mass, added mass, damping and hydrostatic stiffness matrices for the buoy in q coordinates are taken to be:-

$$M_B+M_{BA} = \begin{bmatrix} M+M_{11} & 0 & M_{13} & 0 & m_{15} & 0 \\ 0 & M+m_{11} & 0 & m_{15} & 0 & 0 \\ M_{13} & 0 & M+M_{33} & 0 & 0 & 0 \\ 0 & m_{15} & 0 & I_R+m_{44} & 0 & 0 \\ m_{15} & 0 & 0 & 0 & I_R+m_{44} & 0 \\ 0 & 0 & 0 & 0 & 0 & I_y \end{bmatrix}$$

$$D_B = \begin{bmatrix} \beta_{11} & 0 & 0 & 0 & \beta_{15} & 0 \\ 0 & \beta_{22} & 0 & \beta_{24} & 0 & 0 \\ 0 & 0 & \beta_{33} & 0 & 0 & 0 \\ 0 & \beta_{24} & 0 & \beta_{44} & 0 & 0 \\ \beta_{15} & 0 & 0 & 0 & \beta_{55} & 0 \\ 0 & 0 & 0 & 0 & 0 & 0 \end{bmatrix}$$

$$k_h = \begin{bmatrix} k_1 \sin^2 f_5 & 0 & -k_1 \sin f_5 \cos f_5 & 0 & 0 & 0 \\ 0 & 0 & 0 & 0 & 0 & 0 \\ -k_1 \sin f_5 \cos f_5 & 0 & k_1 \cos^2 f_5 & 0 & 0 & 0 \\ 0 & 0 & 0 & k_2 & 0 & 0 \\ 0 & 0 & 0 & 0 & k_3 & 0 \\ 0 & 0 & 0 & 0 & 0 & 0 \end{bmatrix}$$

where:-

$$M_{11} = m_{11} \cos^2 f_5 + m_{33} \sin^2 f_5$$

$$M_{13} = m_{11} \cos f_5 \sin f_5 - m_{33} \cos f_5 \sin f_5$$

$$M_{33} = m_{11} \sin^2 f_5 + m_{33} \cos^2 f_5$$

and m_{ij} and k_i represent the added masses and hydrostatic stiffnesses of an upright buoy. β_{ij} is a linearised damping coefficient which can be

F I G U R E S

SYSTEM	FIELD	DESIGN WAVE (M)	DESIGN CURRENT (M/S)	WATER DEPTH (M)	TANKER SIZE (DWT)	DATE INSTALLED
SBS	CADLAO	16.8	-	93.0	120,000	
SBS	ASHTART I	12.3	1.29	66.0	70,000	1974
SBS	ASHTART II	12.3	1.29	66.0	135.000	1979
SBS	SOUTH NIDO	12.0	1.03	60.0	70,000	1979
SBS	UDANG	11.7	1.49	91.5	102,000	1979
SBS	POLENG	8.1	1.54	54.0	70.000	1975
SBS	ARDJUNA	8.1	1.80	42.0	66,000	1976
SBS	ARZANAH	7.5	1.54	32.1	252,000	1979
YOKE-CALM	ERWAIN	14.4	-	64.2	85,000	
YOKE-CALM	FATEH	10.8	1.80	39.0	126,000	1980
YOKE-SALM	SANTA BARBARA	12.3	1.03	147.0	50,000	1981
YOKE TOWER	FULMAR	25.5	1.23	81.0	210,000	1980
YOKE TOWER	GAROUPA	15.3	1.80	120.0	54.000	1979
SALS	NILDE	18.0	1.18	93.6	84.000	1979
SALS	CASTELLON	15.6	1.29	116.7	58,000	1977
SALS	PULAI	13.2	1.29	66.0	167.000	1978

FIG. 1.1 YOKE MOORINGS IN SERVICE AROUND THE WORLD

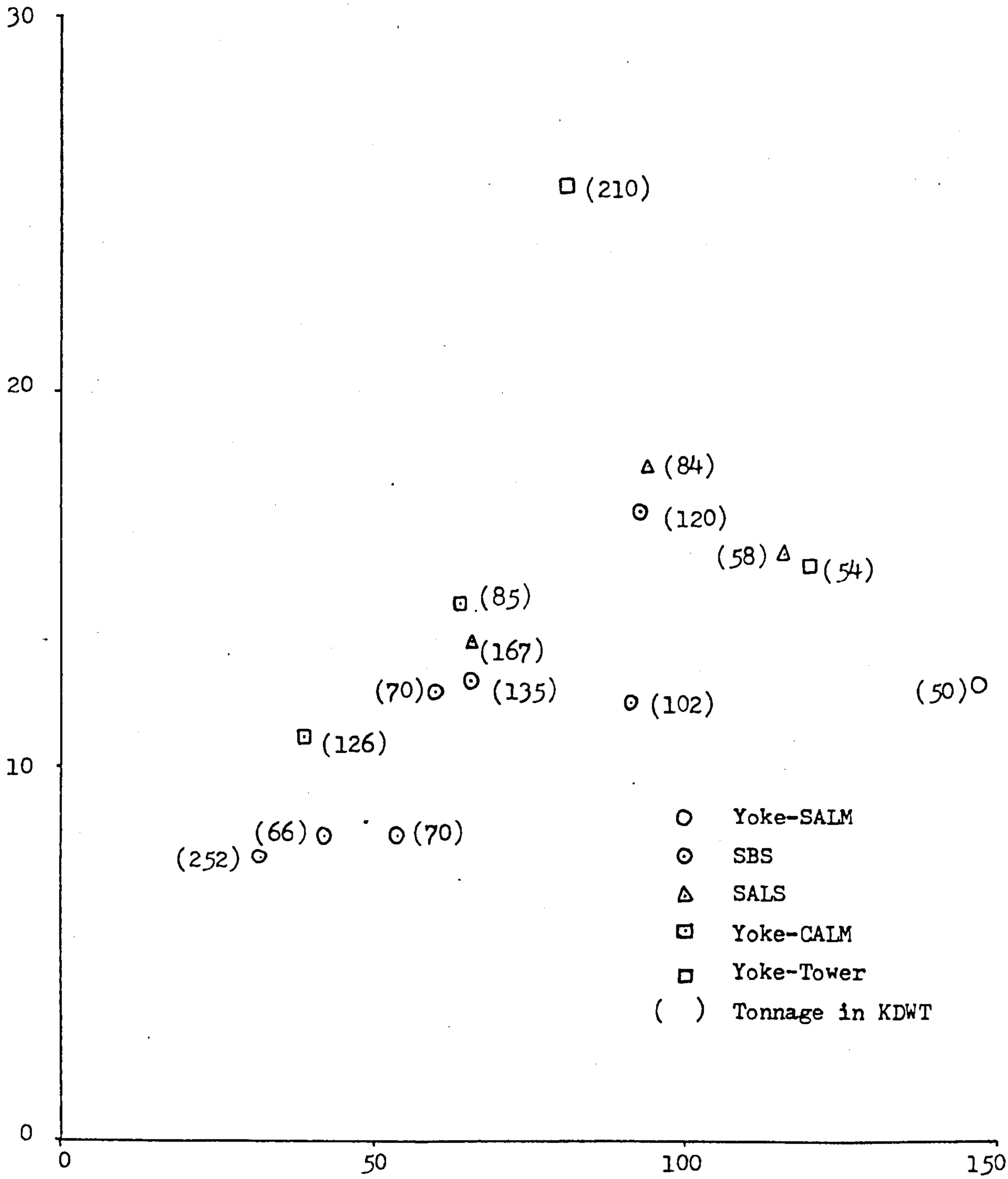

FIG. 1.2 YOKE MOORING SYSTEMS CURRENTLY IN SERVICE

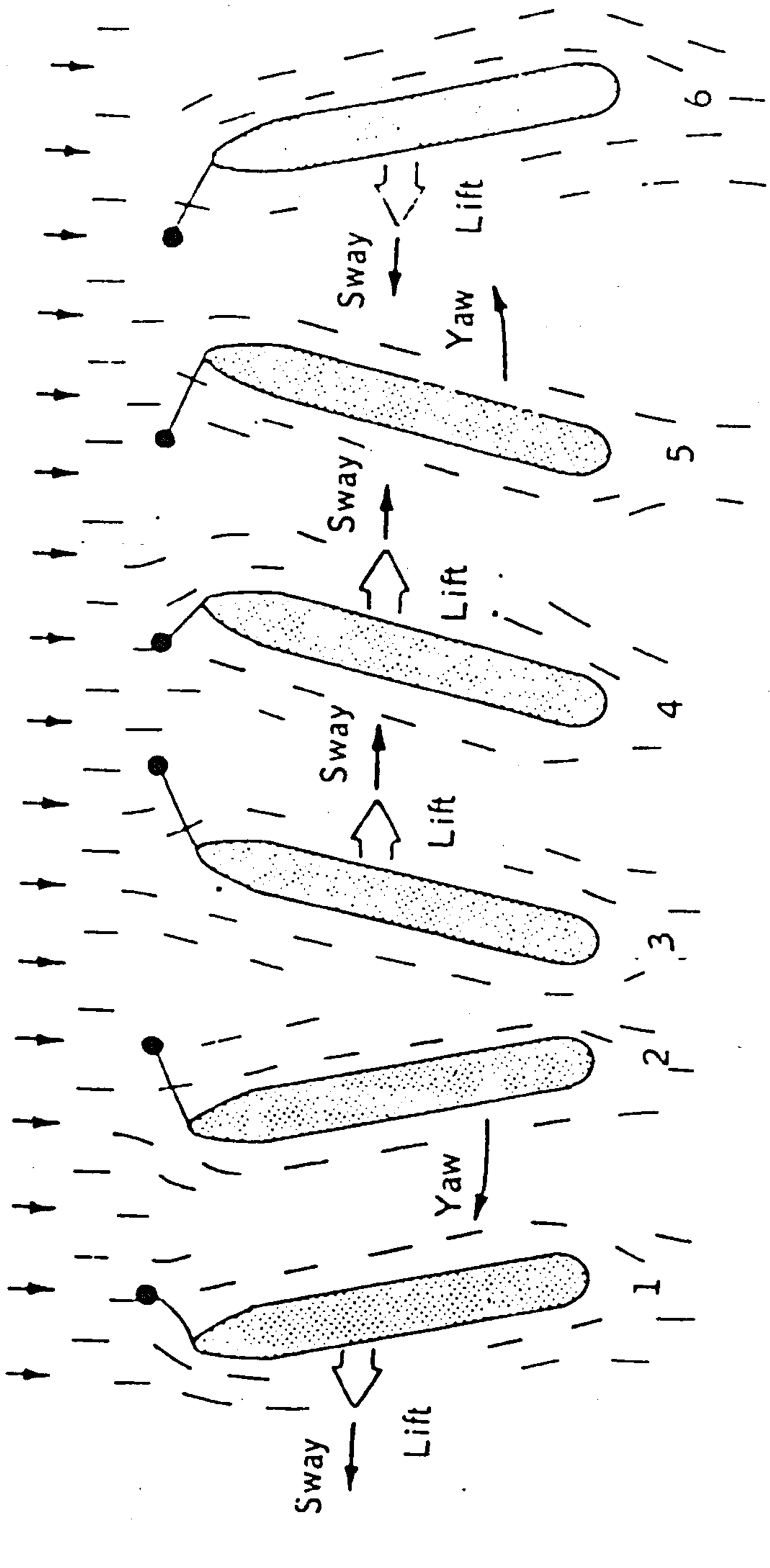

FIG. 1.3 FISHTAILING MOTIONS OF A SINGLE POINT MOORING TERMINAL

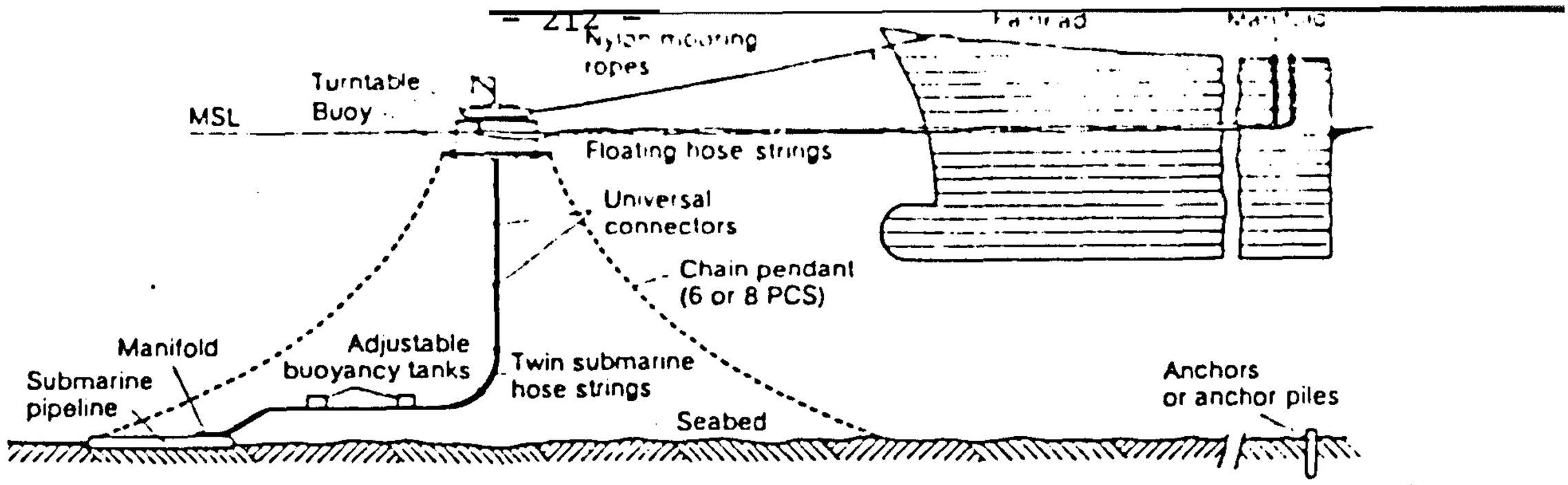

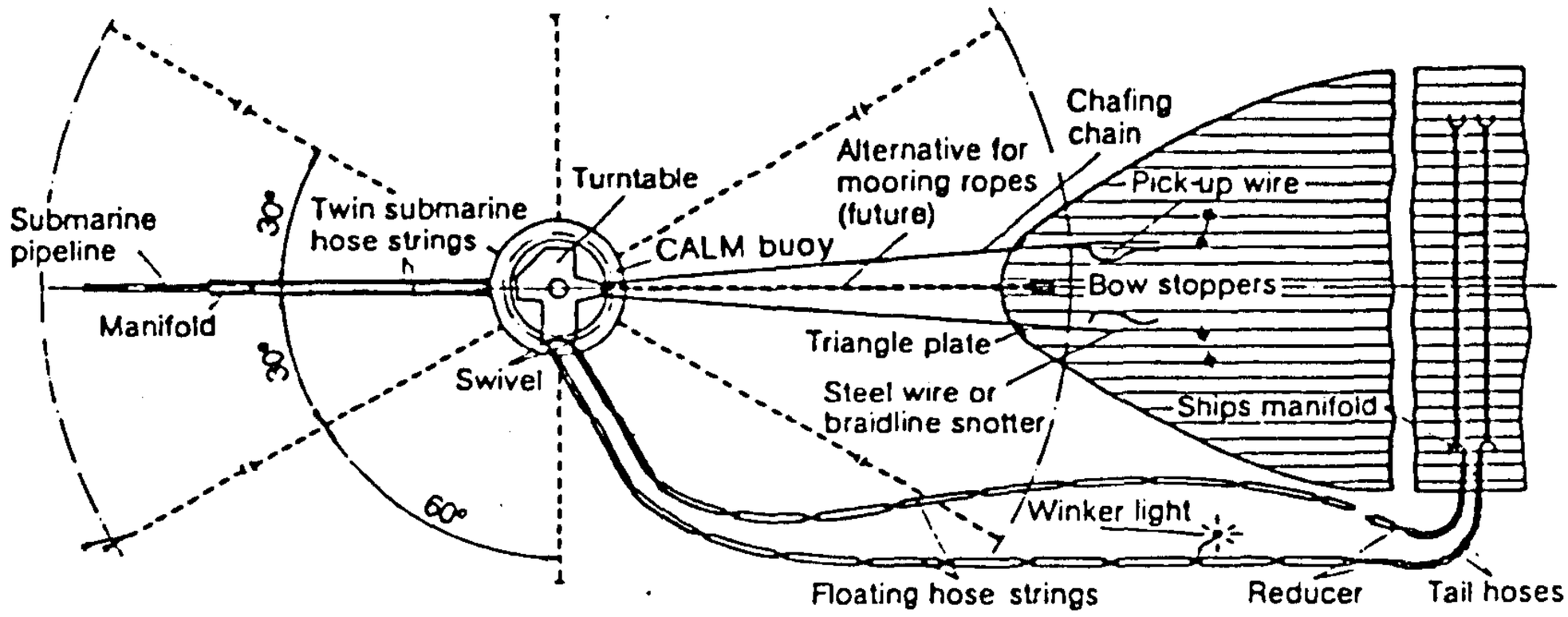

FIG. 1.4 THE CALM SYSTEM

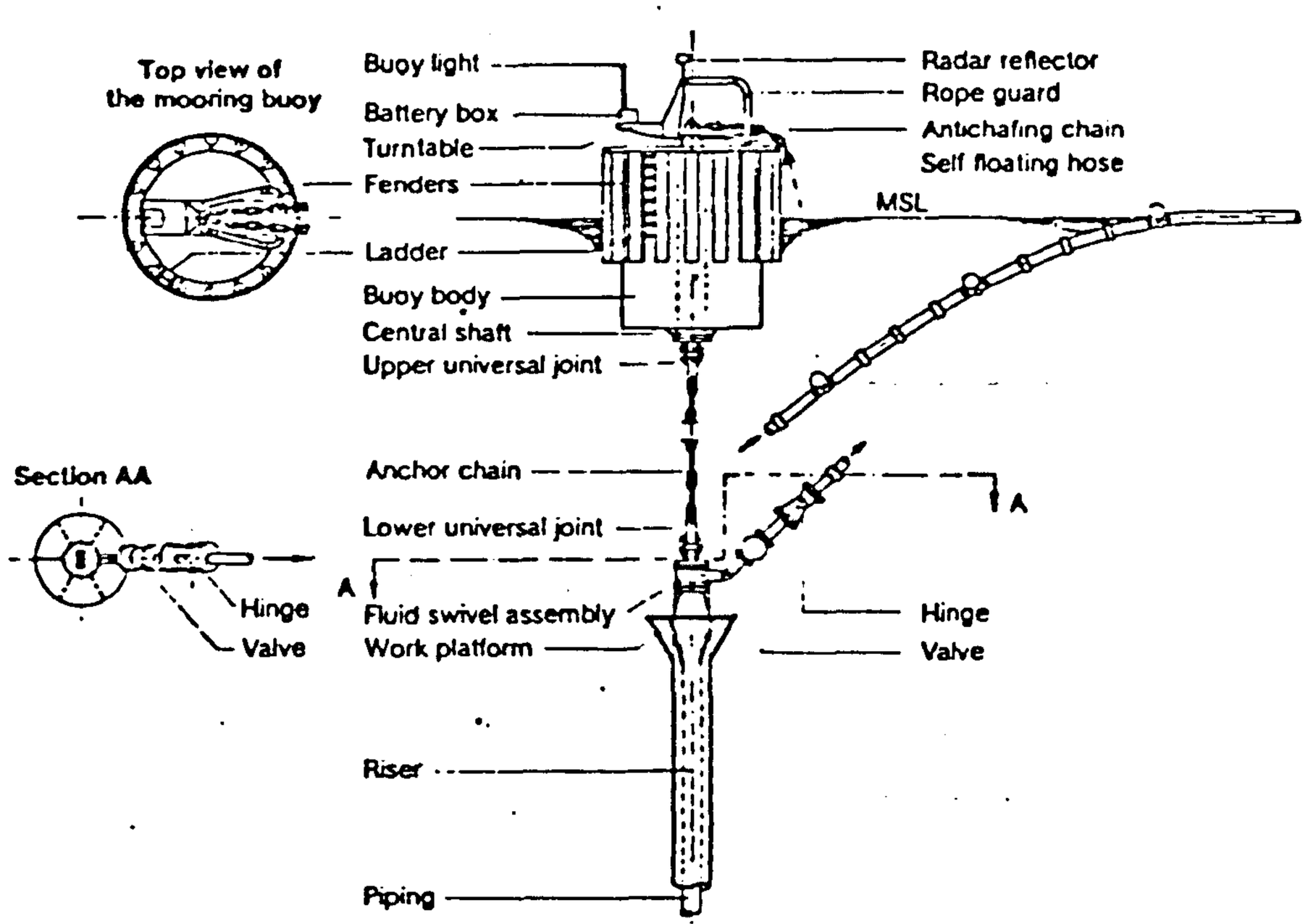

FIG. 1.5 THE SALM SYSTEM

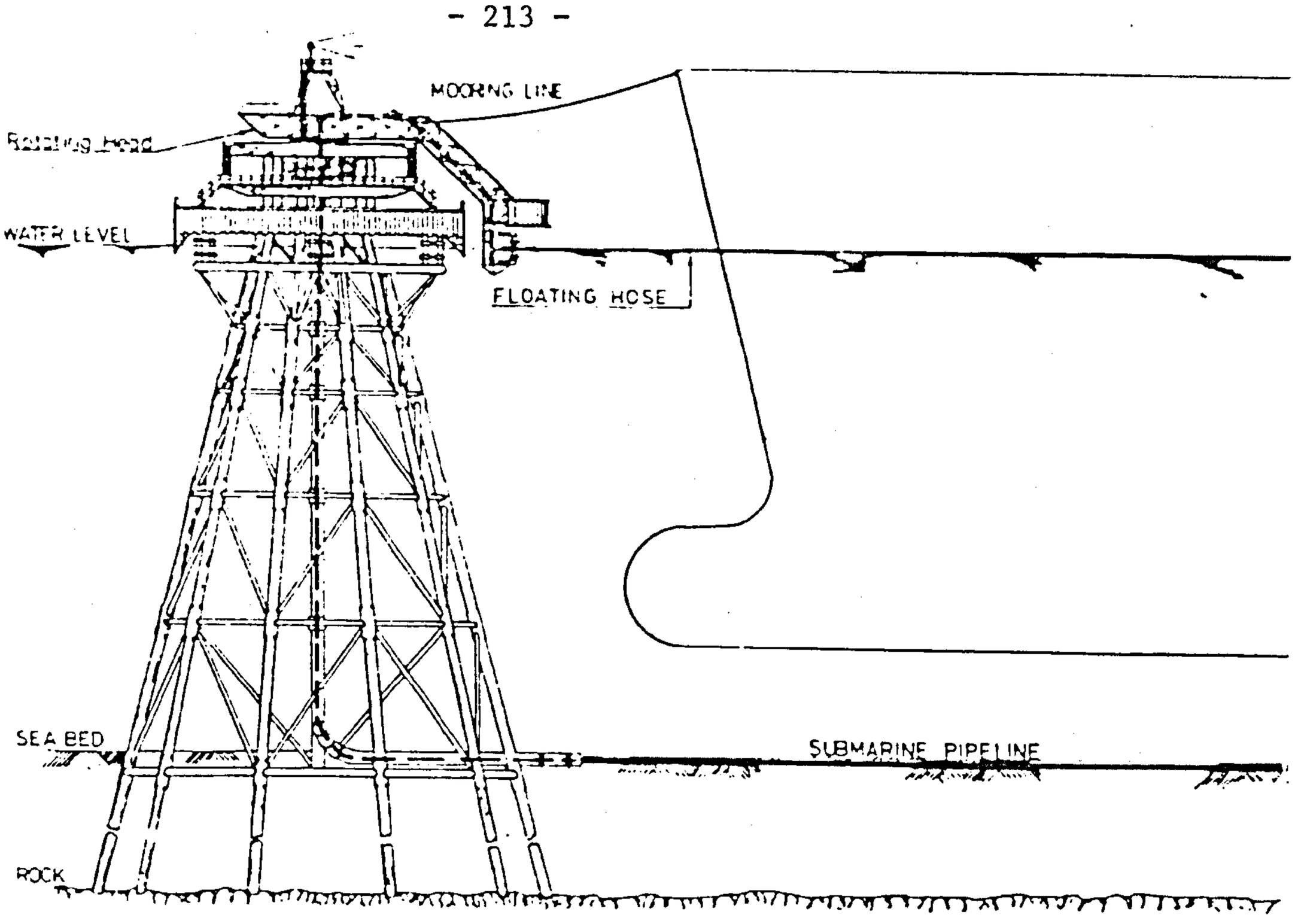

FIG. 1.6 THE FIXED TOWER

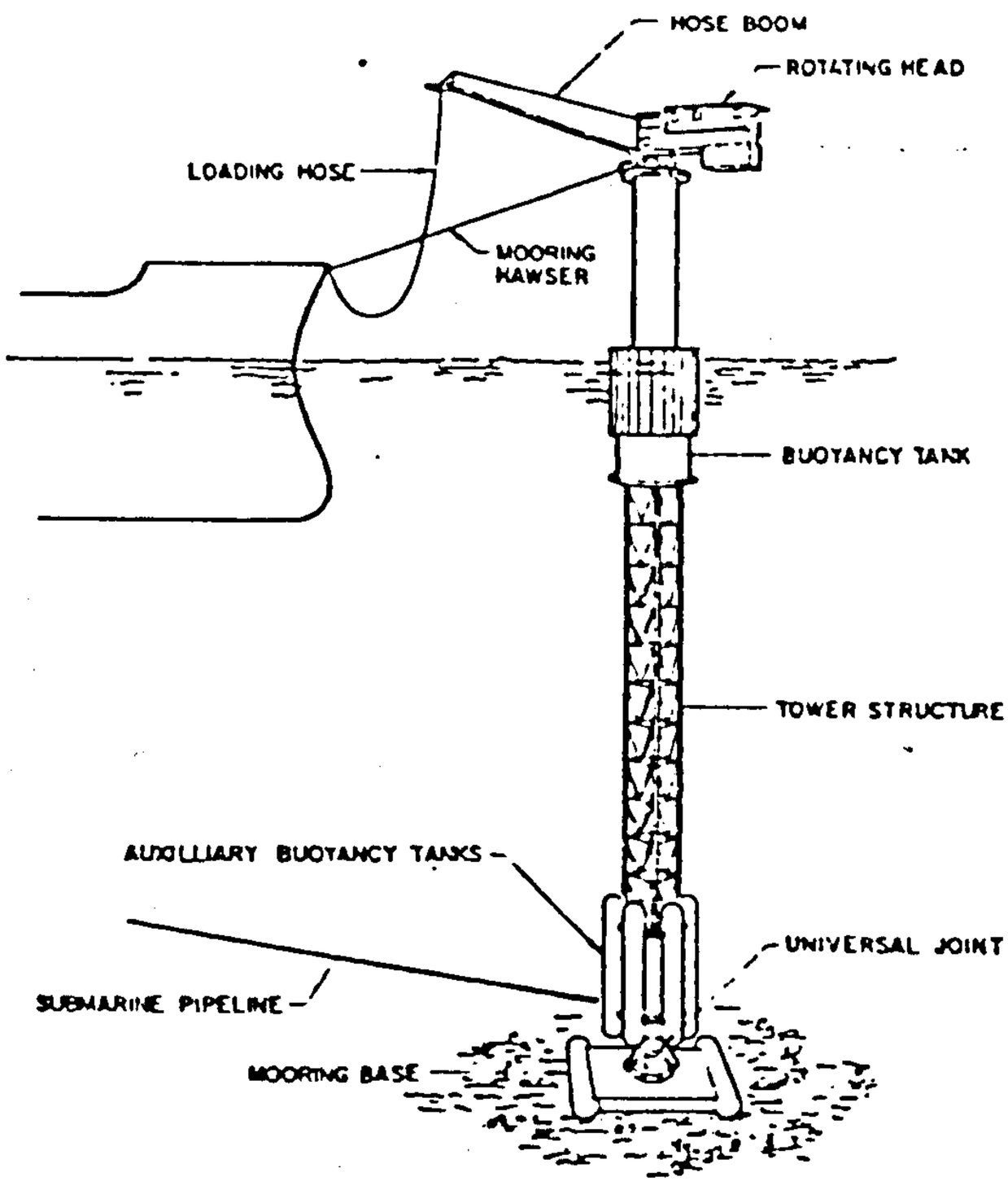

FIG. 1.7 THE ARTICULATED TOWER

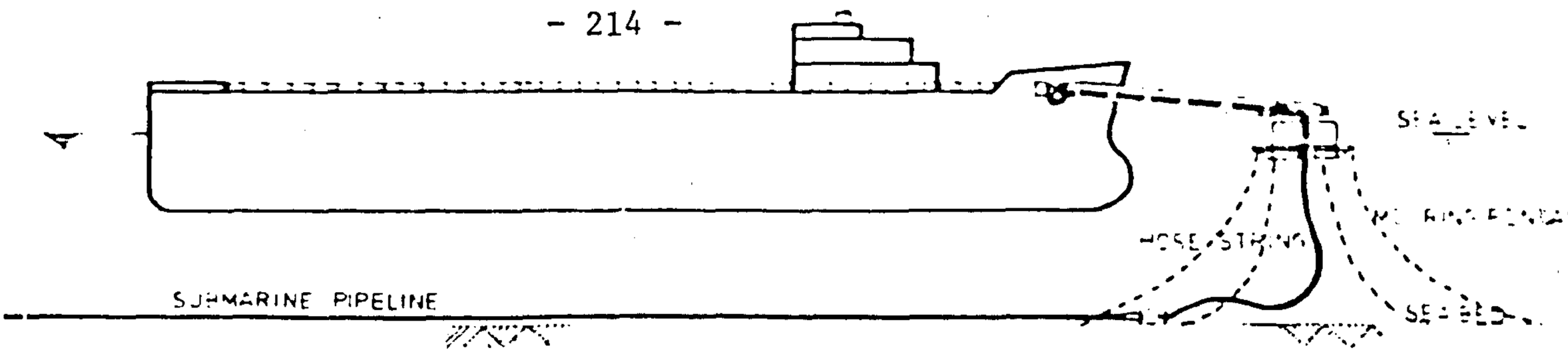

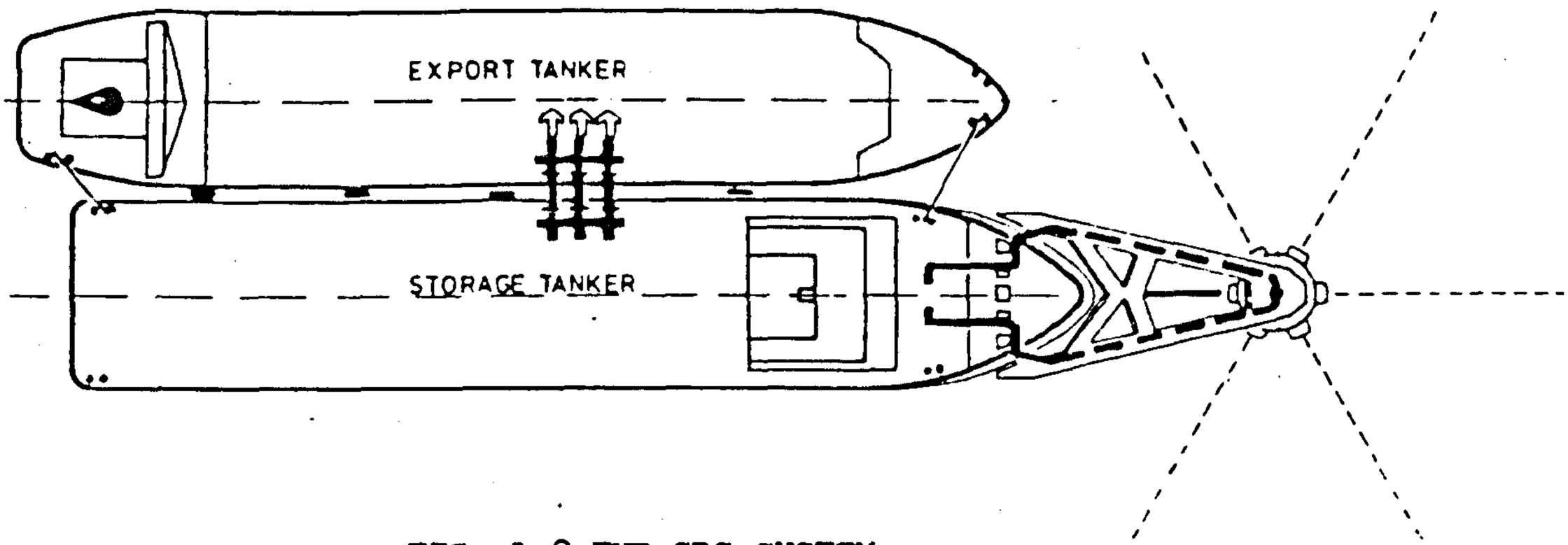

FIG. 1.8 THE SBS SYSTEM

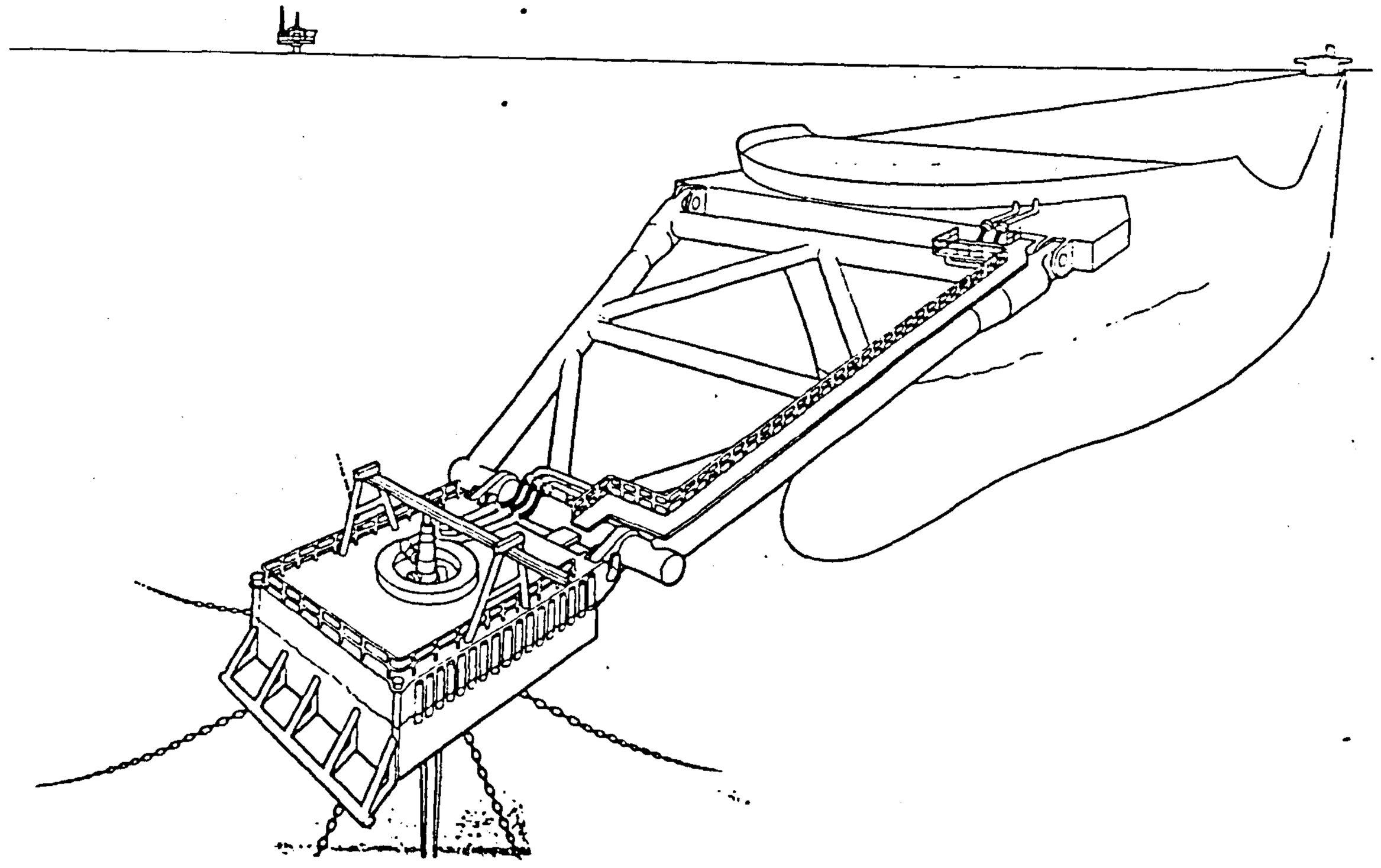

FIG. 1.9 THE YOKE-CALM SYSTEM

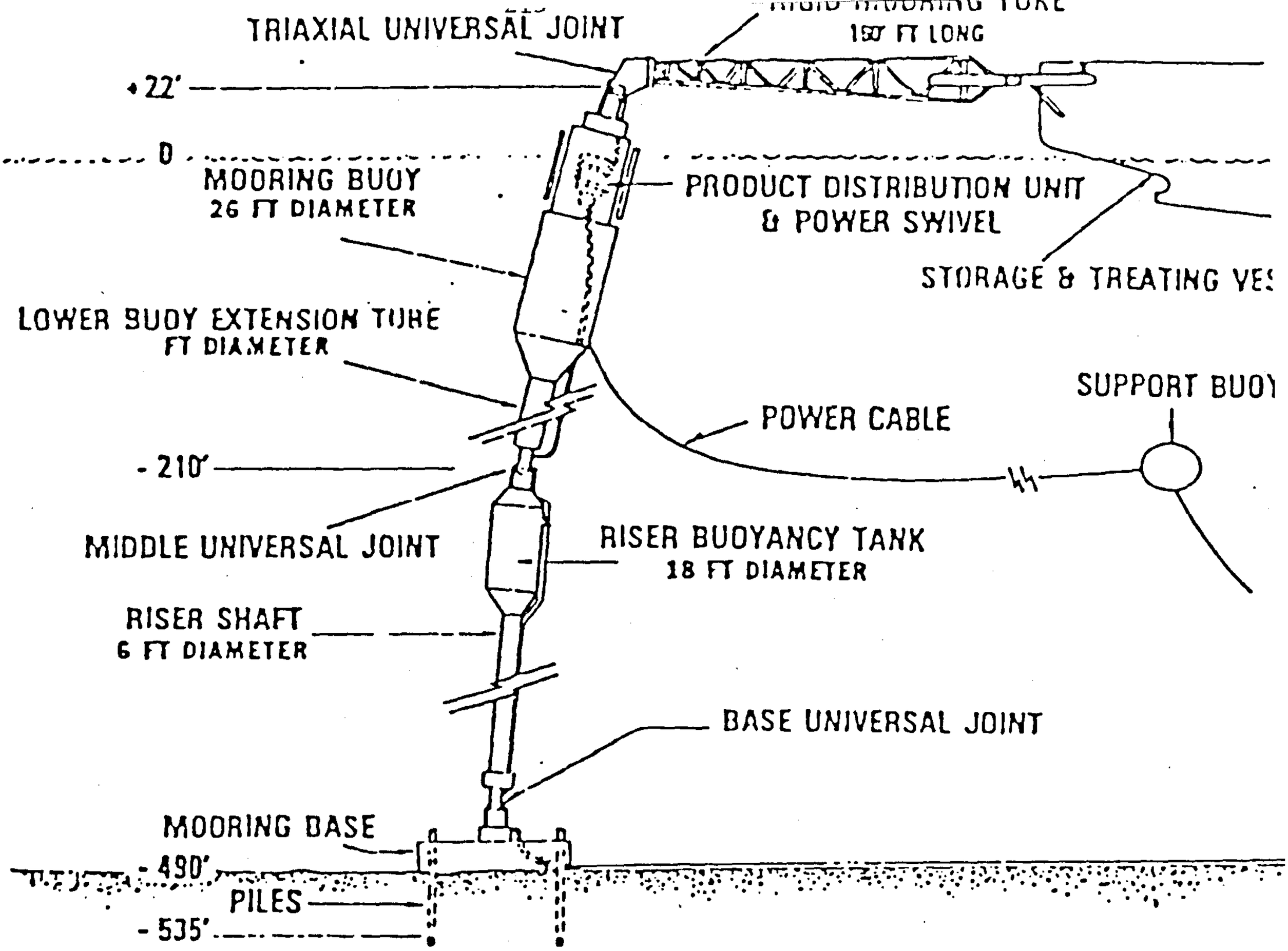

FIG. 1.10 THE YOKE-SALM SYSTEM

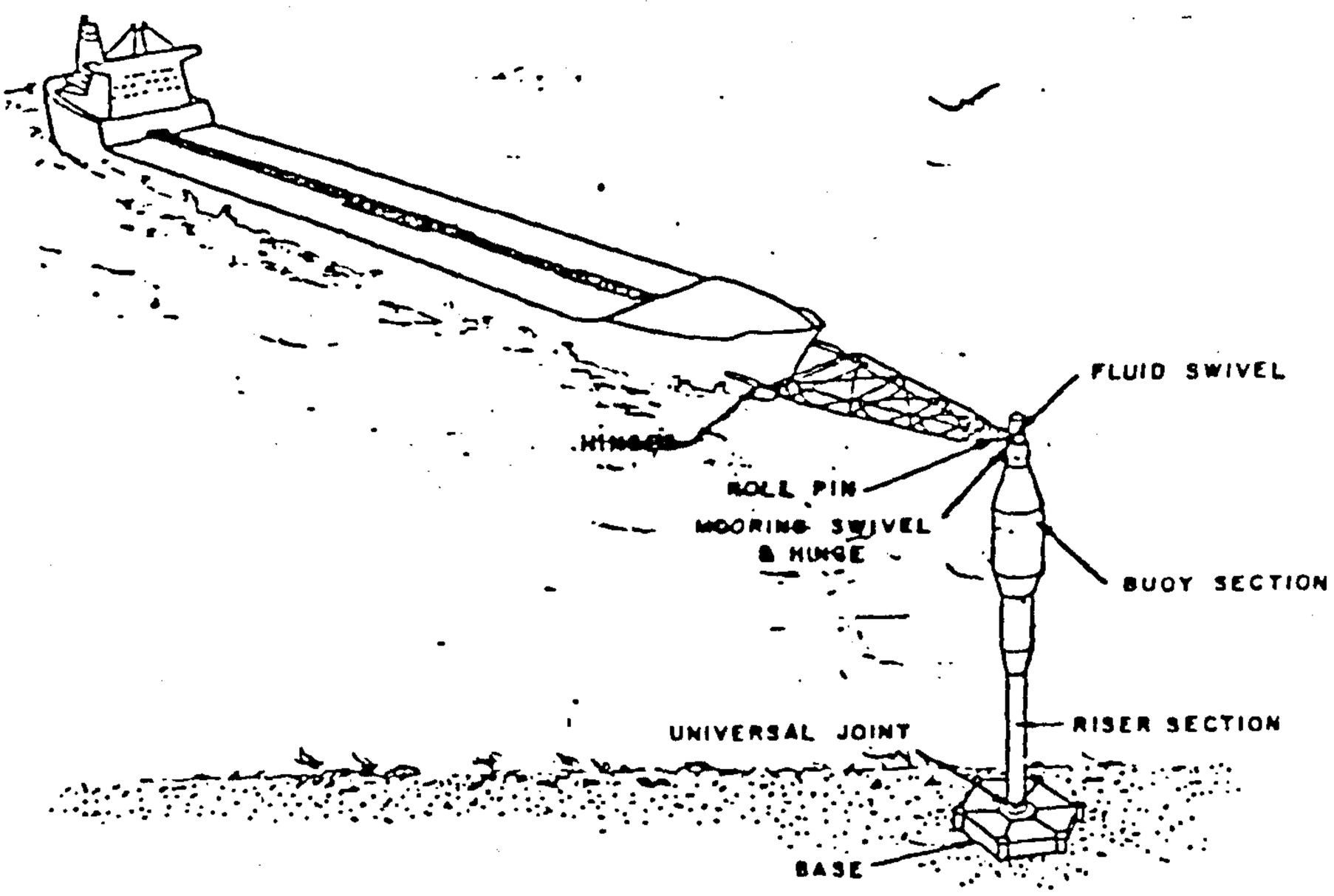

FIG. 1.11 THE YOKE-TOWER SYSTEM

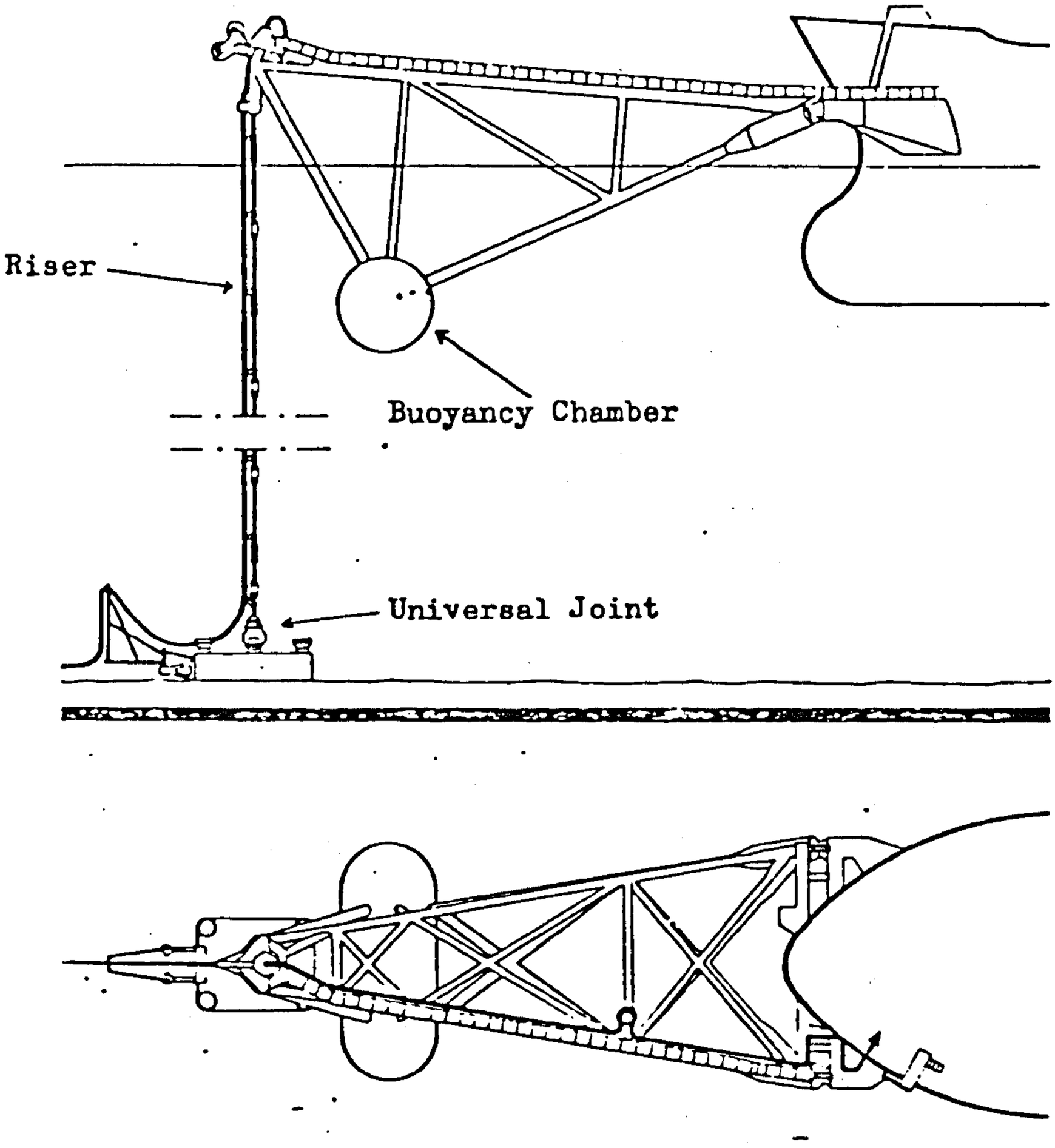

FIG. 1.12 THE SALS SYSTEM

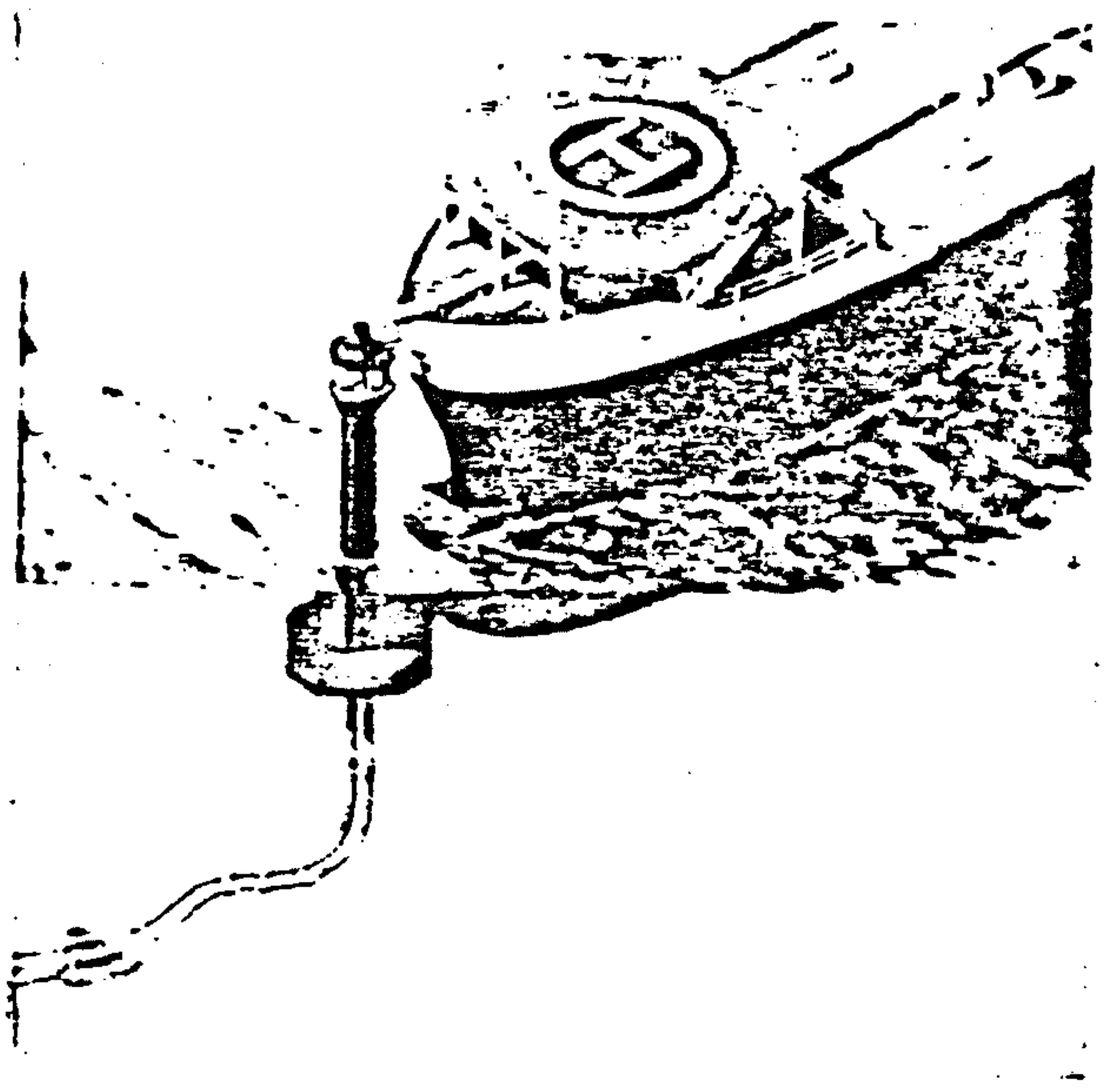

FIG. 1.13 THE IMODCO BOW MOORING SYSTEM

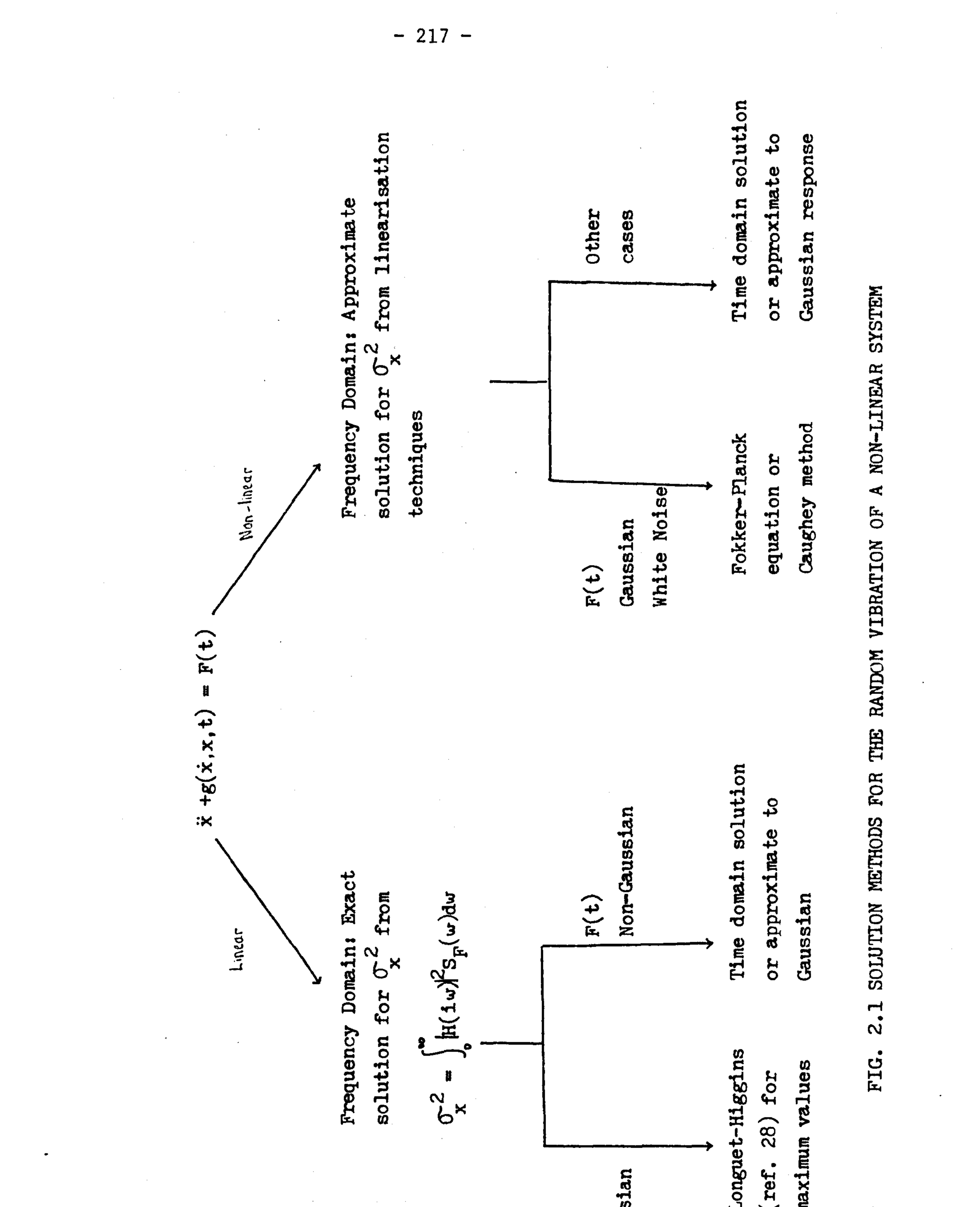

FIG. 2.1 SOLUTION METHODS FOR THE RANDOM VIBRATION OF A NON-LINEAR SYSTEM

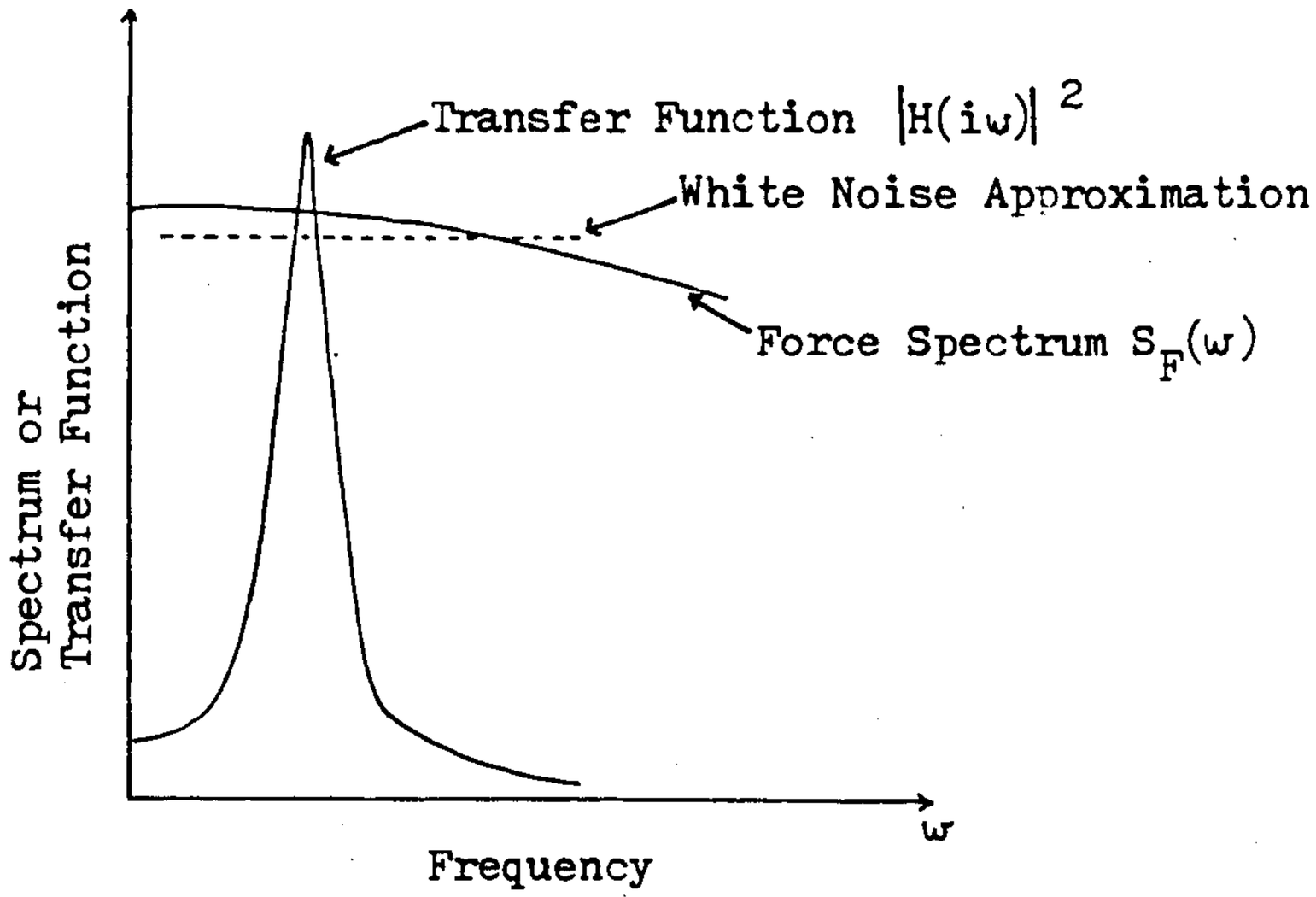

FIG. 2.2 WHITE NOISE APPROXIMATION FOR A LIGHTLY DAMPED SYSTEM

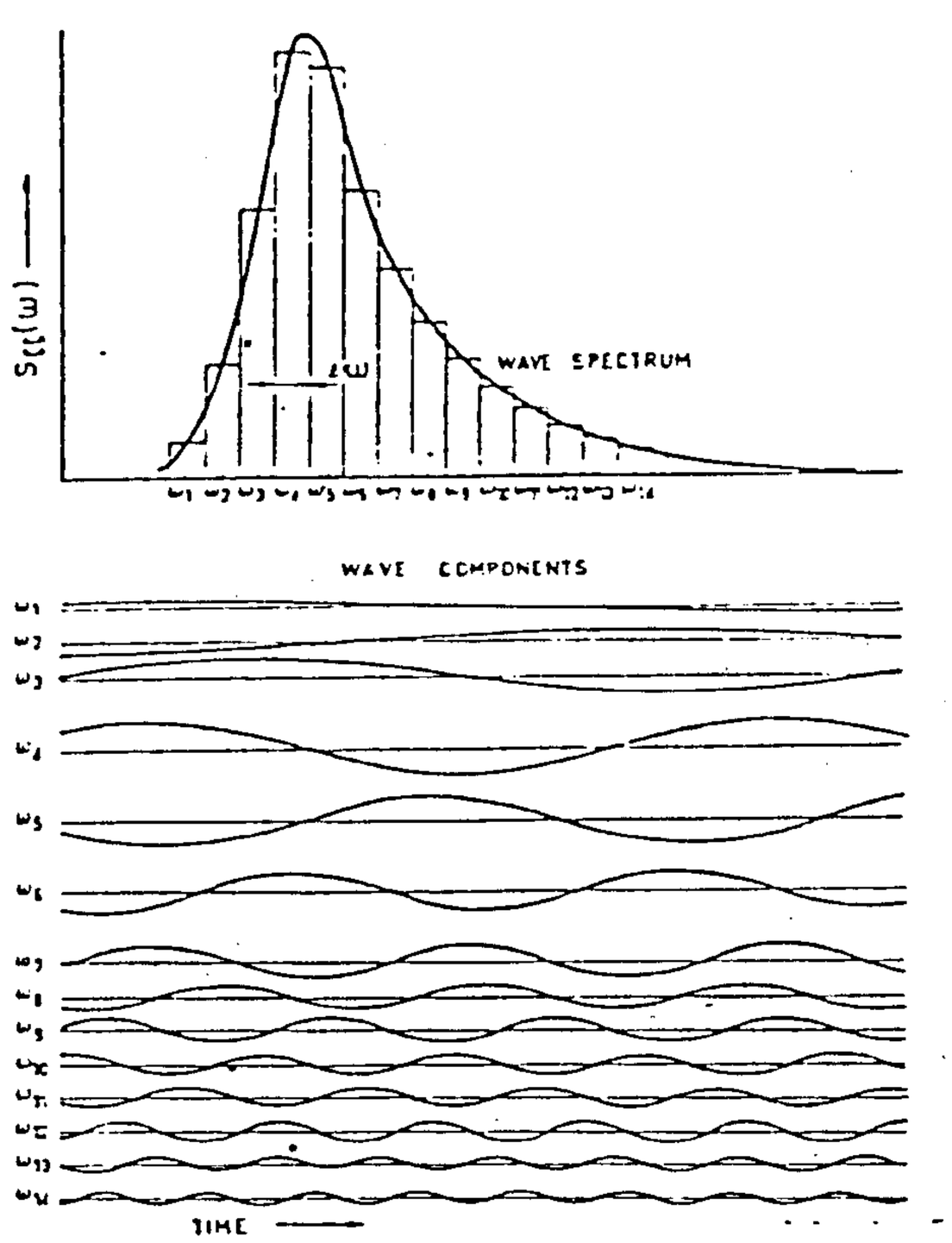

FIG. 2.3 MONTE-CARLO REPRESENTATION OF A RANDOM SEASTATE

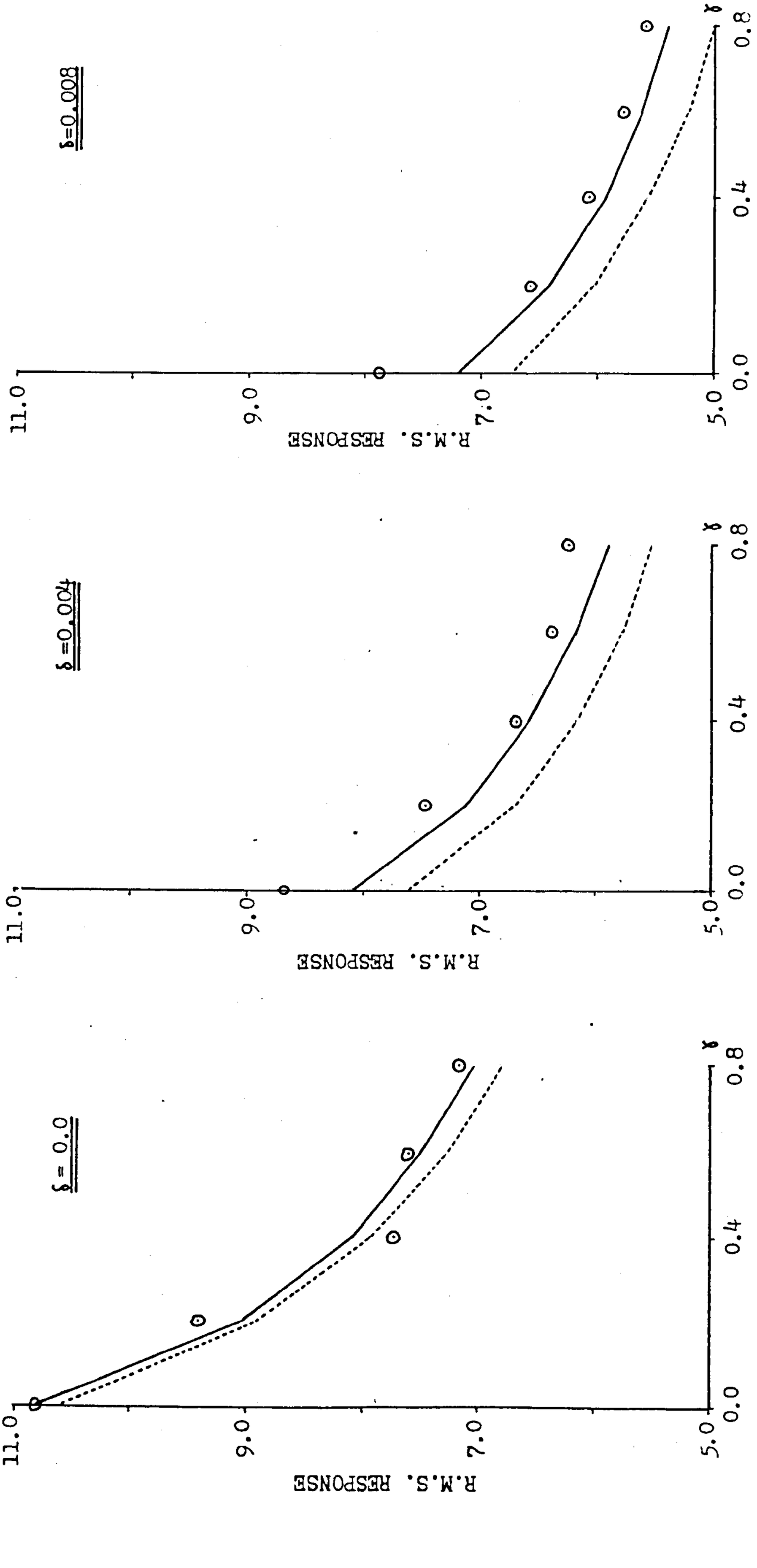

FIG. 2.4 R.M.S. RESPONSE FOR VARIOUS VALUES OF γ AND δ

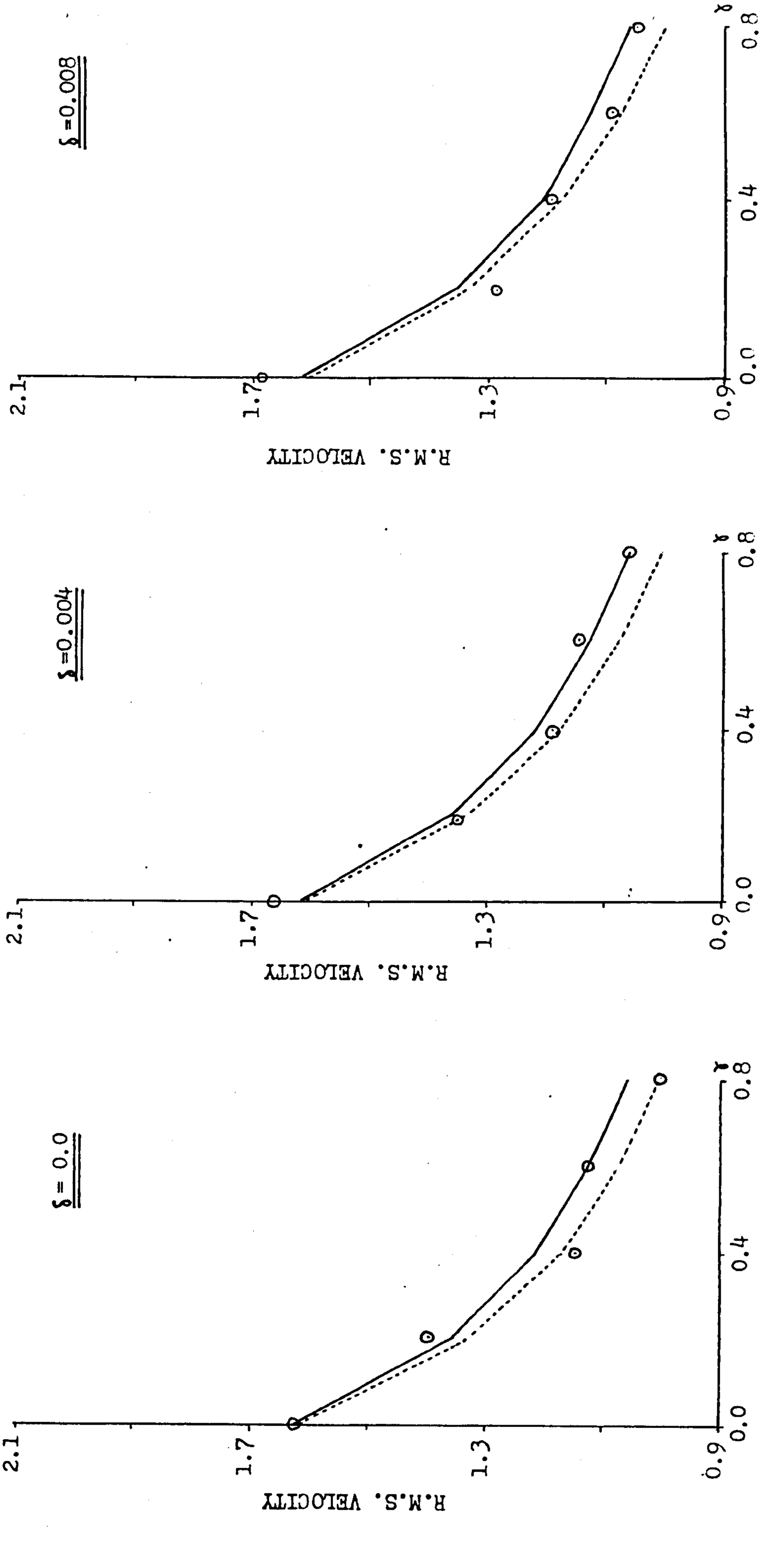

FIG. 2.5 R.M.S. VELOCITY FOR VARIOUS VALUES OF γ AND δ

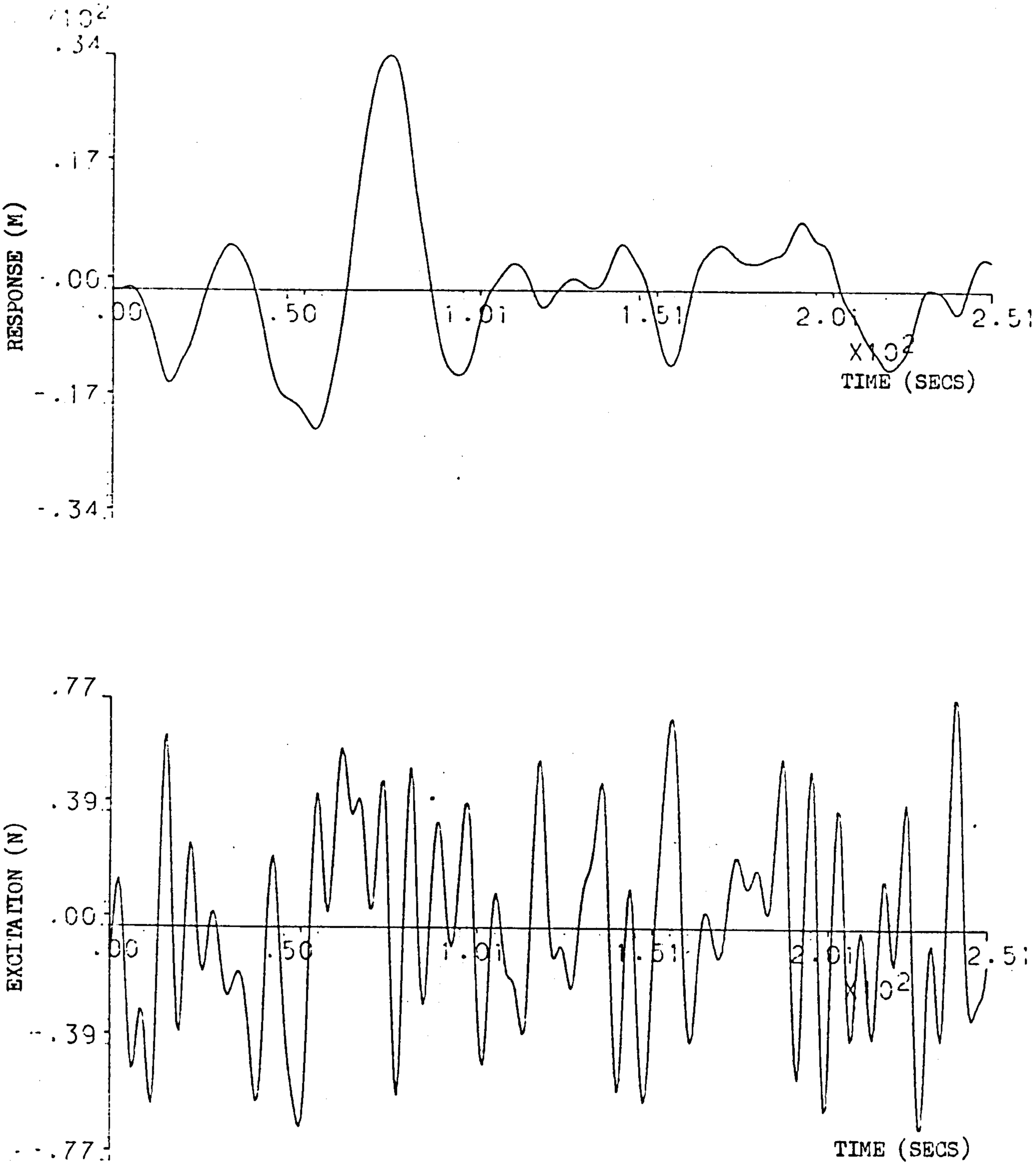

FIG. 2.6 RESPONSE FOR $\gamma = \delta = 0.0$

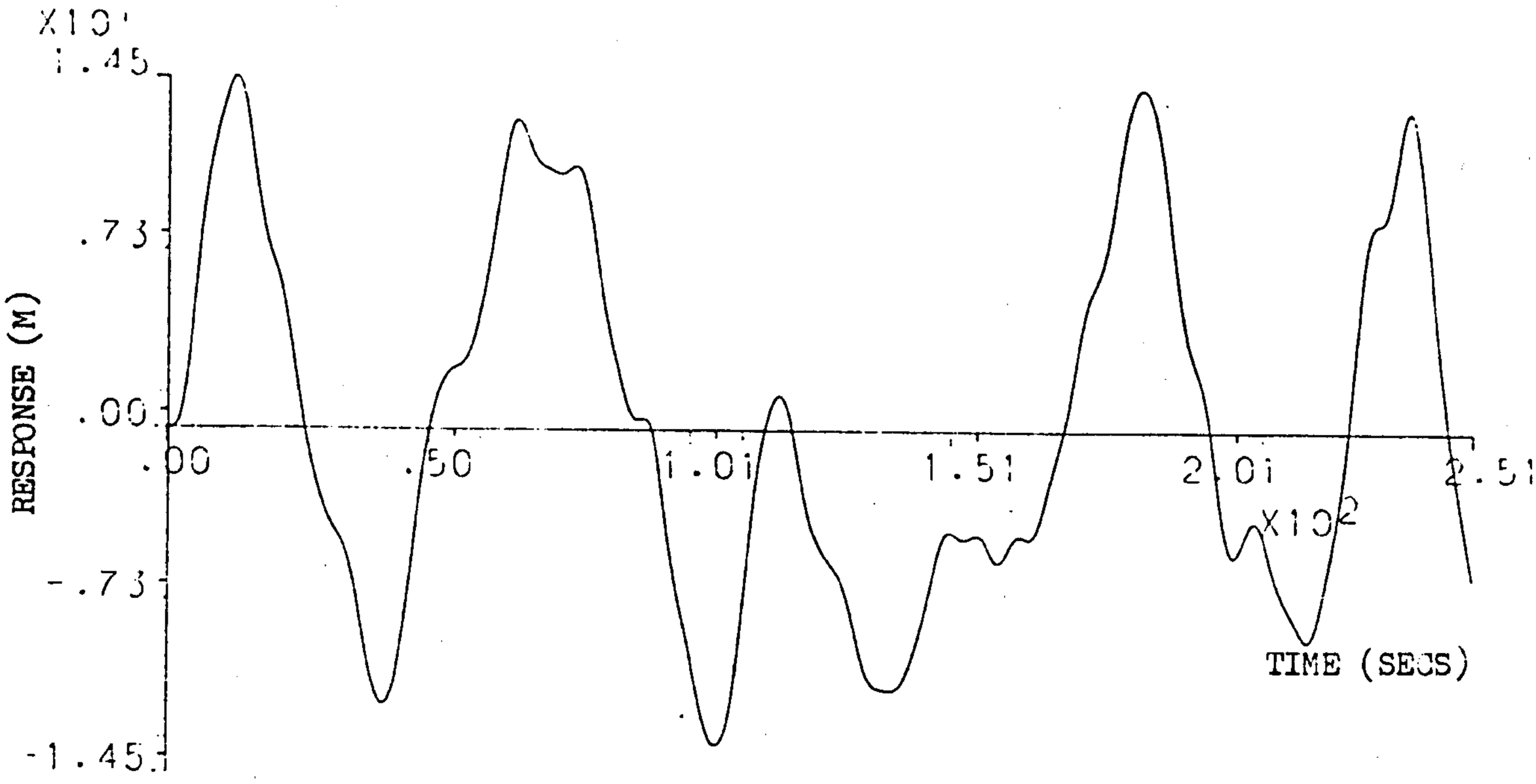

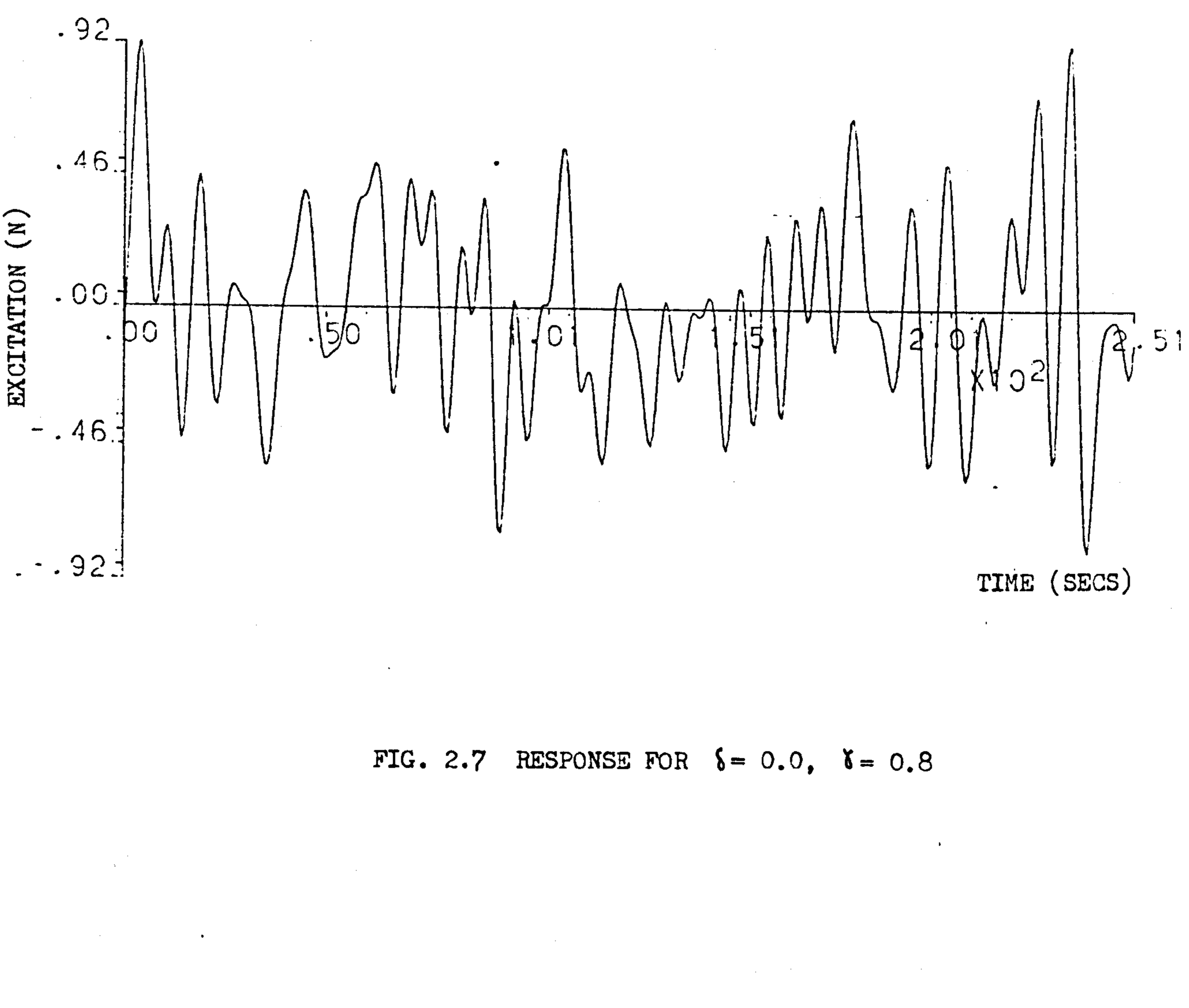

FIG. 2.7 RESPONSE FOR $\zeta = 0.0$, $\gamma = 0.8$

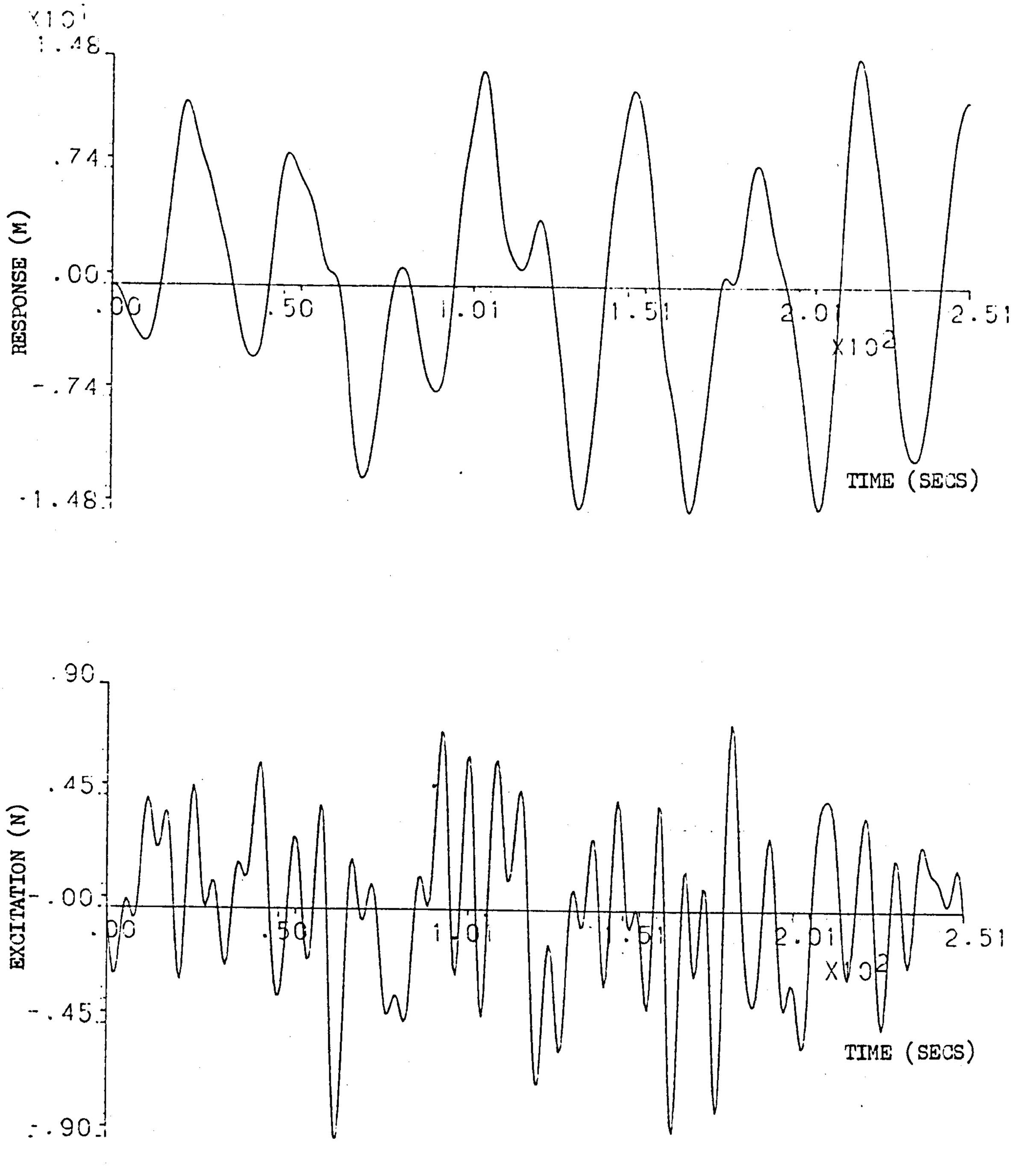

FIG. 2.8 RESPONSE FOR $\delta = 0.008$, $\gamma = 0.0$

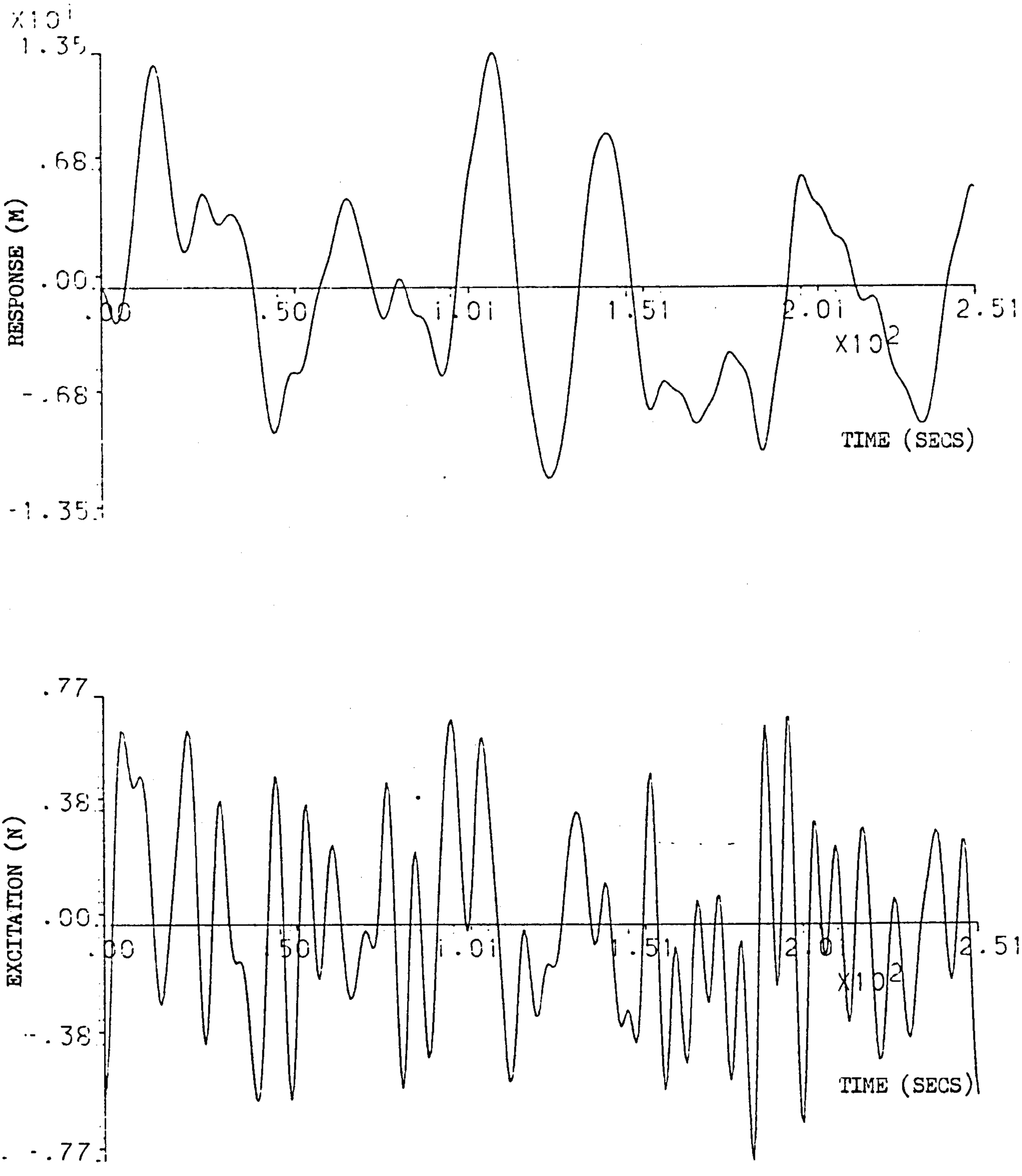

FIG. 2.9 RESPONSE FOR ζ=0.008, γ=0.8

δ \ γ	0.0	0.2	0.4	0.6	0.8
0.0	34.24 30.74	25.54 26.64	22.39 23.64	21.51 23.24	21.62 20.38
0.004	19.93 24.47	18.57 21.29	16.99 18.89	17.83 18.10	16.32 17.78
0.008	18.58 22.19	16.38 18.99	15.07 17.56	13.50 16.63	14.72 15.99

FIG. 2.10 MAXIMUM VALUES
TOP LINE - FROM TIME HISTORIES
BOTTOM LINE - FROM FORMULA $\sqrt{2\ln(N)}$

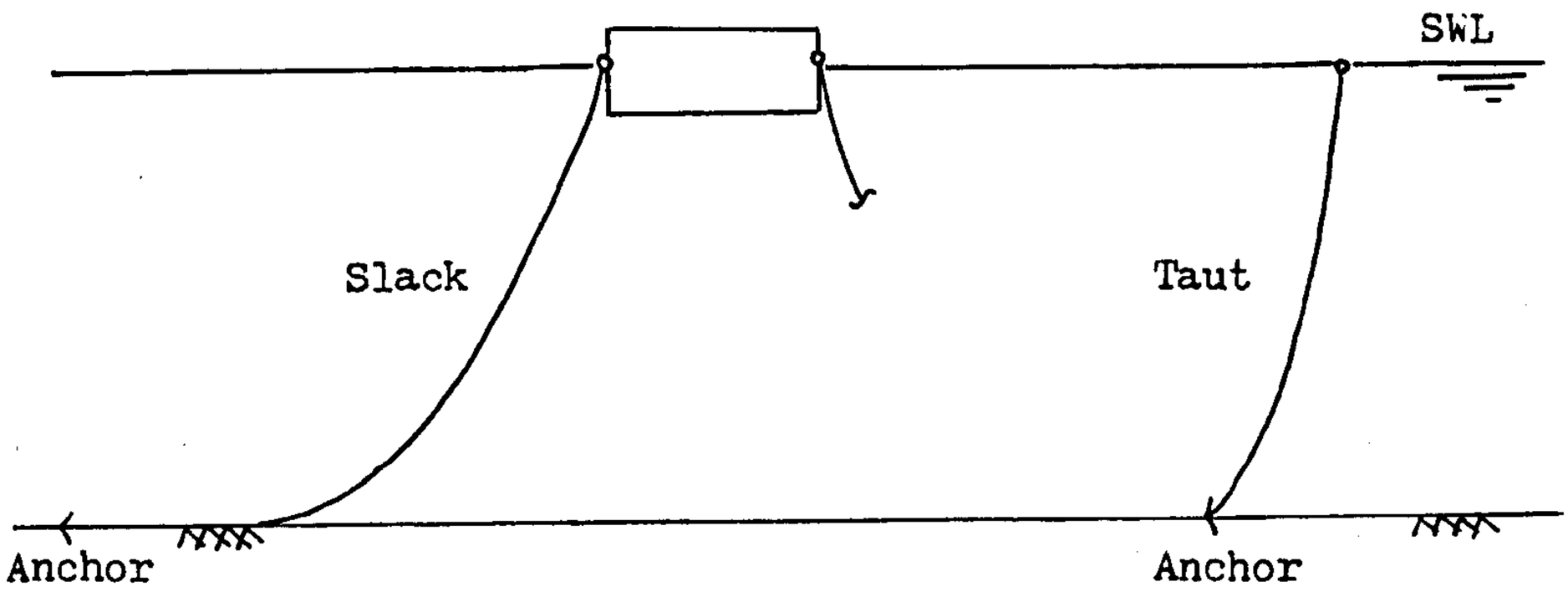

FIG. 3.1 TYPES OF MOORINGS

	Bottom Type	
Anchor Type	Sand	Mud
Stockless	6	2
Lightweight	16	9
Stato	20	15
Boss	-	35

Holding Power = (Max. Horizontal Pull/Anchor Weight)

FIG. 3.2 HOLDING POWER FOR VARIOUS ANCHOR TYPES

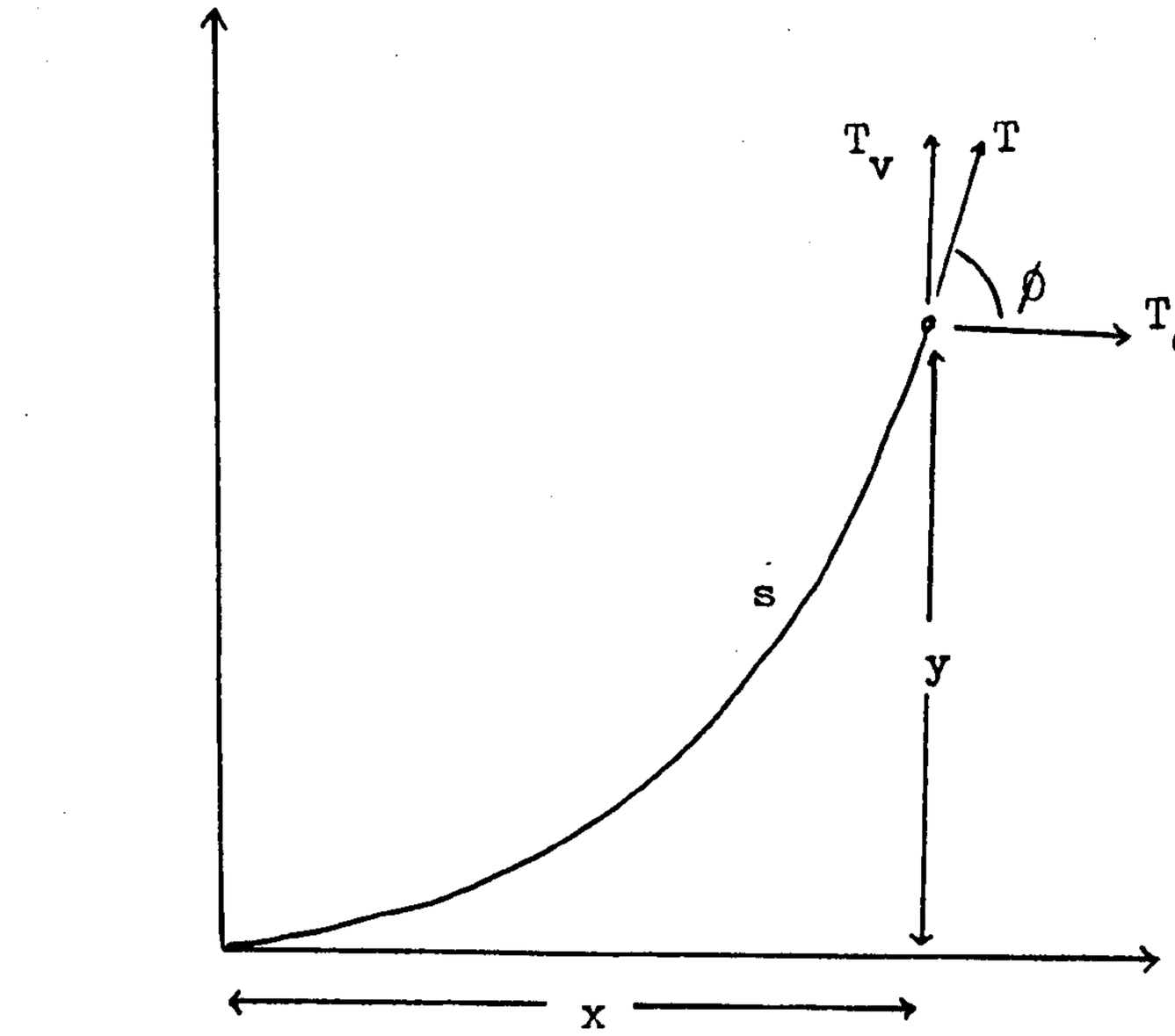

FIG. 3.3 NOTATION USED FOR THE ANALYSIS OF A CATENARY MOORING LINE

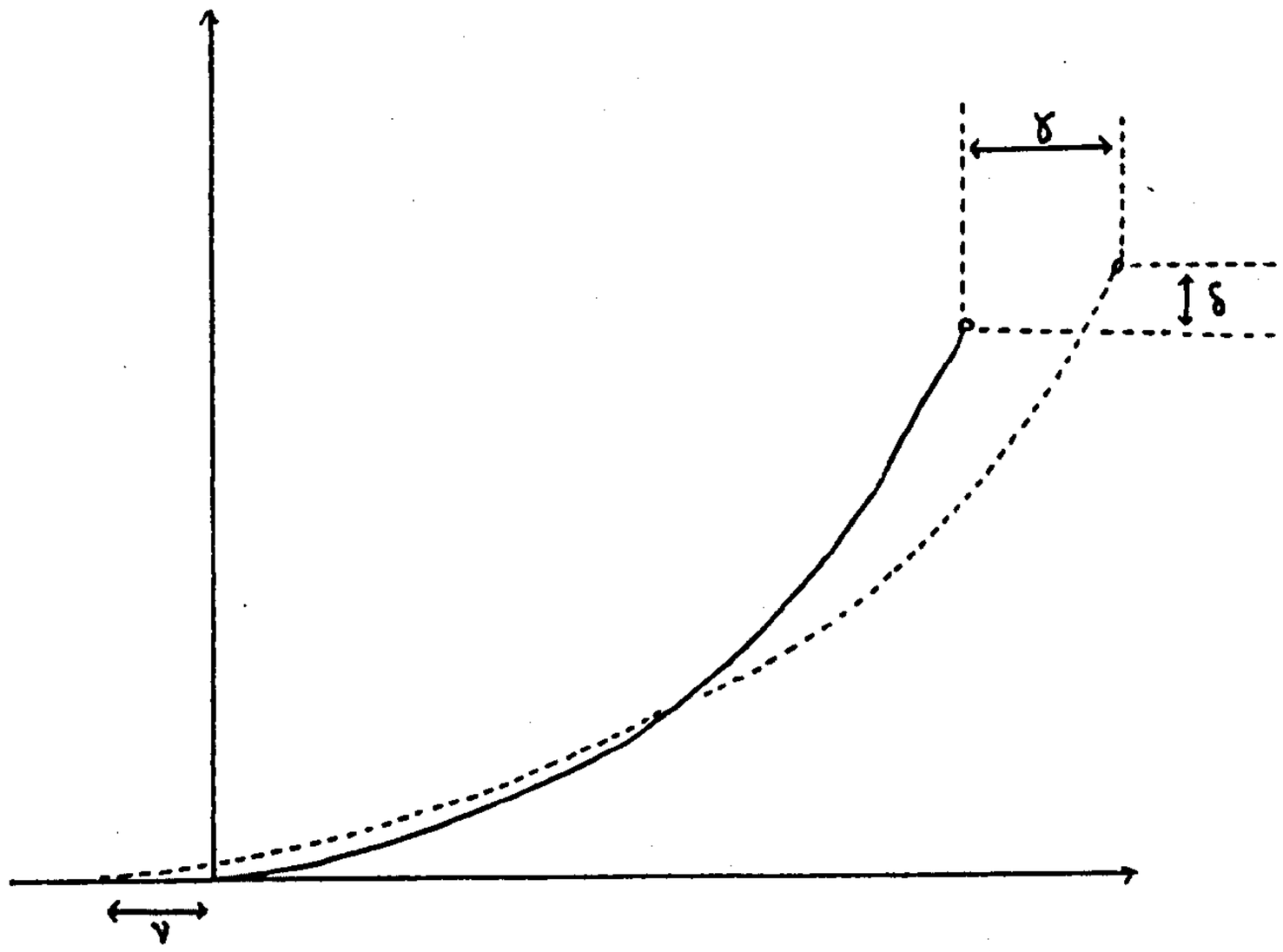

FIG. 3.4 DISPLACEMENTS OF THE MOORING LINE

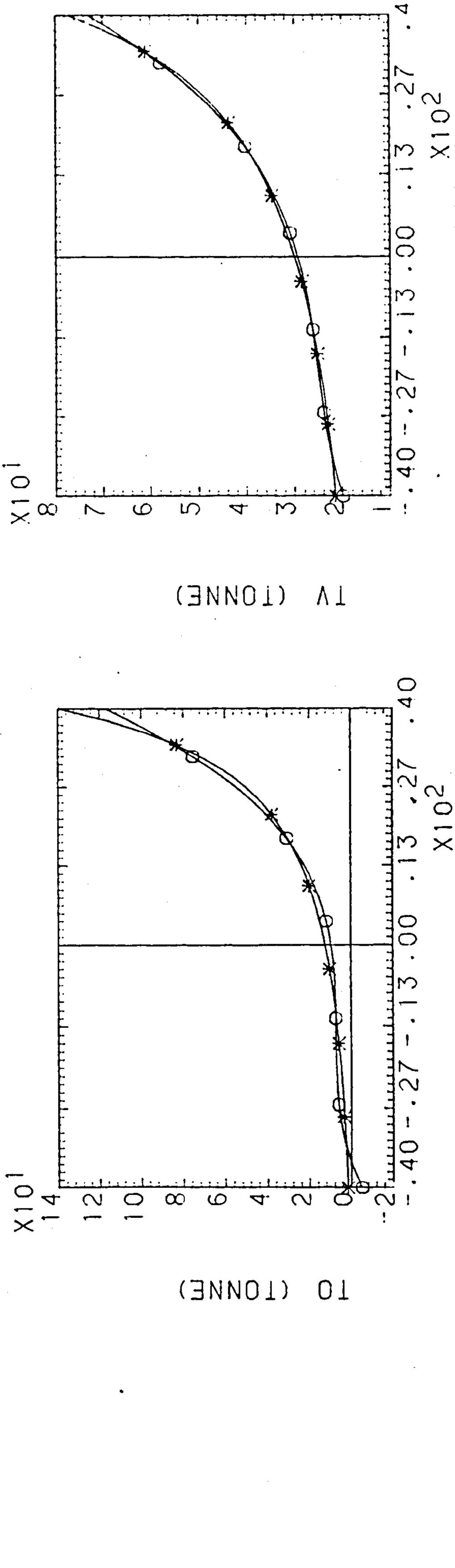

FIG. 3.5 STIFFNESS CURVES FOR AN EXAMPLE CATENARY LINE
(*= Inverse Curve, O = Close Fit Cubic)

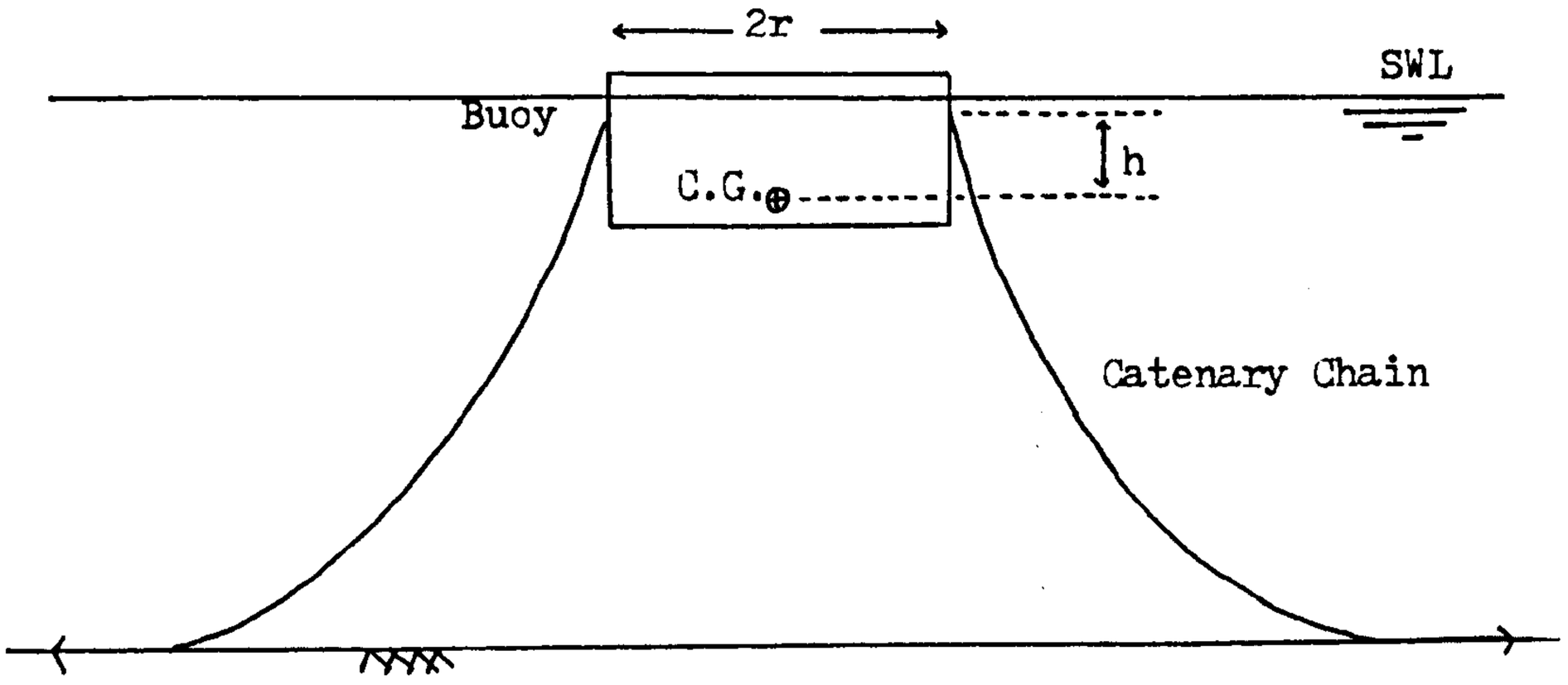

FIG. 3.6 BUOY DIMENSIONS

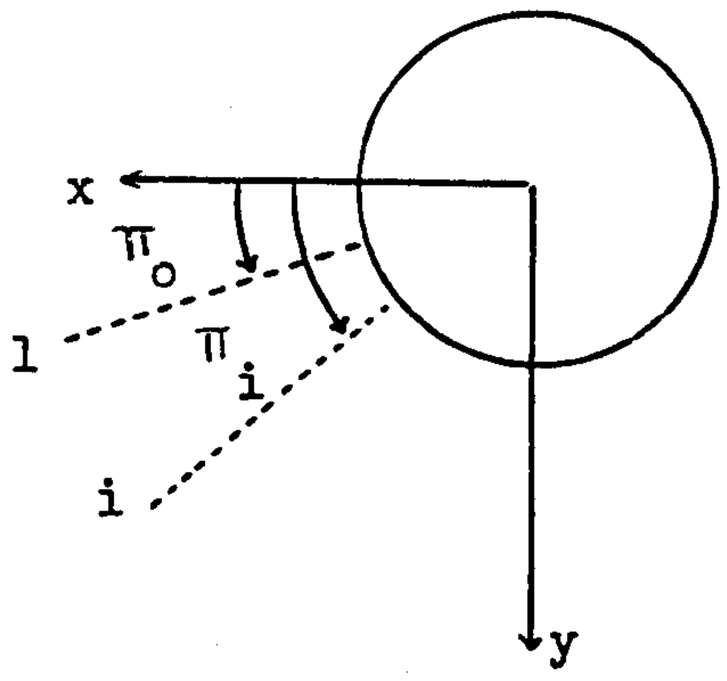

FIG. 3.7 CABLE ANGLES

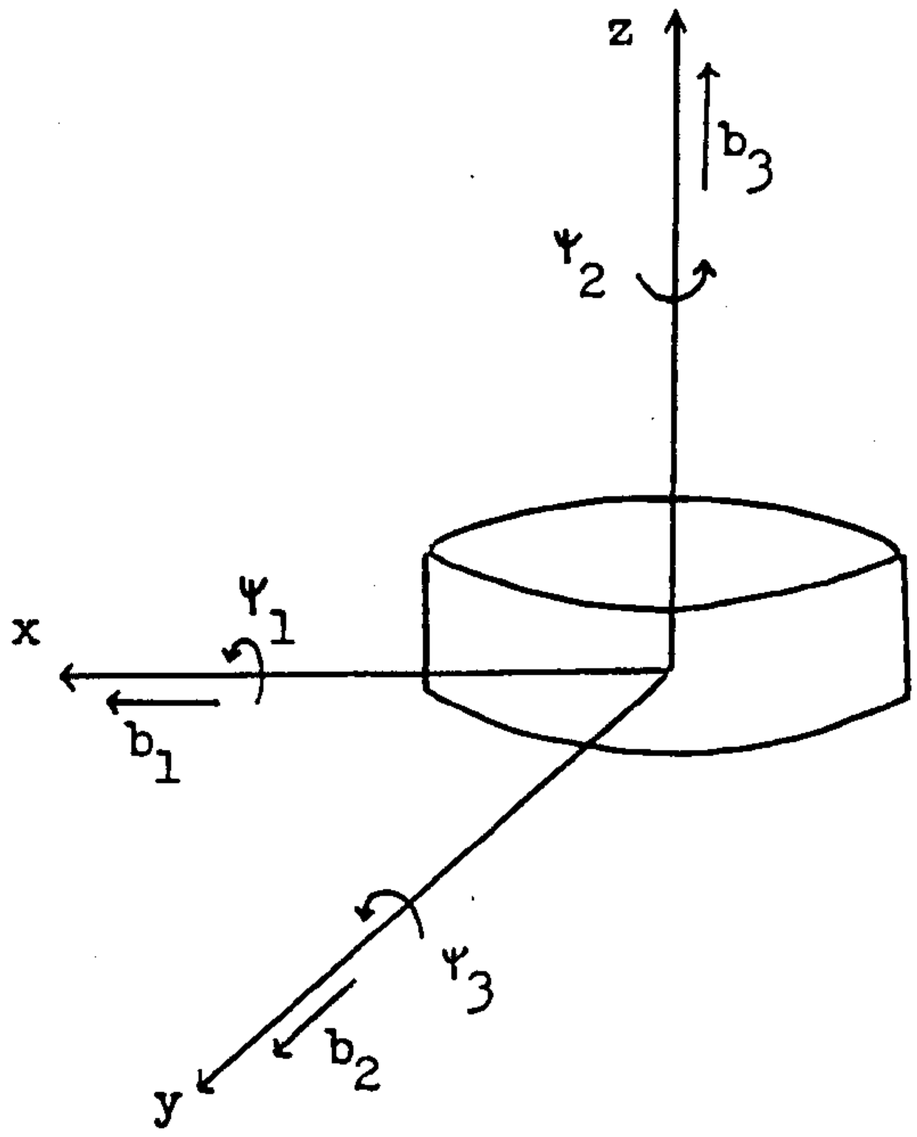

FIG. 3.8 BUOY DISPLACEMENTS

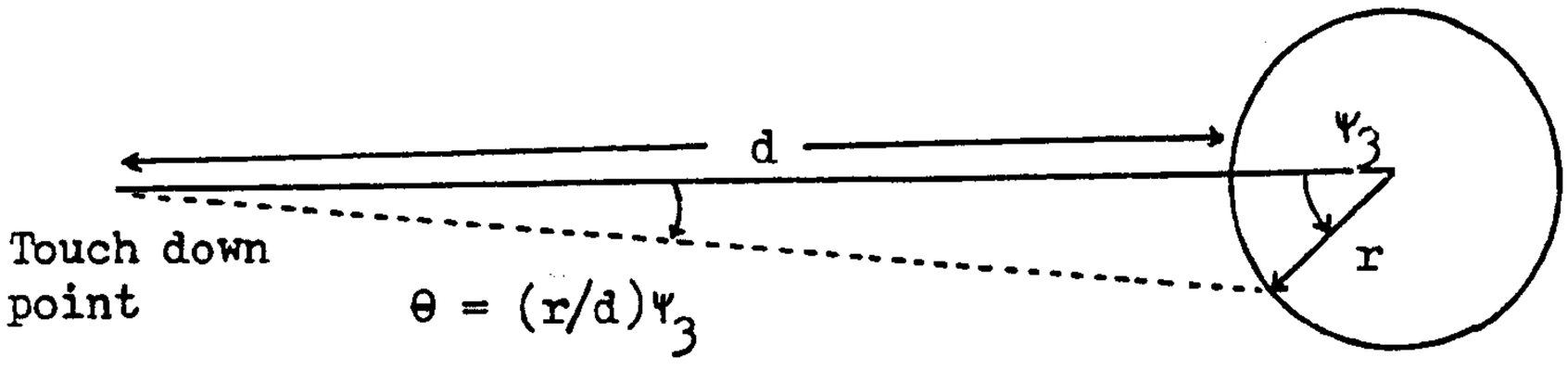

FIG. 3.9 THE EFFECT OF YAW

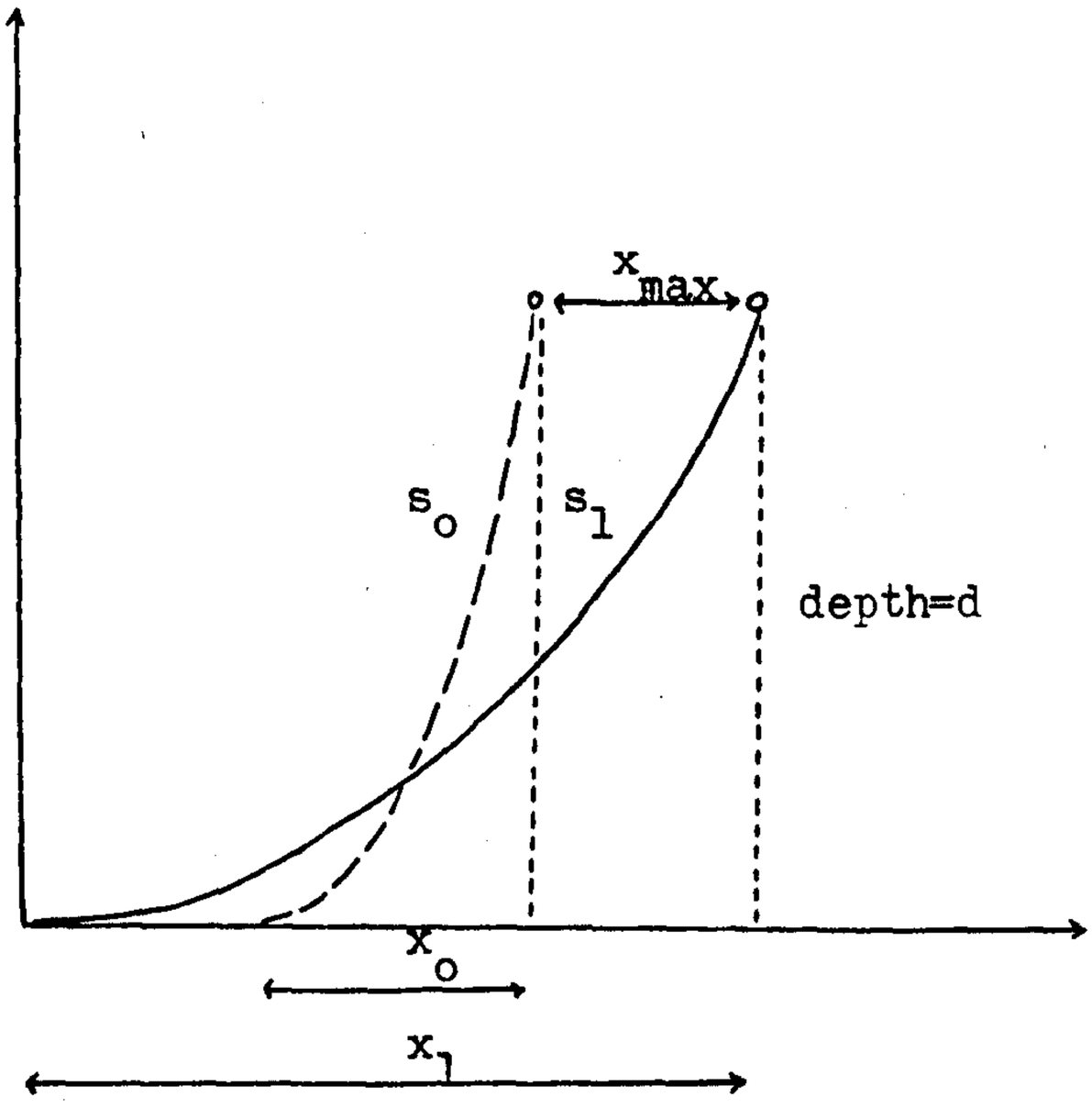

FIG. 3.10 MAXIMUM ALLOWABLE DISPLACEMENT OF CABLE FROM THE EQUILIBRIUM POSITION

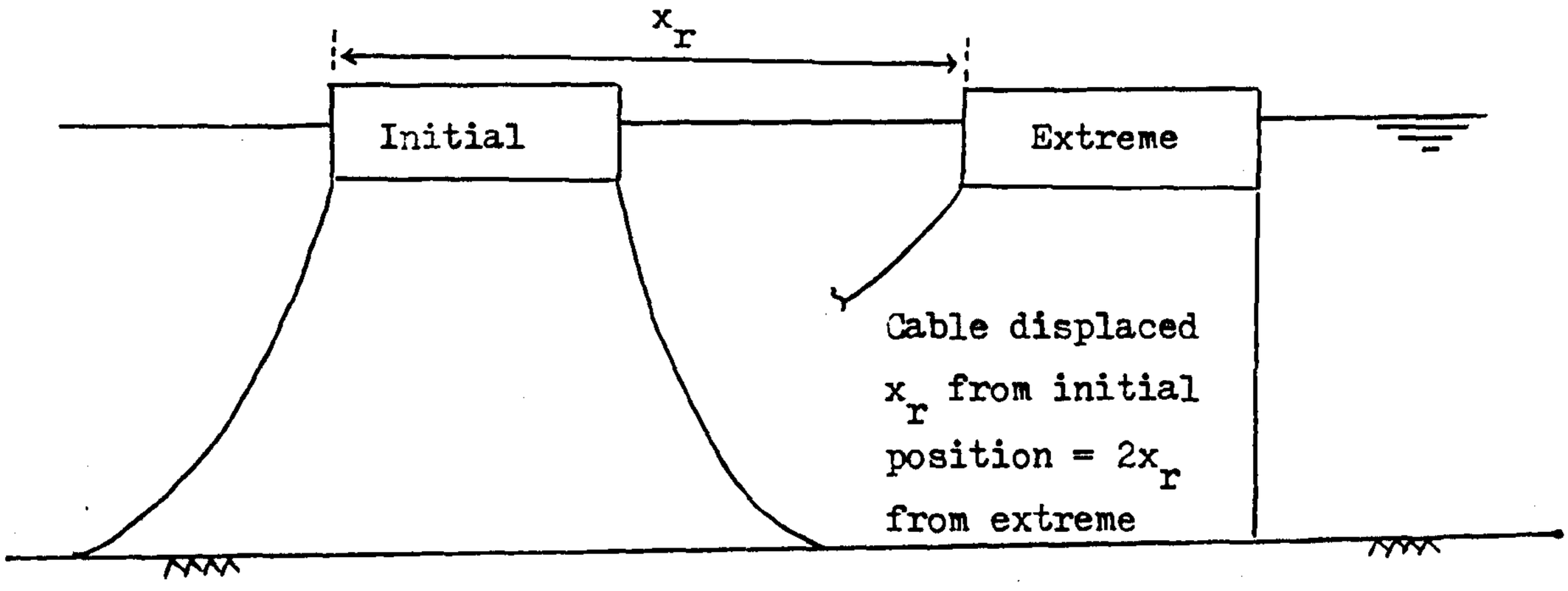

FIG. 3.11 CABLE SLACK AT EXTREME POSITION

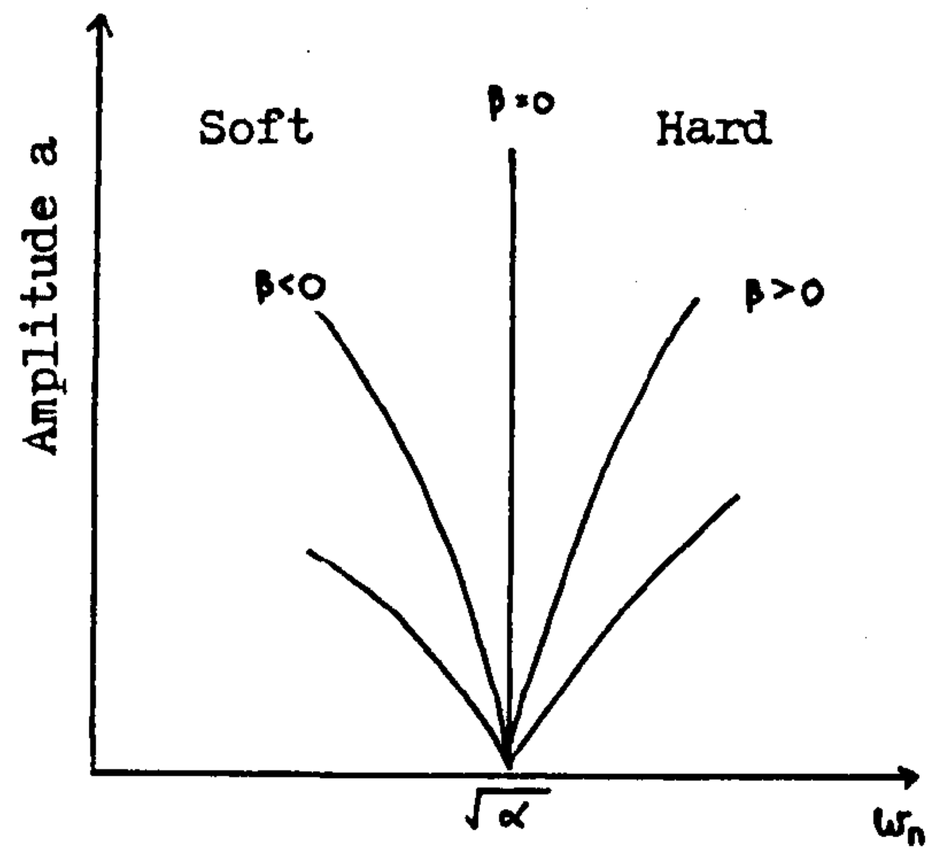

FIG. 3.12 EFFECT OF β ON THE NATURAL FREQUENCY

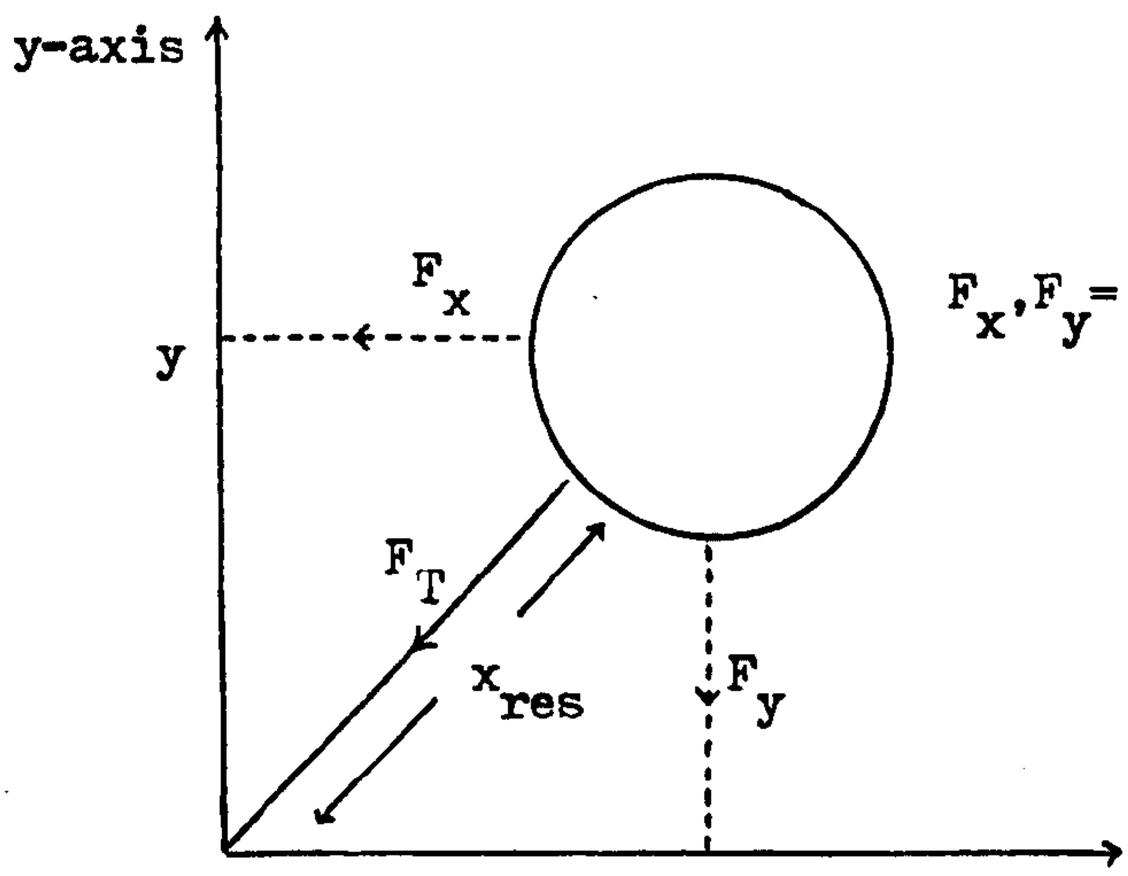

F_x, F_y = x,y components of horizontal restoring force

FIG. 3.13 HORIZONTAL BUOY DISPLACEMENTS

FIG. 3.14 DESIGN TABLES FOR A CATENARY ANCHORING SYSTEM

This Figure is presented in the following four pages, in which the notation used is as follows:-

XR = Maximum allowable horizontal excursion/water depth.
S1 = Length of suspended chain at the maximum horizontal excursion.
S0 = Length of suspended chain at initial configuration.
D = Water depth.
X0 = Horizontal projected length at initial configuration.
P = Wetted weight of chain per unit length.
T0 = Horizontal top tension for initial configuration.
A = Cubic coefficient for stiffness curve.
B = Squared coefficient for stiffness curve.
C = Linear coefficient for stiffness curve.
D = Constant term in the stiffness curve.
FMAX = Horizontal restoring force of mooring system at the maximum excursion.

DESIGN TABLES FOR SLACK MOORINGS
****

TABLE FOR SLACK AT 2*XP
****

XR\S1	0.2000E+01	0.2500E+01	0.3000E+01	0.3500E+01	0.4000E+01
0.1000E+00	0.0000E+00	0.0000E+00	0.0000E+00	0.0000E+00	0.0000E+00
0.1500E+00	0.0000E+00	0.0000E+00	0.0000E+00	0.0000E+00	0.0000E+00
0.2000E+00	0.0000E+00	0.0000E+00	0.0000E+00	0.0000E+00	0.0000E+00
0.2500E+00	0.0000E+00	0.0000E+00	0.0000E+00	0.0000E+00	0.0000E+00
0.3000E+00	0.0000E+00	0.0000E+00	0.0000E+00	0.0000E+00	0.0000E+00
0.3500E+00	0.1000E+01	0.0000E+00	0.0000E+00	0.0000E+00	0.0000E+00
0.4000E+00	0.1000E+01	0.1000E+01	0.1000E+01	0.0000E+00	0.0000E+00
0.4500E+00	0.1000E+01	0.1000E+01	0.1000E+01	0.1000E+01	0.1000E+01
0.5000E+00	0.1000E+01	0.1000E+01	0.1000E+01	0.1000E+01	0.1000E+01

TABLE OF SO/D
****

XR\S1	0.2000E+01	0.2500E+01	0.3000E+01	0.3500E+01	0.4000E+01
0.1000E+00	0.1607E+01	0.1878E+01	0.2121E+01	0.2340E+01	0.2544E+01
0.1500E+00	0.1475E+01	0.1685E+01	0.1866E+01	0.2025E+01	0.2168E+01
0.2000E+00	0.1371E+01	0.1536E+01	0.1675E+01	0.1795E+01	0.1901E+01
0.2500E+00	0.1287E+01	0.1419E+01	0.1529E+01	0.1621E+01	0.1702E+01
0.3000E+00	0.1218E+01	0.1326E+01	0.1413E+01	0.1486E+01	0.1549E+01
0.3500E+00	0.1162E+01	0.1250E+01	0.1321E+01	0.1380E+01	0.1430E+01
0.4000E+00	0.1117E+01	0.1189E+01	0.1246E+01	0.1294E+01	0.1334E+01
0.4500E+00	0.1080E+01	0.1138E+01	0.1186E+01	0.1224E+01	0.1257E+01
0.5000E+00	0.1050E+01	0.1097E+01	0.1136E+01	0.1168E+01	0.1194E+01

TABLE OF XC/D
****

XR\S1	0.2000E+01	0.2500E+01	0.3000E+01	0.3500E+01	0.4000E+01
0.1000E+00	0.1153E+01	0.1501E+01	0.1791E+01	0.2043E+01	0.2273E+01
0.1500E+00	0.9703E+00	0.1256E+01	0.1485E+01	0.1677E+01	0.1846E+01
0.2000E+00	0.8153E+00	0.1056E+01	0.1243E+01	0.1397E+01	0.1528E+01
0.2500E+00	0.6807E+00	0.8887E+00	0.1046E+01	0.1172E+01	0.1279E+01
0.3000E+00	0.5617E+00	0.7444E+00	0.8796E+00	0.9864E+00	0.1075E+01
0.3500E+00	0.4554E+00	0.6154E+00	0.7368E+00	0.8290E+00	0.9045E+00
0.4000E+00	0.3591E+00	0.5061E+00	0.6114E+00	0.6924E+00	0.7581E+00
0.4500E+00	0.2713E+00	0.4052E+00	0.5001E+00	0.5723E+00	0.6305E+00
0.5000E+00	0.1905E+00	0.3134E+00	0.3996E+00	0.4648E+00	0.5169E+00

TABLE OF TO/(P*D)
****

XR\S1	0.2000E+01	0.2500E+01	0.3000E+01	0.3500E+01	0.4000E+01
0.1000E+00	0.7914E+00	0.1264E+01	0.1749E+01	0.2237E+01	0.2735E+01
0.1500E+00	0.5883E+00	0.9196E+00	0.1241E+01	0.1549E+01	0.1851E+01
0.2000E+00	0.4394E+00	0.6796E+00	0.9029E+00	0.1111E+01	0.1307E+01
0.2500E+00	0.3278E+00	0.5070E+00	0.6683E+00	0.8144E+00	0.9488E+00
0.3000E+00	0.2423E+00	0.3786E+00	0.4983E+00	0.6045E+00	0.7003E+00
0.3500E+00	0.1761E+00	0.2815E+00	0.3724E+00	0.4516E+00	0.5222E+00
0.4000E+00	0.1241E+00	0.2065E+00	0.2765E+00	0.3369E+00	0.3901E+00
0.4500E+00	0.8331E-01	0.1480E+00	0.2028E+00	0.2495E+00	0.2903E+00
0.5000E+00	0.5121E-01	0.1021E+00	0.1450E+00	0.1815E+00	0.2123E+00

TABLE OF (A*D*C)/P
****

XR\S1	0.2000E+01	0.2500E+01	0.3000E+01	0.3500E+01	0.4000E+01
0.1000E+00	0.4533E+02	0.1171E+03	0.2292E+03	0.4235E+03	0.7187E+03
0.1500E+00	0.2922E+02	0.7007E+02	0.1341E+03	0.2244E+03	0.3532E+03
0.2000E+00	0.1973E+02	0.4445E+02	0.8103E+02	0.1305E+03	0.1970E+03
0.2500E+00	0.1383E+02	0.2979E+02	0.5235E+02	0.8176E+02	0.1196E+03
0.3000E+00	0.9959E+01	0.2072E+02	0.3535E+02	0.5387E+02	0.7699E+02
0.3500E+00	0.7179E+01	0.1491E+02	0.2486E+02	0.3717E+02	0.5215E+02
0.4000E+00	0.5368E+01	0.1083E+02	0.1791E+02	0.2643E+02	0.3656E+02
0.4500E+00	0.4300E+01	0.8174E+01	0.1322E+02	0.1927E+02	0.2639E+02
0.5000E+00	0.3550E+01	0.6409E+01	0.1009E+02	0.1444E+02	0.1953E+02

TABLE OF (3*D)/P
****

XR\S1	0.2000E+01	0.2500E+01	0.3000E+01	0.3500E+01	0.4000E+01
0.1000E+00	0.1613E+02	0.3445E+02	0.6115E+02	0.9696E+02	0.1450E+03
0.1500E+00	0.1126E+02	0.2280E+02	0.3845E+02	0.5928E+02	0.8337E+02
0.2000E+00	0.8315E+01	0.1591E+02	0.2582E+02	0.3800E+02	0.5279E+02
0.2500E+00	0.6315E+01	0.1163E+02	0.1832E+02	0.2631E+02	0.3574E+02
0.3000E+00	0.4931E+01	0.8776E+01	0.1349E+02	0.1899E+02	0.2536E+02
0.3500E+00	0.3994E+01	0.6832E+01	0.1026E+02	0.1424E+02	0.1874E+02
0.4000E+00	0.3311E+01	0.5479E+01	0.8044E+01	0.1096E+02	0.1425E+02
0.4500E+00	0.2752E+01	0.4485E+01	0.6474E+01	0.8695E+01	0.1116E+02
0.5000E+00	0.2236E+01	0.3697E+01	0.5278E+01	0.7013E+01	0.8921E+01

TABLE OF C/P
****

XR\S1	0.2000E+01	0.2500E+01	0.3000E+01	0.3500E+01	0.4000E+01
0.1000E+00	0.4675E+01	0.8120E+01	0.1219E+02	0.1676E+02	0.2171E+02
0.1500E+00	0.3360E+01	0.5484E+01	0.7780E+01	0.1015E+02	0.1250E+02
0.2000E+00	0.2473E+01	0.3831E+01	0.5178E+01	0.6464E+01	0.7617E+01
0.2500E+00	0.1853E+01	0.2743E+01	0.3551E+01	0.4249E+01	0.4795E+01
0.3000E+00	0.1403E+01	0.1994E+01	0.2478E+01	0.2843E+01	0.3062E+01
0.3500E+00	0.1075E+01	0.1464E+01	0.1745E+01	0.1912E+01	0.1950E+01
0.4000E+00	0.8097E+00	0.1083E+01	0.1232E+01	0.1277E+01	0.1212E+01
0.4500E+00	0.5827E+00	0.7805E+00	0.8583E+00	0.8354E+00	0.7126E+00
0.5000E+00	0.3970E+00	0.5336E+00	0.5630E+00	0.5025E+00	0.3545E+00

TABLE OF D/(P*C)
****

XR\S1	0.2000E+01	0.2500E+01	0.3000E+01	0.3500E+01	0.4000E+01
0.1000E+00	0.7887E+00	0.1253E+01	0.1735E+01	0.2212E+01	0.2691E+01
0.1500E+00	0.5835E+00	0.9075E+00	0.1217E+01	0.1506E+01	0.1779E+01
0.2000E+00	0.4316E+00	0.6607E+00	0.8662E+00	0.1049E+01	0.1208E+01
0.2500E+00	0.3167E+00	0.4810E+00	0.6194E+00	0.7340E+00	0.8255E+00
0.3000E+00	0.2276E+00	0.3457E+00	0.4384E+00	0.5087E+00	0.5575E+00
0.3500E+00	0.1570E+00	0.2419E+00	0.3026E+00	0.3427E+00	0.3636E+00
0.4000E+00	0.1013E+00	0.1599E+00	0.1979E+00	0.2173E+00	0.2193E+00
0.4500E+00	0.5940E-01	0.9619E-01	0.1159E+00	0.1199E+00	0.1090E+00
0.5000E+00	0.2819E-01	0.4755E-01	0.5333E-01	0.4551E-01	0.2454E-01

TABLES OF FMAX/(P*D) FOR 4, 6 AND 8 CABLES

XR\S1	0.2000E+01	0.2500E+01	0.3000E+01	0.3500E+01	0.4000E+01
0.1000E+00	0.1027E+01	0.1561E+01	0.2924E+01	0.4215E+01	0.5524E+01
0.1500E+00	0.1209E+01	0.2129E+01	0.3264E+01	0.4603E+01	0.6246E+01
0.2000E+00	0.1312E+01	0.2266E+01	0.3420E+01	0.4776E+01	0.6402E+01
0.2500E+00	0.1373E+01	0.2344E+01	0.3502E+01	0.4848E+01	0.6447E+01
0.3000E+00	0.1402E+01	0.2379E+01	0.3529E+01	0.4855E+01	0.6421E+01
0.3500E+00	0.1399E+01	0.2391E+01	0.3536E+01	0.4846E+01	0.6382E+01
0.4000E+00	0.1366E+01	0.2367E+01	0.3505E+01	0.4800E+01	0.6309E+01
0.4500E+00	0.1375E+01	0.2345E+01	0.3467E+01	0.4741E+01	0.6223E+01
0.5000E+00	0.1361E+01	0.2319E+01	0.3424E+01	0.4674E+01	0.6125E+01

XR\S1	0.2000E+01	0.2500E+01	0.3000E+01	0.3500E+01	0.4000E+01
0.1000E+00	0.1506E+01	0.2703E+01	0.4205E+01	0.6001E+01	0.8186E+01
0.1500E+00	0.1738E+01	0.3012E+01	0.4543E+01	0.6327E+01	0.8436E+01
0.2000E+00	0.1842E+01	0.3125E+01	0.4626E+01	0.6345E+01	0.8349E+01
0.2500E+00	0.1892E+01	0.3152E+01	0.4607E+01	0.6253E+01	0.8154E+01
0.3000E+00	0.1893E+01	0.3125E+01	0.4529E+01	0.6104E+01	0.7914E+01
0.3500E+00	0.1856E+01	0.3074E+01	0.4436E+01	0.5954E+01	0.7691E+01
0.4000E+00	0.1804E+01	0.2987E+01	0.4312E+01	0.5783E+01	0.7458E+01
0.4500E+00	0.1742E+01	0.2903E+01	0.4189E+01	0.5613E+01	0.7234E+01
0.5000E+00	0.1676E+01	0.2806E+01	0.4064E+01	0.5445E+01	0.7014E+01

XR\S1	0.2000E+01	0.2500E+01	0.3000E+01	0.3500E+01	0.4000E+01
0.1000E+00	0.2007E+01	0.3601E+01	0.5599E+01	0.7982E+01	0.1086E+02
0.1500E+00	0.2314E+01	0.4004E+01	0.6025E+01	0.8378E+01	0.1113E+02
0.2000E+00	0.2455E+01	0.4141E+01	0.6109E+01	0.8348E+01	0.1092E+02
0.2500E+00	0.2507E+01	0.4159E+01	0.6048E+01	0.8164E+01	0.1057E+02
0.3000E+00	0.2500E+01	0.4103E+01	0.5905E+01	0.7901E+01	0.1015E+02
0.3500E+00	0.2444E+01	0.4012E+01	0.5739E+01	0.7634E+01	0.9759E+01
0.4000E+00	0.2351E+01	0.3875E+01	0.5525E+01	0.7345E+01	0.9362E+01
0.4500E+00	0.2255E+01	0.3722E+01	0.5327E+01	0.7061E+01	0.8987E+01
0.5000E+00	0.2163E+01	0.3570E+01	0.5103E+01	0.6763E+01	0.8608E+01

TABLES OF (A*D*C)/P FOR 4, 6 AND 8 CABLES

XR\S1	0.2000E+01	0.2500E+01	0.3000E+01	0.3500E+01	0.4000E+01
0.1000E+00	0.9066E+02	0.2342E+03	0.4785E+03	0.8470E+03	0.1437E+04
0.1500E+00	0.5864E+02	0.1401E+03	0.2682E+03	0.4487E+03	0.7065E+03
0.2000E+00	0.3946E+02	0.8890E+02	0.1621E+03	0.2611E+03	0.3939E+03
0.2500E+00	0.2767E+02	0.5958E+02	0.1047E+03	0.1635E+03	0.2391E+03
0.3000E+00	0.1992E+02	0.4145E+02	0.7071E+02	0.1077E+03	0.1540E+03
0.3500E+00	0.1436E+02	0.2982E+02	0.4975E+02	0.7434E+02	0.1043E+03
0.4000E+00	0.1074E+02	0.2165E+02	0.3582E+02	0.5286E+02	0.7312E+02
0.4500E+00	0.8601E+01	0.1635E+02	0.2644E+02	0.3853E+02	0.5278E+02
0.5000E+00	0.7099E+01	0.1282E+02	0.2015E+02	0.2888E+02	0.3906E+02

XR\S1	0.2000E+01	0.2500E+01	0.3000E+01	0.3500E+01	0.4000E+01
0.1000E+00	0.1020E+03	0.2635E+03	0.5383E+03	0.9528E+03	0.1617E+04
0.1500E+00	0.6597E+02	0.1577E+03	0.3017E+03	0.5048E+03	0.7948E+03
0.2000E+00	0.4439E+02	0.1000E+03	0.1823E+03	0.2937E+03	0.4432E+03
0.2500E+00	0.3113E+02	0.6703E+02	0.1179E+03	0.1840E+03	0.2690E+03
0.3000E+00	0.2241E+02	0.4663E+02	0.7955E+02	0.1212E+03	0.1732E+03
0.3500E+00	0.1615E+02	0.3354E+02	0.5597E+02	0.8364E+02	0.1173E+03
0.4000E+00	0.1208E+02	0.2436E+02	0.4030E+02	0.5947E+02	0.8226E+02
0.4500E+00	0.9676E+01	0.1839E+02	0.2974E+02	0.4335E+02	0.5937E+02
0.5000E+00	0.7987E+01	0.1442E+02	0.2267E+02	0.3249E+02	0.4394E+02

XR\S1	0.2000E+01	0.2500E+01	0.3000E+01	0.3500E+01	0.4000E+01
0.1000E+00	0.1360E+03	0.3513E+03	0.7177E+03	0.1270E+04	0.2156E+04
0.1500E+00	0.8796E+02	0.2102E+03	0.4023E+03	0.6731E+03	0.1060E+04
0.2000E+00	0.5919E+02	0.1333E+03	0.2431E+03	0.3916E+03	0.5909E+03
0.2500E+00	0.4150E+02	0.8933E+02	0.1570E+03	0.2453E+03	0.3587E+03
0.3000E+00	0.2988E+02	0.6217E+02	0.1061E+03	0.1616E+03	0.2310E+03
0.3500E+00	0.2154E+02	0.4473E+02	0.7463E+02	0.1115E+03	0.1564E+03
0.4000E+00	0.1610E+02	0.3248E+02	0.5373E+02	0.7929E+02	0.1097E+03
0.4500E+00	0.1290E+02	0.2452E+02	0.3966E+02	0.5780E+02	0.7916E+02
0.5000E+00	0.1065E+02	0.1923E+02	0.3023E+02	0.4331E+02	0.5859E+02

TABLES OF C/P FOR 4, 6 AND 8 CABLES

****

XR\S1	0.2000E+01	0.2500E+01	0.3000E+01	0.3500E+01	0.4000E+01
0.1000E+00	0.9350E+01	0.1624E+02	0.2439E+02	0.3352E+02	0.4343E+02
0.1500E+00	0.6721E+01	0.1097E+02	0.1556E+02	0.2029E+02	0.2500E+02
0.2000E+00	0.4946E+01	0.7661E+01	0.1036E+02	0.1293E+02	0.1523E+02
0.2500E+00	0.3705E+01	0.5487E+01	0.7103E+01	0.8499E+01	0.9589E+01
0.3000E+00	0.2805E+01	0.3969E+01	0.4957E+01	0.5635E+01	0.6124E+01
0.3500E+00	0.2150E+01	0.2923E+01	0.3491E+01	0.3825E+01	0.3900E+01
0.4000E+00	0.1619E+01	0.2165E+01	0.2465E+01	0.2554E+01	0.2424E+01
0.4500E+00	0.1165E+01	0.1562E+01	0.1717E+01	0.1671E+01	0.1425E+01
0.5000E+00	0.7939E+00	0.1067E+01	0.1126E+01	0.1005E+01	0.7089E+00

XR\S1	0.2000E+01	0.2500E+01	0.3000E+01	0.3500E+01	0.4000E+01
0.1000E+00	0.1403E+02	0.2436E+02	0.3658E+02	0.5028E+02	0.6514E+02
0.1500E+00	0.1008E+02	0.1645E+02	0.2334E+02	0.3044E+02	0.3750E+02
0.2000E+00	0.7419E+01	0.1149E+02	0.1553E+02	0.1939E+02	0.2285E+02
0.2500E+00	0.5558E+01	0.8230E+01	0.1065E+02	0.1275E+02	0.1438E+02
0.3000E+00	0.4208E+01	0.5983E+01	0.7435E+01	0.8528E+01	0.9186E+01
0.3500E+00	0.3224E+01	0.4392E+01	0.5236E+01	0.5737E+01	0.5850E+01
0.4000E+00	0.2429E+01	0.3248E+01	0.3697E+01	0.3831E+01	0.3636E+01
0.4500E+00	0.1748E+01	0.2342E+01	0.2575E+01	0.2506E+01	0.2138E+01
0.5000E+00	0.1191E+01	0.1601E+01	0.1639E+01	0.1508E+01	0.1063E+01

XR\S1	0.2000E+01	0.2500E+01	0.3000E+01	0.3500E+01	0.4000E+01
0.1000E+00	0.1870E+02	0.3248E+02	0.4877E+02	0.6704E+02	0.8685E+02
0.1500E+00	0.1344E+02	0.2194E+02	0.3112E+02	0.4059E+02	0.4999E+02
0.2000E+00	0.9893E+01	0.1532E+02	0.2071E+02	0.2586E+02	0.3047E+02
0.2500E+00	0.7411E+01	0.1097E+02	0.1421E+02	0.1700E+02	0.1918E+02
0.3000E+00	0.5610E+01	0.7978E+01	0.9913E+01	0.1137E+02	0.1225E+02
0.3500E+00	0.4299E+01	0.5856E+01	0.6981E+01	0.7649E+01	0.7800E+01
0.4000E+00	0.3239E+01	0.4331E+01	0.4929E+01	0.5109E+01	0.4848E+01
0.4500E+00	0.2331E+01	0.3123E+01	0.3433E+01	0.3342E+01	0.2851E+01
0.5000E+00	0.1588E+01	0.2134E+01	0.2252E+01	0.2010E+01	0.1418E+01

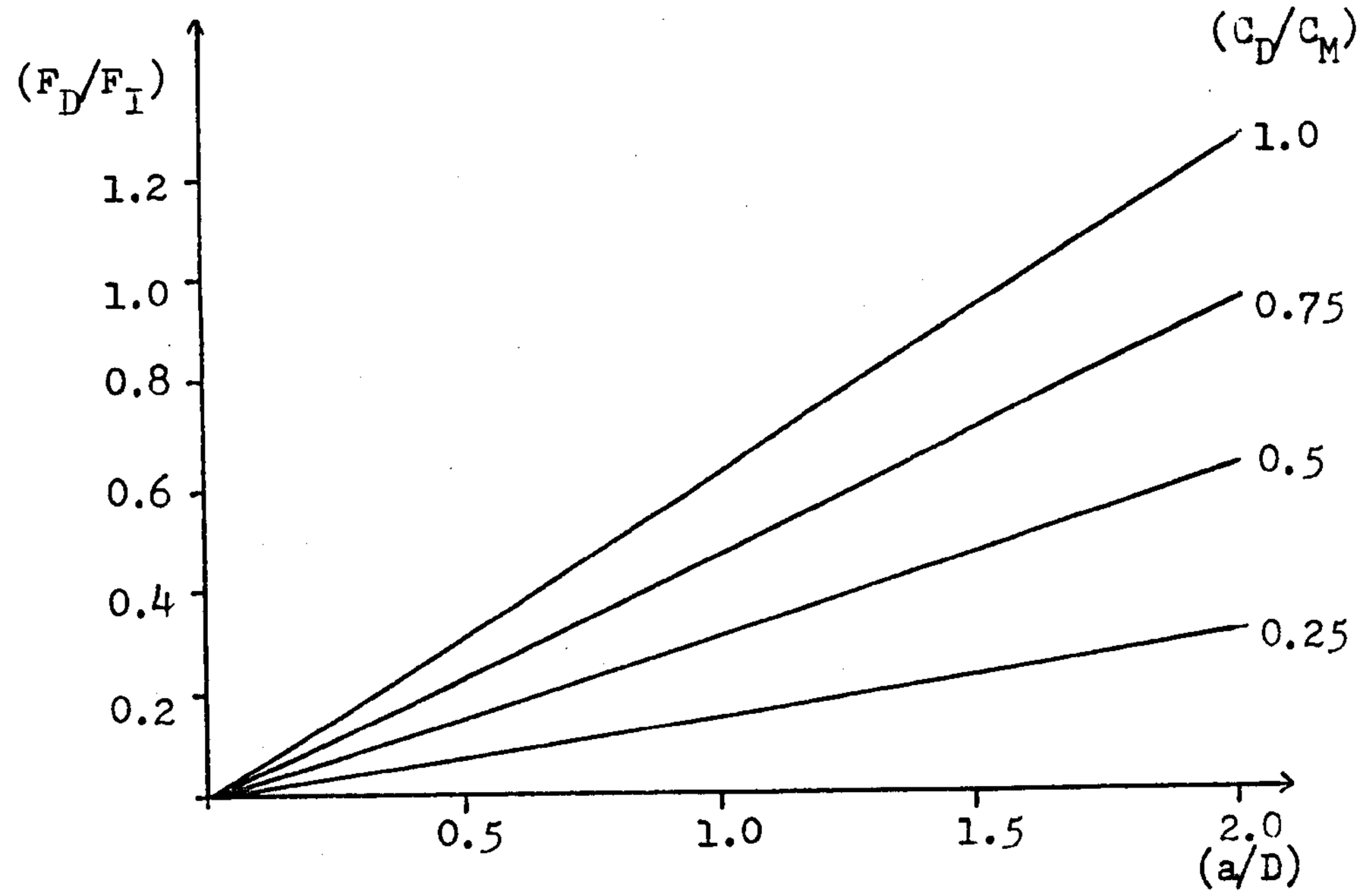

FIG. 4.1 (DRAG/INERTIA) FORCE RATIO FOR A MOORING BUOY

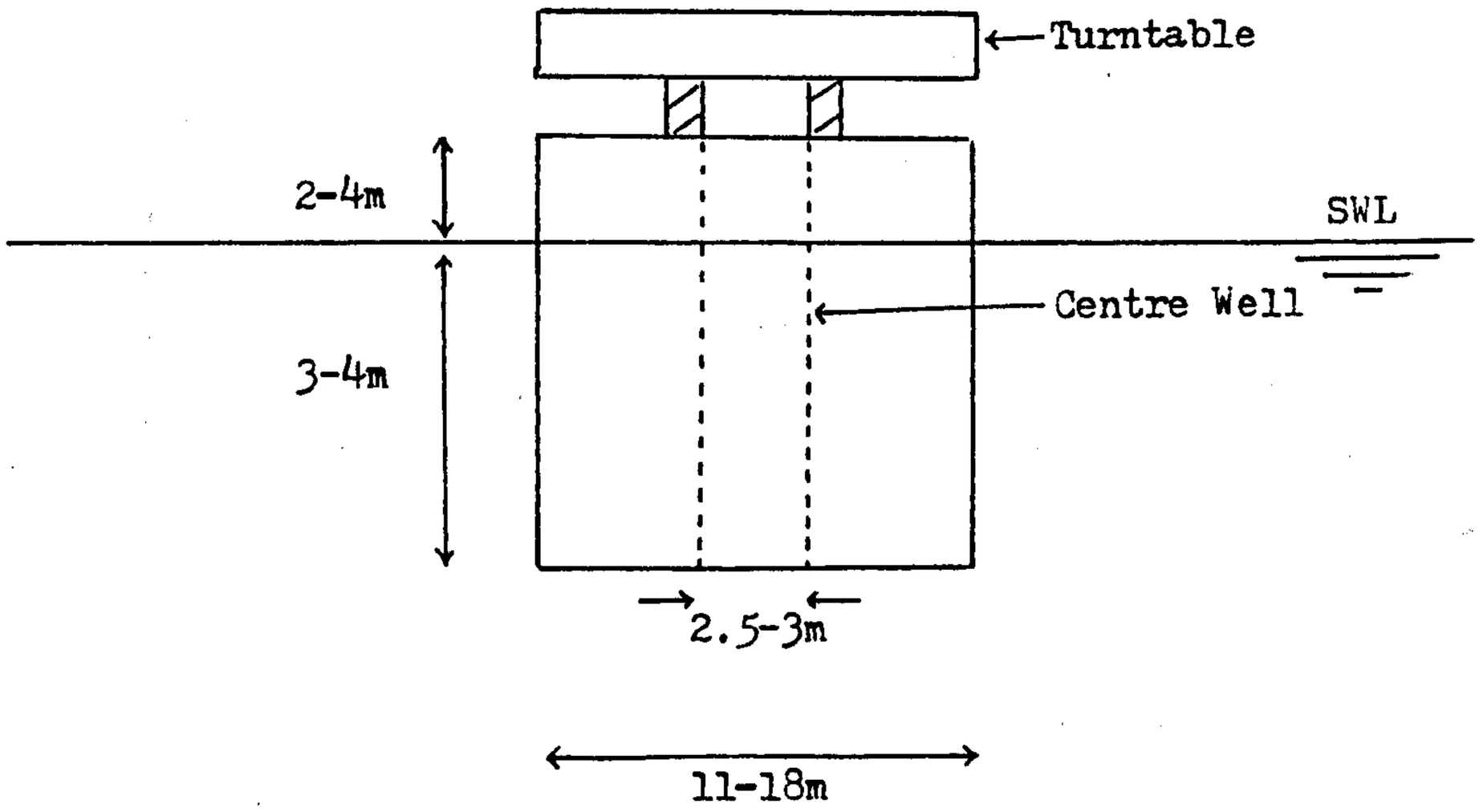

FIG. 4.2 TYPICAL DIMENSIONS FOR A MOORING BUOY

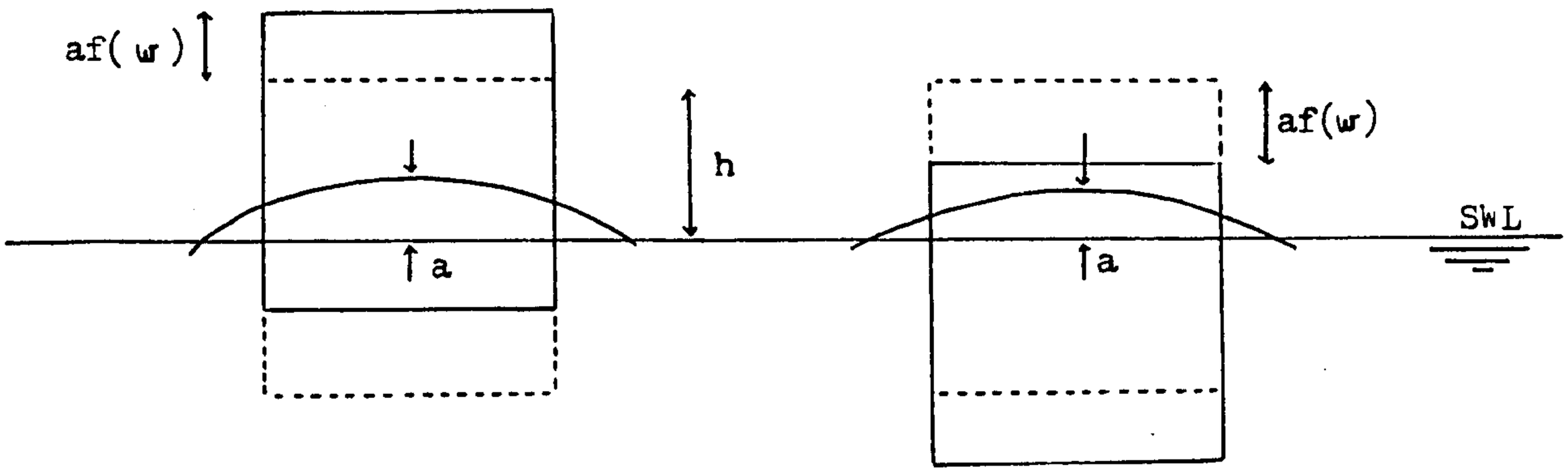

FIG. 4.3 BUOY SUBMERGENCE

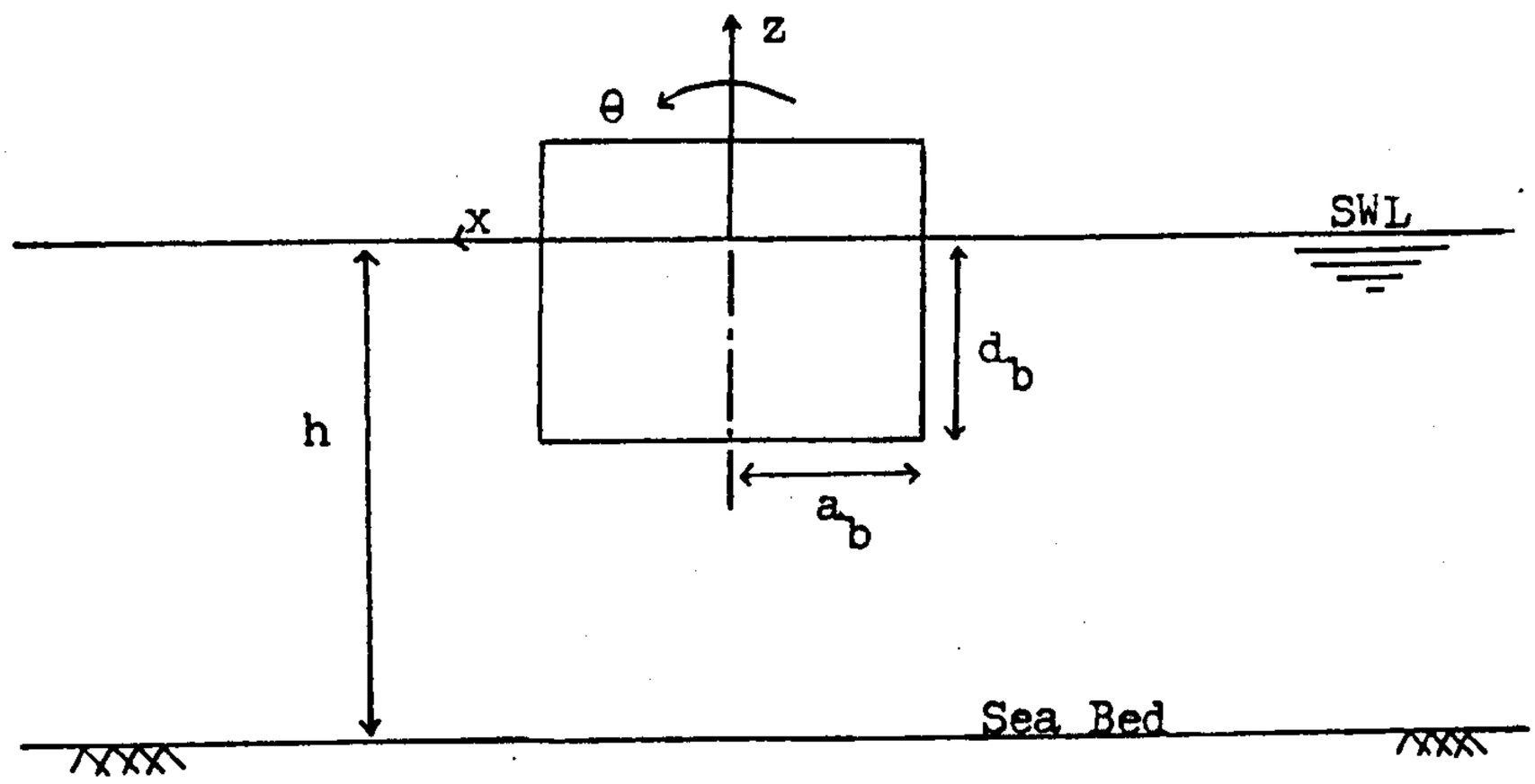

$$\overline{m}_{xx} = \rho \pi a_b^2 d_b \qquad \overline{m}_{\theta\theta} = \overline{m}_{xx} d_b^2/4 + 2\rho a_b^5/15$$

$$\overline{m}_{zz} = 2\pi a_b^3 \rho/3 \qquad \overline{m}_{\theta x} = -\overline{m}_{xx} 4d_b/(3\pi)$$

FIG. 4.4 NOTATION FOR FIGURE 4.5

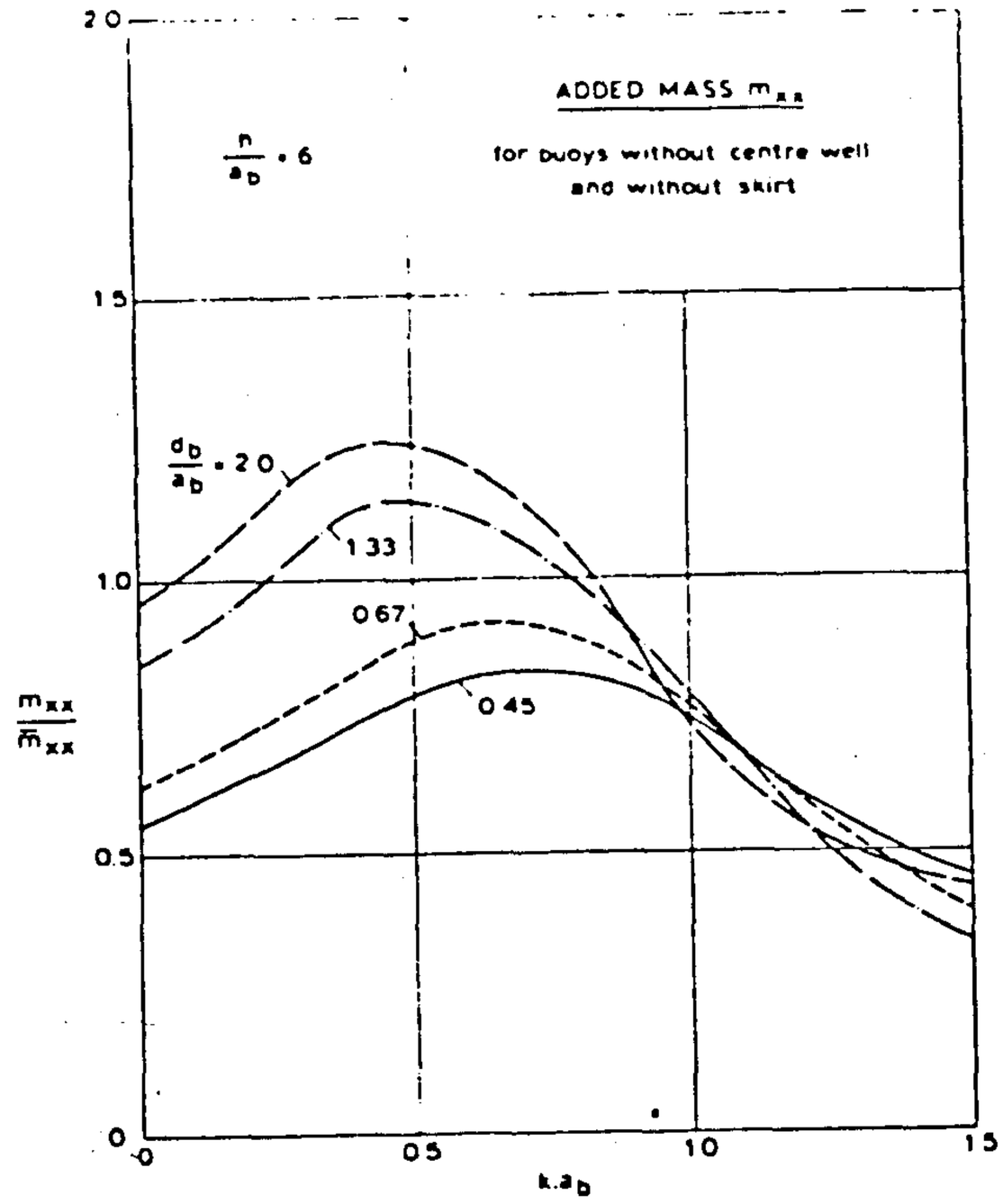

FIG. 4.5.1 SURGE ADDED MASS OF A MOORING BUOY

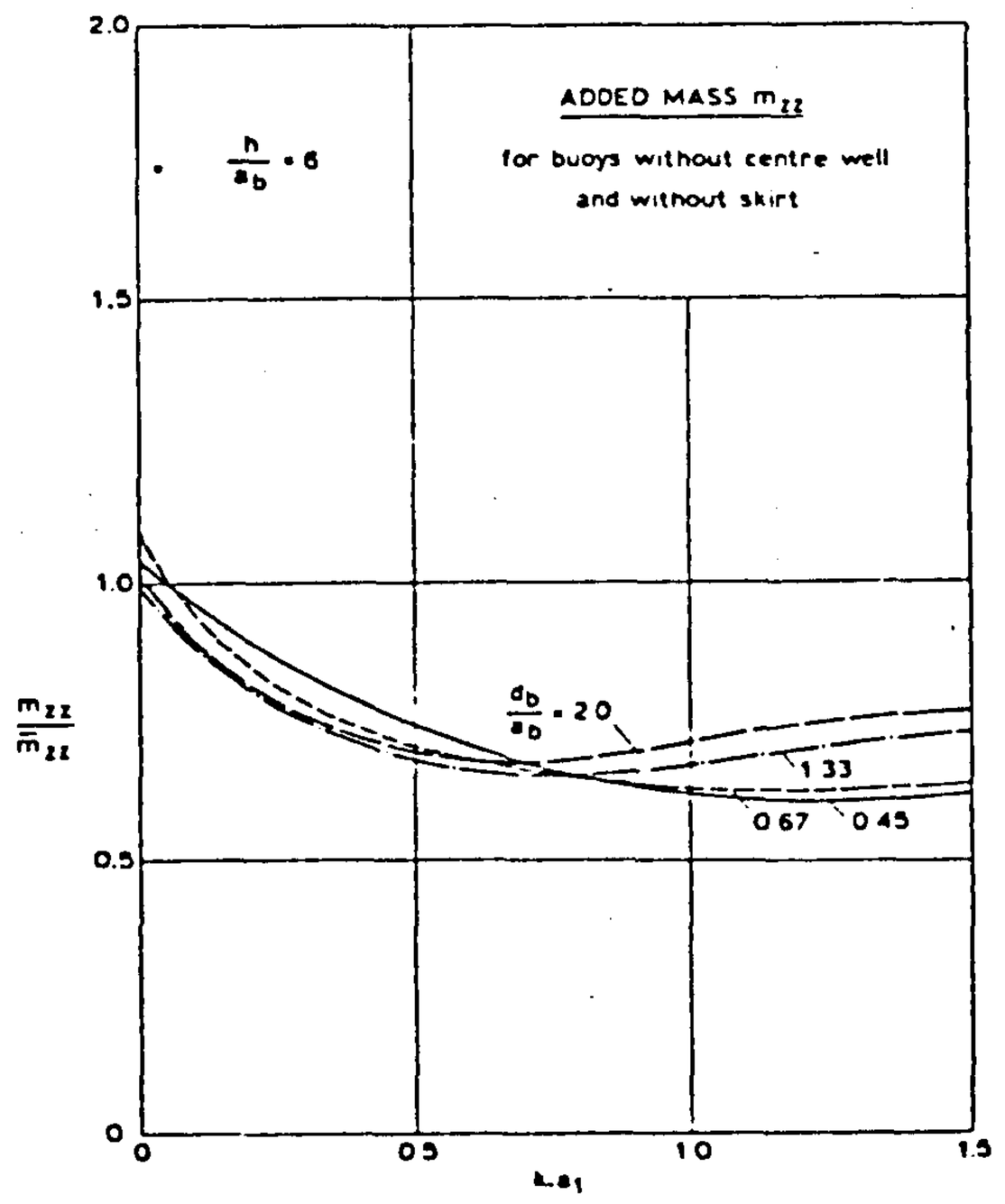

FIG. 4.5.2 HEAVE ADDED MASS OF A MOORING BUOY

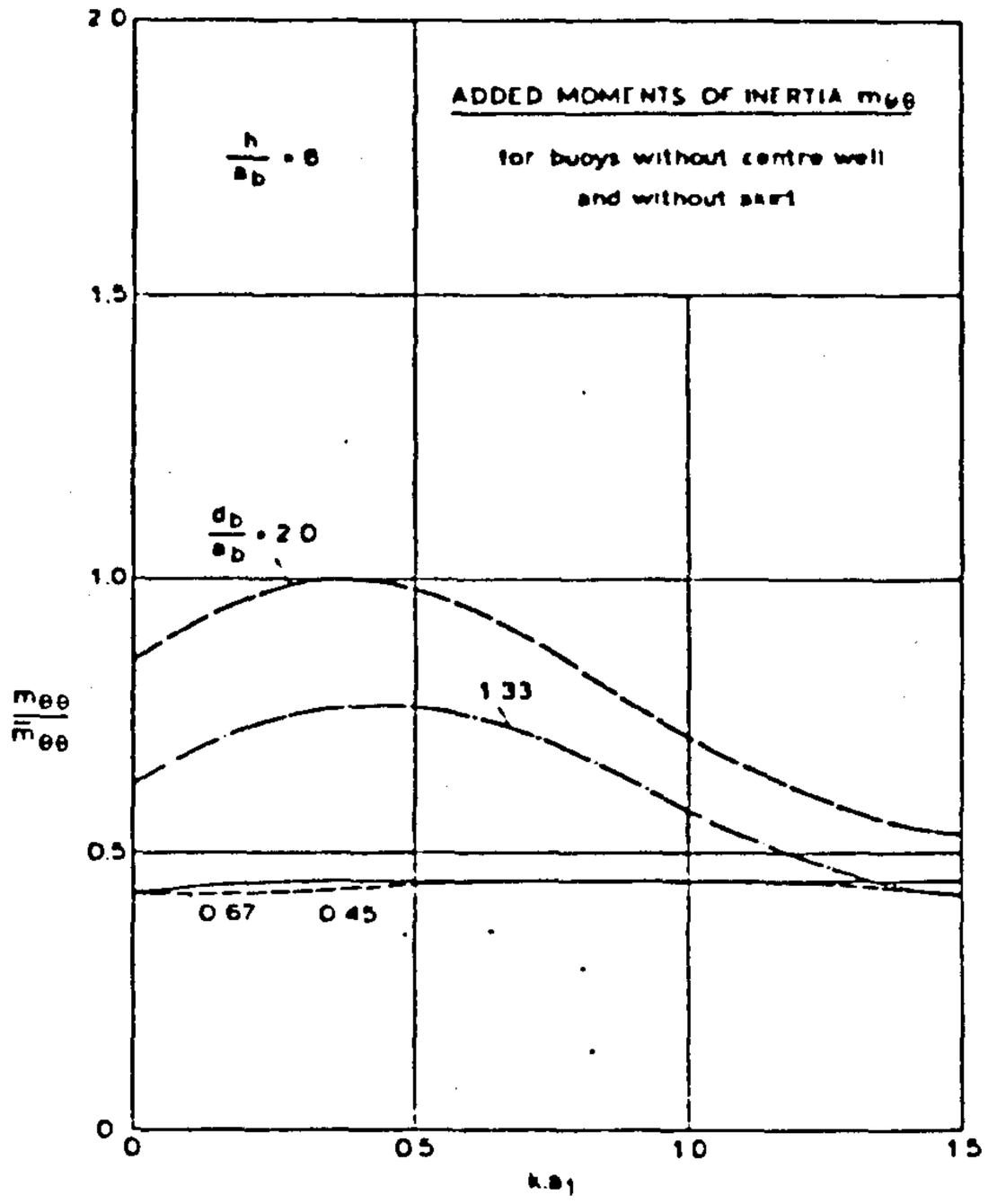

FIG. 4.5.3 PITCH ADDED MASS OF A MOORING BUOY

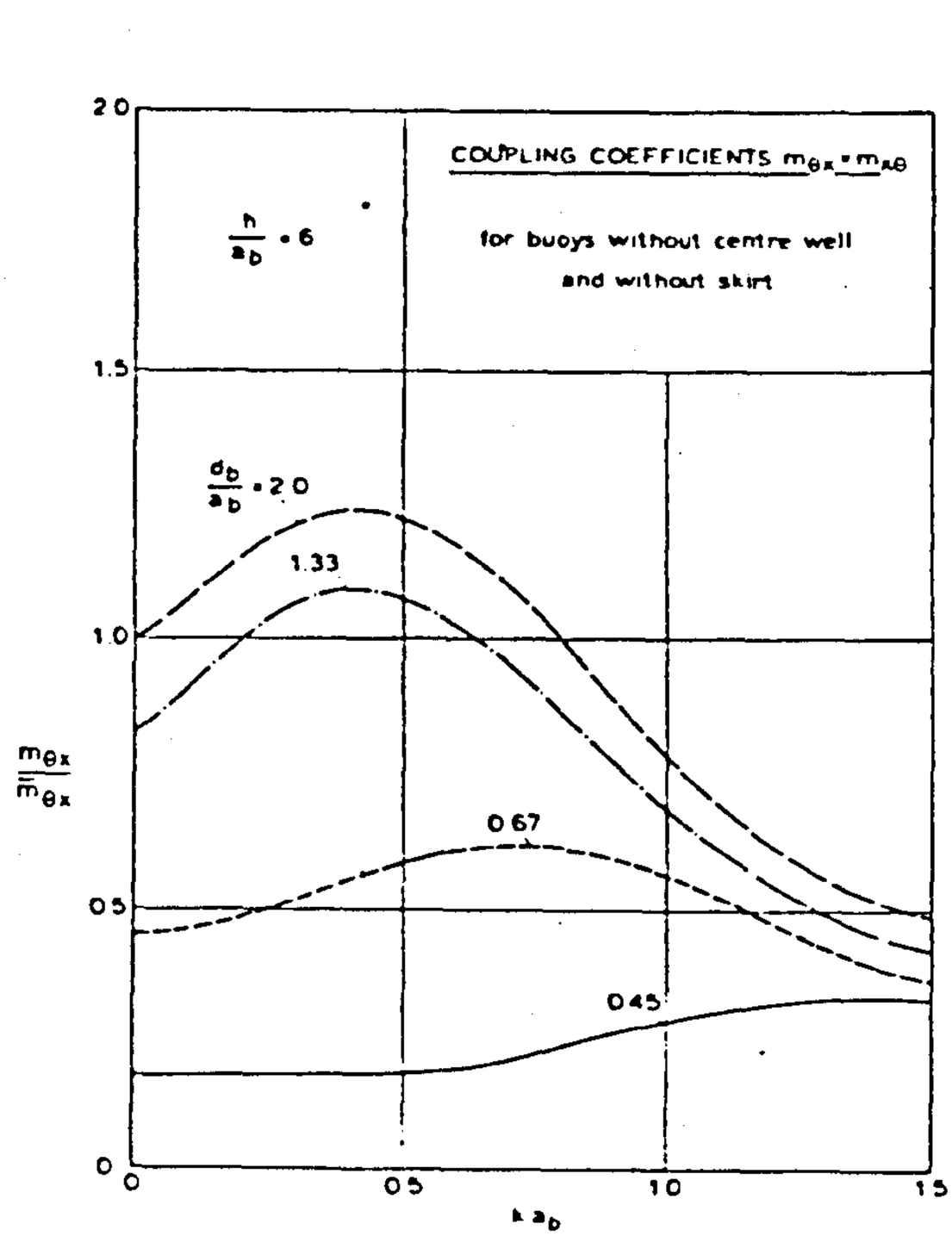

FIG. 4.5.4 PITCH-SURGE ADDED MASS OF A MOORING BUOY

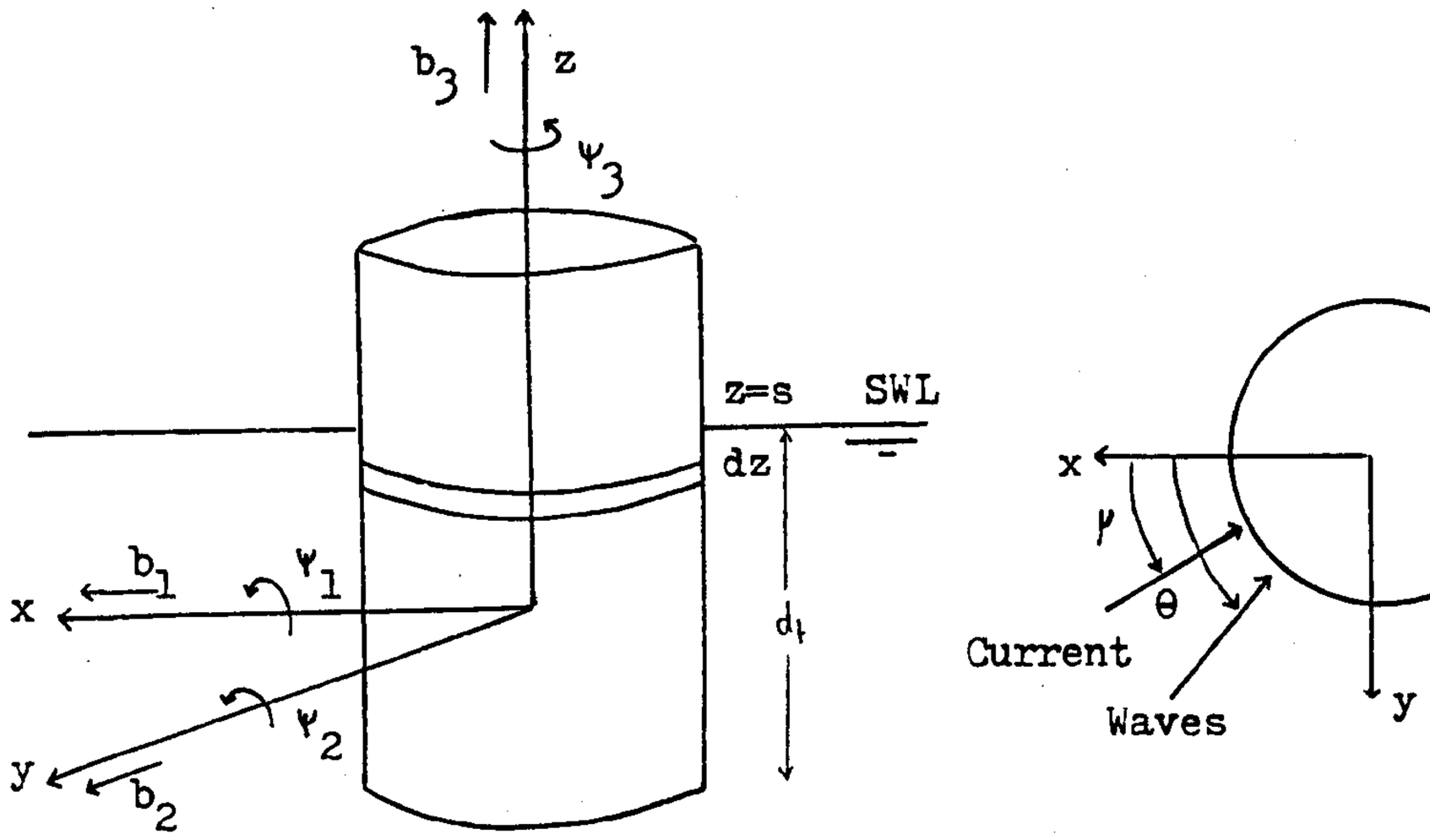

FIG. 4.6 NOTATION FOR THE ANALYSIS OF DRAG FORCES ACTING ON THE BUOY

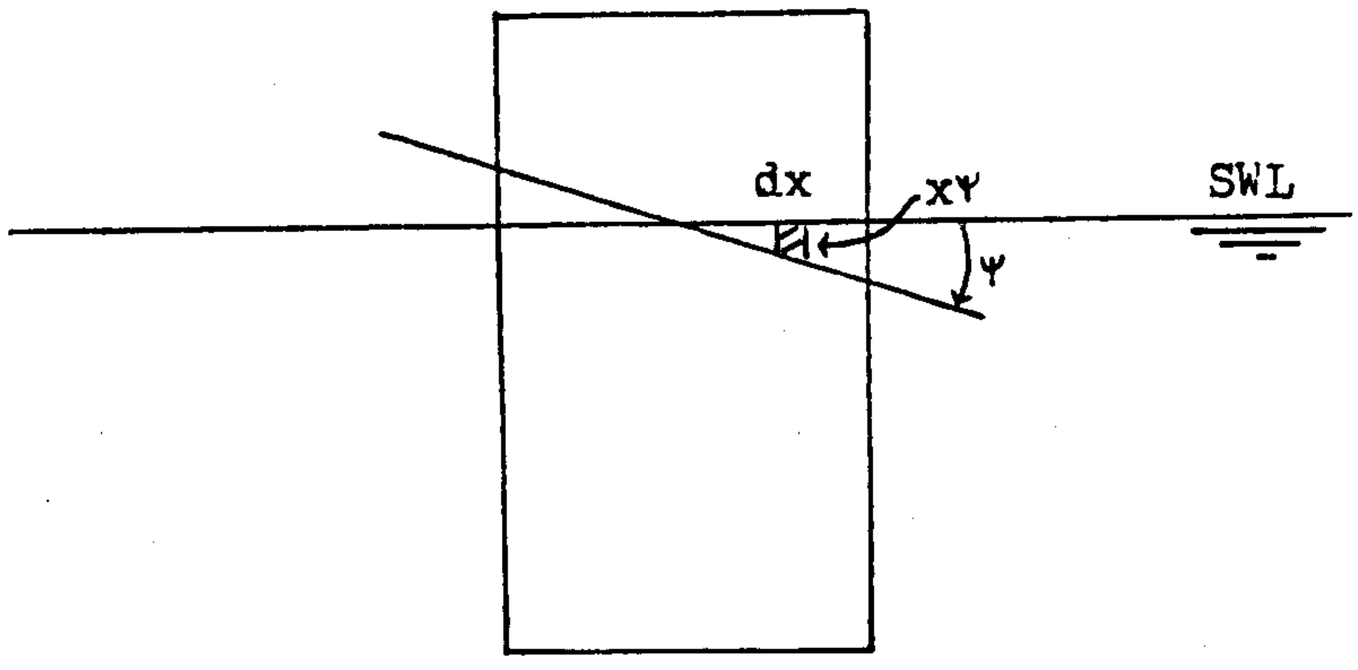

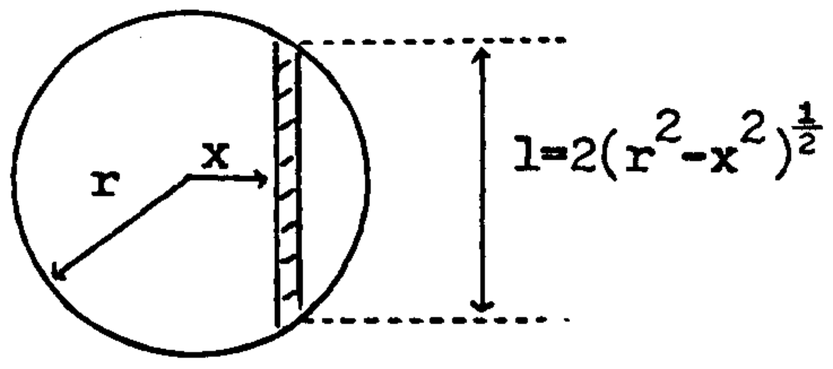

FIG. 4.7 CHANGE IN BUOYANCY DUE TO ROLL OR PITCH

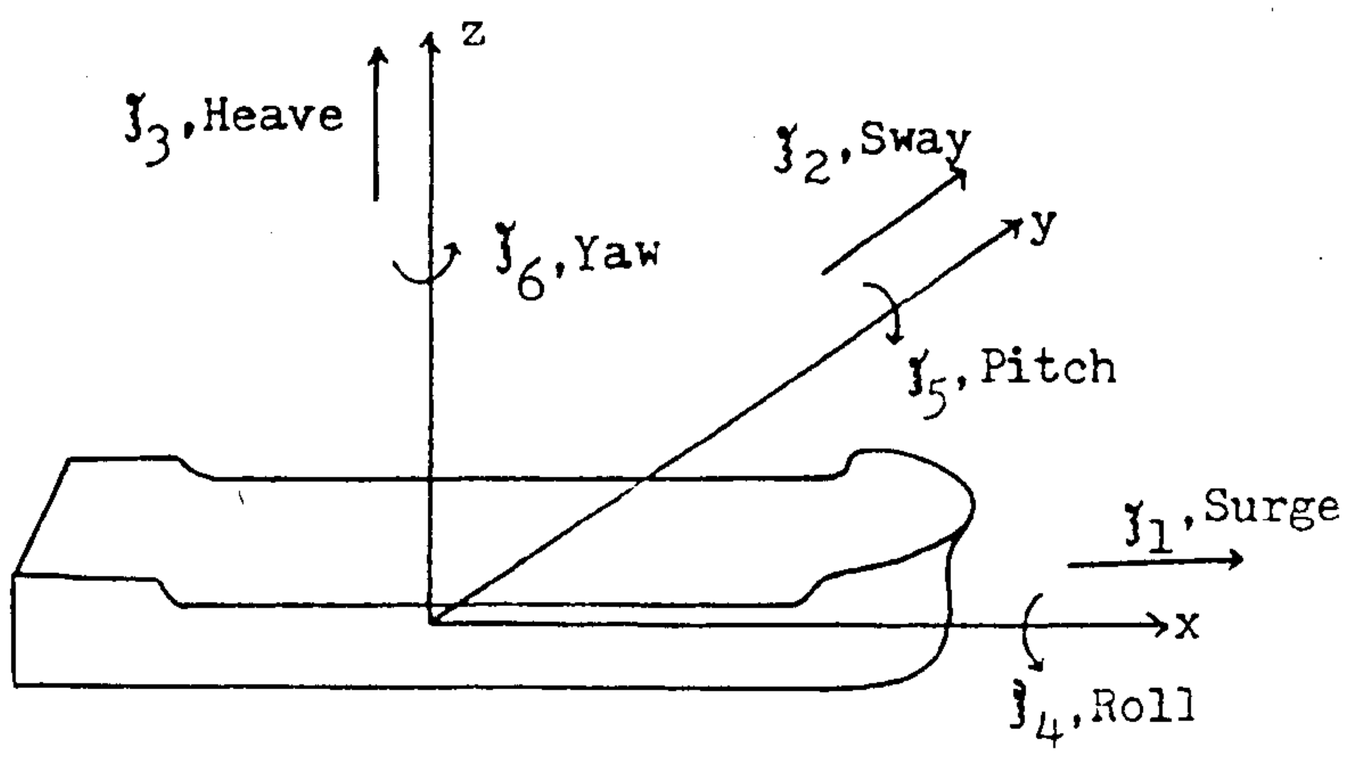

FIG. 5.1 VESSEL DEGREES OF FREEDOM

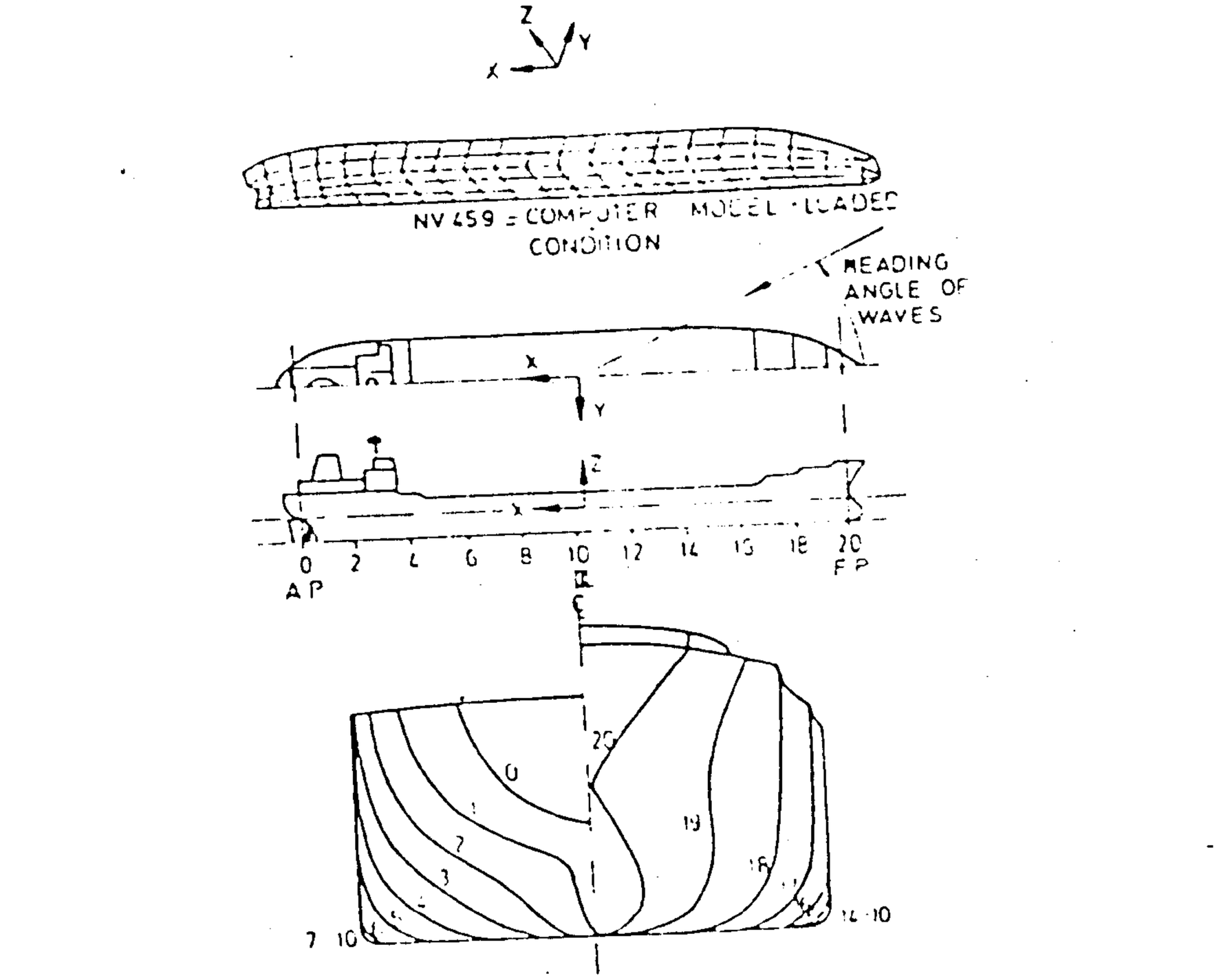

Tanker – displacement of 155,000 tons

FIG. 5.2 MESH FOR USE IN A DIFFRACTION PROGRAM

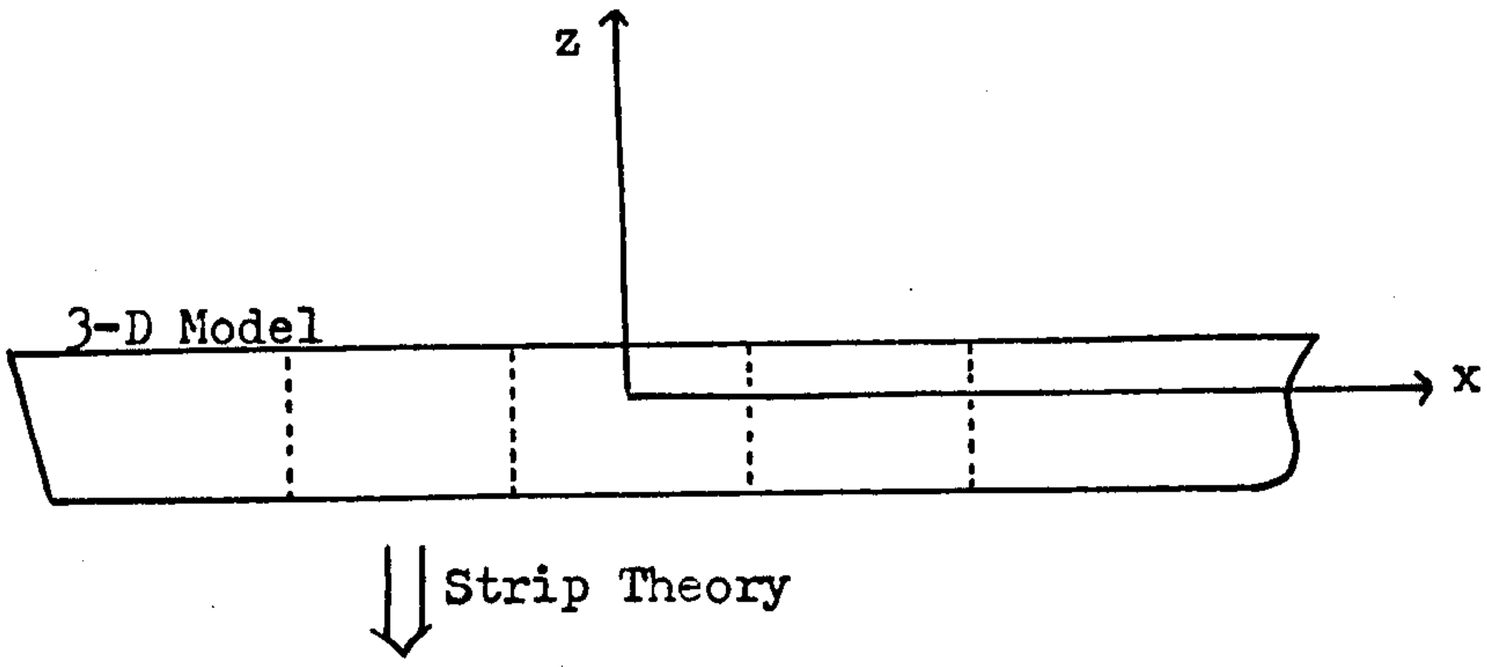

FIG. 5.3 STRIP THEORY

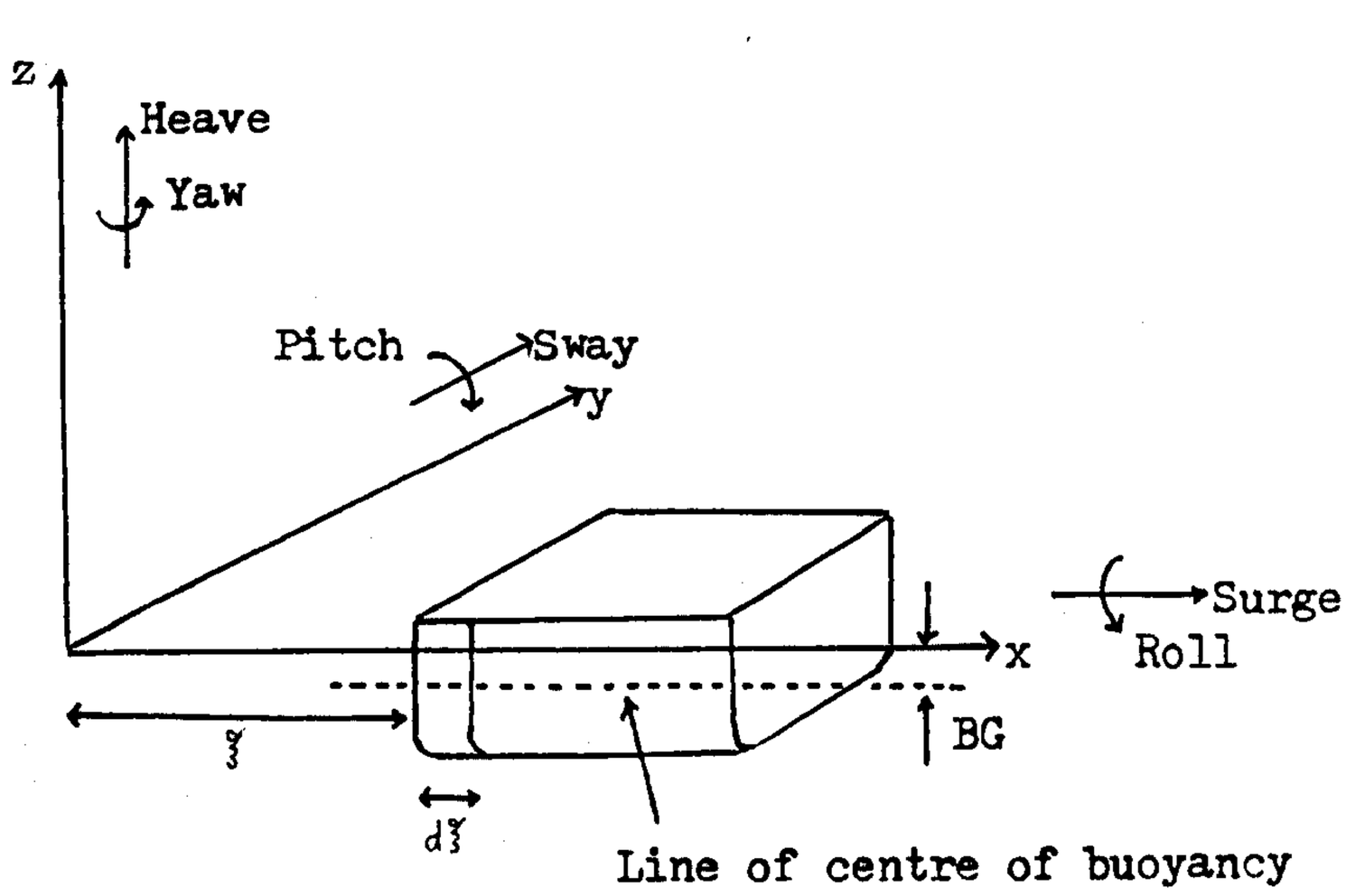

FIG. 5.4 SHIP SECTION

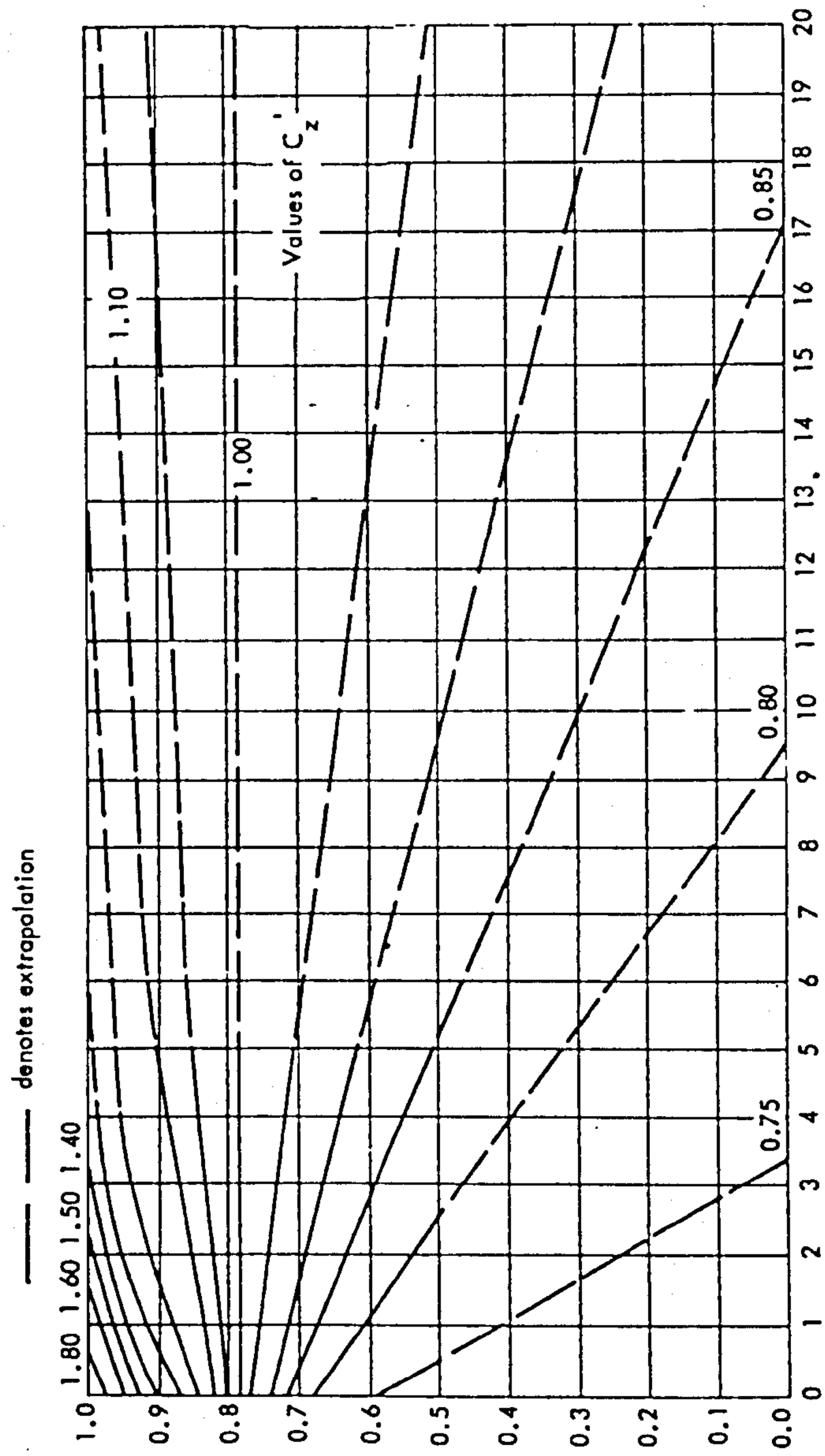

FIG. 5.5 THE COEFFICIENT C_Z' AS GIVEN BY PROHASKA, REF. 57

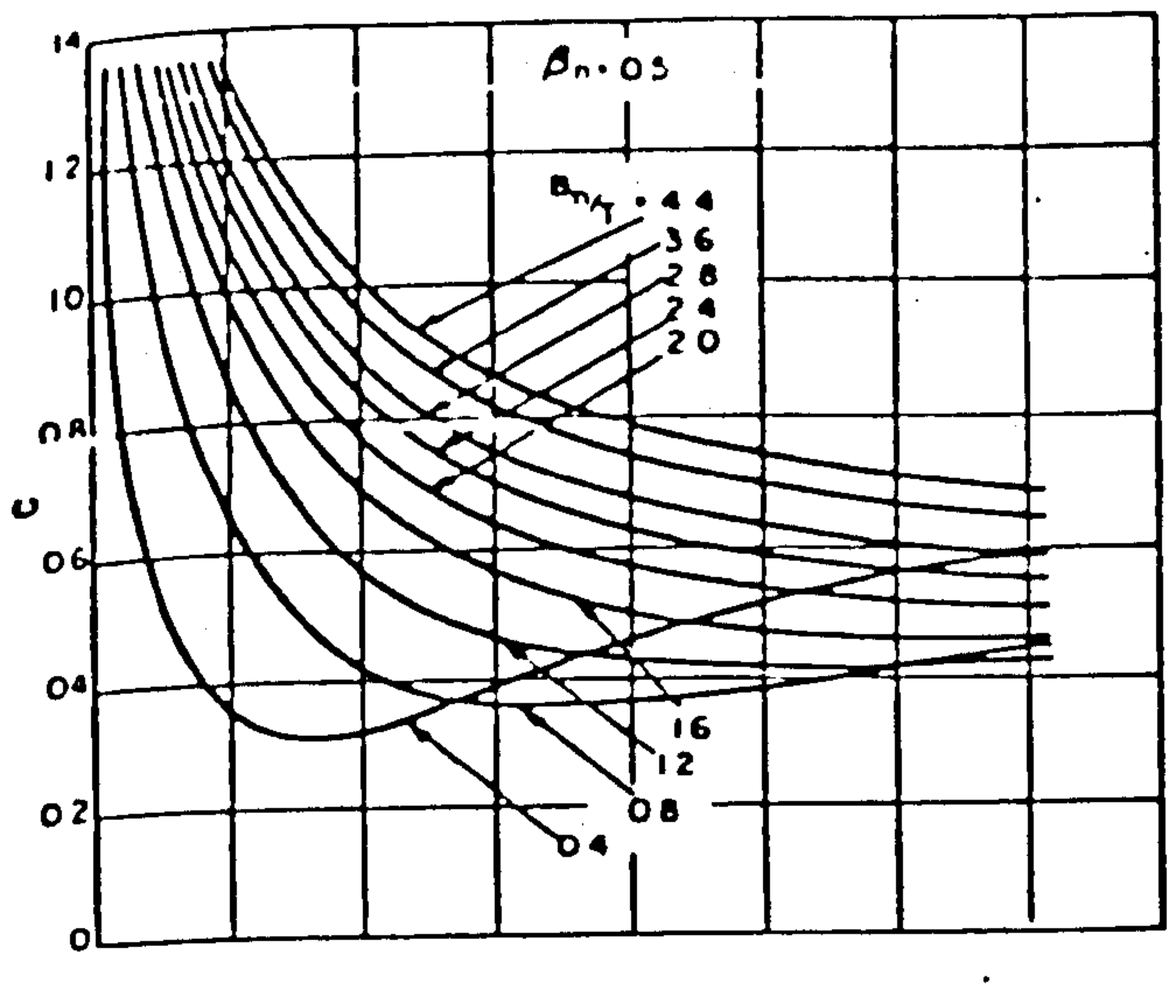

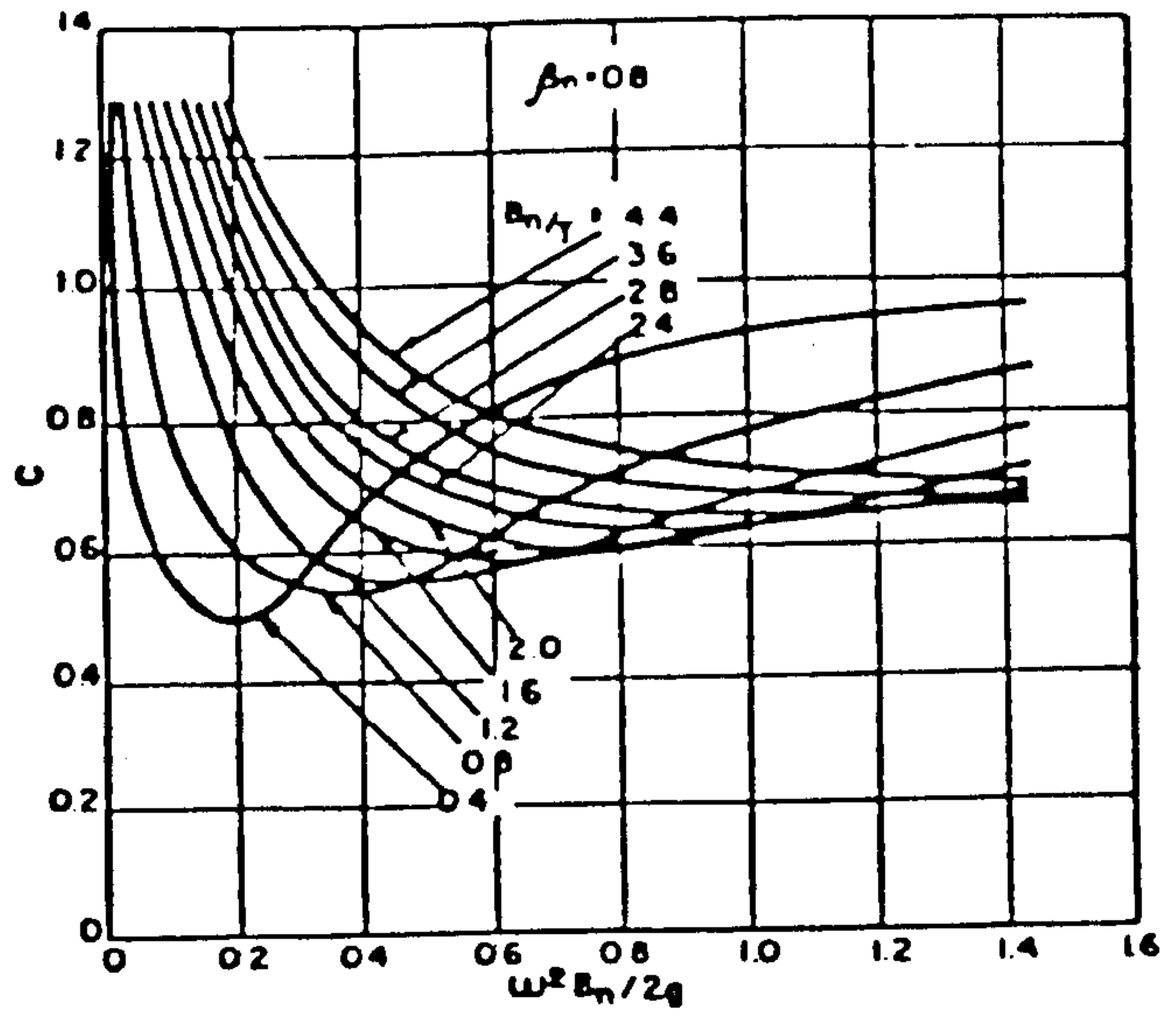

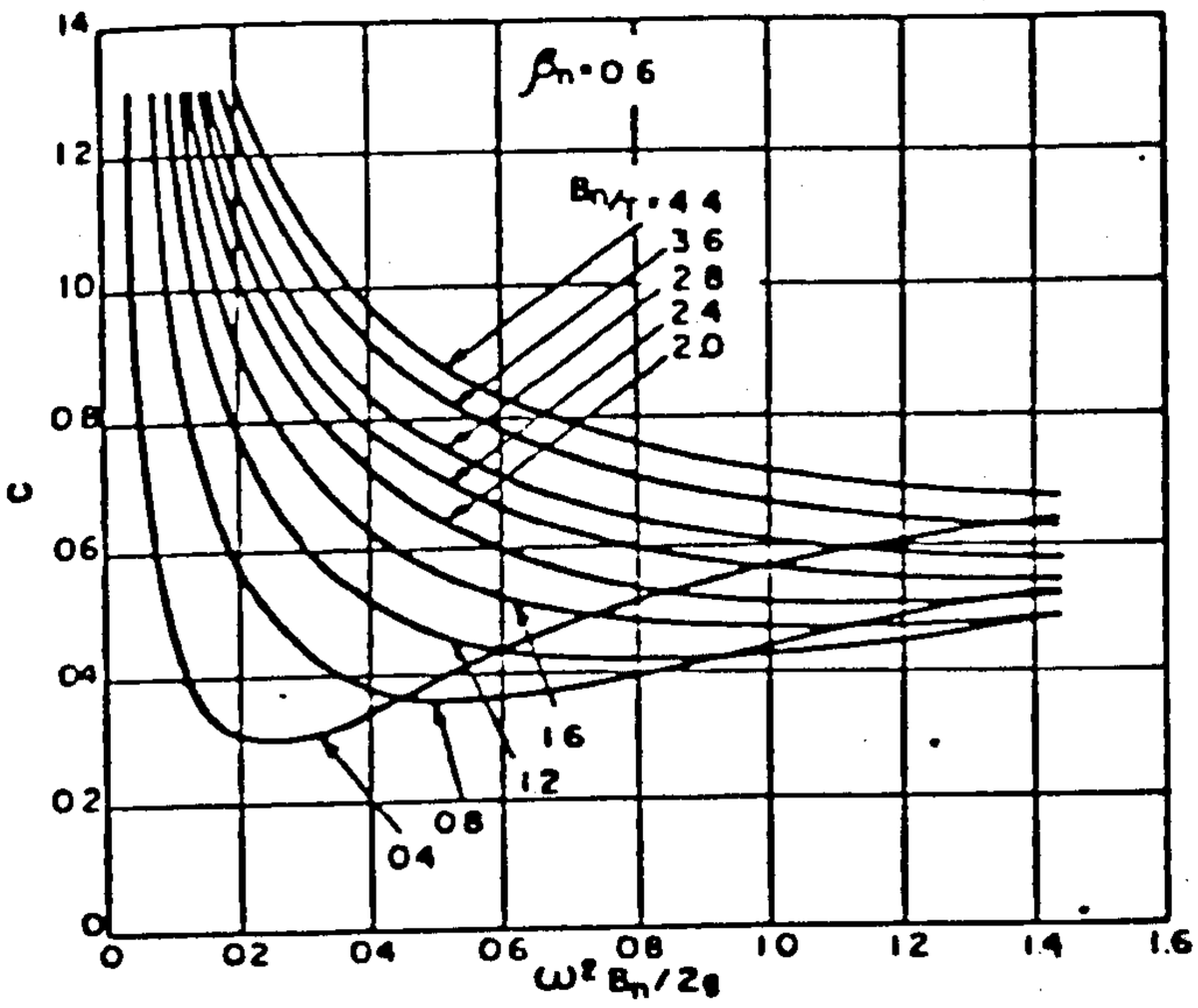

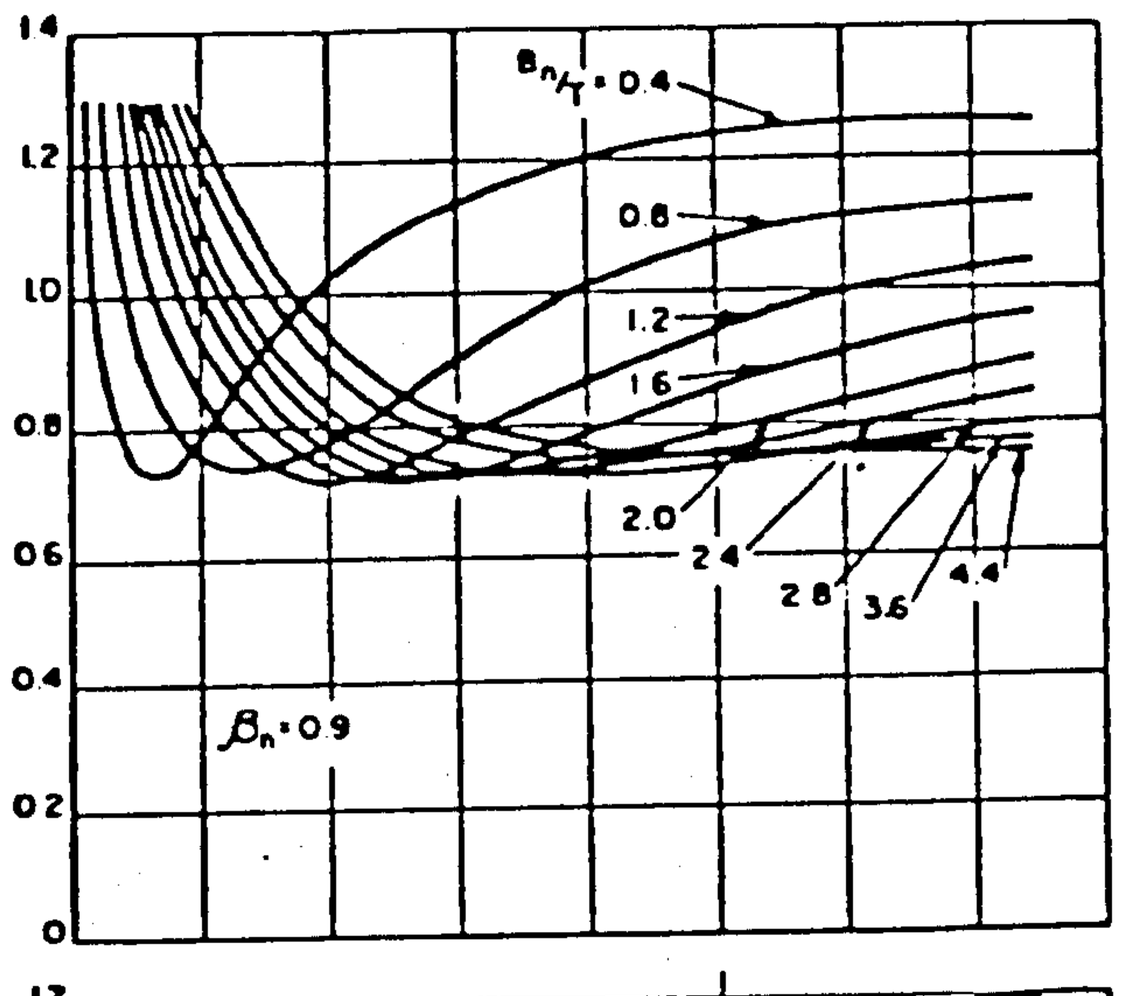

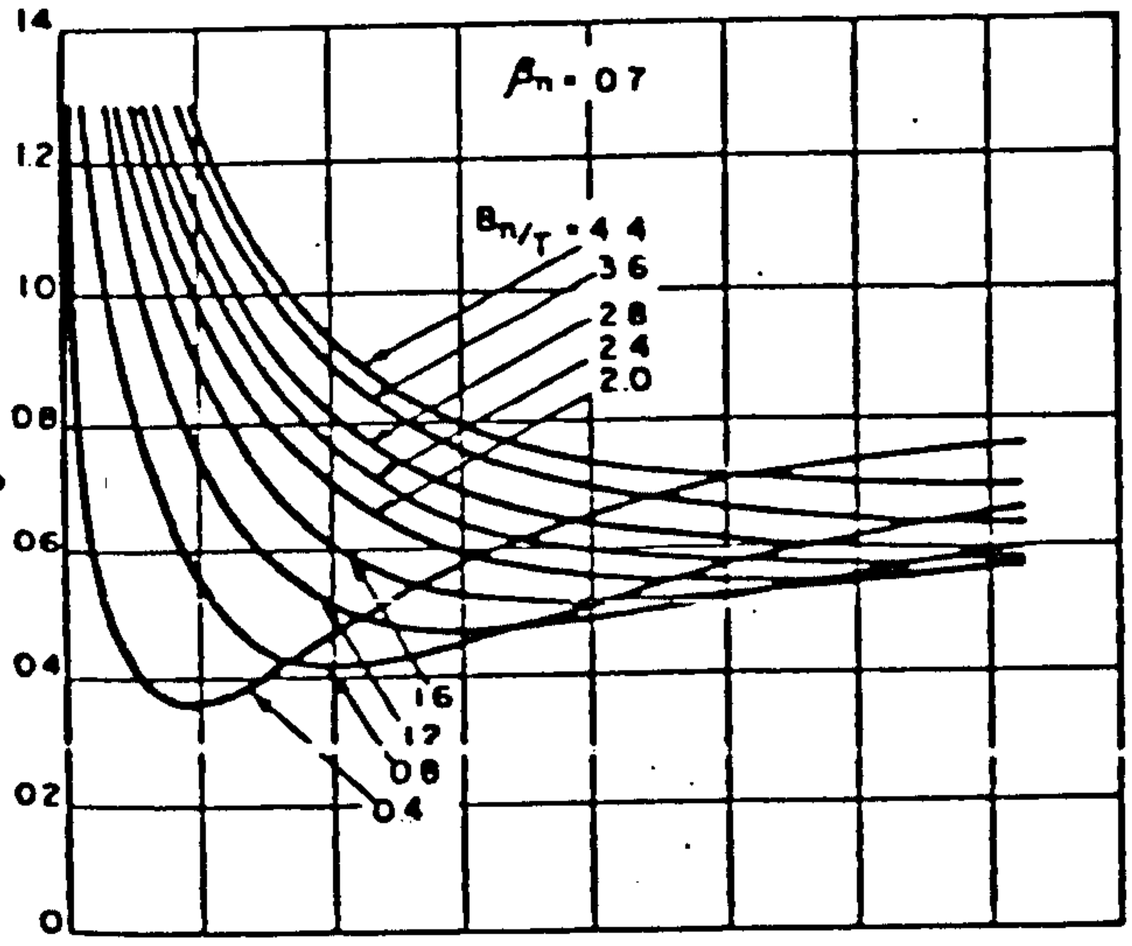

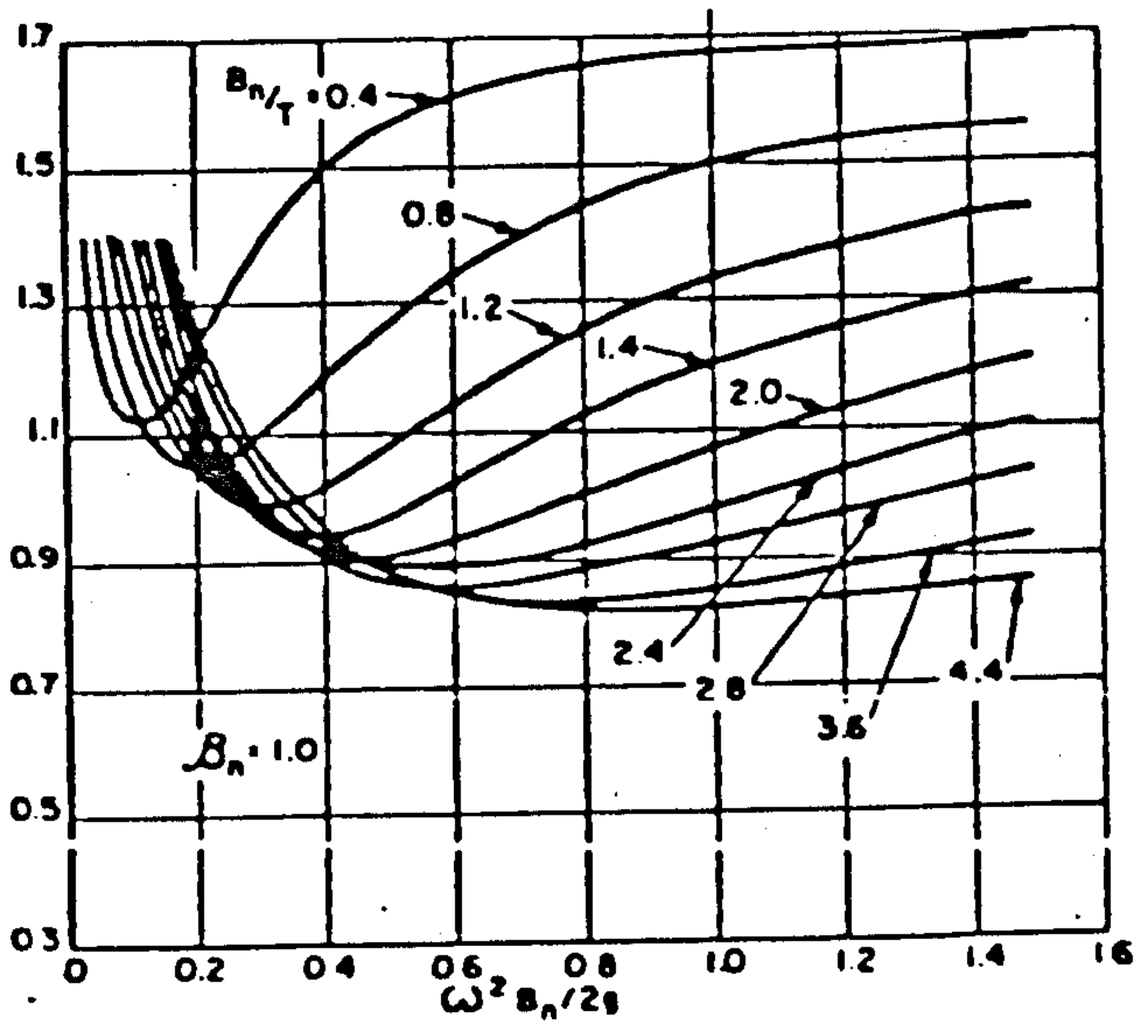

FIG. 5.6 GRIM'S DATA FOR THE ADDED MASS OF A SHIP SECTION
(REF. 66)

	1	2	3	4	5	6
1	Sommet or Wichers and Sluijs					
2	0	Prohaska + k'_4 from Kaplan				
3	0	0	Grim's data			
4	0	$BG.A'_{22}$	0	$V'K^2_{xx}$		
5	$-BG.A_{11}$	0	$\frac{}{}A'_{33}$	0	$\frac{}{}^2A'_{33}$	
6	0	$\frac{}{}A'_{22}$	0	$\frac{}{}A'_{42}$	0	$\frac{}{}^2A'_{22}$

1 = Surge
2 = Sway
3 = Heave
4 = Roll
5 = Pitch
6 = Yaw

FIG. 5.7 SUMMARY OF ADDED MASS TERMS

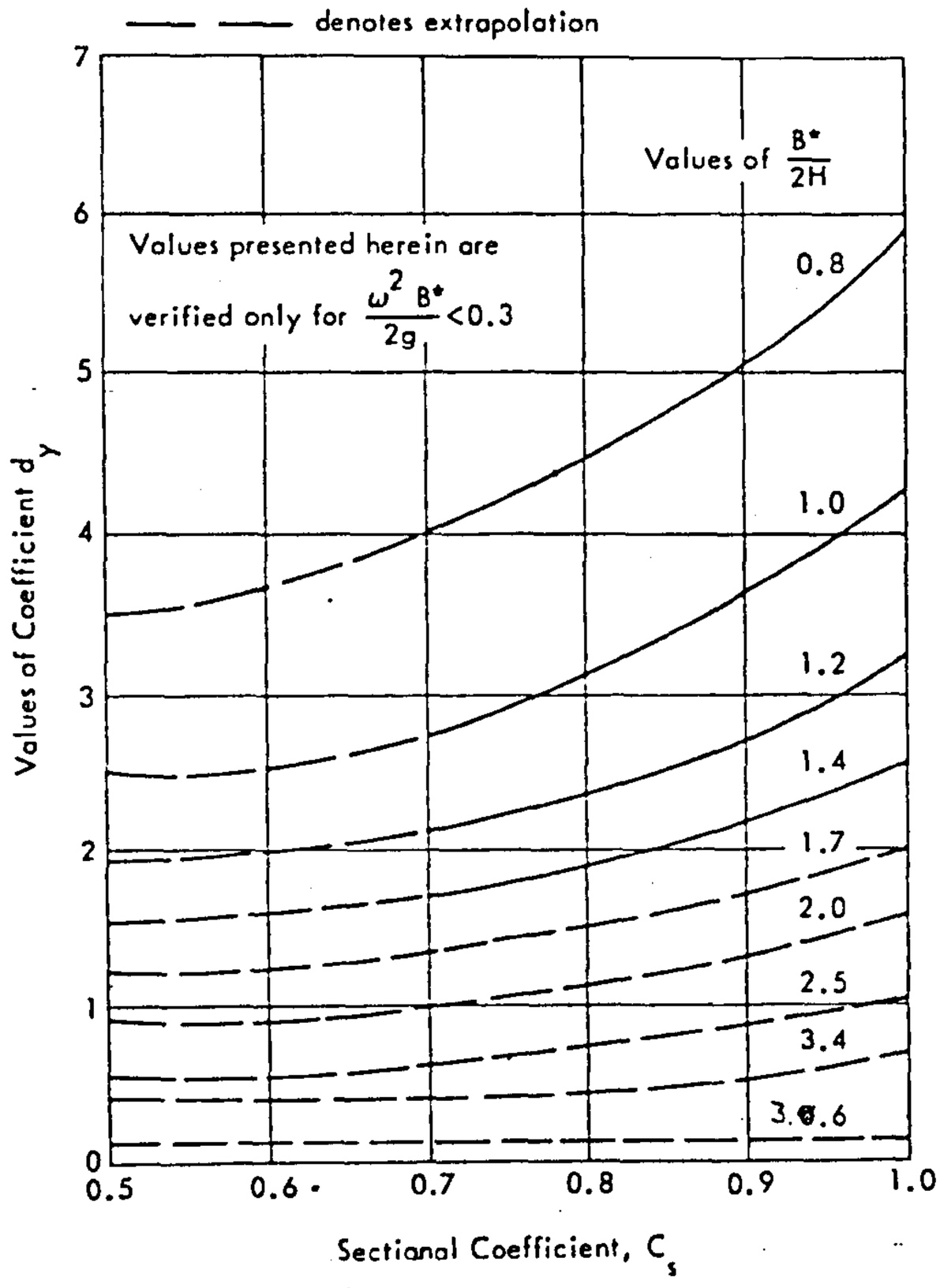

FIG. 5.8 THE COEFFICIENT d_y AS GIVEN BY VOSSERS, REF. 62

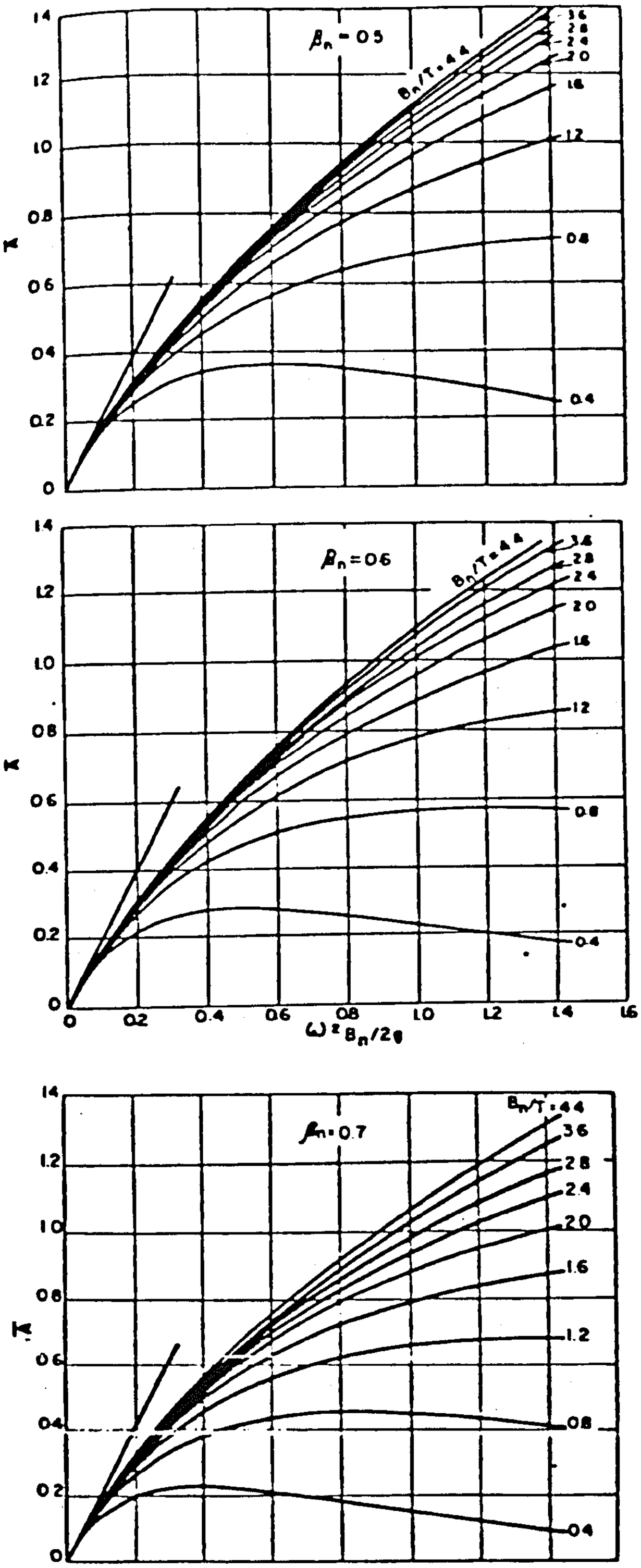

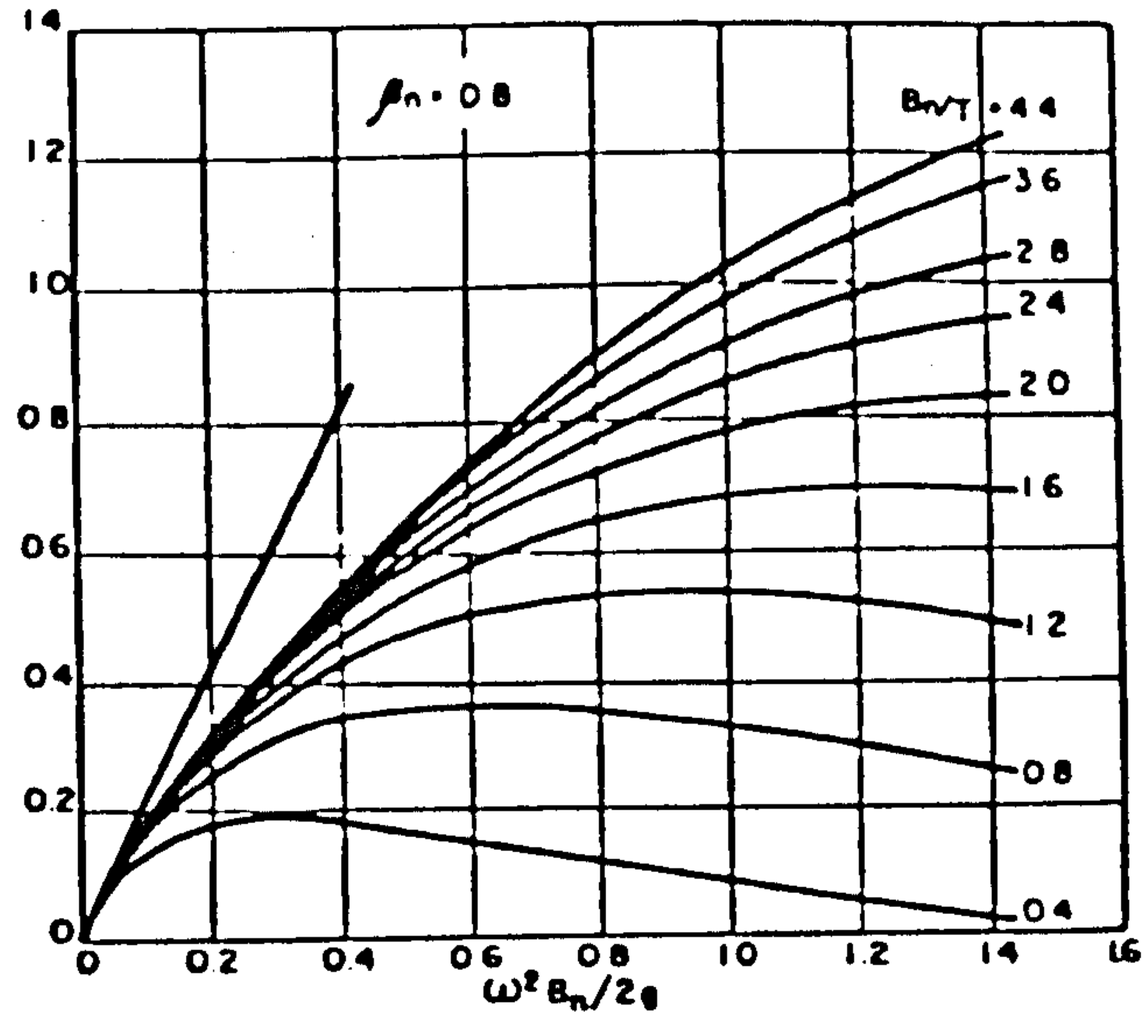

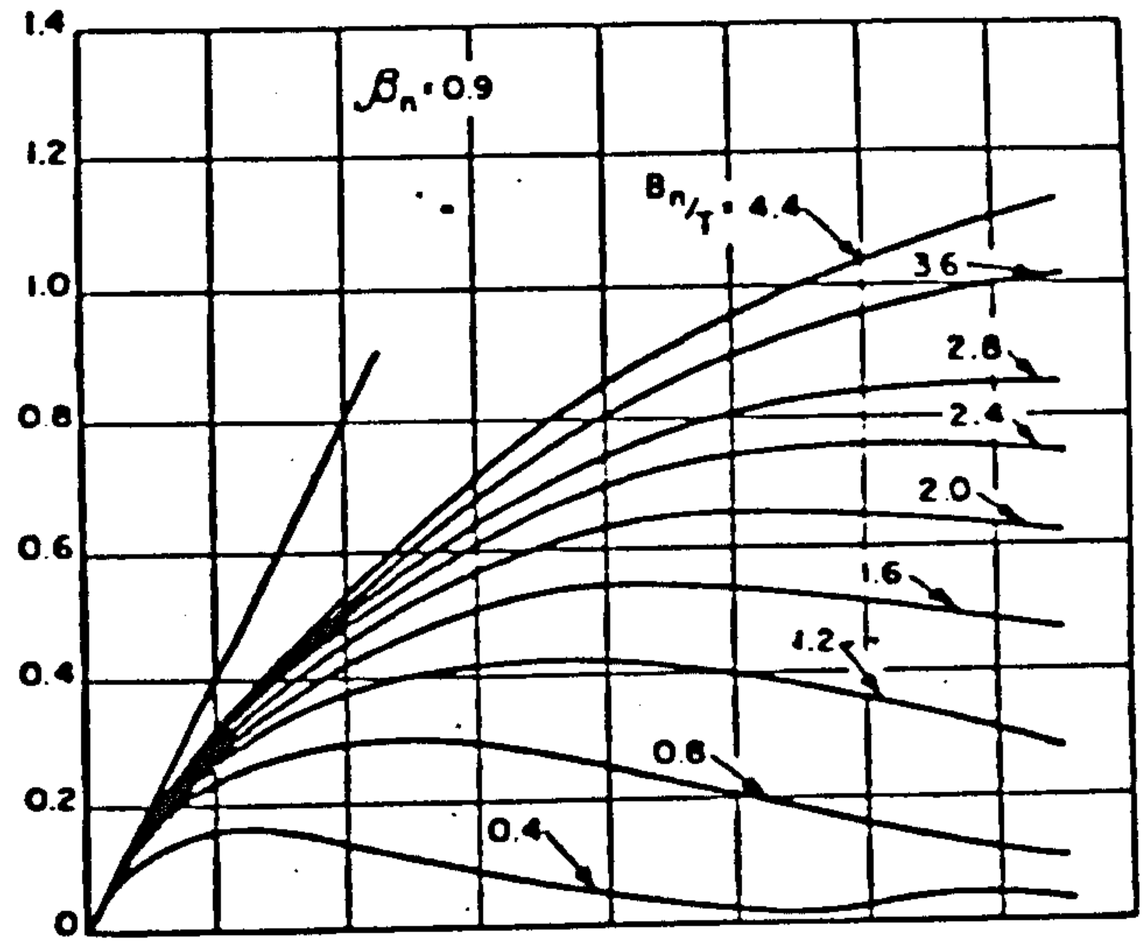

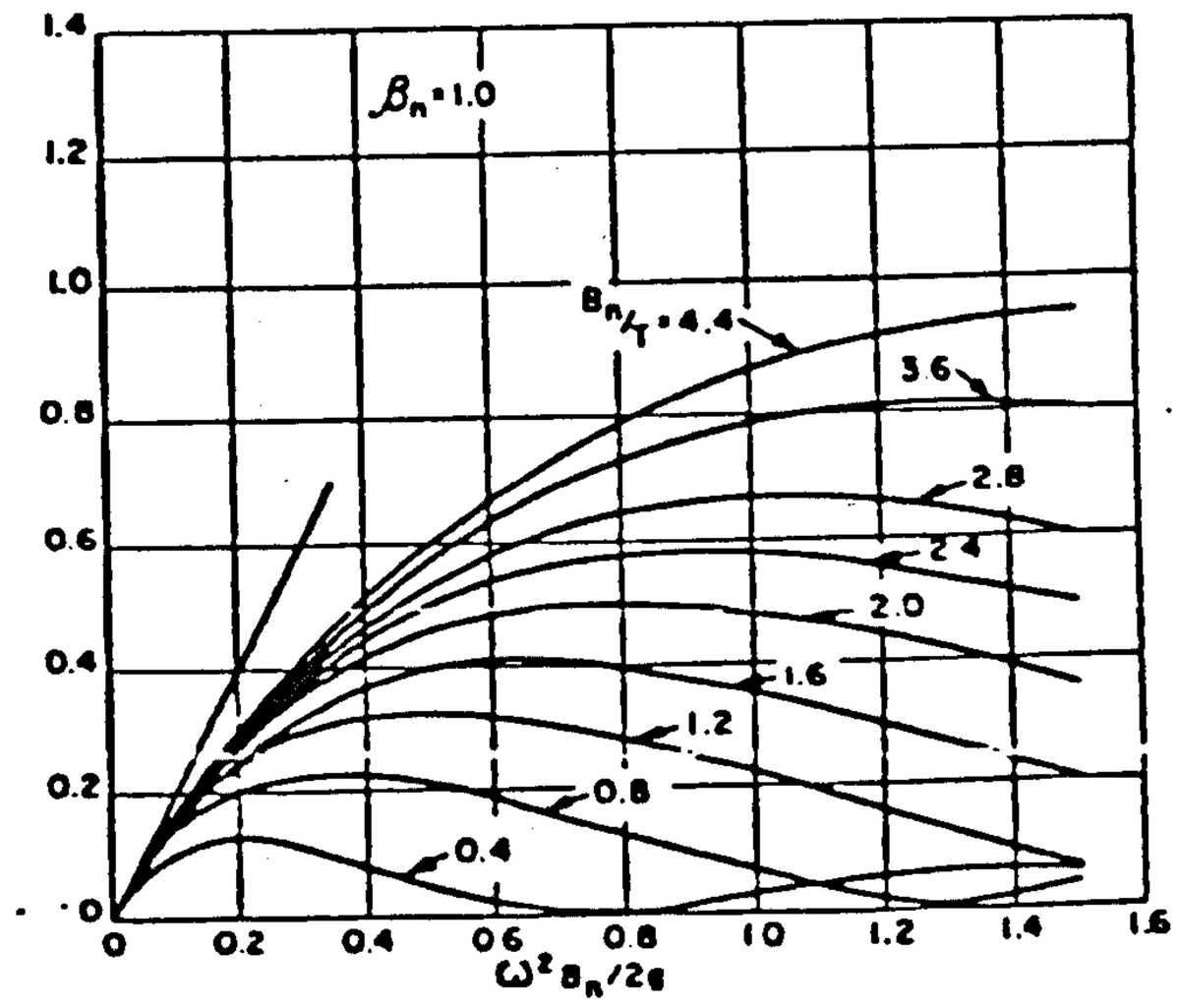

FIG. 5.9 GRIM'S DATA FOR THE POTENTIAL DAMPING OF A SHIP SECTION (REF. 66)

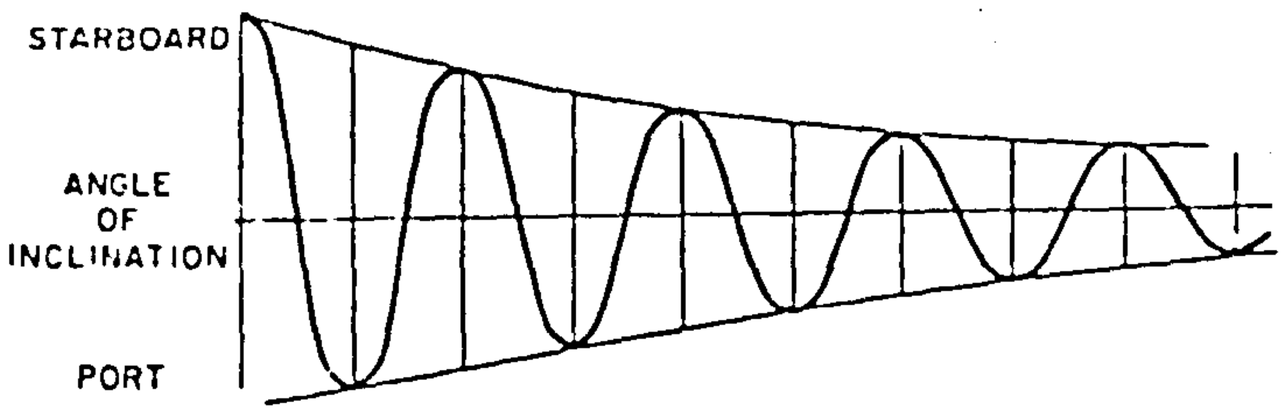

Motion of ship due to resisted rolling in still water.

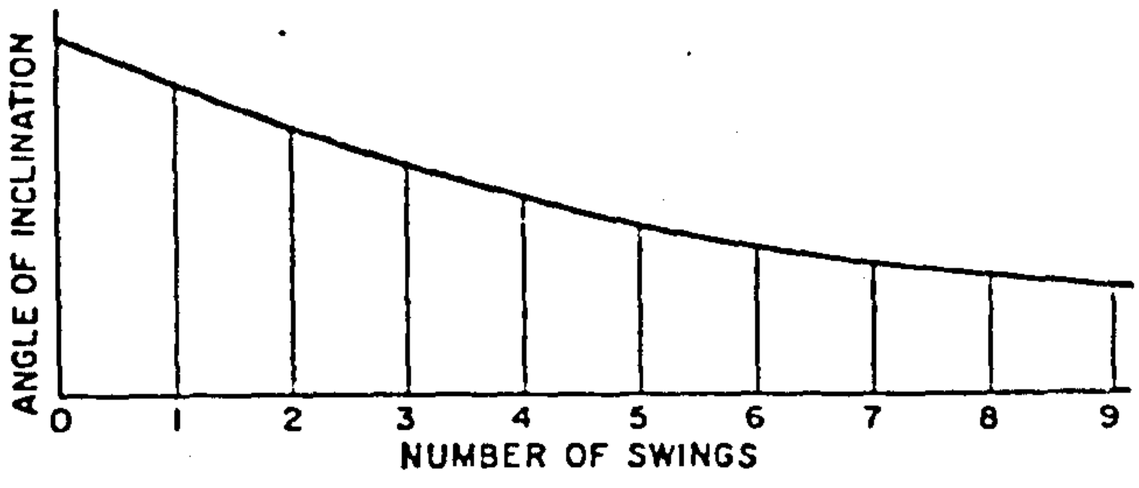

Curve of declining angles in still water

Name	Bilge keels	Period of roll, sec	K_1	K_2	Δ, tons
Greyhound.....	None	8.70	0.0440	0.0032	1160
Greyhound.....	Yes	8.66	0.0350	0.0500	1160
Revenge.....	None	16.00	0.0150	0.0028	13370
Revenge.....	Yes	16.80	0.0840	0.0190	13370
Revenge.....	None	15.20	0.0123	0.0025	14300
Revenge.....	Yes	15.50	0.0650	0.0170	14300
Oregon.....	None	15.20	0.0110	0.0021	9810
Oregon.....	Yes	15.66	0.0450	0.0230	9790

FIG. 5.10 ROLL EXTINCTION CURVE AND THE COEFFICIENTS K_1 AND K_2

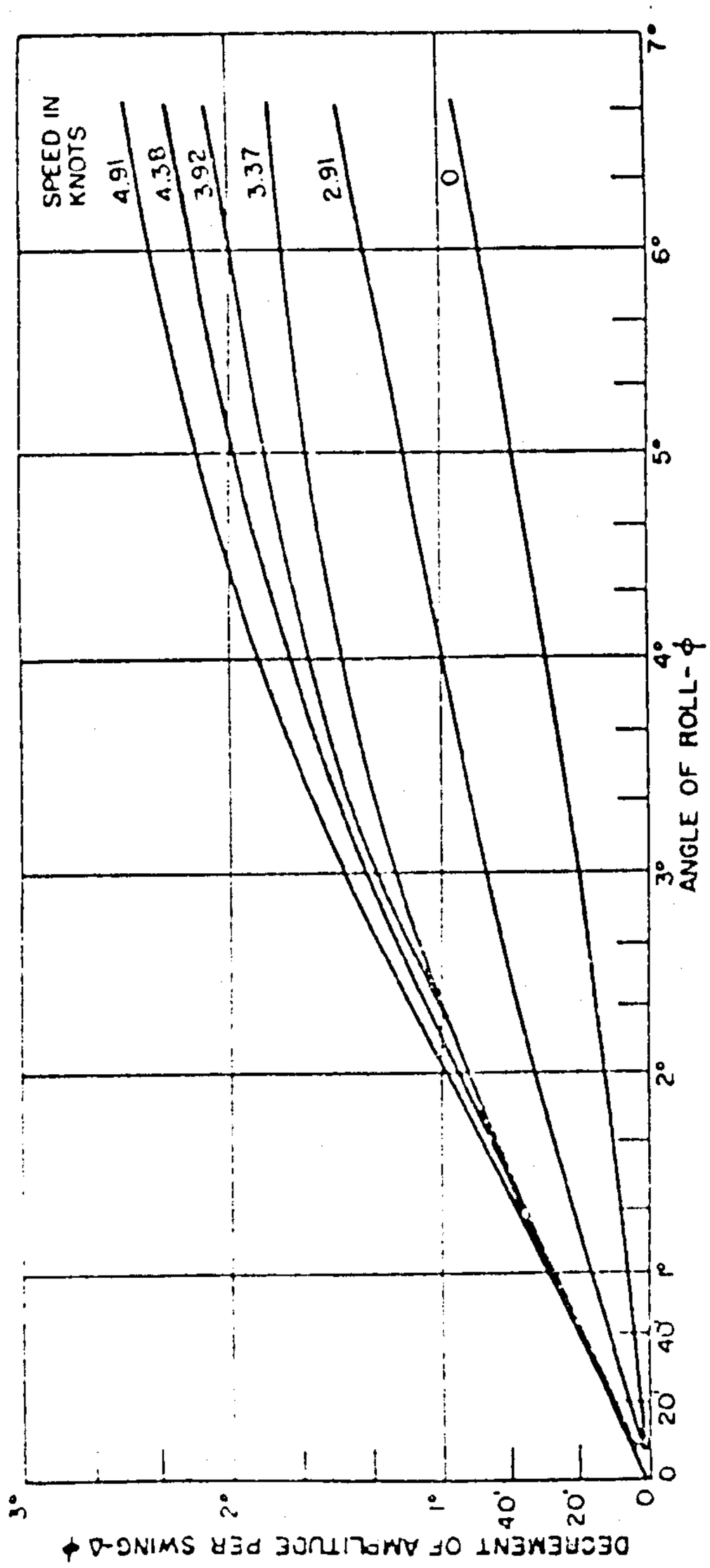

FIG. 5.11 THE EFFECT OF FORWARD SPEED ON ROLL DAMPING

	1	2	3	4	5	6
1	Wichers and Sluijs or 10% of heave damping					
2	0	N'_{yy} -Vossers C_{22} -Kaplan				
3	0	0	C_{33} -Havelock N'_{33} -Grim			
4	0	$N'_{24}=BG.N'_{22}$ $C_{24}=C_{22}$	0	Model Tests		
5	0	0	$N'_{35}= \gamma N'_{33}$ $C_{35}= 1$	0	$N'_{55}= \gamma^2 N'_{22}$ $C_{55}= C_{22}$	
6	0	$N'_{62}= \gamma N'_{22}$ $C_{62}= 1$	0	$N'_{46}= \gamma N'_{42}$ $C_{46}= 1$	0	$N'_{66}= \gamma^2 N'_{22}$ C_{66} -Kaplan

FIG. 5.12 SUMMARY OF DAMPING TERMS (NOTATION AS IN FIG. 5.7)

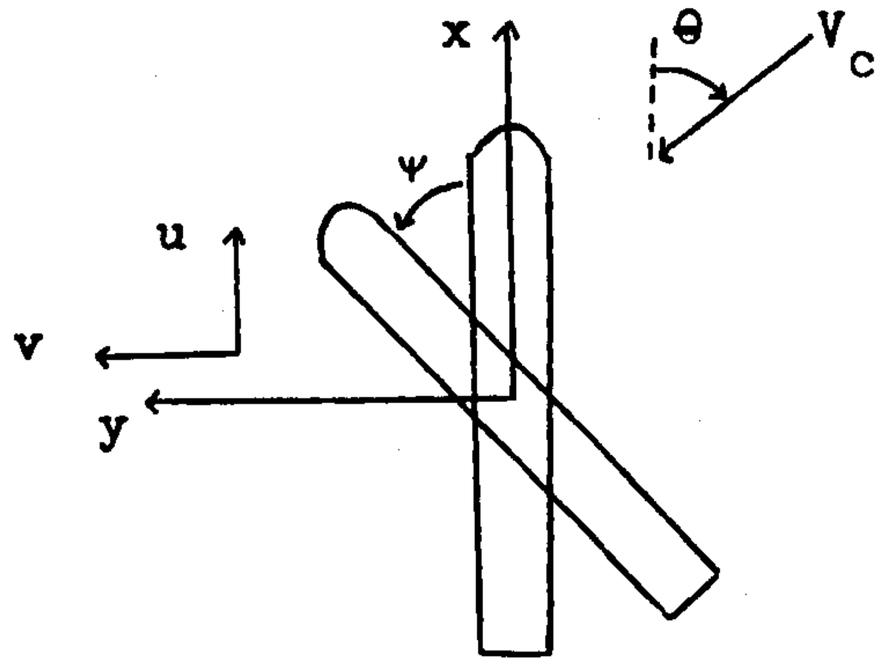

FIG. 5.13 CURRENT DAMPING

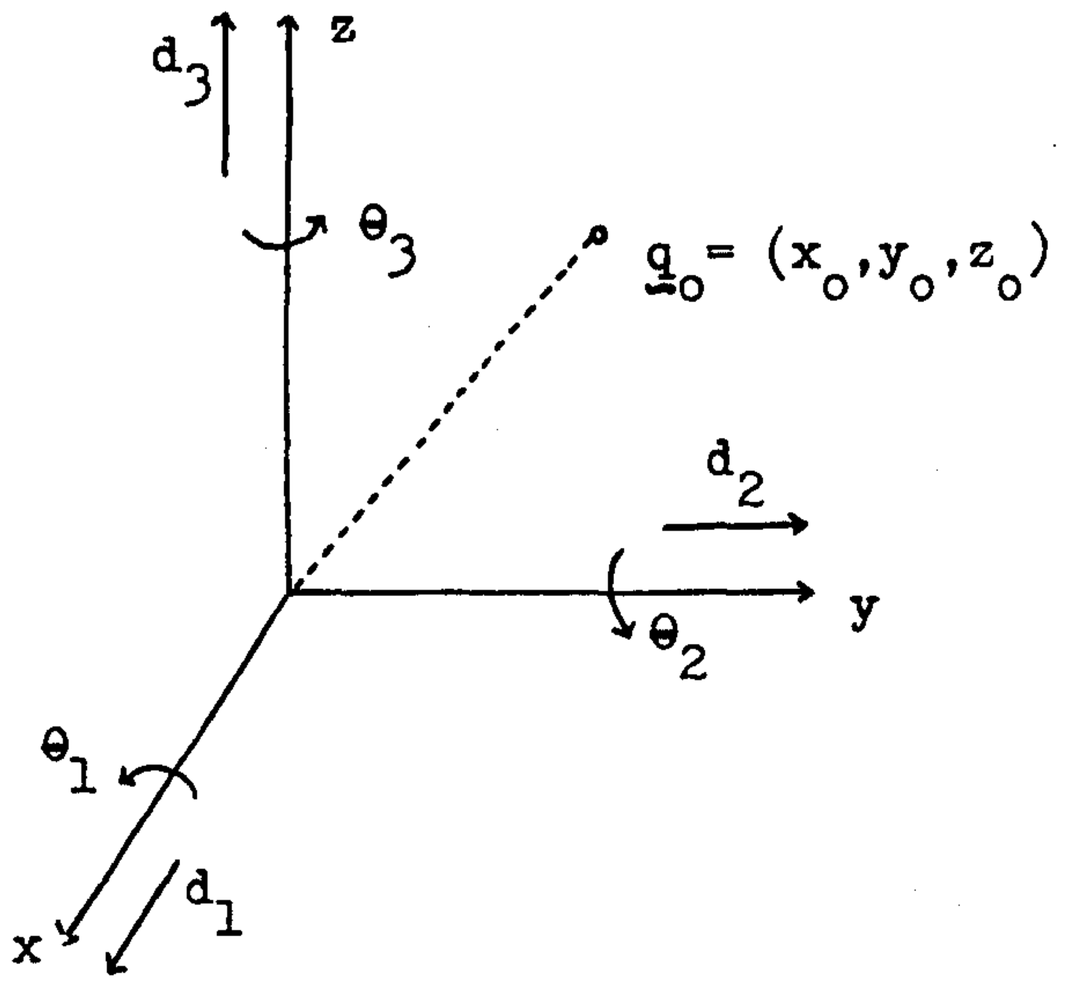

FIG. 6.1 COORDINATE SYSTEM FOR A FLOATING BODY

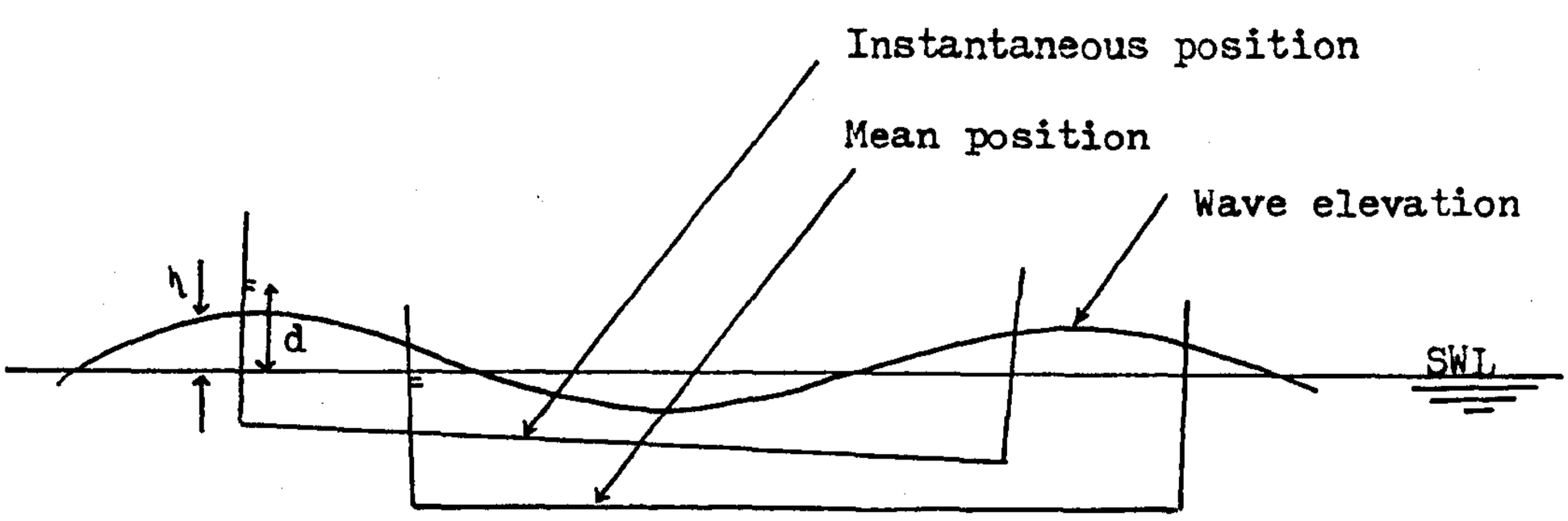

FIG. 6.2 WATERLINE DISPLACEMENT OF A FLOATING BODY

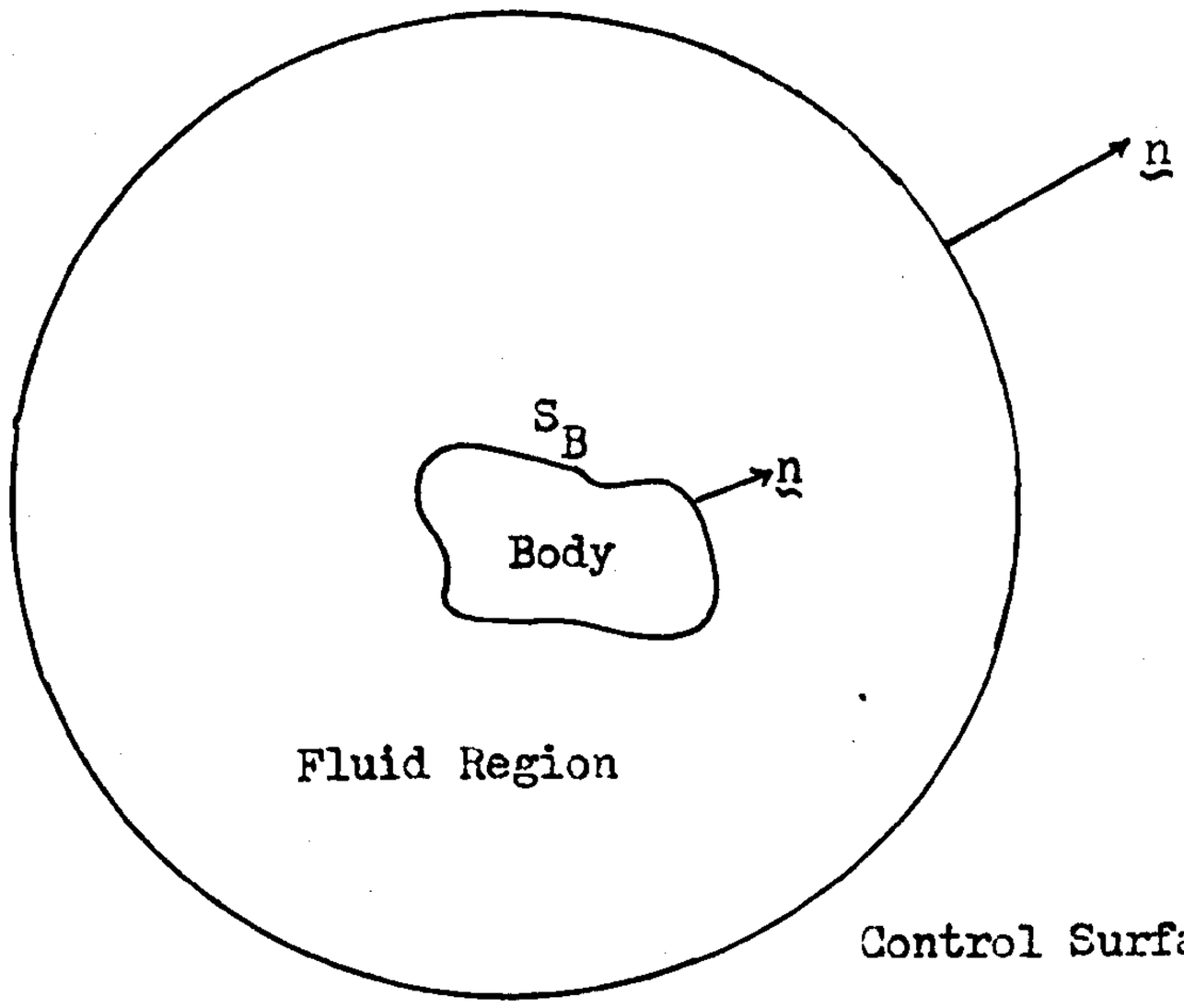

FIG. 6.3 NOTATION USED FOR THE CALCULATION OF THE FORCES ACTING ON A SUBMERGED BODY

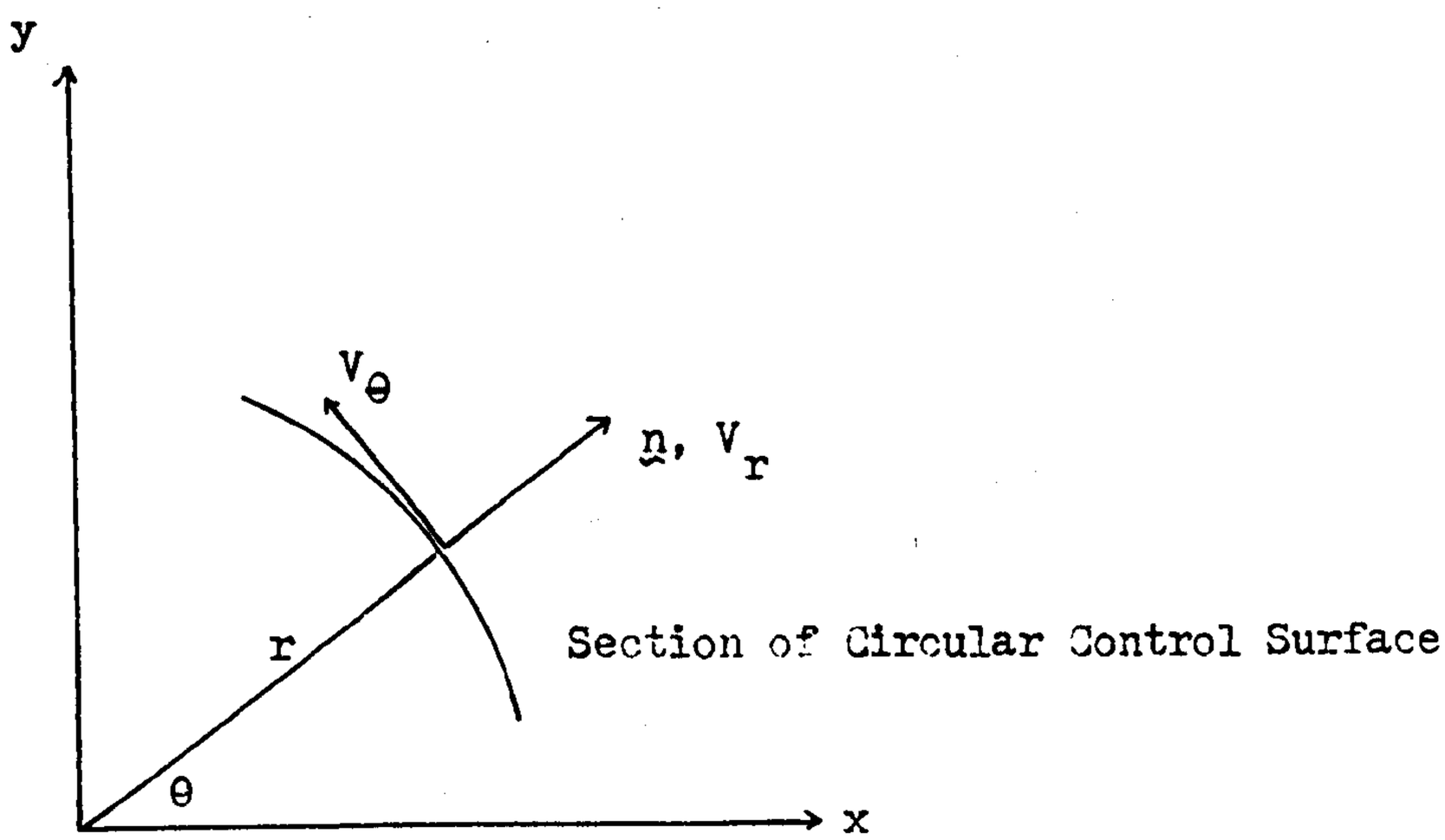

FIG. 6.4 CONTROL SURFACE FOR THE NEWMAN METHOD OF CALCULATING THE MEAN DRIFT FORCES

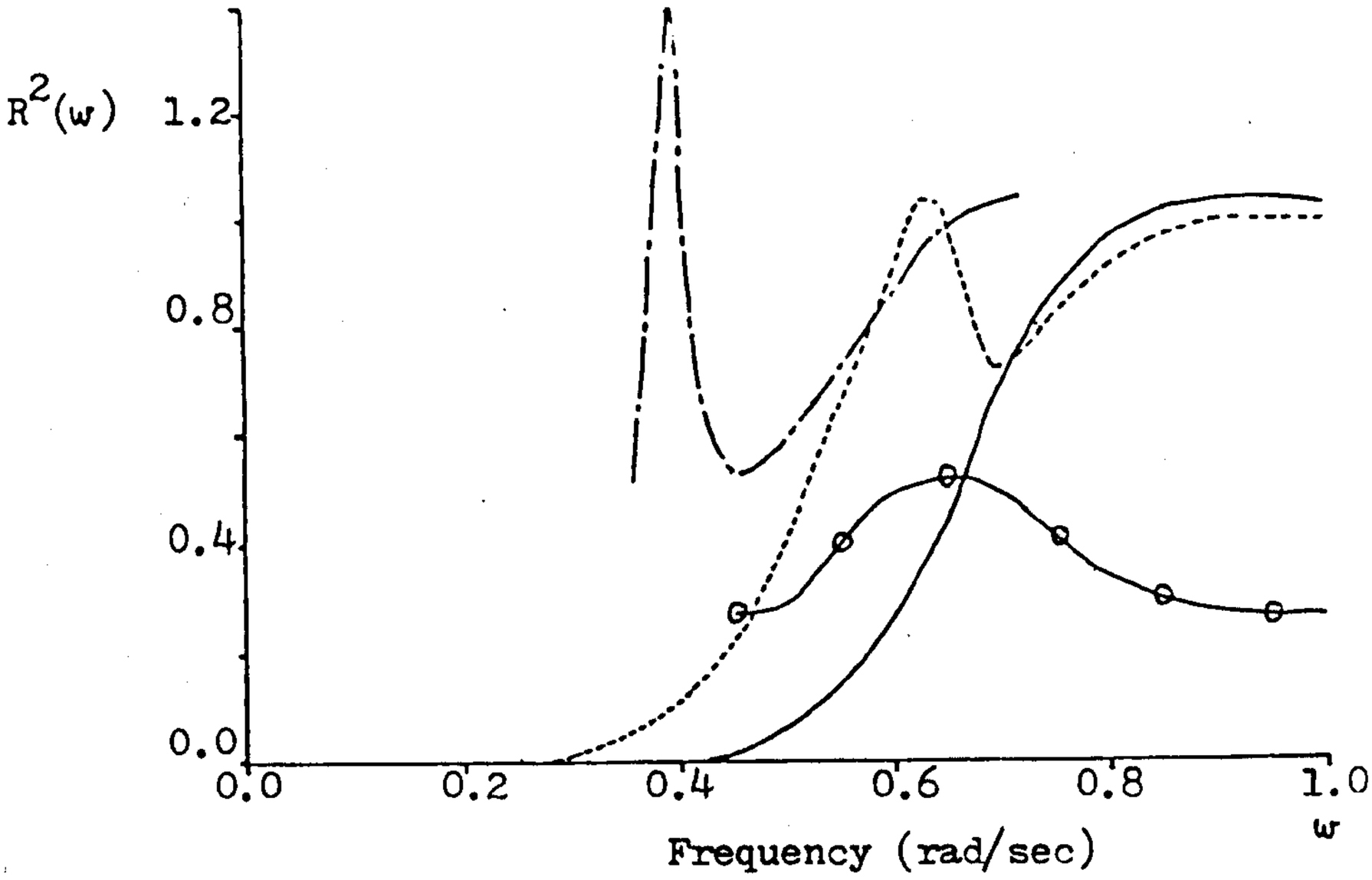

FIG. 6.5 SURGE REFLECTION COEFFICIENTS
(DIMENSIONS ARE BEAMxLENGTHxDRAFT)

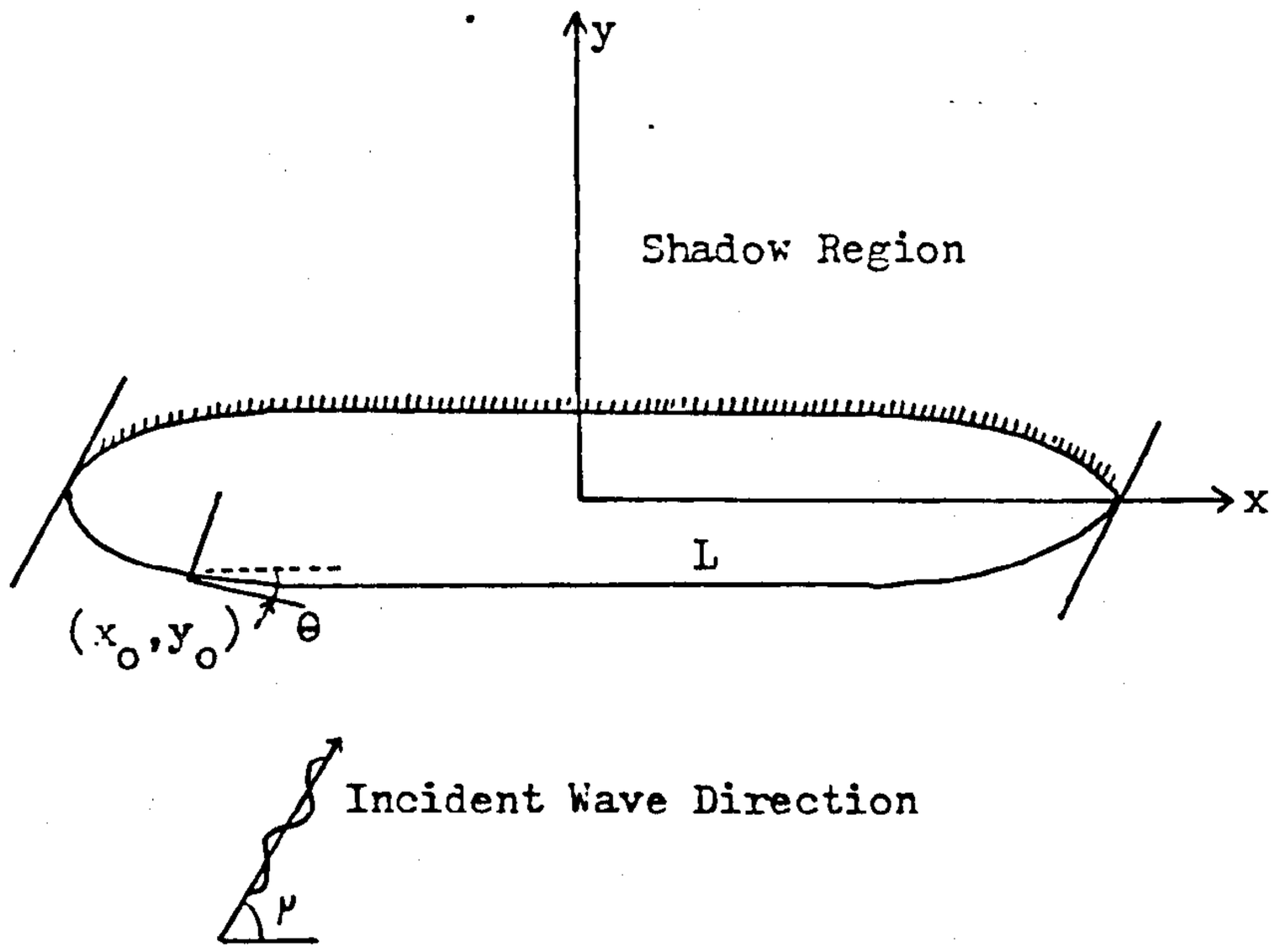

FIG. 6.6 IDEALISATION FOR HIGH FREQUENCY WAVES INCIDENT ON A FLOATING BODY

Table 8 *Numerical calculations of T^{1}_{ij} (ρg) for a rectangular cylinder in beam sea (b/d = 20/15)*

$\omega_i(d/g)^{1/2}$	$\omega_j(d/g)^{1/2}$ 1.53	1.37	0.97	0.93	0.87	0.85	0.79	0.74
1.53	0.387	0.231	0.323	0.400	0.442	0.455	0.470	0.505
1.37	0.231	0.300	0.178	0.199	0.223	0.239	0.299	0.39
0.97	0.323	0.178	0.240	0.257	0.272	0.277	0.137	0.087
0.93	0.397	0.199	0.257	0.293	0.326	0.348	0.192	0.117
0.87	0.442	0.223	0.272	0.326	0.380	0.424	0.270	0.173
0.85	0.455	0.239	0.277	0.348	0.424	0.493	0.361	0.252
0.79	0.470	0.300	0.137	0.192	0.270	0.361	0.273	0.160
0.74	0.505	0.389	0.088	0.117	0.173	0.252	0.160	0.025

Table 9. *Numerical calculations of $T^{s}_{ij}/(\rho g)$ for a rectangular cylinder in beam sea* (b/d = 20/15)

$\omega_i(d/g)^{1/2}$	$\omega_j(d/g)^{1/2}$ 1.53	1.37	0.97	0.93	0.87	0.85	0.79	0.74
1.53	0.0	0.085	0.007	−0.008	−0.022	−0.026	0.027	0.036
1.37	−0.085	0.0	0.027	−0.015	−0.062	−0.101	−0.103	−0.137
0.97	−0.007	−0.027	0.0	0.0	−0.024	−0.083	−0.181	−0.13
0.93	0.008	0.015	0.0	0.0	−0.021	−0.085	−0.209	−0.141
0.87	0.022	0.062	0.024	0.021	0.0	−0.067	−0.223	−0.145
0.85	0.026	0.107	0.083	0.084	0.067	0.0	−0.183	−0.105
0.79	−0.027	0.103	0.181	0.204	0.223	0.183	0.0	0.094
0.74	−0.036	0.137	0.130	0.141	0.145	0.105	−0.094	0.0

FIG. 6.7 SECOND ORDER TRANSFER FUNCTIONS FOR A CYLINDER IN BEAM SEAS, AS GIVEN BY FALTINSEN AND LOKEN, REF. 76

ω_2 \ ω_1	0.354	0.444	0.523	0.600	0.713	0.803	0.887
0.354	2.0	8.7	10.4	24.5	10.0	38.4	37.5
0.444		7.0	20.8	19.4	25.7	12.1	35.2
0.523			12.4	16.4	8.3	14.3	14.2
0.600				14.0	9.5	18.0	14.9
0.713					8.6	4.3	6.7
0.803						9.2	4.7
0.887							8.6

T_{12} in tf/m^2

Frequencies in rad./sec.

FIG. 6.8 SECOND ORDER COSINE TRANSFER FUNCTION FOR A TANKER IN HEAD SEAS, AS GIVEN BY PINKSTER , REF. 75

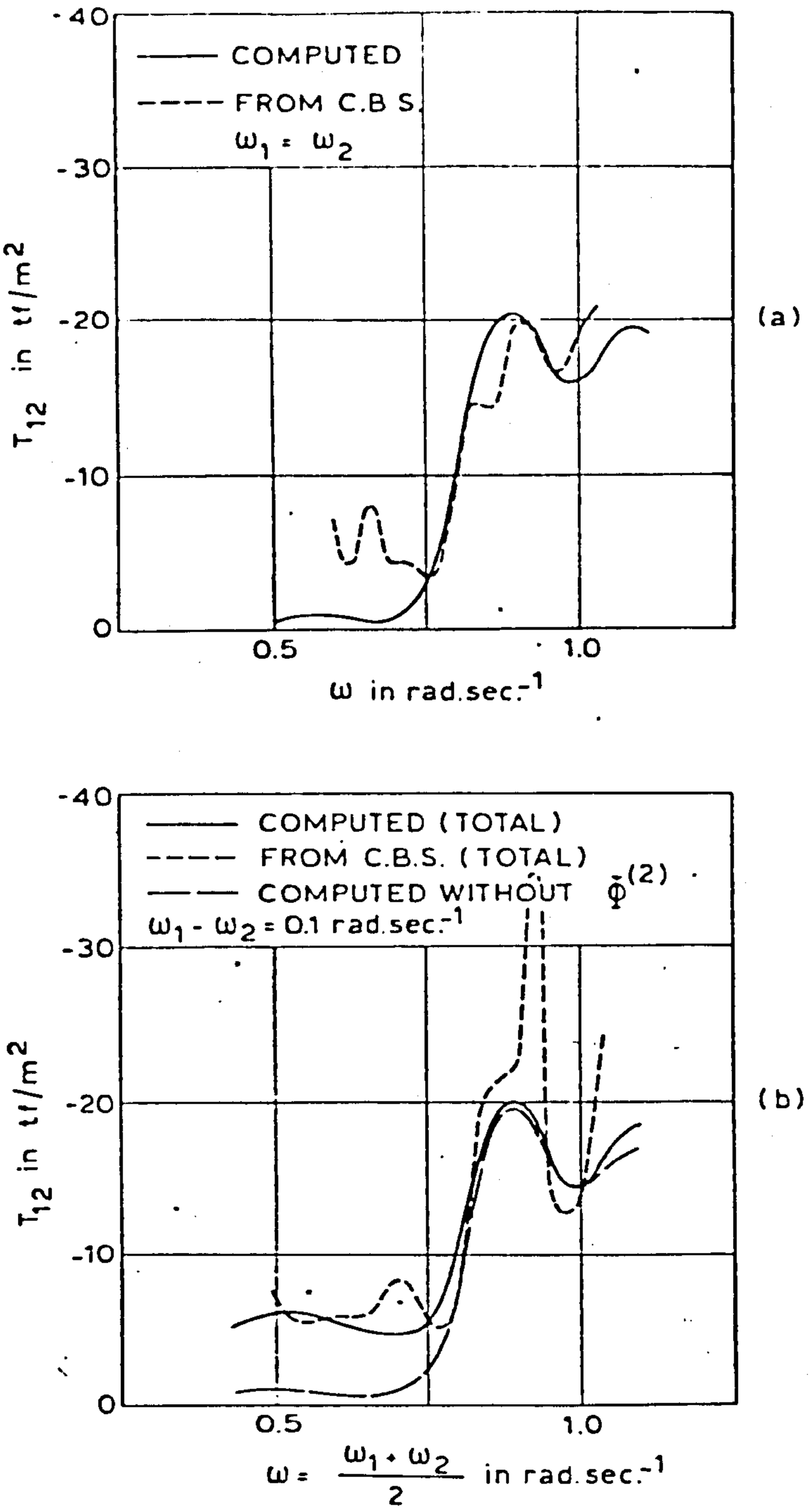

FIG. 6.9 REFLECTION COEFFICIENTS FOR A SEMISUBMERSIBLE IN REGULAR WAVES (A), AND REGULAR WAVE GROUPS (B) (C.B.S.= MODEL TESTS)

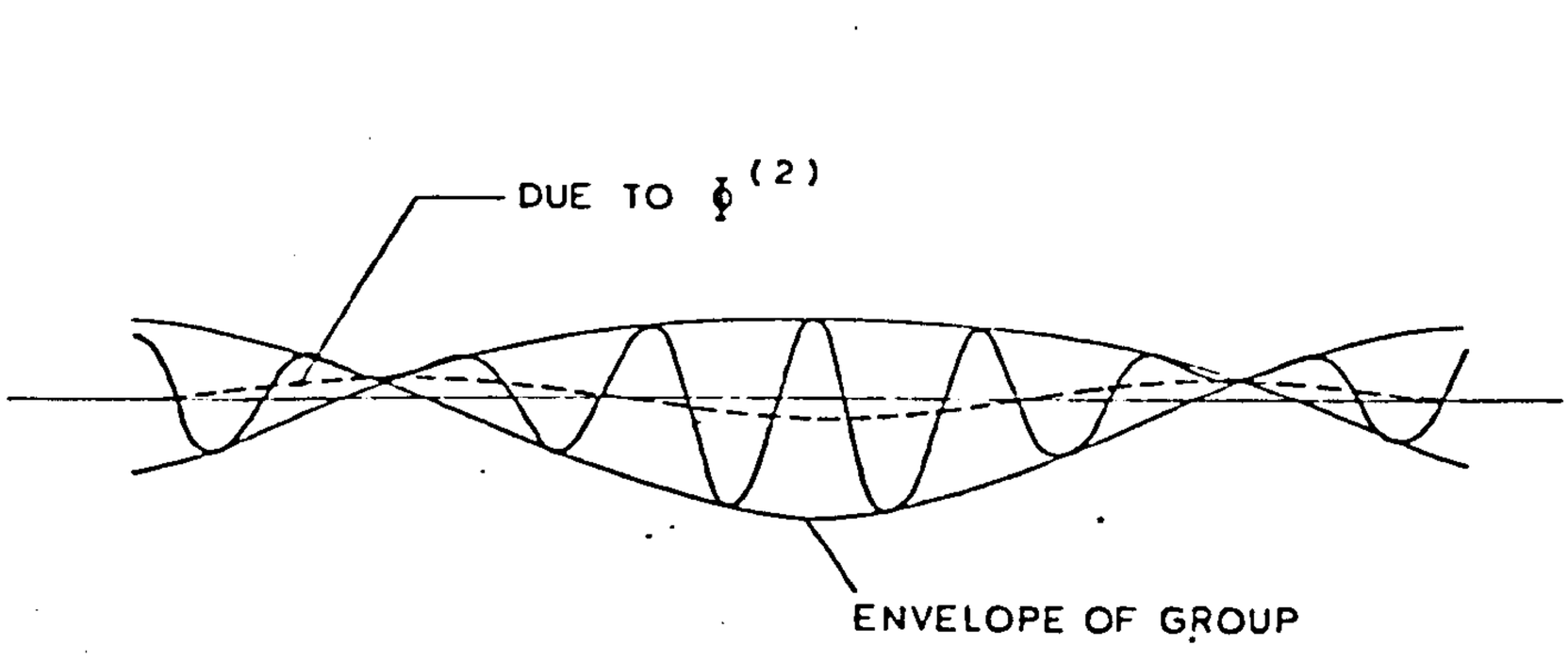

FIG. 6.10 THE WAVE ENVELOPE

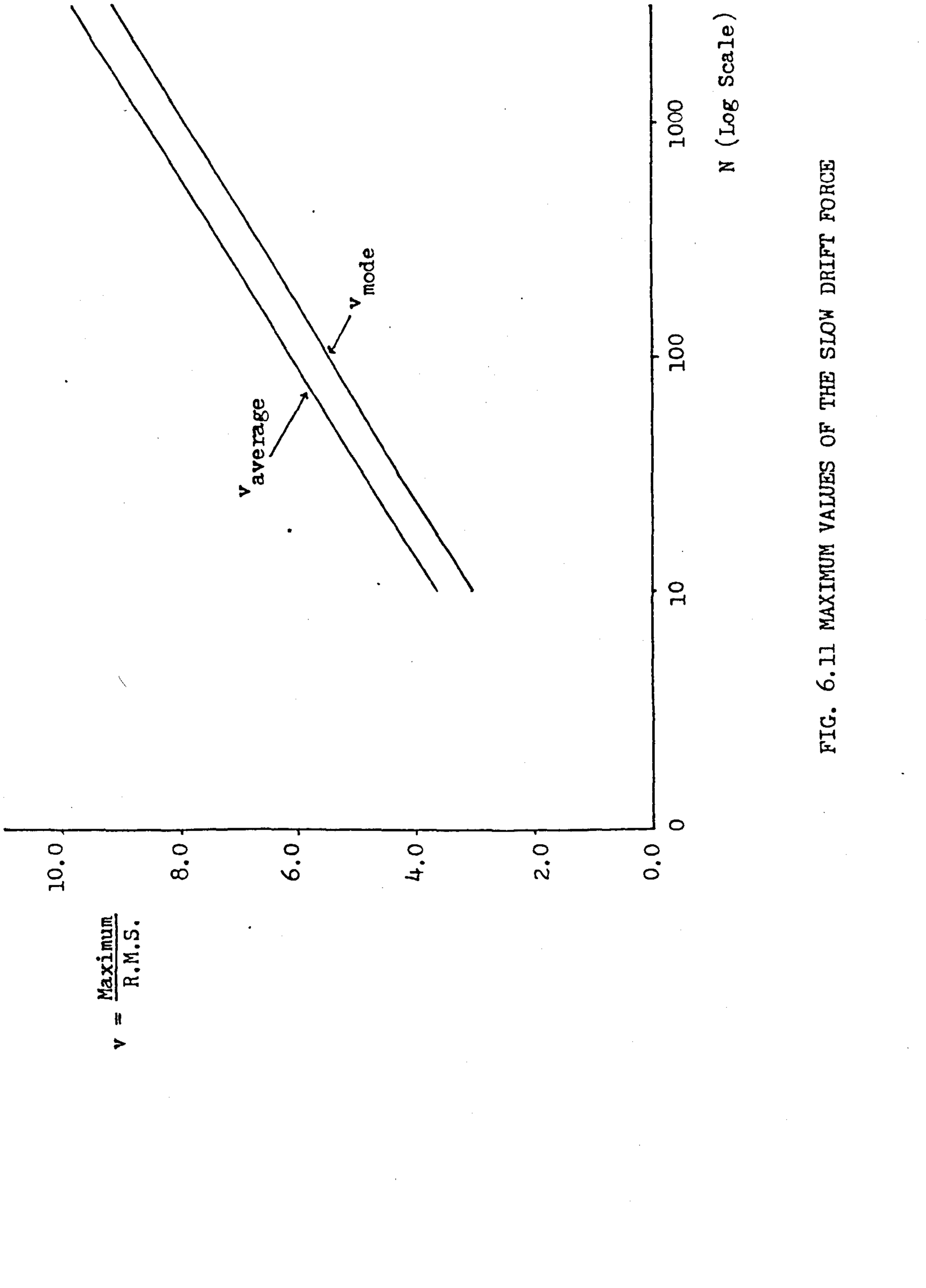

FIG. 6.11 MAXIMUM VALUES OF THE SLOW DRIFT FORCE

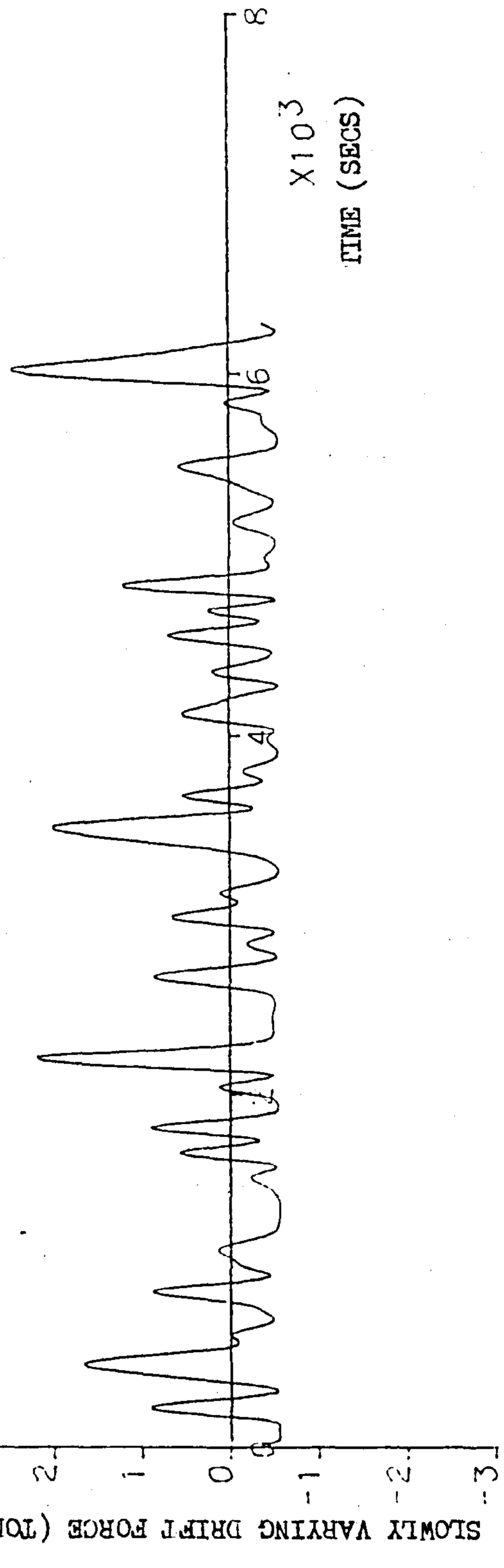

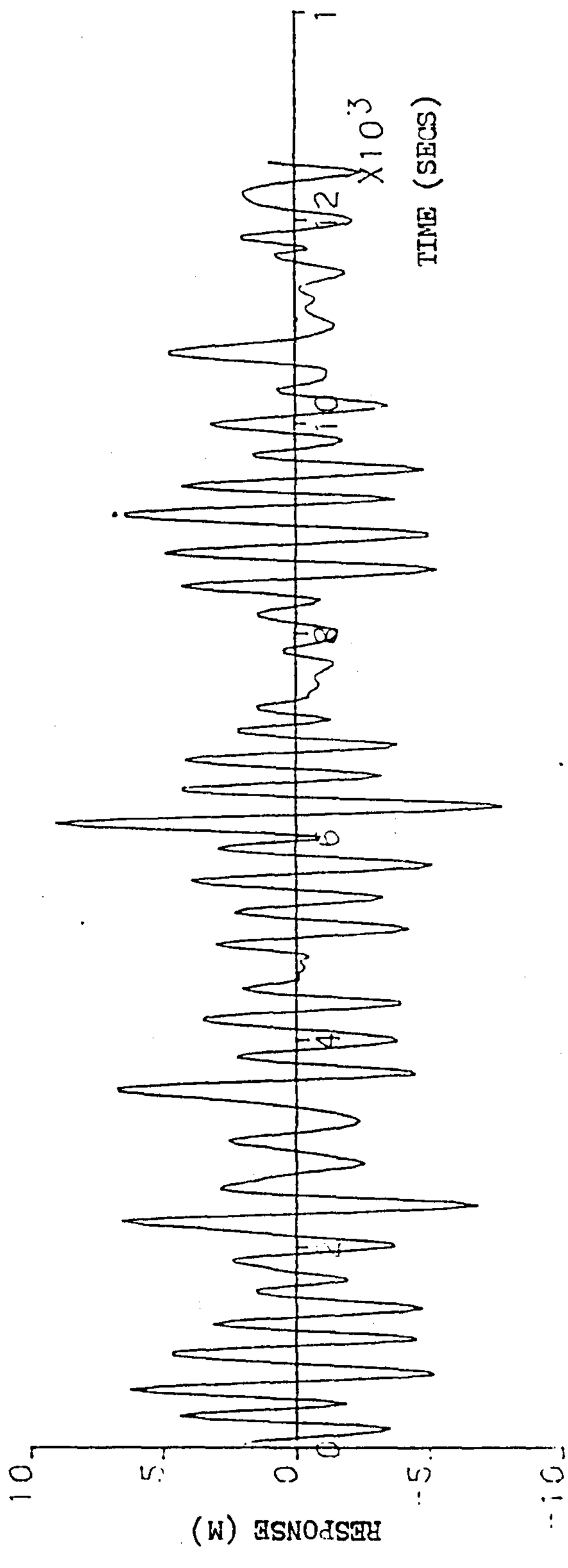

FIG. 6.12 EXAMPLE TIME HISTORY OF SLOW DRIFT FORCE AND RESPONSE

N	$\bar{v}$ From Time Domain Prog.	$\bar{v}$ From Eqn. (6.59)	v-mode From Eqn. (6.58)
15	4.28	4.08	3.49
30	4.52	4.85	4.25
45	4.71	5.29	4.69

FIG. 6.13 RESULTS FOR V

Range of v	No. for N=15	No. for N=30	No. for N=45
2.0-2.5	2	0	0
2.5-3.0	3	0	0
3.0-3.5	3	6	1
3.5-4.0	3	6	5
4.0-4.5	6	2	7
4.5-5.0	5	8	9
5.0-5.5	6	4	5
5.5-6.0	1	1	2
6.0-6.5	0	1	0
6.5-7.0	0	2	0
7.0-7.5	0	0	0
7.5-8.0	1	0	0
9.0-9.5	0	0	1

FIG. 6.14 COMPUTER RESULTS FOR V

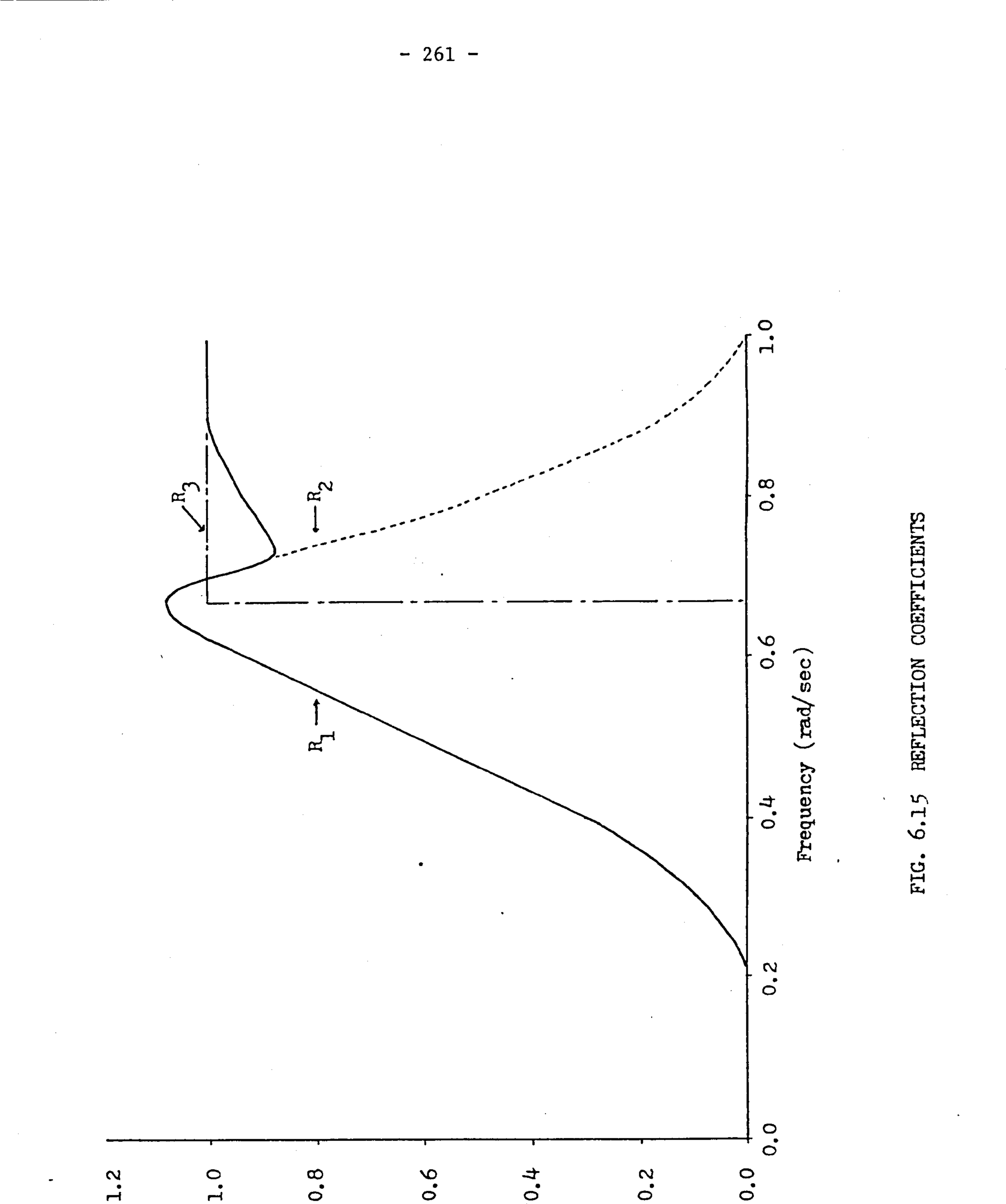

FIG. 6.15 REFLECTION COEFFICIENTS

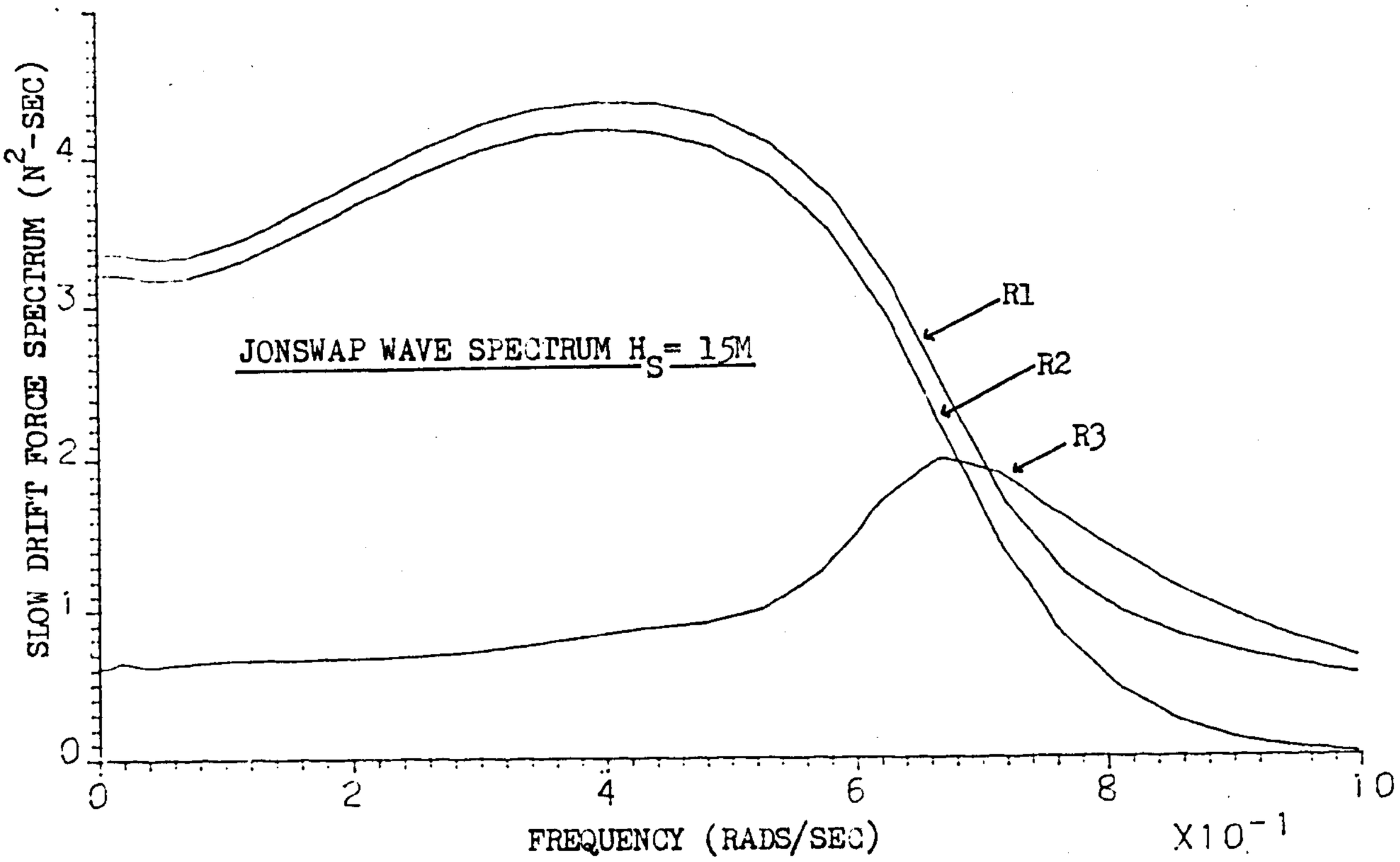

FIG. 6.16 SLOW DRIFT SPECTRA FOR VARIOUS REFLECTION COEFFICIENTS (SEE FIG. 6.15)

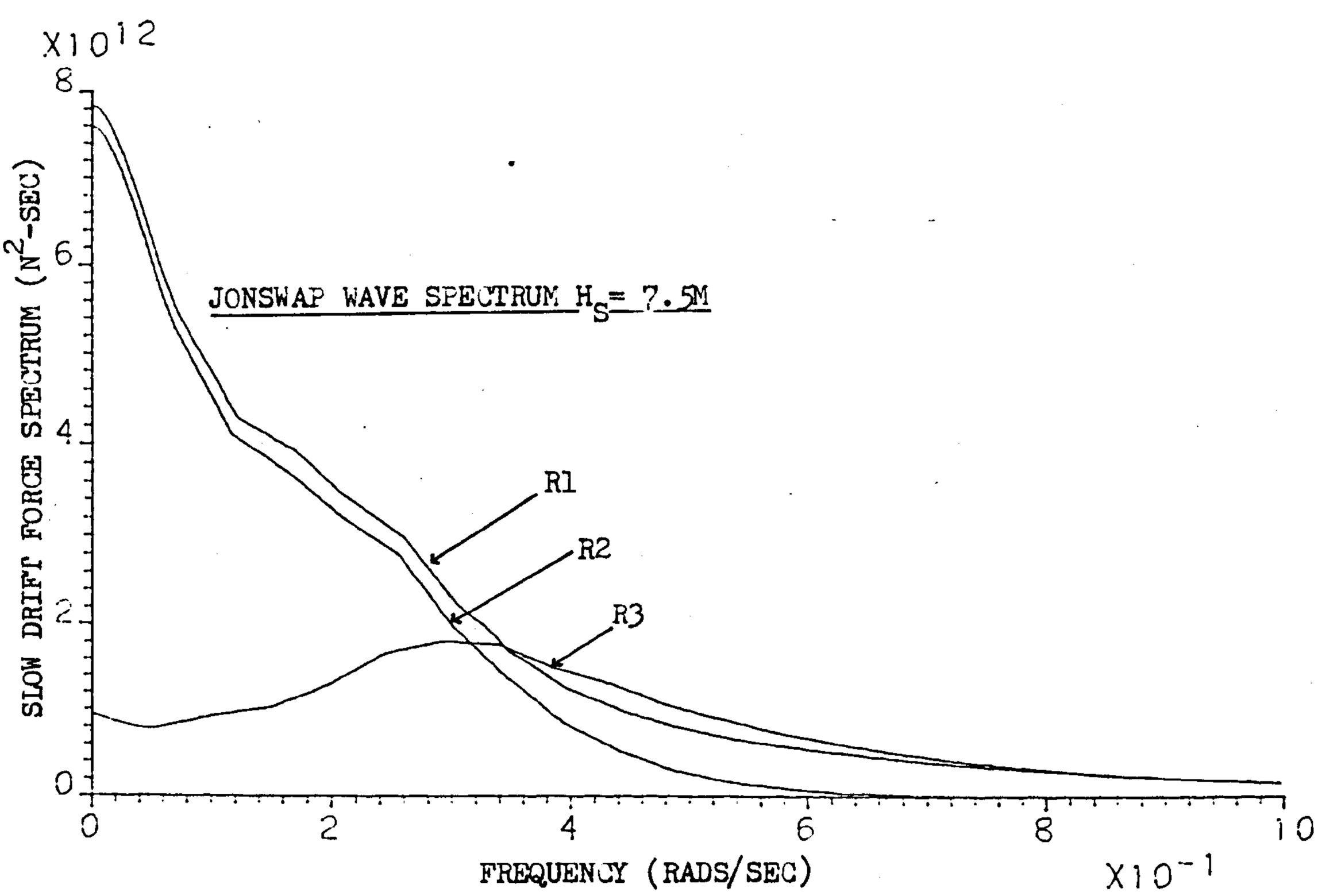

FIG. 6.17 SLOW DRIFT SPECTRA FOR VARIOUS REFLECTION COEFFICIENTS (SEE FIG. 6.15)

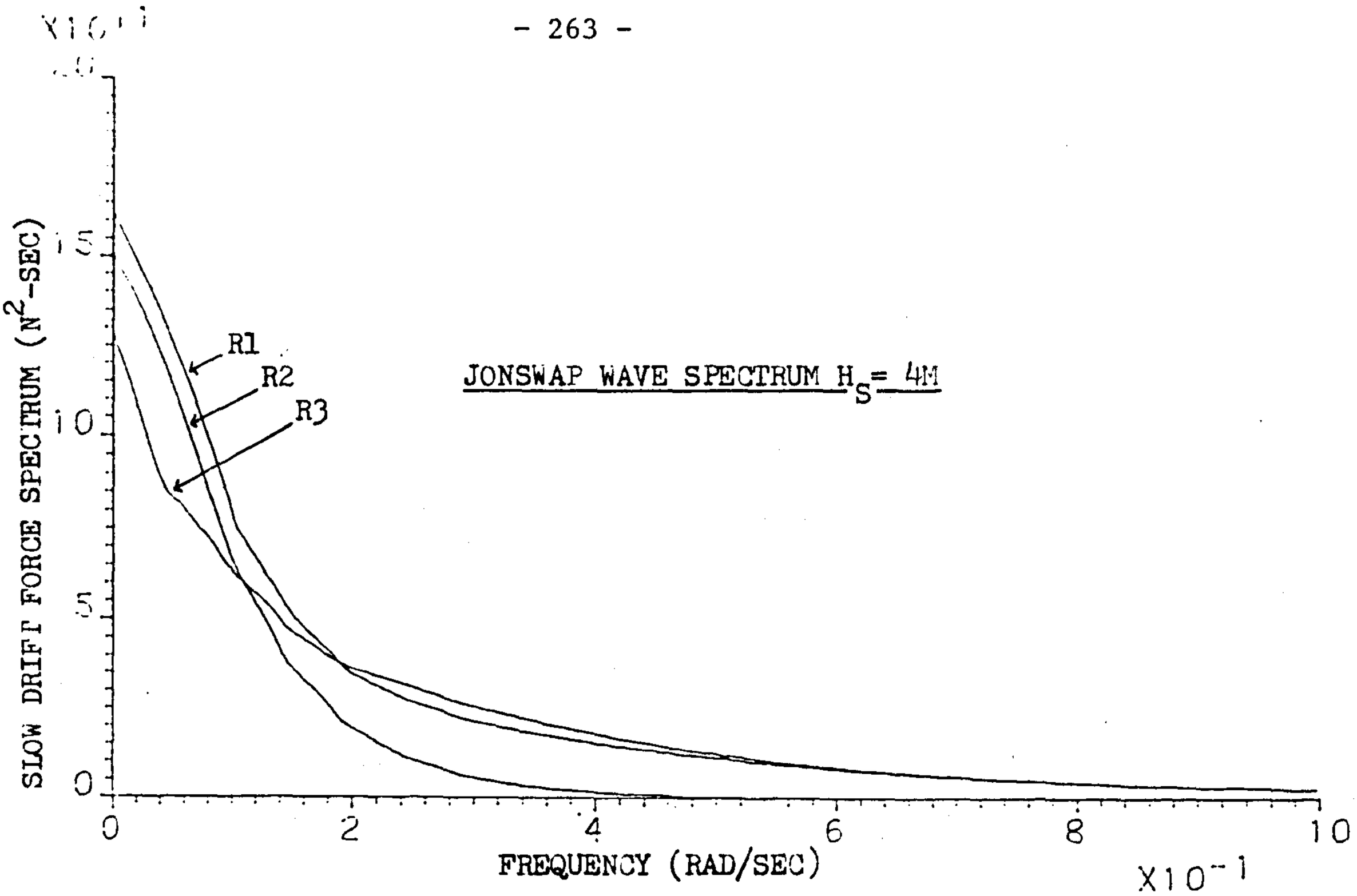

FIG. 6.18 SLOW DRIFT SPECTRA FOR VARIOUS REFLECTION COEFFICIENTS (SEE FIG. 6.15)

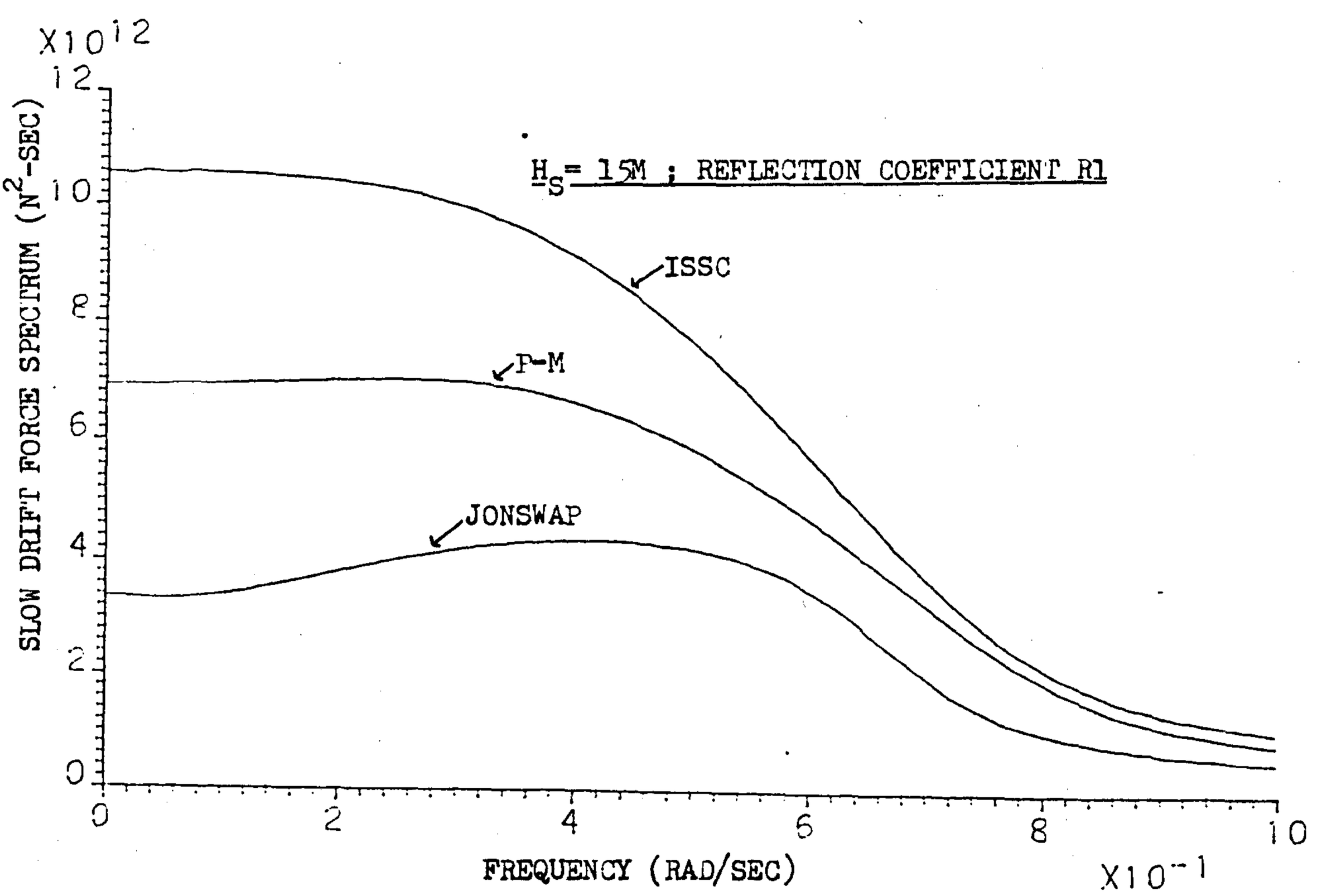

FIG. 6.19 SLOW DRIFT SPECTRA FOR VARIOUS TYPES OF WAVE SPECTRUM

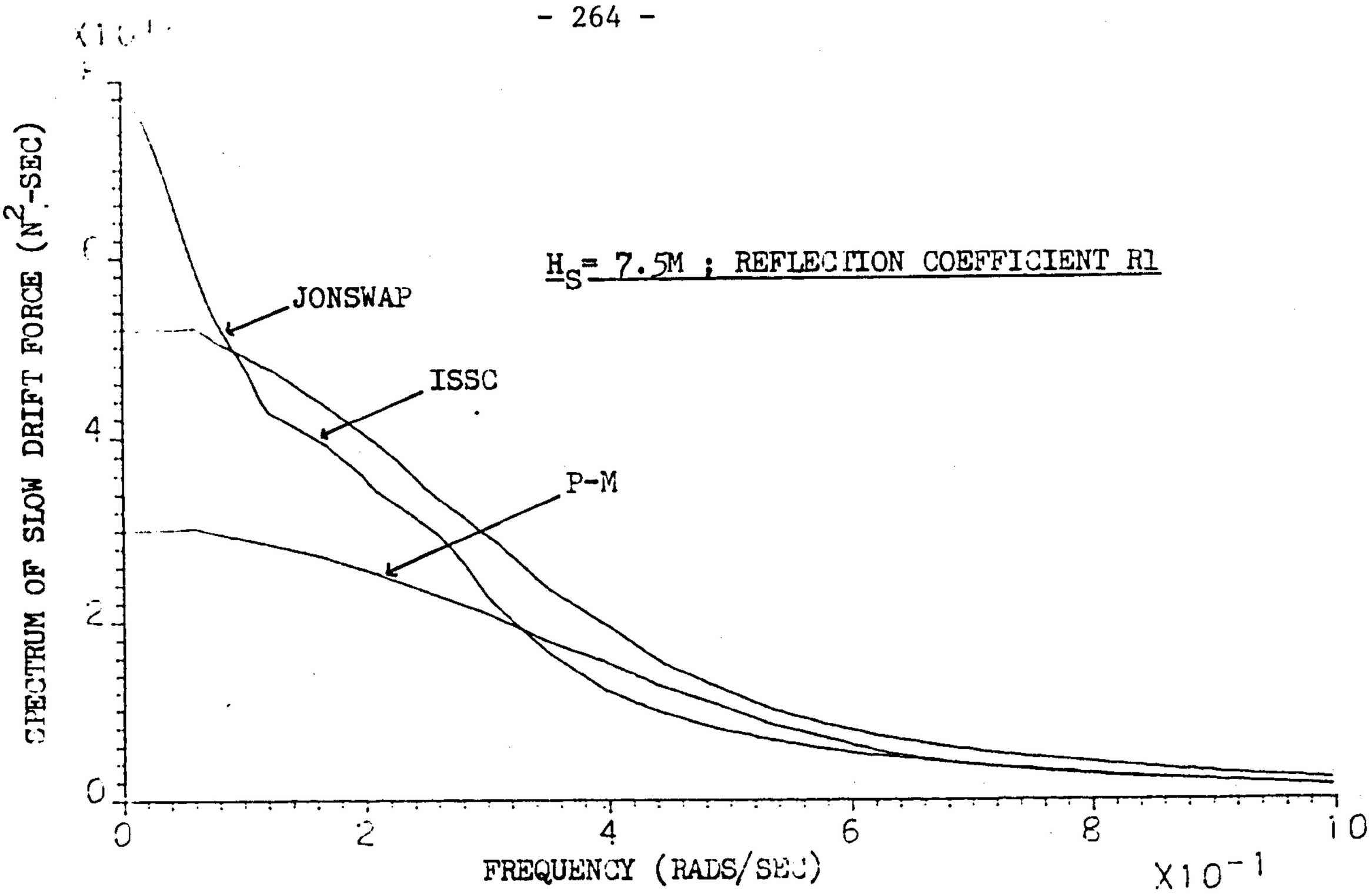

FIG. 6.20 SLOW DRIFT SPECTRA FOR VARIOUS TYPES OF WAVE SPECTRUM

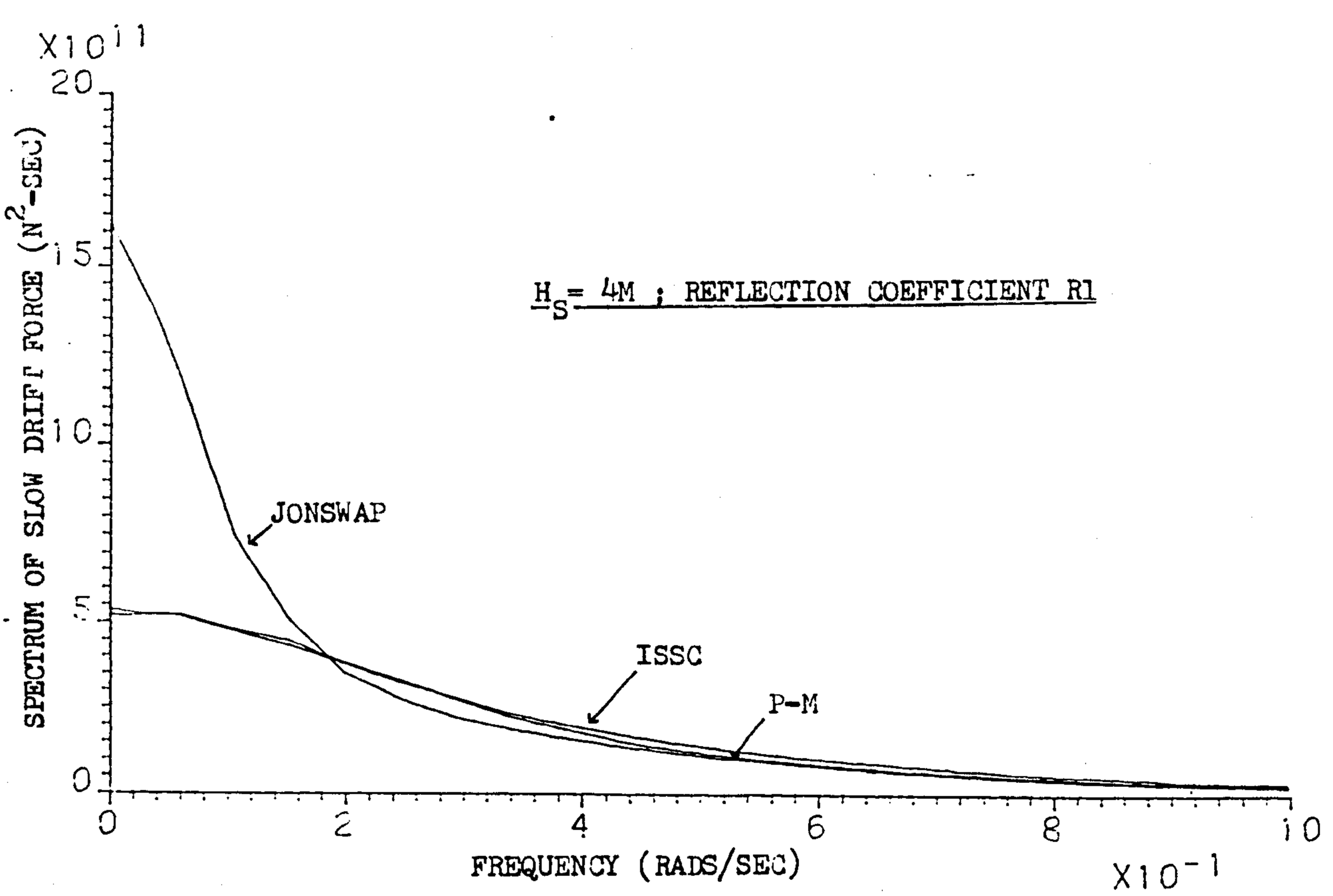

FIG. 6.21 SLOW DRIFT SPECTRA FOR VARIOUS TYPES OF WAVE SPECTRUM

FIG. NO.	SPECTRUM TYPE/H_S(M)	REF. COEFF. TYPE	LIN. STIFFNESS (TONNE/M)	MEAN DRIFT FORCE (TONNE)	R.M.S. RESPONSE (M)
6.16	JONSWAP/15.0	1	17.67	64.02	8.40
	JONSWAP/15.0	2	16.53	54.96	8.49
	JONSWAP/15.0	3	7.70	24.19	5.51
6.17	JONSWAP/7.5	1	22.79	64.68	10.47
	JONSWAP/7.5	2	20.58	44.82	10.86
	JONSWAP/7.5	3	9.54	37.28	5.61
6.18	JONSWAP/4.0	1	11.16	38.10	6.84
	JONSWAP/4.0	2	9.51	25.06	7.16
	JONSWAP/4.0	3	9.57	32.54	6.23
6.19	JONSWAP/15.0	1	17.67	64.02	8.40
	P-M/15.0	1	24.30	75.26	10.45
	ISSC/15.0	1	29.42	81.41	11.83
6.20	JONSWAP/7.5	1	22.79	64.68	10.47
	P-M/7.5	1	17.08	63.62	8.14
	ISSC/7.5	1	22.18	79.12	9.45
6.21	JONSWAP/4.0	1	11.16	38.10	6.84
	P-M/4.0	1	8.56	36.24	4.74
	ISSC/4.0	1	8.75	38.34	4.68

FIG. 6.22 SLOW DRIFT RESULTS FOR A TANKER MOORED IN HEAD SEAS

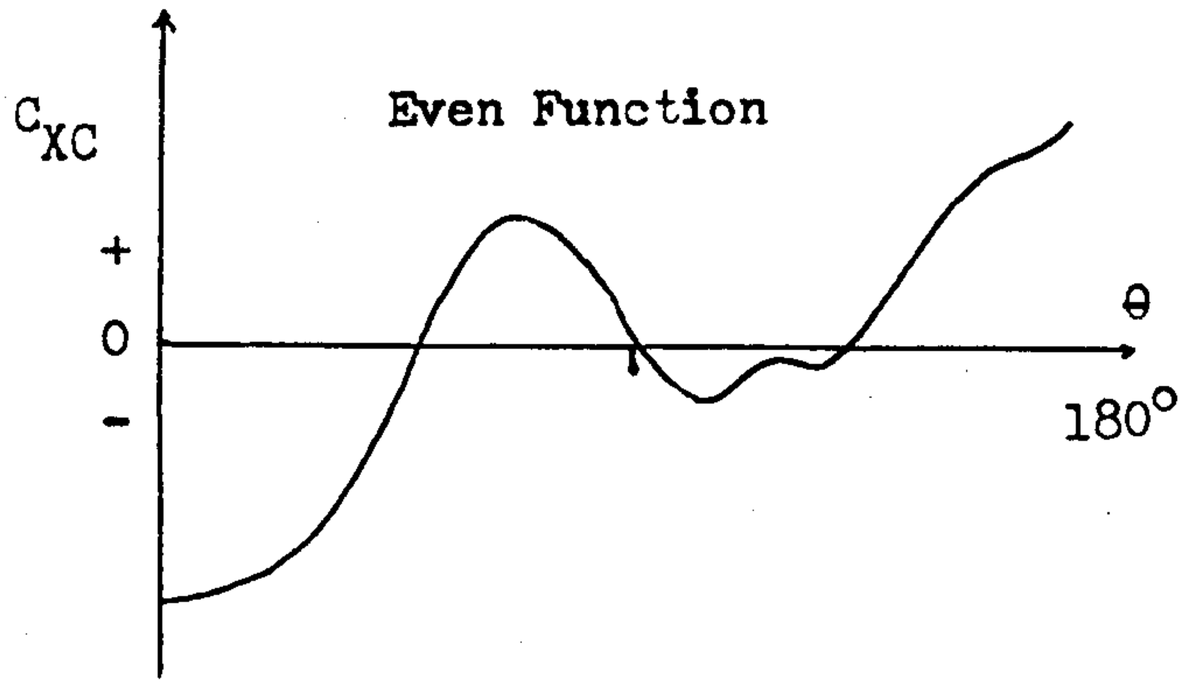

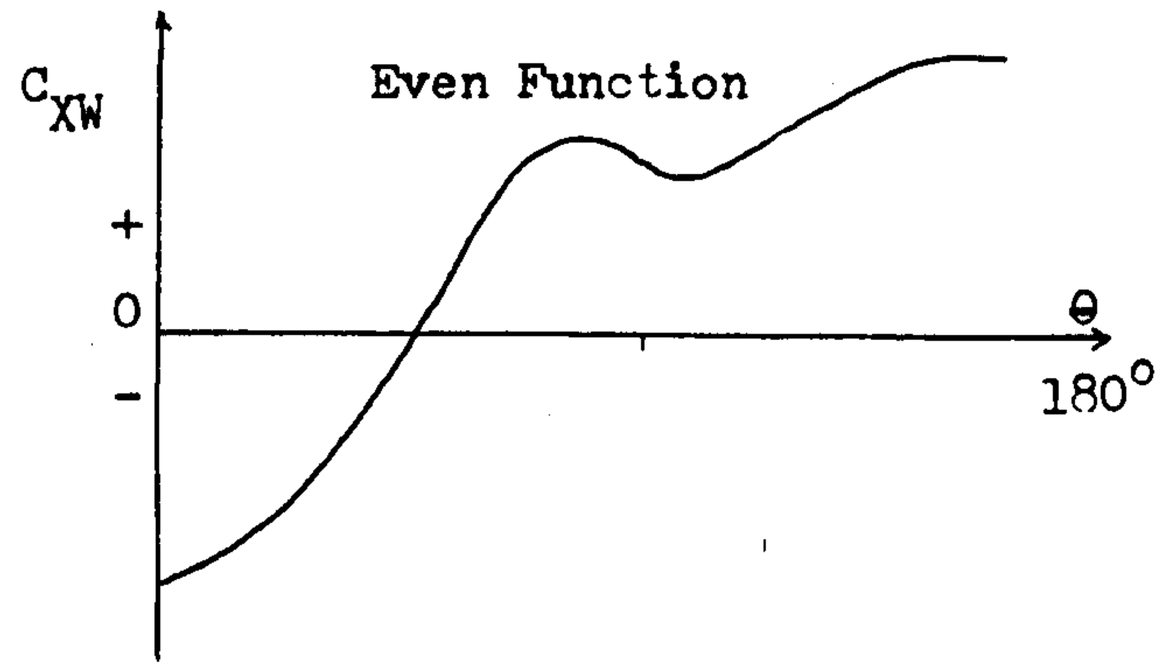

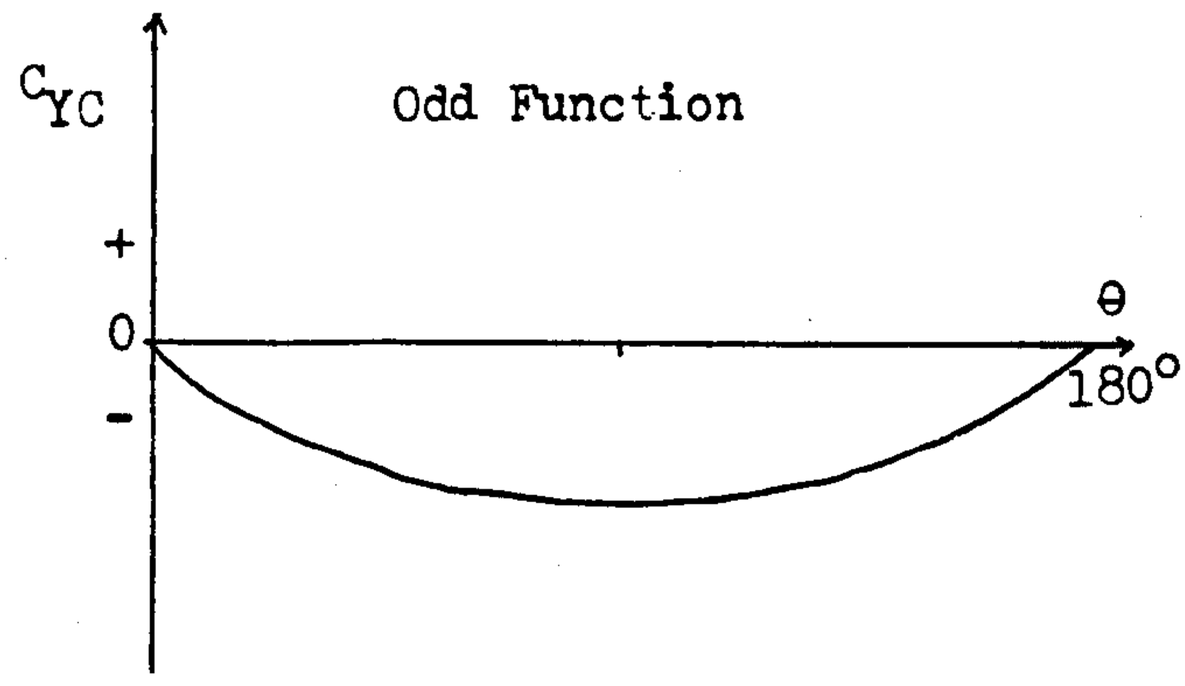

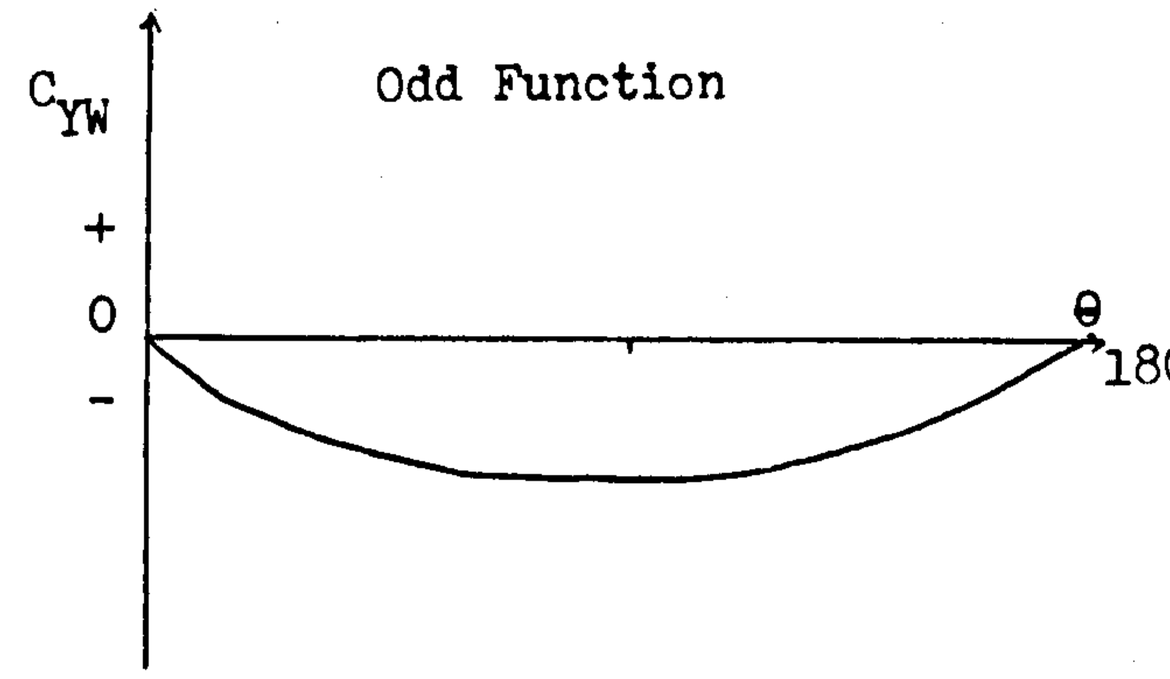

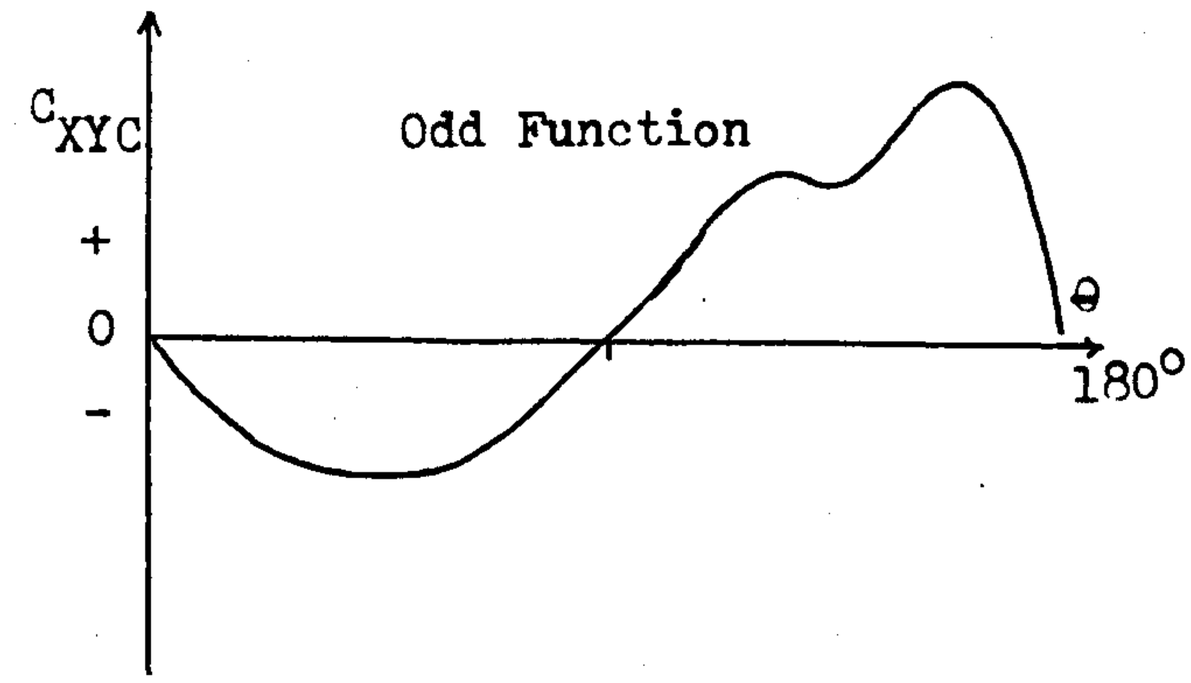

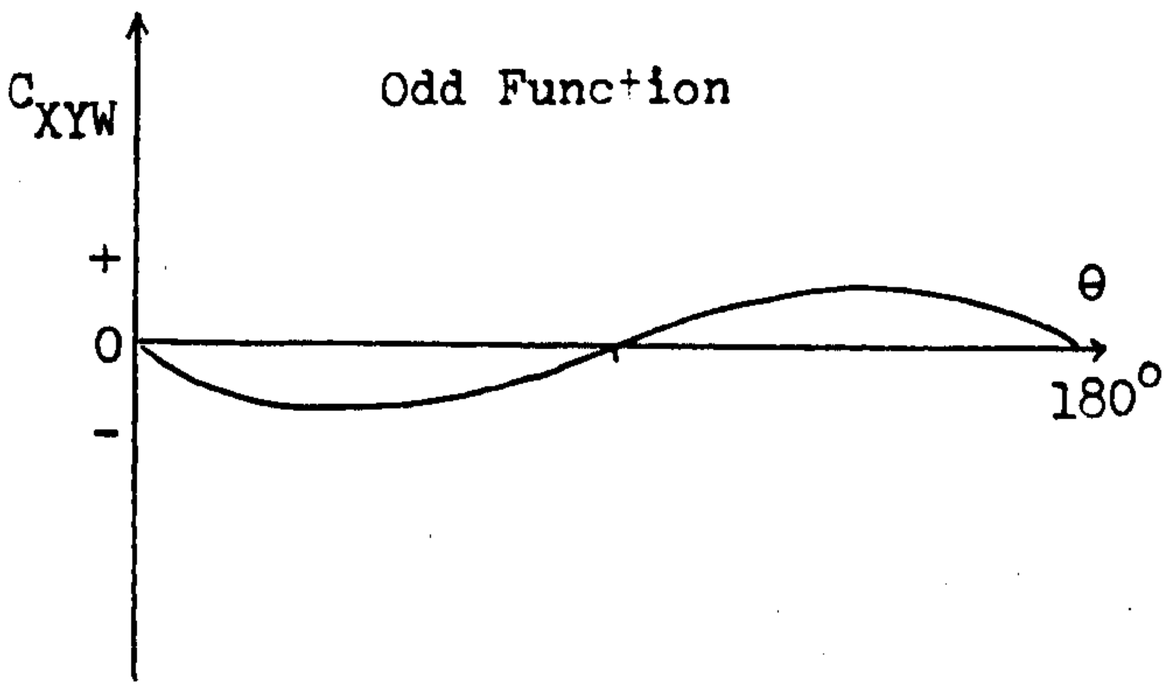

CURRENT WIND

FIG. 7.1 TYPICAL SHAPES OF THE OCIMF CURVES (REF. 68)

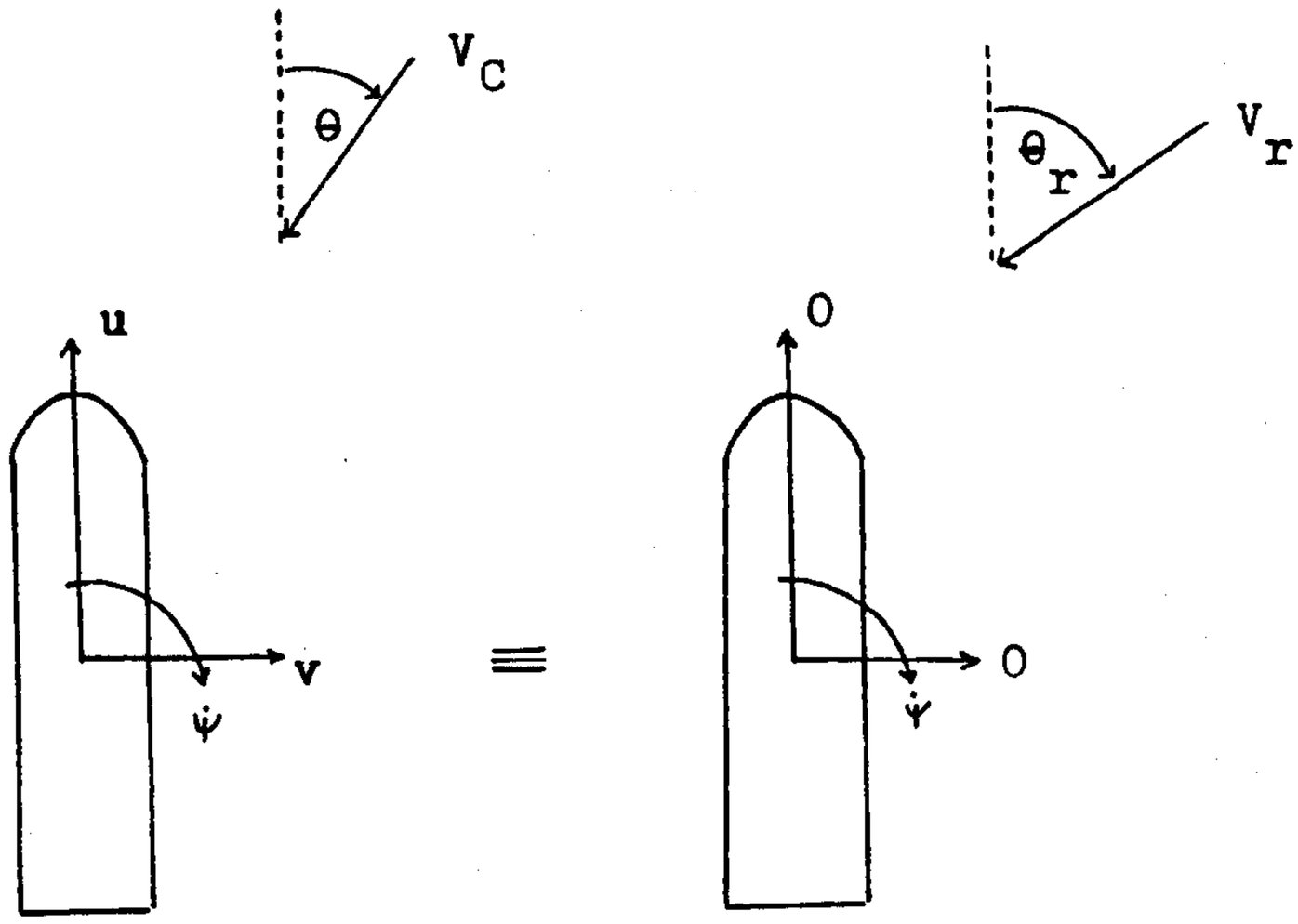

$$V_r^2 = (u + V_C\cos\theta)^2 + (v + V_C\sin\theta)^2$$

$$\theta_r = \tan^{-1}\{(v + V_C\sin\theta)/(u + V_C\cos\theta)\}$$

FIG. 7.2 A VLCC MOVING IN A CURRENT

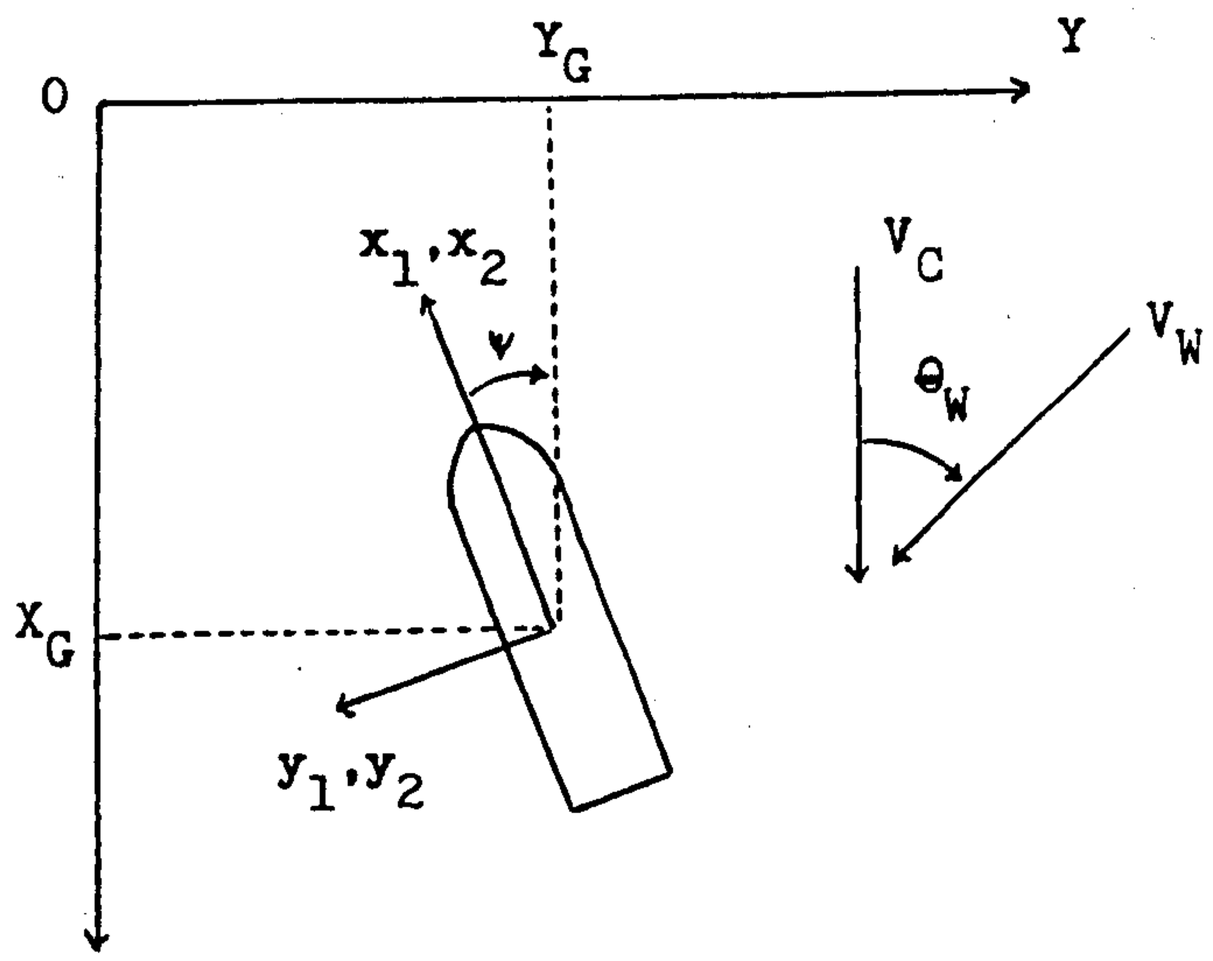

FIG. 7.3 COORDINATE SYSTEMS

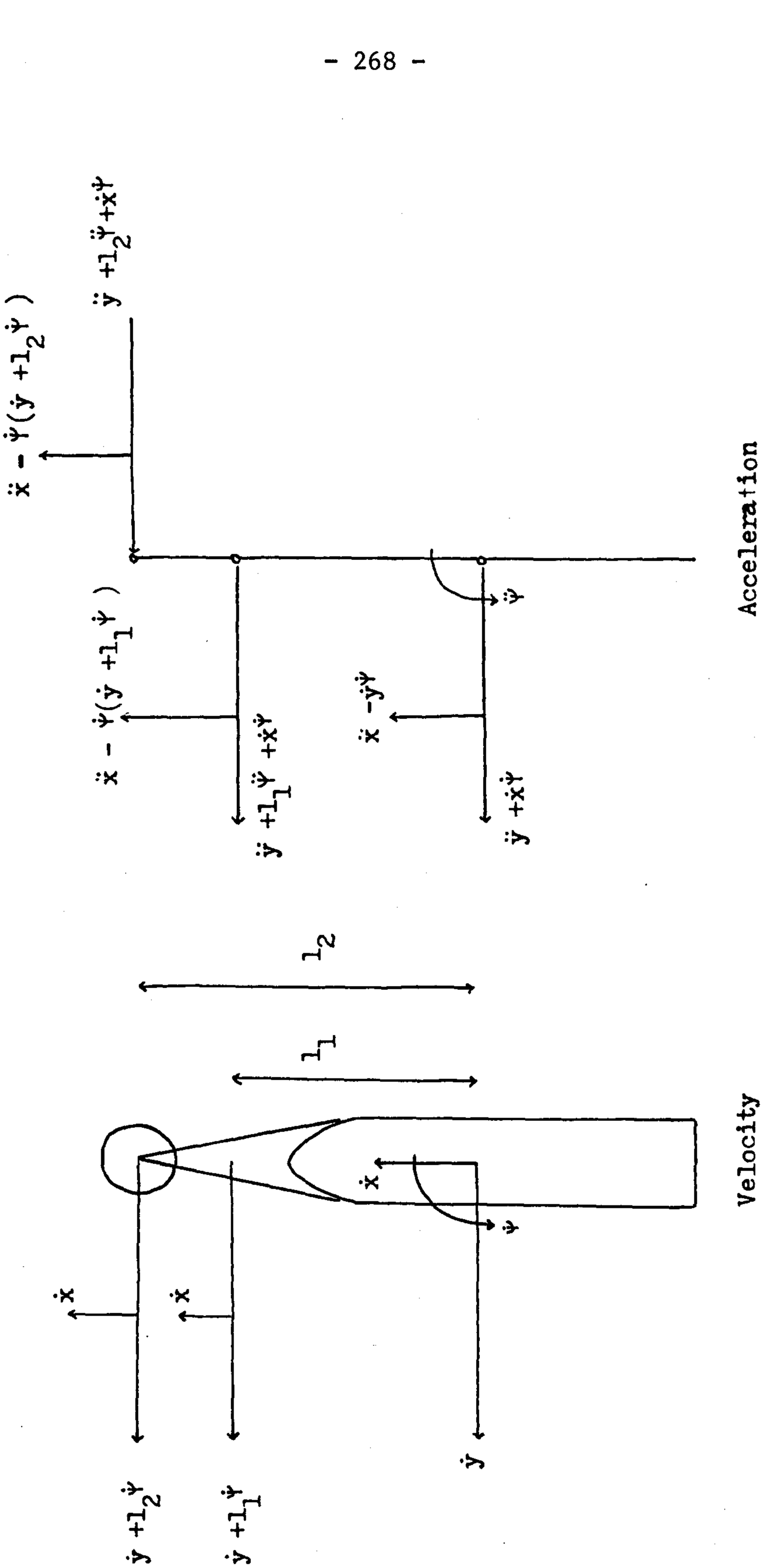

FIG. 7.4 VELOCITY AND ACCELERATION DIAGRAMS FOR THE MOTION OF A SBS SYSTEM

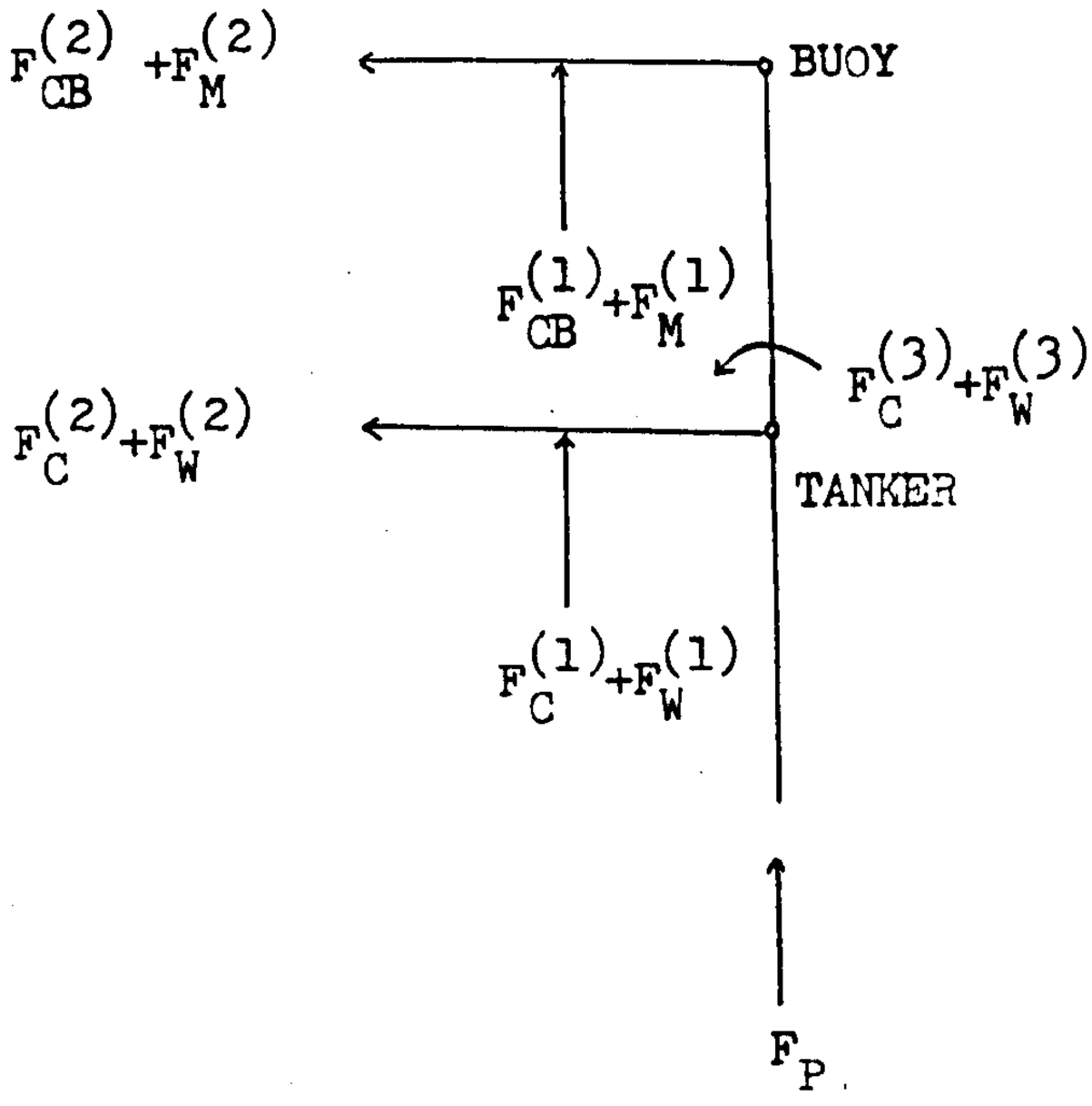

F_C= CURRENT FORCE/MOMENT
F_W= WIND FORCE/MOMENT
F_M= MOORING FORCE
F_P= PROPULSION (ASTERN THRUST)

FIG. 7.5 FORCES ACTING ON THE SYSTEM

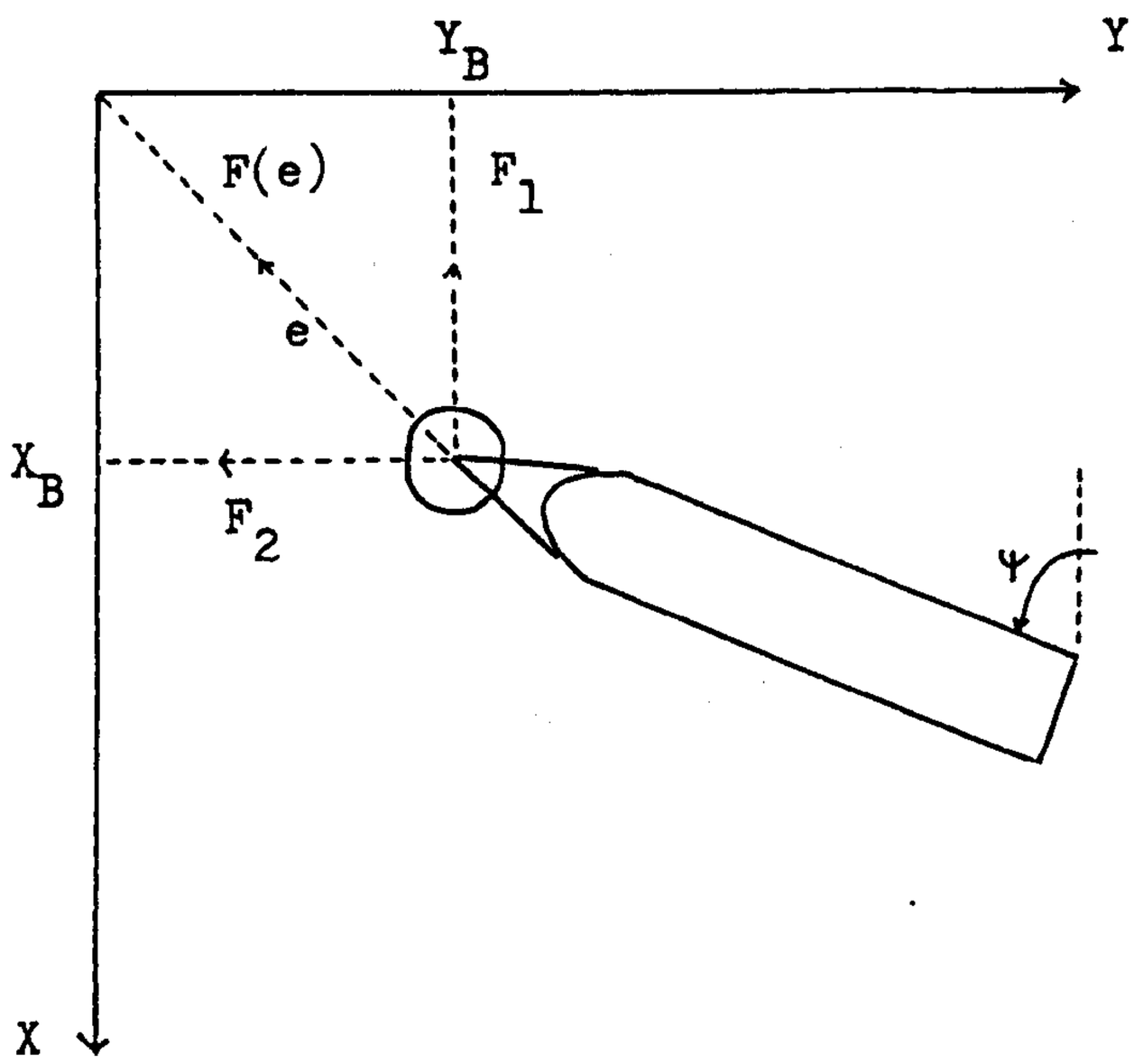

FIG. 7.6 MOORING FORCES

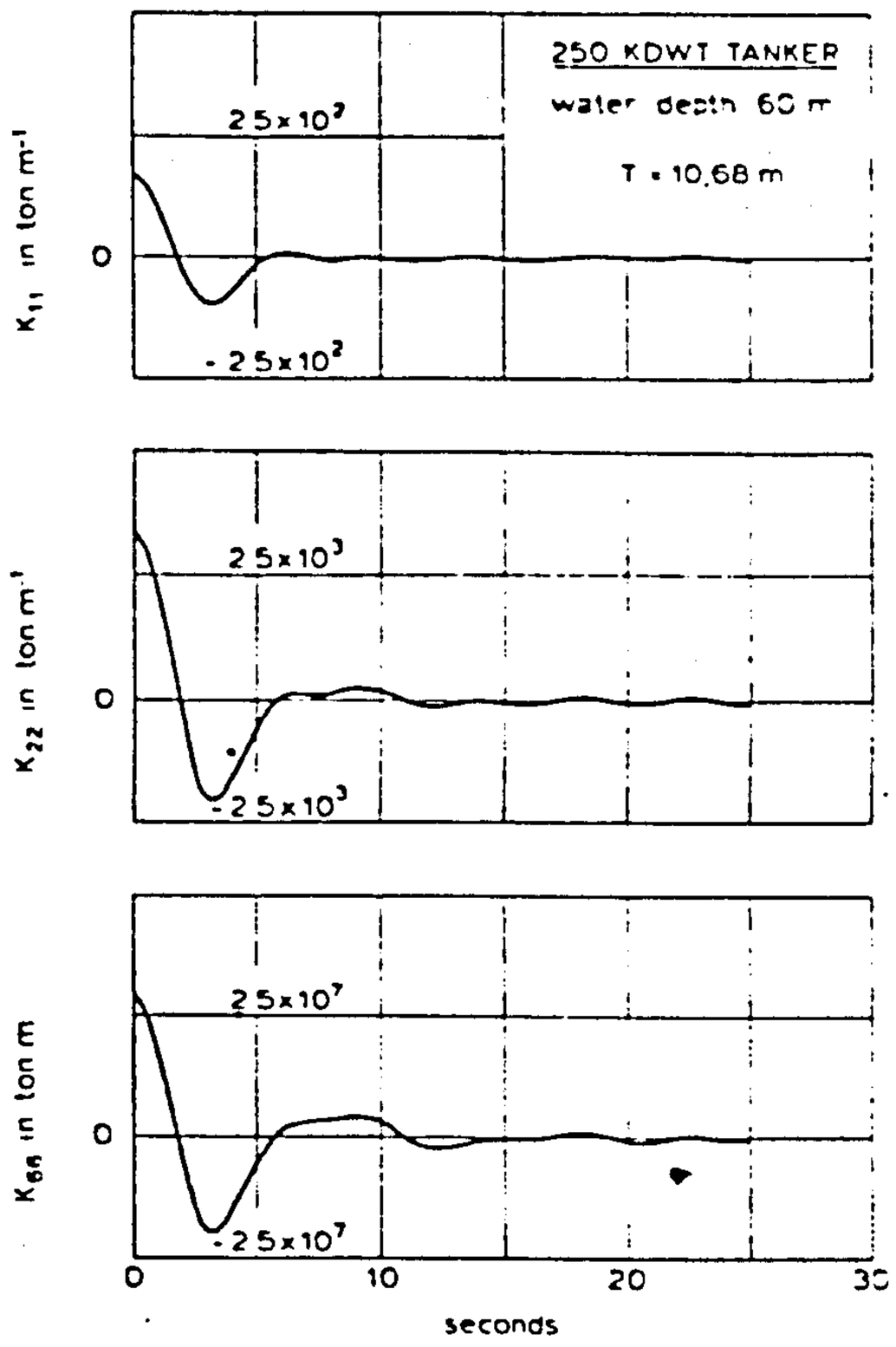

FIG. 7.7 RETARDATION FUNCTIONS (GIVEN BY WICHERS, REF. 17)

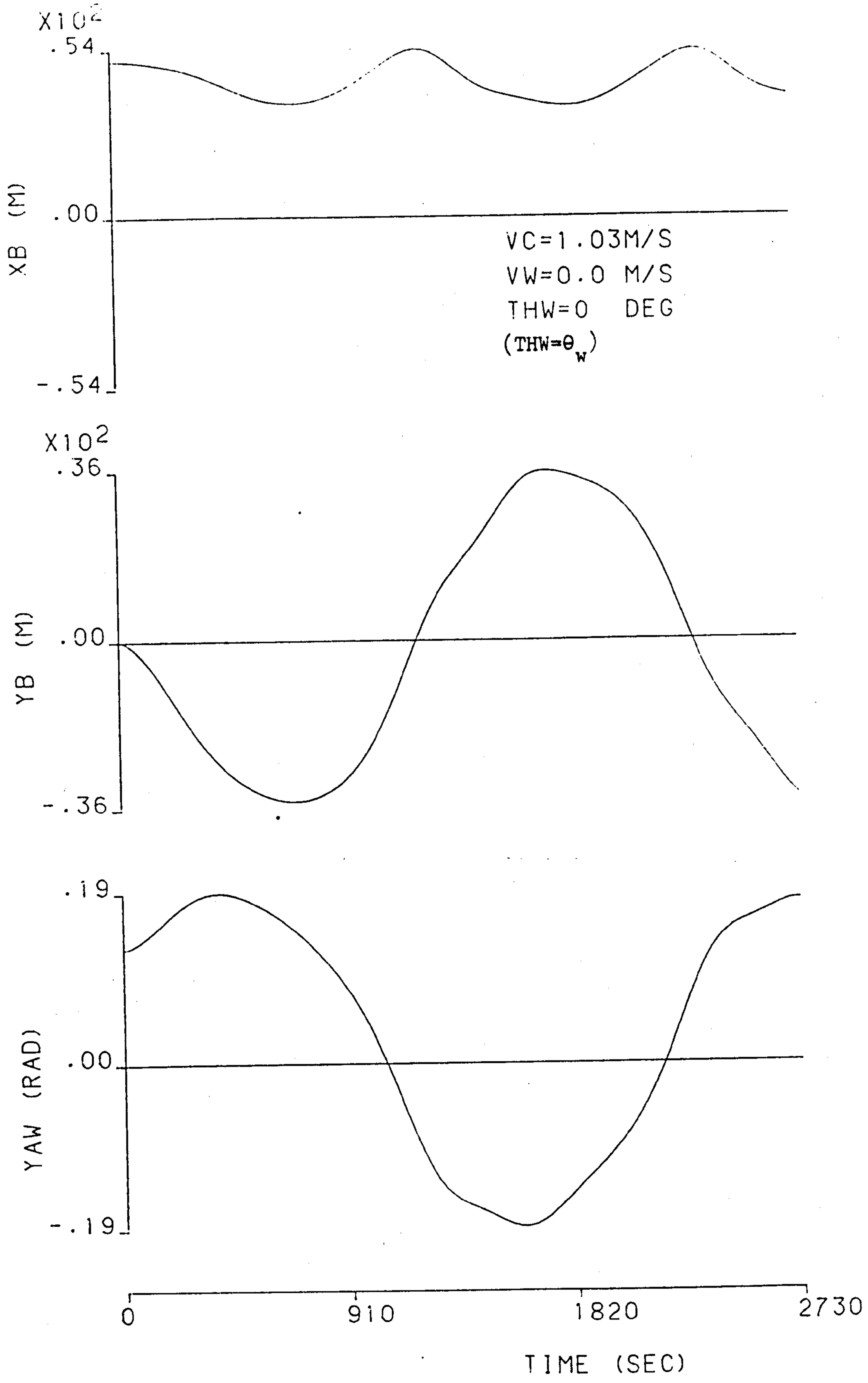

FIG. 7.8 FISHTAILING MOTIONS OF A TANKER MOORED BY A BOW HAWSER

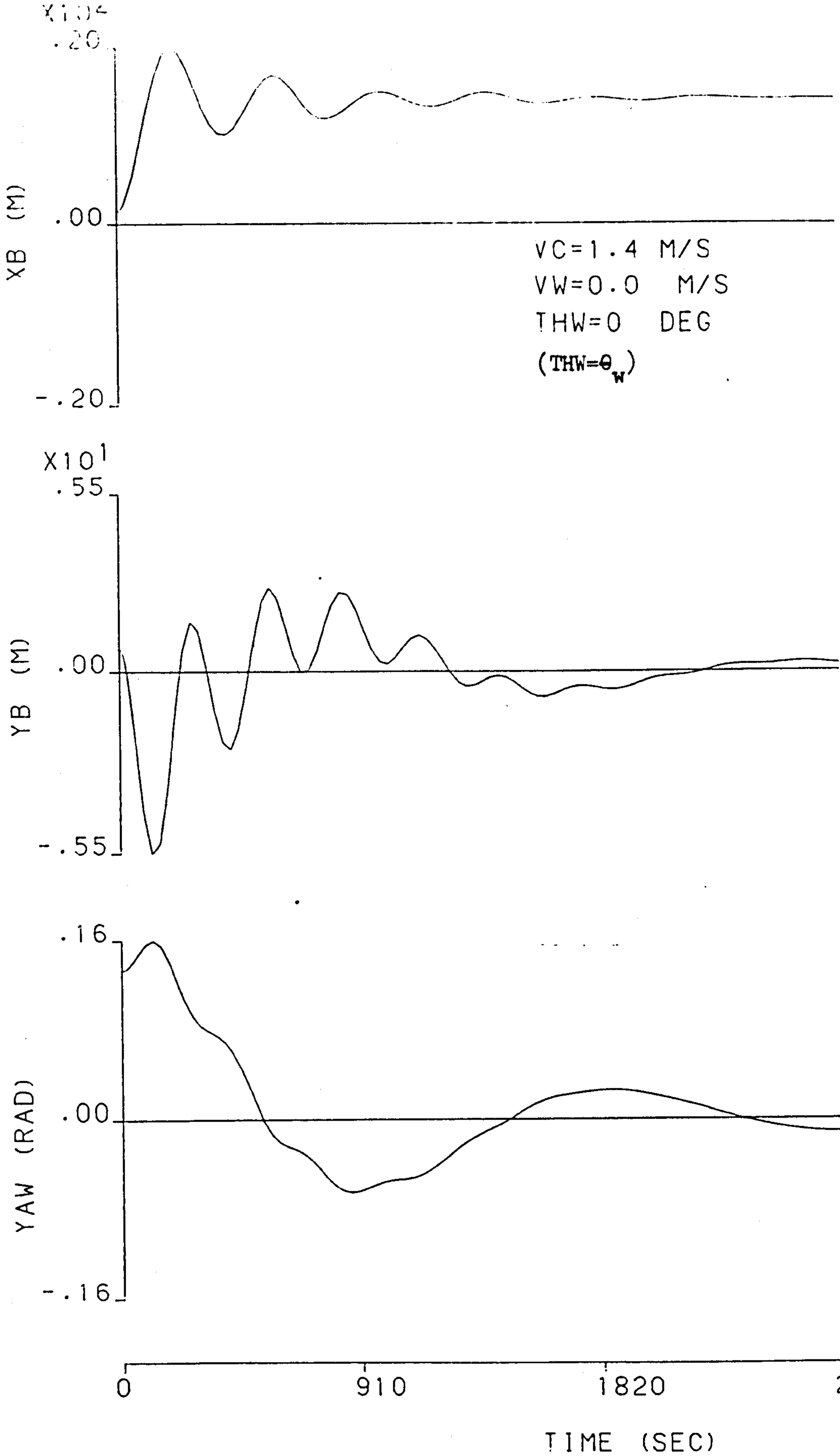

FIG. 7.9 MOTIONS OF A SBS SYSTEM IN WIND AND CURRENT ALONE

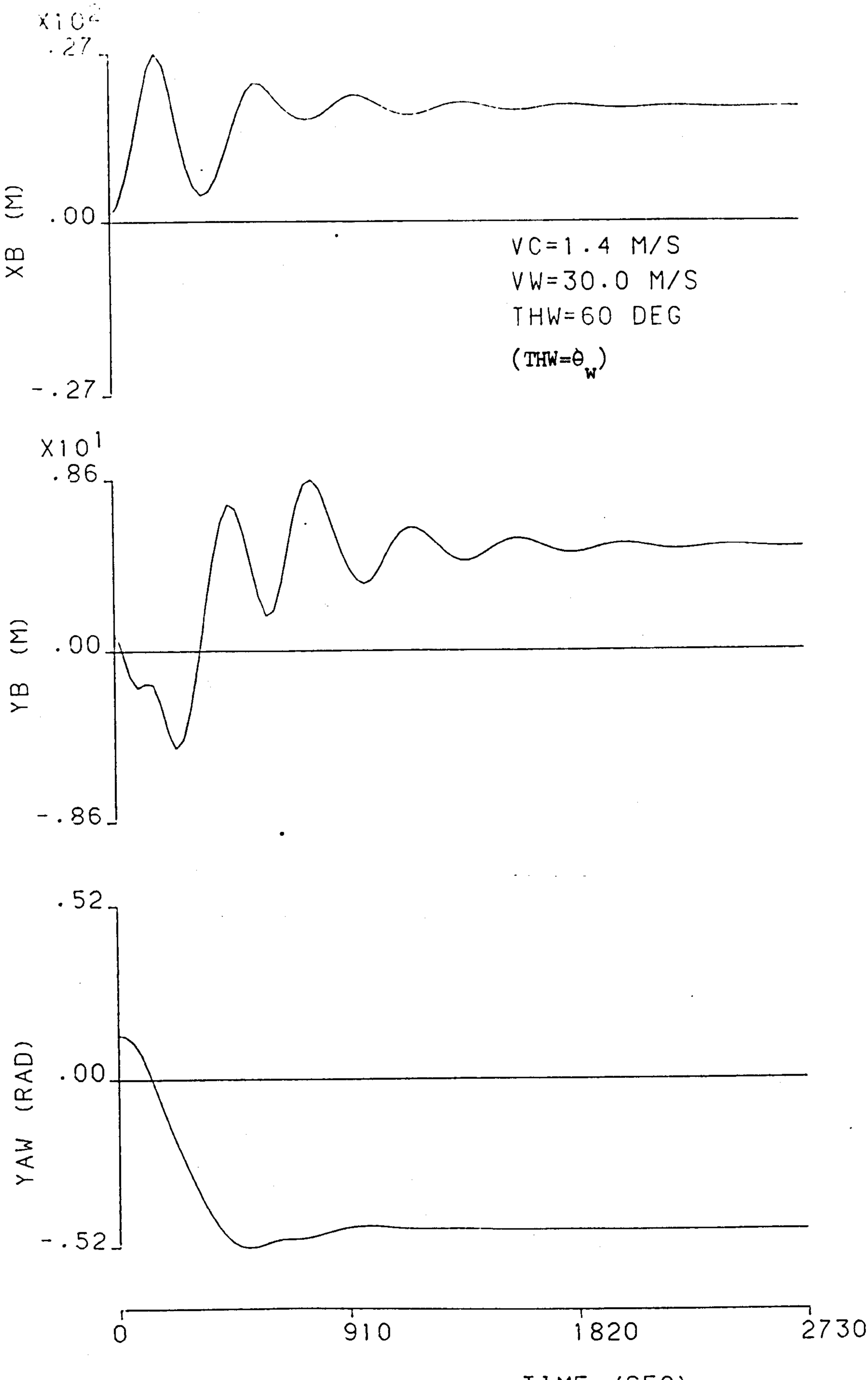

FIG. 7.10 MOTION OF A SBS SYSTEM IN WIND AND CURRENT ALONE

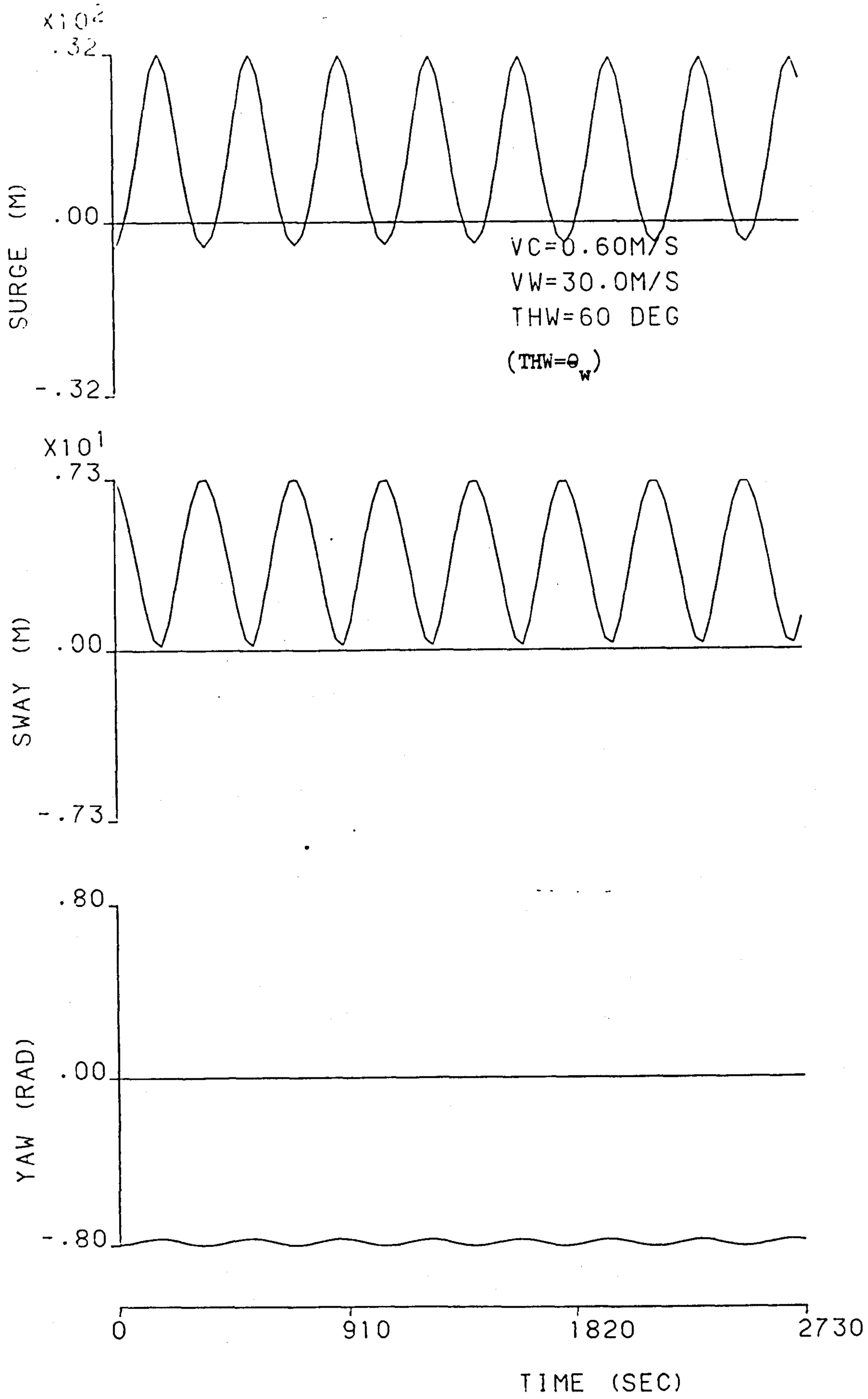

FIG. 7.11 MOTION OF A SBS SYSTEM IN WIND AND CURRENT ALONE

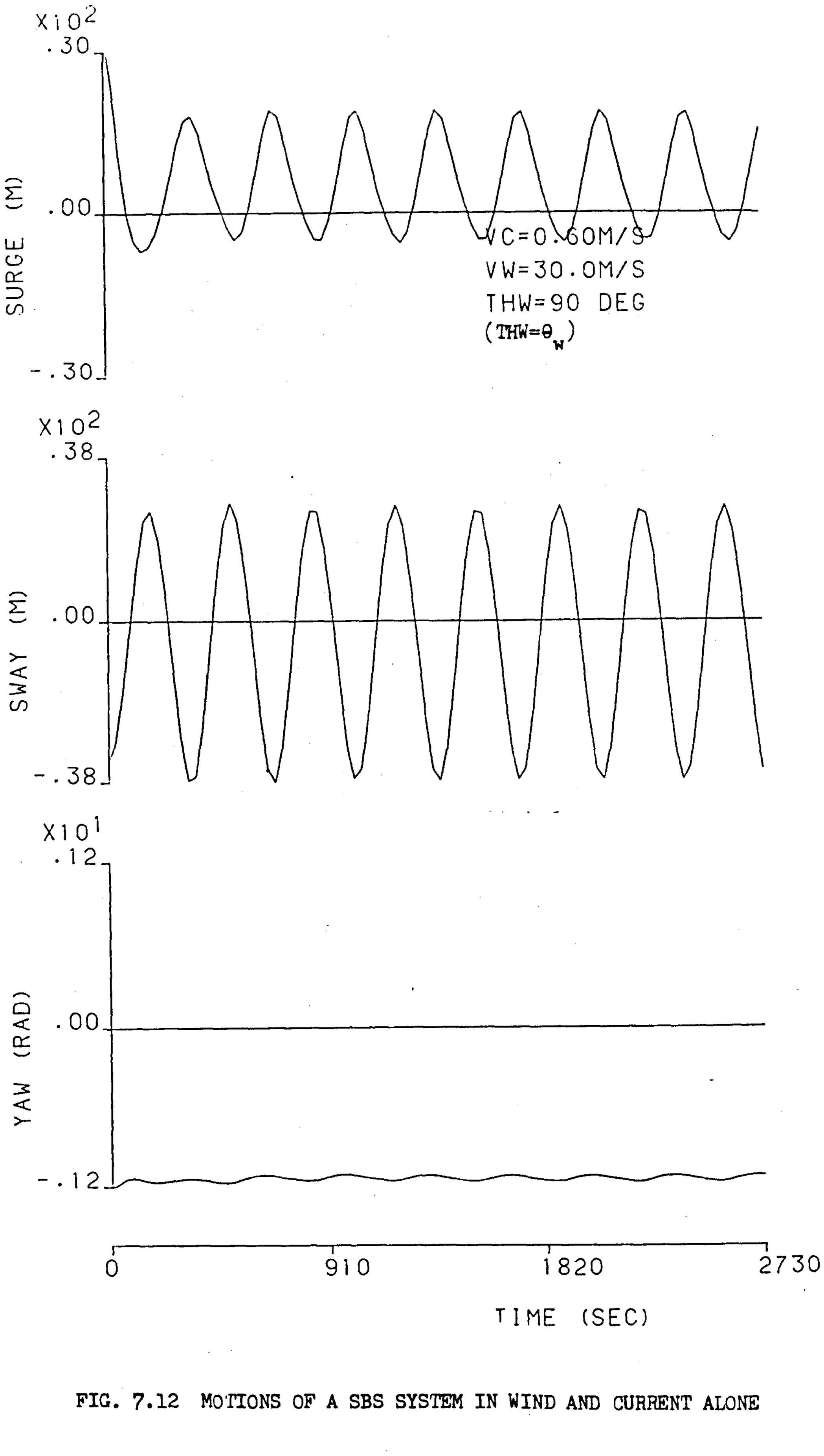

FIG. 7.12 MOTIONS OF A SBS SYSTEM IN WIND AND CURRENT ALONE

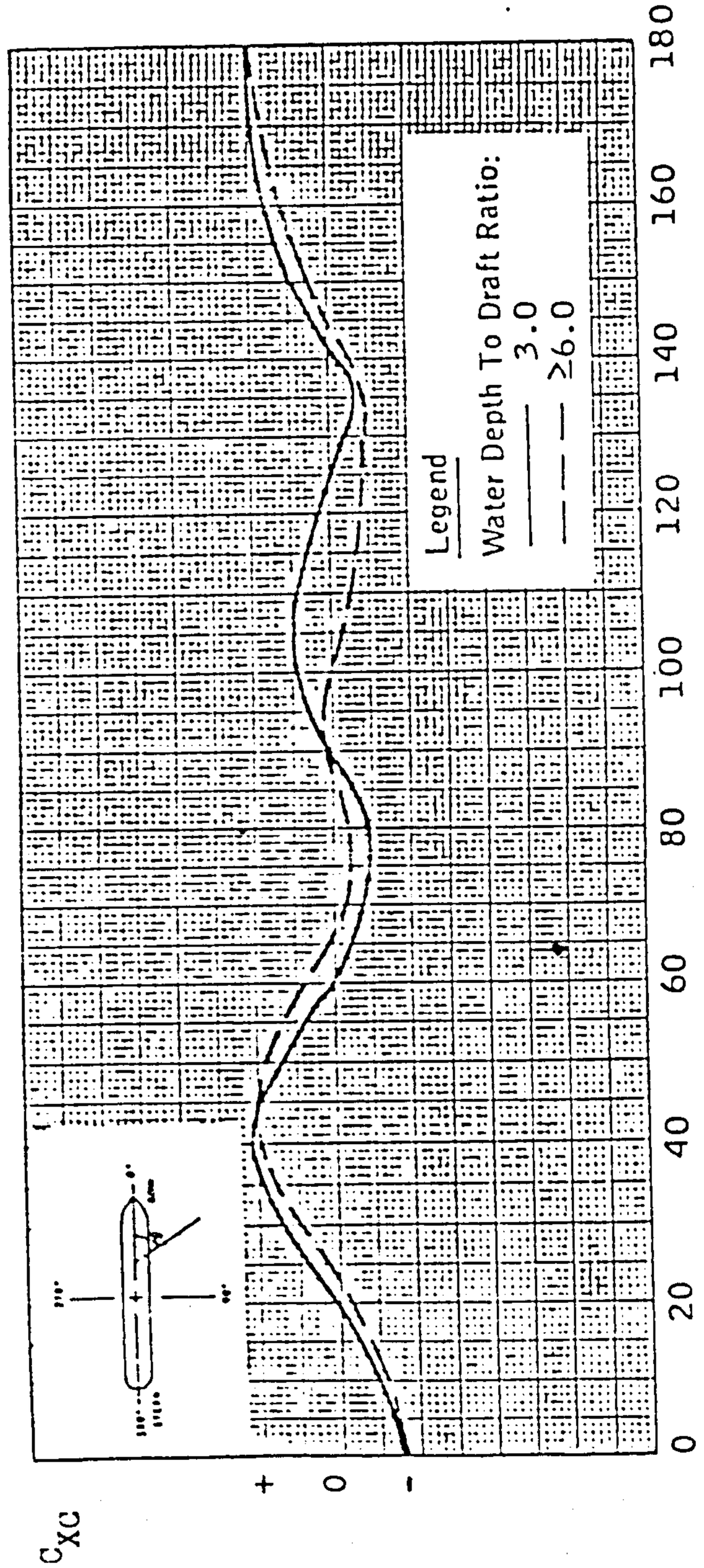

FIG. 7.13 OCIMF DATA FOR THE SURGE CURRENT FORCE COEFFICIENT C_{XC} (REF. 68)

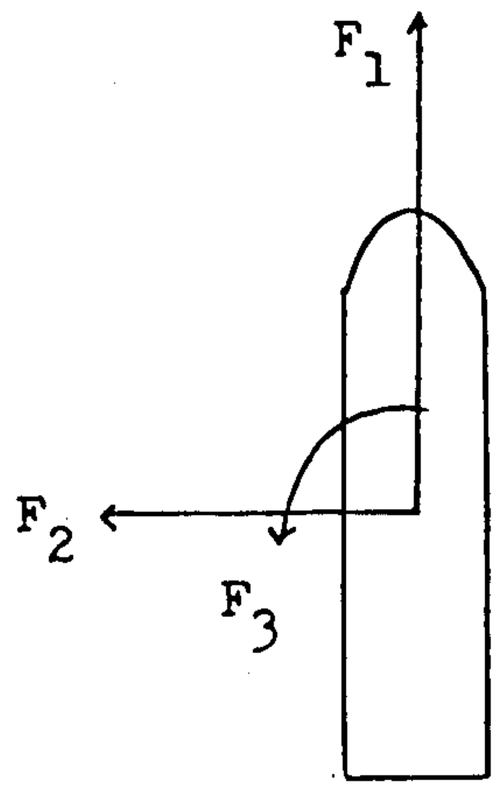

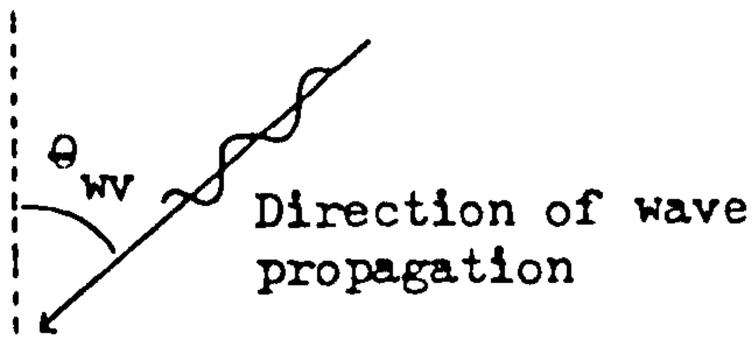

FIG. 7.14 SIGN CONVENTION FOR THE MEAN DRIFT FORCES

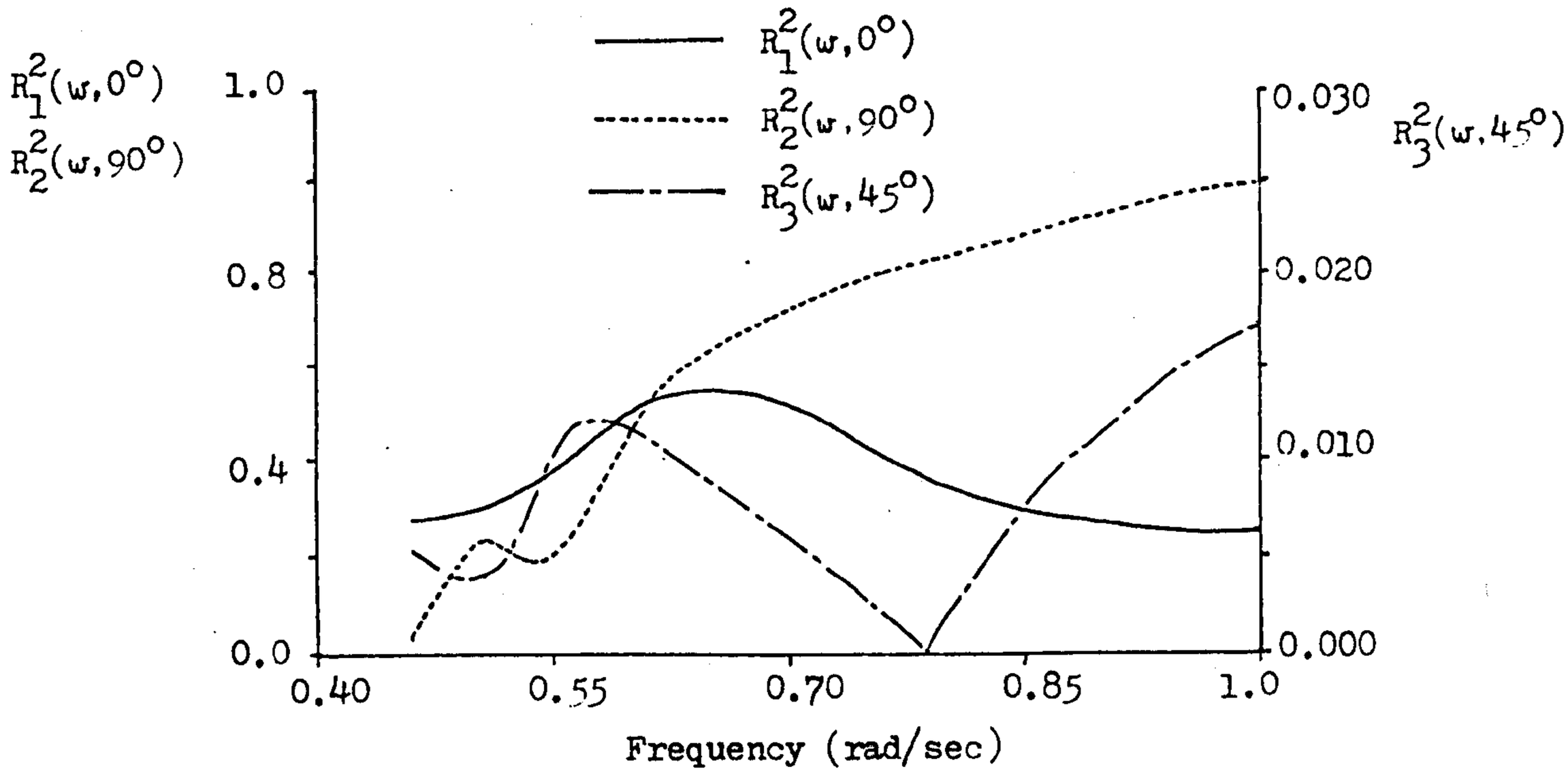

FIG. 7.15 TANKER REFLECTION COEFFICIENTS

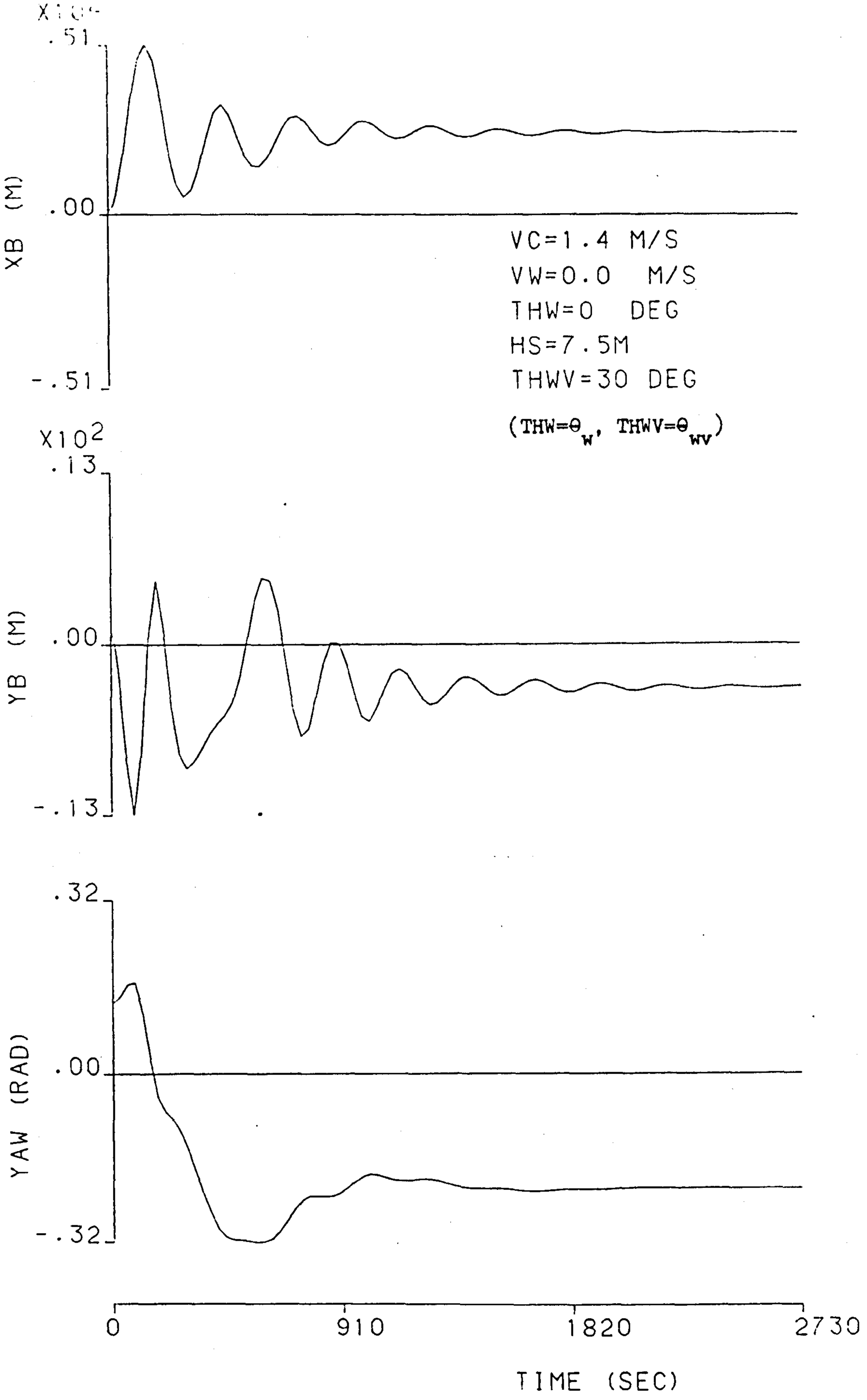

FIG. 7.16 MOTIONS OF A SBS SYSTEM IN WIND AND CURRENT, MEAN DRIFT FORCES INCLUDED

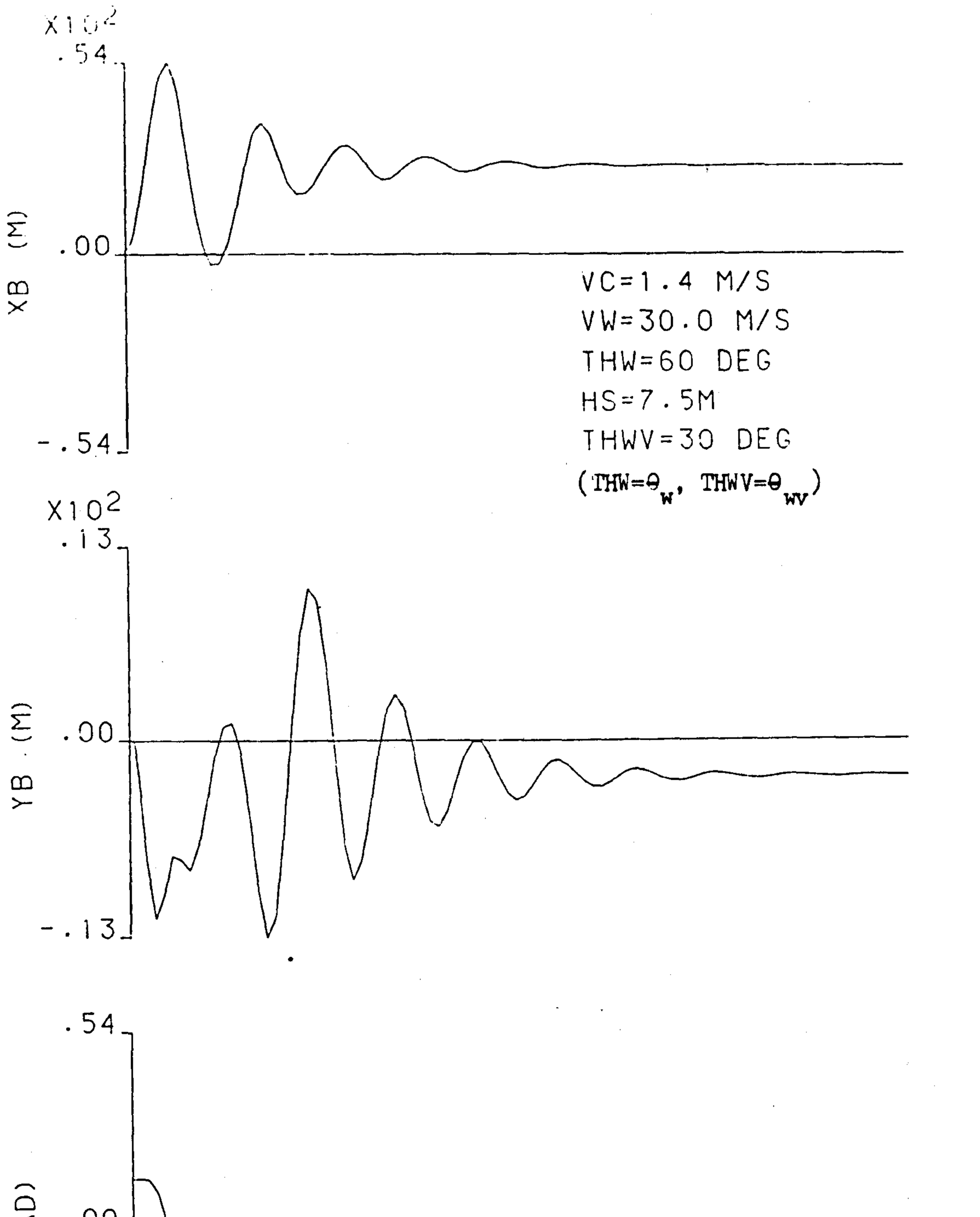

FIG. 7.17 MOTIONS OF A SBS SYSTEM IN WIND AND CURRENT, MEAN DRIFT FORCES INCLUDED

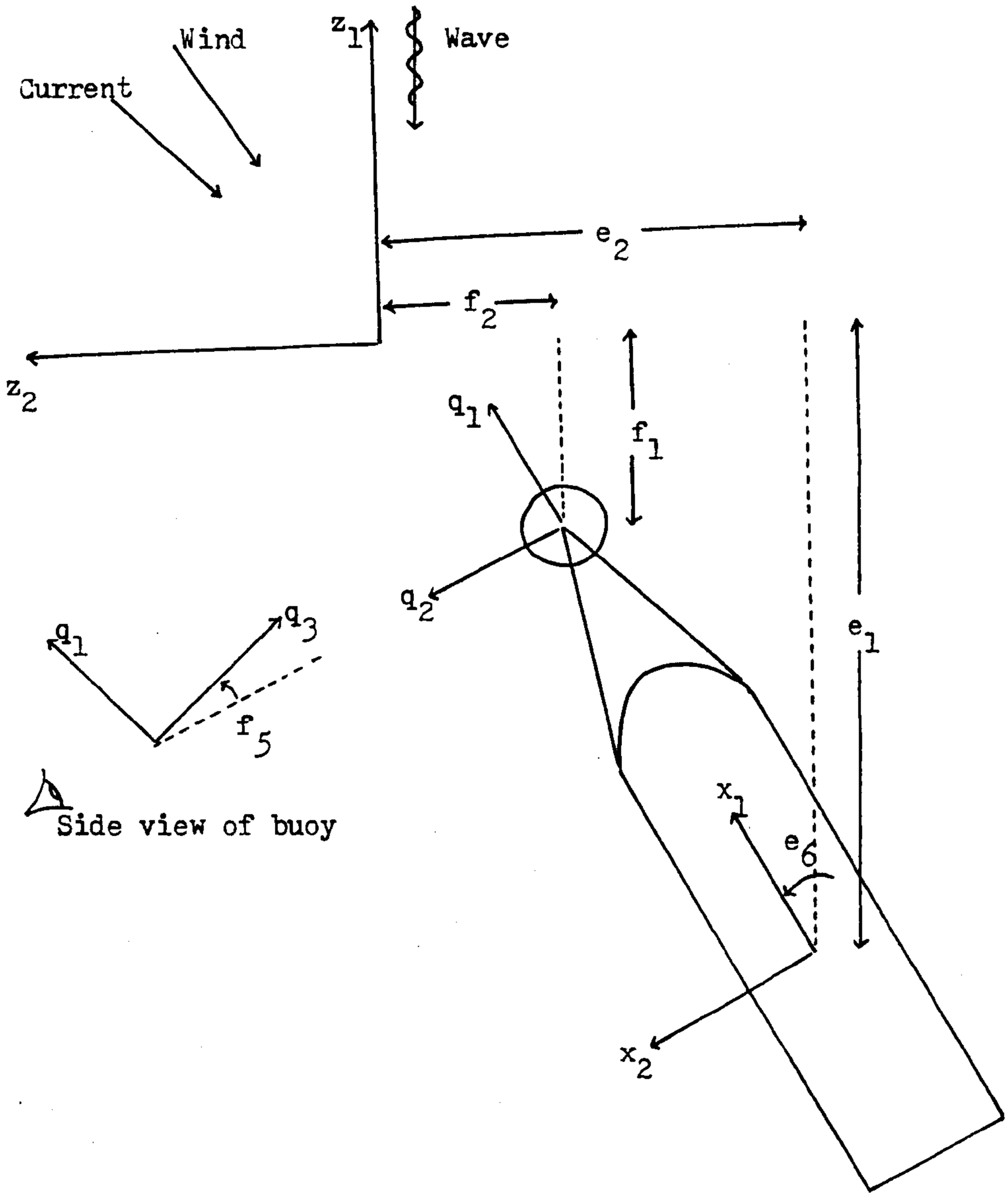

Additional static displacements : e_3, f_3 = depth below SWL of tanker and buoy CG's

FIG. 8.1 COORDINATE SYSTEMS AND STATIC DISPLACEMENTS

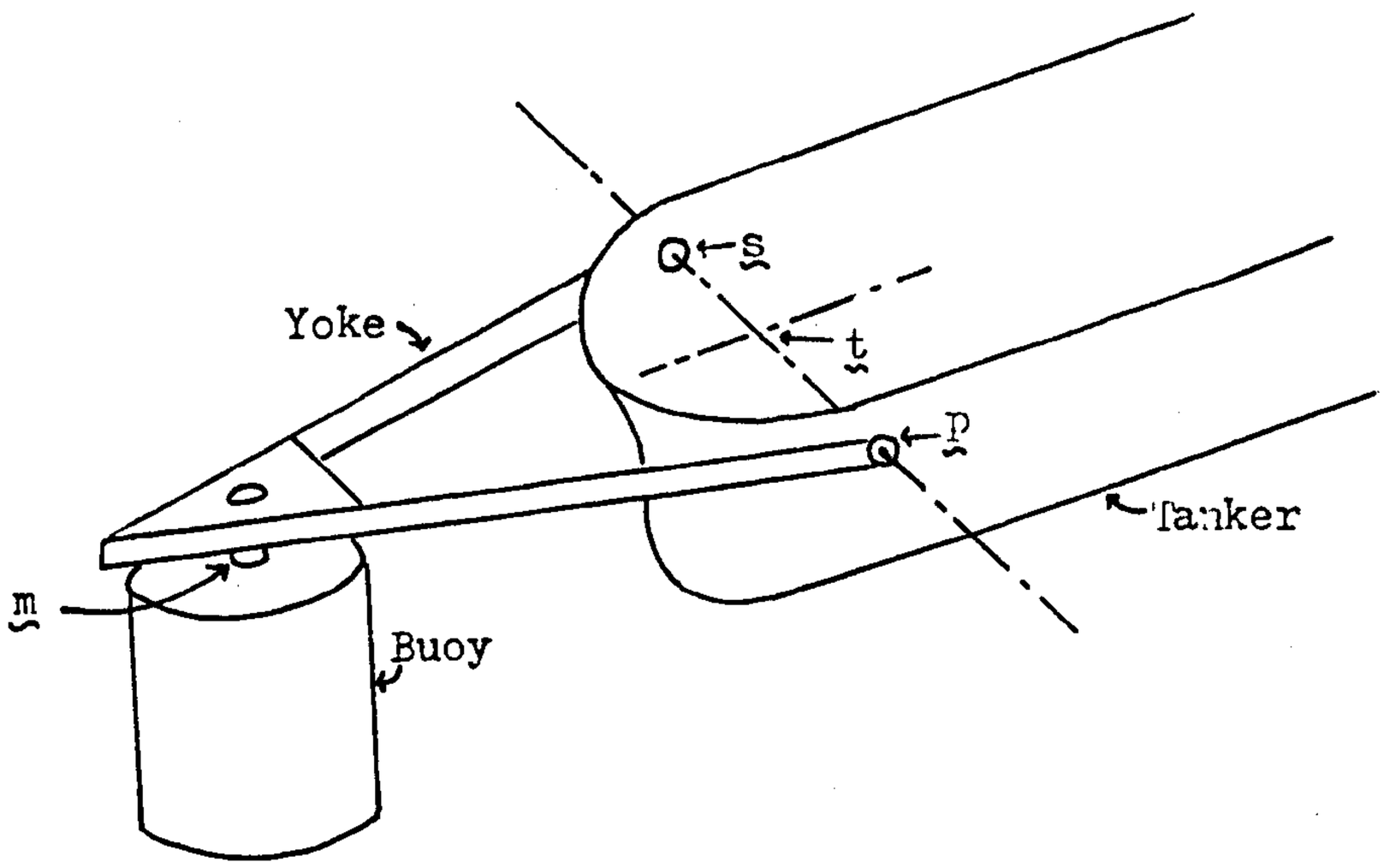

FIG. 8.2 POINTS ON THE YOKE/TANKER SYSTEM

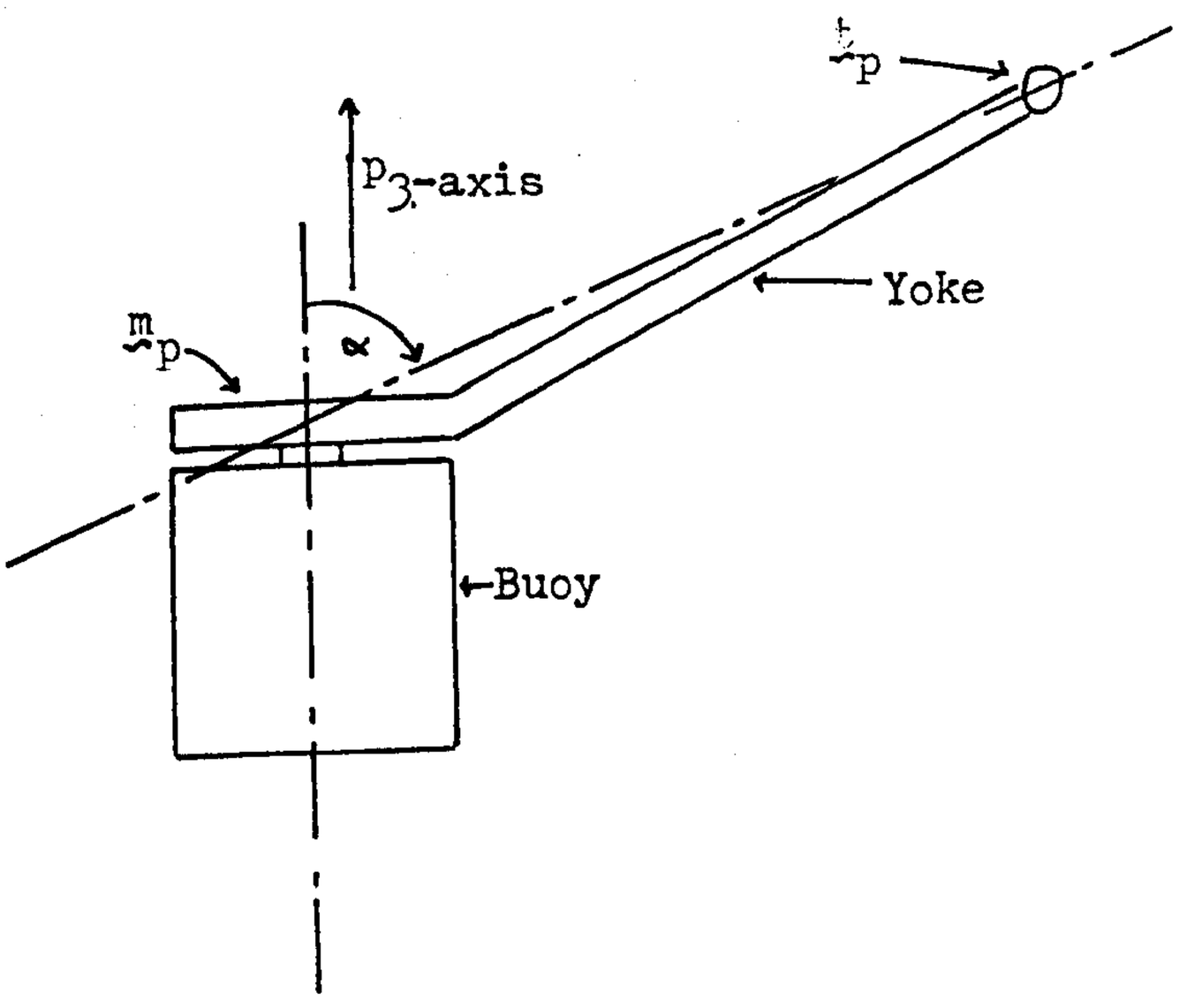

FIG. 8.3 CONSTRAINT BETWEEN THE YOKE AND THE BUOY

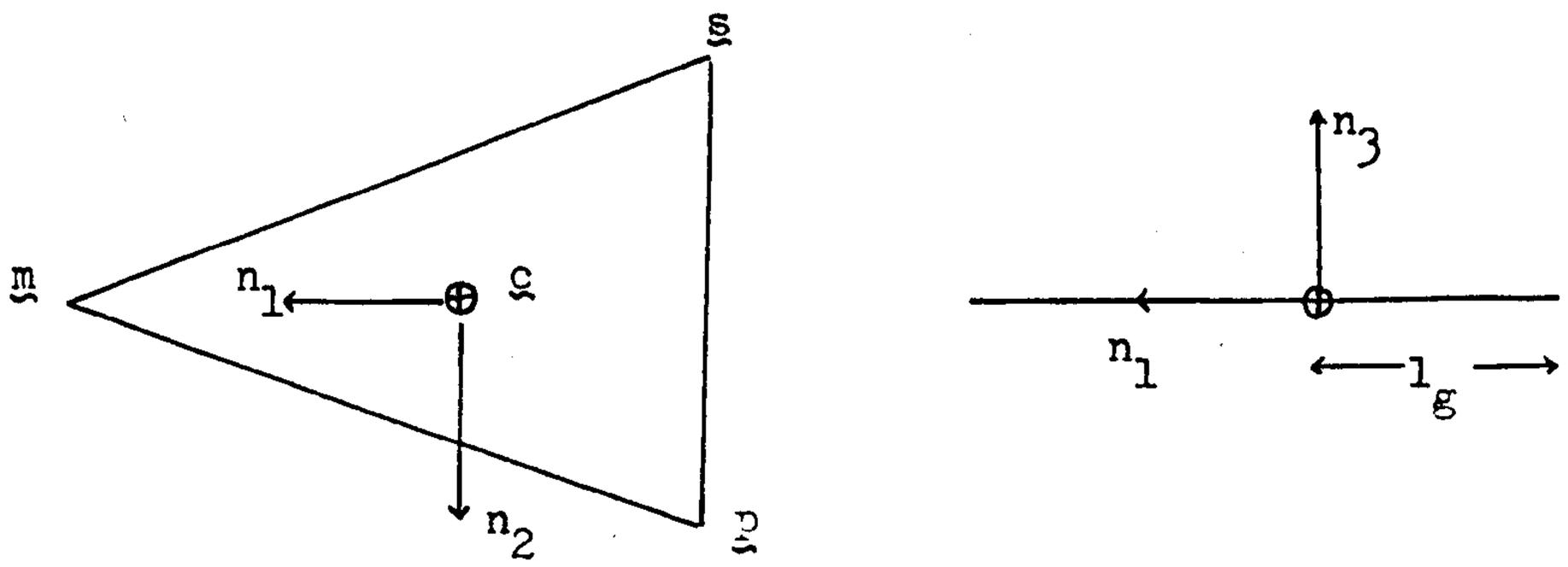

FIG. 8.4 YOKE COORDINATE SYSTEM

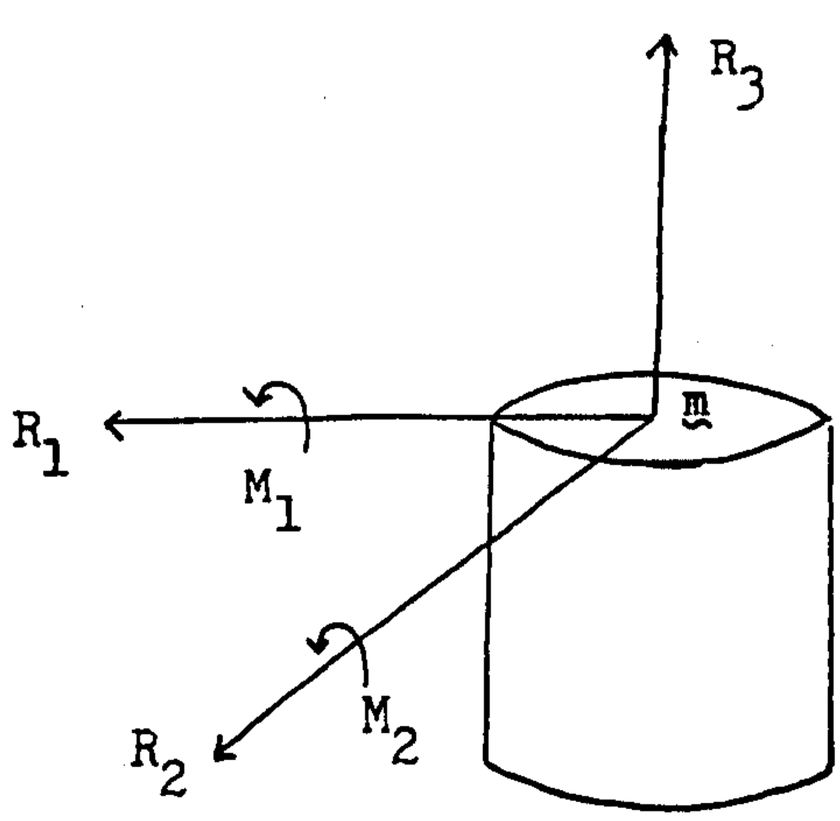

FIG. 8.5 REACTIONS AND MOMENTS AT THE BUOY

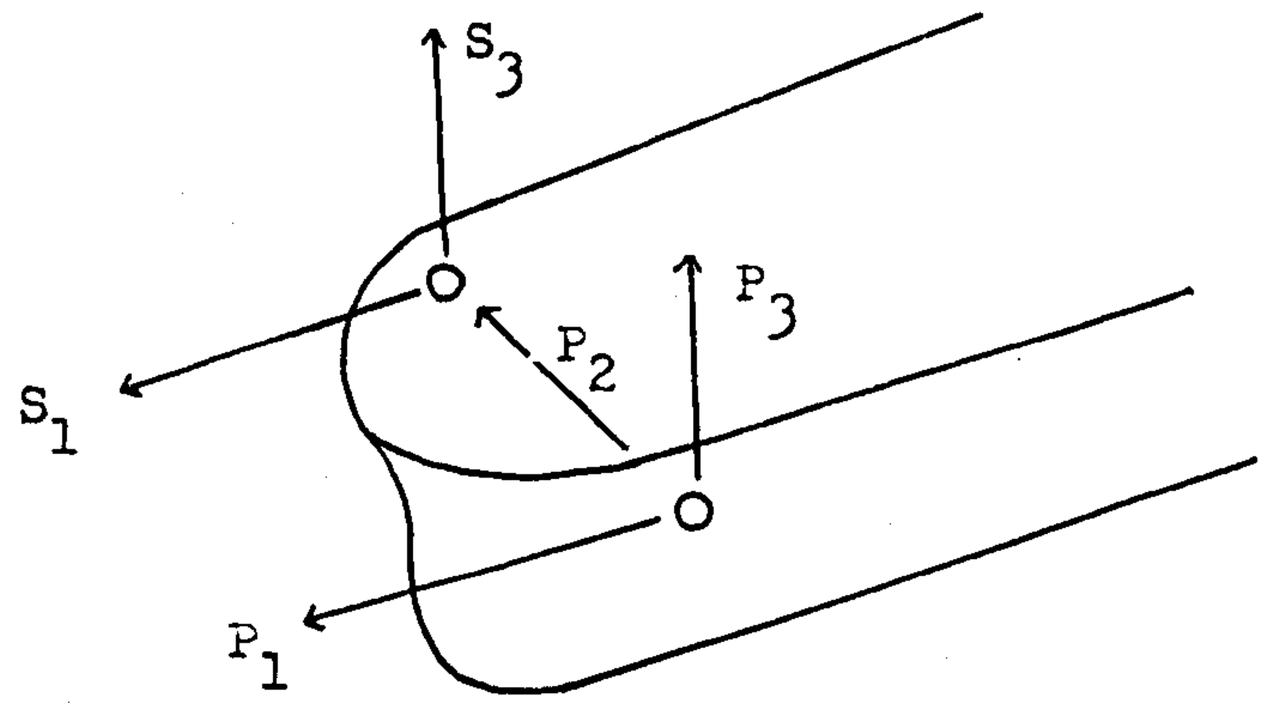

FIG. 8.6 REACTIONS AT THE TANKER

Item	Vessel				
	1	2	3	4	5
Length between perpendiculars (m)	285.6	285.6	285.6	285.6	310.0
Beam (m)	46.71	46.71	46.71	46.71	47.20
Mean draft (m)	13.82	5.94	5.94	5.94	18.90
Displacement (kg)	1.55×10^8	6.18×10^7	6.18×10^7	6.18×10^7	2.41×10^8
C.G. position, fore of midships (m)	6.46	0.0	60.0	-60.0	10.0
C.G. position, above baseline (m)	11.03	9.73	9.73	9.73	13.32
Ht. of yoke pivots above baseline (m)	23.82	23.82	23.82	23.82	28.90
Roll M.I. ($kg\text{-}m^2$)	4.14×10^{10}	1.65×10^{10}	1.65×10^{10}	1.65×10^{10}	6.96×10^{10}
Pitch M.I. ($kg\text{-}m^2$)	7.90×10^{11}	3.15×10^{11}	5.37×10^{11}	5.37×10^{11}	1.45×10^{12}
Yaw M.I. ($kg\text{-}m^2$)	7.90×10^{11}	3.15×10^{11}	5.37×10^{11}	5.37×10^{11}	1.45×10^{12}
Heave-pitch mass coupling, M_{35} (kg-m)	0.0	0.0	-3.7×10^9	3.7×10^9	0.0
Sway-yaw mass coupling, M_{26} (kg-m)	0.0	0.0	3.7×10^9	-3.7×10^9	0.0
Roll metacentric ht. (m)	8.97	21.5	21.5	21.5	5.78
Pitch metacentric ht. (m)	491.84	1137.56	1137.56	1137.56	423.72

1 = 130,000DWT Tanker at full draft

2 = 130,000DWT Tanker at half draft with C.G. midships

3 = 130,000DWT Tanker at half draft with C.G. 60m fore of midships

4 = 130 000DWT Tanker at half draft with C.G. 60m aft of midships

5 = 200 000DWT Tanker at full draft

FIG. 9.1 DIMENSIONS OF THE VESSELS CONSIDERED

FIG. 9.2 MOORING CONFIGURATION TYPE 1

Stiffness Properties of Catenary Mooring System

Linear stiffness matrix non-zero entries (SI Units):-

k_{11}= 1.145x10^4 k_{15}= 2.51x10^5 k_{22}= 1.145x10^4
k_{24}= -2.51x10^5 k_{33}= 5.73x10^4 k_{42}= -2.51x10^5
k_{44}= 4.46x10^6 k_{51}= 2.51x10^5 k_{55}= 4.46x10^6
k_{66} 2.81x10^5

Horizontal cubic coefficient = 44.3

Static Configuration of Catenaries

Water depth = 95m
Wetted wt./unit length = 0.415tonnes/m
Horizontal span = 72.02m
Suspended length = 126.73m
Horizontal pre-tension = 15.38tonnes
Vertical pre-tension = 52.59tonnes

Yoke and Buoy Dimensions

Yoke: Mass = 9.75x10^{5}kg Roll M.I. = 9.95x10^{7}kg-m^2
Yaw M.I. = 3.73x10^{8}kg-m^2 Pitch M.I. = 2.98x10^{8}kg-m^2
l_3 = 53m l_1 = 35m
l_2 = 20.17m

Buoy: Mass = 3.25x10^{5}kg Diameter = 19m
Yaw M.I. = 2.01x10^{7}kg-m^2 Draft = 4.5m
Roll M.I. = 6.68x10^{6}kg-m^2
Pitch M.I. = 6.68x10^{6}kg-m^2

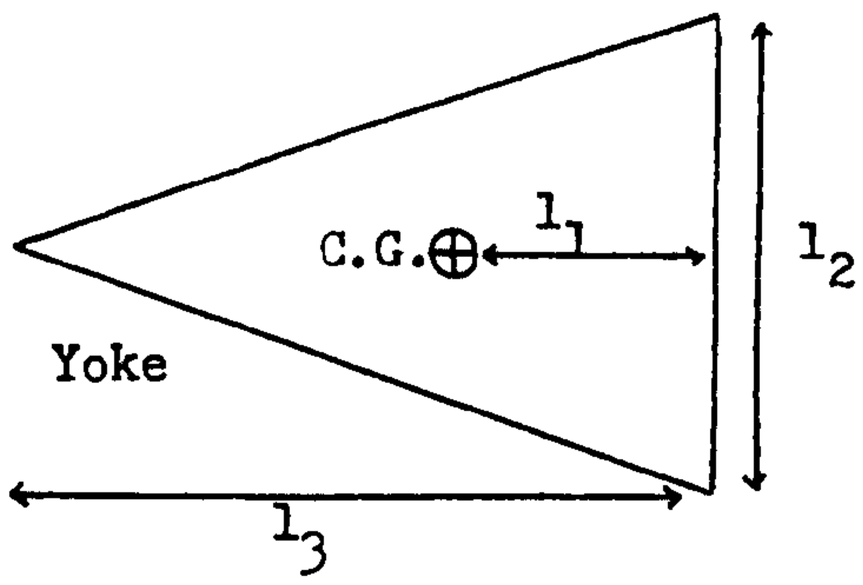

FIG. 9.3 MOORING CONFIGURATION TYPE 2

Stiffness Properties of Catenary Mooring System

Linear stiffness matrix non-zero entries (SI Units):-

k_{11}= 3.627x10^4
k_{15}= 4.76x10^5
k_{22}= 3.627x10^4
k_{24}= -4.76x10^5
k_{33}= 6.98x10^4
k_{42}= -4.76x10^5
k_{44}= 6.58x10^6
k_{51}= 4.76x10^5
k_{55}= 6.58x10^6
k_{66}= 7.66x10^5

Horizontal cubic coefficient = 89.09

Static Configuration of Catenaries

Water depth	= 95m
Wetted wt./unit length	= 0.415tonnes/m
Horizontal span	= 102.13m
Suspended length	= 147.16m
Horizontal pre-tension	= 27.61tonnes
Vertical pre-tension	= 61.07tonnes

Yoke and Buoy Dimensions

As in Figure 9.2

FIG. 9.4 MOORING CONFIGURATION TYPE 3

Stiffness Properties of Catenary Mooring System

Linear stiffness matrix non-zero entries (SI Units):-

k_{11}= 9.36x10^4
k_{15}= 9.52x10^5
k_{22}= 9.36x10^4
k_{24}= -9.52x10^5
k_{33}= 8.90x10^4
k_{24}= -9.52x10^5
k_{44}= 1.06x10^7
k_{15}= 9.52x10^5
k_{55}= 1.06x10^7
k_{66}= 1.41x10^6

Horizontal cubic coefficient = 229.3

Static Configuration of Catenaries

Water depth	= 95m
Wetted wt./unit length	= 0.415tonnes/m
Horizontal span	= 145.16m
Suspended length	= 180.6m
Horizontal pre-tension	= 51.53tonnes
Vertical pre-tension	= 74.95tonnes

Yoke and Buoy Dimensions

As in Figure 9.2

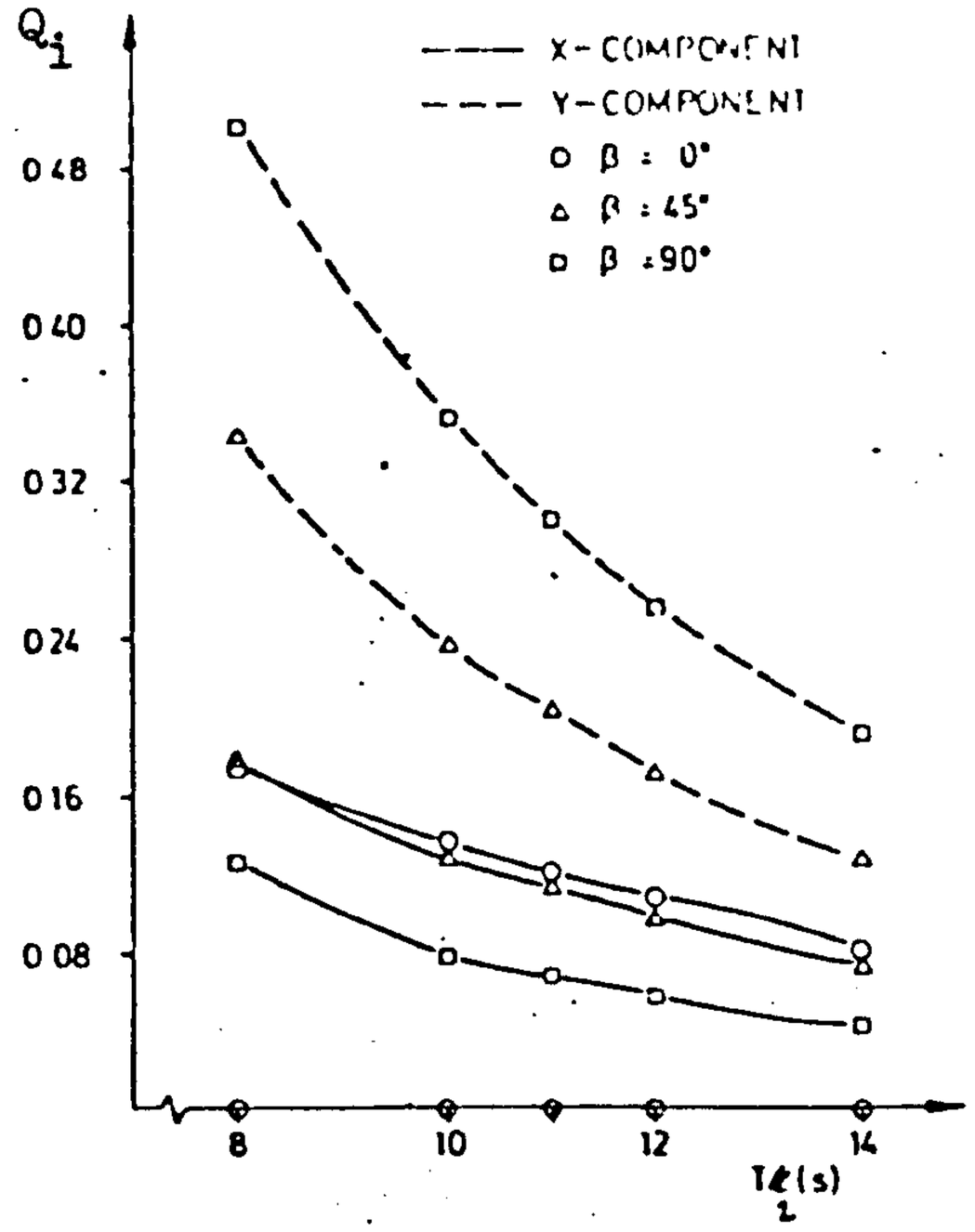

Wave drift forces in irregular waves on tanker.

FIG. 9.5 THE MEAN DRIFT FORCES ON A VLCC

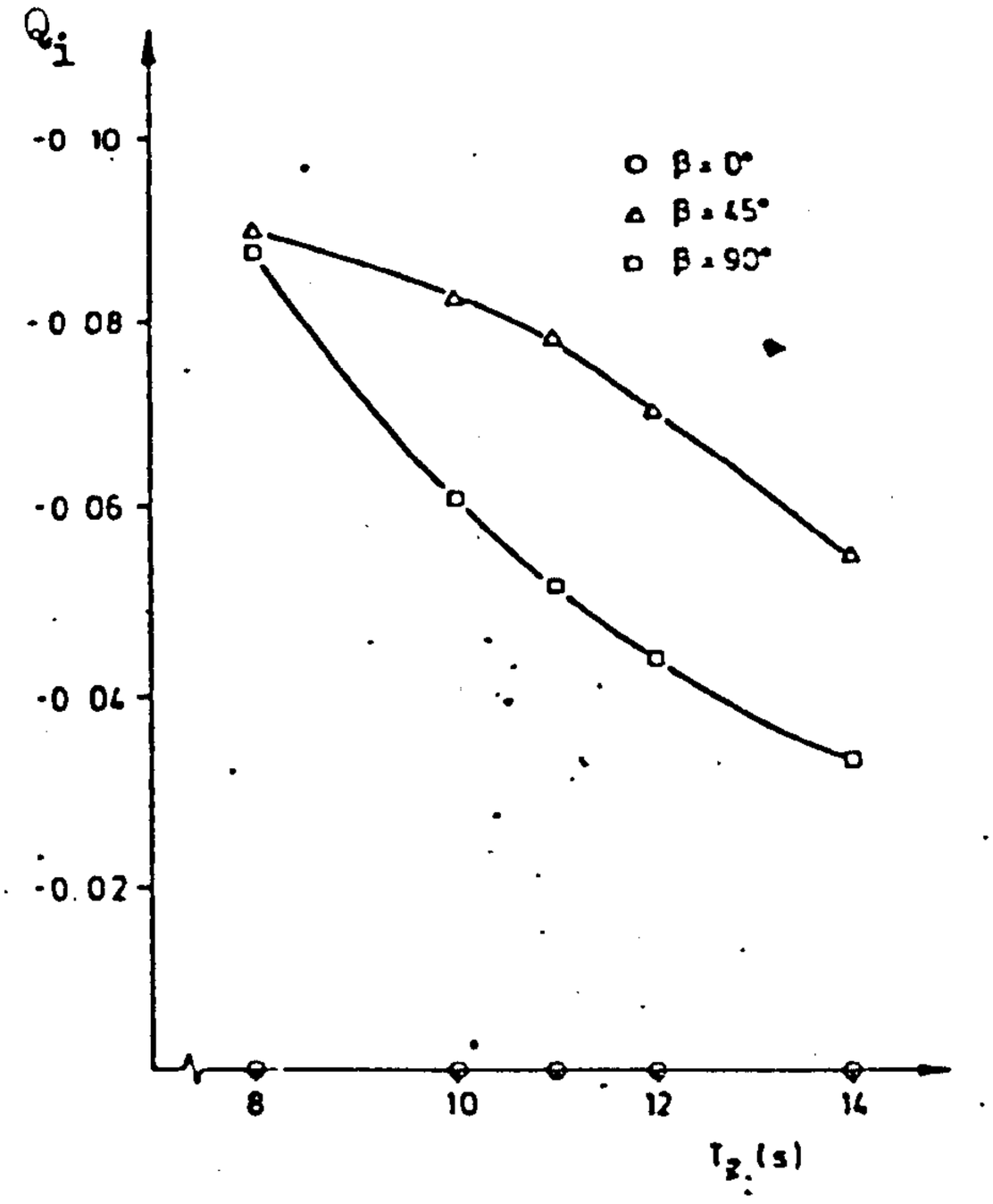

Wave drift moments in irregular waves on tanker.

FIG. 9.6 THE MEAN DRIFT MOMENT ON A VLCC

VESSEL (SEE FIG 9.1)	CASE	SURGE	SWAY-YAW IN PHASE	SWAY-YAW OUT OF PHASE	ROLL	HEAVE-PITCH IN PHASE	HEAVE-PITCH OUT OF PHASE	YOKE
1	1	0.01553	0.03168	0.0	0.4684	0.6054	0.5619	1.063
	2	0.01550	0.03077	0.004149	0.4684	0.6054	0.5619	1.063
	3	0.02638	0.04012	0.004092	0.4684	0.6054	0.5619	1.064
2	1	0.02466	0.05651	0.0	0.7267	0.5907	0.6189	1.047
	2	0.02466	0.05594	0.004907	0.7267	0.5907	0.6189	1.047
	3	0.03287	0.06355	0.004895	0.7267	0.5907	0.6190	1.047
5	1	0.01225	0.02379	0.0	0.3646	0.5602	0.5143	1.063
	2	0.01227	0.02305	0.003642	0.3646	0.5602	0.5143	1.063
	3	0.02107	0.03061	0.003566	0.3646	0.5602	0.5143	1.064

CASES: (1) STILL WATER
(2) 1M/S CURRENT
(3) 1M/S CURRENT, LINEARISED STIFFNESSES

FIG. 9.7 THE EFFECT OF VESSEL SIZE ON THE NATURAL FREQUENCIES OF A SBS SYSTEM
(ALL FIGURES ARE FREQUENCIES, IN RAD/SEC)

VESSEL (SEE FIG. 9.1)	CASE	SURGE	SWAY-YAW IN PHASE	SWAY-YAW OUT OF PHASE	ROLL	HEAVE-PITCH IN PHASE	HEAVE-PITCH OUT OF PHASE	YOKE
2	1	0.02466	0.05651	0.0	0.7267	0.5907	0.6189	1.047
	2	0.02466	0.05594	0.004907	0.7267	0.5907	0.6189	1.047
	3	0.03287	0.06355	0.004895	0.7267	0.5907	0.6190	1.047
3	1	0.02467	0.04294	0.0	0.7278	0.6348	0.5508	1.047
	2	0.02465	0.04256	0.006225	0.7278	0.6348	0.5508	1.047
	3	0.03295	0.04953	0.006216	0.7278	0.6348	0.5509	1.047
4	1	0.02468	0.06365	0.0	0.7279	0.5198	0.6487	1.047
	2	0.02469	0.06304	0.003954	0.7279	0.5198	0.6487	1.047
	3	0.03293	0.06977	0.003944	0.7279	0.5198	0.6488	1.047

CASES: (1) STILL WATER
(2) 1M/S CURRENT
(3) 1M/S CURRENT, LINEARISED STIFFNESSES

FIG. 9.8 EFFECT OF VESSEL LOADING CONDITIONS ON THE NATURAL FREQUENCIES OF A SBS SYSTEM (ALL FIGURES ARE FREQUENCIES. IN RAD/SEC)

VESSEL (SEE FIG. 9.1)	CASE	SURGE	SWAY-YAW IN PHASE	SWAY-YAW OUT OF PHASE	ROLL	HEAVE-PITCH IN PHASE	HEAVE-PITCH OUT OF PHASE	YOKE
1	1	0.008341	0.01693	0.0	0.4683	0.6054	0.5619	1.061
MOORING (9.2)	2	0.008341	0.01497	0.004544	0.4683	0.6054	0.5619	1.061
	3	0.02120	0.02958	0.004149	0.4683	0.6054	0.5619	1.061
1	1	0.01553	0.03168	0.0	0.4684	0.6054	0.5619	1.063
MOORING (9.3)	2	0.01550	0.03077	0.004149	0.4684	0.6054	0.5619	1.063
	3	0.02638	0.04012	0.004092	0.4684	0.6054	0.5619	1.064
1	1	0.02385	0.04834	0.0	0.4686	0.6054	0.5619	1.067
MOORING (9.4)	2	0.02385	0.04774	0.004071	0.4686	0.6054	0.5619	1.067
	3	0.03479	0.05729	0.004055	0.4686	0.6054	0.5619	1.068

CASES: (1) STILL WATER
(2) 1M/S CURRENT
(3) 1M/S CURRENT, LINEARISED STIFFNESSES

FIG. 9.9 THE EFFECT OF THE MOORING CONFIGURATION ON THE NATURAL FREQUENCIES OF A SBS SYSTEM
(ALL FIGURES ARE FREQUENCIES. IN RAD/SEC)

AMPLITUDE (M)	NATURAL FREQUENCY (RAD/SEC)
0.0	0.008341
4.0	0.008532
12.0	0.009914
20.0	0.01219
28.0	0.01494
36.0	0.01796
44.0	0.02113
52.0	0.02439

FIG. 9.10 NATURAL FREQUENCY FOR VARIOUS AMPLITUDES OF FREE VIBRATION

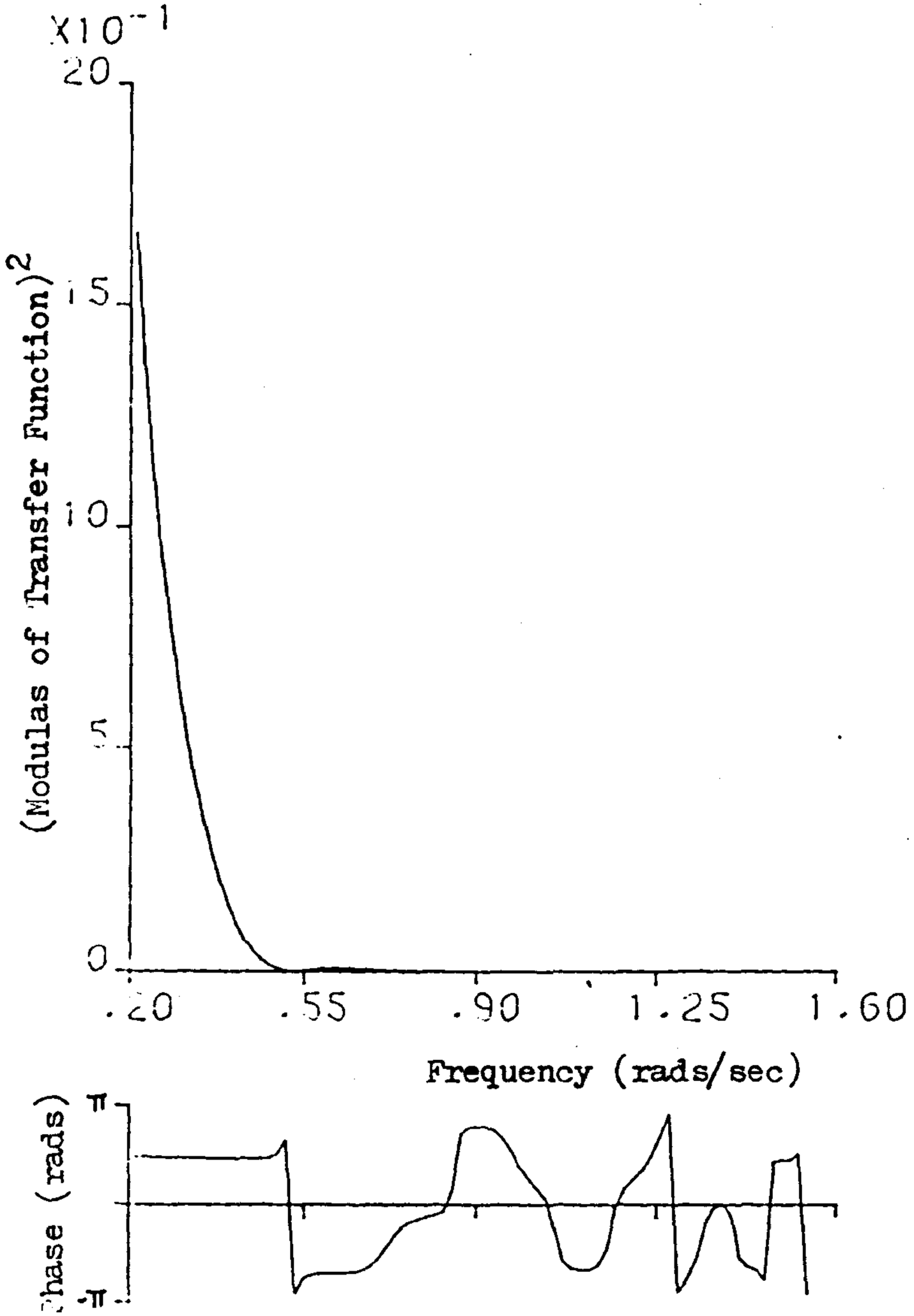

9.11.1 Surge

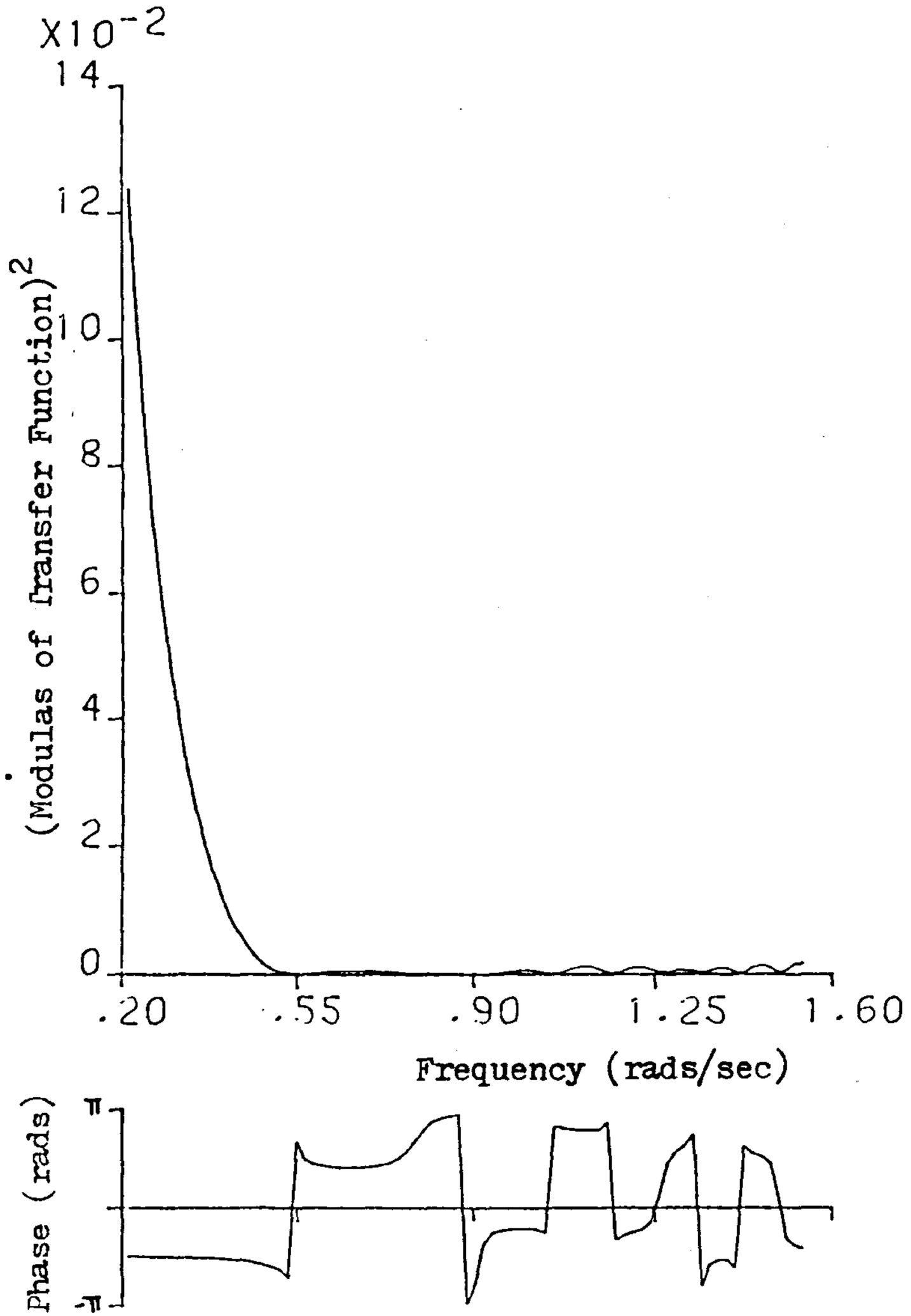

9.11.2 Sway

FIG. 9.11 SBS TRANSFER FUNCTIONS - 130,000DWT TANKER AT FULL DRAFT

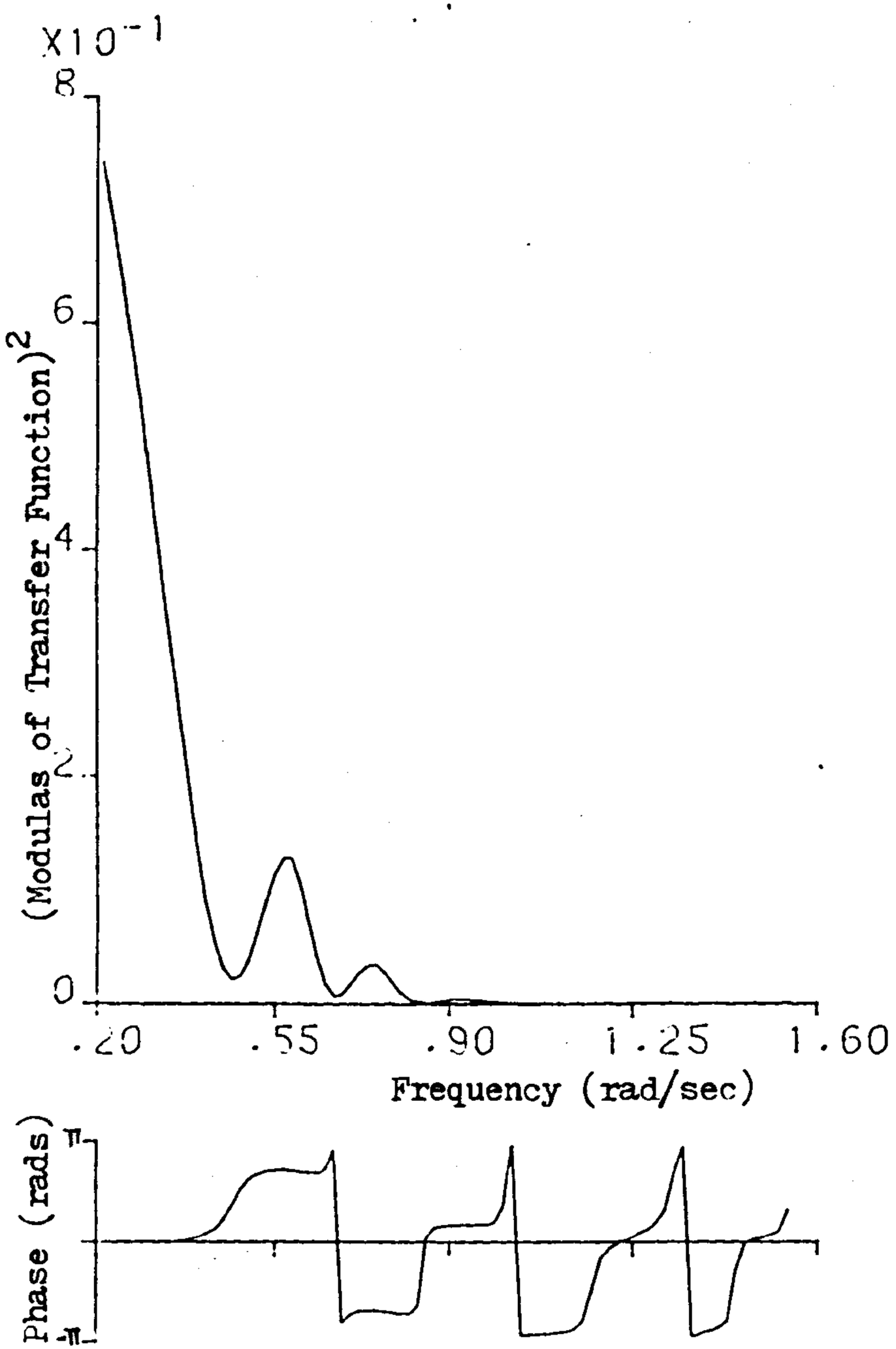

9.11.3 Heave

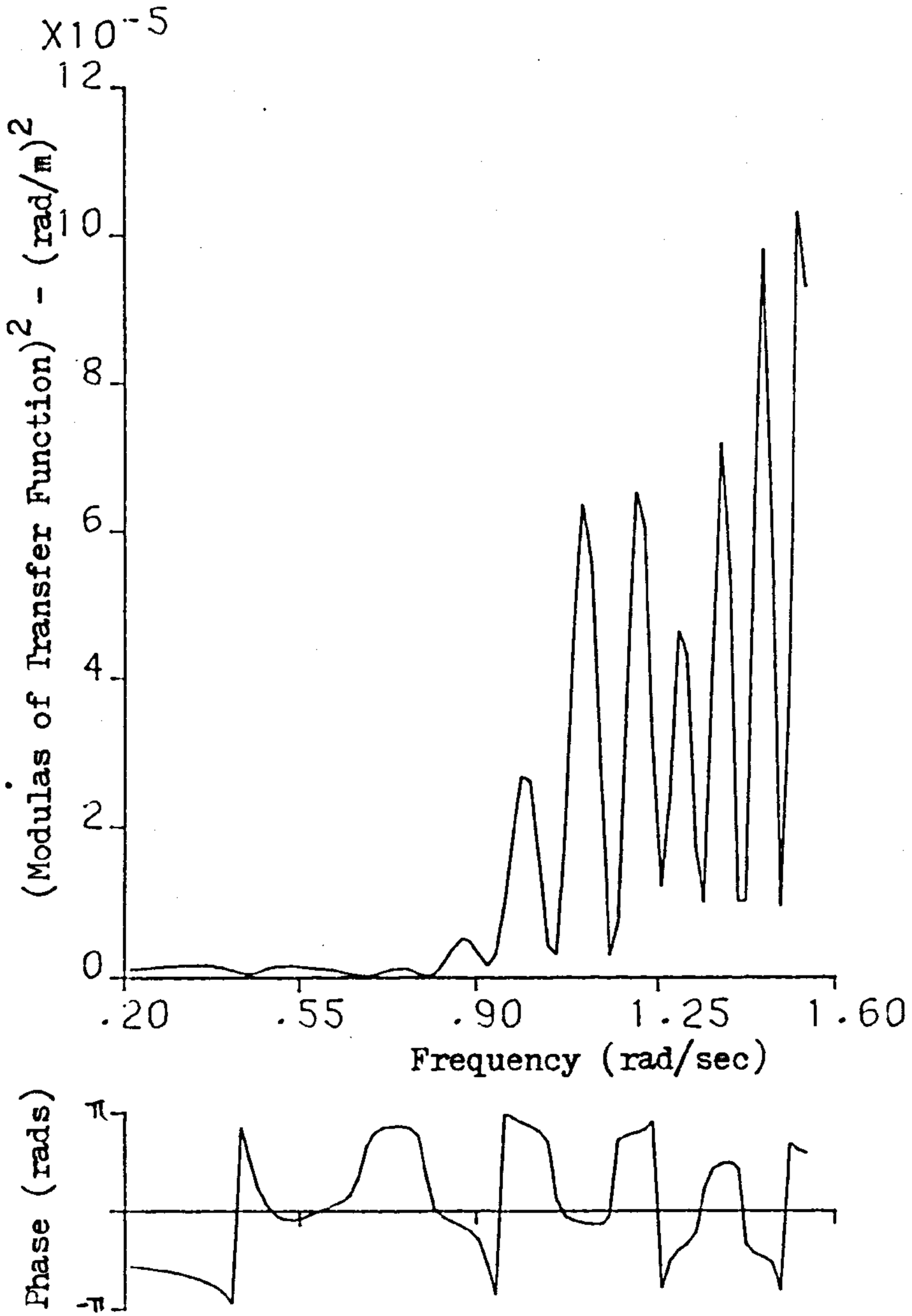

9.11.4 Roll

FIG. 9.11 SBS TRANSFER FUNCTIONS - 130,000DWT TANKER AT FULL DRAFT

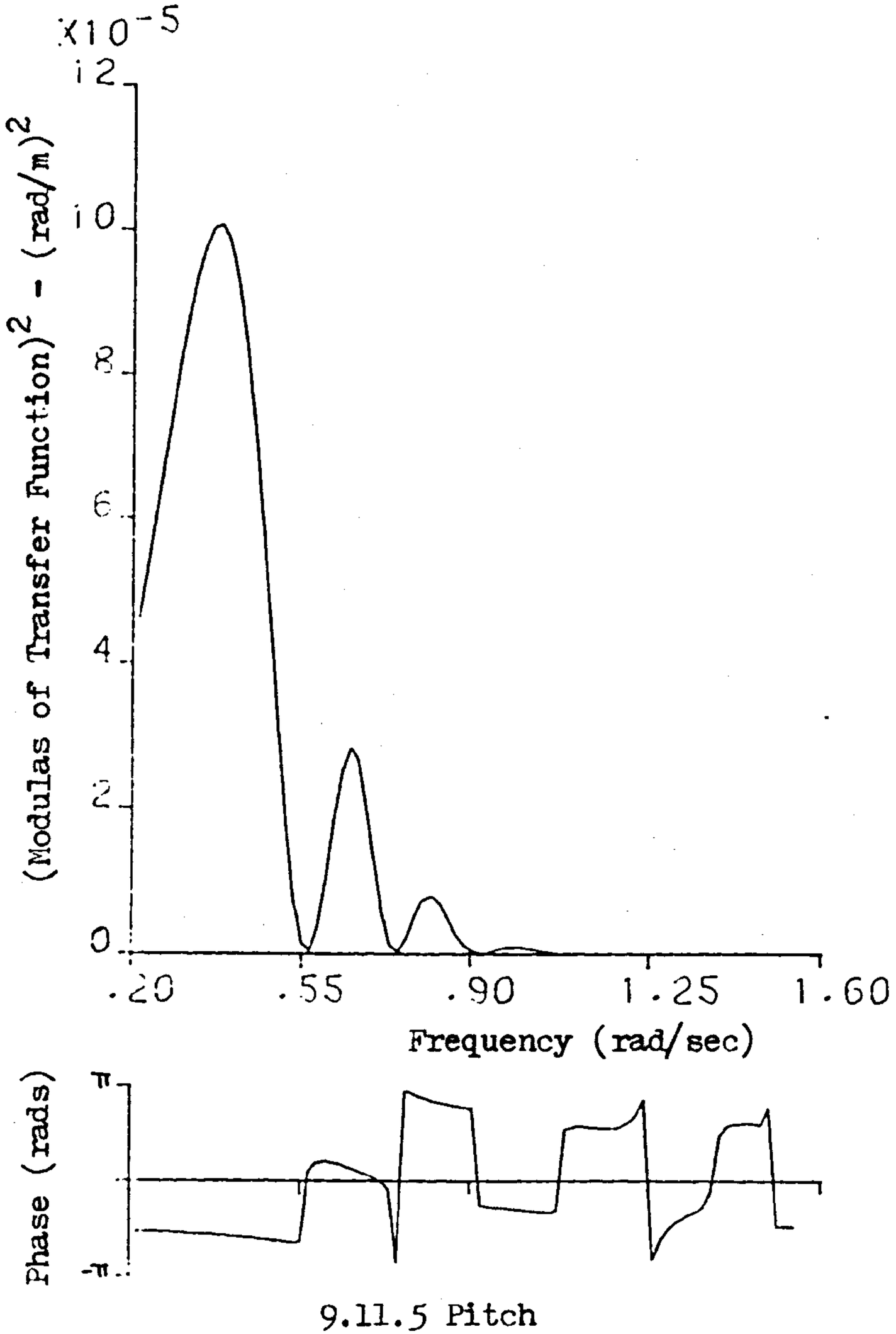

9.11.5 Pitch

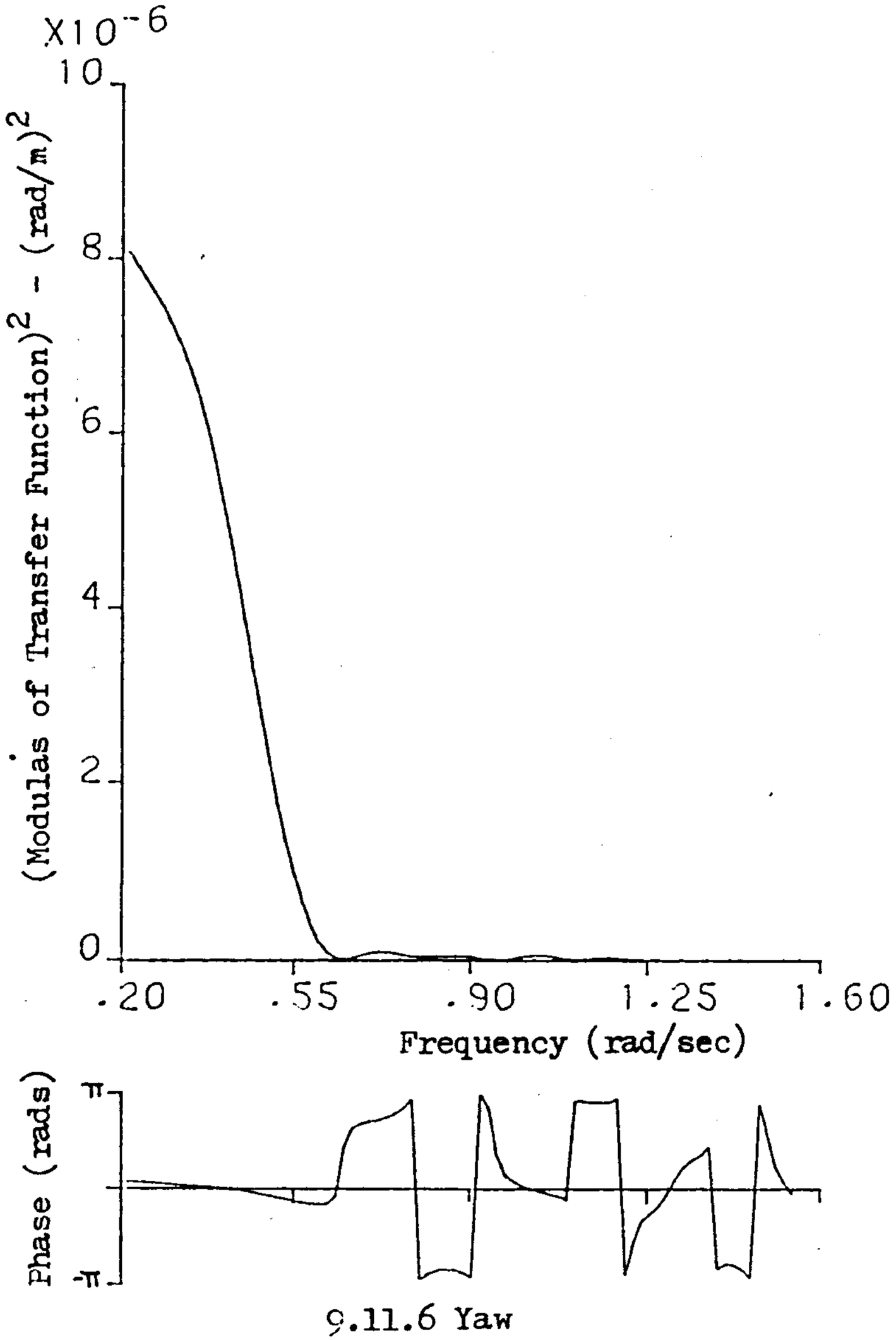

9.11.6 Yaw

FIG. 9.11 SBS TRANSFER FUNCTIONS - 130,000DWT TANKER AT FULL DRAFT

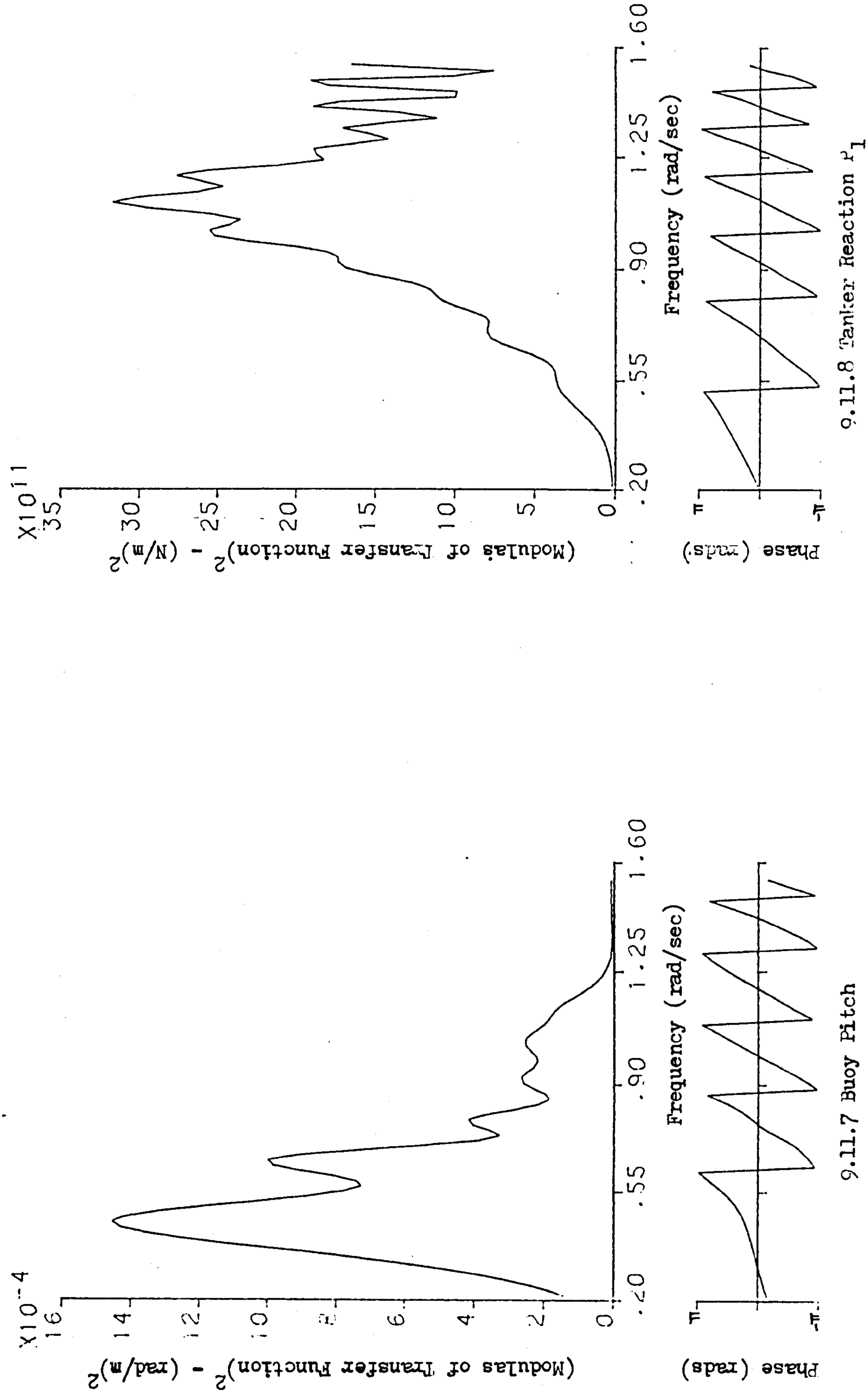

FIG. 9.11 SBS TRANSFER FUNCTIONS - 130,000DWT TANKER AT FULL DRAFT

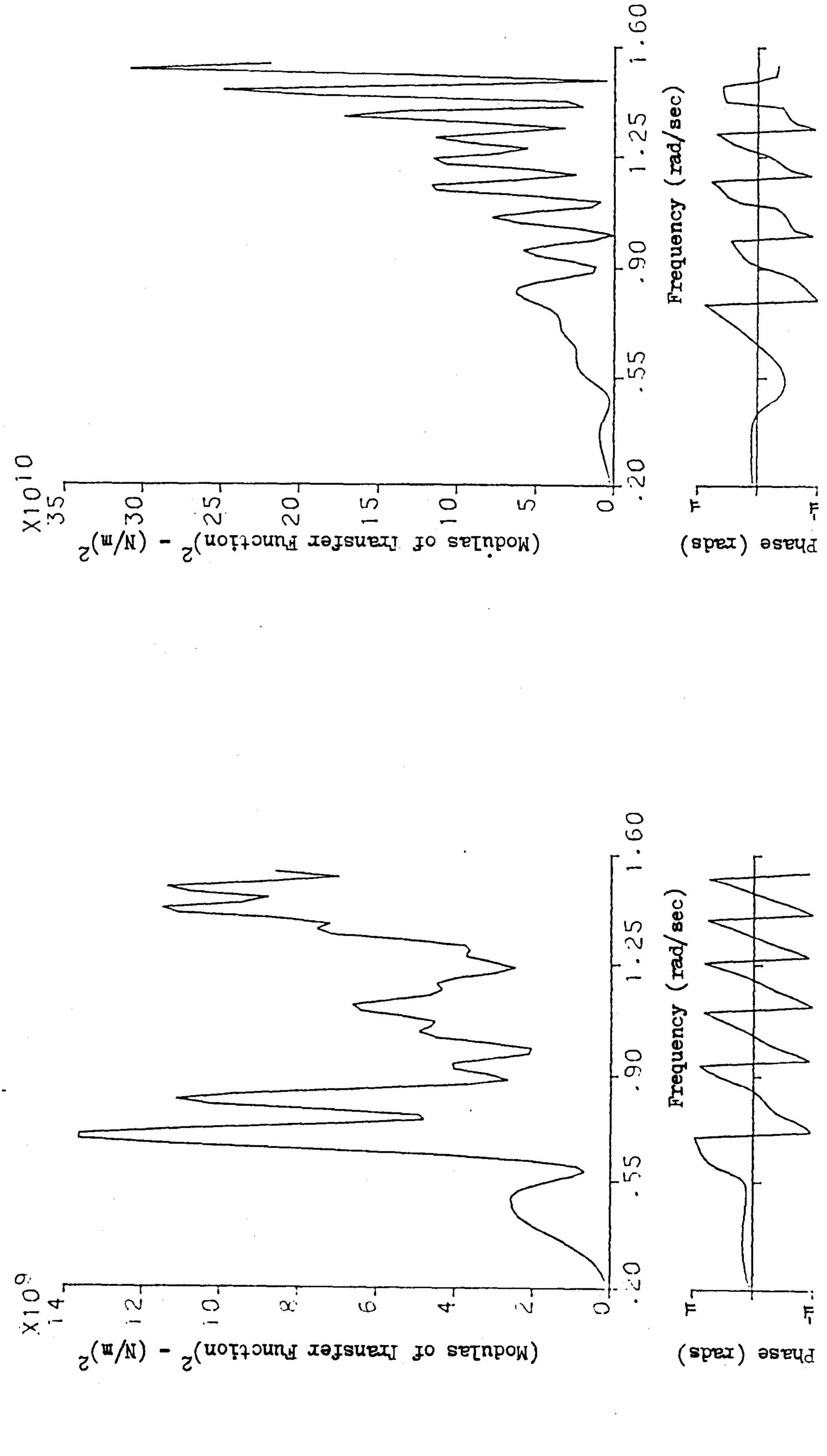

FIG. 9.11 SBS TRANSFER FUNCTIONS - 130,000DWT TANKER AT FULL DRAFT

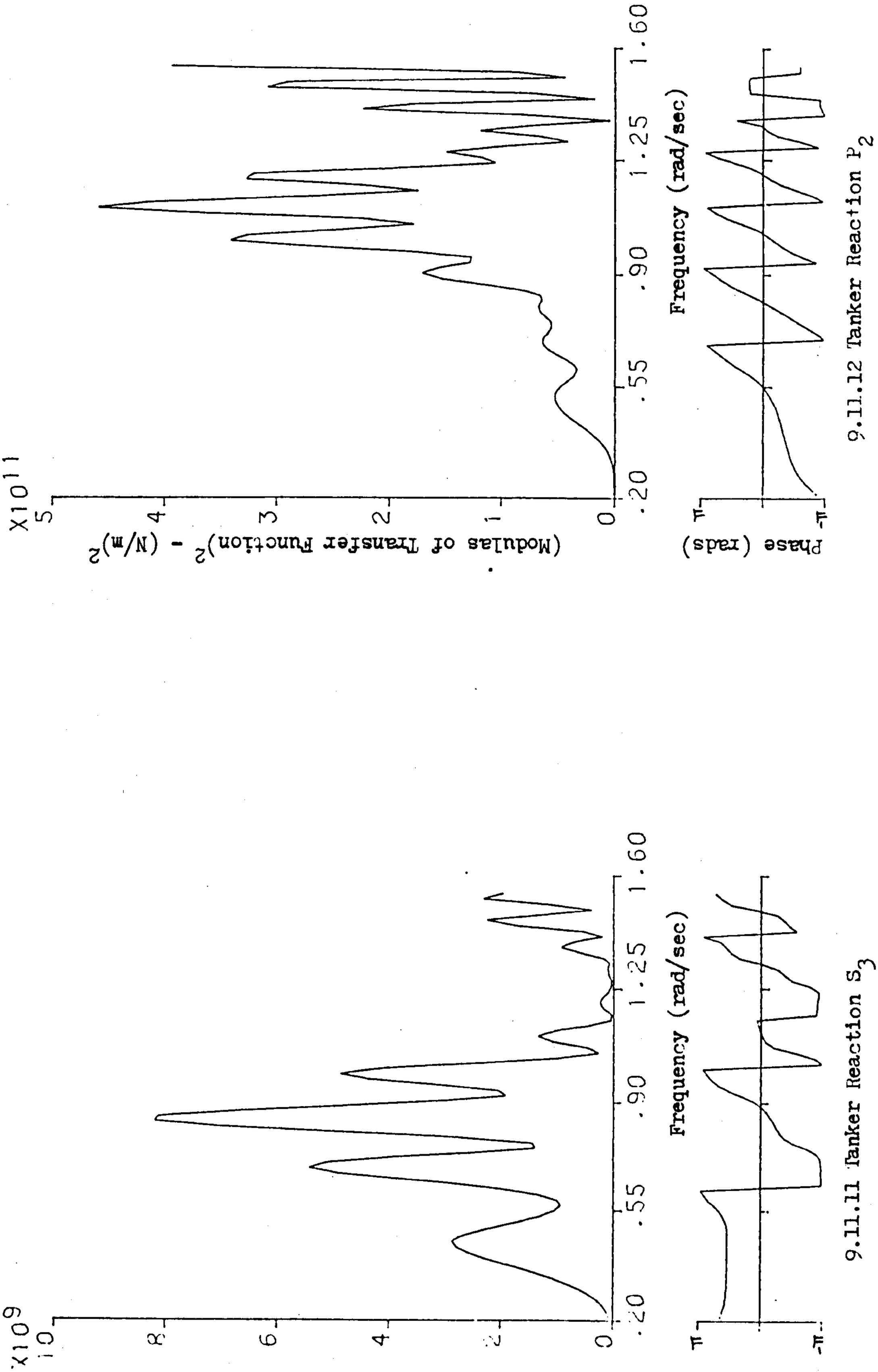

FIG. 9.11 SBS TRANSFER FUNCTIONS - 130,000DWT TANKER AT FULL DRAFT

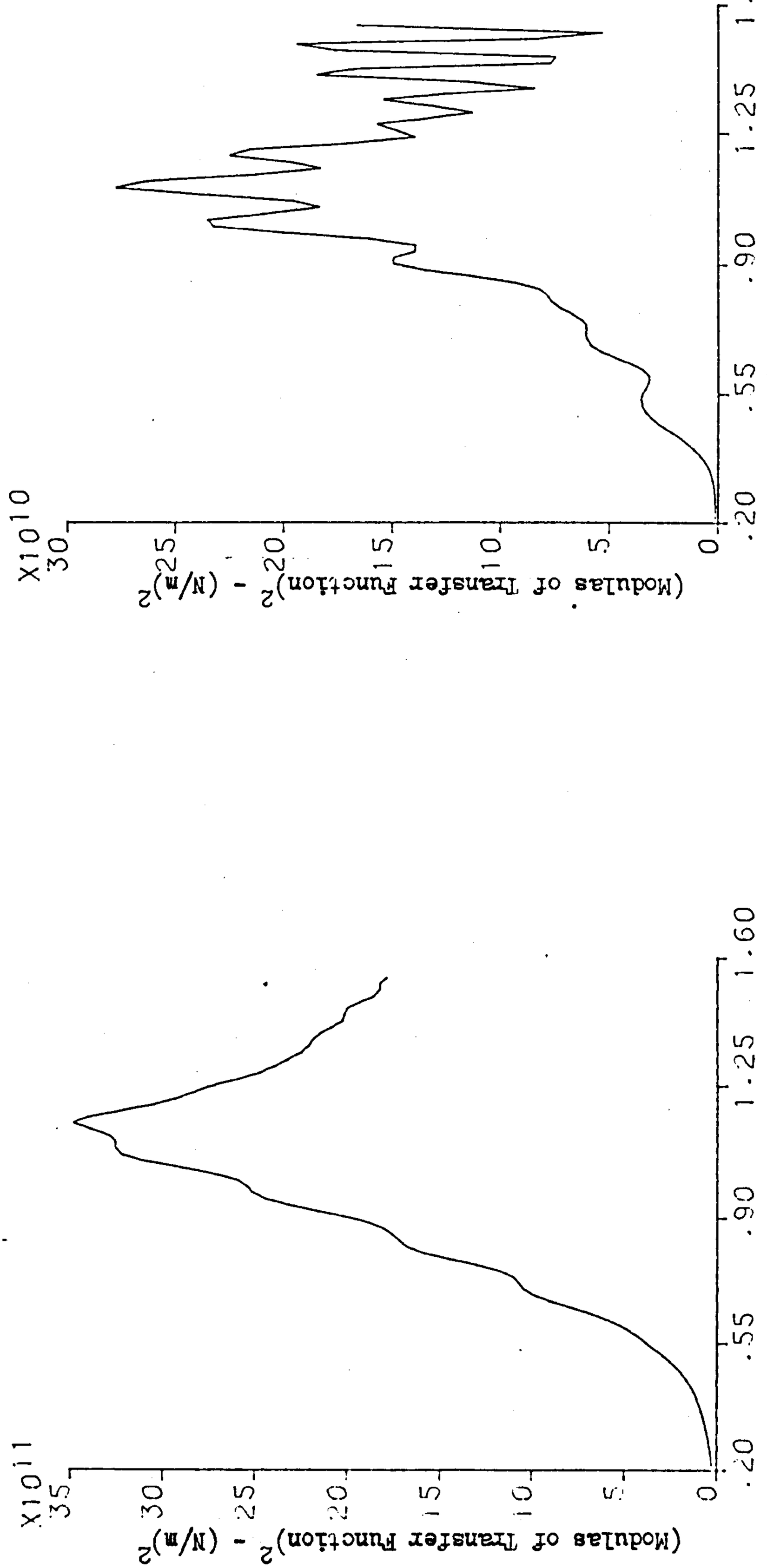

FIG. 9.11 SBS TRANSFER FUNCTIONS - 130,000DWT TANKER AT FULL DRAFT

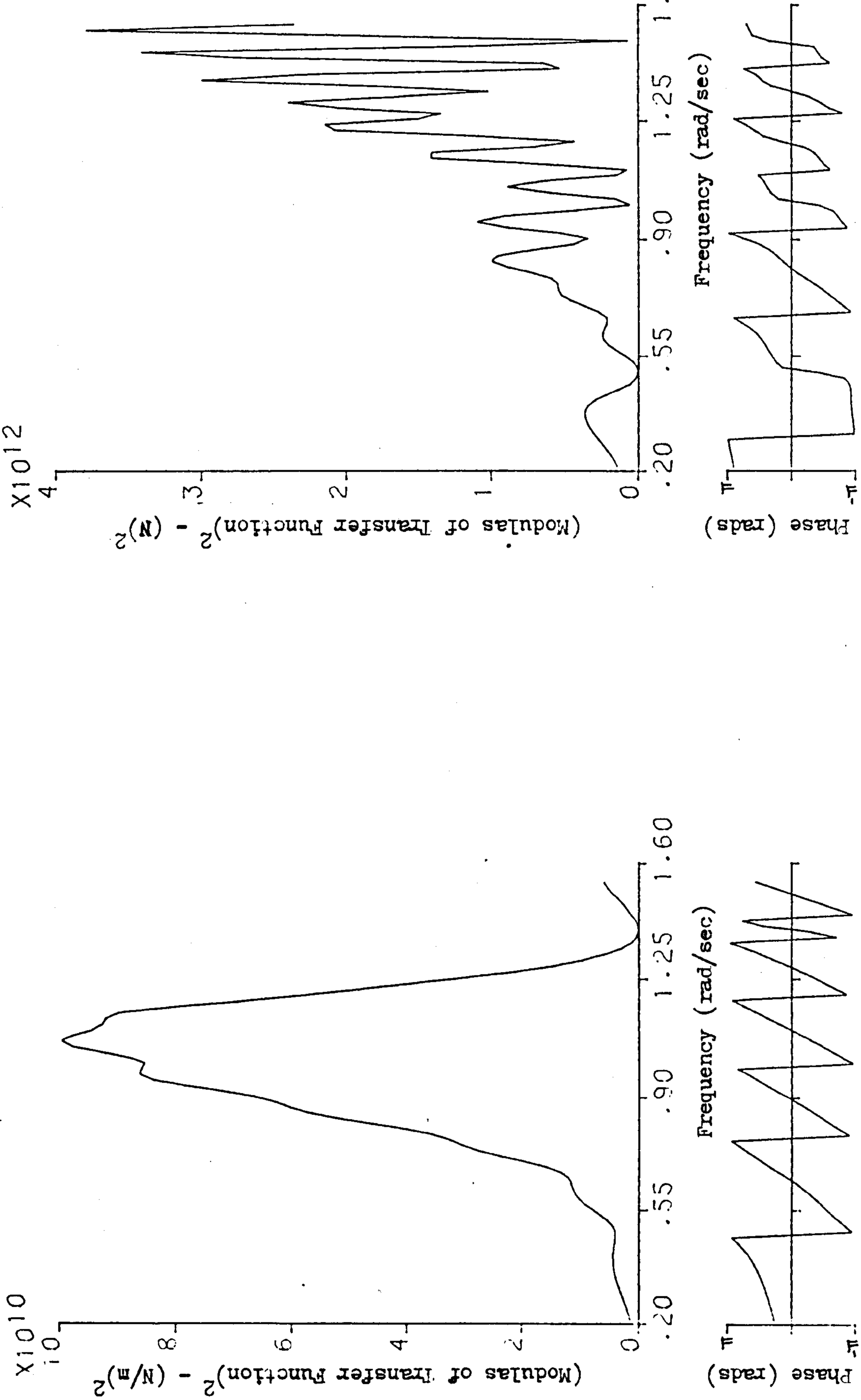

FIG. 9.11 SBS TRANSFER FUNCTIONS - 130,000DWT TANKER AT FULL DRAFT

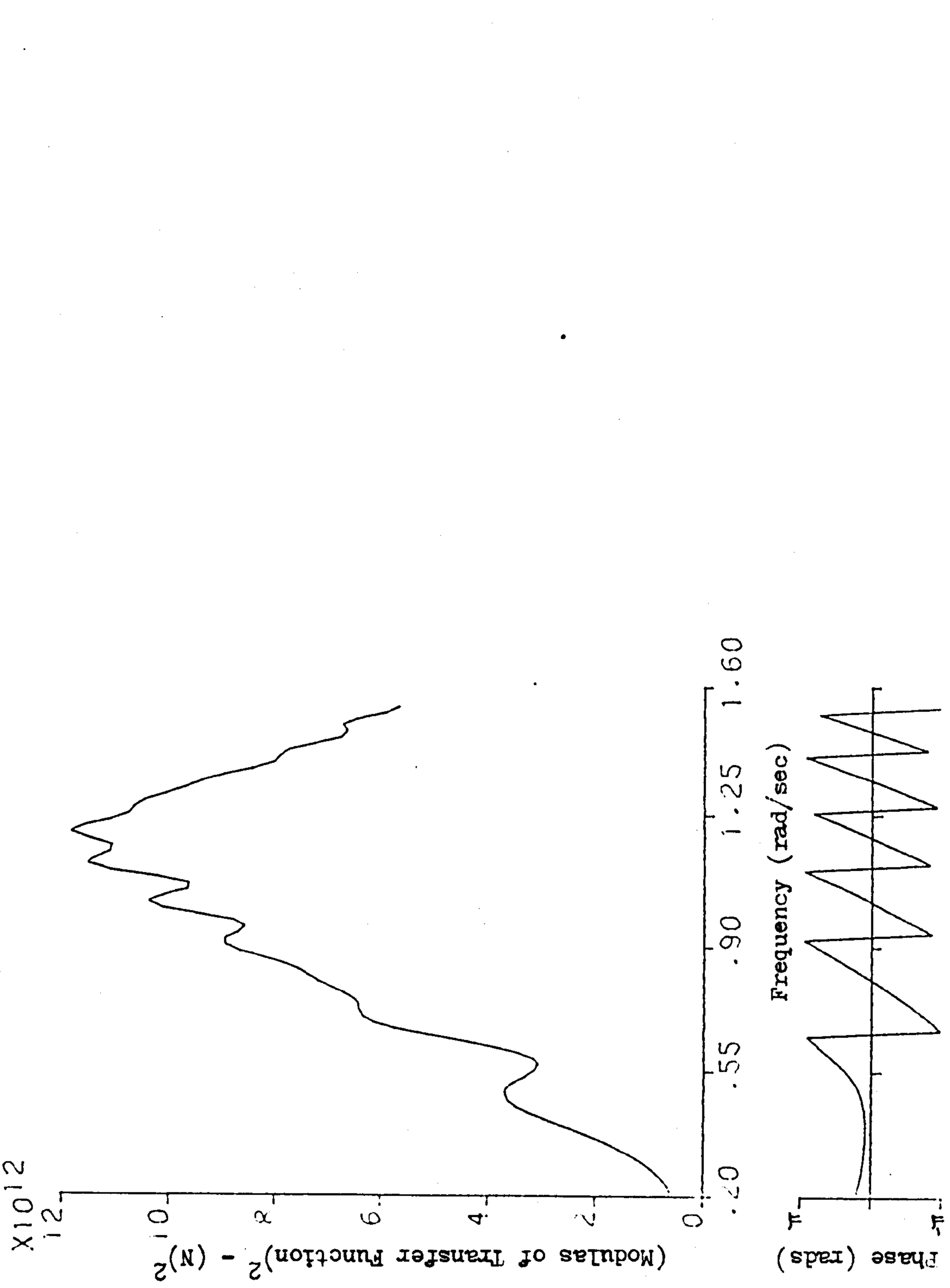

FIG. 9.11 SBS SYSTEM TRANSFER FUNCTIONS - 130,000DWT TANKER AT FULL DRAFT

9.11.17 Buoy Moment M_2

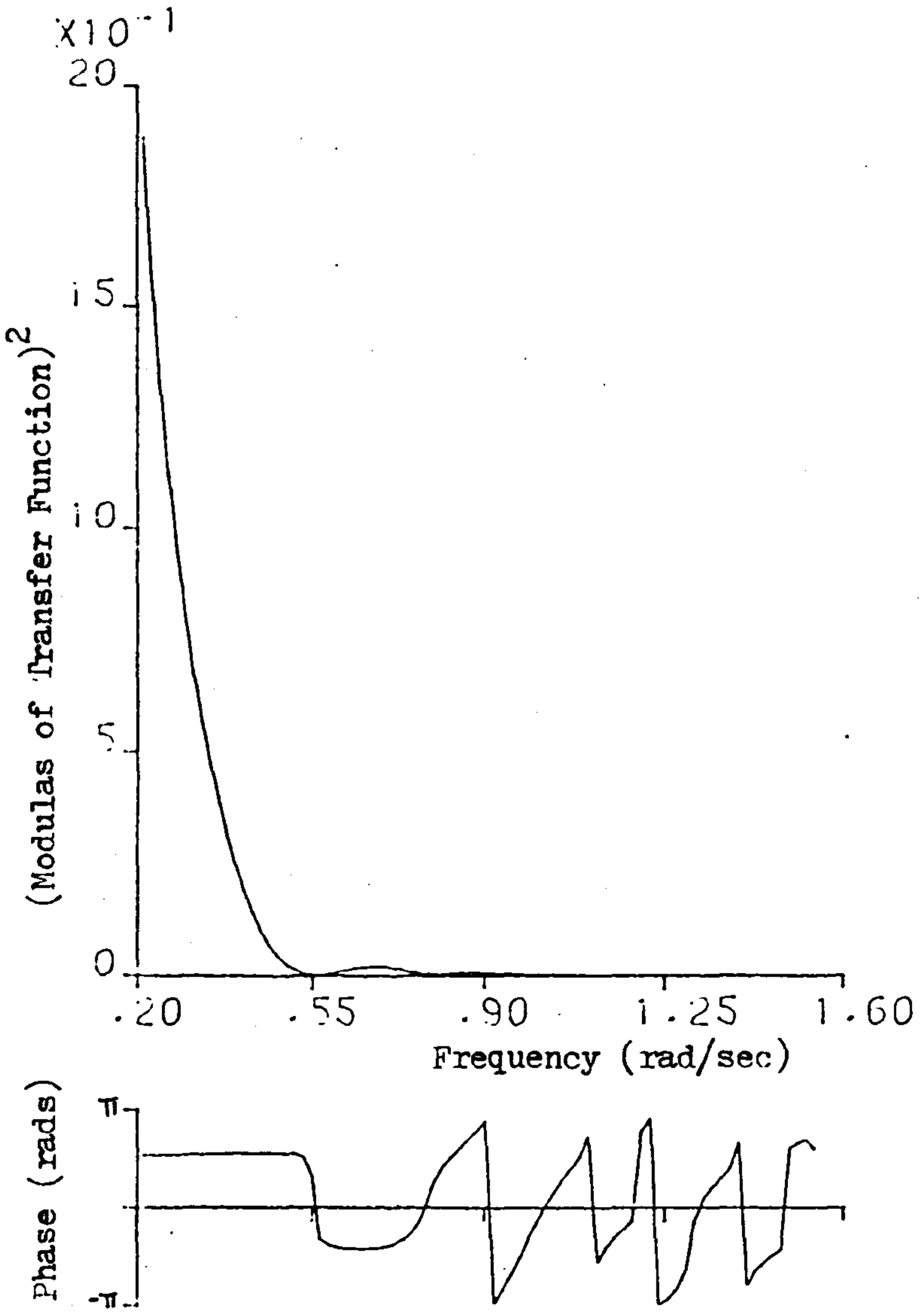

9.12.1 Surge

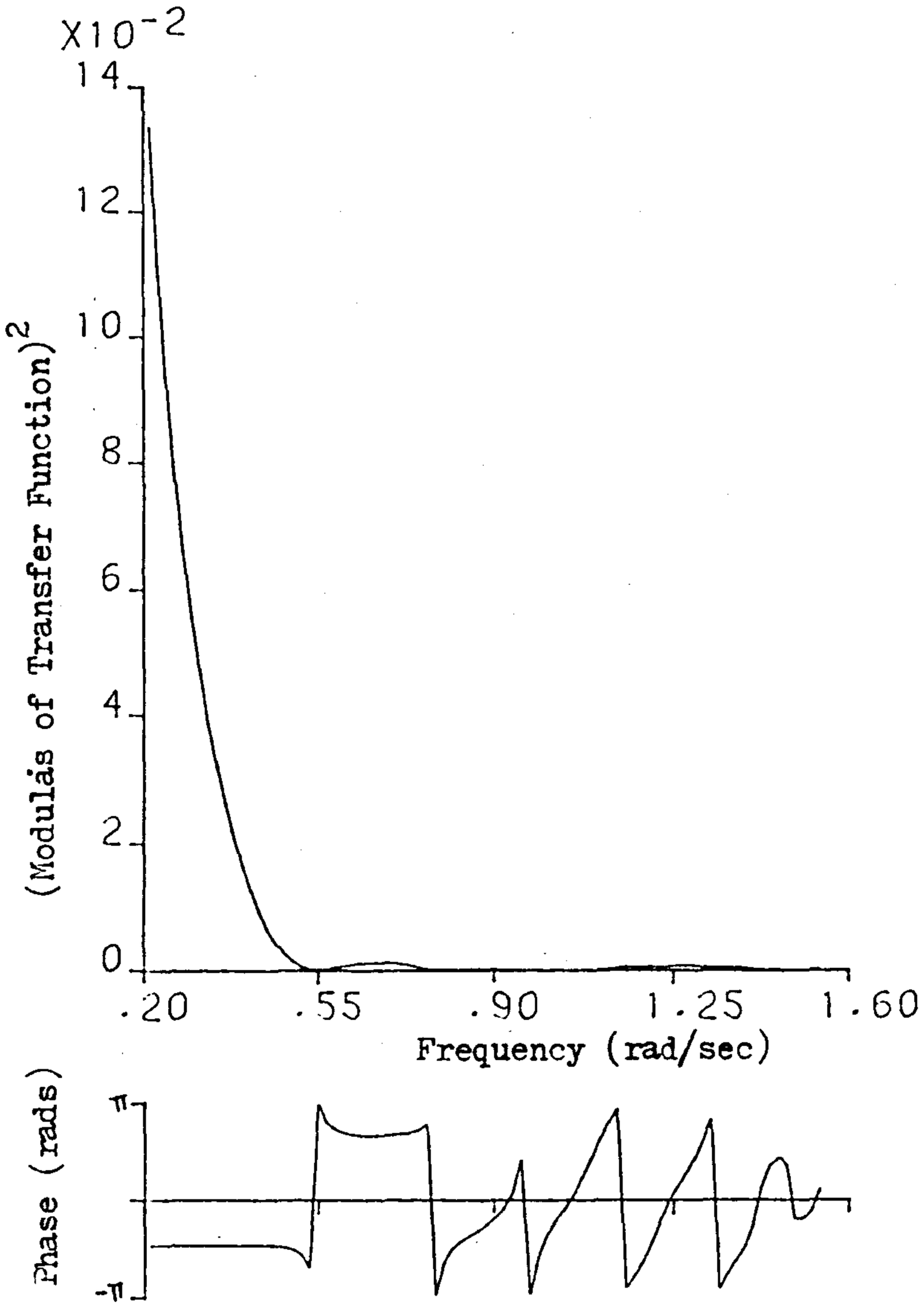

9.12.2 Sway

FIG. 9.12 SBS SYSTEM TRANSFER FUNCTIONS - 130,000DWT TANKER AT HALF DRAFT WITH C.G. MIDSHIPS

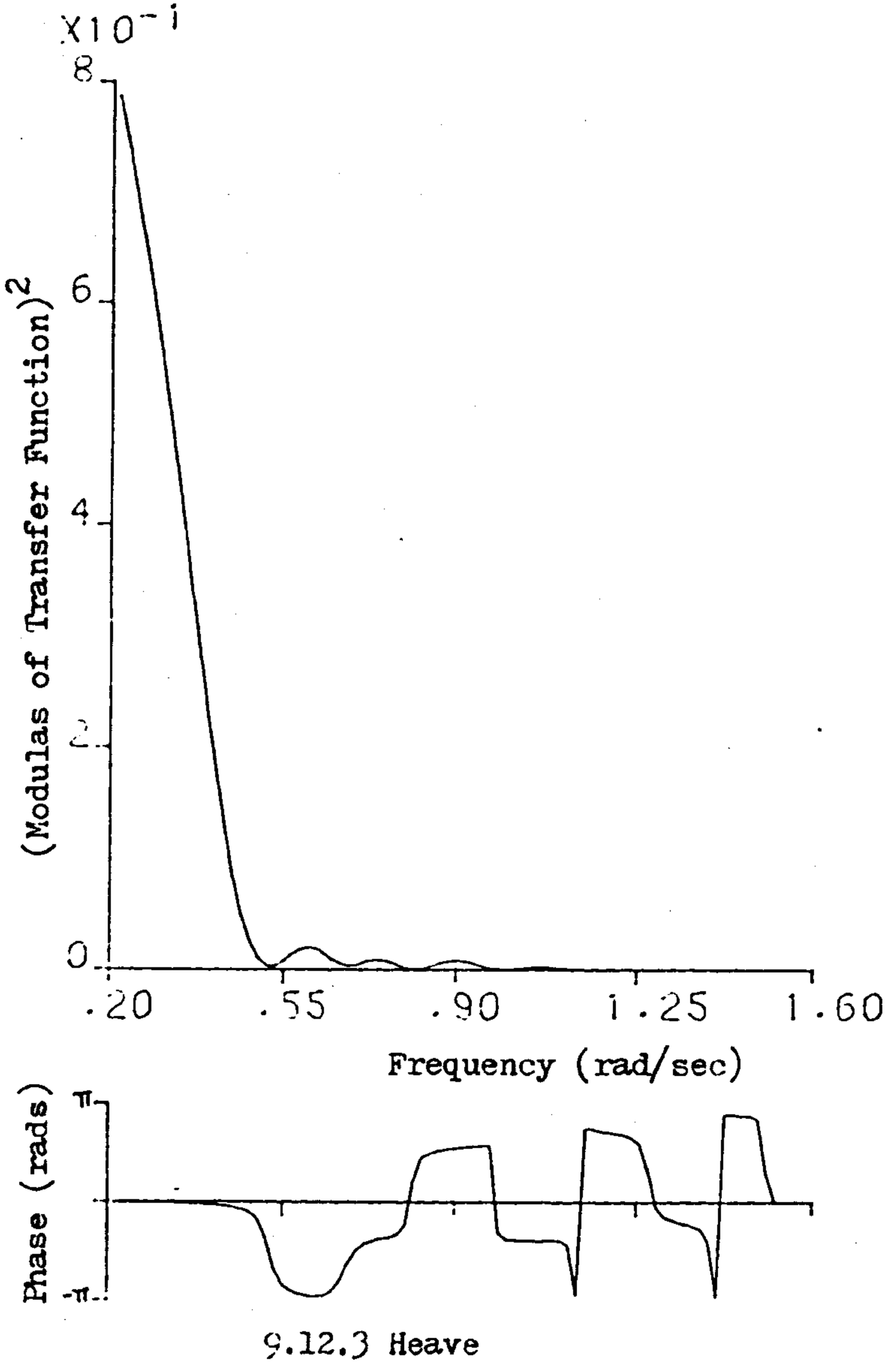

9.12.3 Heave

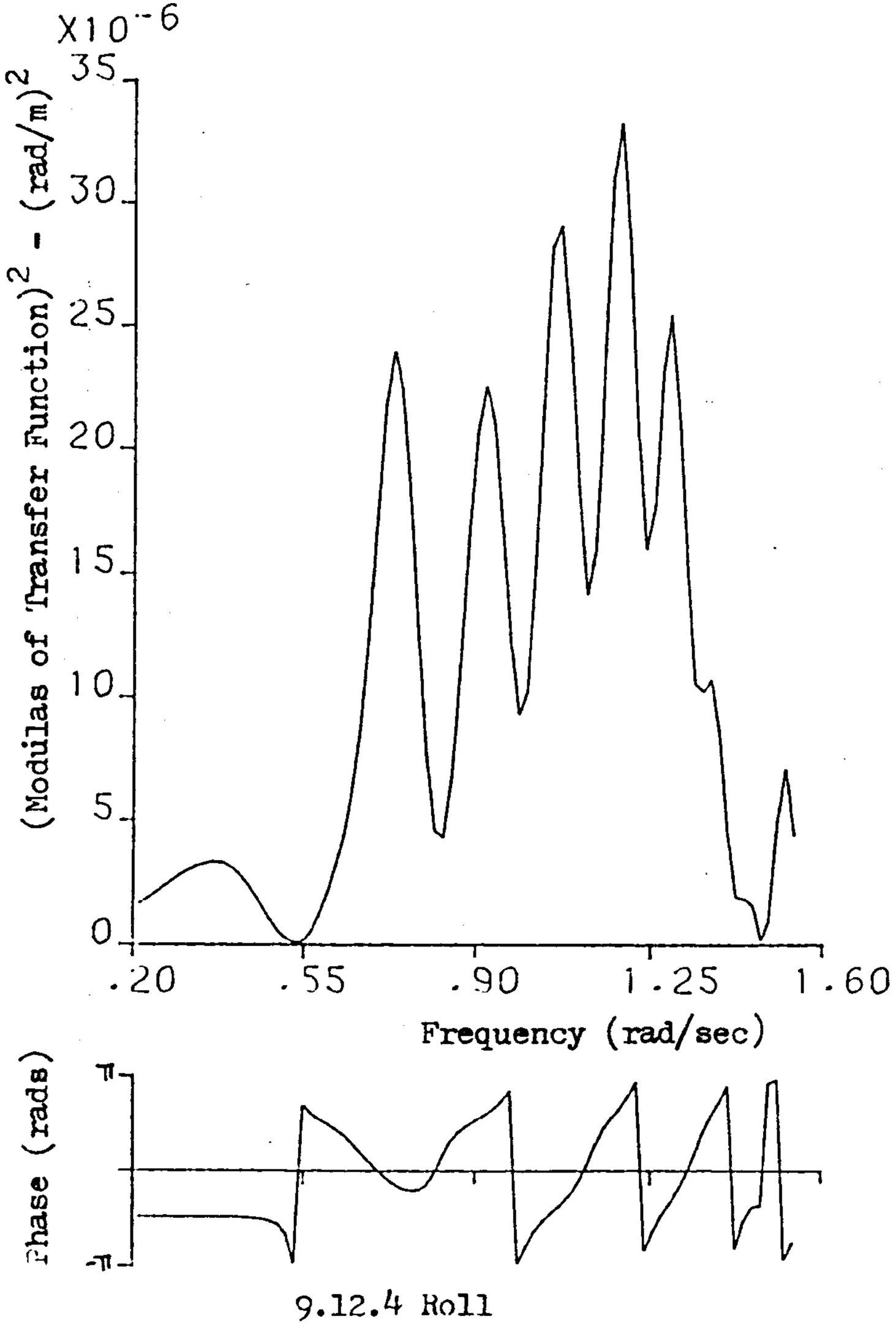

9.12.4 Roll

FIG. 9.12 SBS SYSTEM TRANSFER FUNCTIONS - 130,000DWT TANKER AT HALF DRAFT WITH C.G. MIDSHIPS

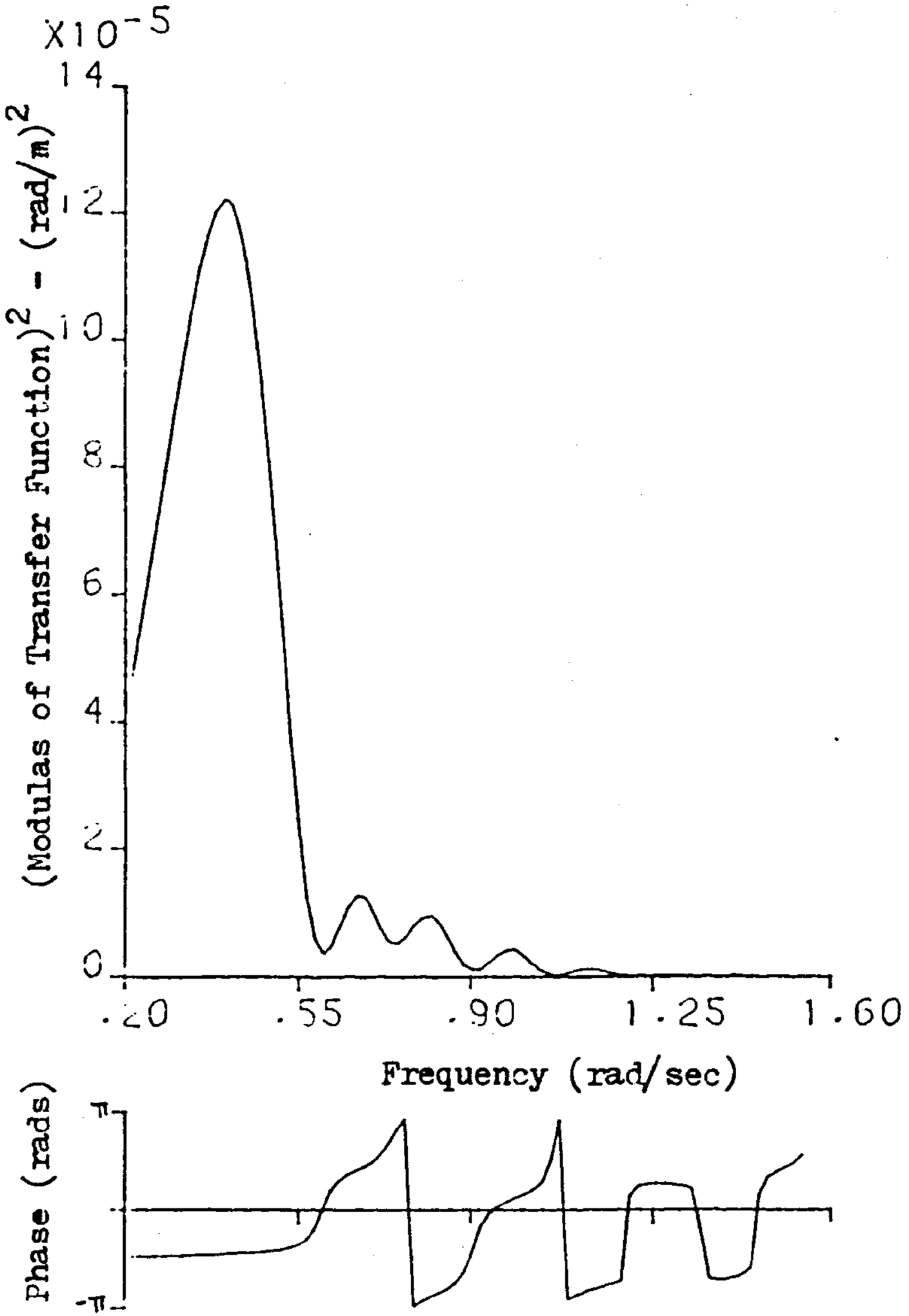

9.12.5 Pitch

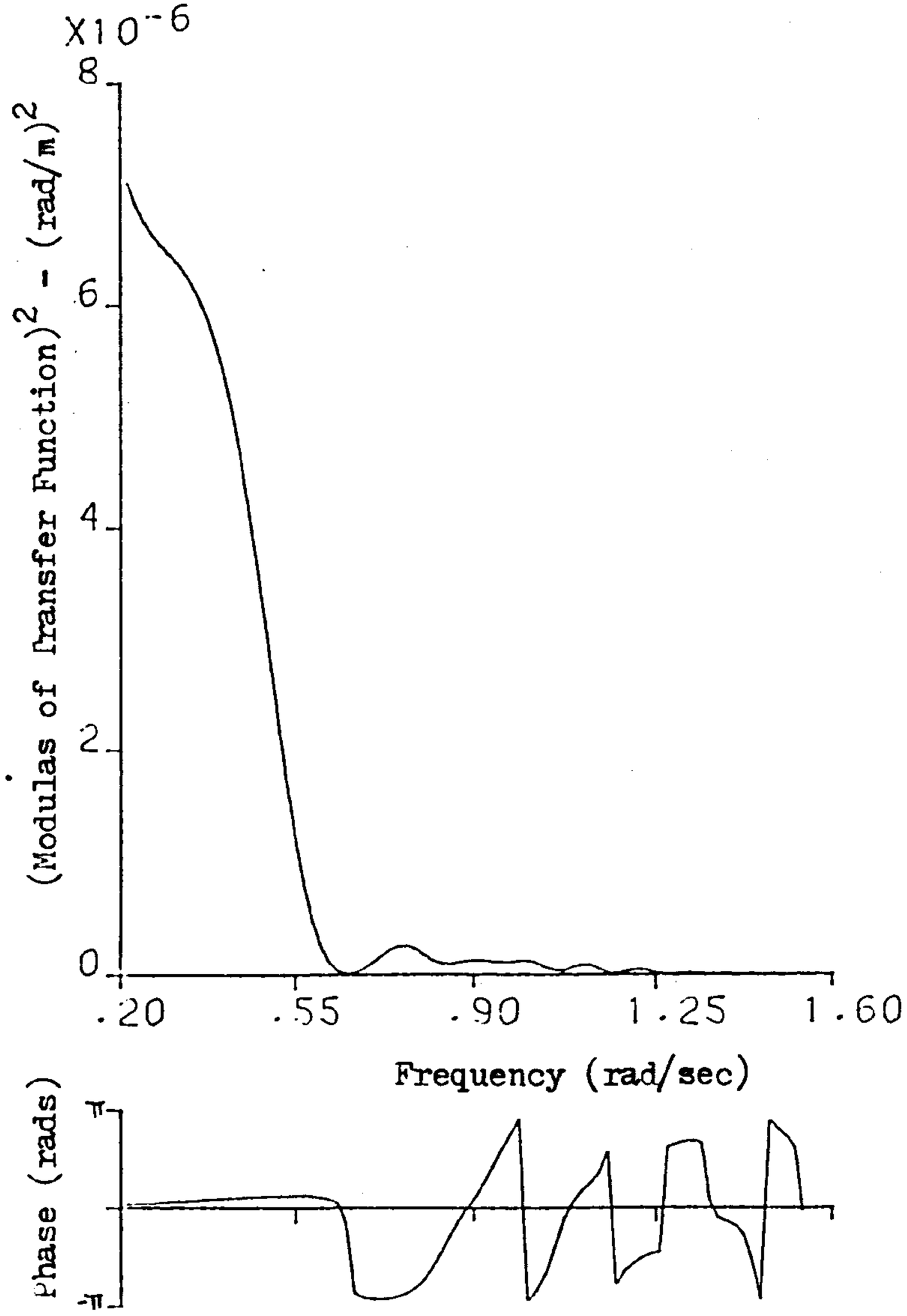

9.12.6 Yaw

FIG. 9.12 SBS SYSTEM TRANSFER FUNCTIONS - 130,000DWT TANKER AT HALF DRAFT WITH C.G. MIDSHIPS

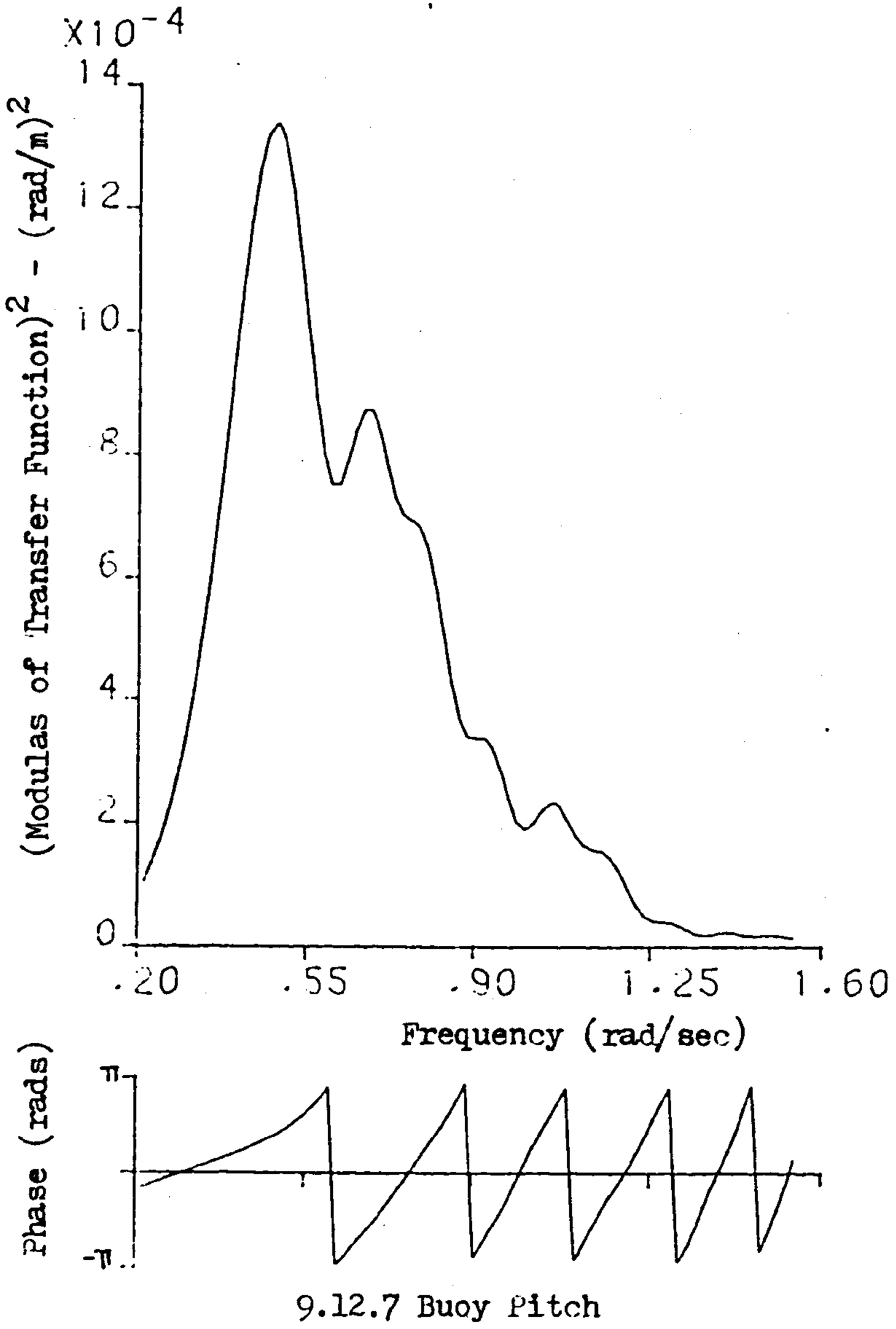

9.12.7 Buoy Pitch

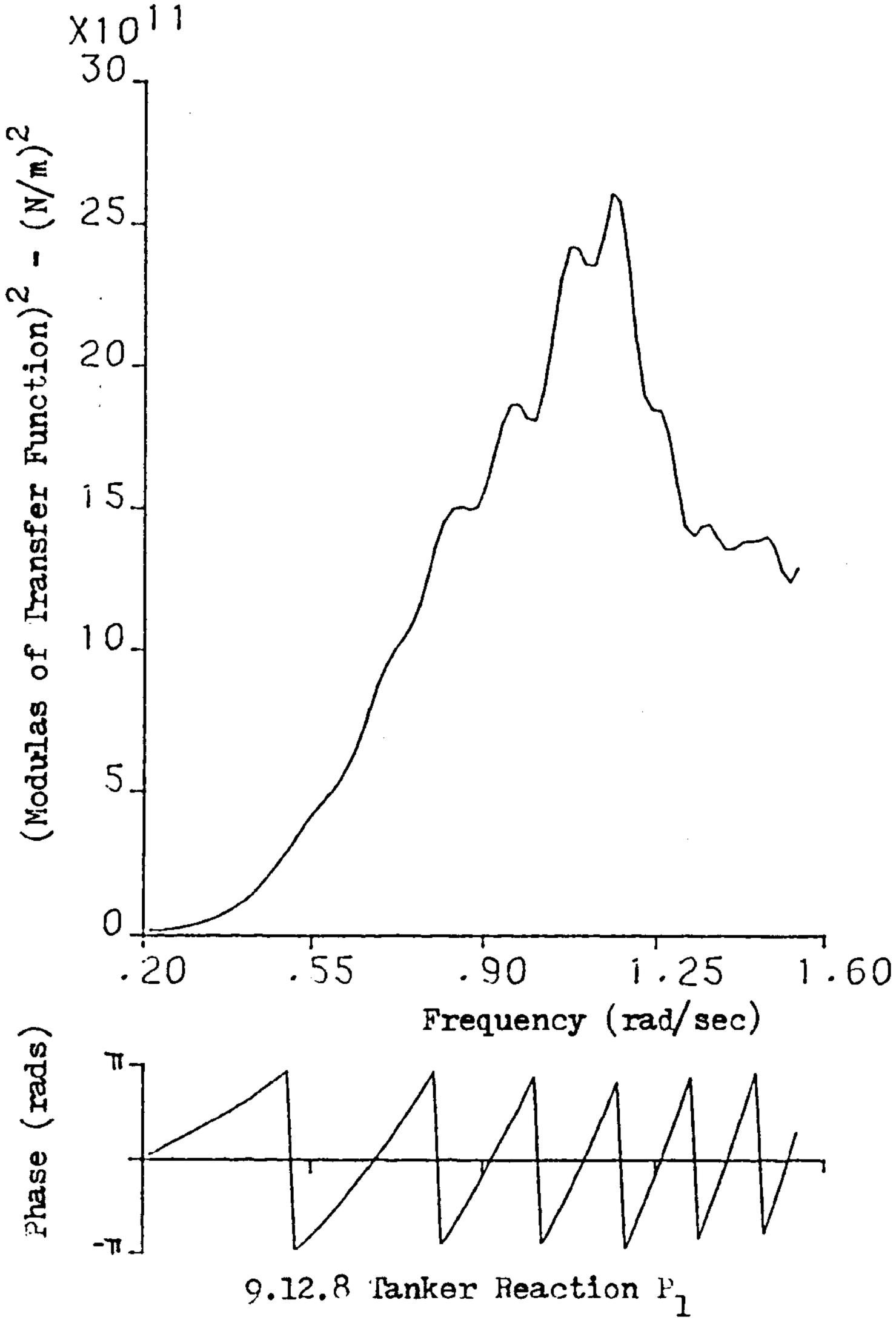

9.12.8 Tanker Reaction F_1

FIG. 9.12 SBS SYSTEM TRANSFER FUNCTIONS - 130,000DWT TANKER AT HALF DRAFT WITH C.G. MIDSHIPS

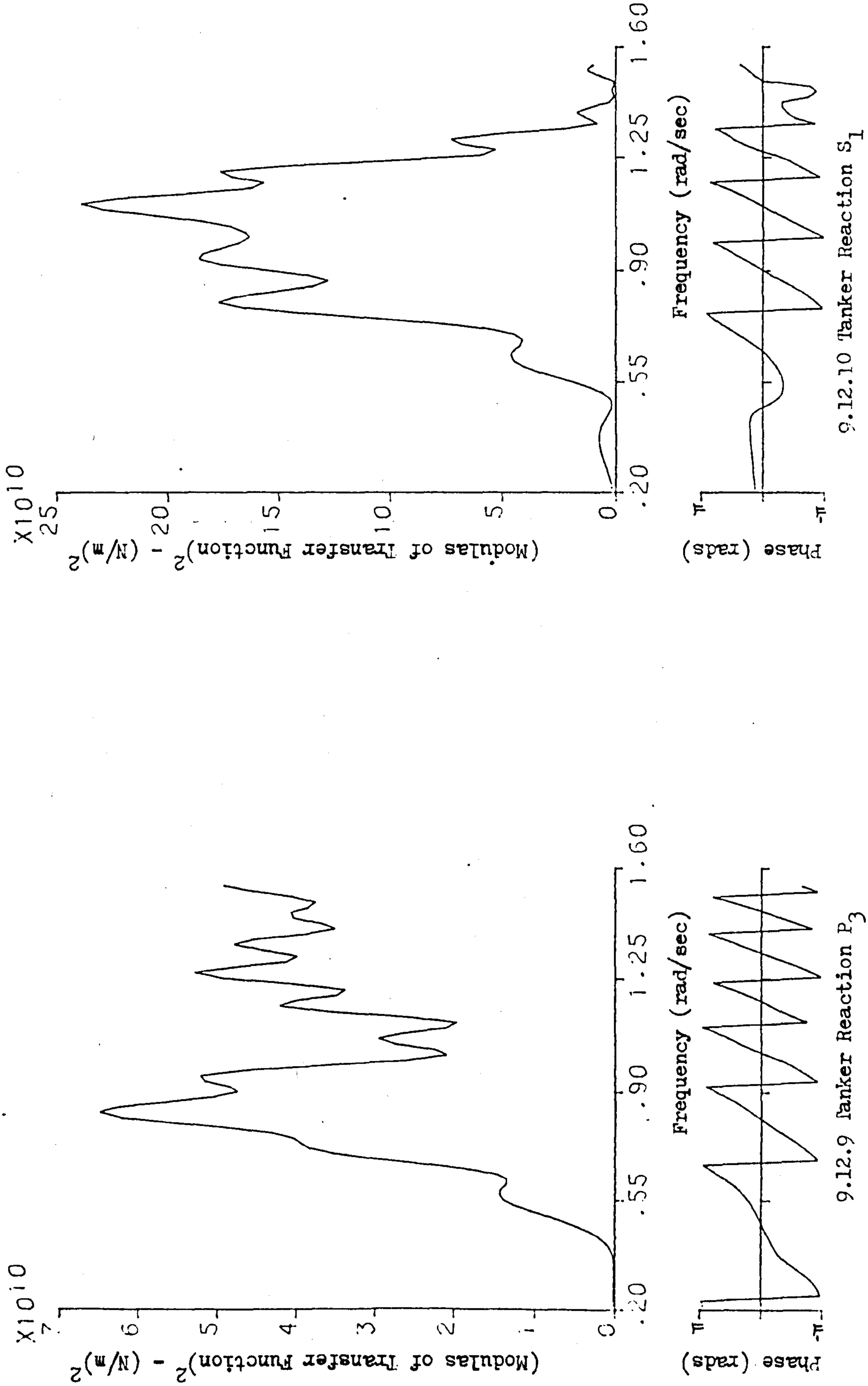

FIG. 9.12 SBS SYSTEM TRANSFER FUNCTIONS - 130,000DWT TANKER AT HALF DRAFT WITH C.G. MIDSHIPS

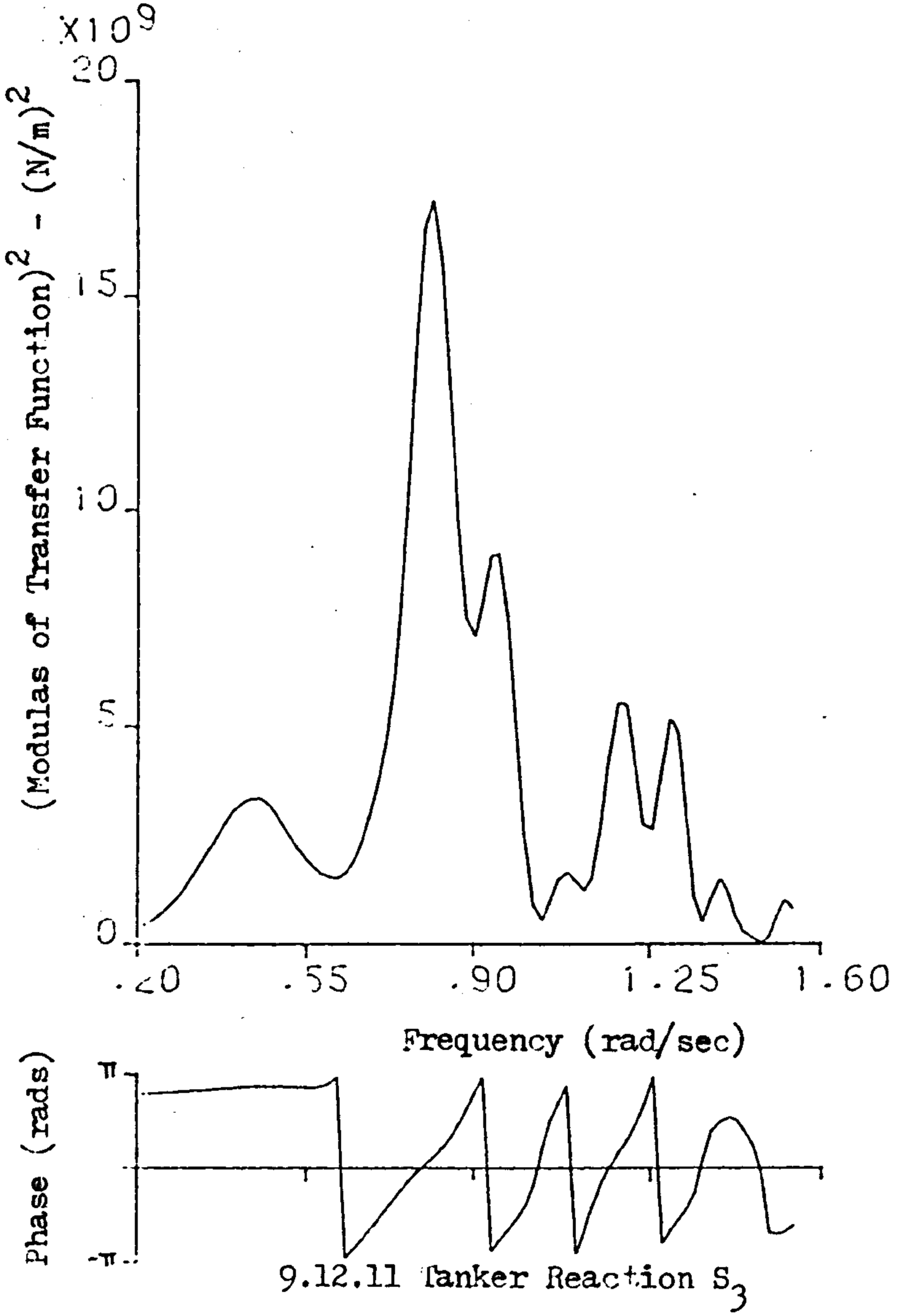

9.12.11 Tanker Reaction S_3

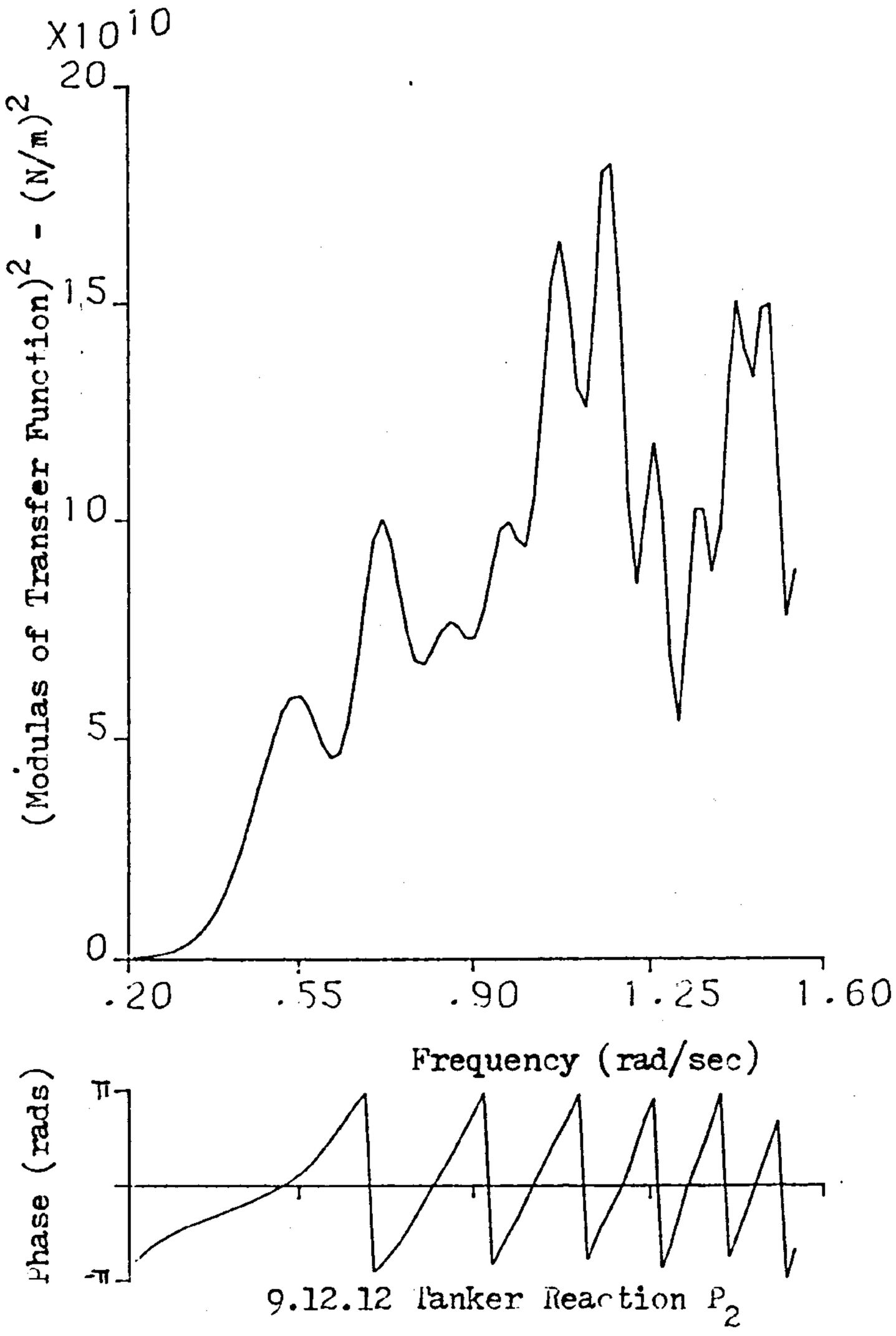

9.12.12 Tanker Reaction P_2

FIG. 9.12 SBS SYSTEM TRANSFER FUNCTIONS - 130,000DWT TANKER AT HALF DRAFT WITH C.G. MIDSHIPS

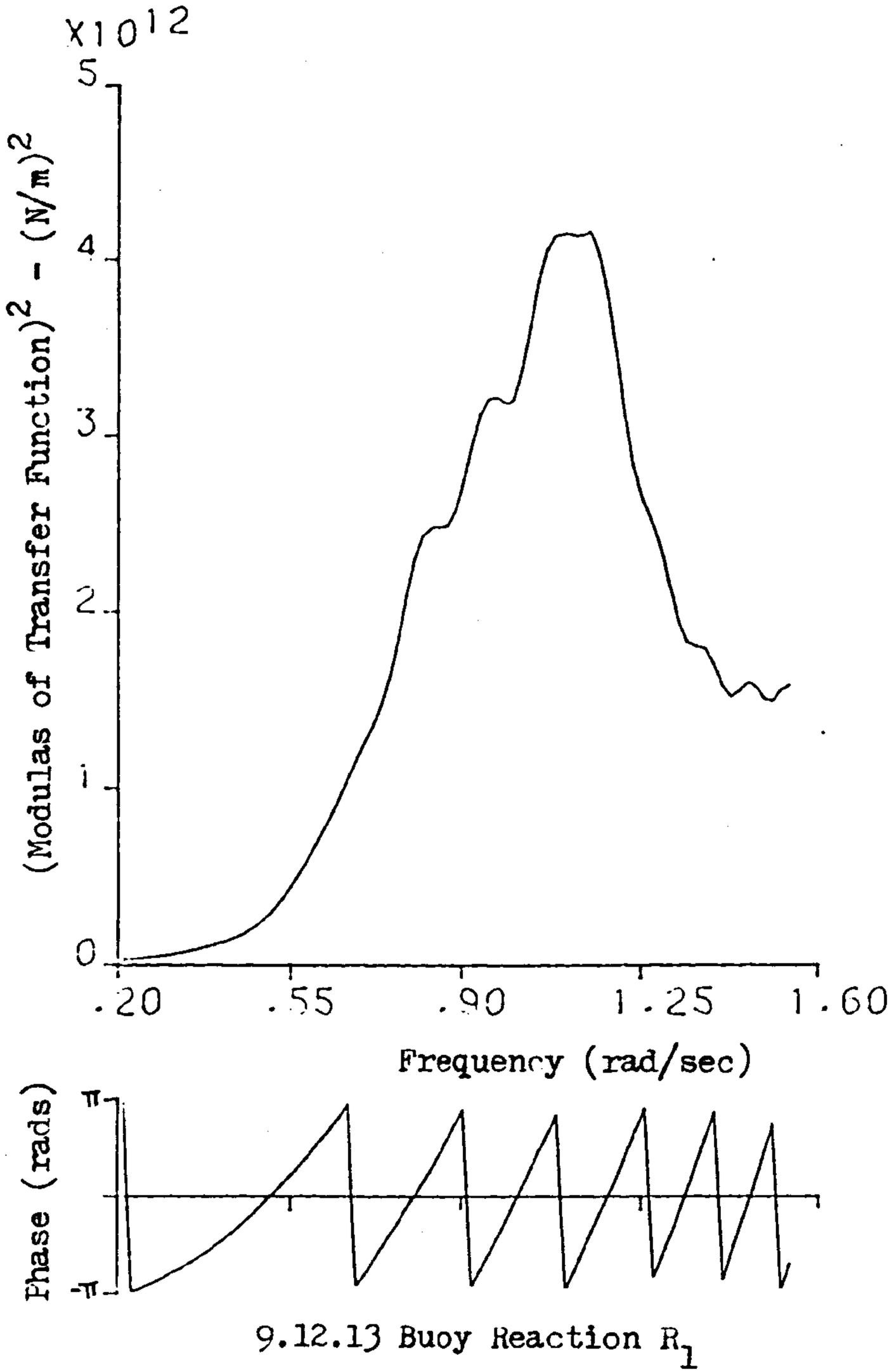

9.12.13 Buoy Reaction R_1

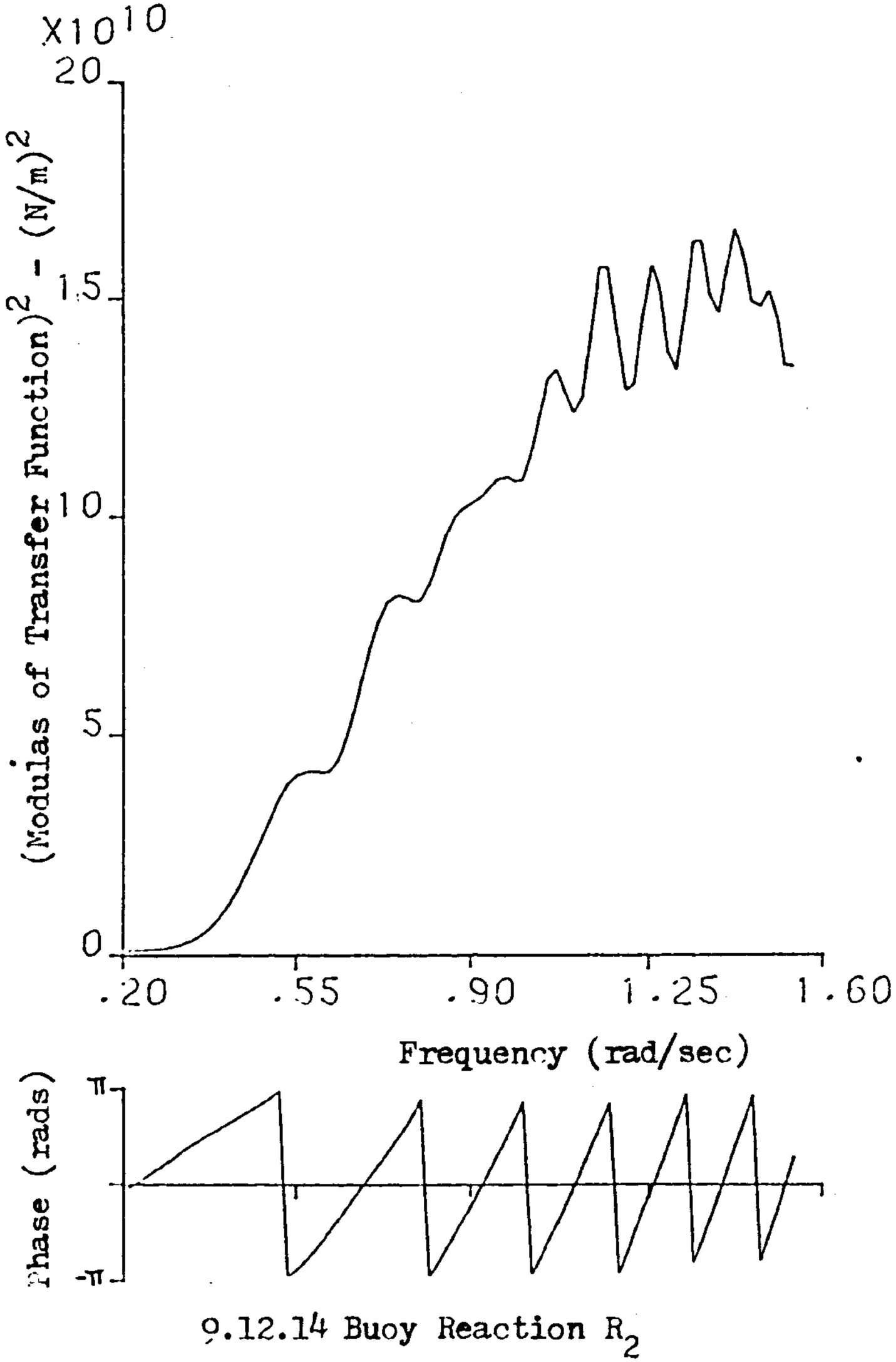

9.12.14 Buoy Reaction R_2

FIG. 9.12 SBS SYSTEM TRANSFER FUNCTIONS - 130,000DWT TANKER AT HALF DRAFT WITH C.G. MIDSHIPS

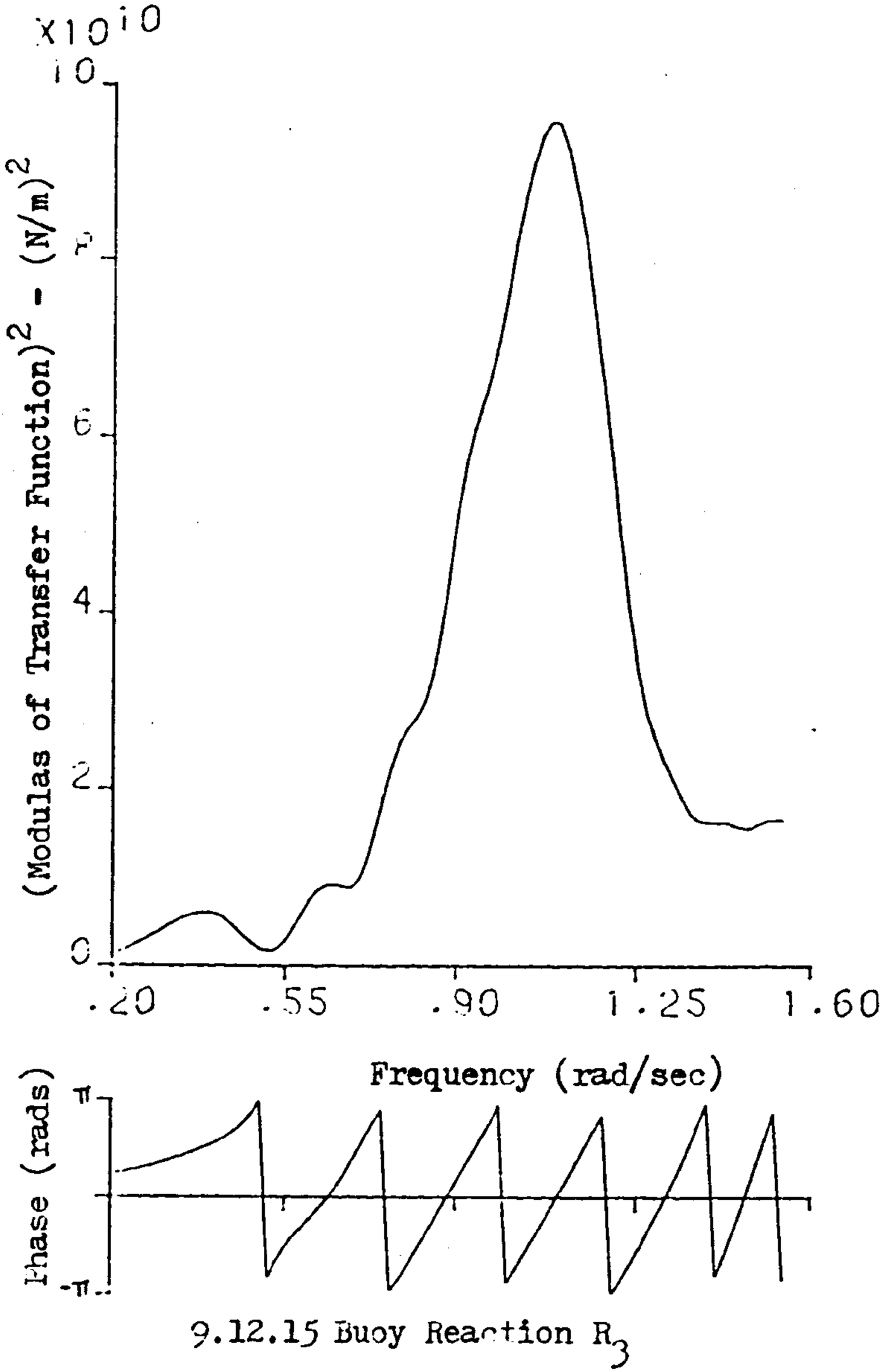

9.12.15 Buoy Reaction R_3

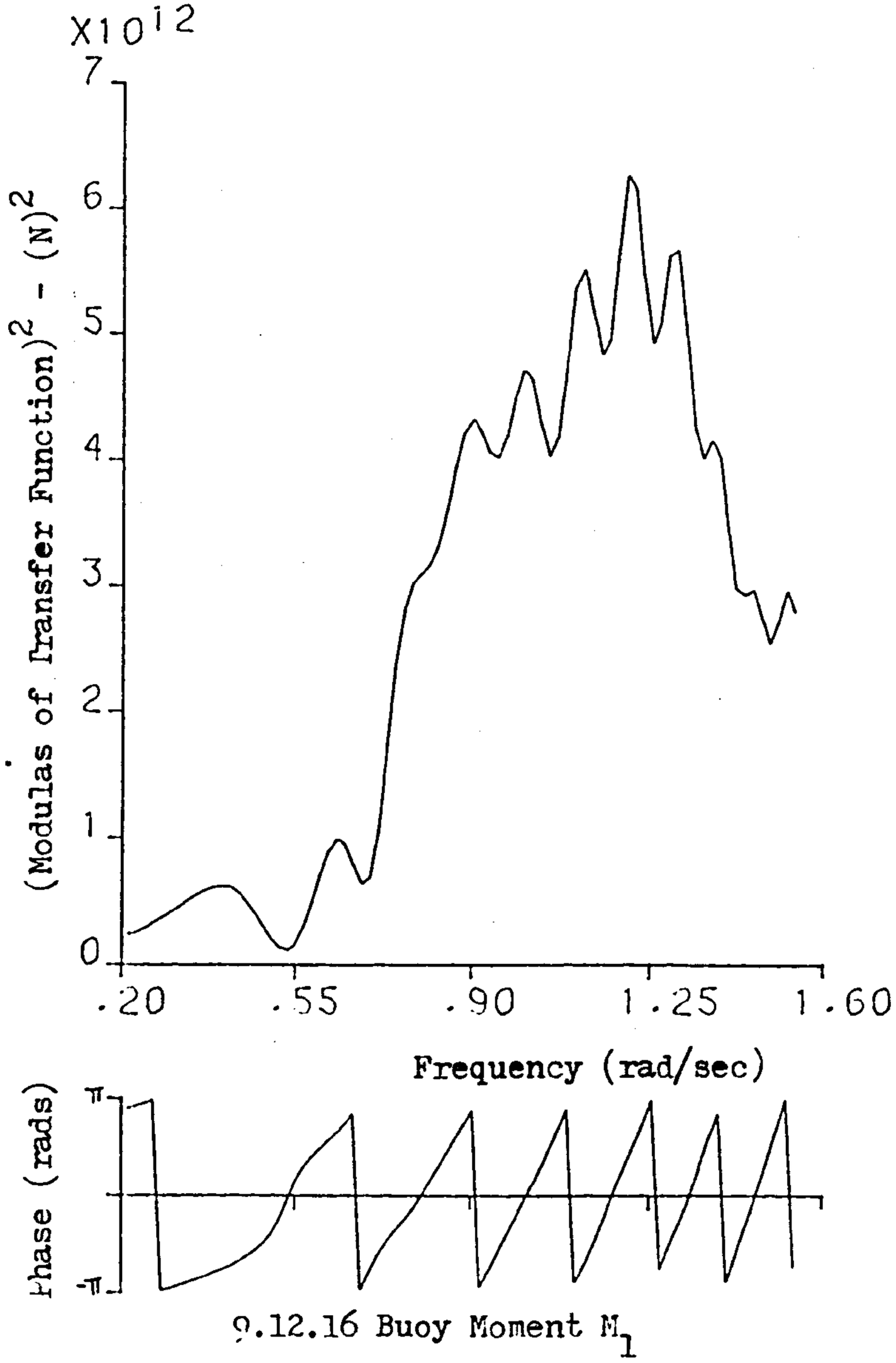

9.12.16 Buoy Moment M_1

FIG. 9.12 SBS SYSTEM TRANSFER FUNCTIONS - 130,000DWT TANKER AT HALF DRAFT WITH C.G. MIDSHIPS

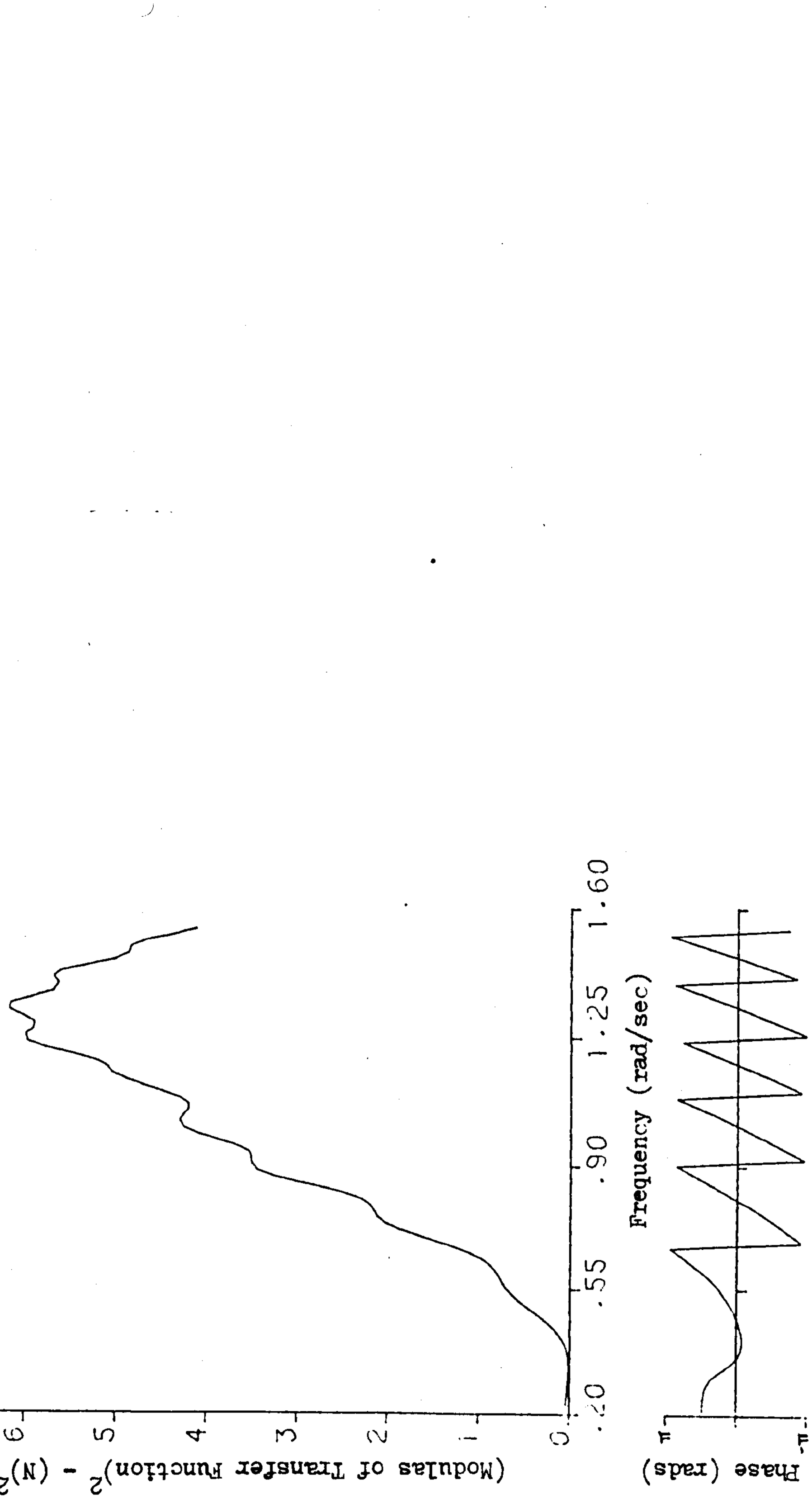

9.12.17 Buoy Moment M_2

FIG. 9.12 SBS SYSTEM TRANSFER FUNCTIONS - 130,000 DWT TANKER AT HALF DRAFT WITH C.G. MIDSHIPS

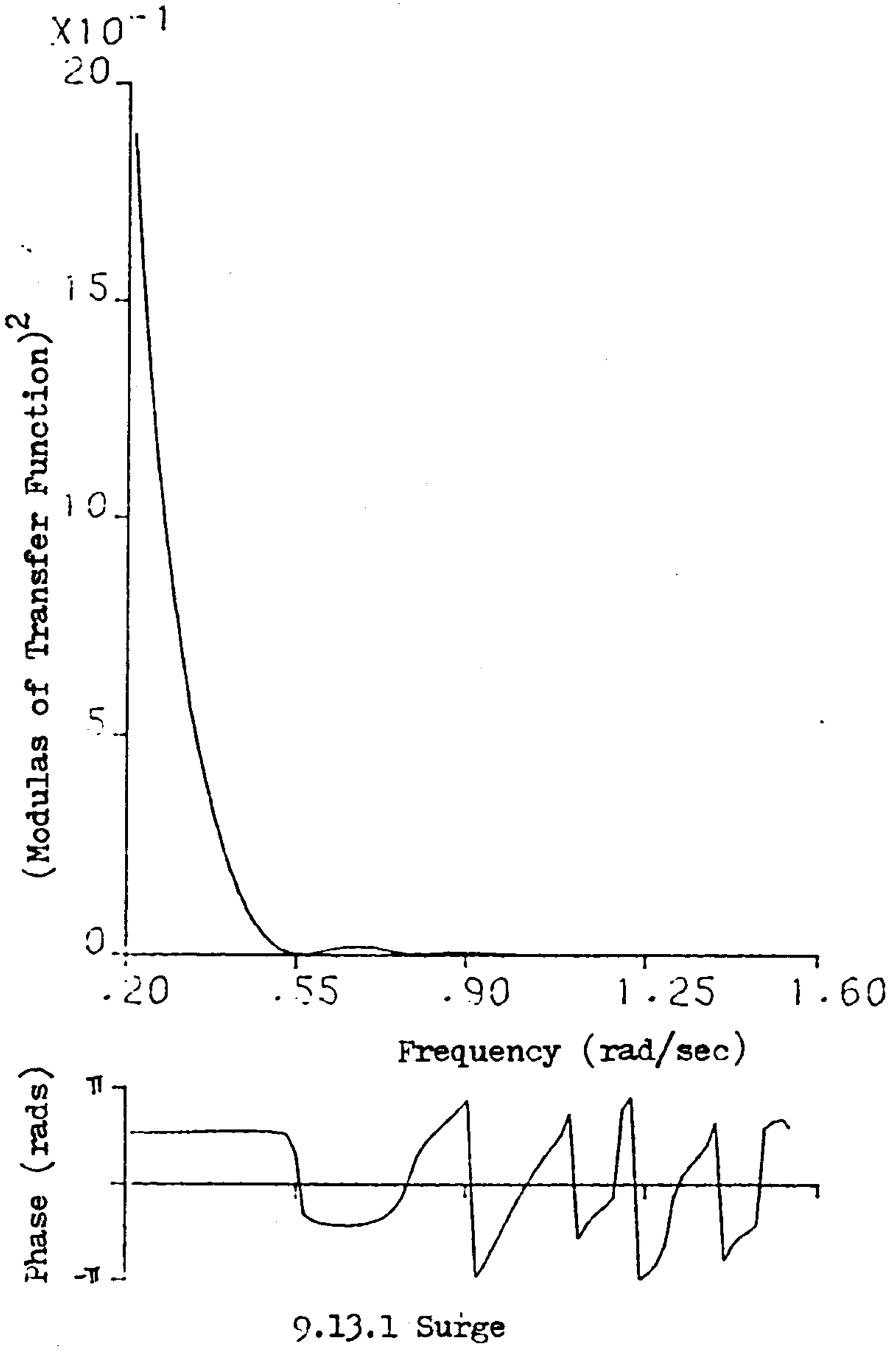

9.13.1 Surge

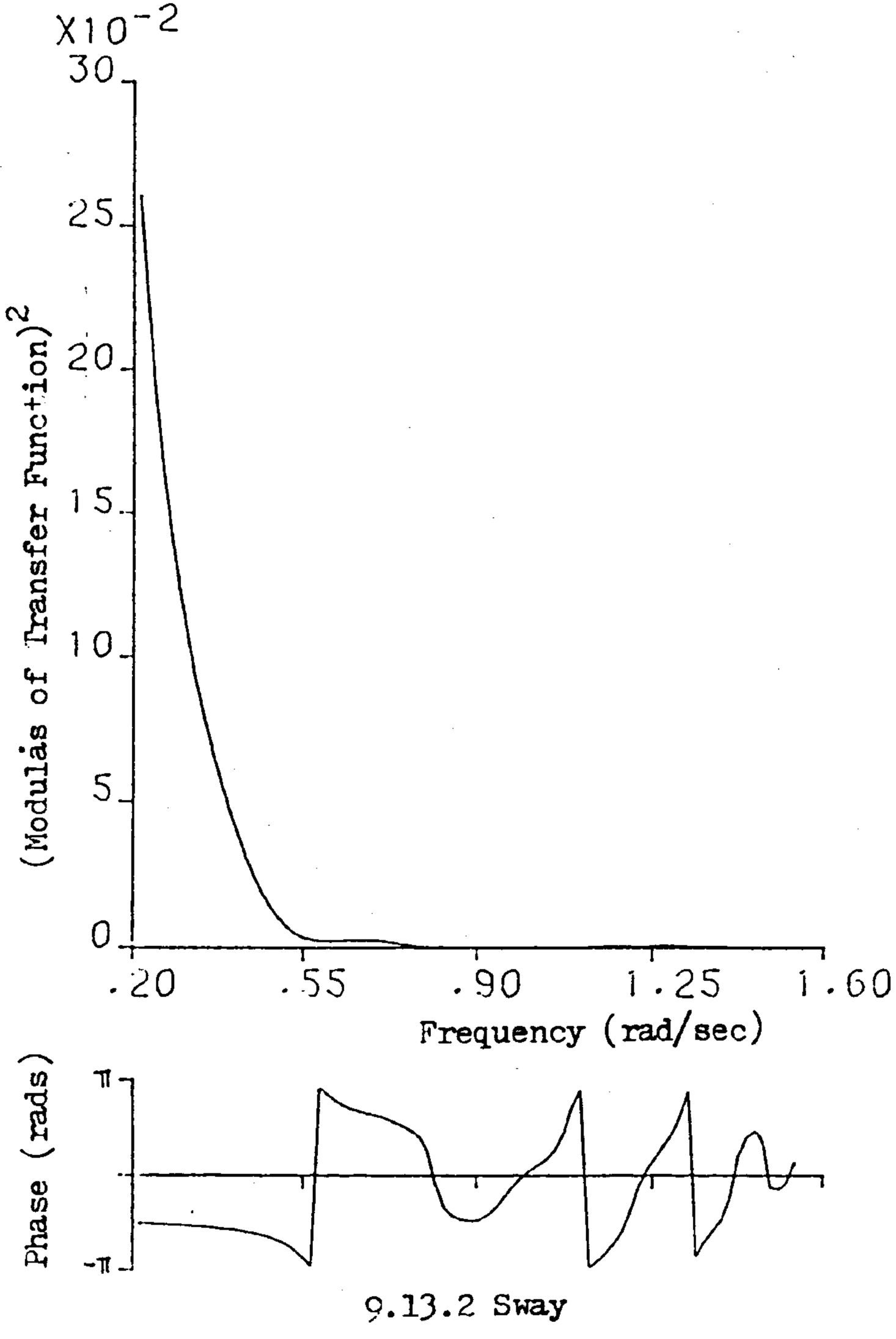

9.13.2 Sway

FIG. 9.13 SBS SYSTEM TRANSFER FUNCTIONS - 130,000DWT TANKER AT HALF DRAFT WITH C.G. 60M FORE OF MIDSHIPS

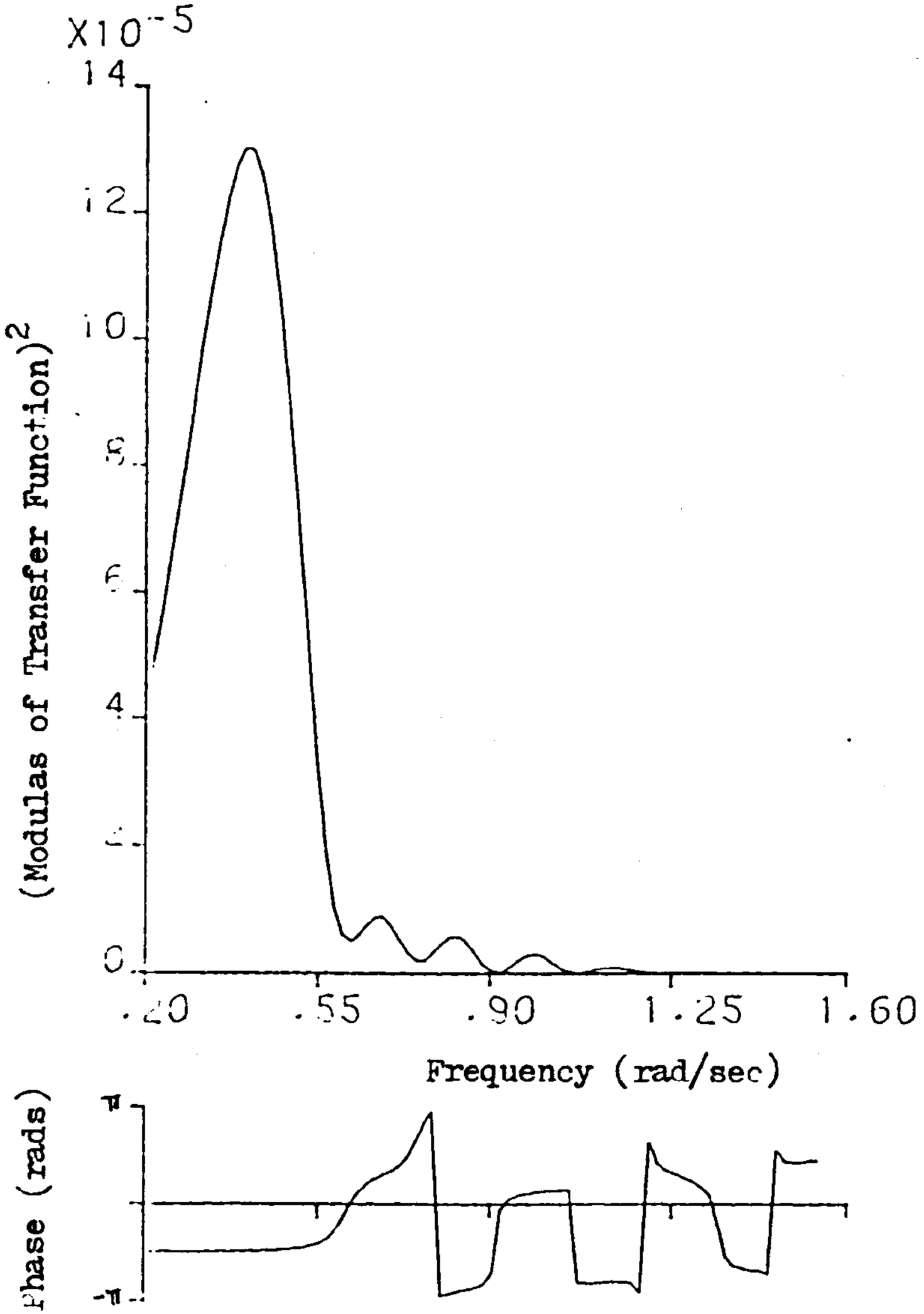

9.13.3 Heave

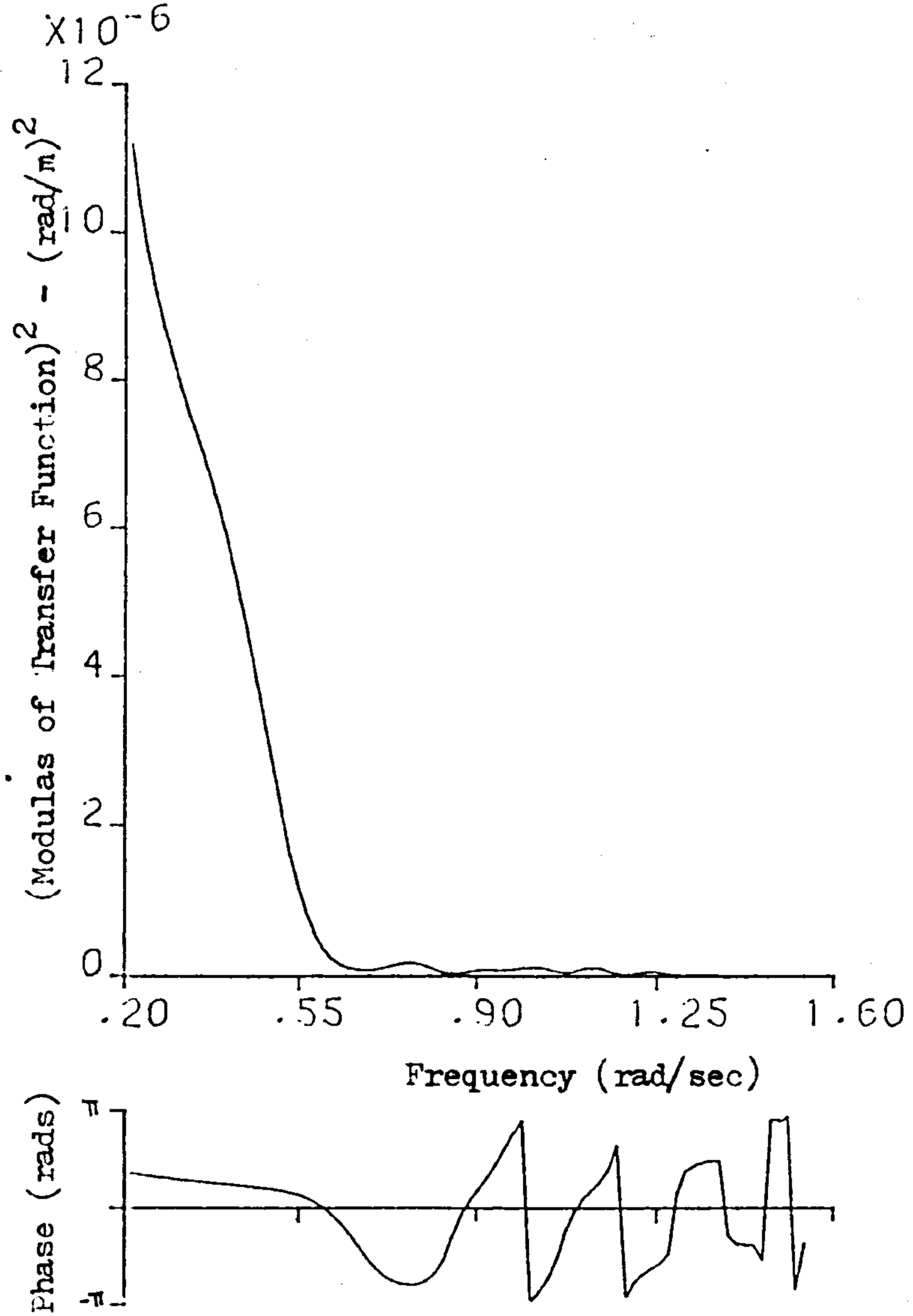

9.13.4 Roll

FIG. 9.13 SBS SYSTEM TRANSFER FUNCTIONS - 130,000DWT TANKER AT HALF DRAFT WITH C.G. 60M FORE OF MIDSHIPS

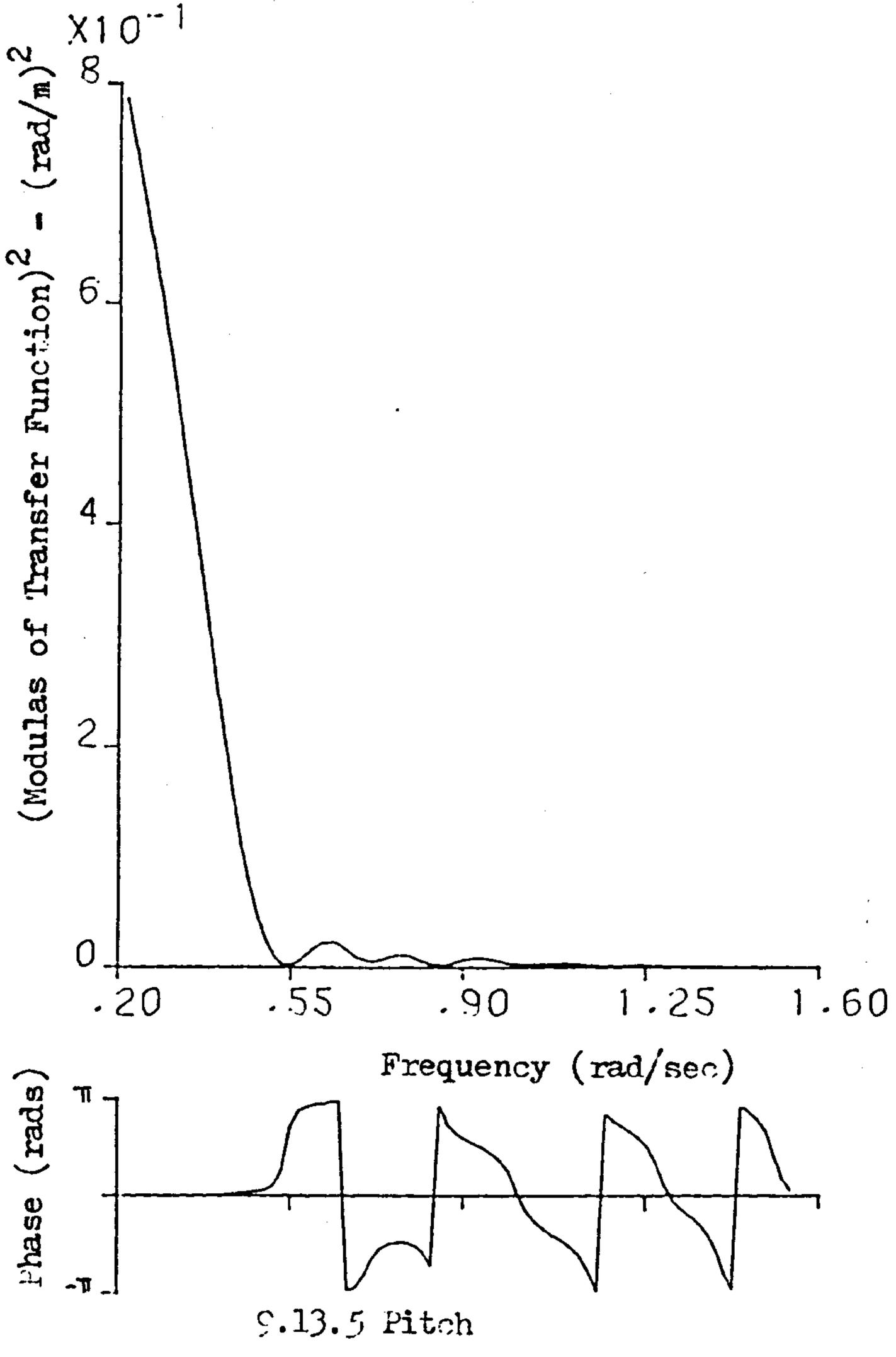

9.13.5 Pitch

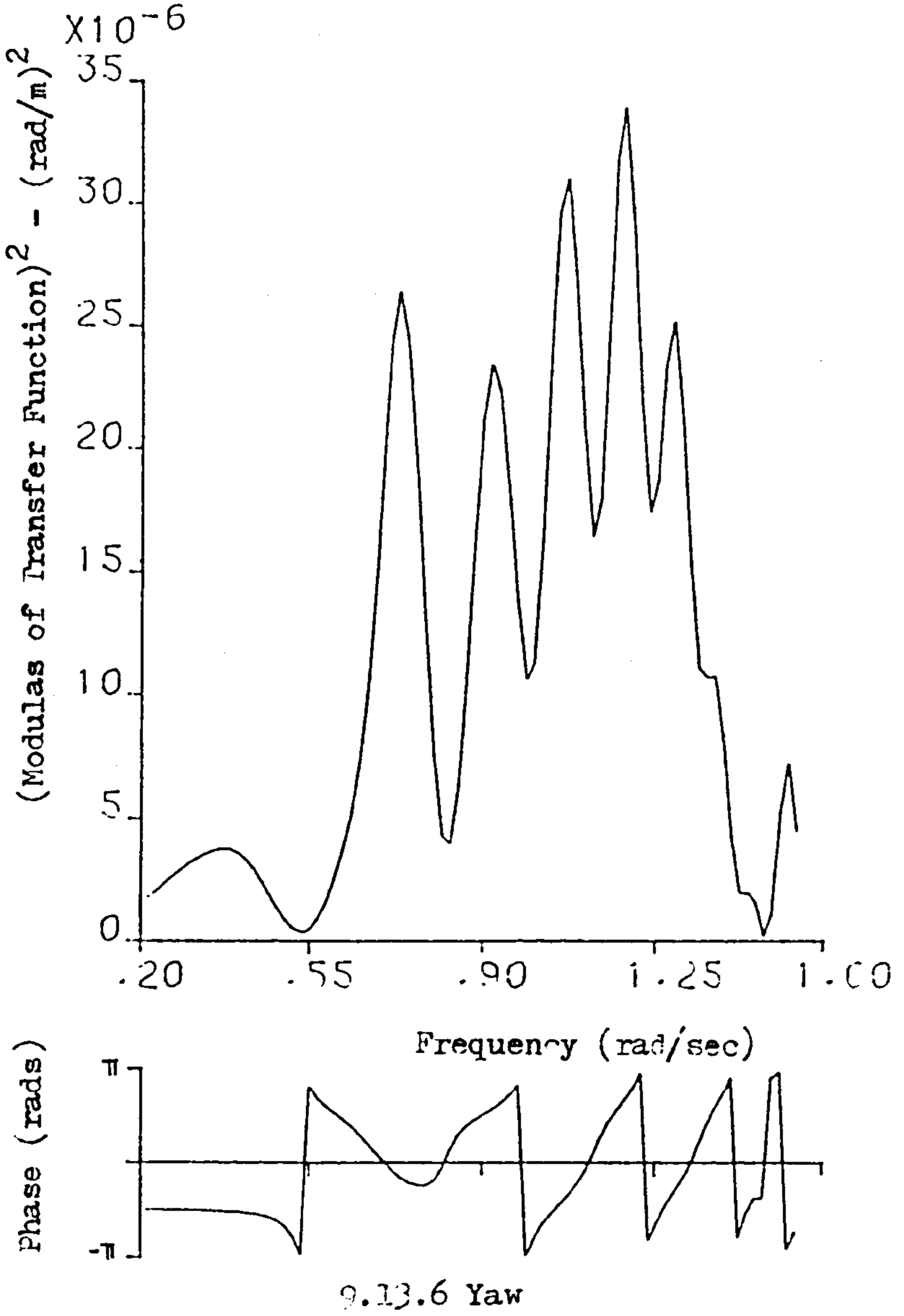

9.13.6 Yaw

FIG. 9.13 SBS SYSTEM TRANSFER FUNCTIONS - 130,000DWT TANKER AT HALF DRAFT WITH C.G. 60M FORE OF MIDSHIPS

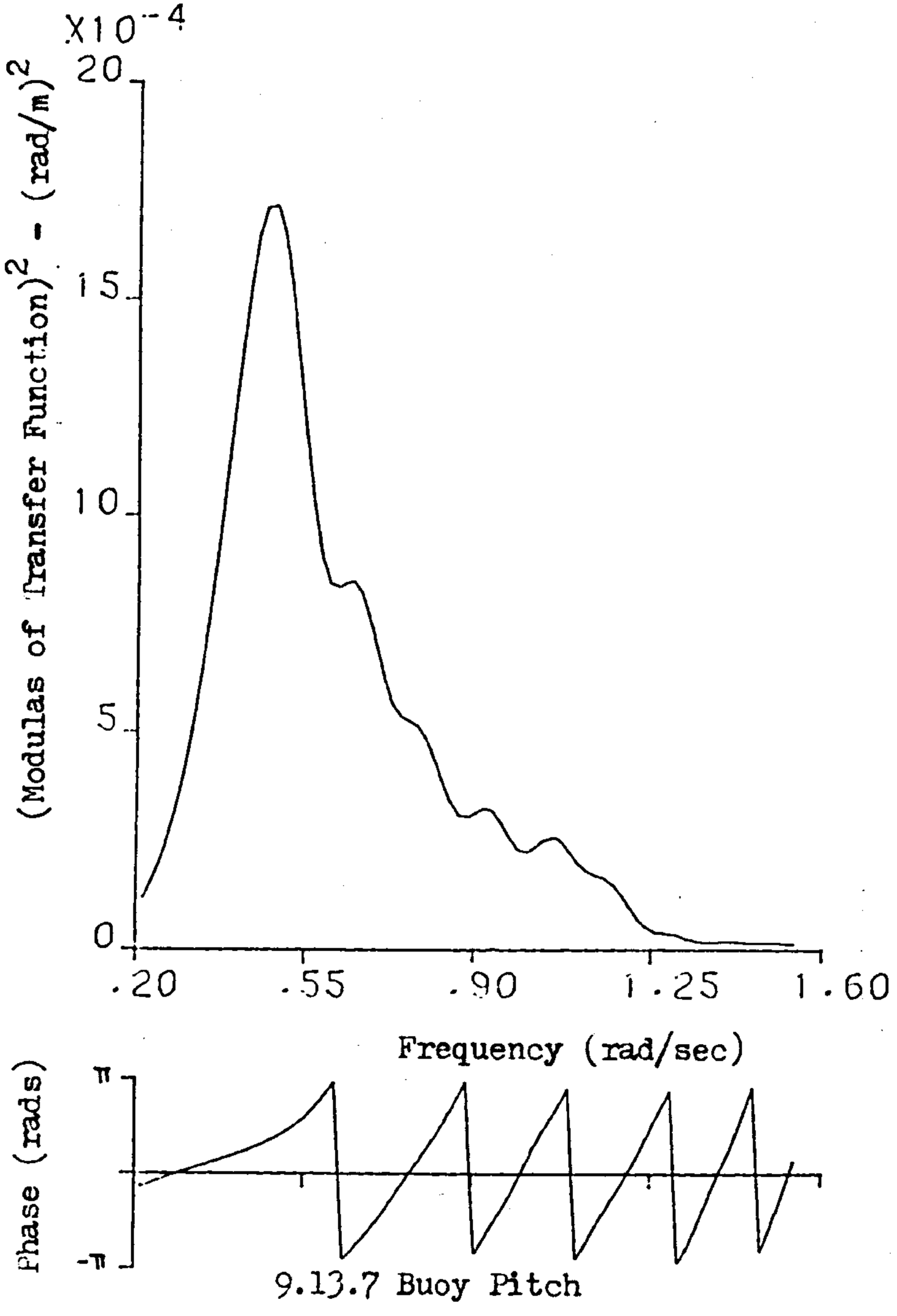

9.13.7 Buoy Pitch

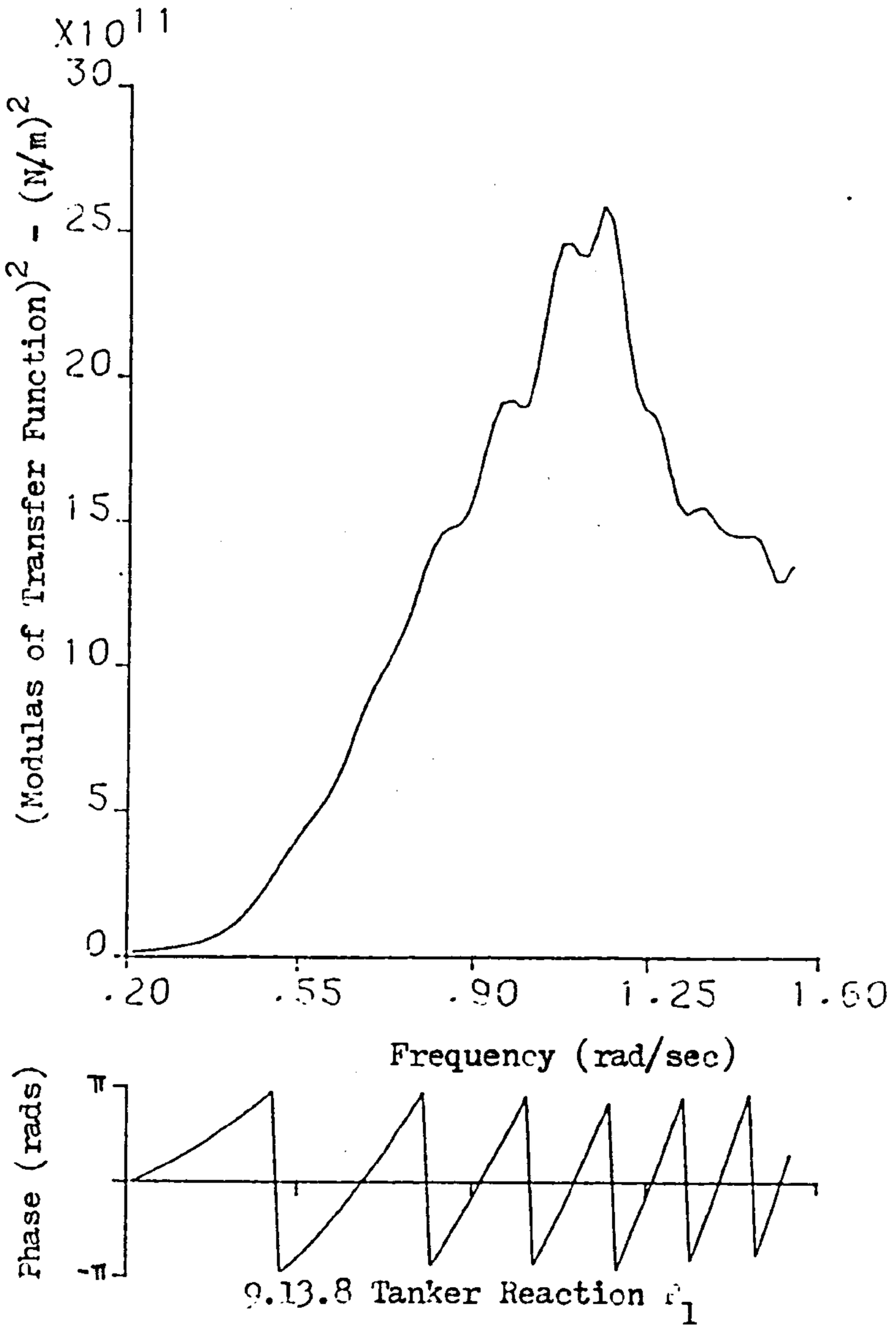

9.13.8 Tanker Reaction F_1

FIG. 9.13 SBS SYSTEM TRANSFER FUNCTIONS - 130,000DWT TANKER AT HALF DRAFT WITH C.G. 60M FORE OF MIDSHIPS

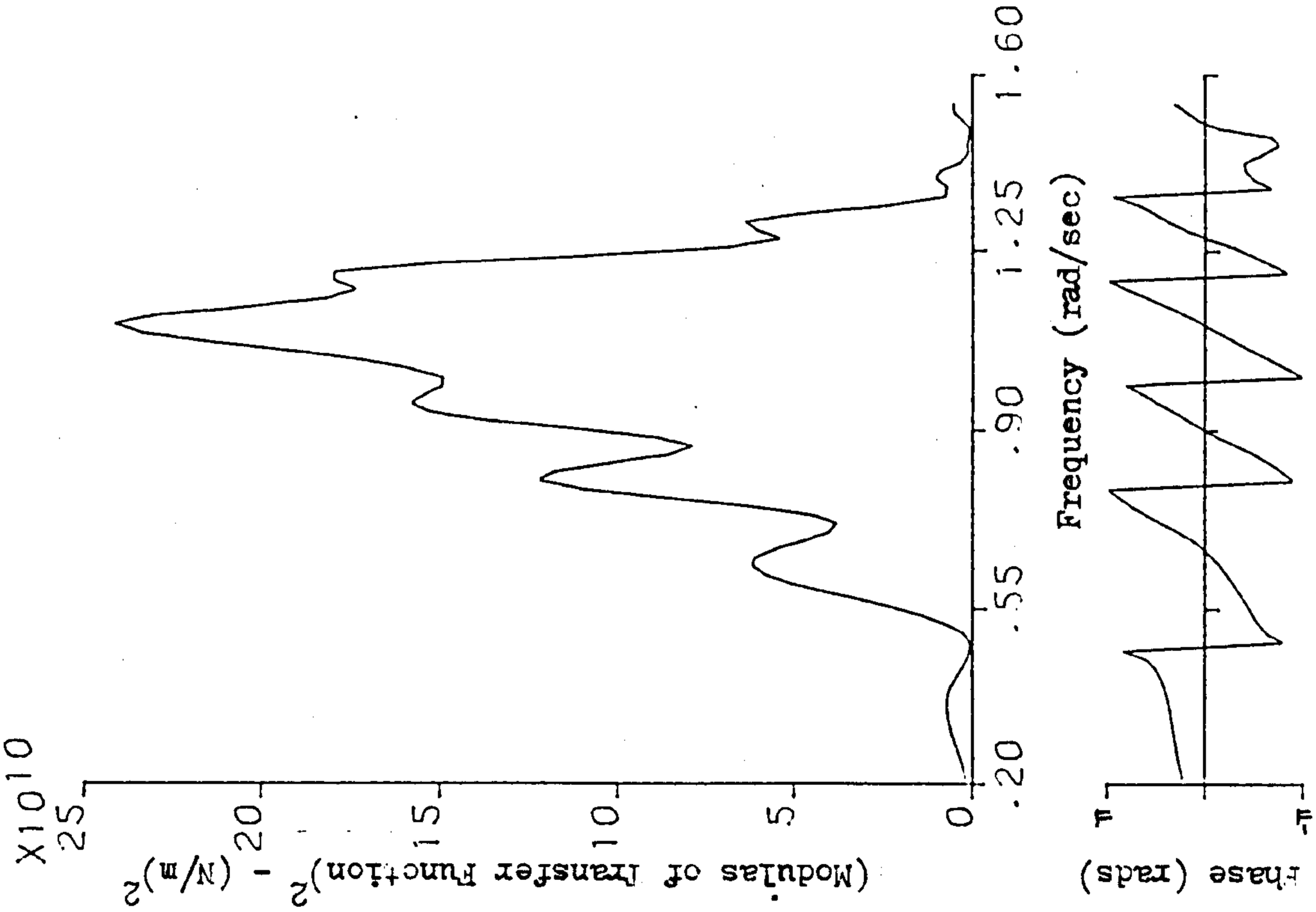

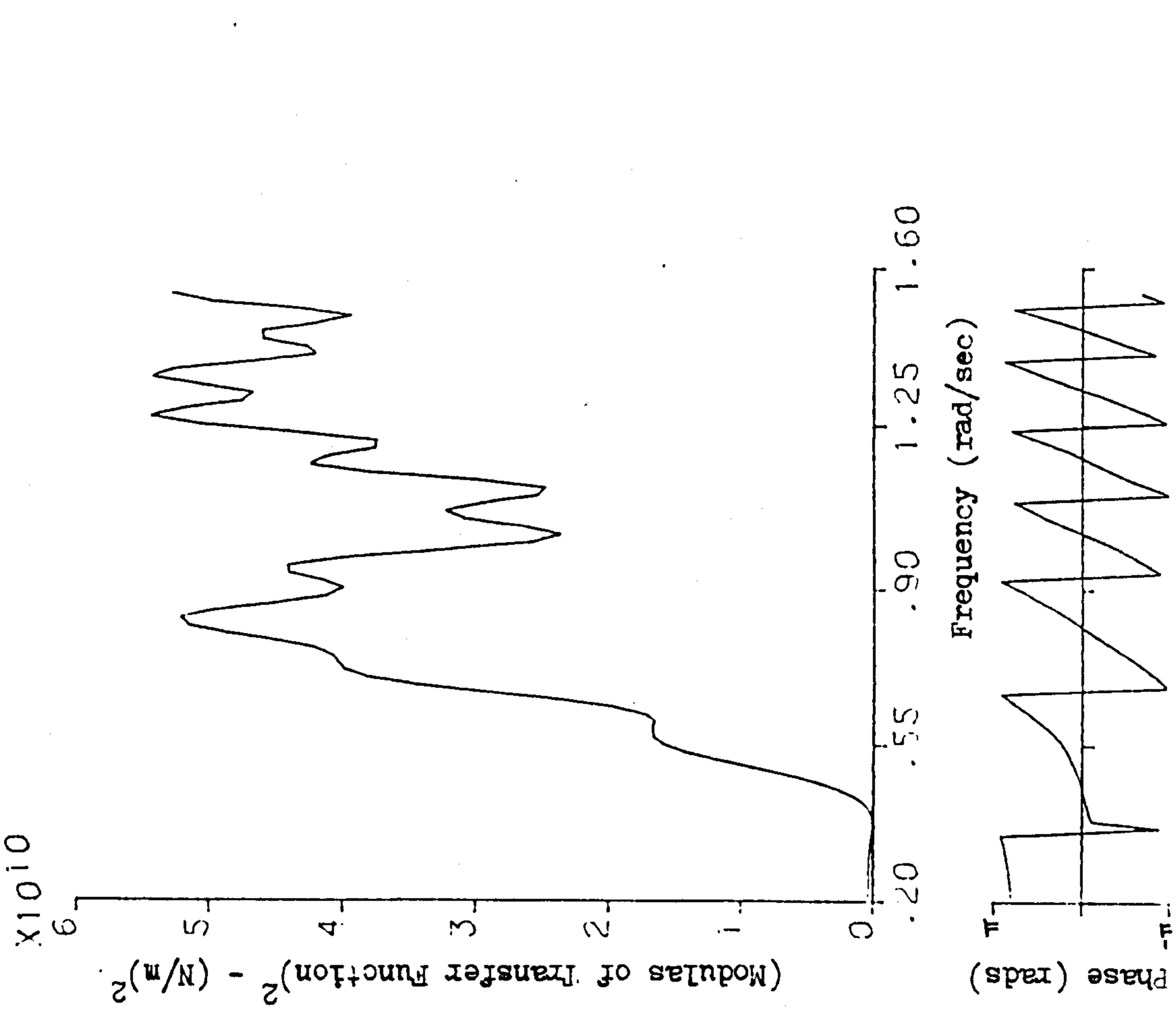

FIG. 9.13 SBS SYSTEM TRANSFER FUNCTIONS - 130,000DWT TANKER AT HALF DRAFT WITH C.G. 60M FORE OF MIDSHIPS

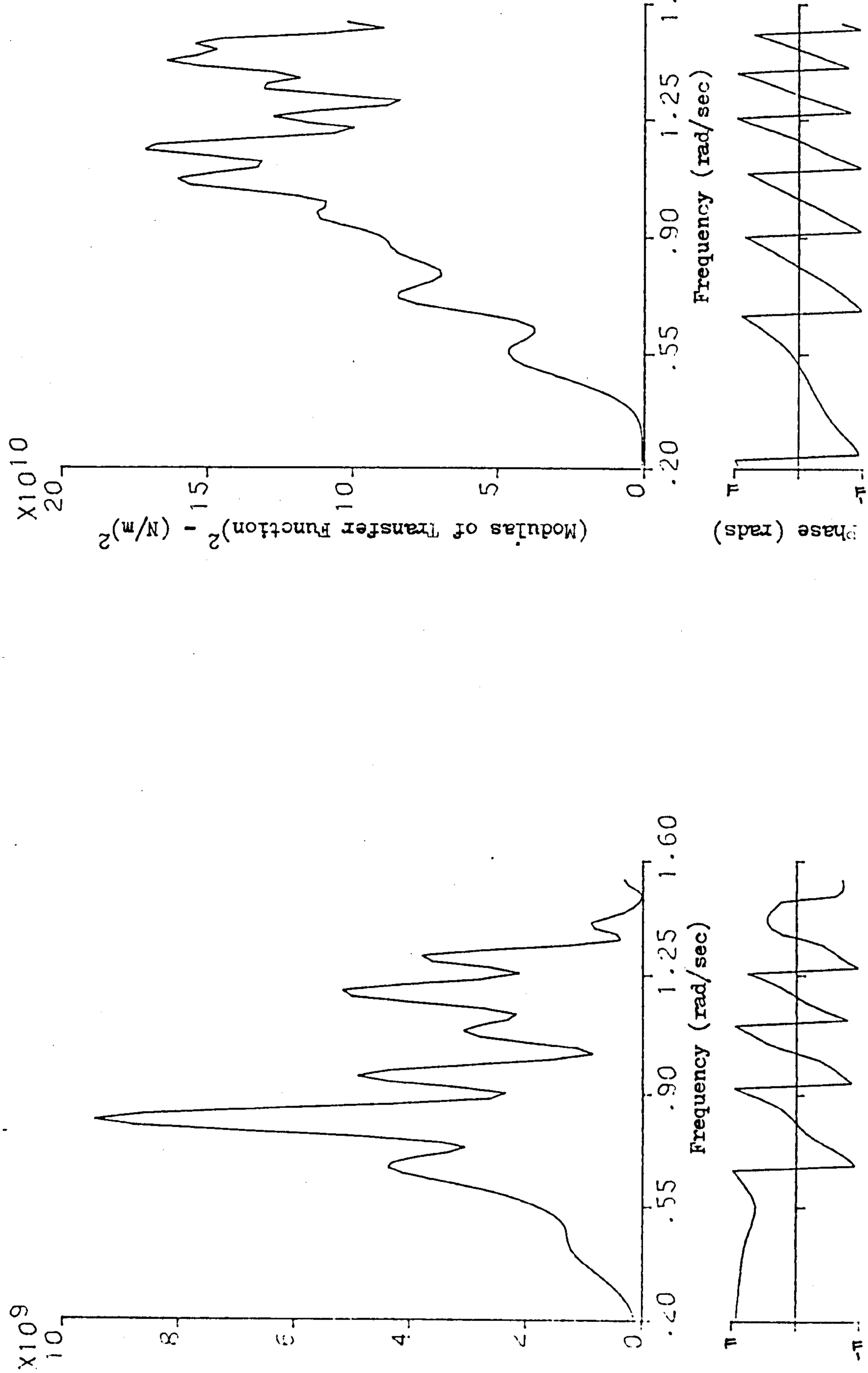

FIG. 9.13 SBS SYSTEM TRANSFER FUNCTIONS - 130,000DWT TANKER AT HALF DRAFT WITH C.G. 60M FORE OF MIDSHIPS

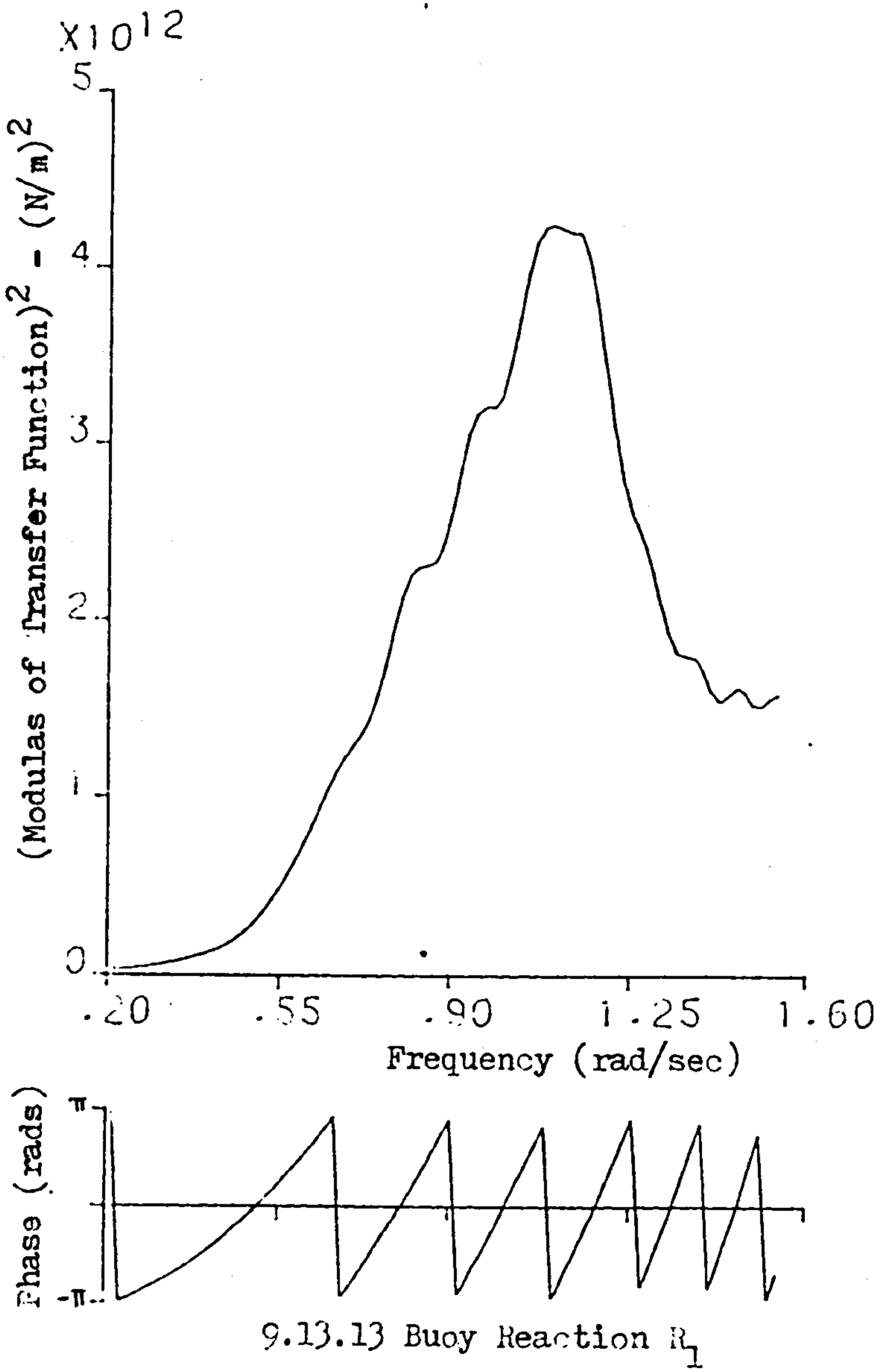

9.13.13 Buoy Reaction R_1

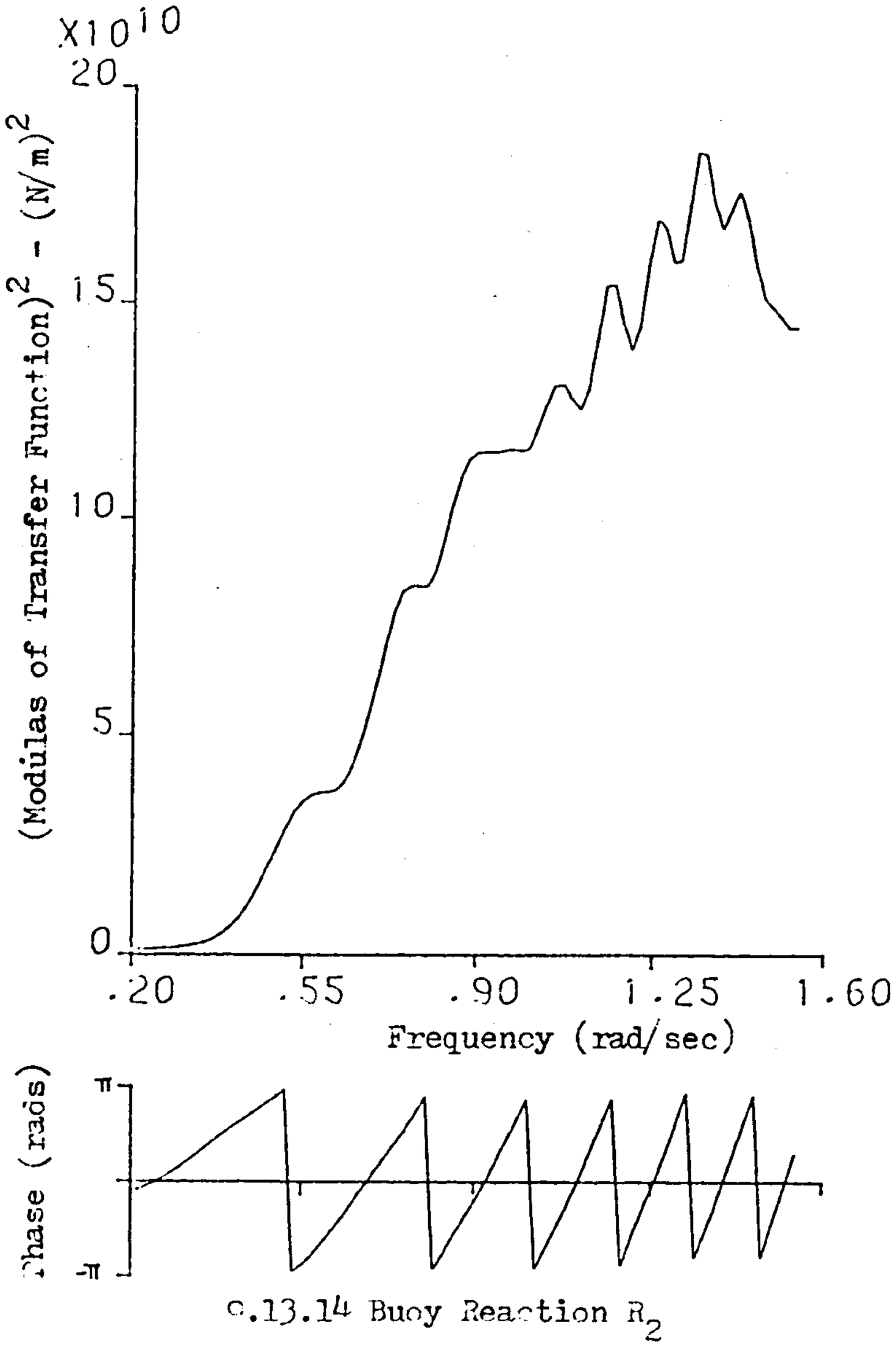

9.13.14 Buoy Reaction R_2

FIG. 9.13 SBS SYSTEM TRANSFER FUNCTIONS - 130,000DWT TANKER AT HALF DRAFT WITH C.G. 60ft FORE OF MIDSHIPS

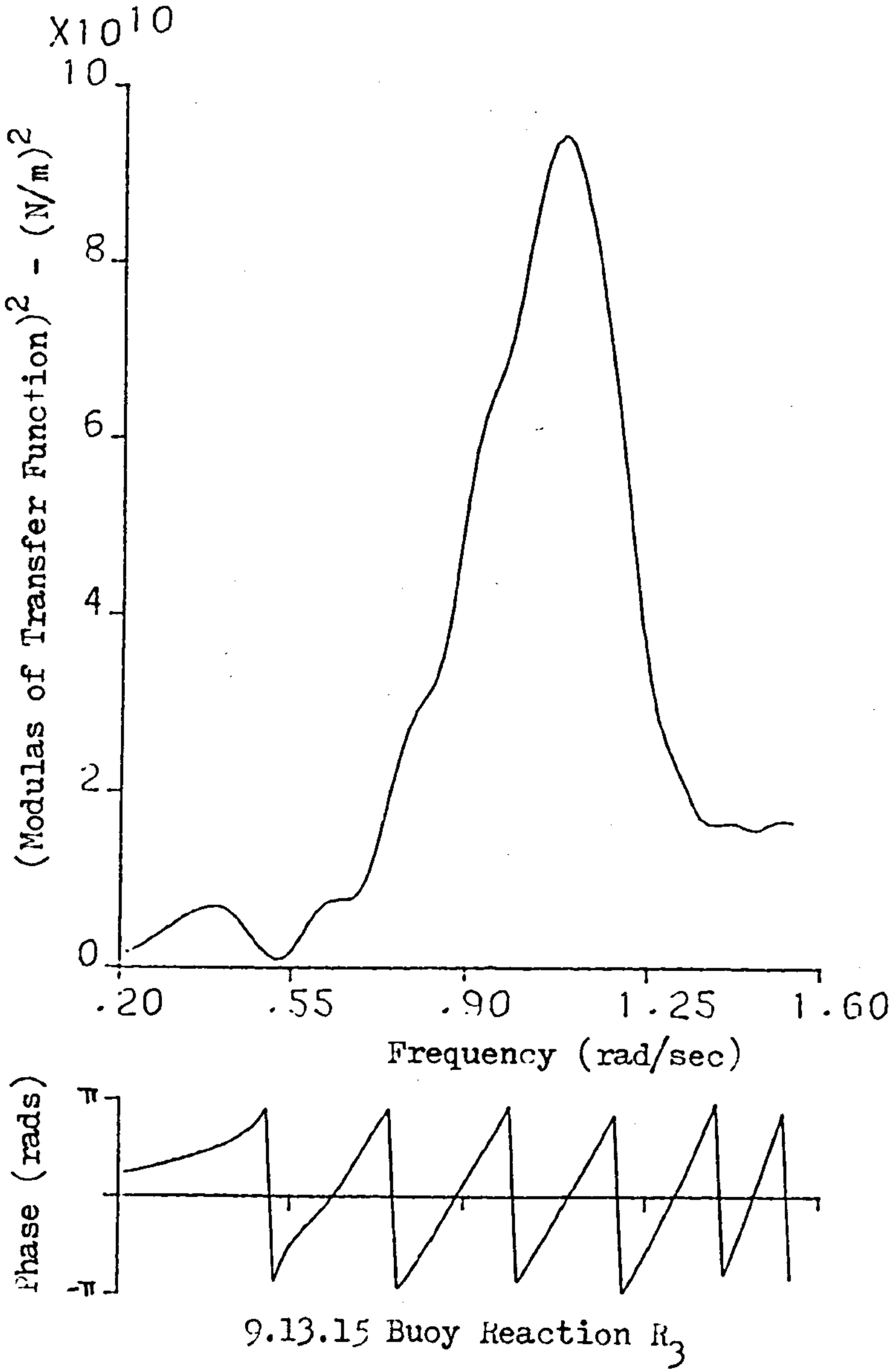

9.13.15 Buoy Reaction R_3

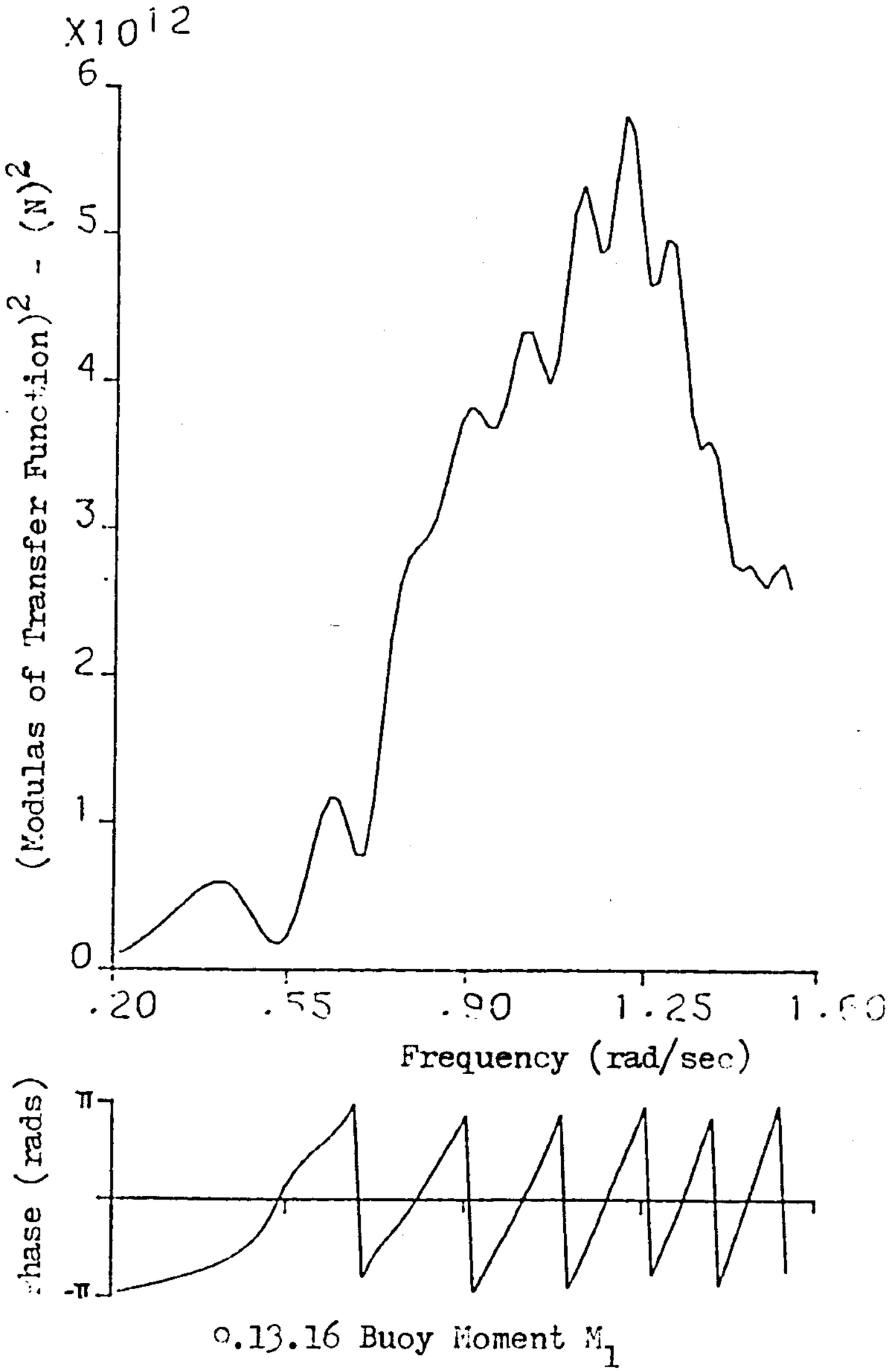

9.13.16 Buoy Moment M_1

FIG. 9.13 SBS SYSTEM TRANSFER FUNCTIONS - 130,000DWT TANKER AT HALF DRAFT WITH C.G. 60M FORE OF MIDSHIPS

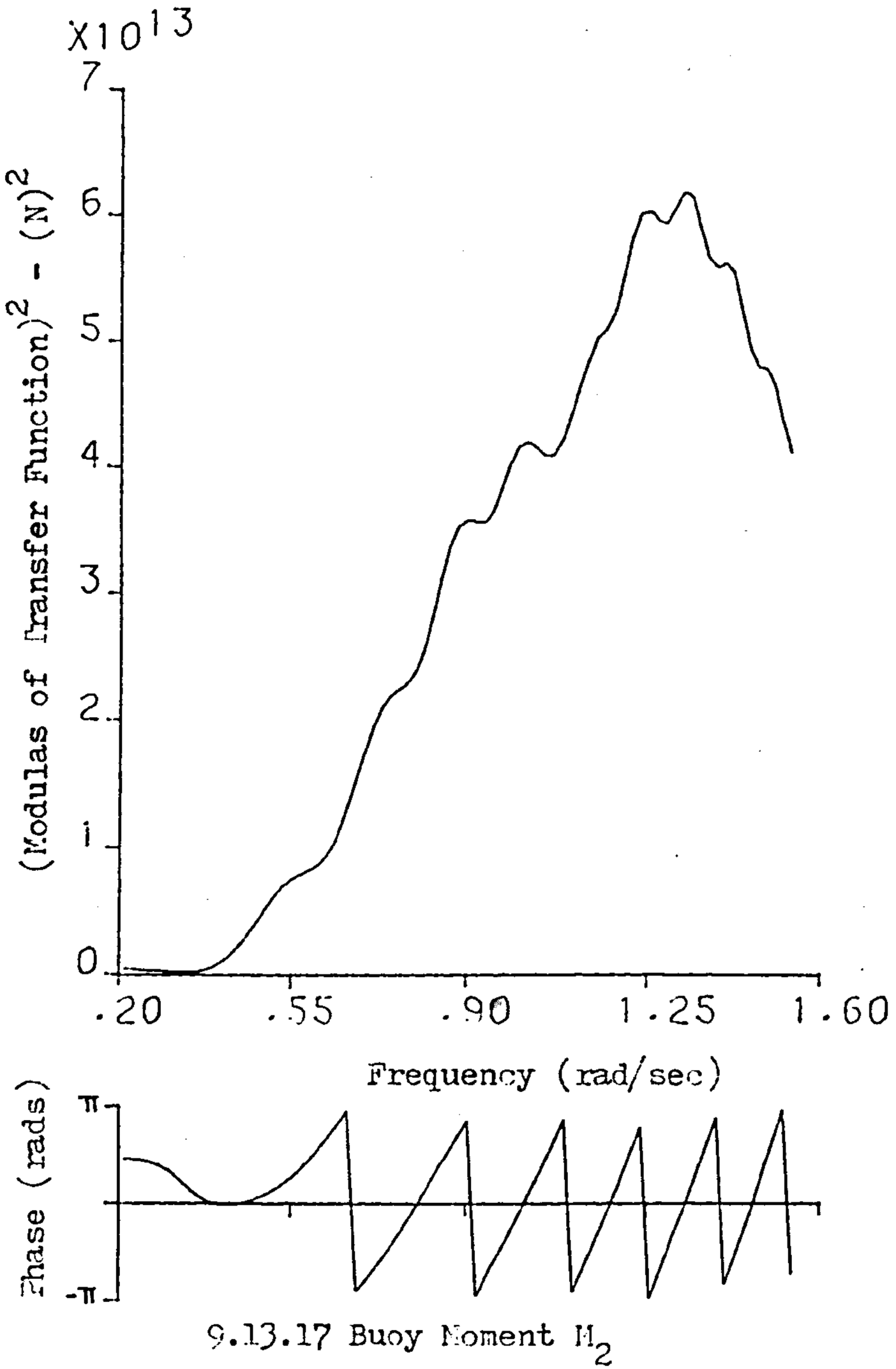

9.13.17 Buoy Moment M_2

FIG. 9.13 SBS SYSTEM TRANSFER FUNCTIONS - 130,000DWT TANKER AT HALF DRAFT WITH C.G. 60N FORE OF MIDSHIPS

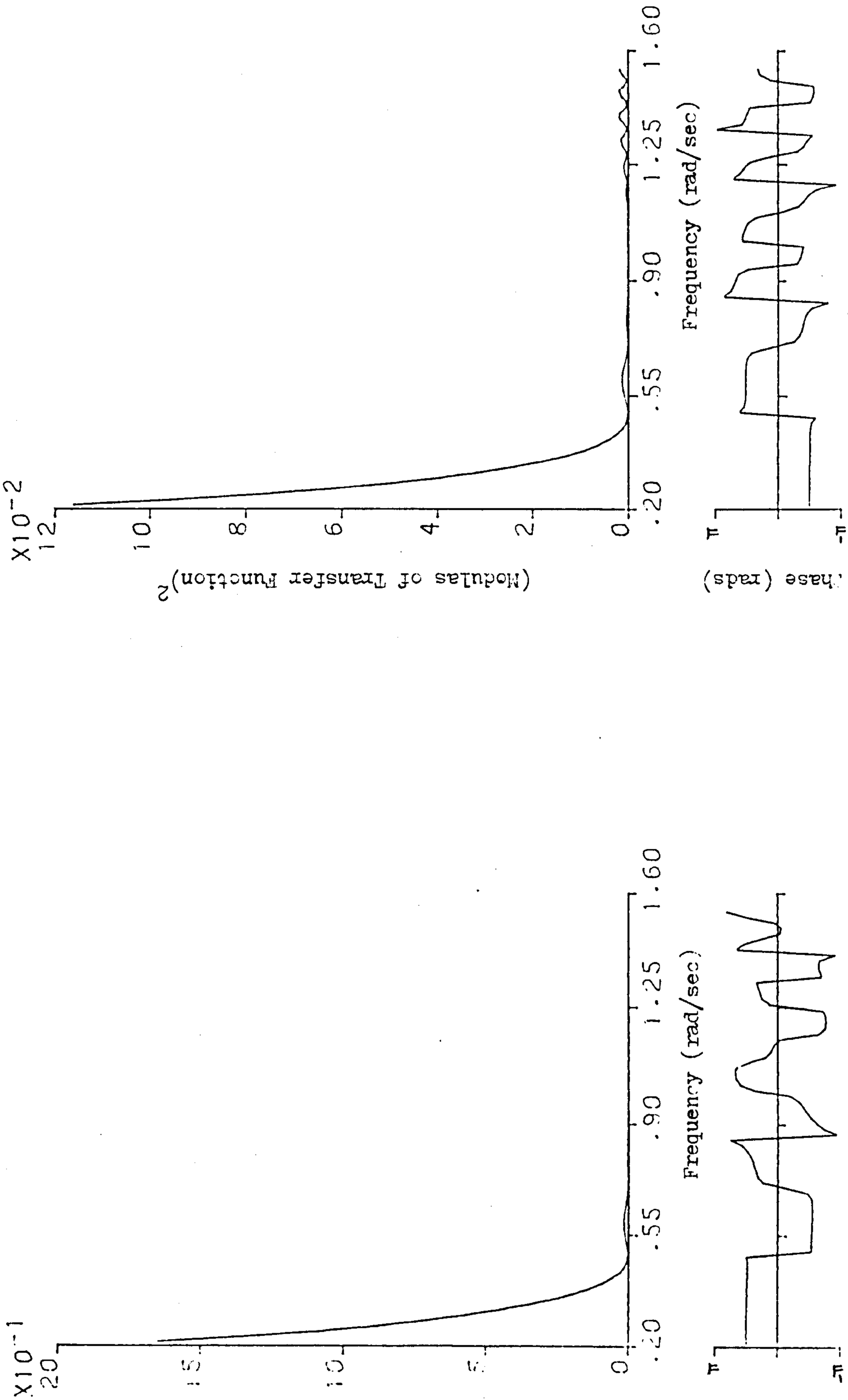

FIG. 9.14 SBS SYSTEM TRANSFER FUNCTIONS - 220,000DWT TANKER AT FULL DRAFT

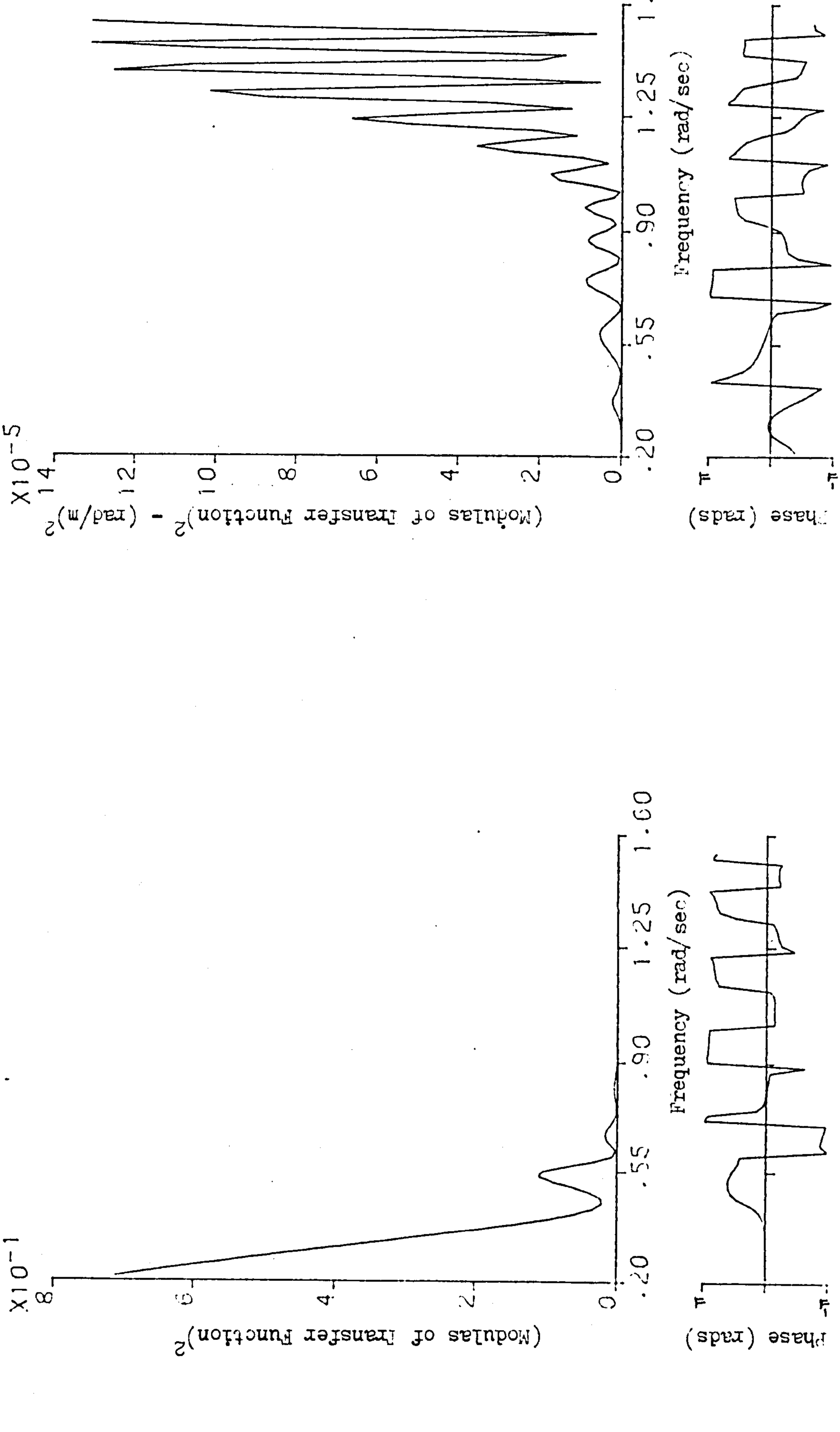

FIG. 9.14 SBS SYSTEM TRANSFER FUNCTIONS - 200,000DWT TANKER AT FULL DRAFT

9.14.3 Heave

9.14.4 Roll

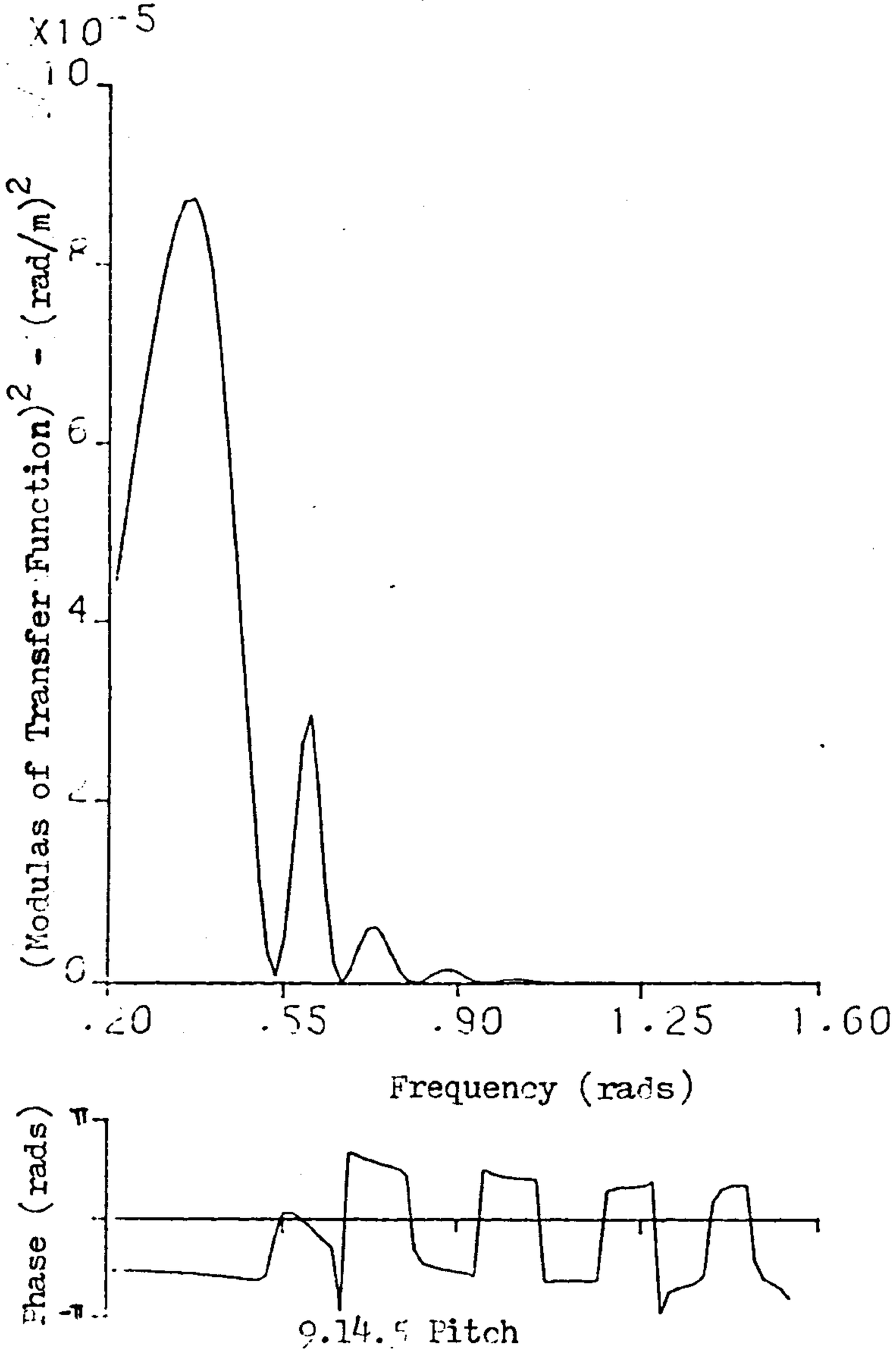

9.14.5 Pitch

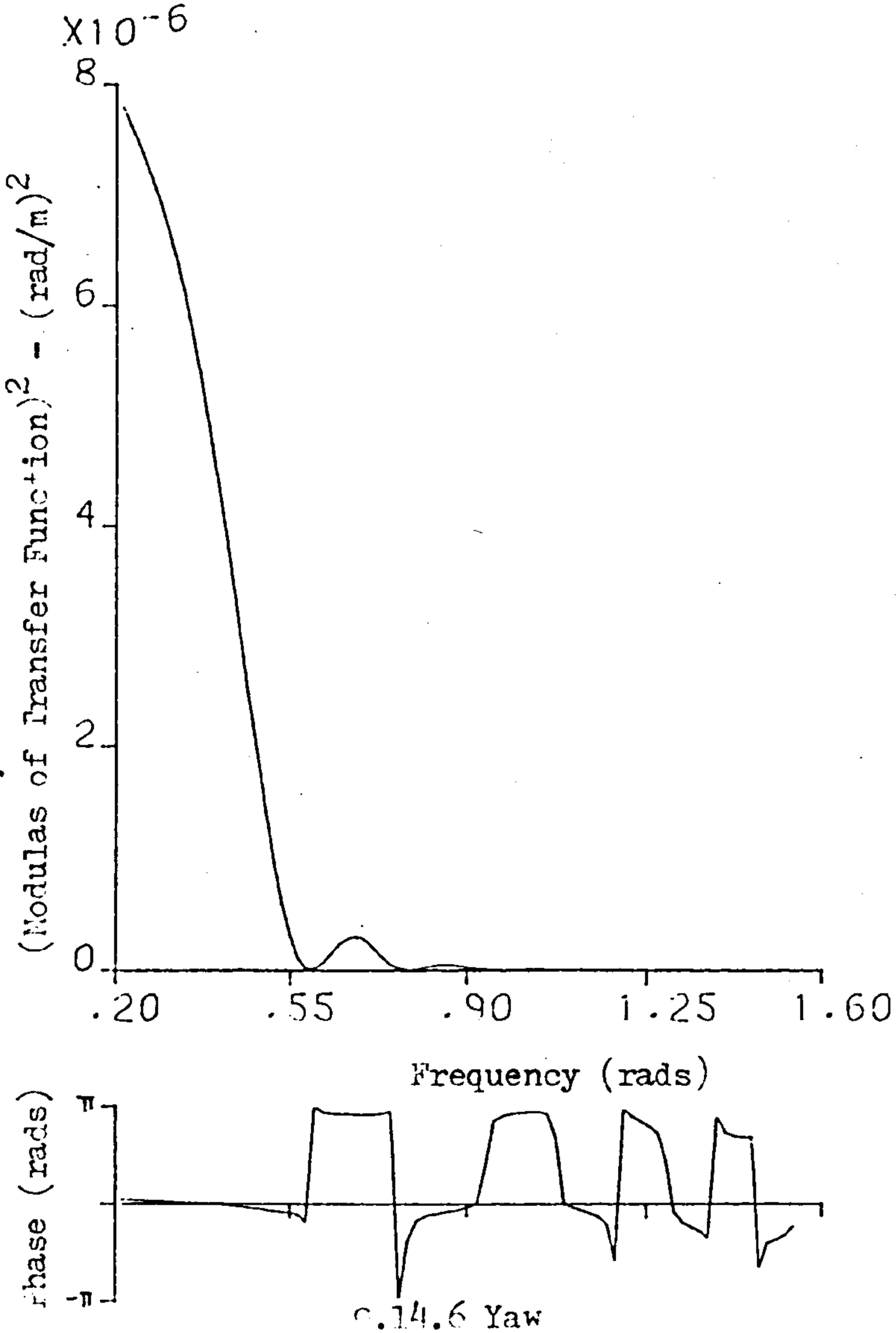

9.14.6 Yaw

FIG. 9.14 SBS SYSTEM TRANSFER FUNCTIONS - 200,000DWT TANKER AT FULL DRAFT

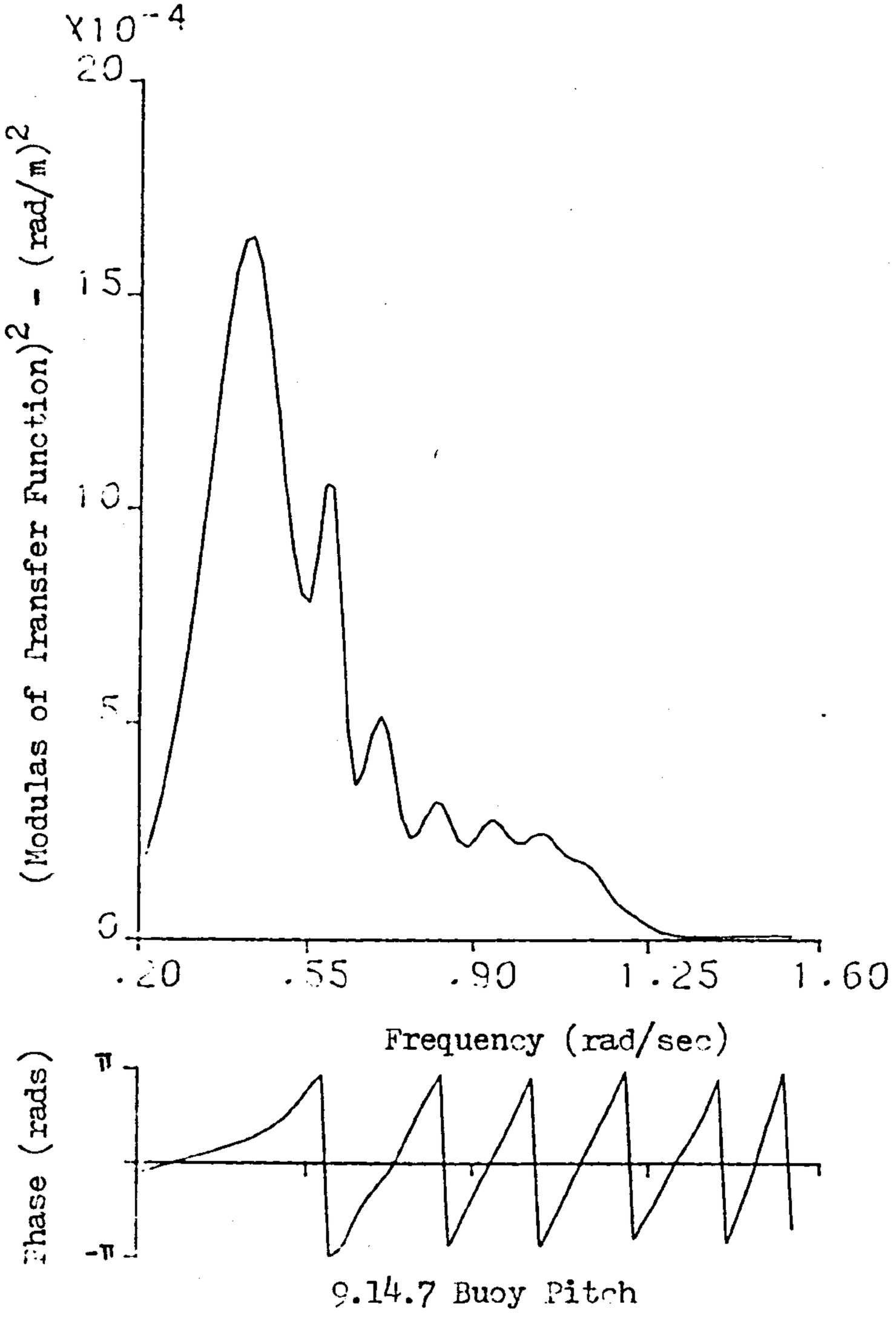

9.14.7 Buoy Pitch

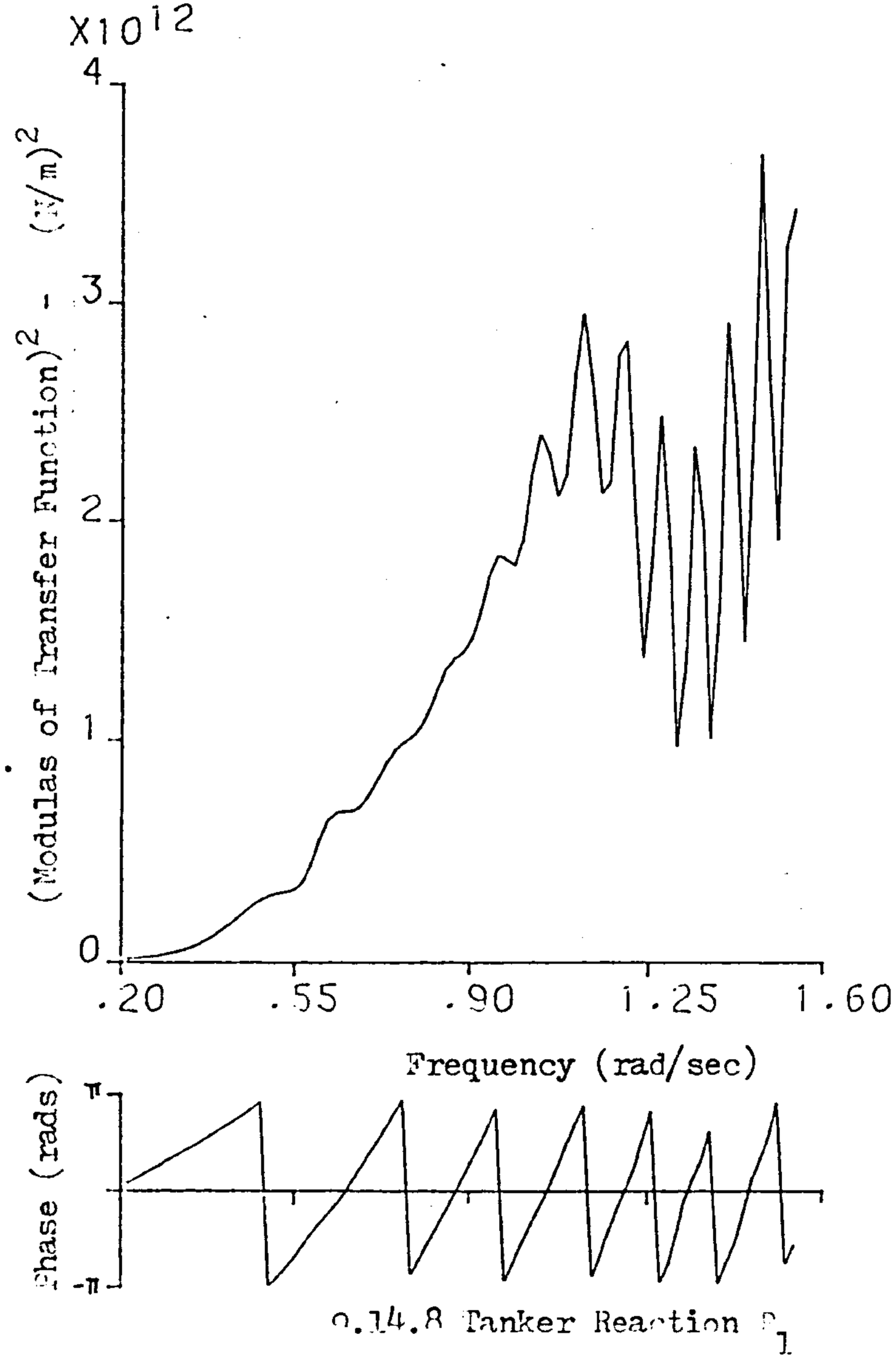

9.14.8 Tanker Reaction F$_1$

FIG. 9.14 SBS SYSTEM TRANSFER FUNCTIONS - 200,000DWT TANKER AT FULL DRAFT

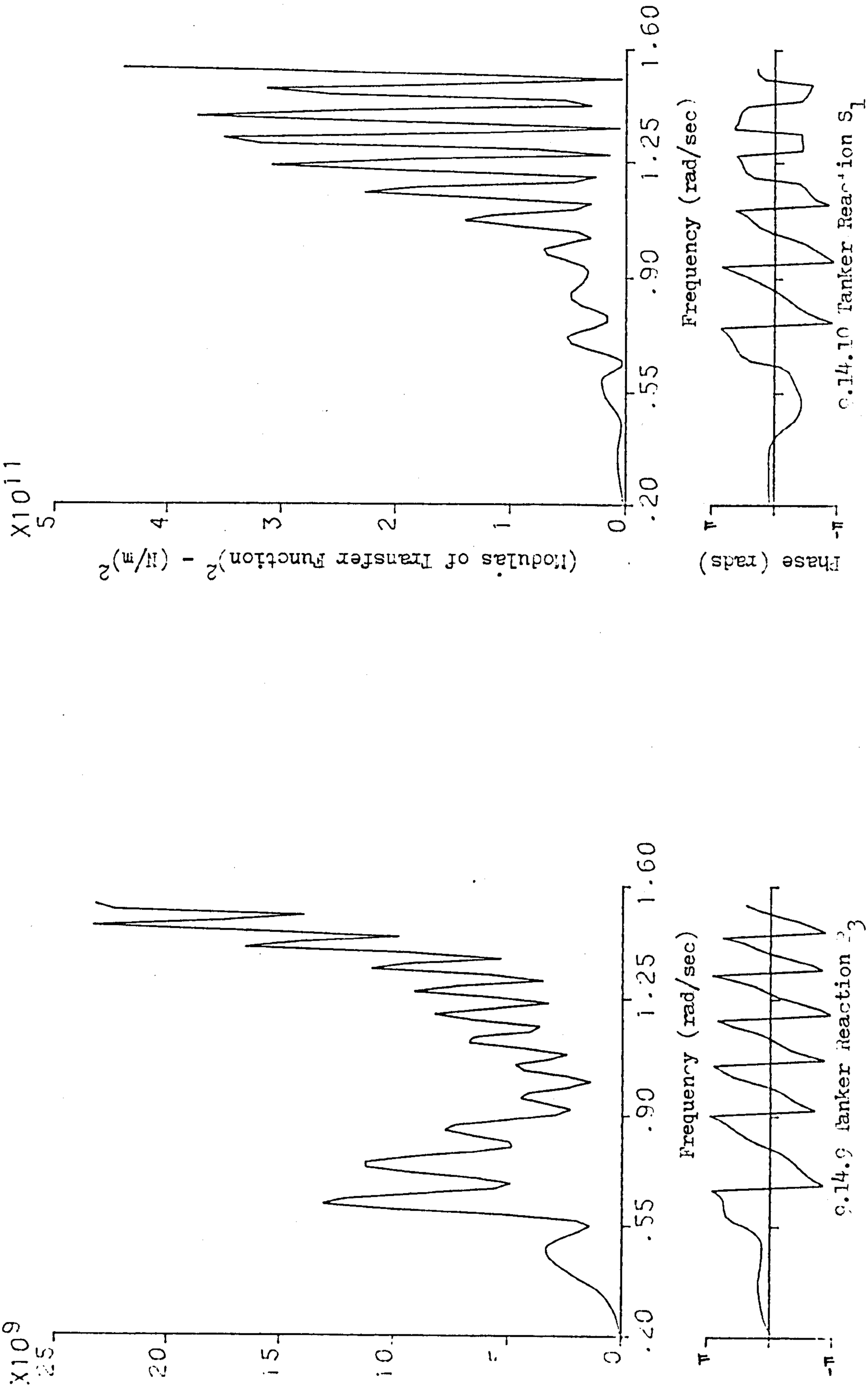

FIG. 6.14 SBS SYSTEM TRANSFER FUNCTIONS - 200,000DWT TANKER AT FULL DRAFT

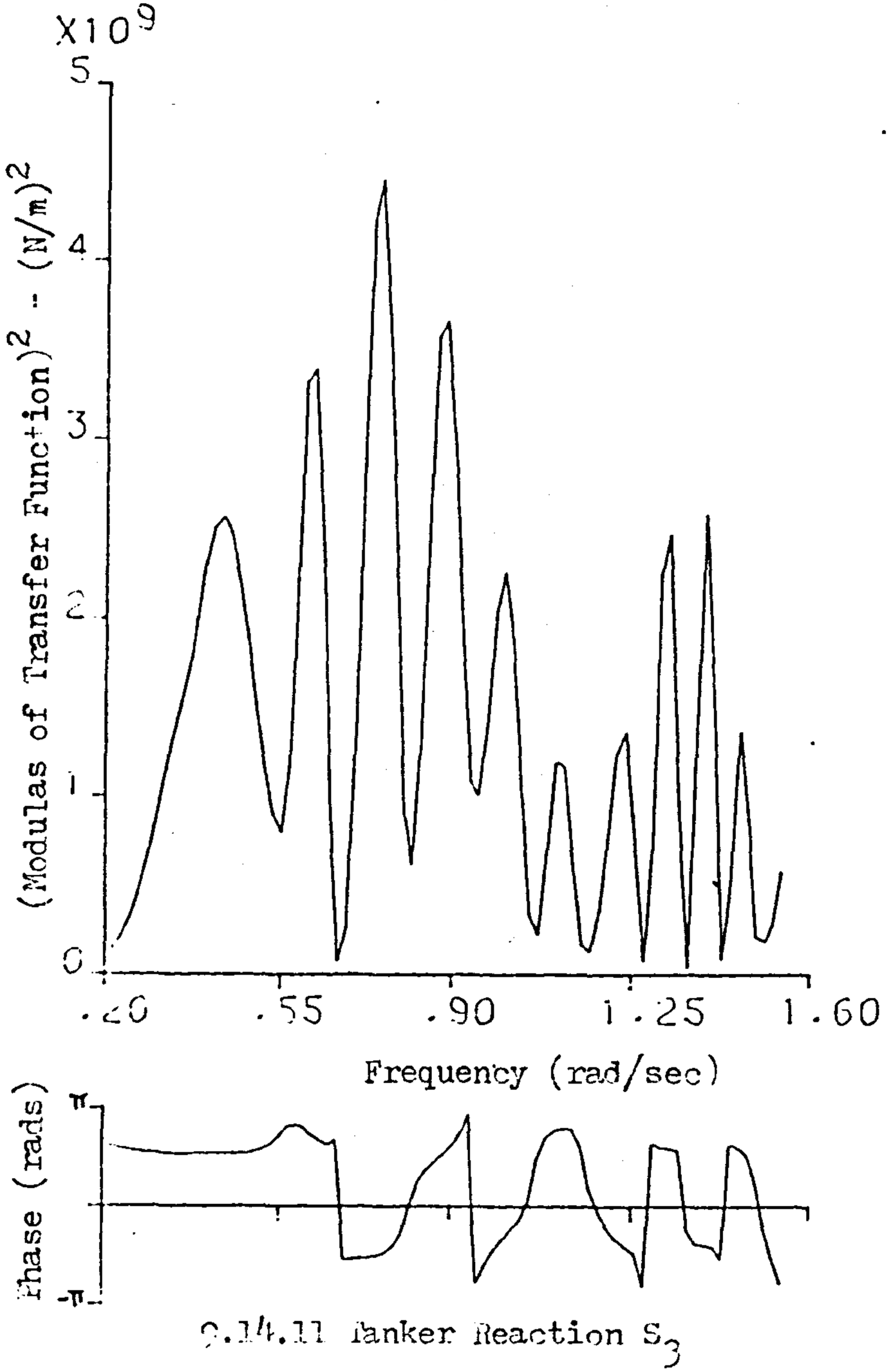

9.14.11 Tanker Reaction S_3

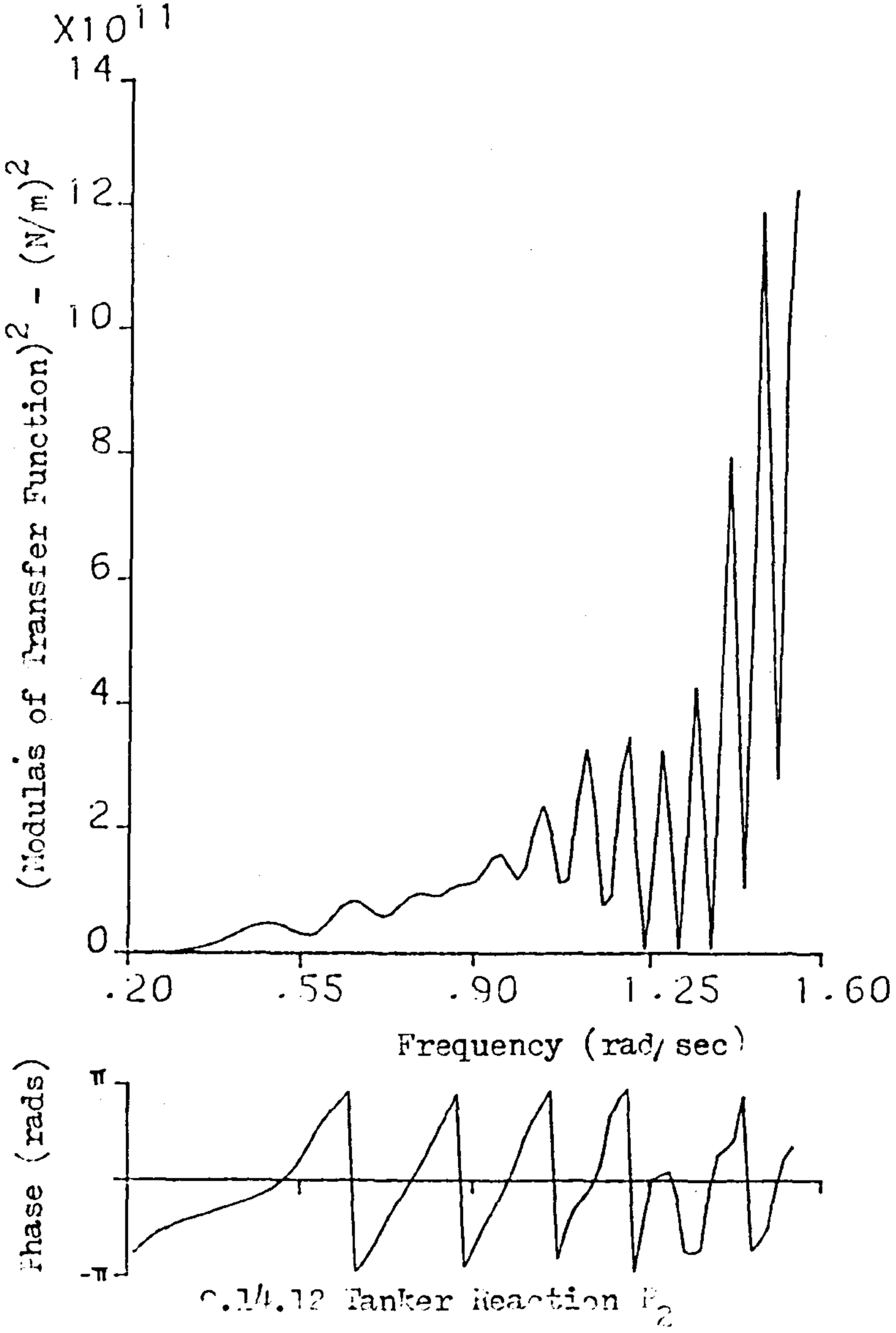

9.14.12 Tanker Reaction R_2

FIG. 9.14 SBS SYSTEM TRANSFER FUNCTIONS - 200,000DWT TANKER AT FULL DRAFT

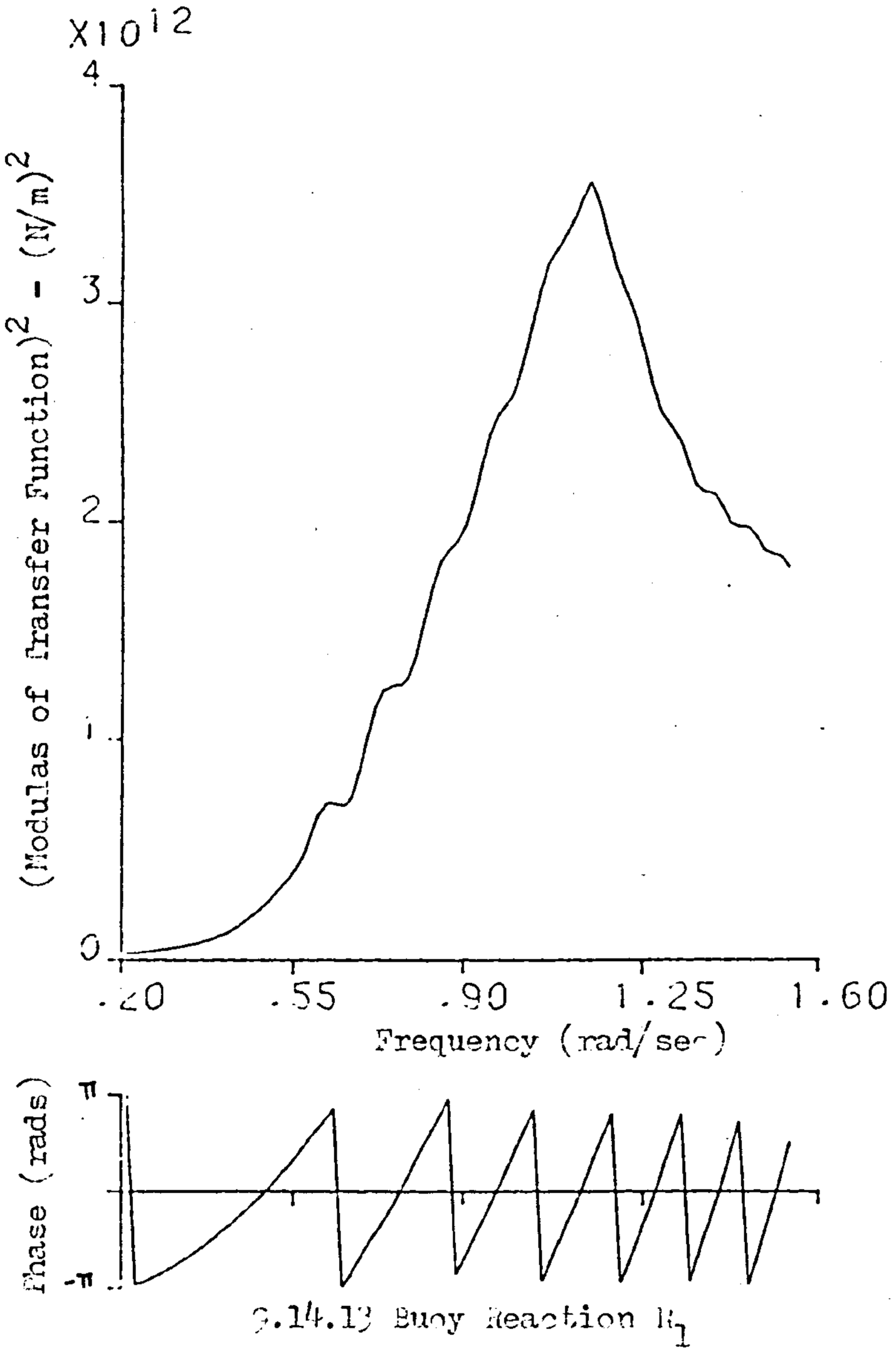

9.14.13 Buoy Reaction R_1

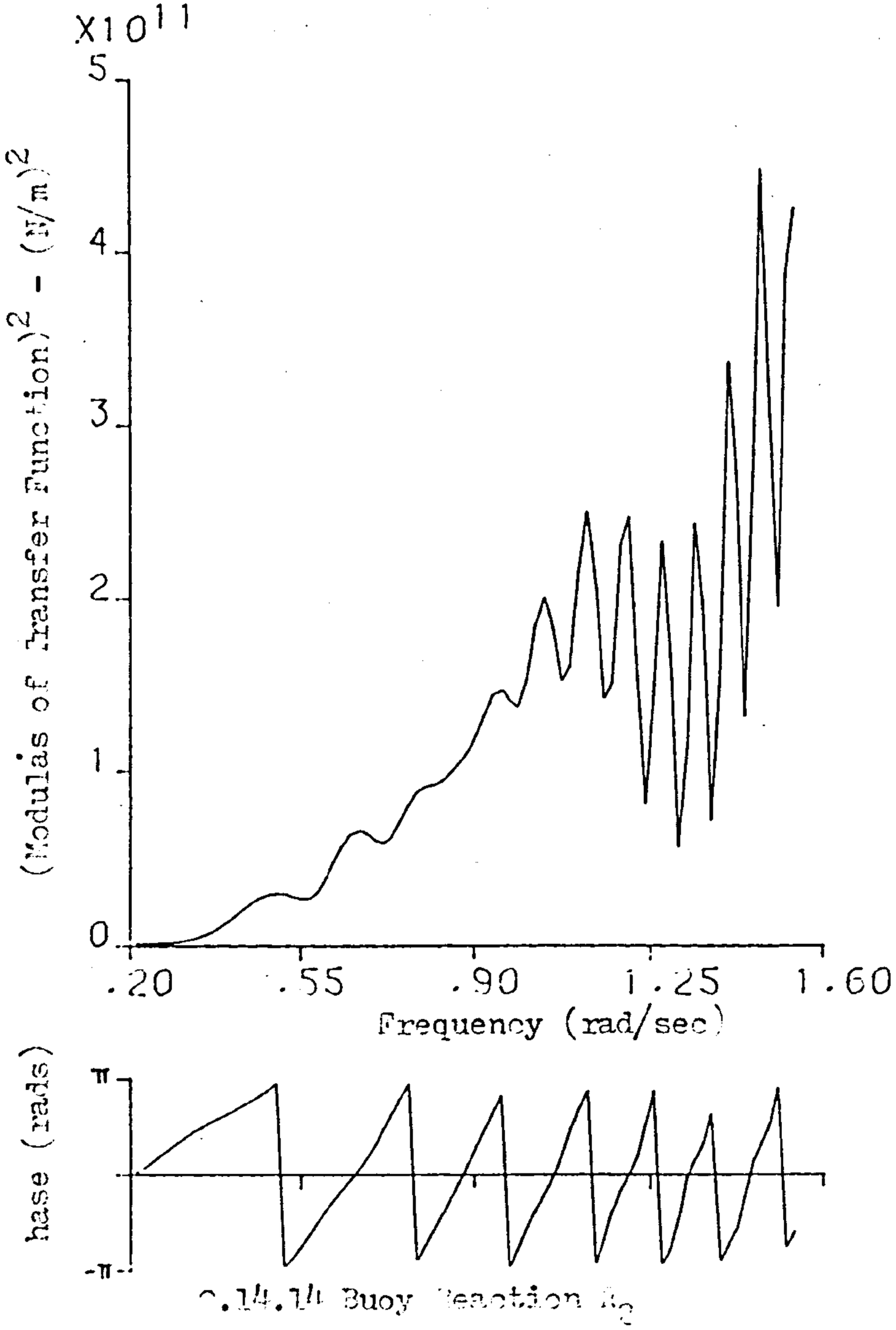

9.14.14 Buoy Reaction R_2

FIG. 9.14 SBS SYSTEM TRANSFER FUNCTIONS - 200 000DWT TANKER AT FULL DRAF

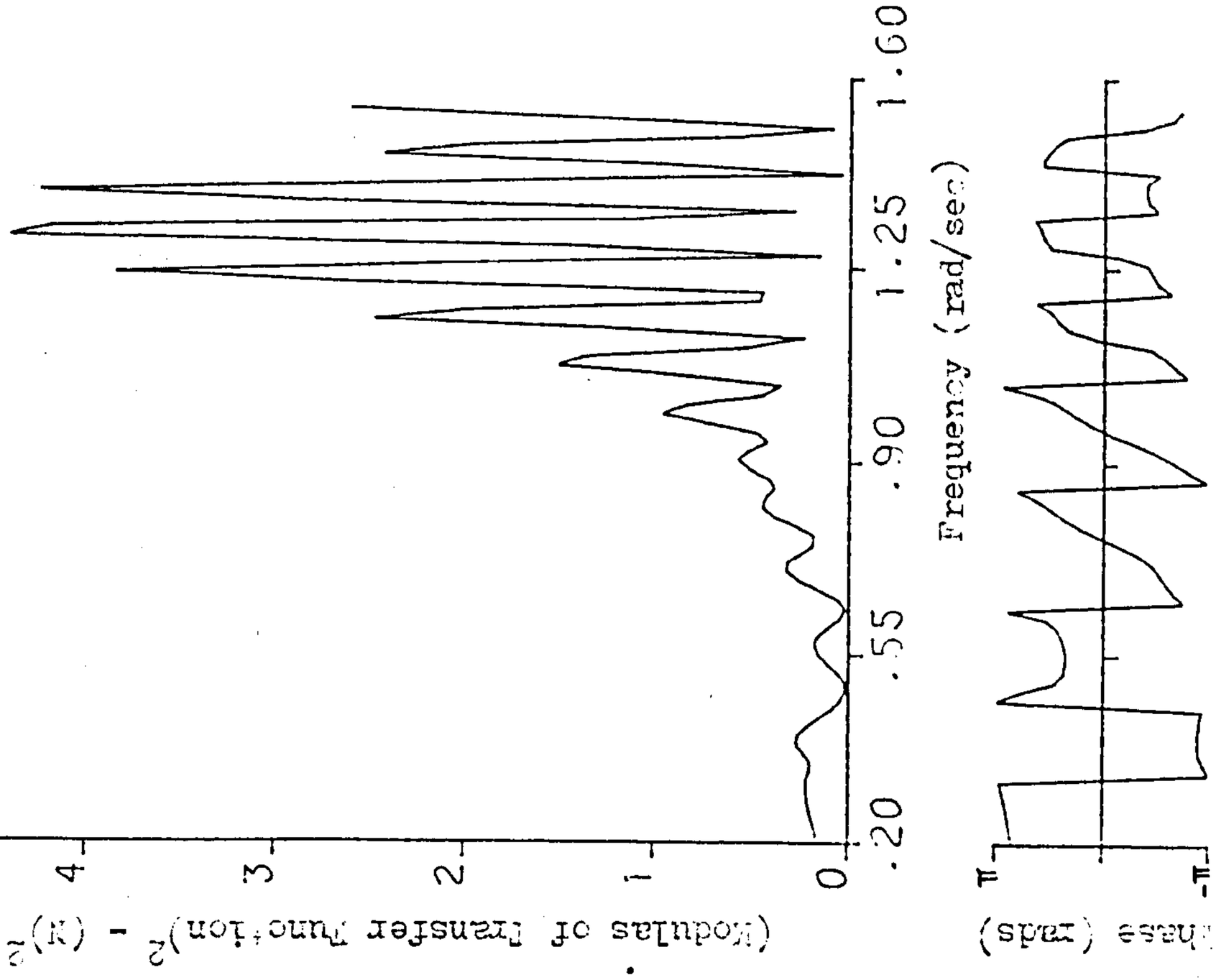

c.14.16 Buoy Reaction Mass System Transfer Functions - Tanker at Full Draft

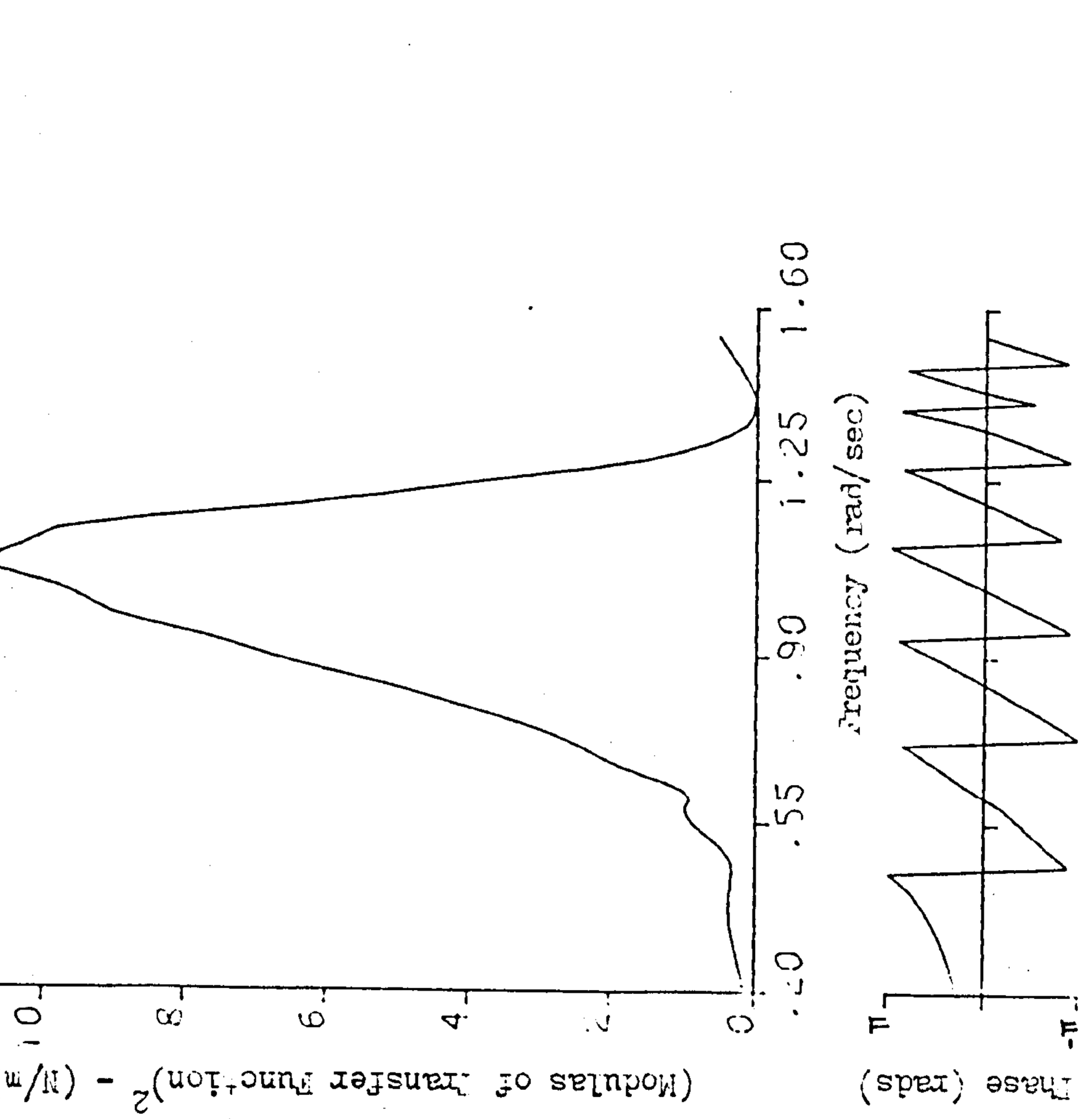

c.14.17 Buoy Reaction Mass System Transfer Functions - Tanker at Ballast Draft

FIG. c.14 CBS SYSTEM TRANSFER FUNCTIONS - 250,000 DWT TANKER AT FULL DRAFT

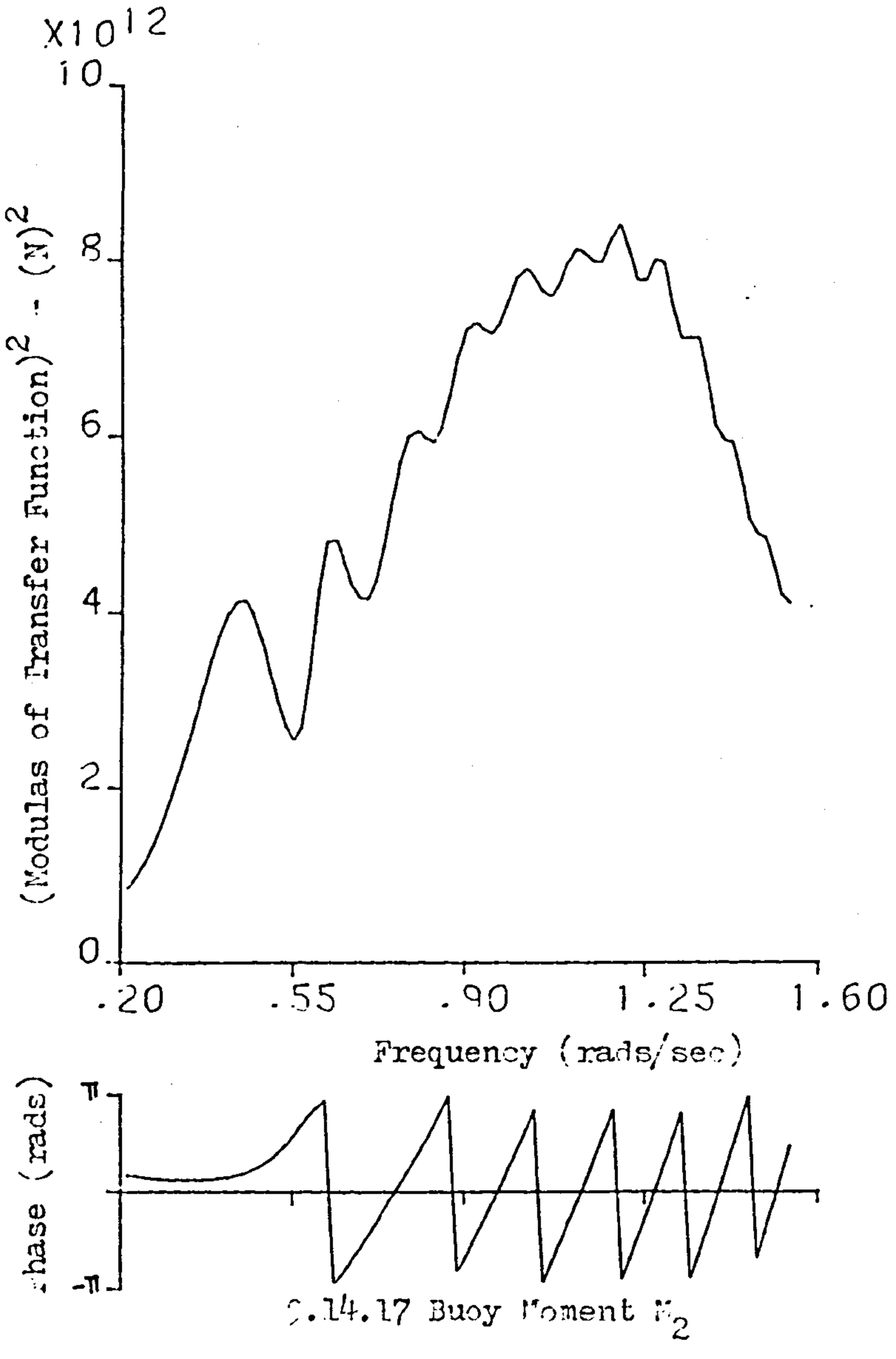

9.14.17 Buoy Moment M_2

FIG. 9.14 SBS SYSTEM TRANSFER FUNCTIONS - 200,000DWT TANKER AT FULL DRAF

FIG. 9.15 ANGULAR DEPENDENCE OF THE FIRST ORDER TRANSFER FUNCTIONS

This Figure is presented as a series of 3-D plots in the following five pages. The axes of these plots are as follows:-

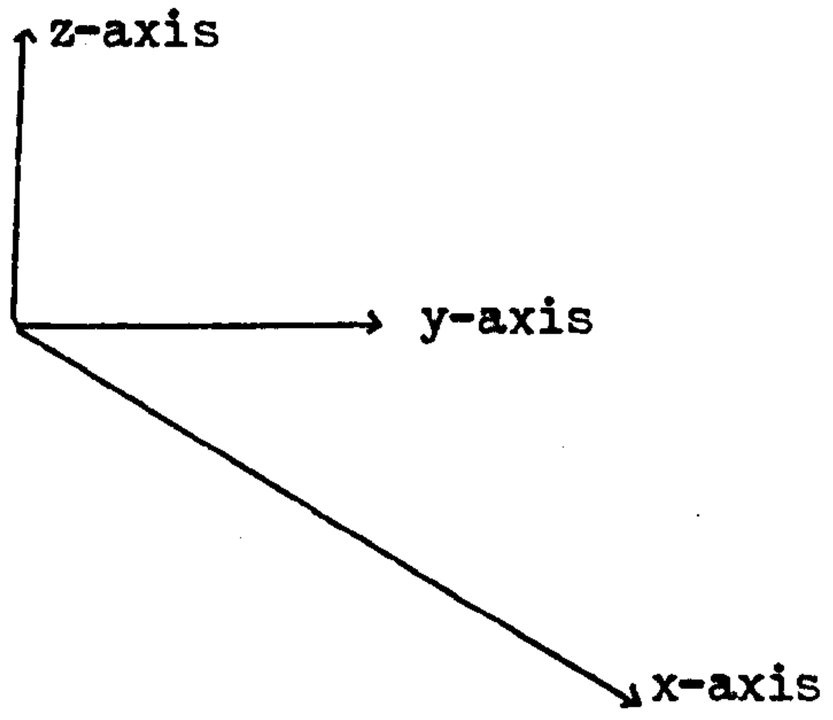

z-axis: (Modulas of the Transfer Function)^2 in SI Units. i.e. non-dimensional for translations, (rad/m)^2 for rotations, (N/m)^2 for forces and N^2 for moments.

y-axis: Angle of incidence of the wave to the bow of the vessel, in radians.

x-axis: Wave frequency, in rad/sec.

The Figure concerns a SBS system which moors a 130,000DWT tanker loaded to full draft.

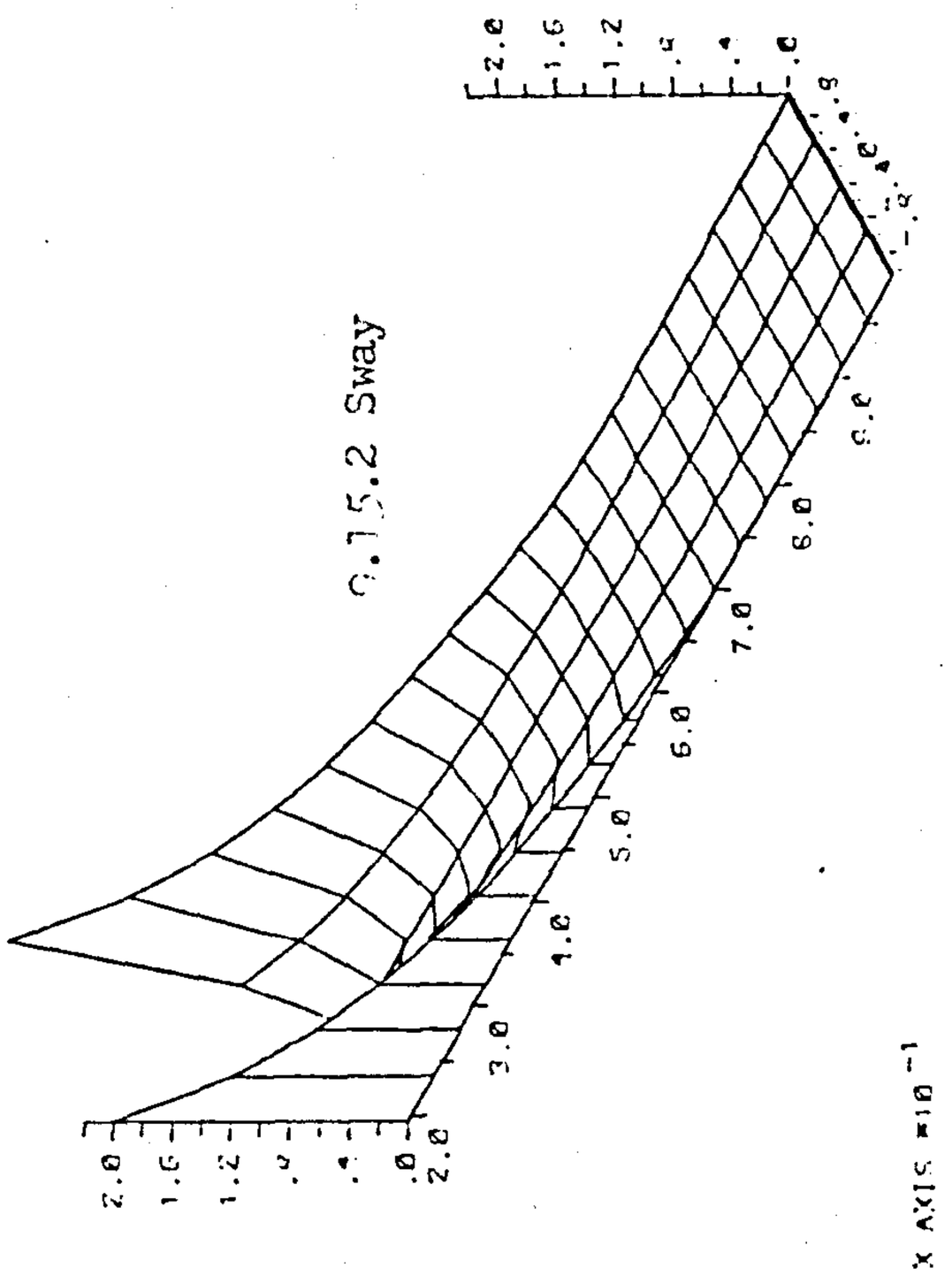
0.15.2 Sway
X AXIS ×10⁻¹

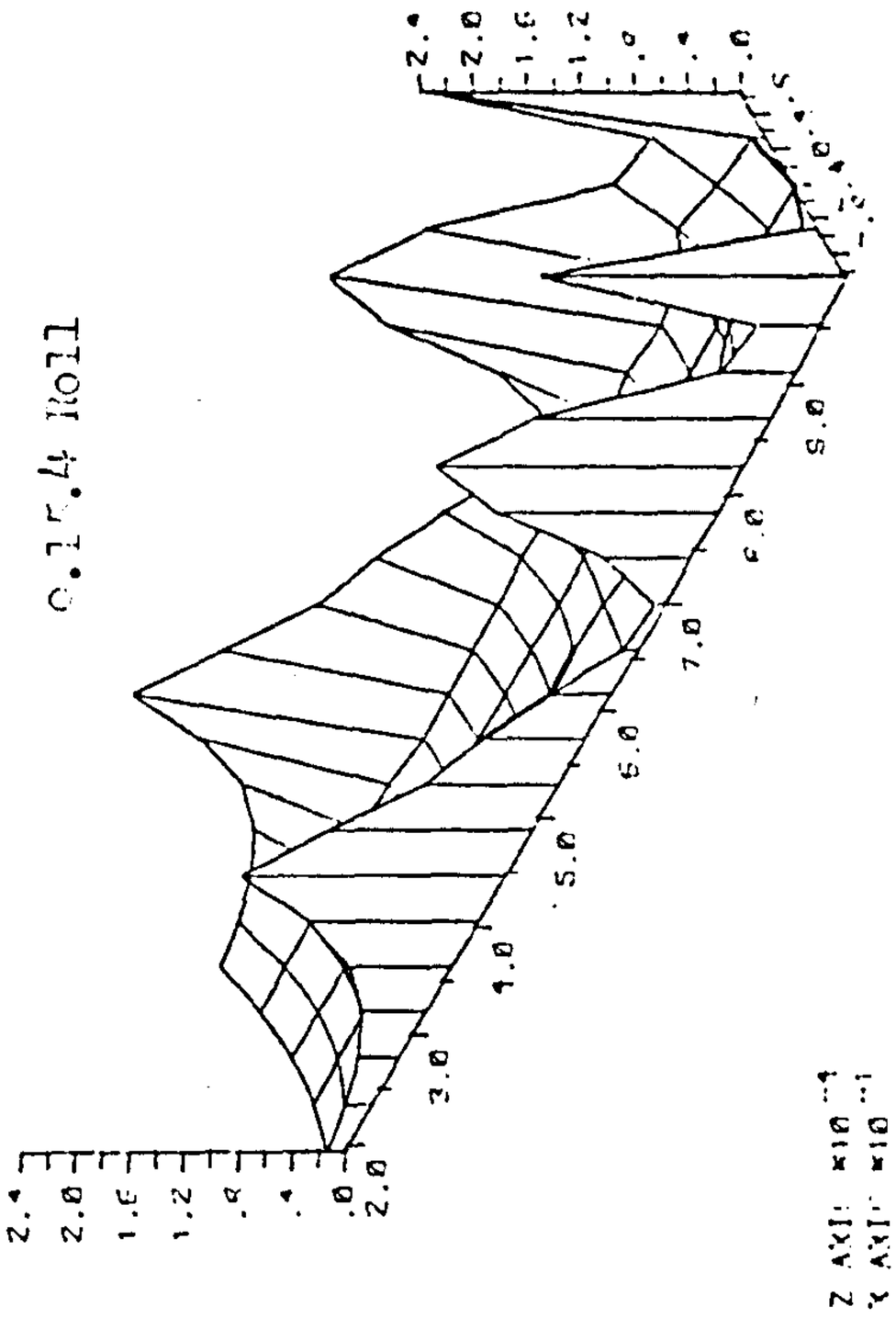
0.15.4 Roll
Z AXIS ×10⁻¹
X AXIS ×10⁻¹

SEE PAGE 329

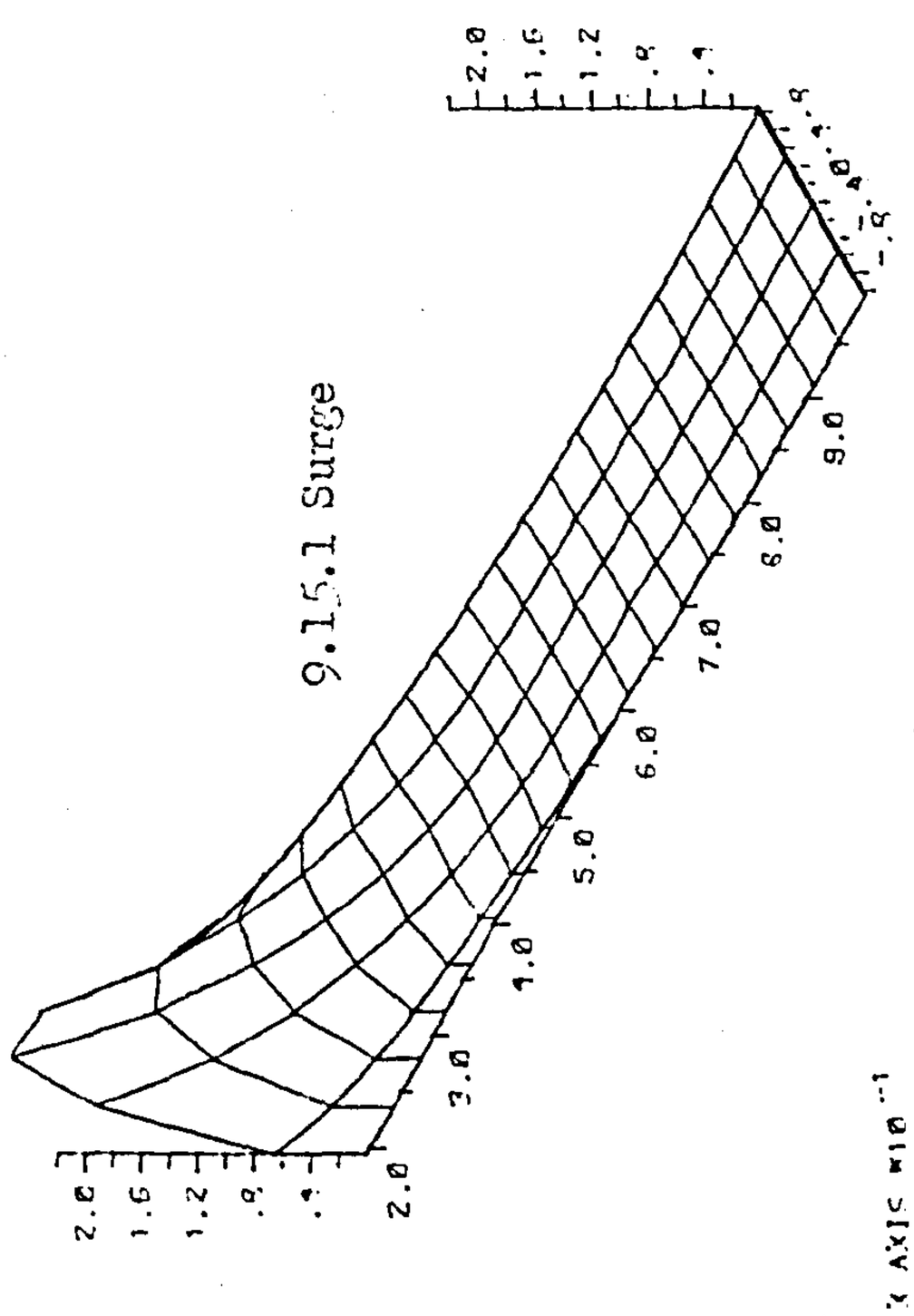
9.15.1 Surge
X AXIS ×10⁻¹

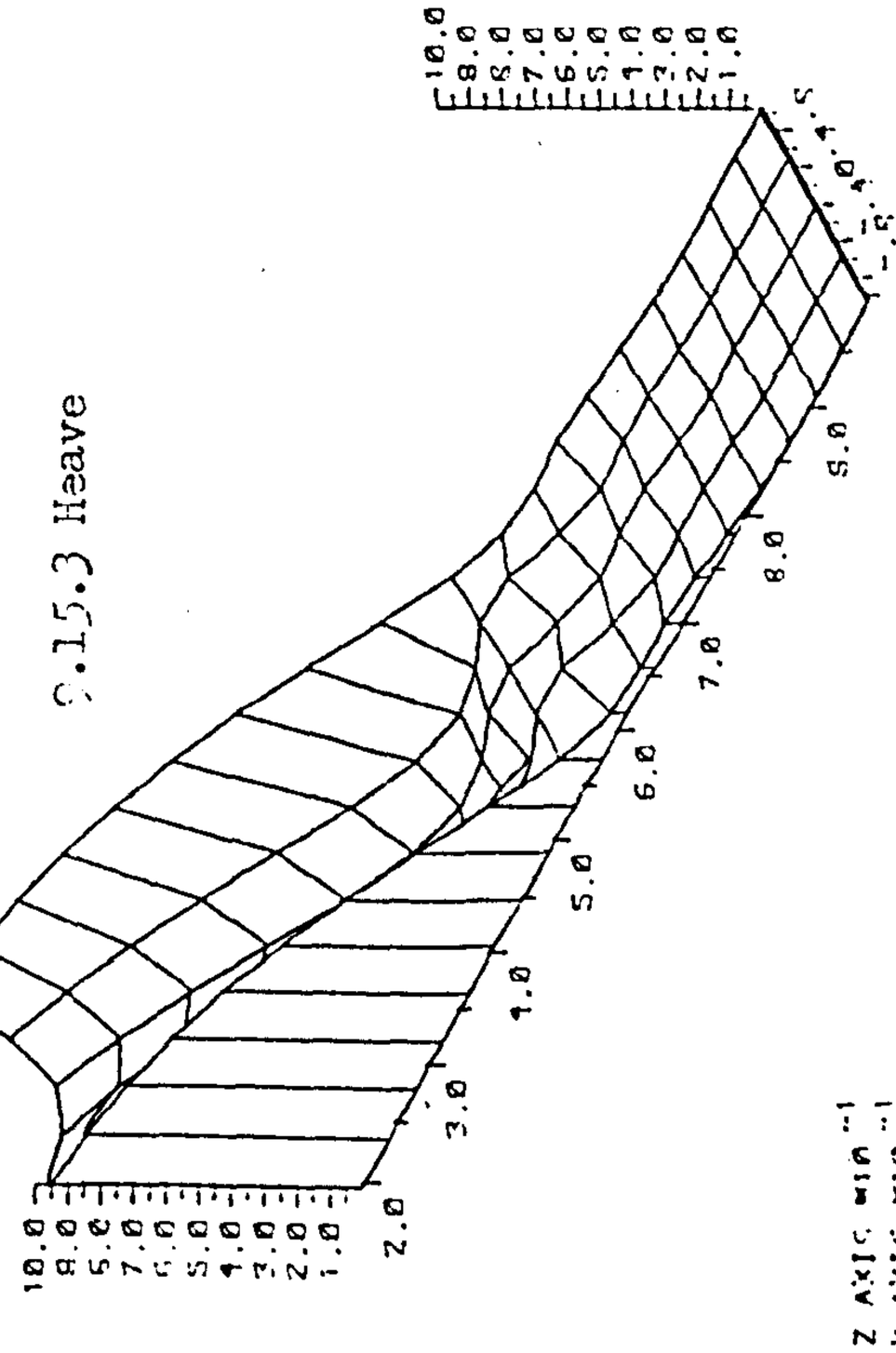
9.15.3 Heave
Z AXIS ×10⁻¹
X AXIS ×10⁻¹

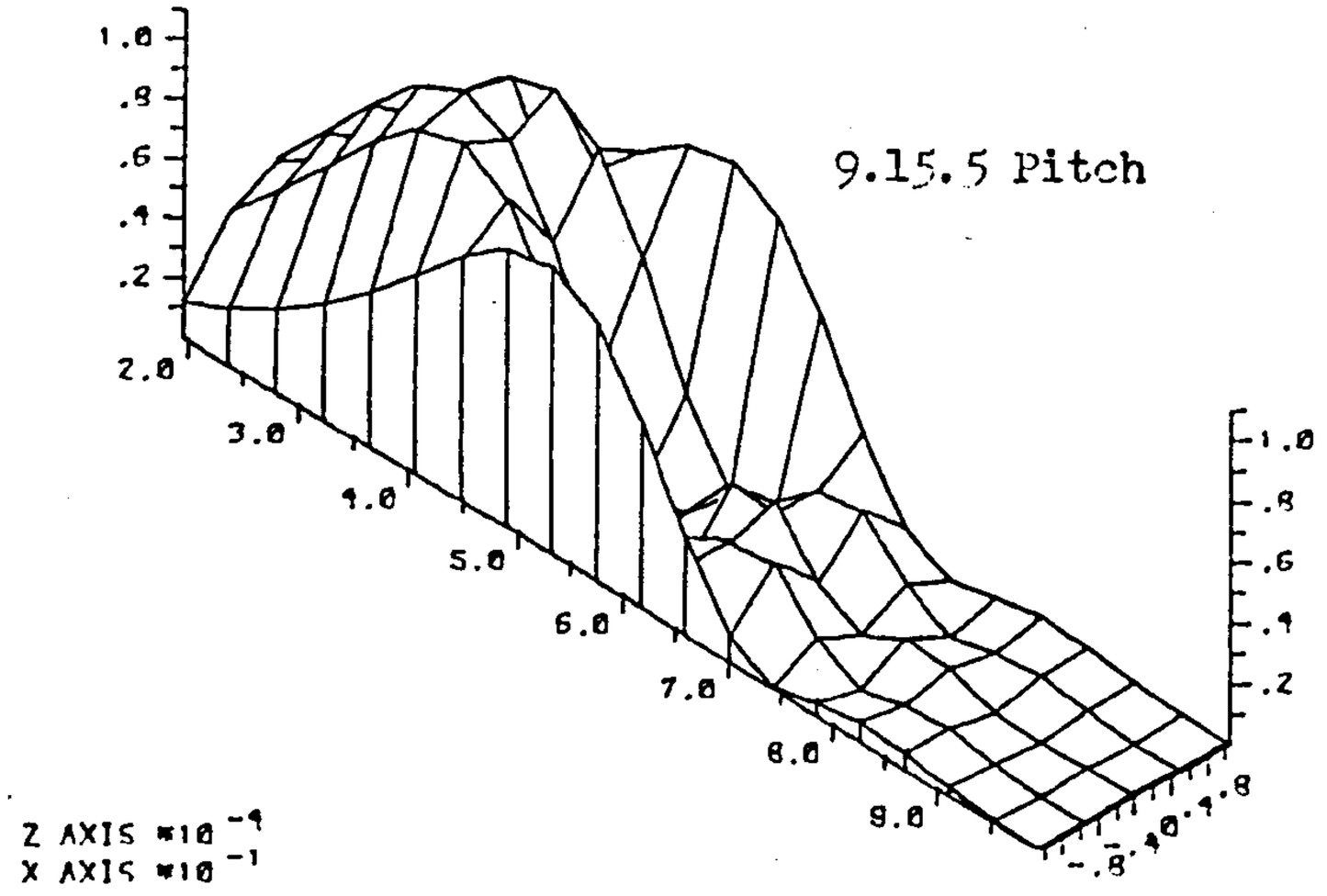

9.15.5 Pitch

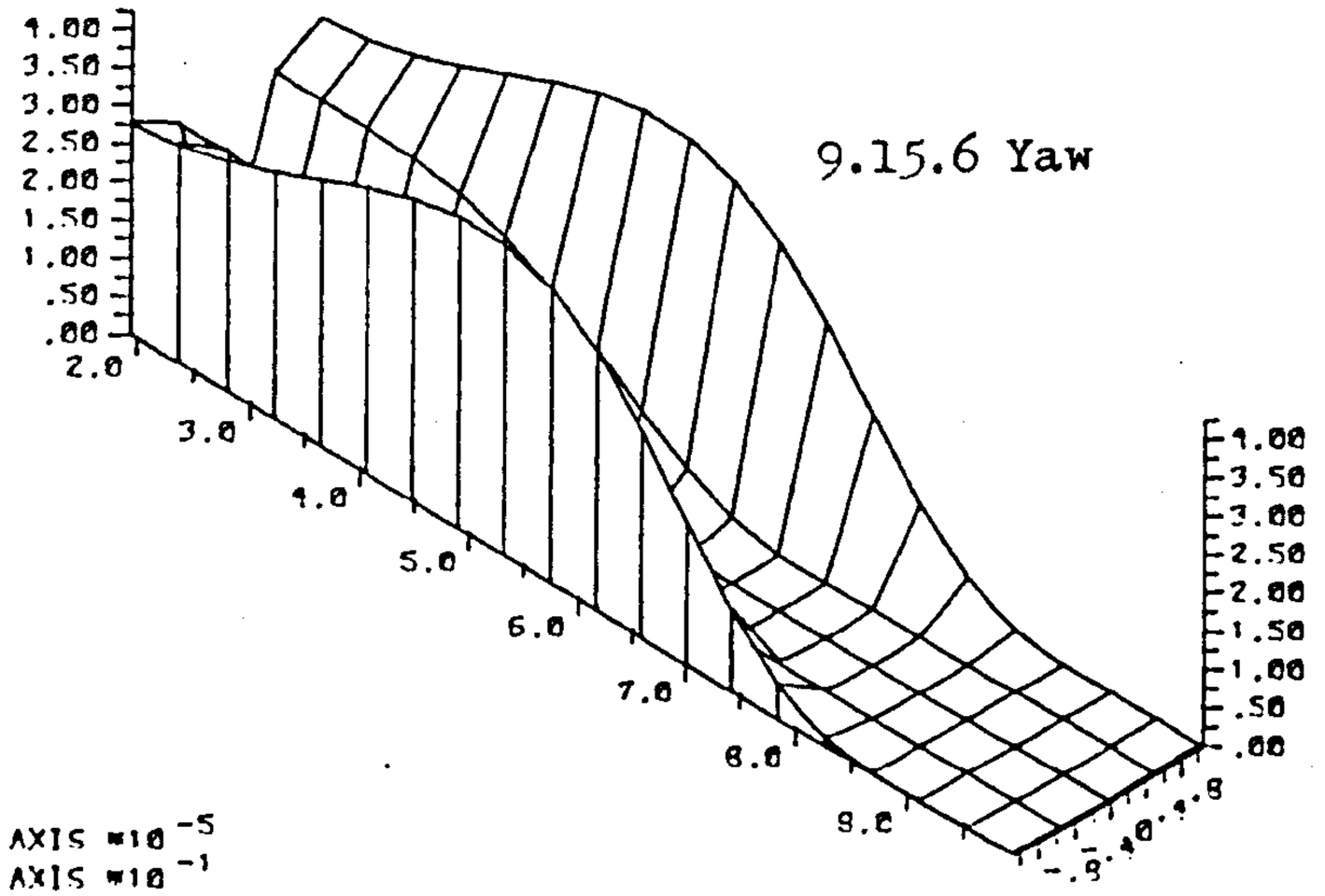

9.15.6 Yaw

SEE PAGE 329

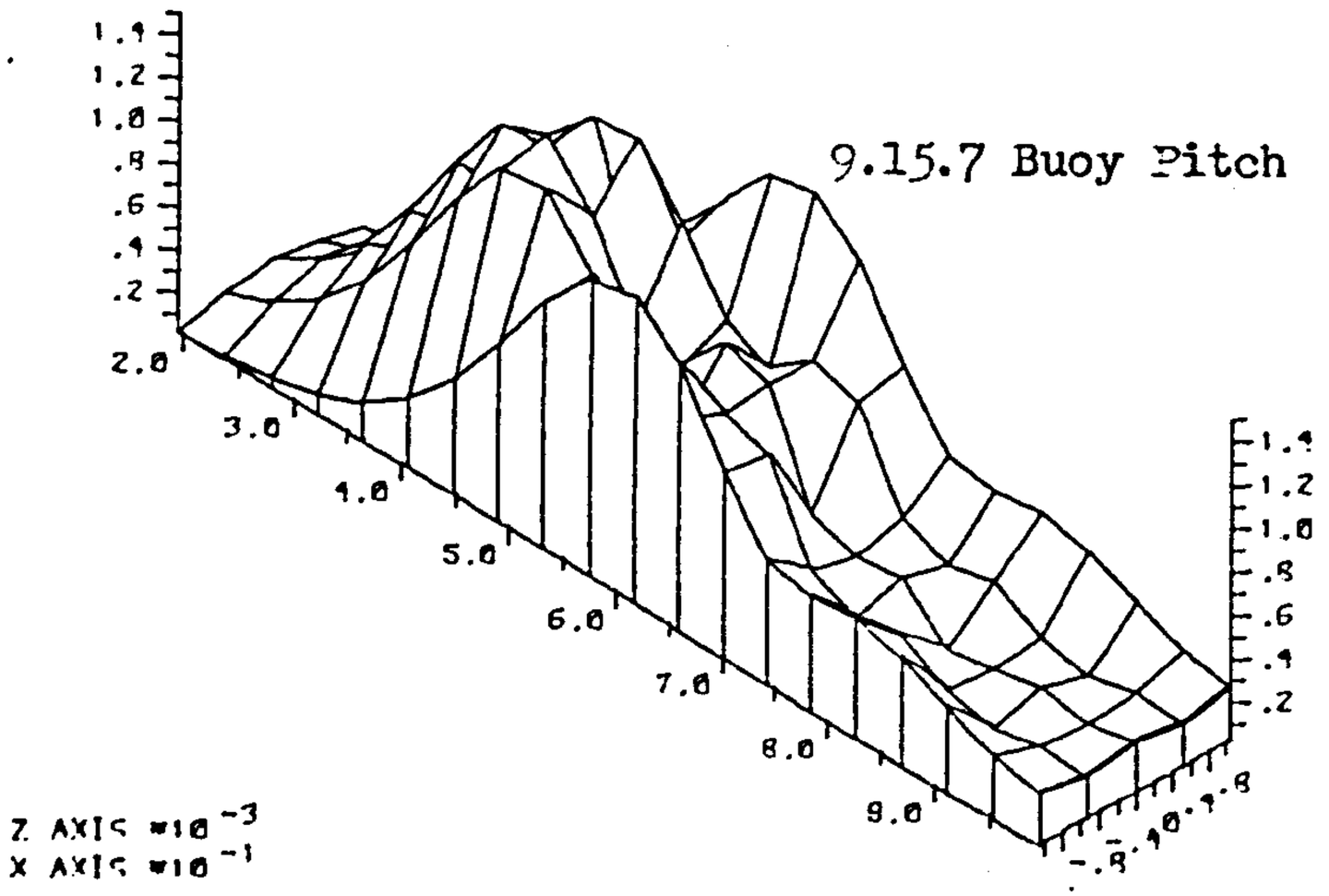

9.15.7 Buoy Pitch

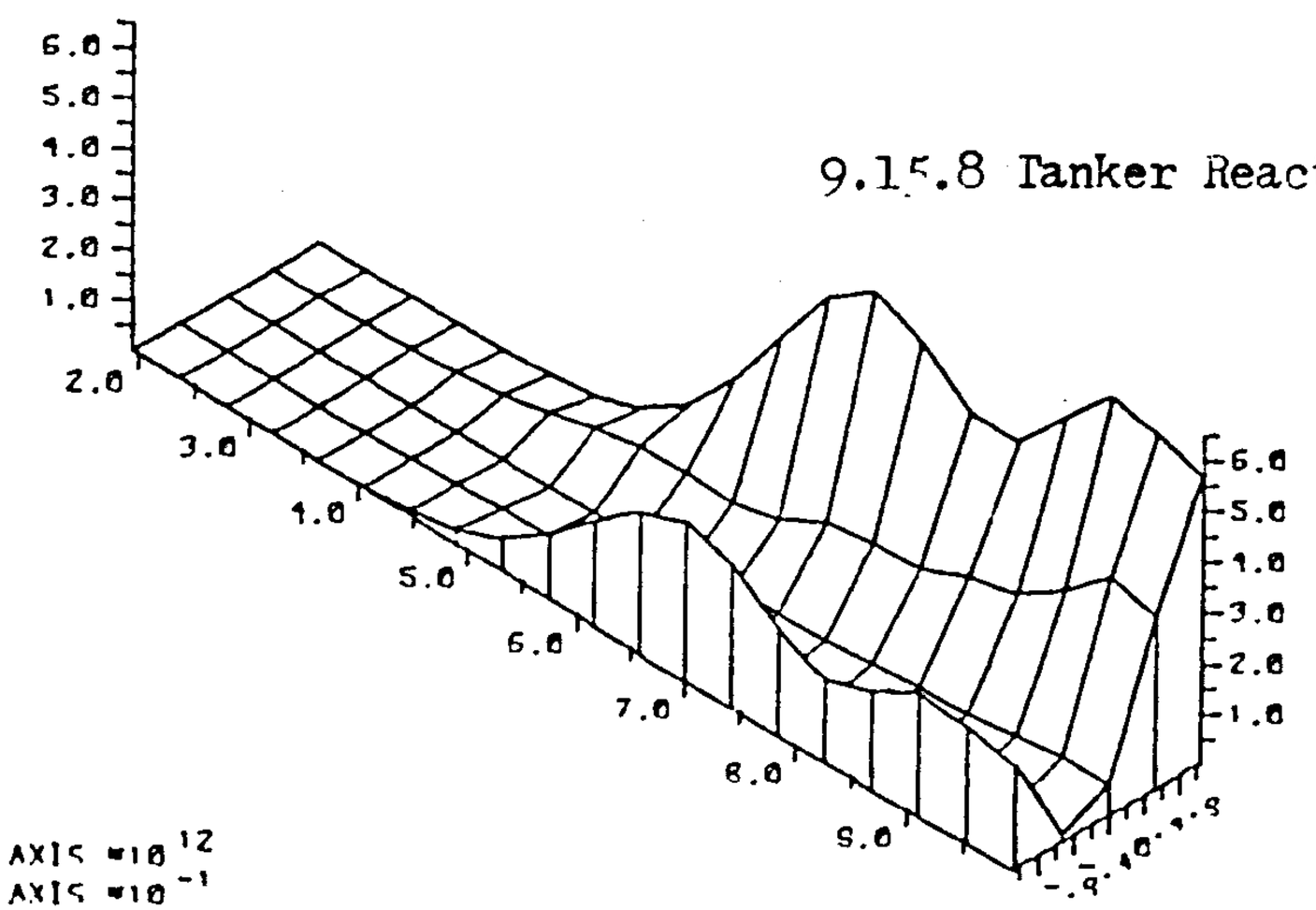

9.15.8 Tanker Reaction P_1

9.15.10 Tanker Reaction S_1

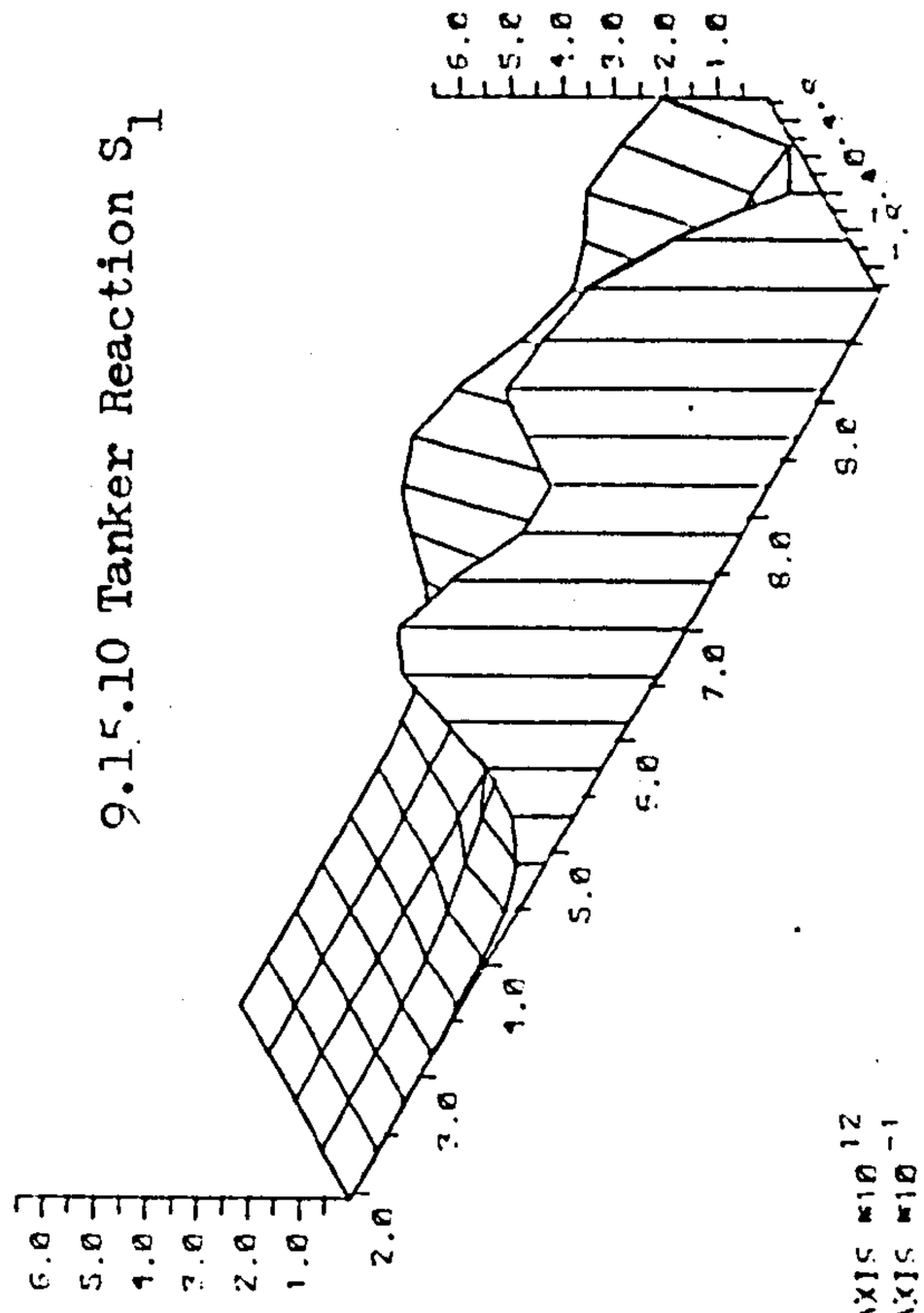

Z AXIS $\times 10^{12}$
X AXIS $\times 10^{-1}$

9.15.12 Tanker Reaction P_2

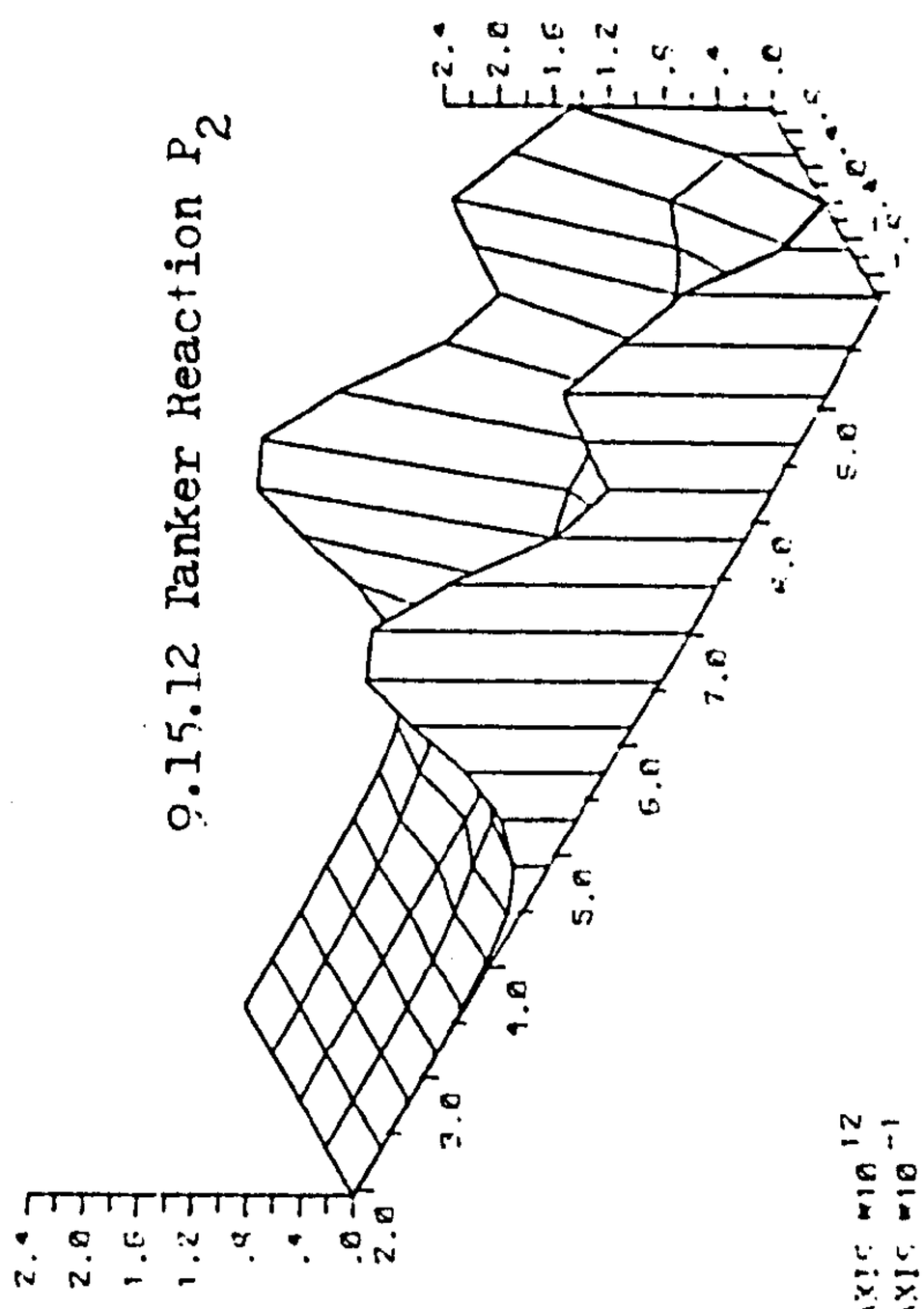

Z AXIS $\times 10^{12}$
X AXIS $\times 10^{-1}$

SEE PAGE 329

9.15.9 Tanker Reaction P_3

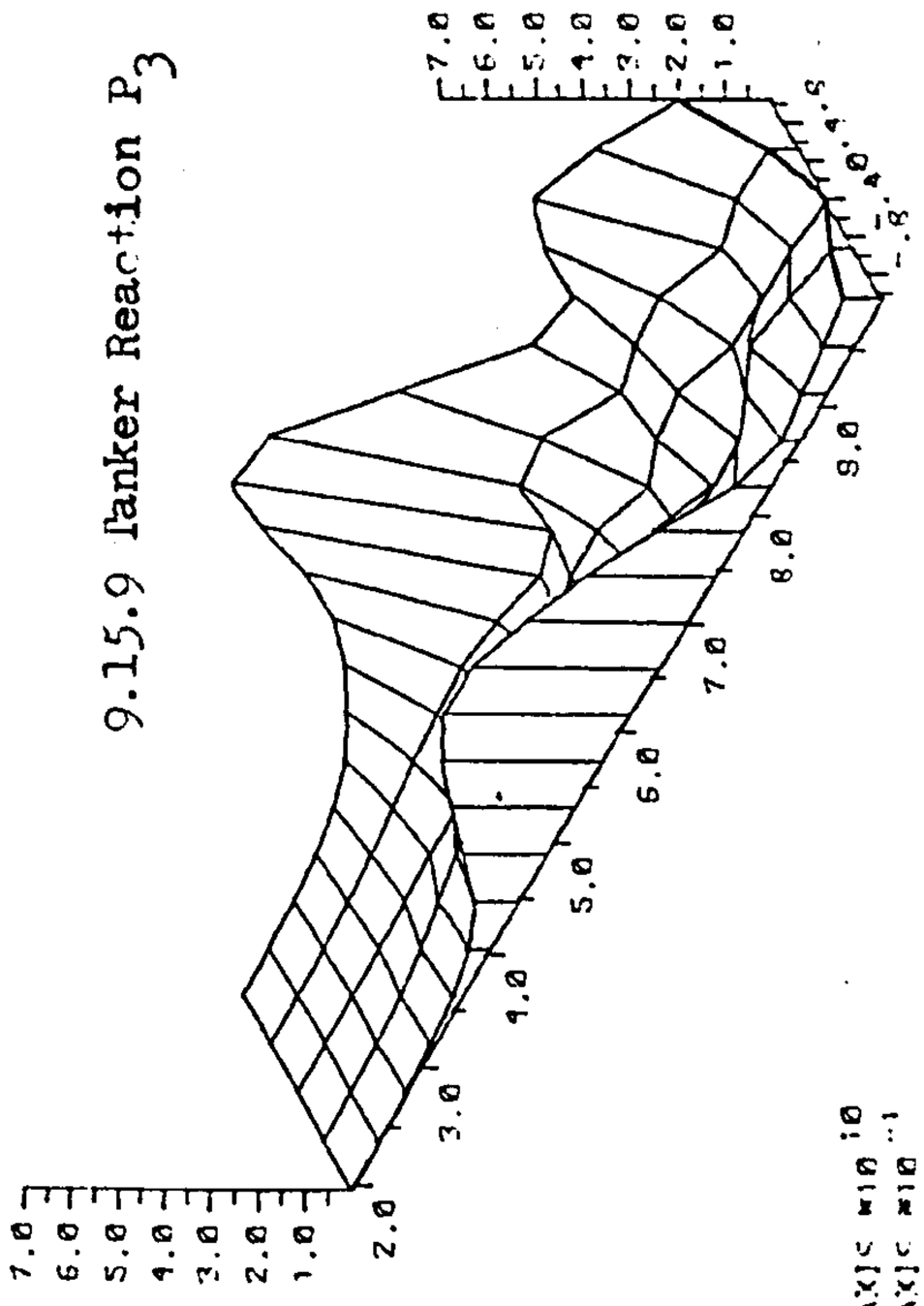

Z AXIS $\times 10^{10}$
X AXIS $\times 10^{-1}$

9.15.11 Tanker Reaction S_3

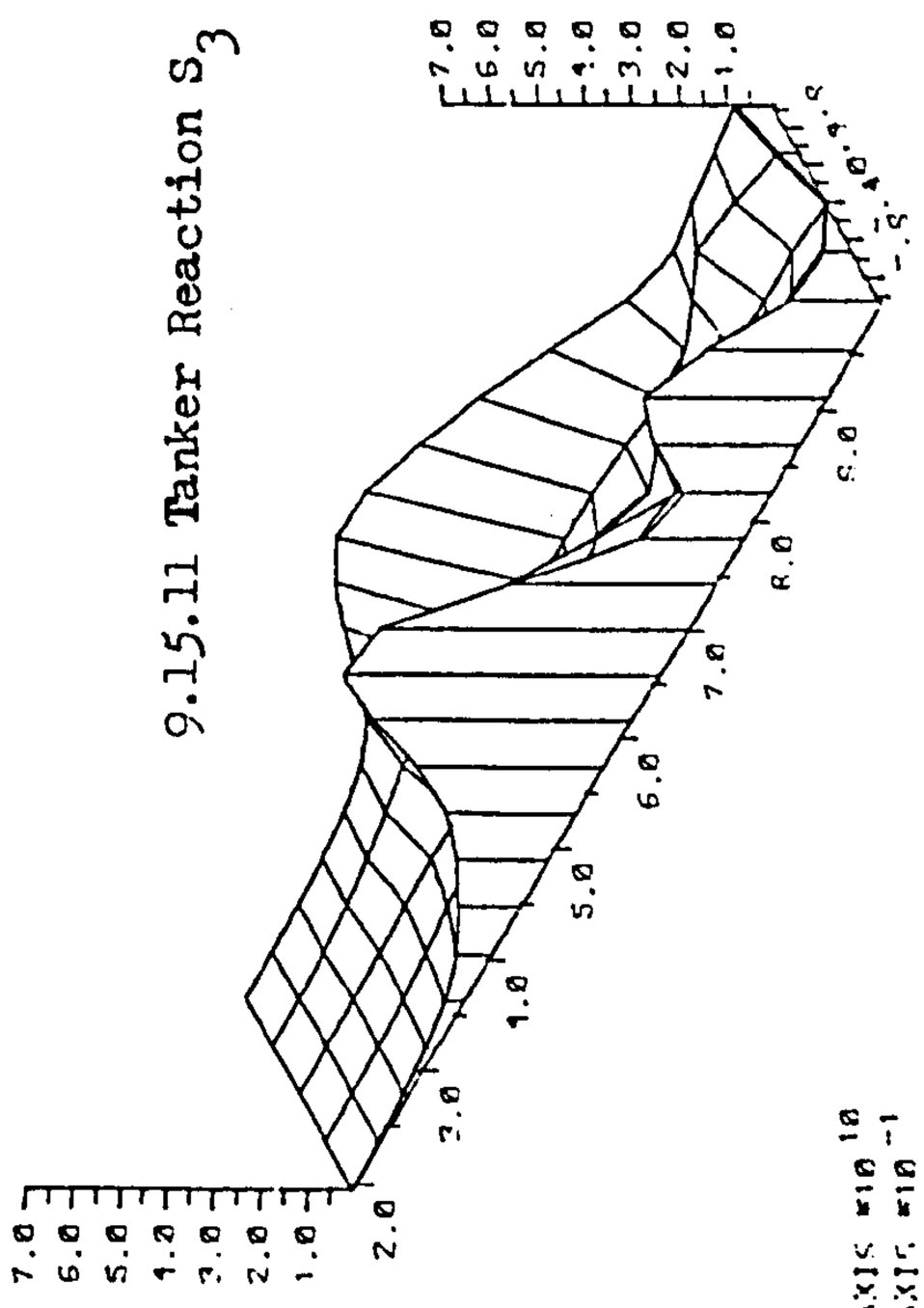

Z AXIS $\times 10^{10}$
X AXIS $\times 10^{-1}$

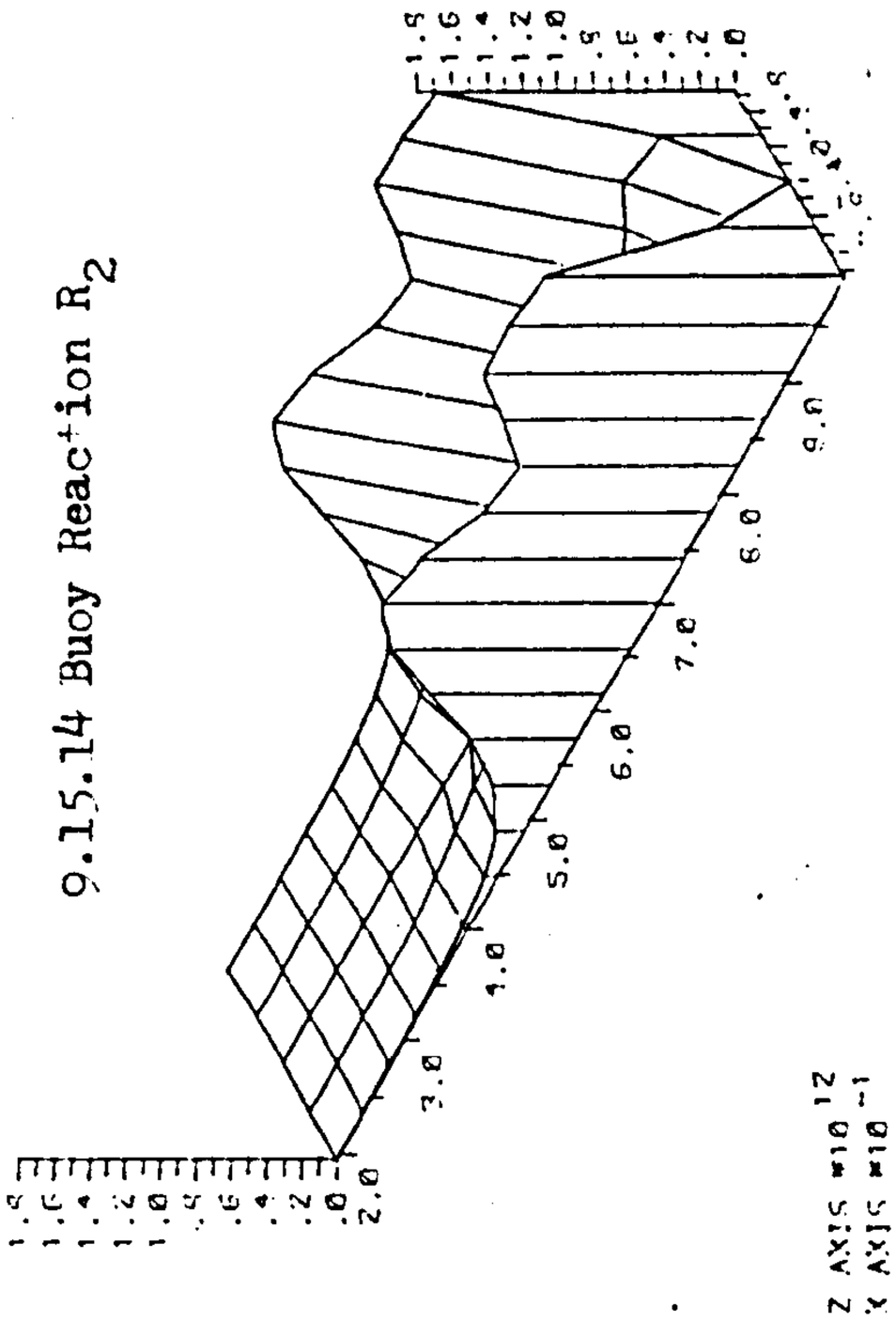
9.15.14 Buoy Reaction R_2
Z AXIS =10^12
X AXIS =10^-1

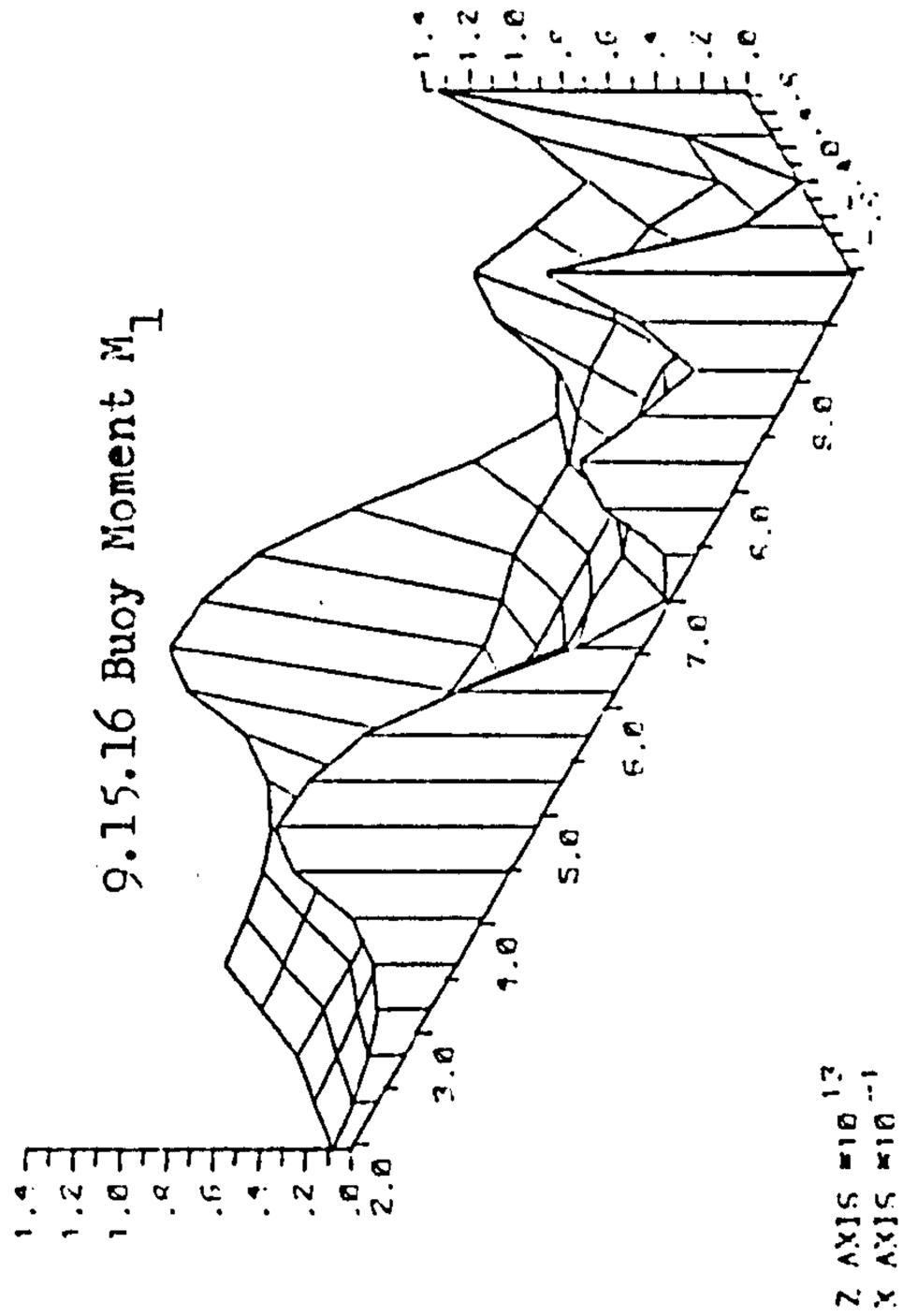
9.15.16 Buoy Moment M_1
Z AXIS =10^12
X AXIS =10^-1

SEE PAGE 329

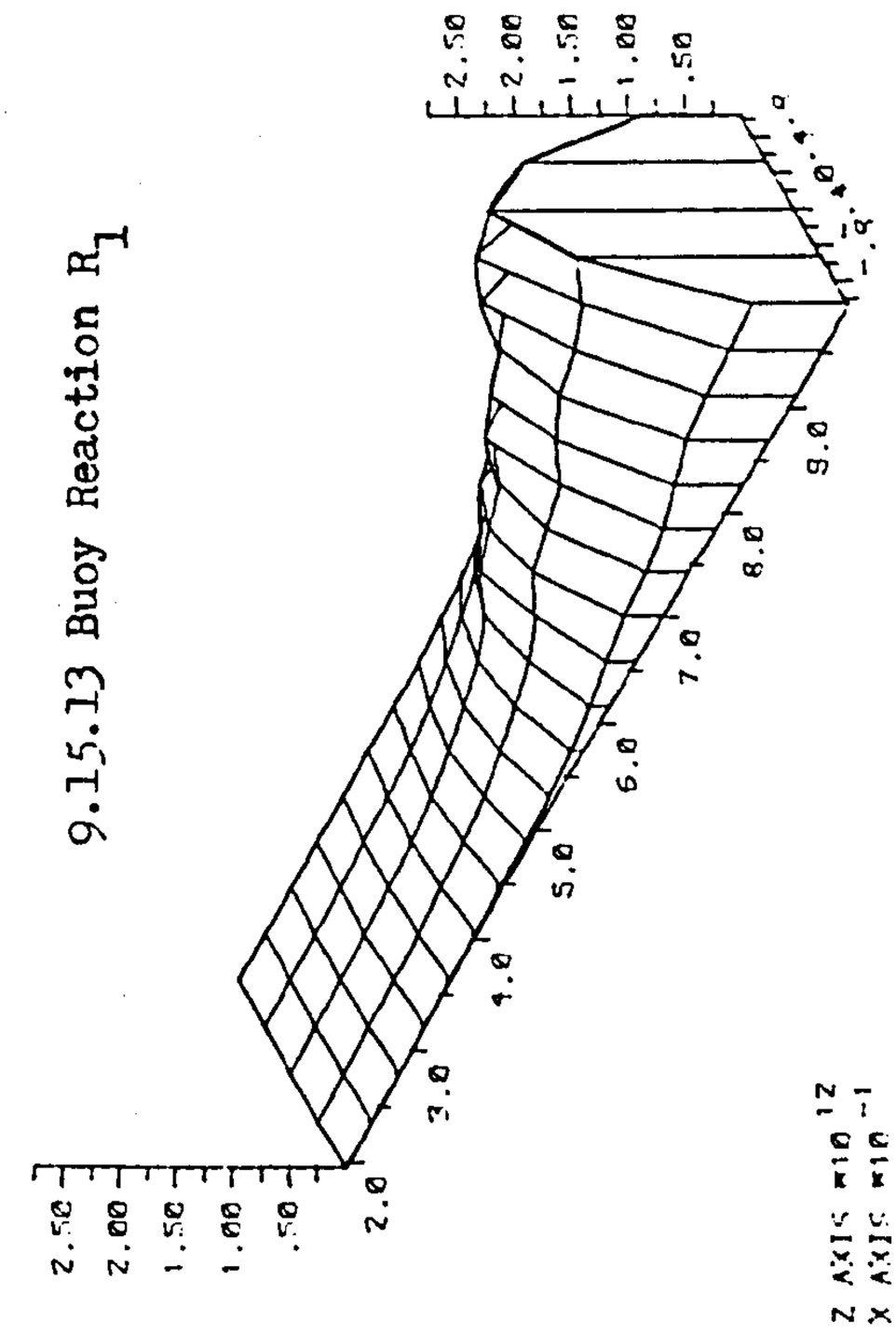
9.15.13 Buoy Reaction R_1
Z AXIS =10^12
X AXIS =10^-1

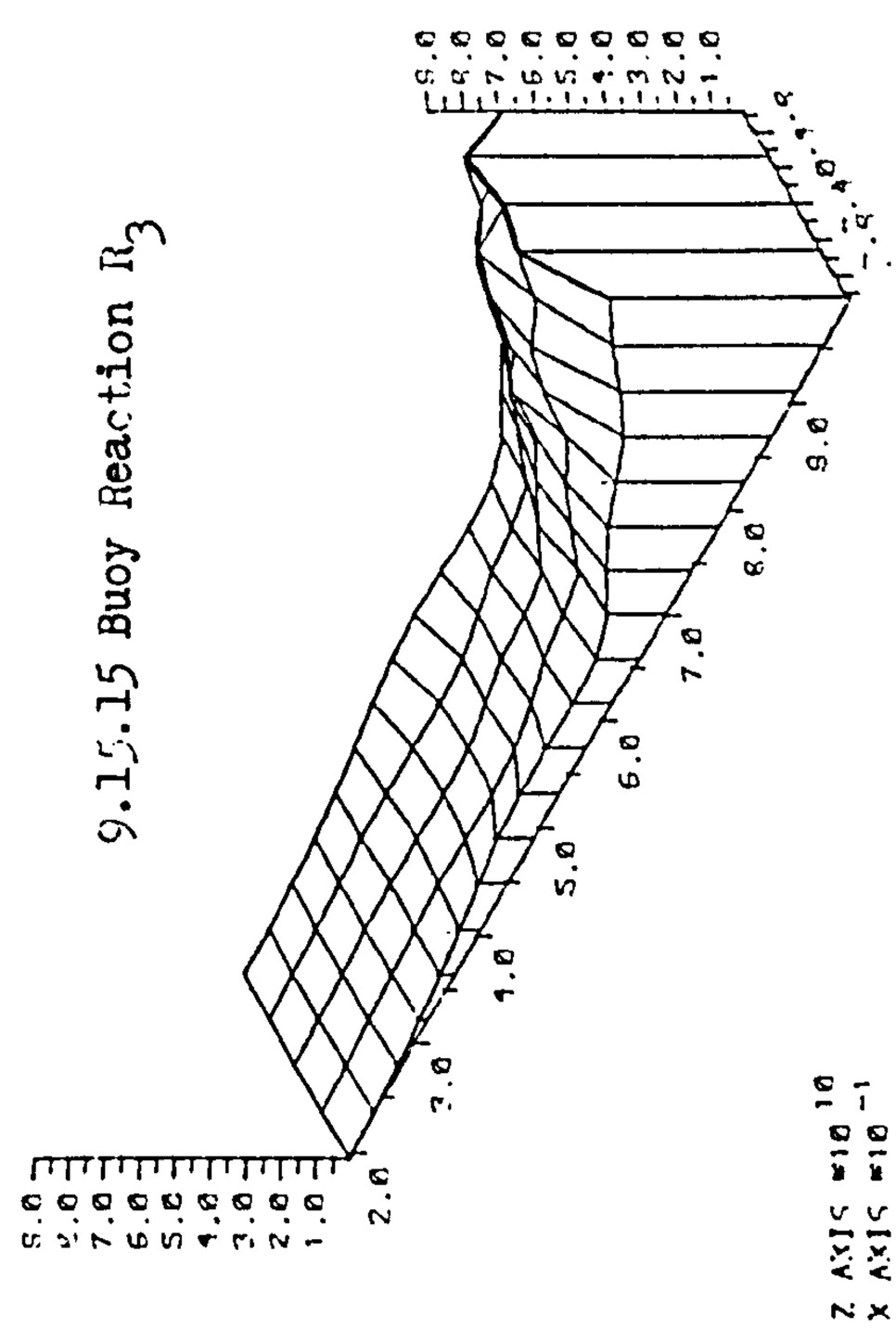
9.15.15 Buoy Reaction R_3
Z AXIS =10^10
X AXIS =10^-1

SEE PAGE 329

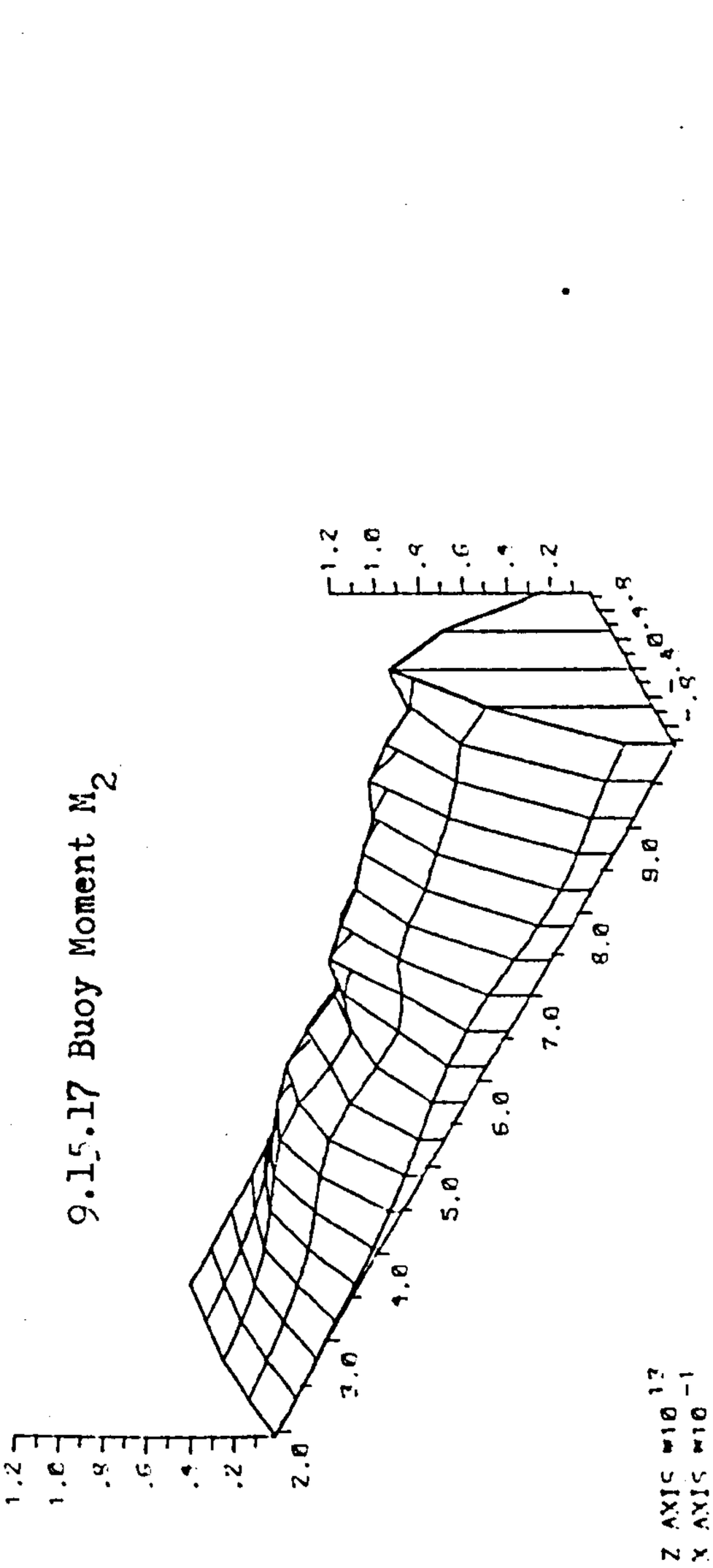
9.15.17 Buoy Moment M_2
1.2
1.0
.8
.6
.4
.2
2.0
3.0
4.0
5.0
6.0
7.0
8.0
9.0
Z AXIS *10 17
X AXIS *10 -1

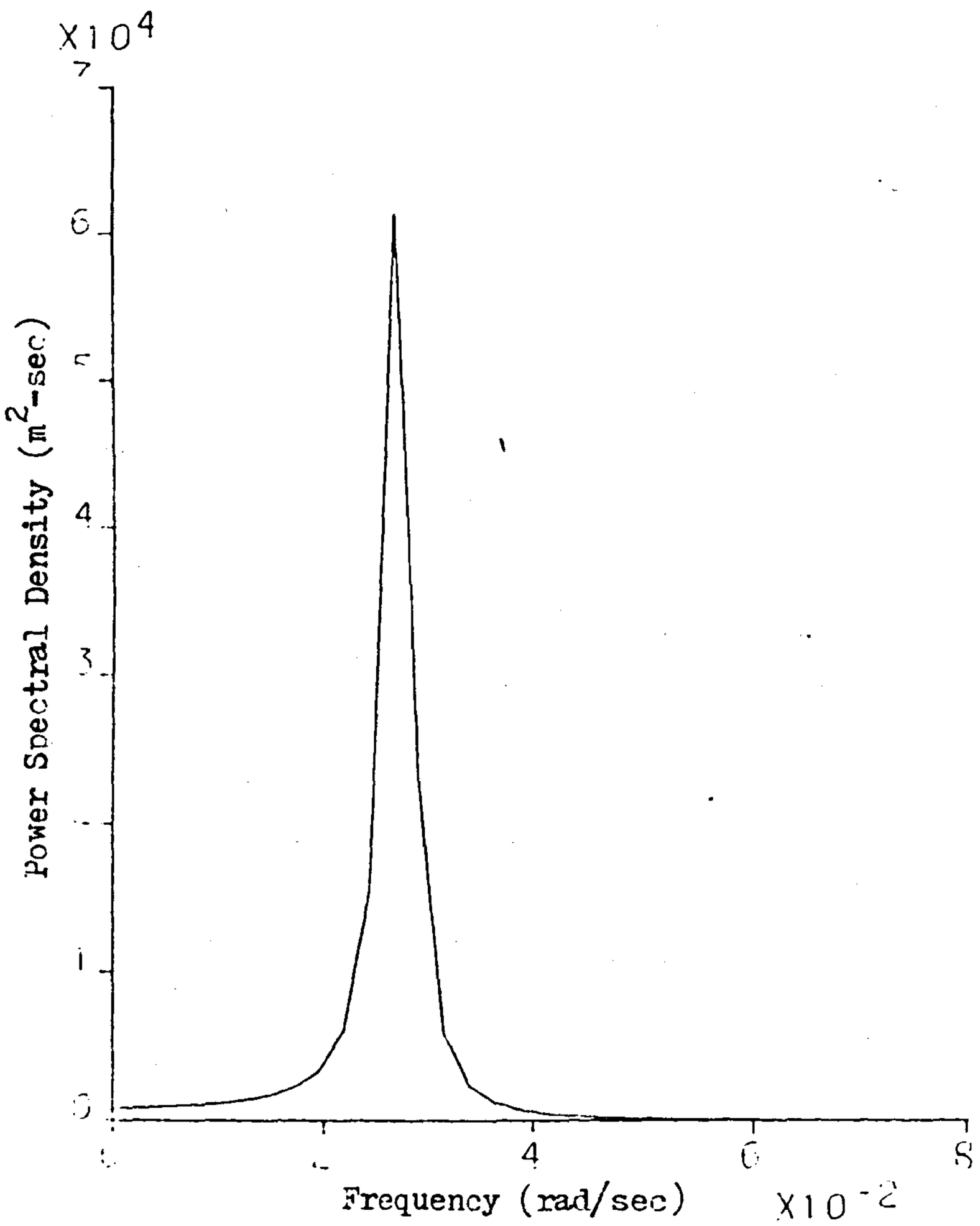

FIG. 9.16 SPECTRUM OF SECOND ORDER SURGE
H_S= 15M

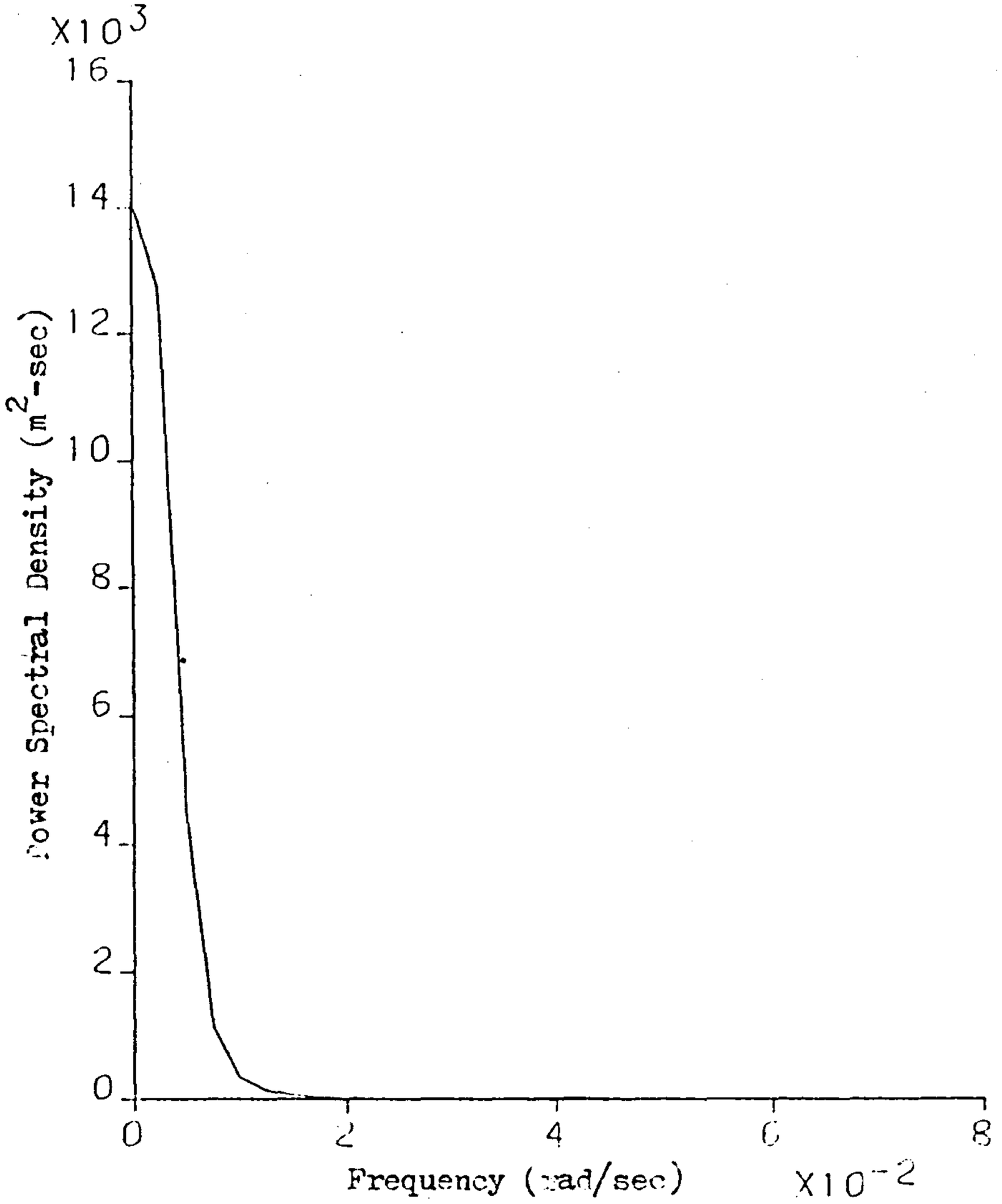

FIG. 9.17 SPECTRUM OF SECOND ORDER SWAY
H_S= 15M

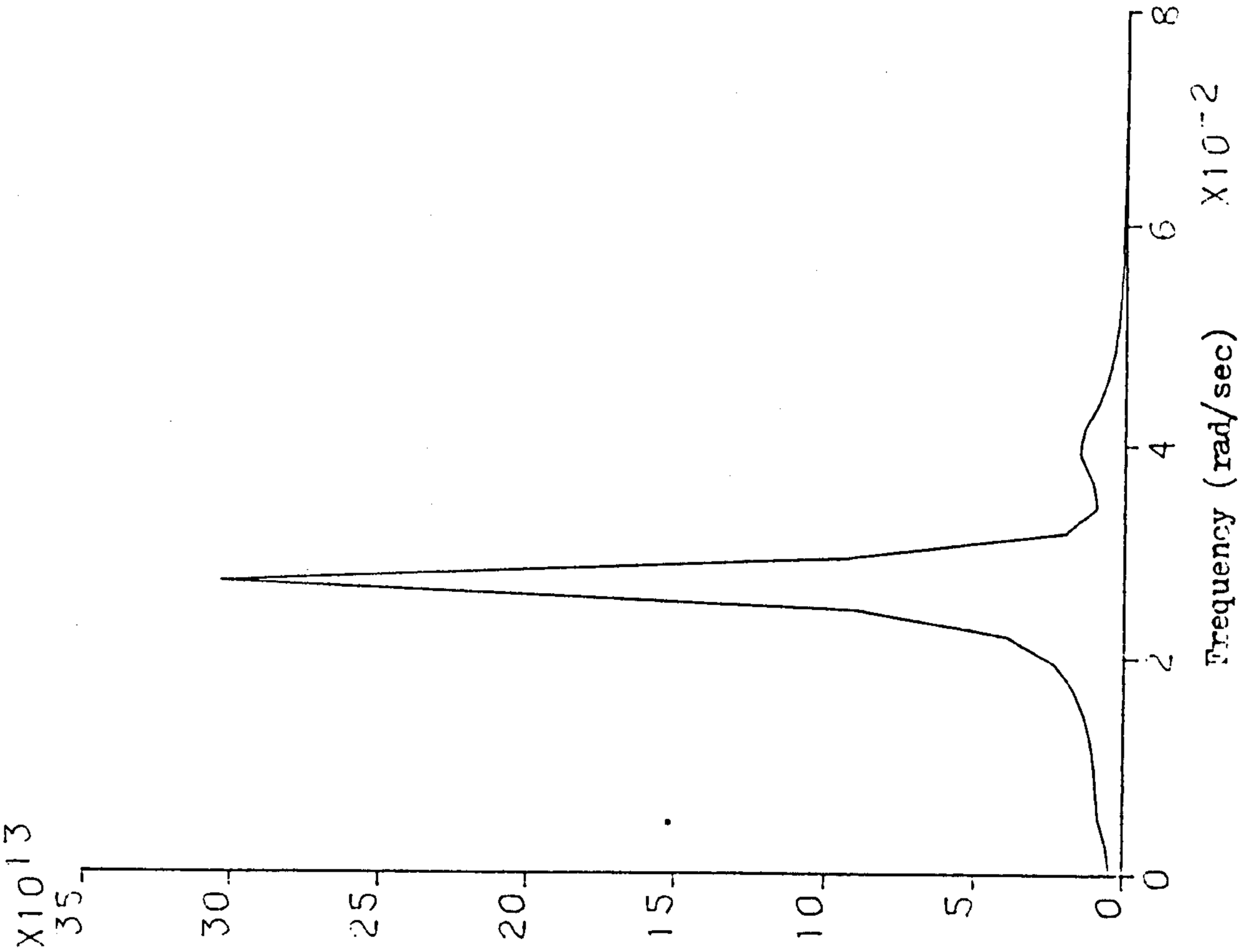

FIG. 9.16 SPECTRUM OF SECOND ORDER YAW REACTION F_1, H_S= 15M

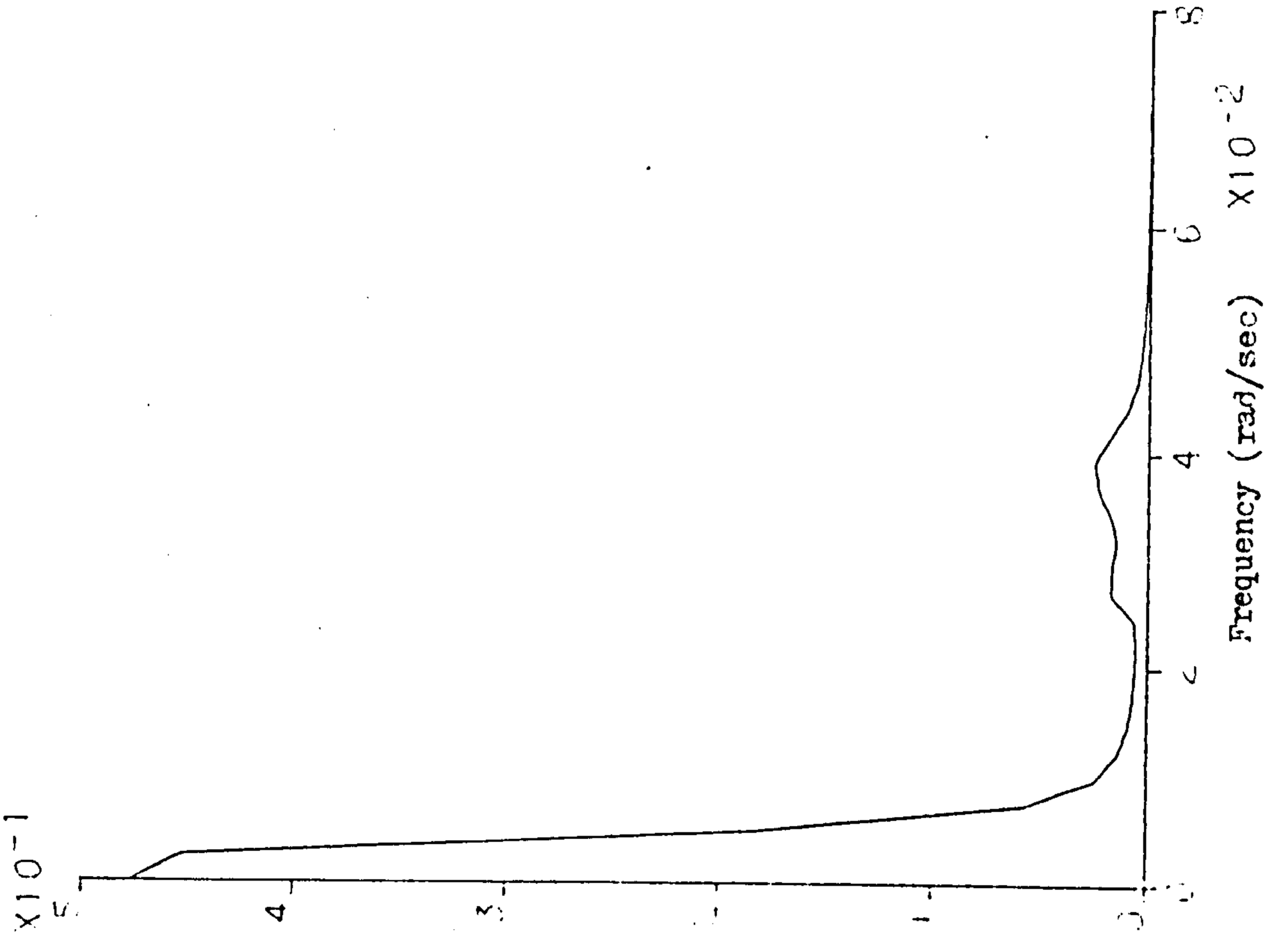

FIG. 9.18 SPECTRUM OF SECOND ORDER YAW H_S= 15M

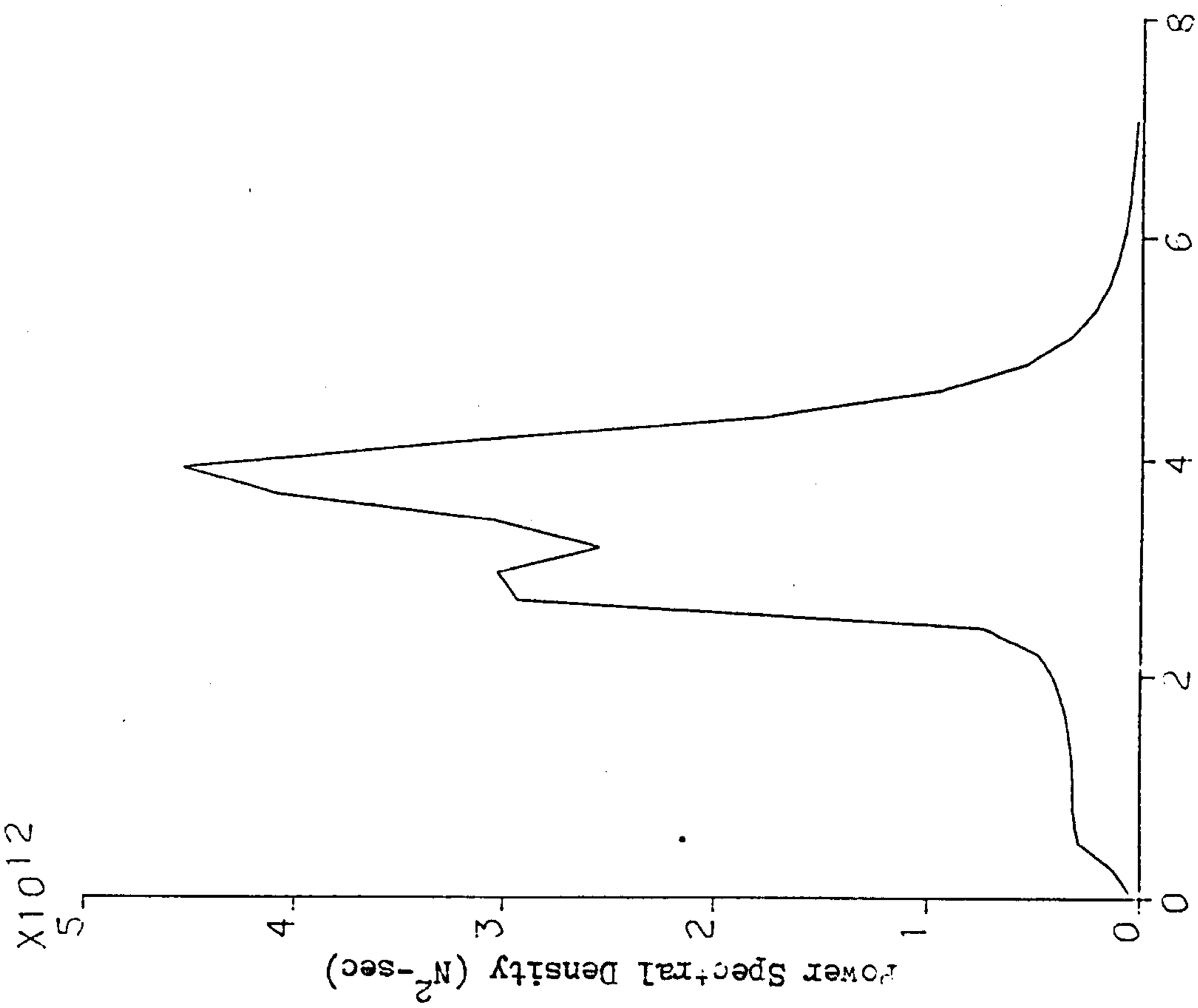

FIG. 9.21 SPECTRUM OF SECOND ORDER TANKER
REACTION P_2, H_S= 15M

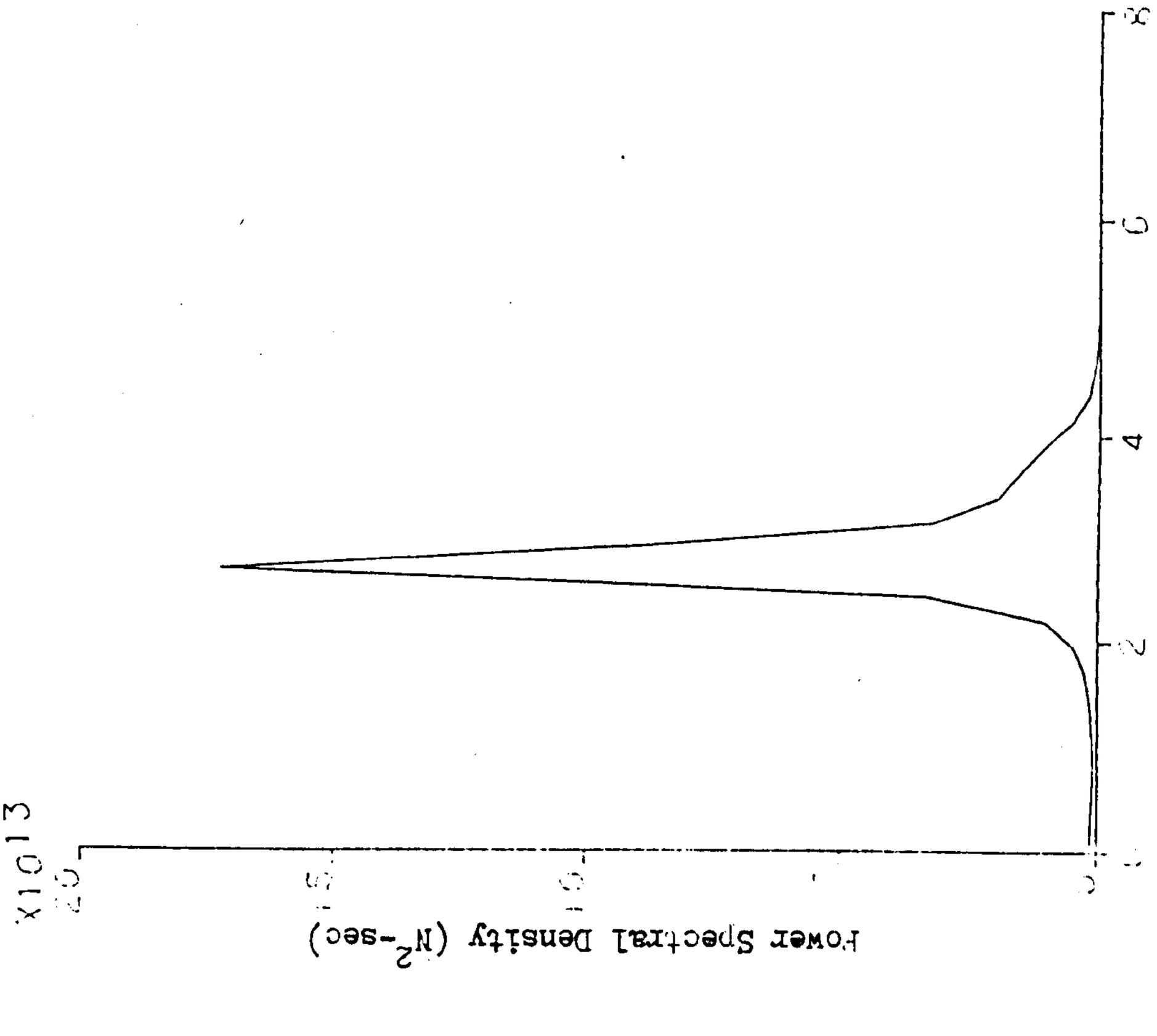

FIG. 9.20 SPECTRUM OF SECOND ORDER TANKER
REACTION S_1, H_S= 15M

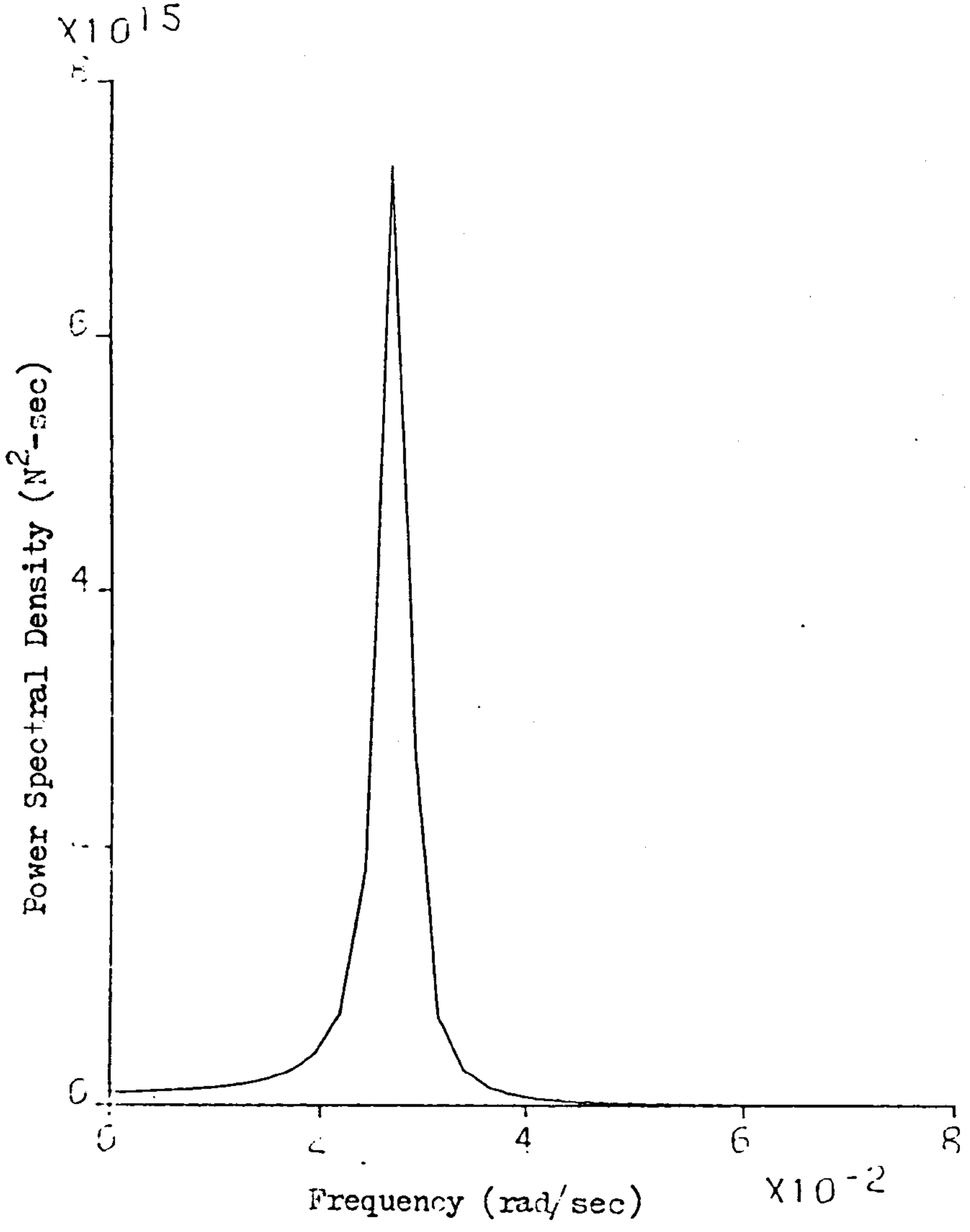

FIG. 9.22 SPECTRUM OF SECOND ORDER BUOY REACTION R_1, H_S= 15M

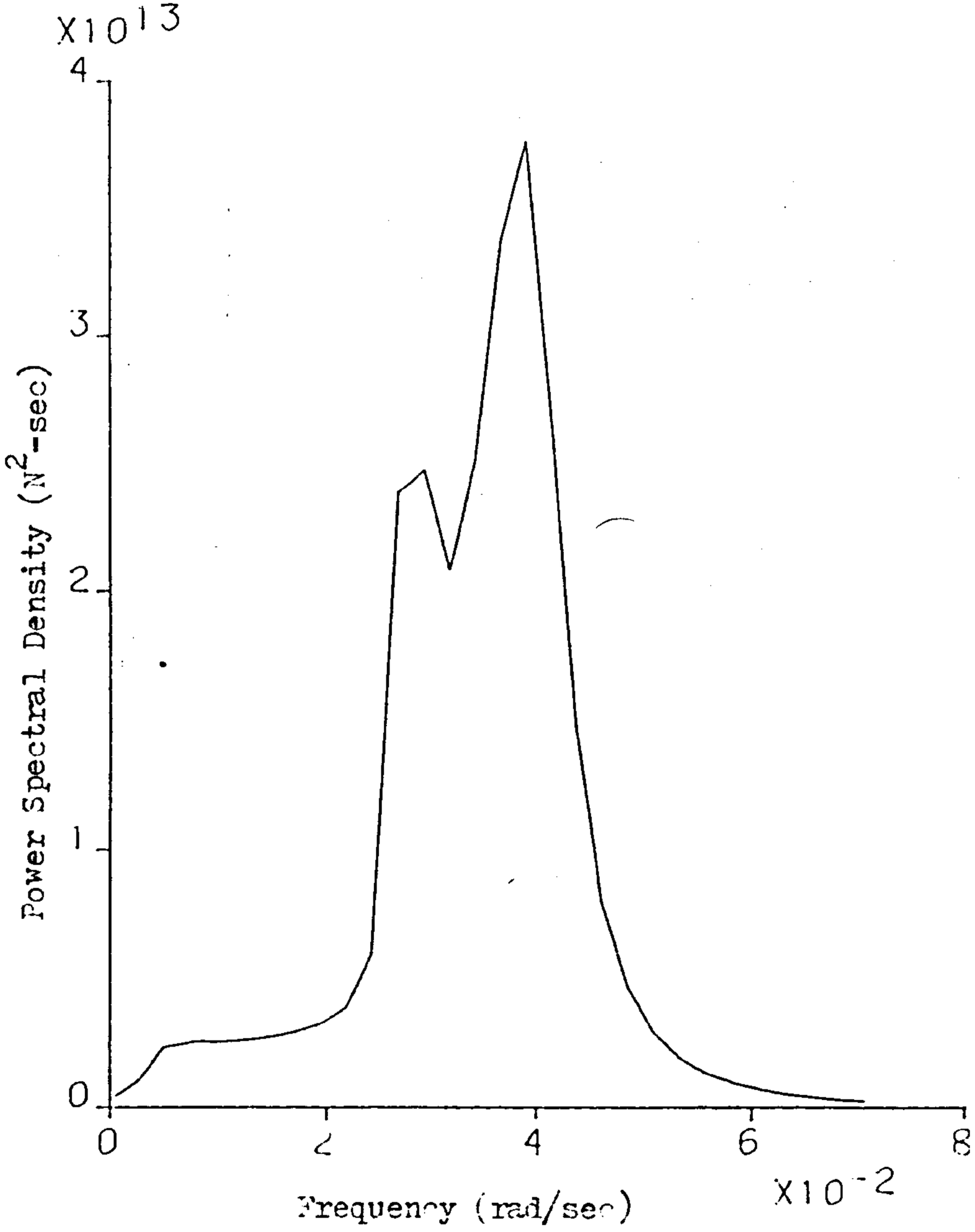

FIG. 9.23 SPECTRUM OF SECOND ORDER BUOY REACTION R_2, H_S=15M

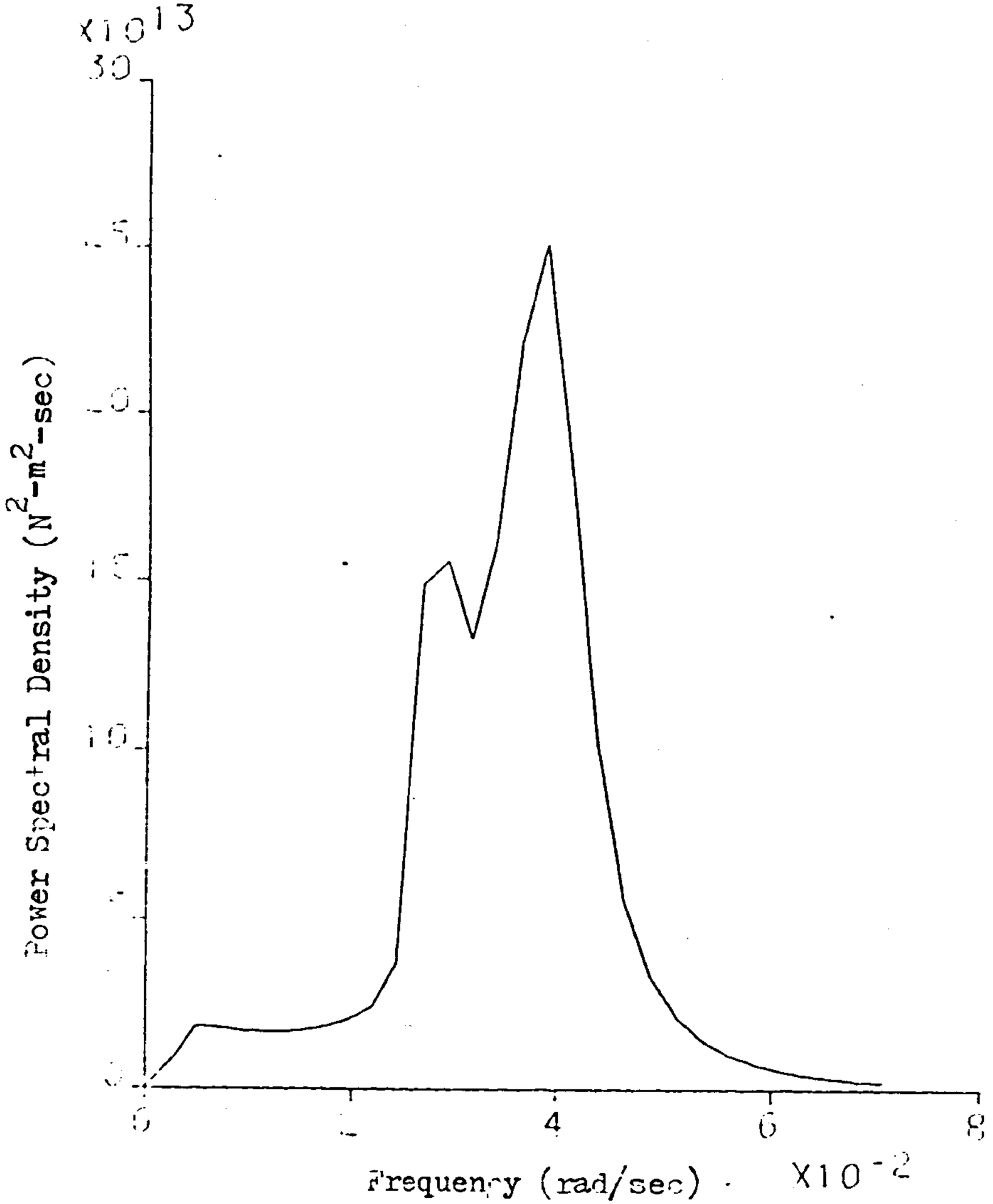

FIG. 9.24 SPECTRUM OF SECOND ORDER BUOY MOMENT M_1, H_S= 15M

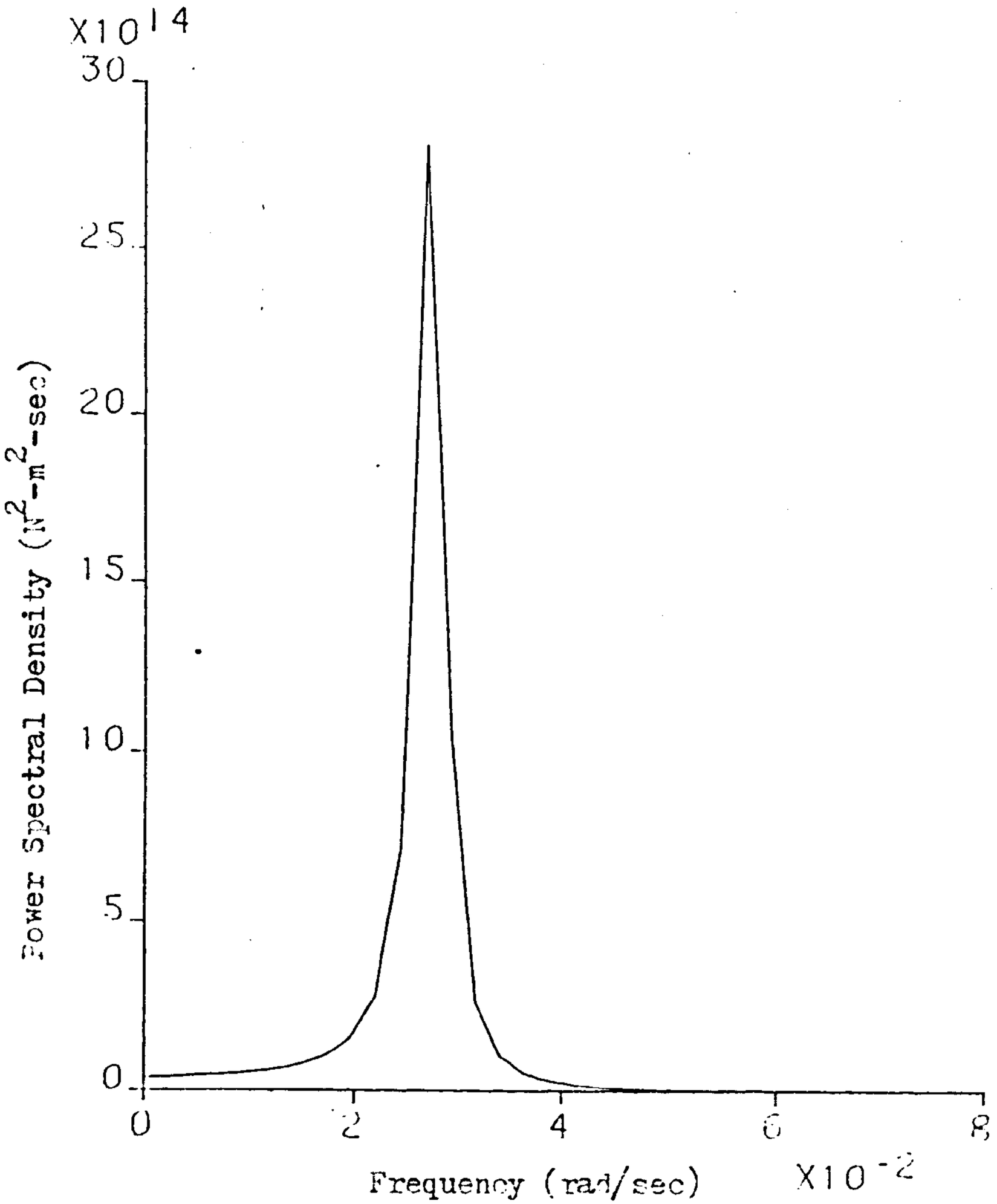

FIG. 9.25 SPECTRUM OF SECOND ORDER BUOY MOMENT M_2. H_S=15M

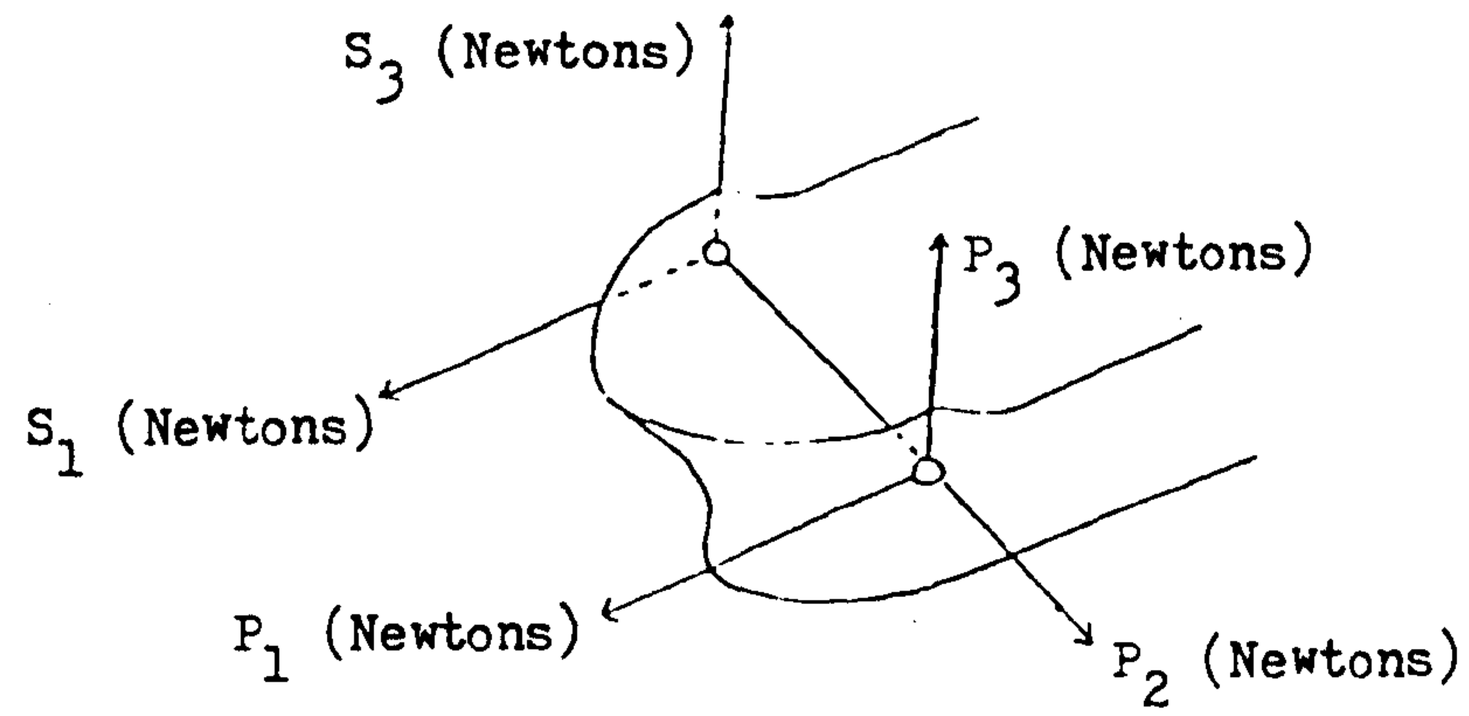

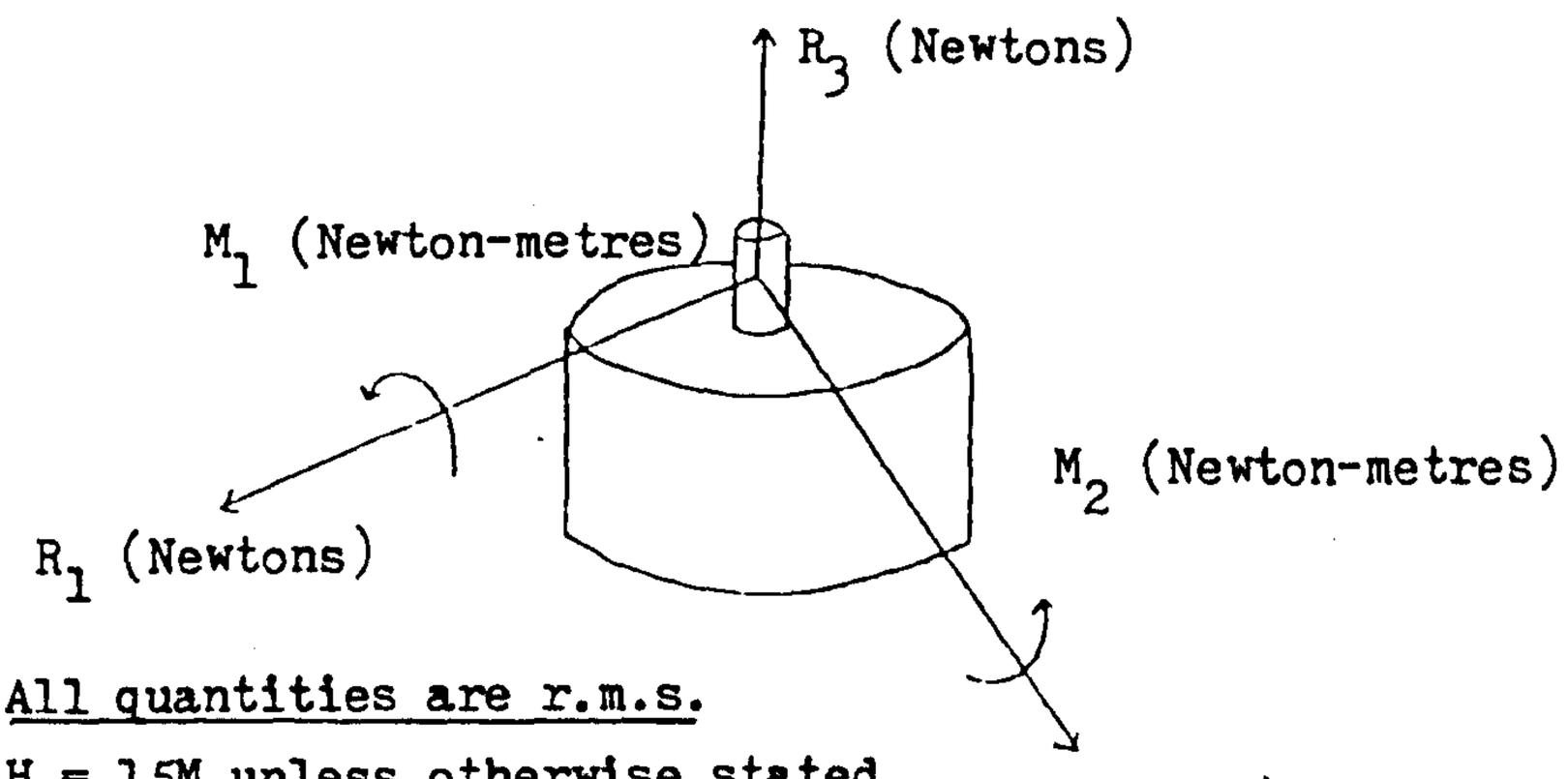

Note: (1) All quantities are r.m.s.

(2) H_S = 15M unless otherwise stated

(3) Details given in (9.4)-(9.6)

(4) 0.1234E+03 = 0.1234×10^3

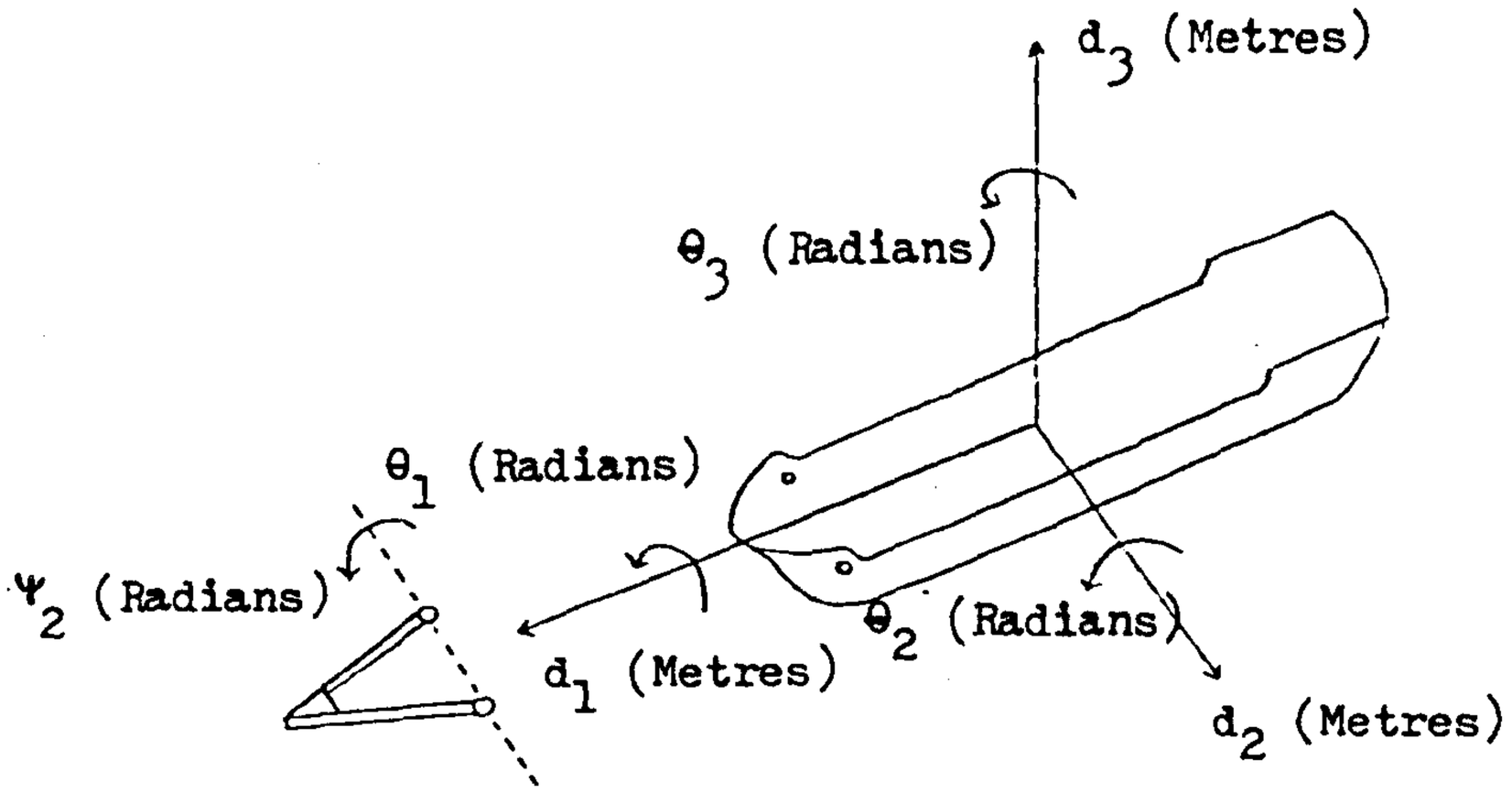

FIG. 9.26 KEY FOR THE FOLLOWING FIGURES

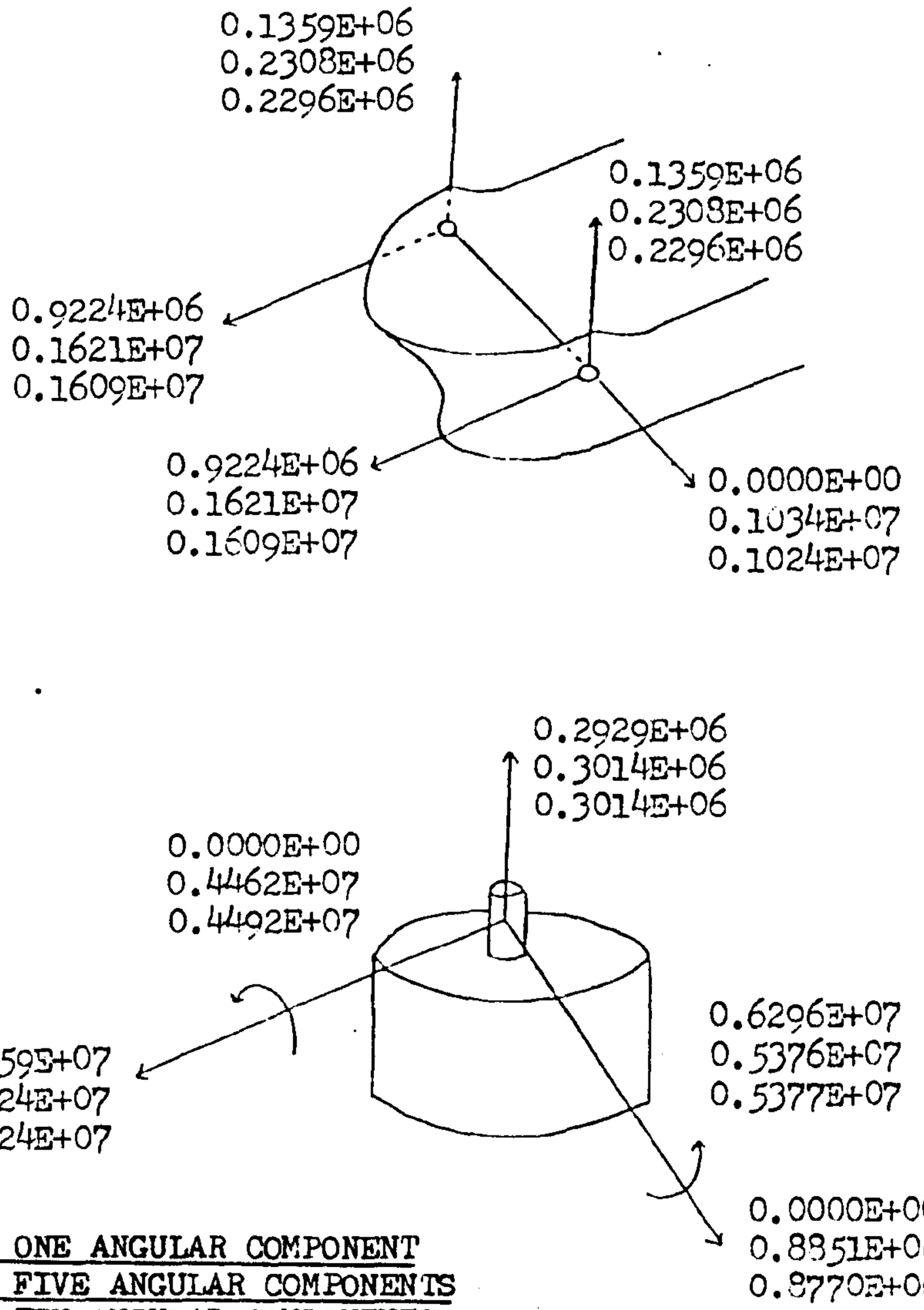

UPPER - ONE ANGULAR COMPONENT
MIDDLE - FIVE ANGULAR COMPONENTS
LOWER - TEN ANGULAR COMPONENTS

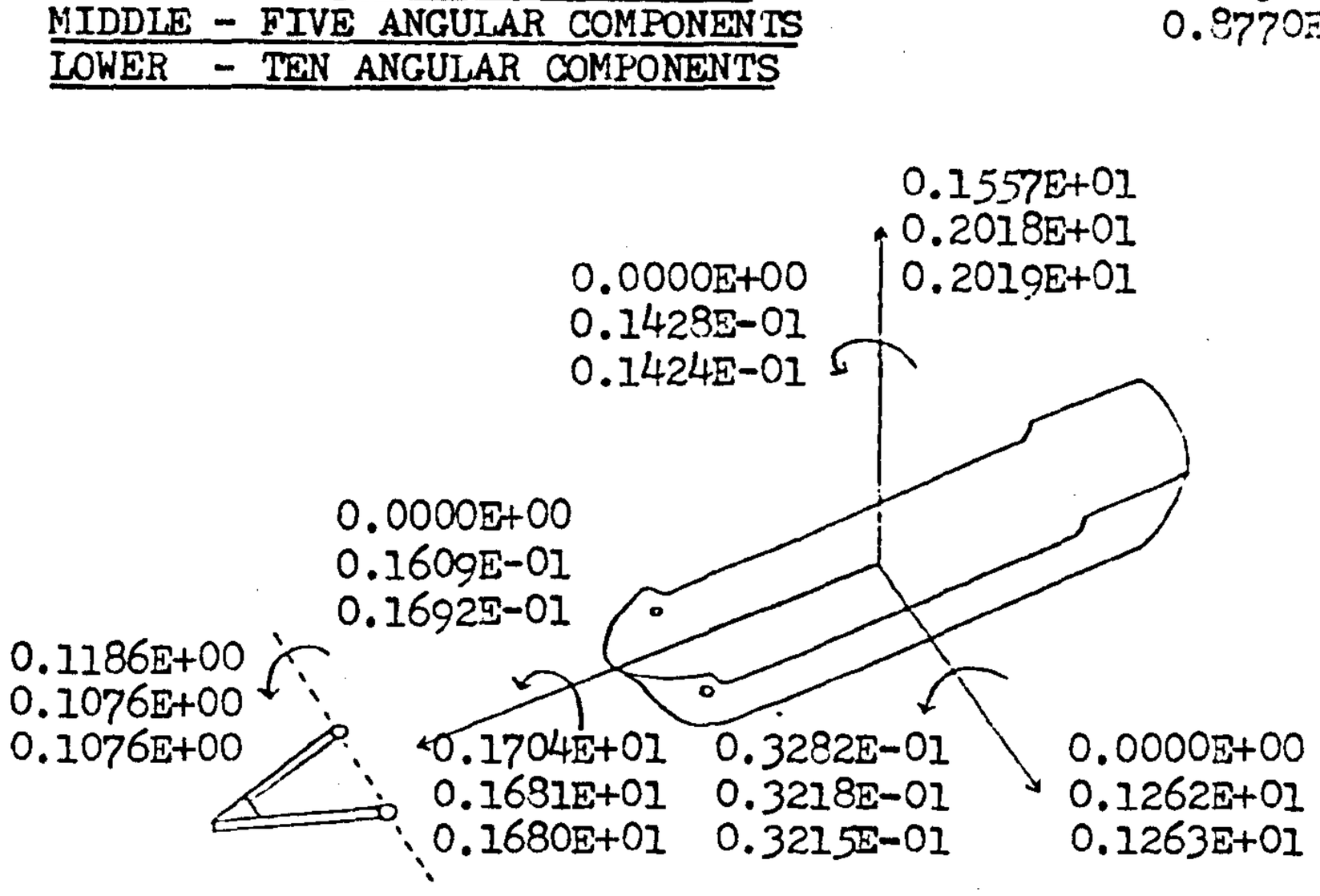

FIG. 9.27 THE EFFECT OF THE SPREADING FUNCTION ON THE FIRST ORDER RESPONSE - HEAD SEAS
(FOR KEY SEE FIG. 9.26)

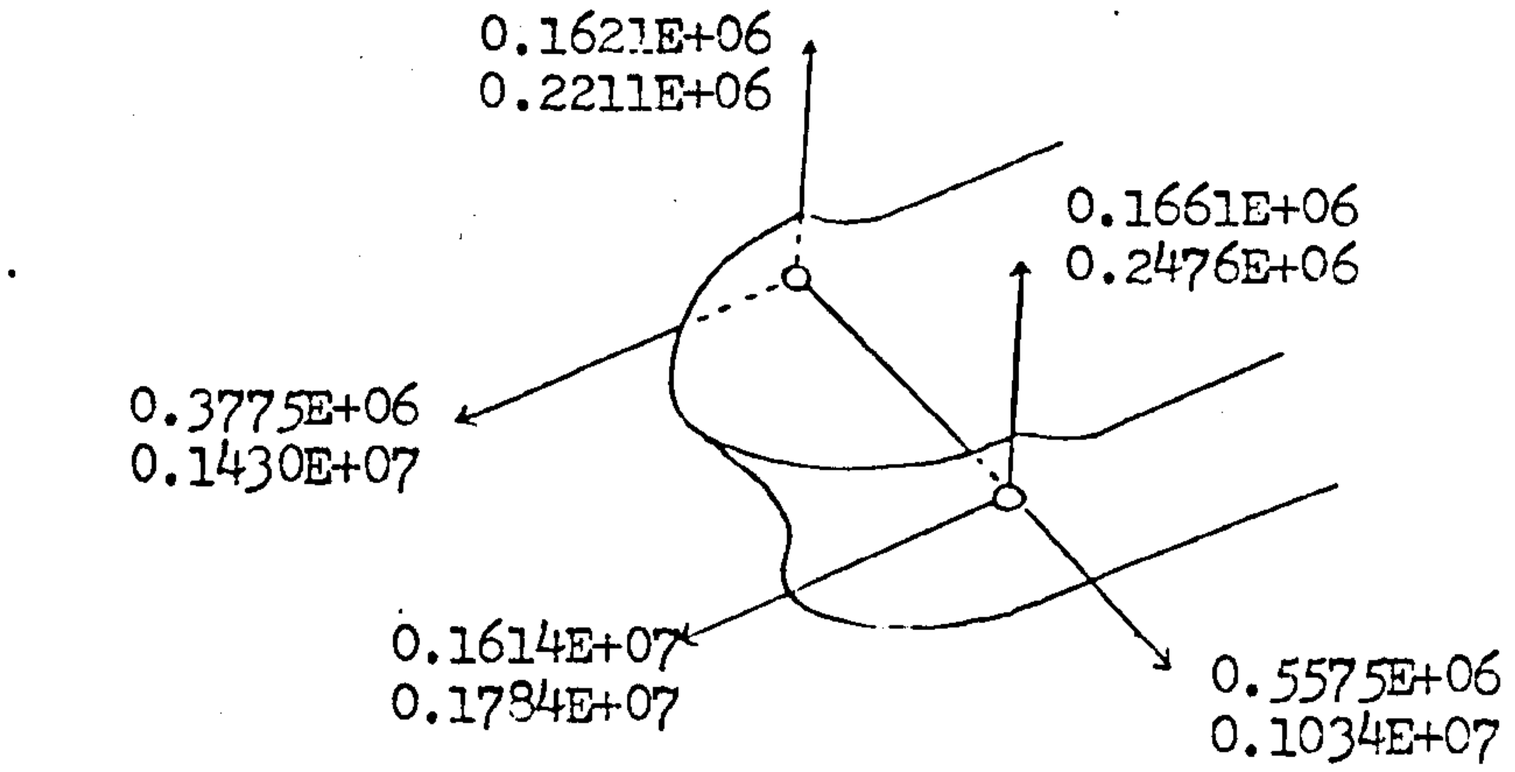

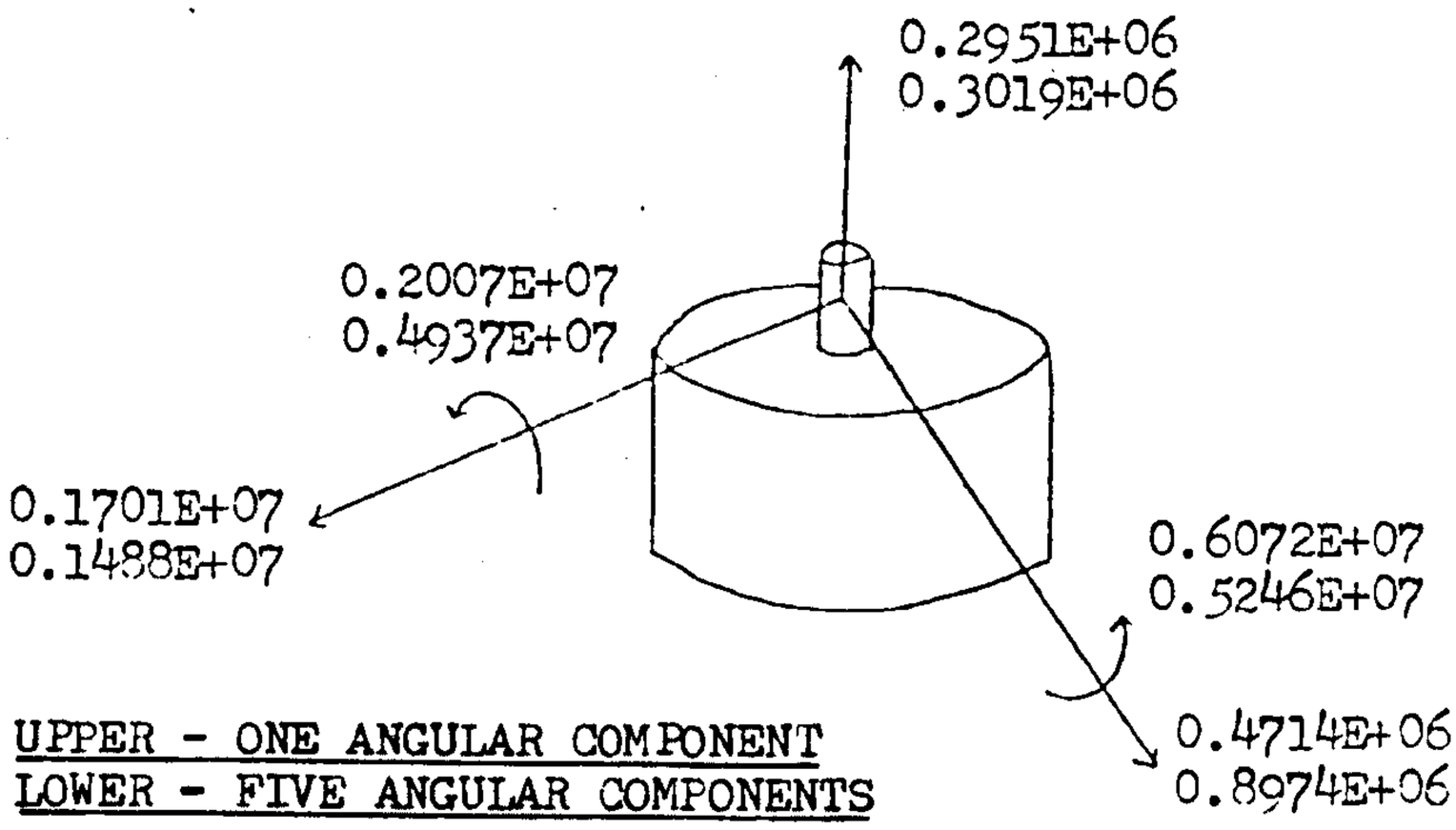

UPPER - ONE ANGULAR COMPONENT
LOWER - FIVE ANGULAR COMPONENTS

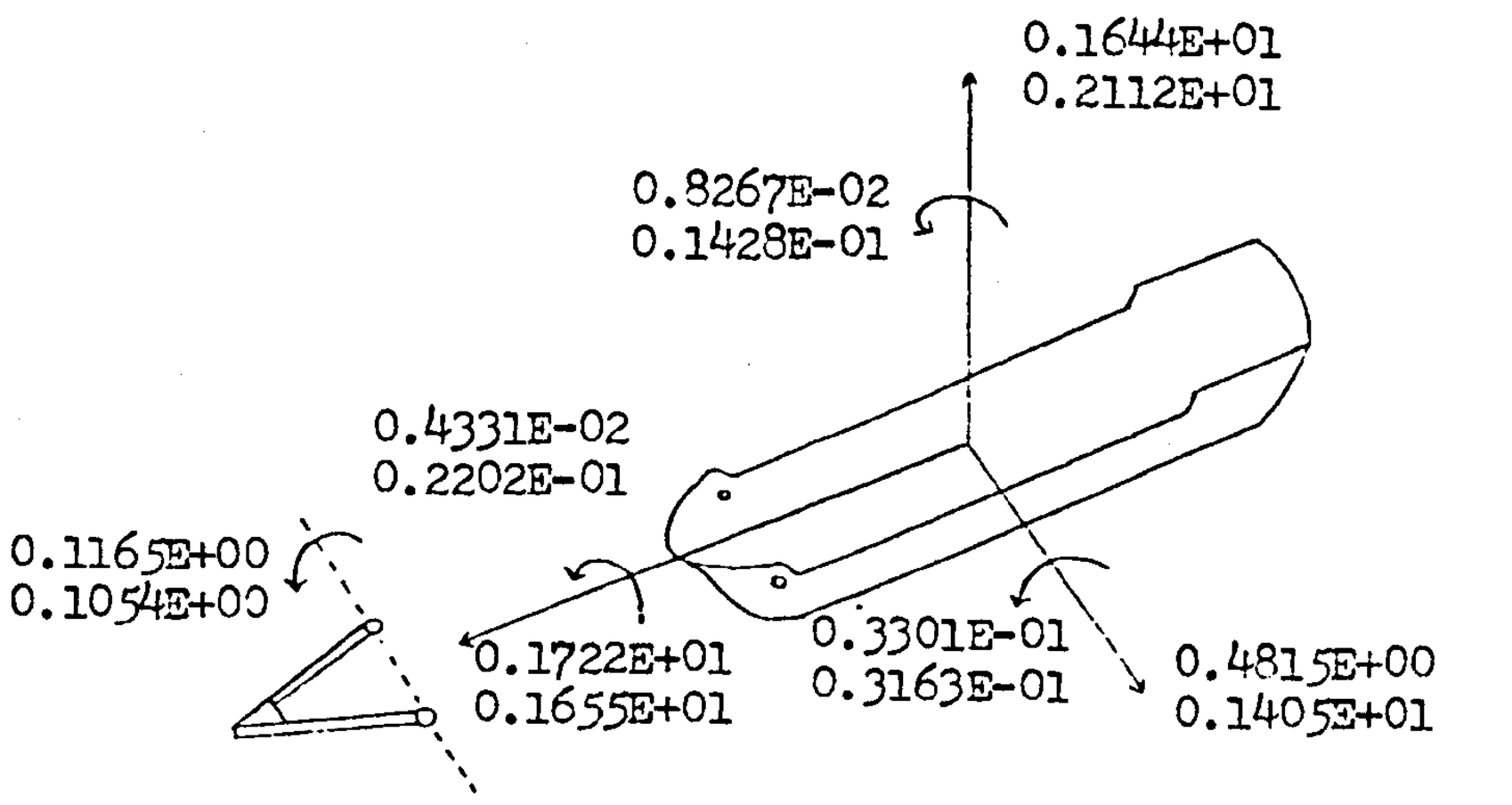

FIG. 9.28 THE EFFECT OF THE SPREADING FUNCTION ON THE FIRST ORDER RESPONSE - 15 DEG. SEAS
(FOR KEY SEE FIG. 9.26)

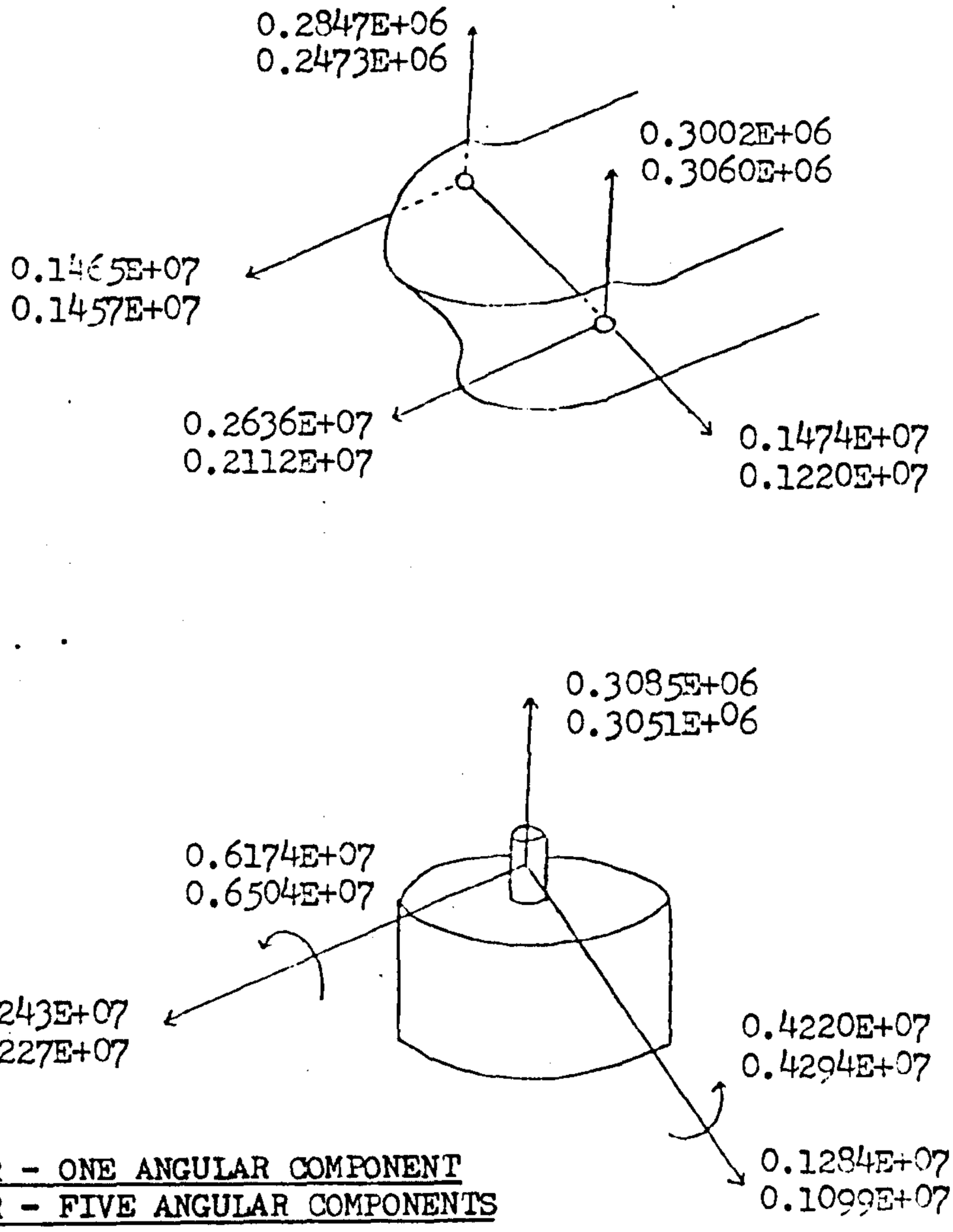

UPPER - ONE ANGULAR COMPONENT
LOWER - FIVE ANGULAR COMPONENTS

FIG. 9.29 THE EFFECT OF THE SPREADING FUNCTION ON THE FIRST ORDER RESPONSE - 45 DEG. SEAS
(FOR KEY SEE FIG. 9.26)

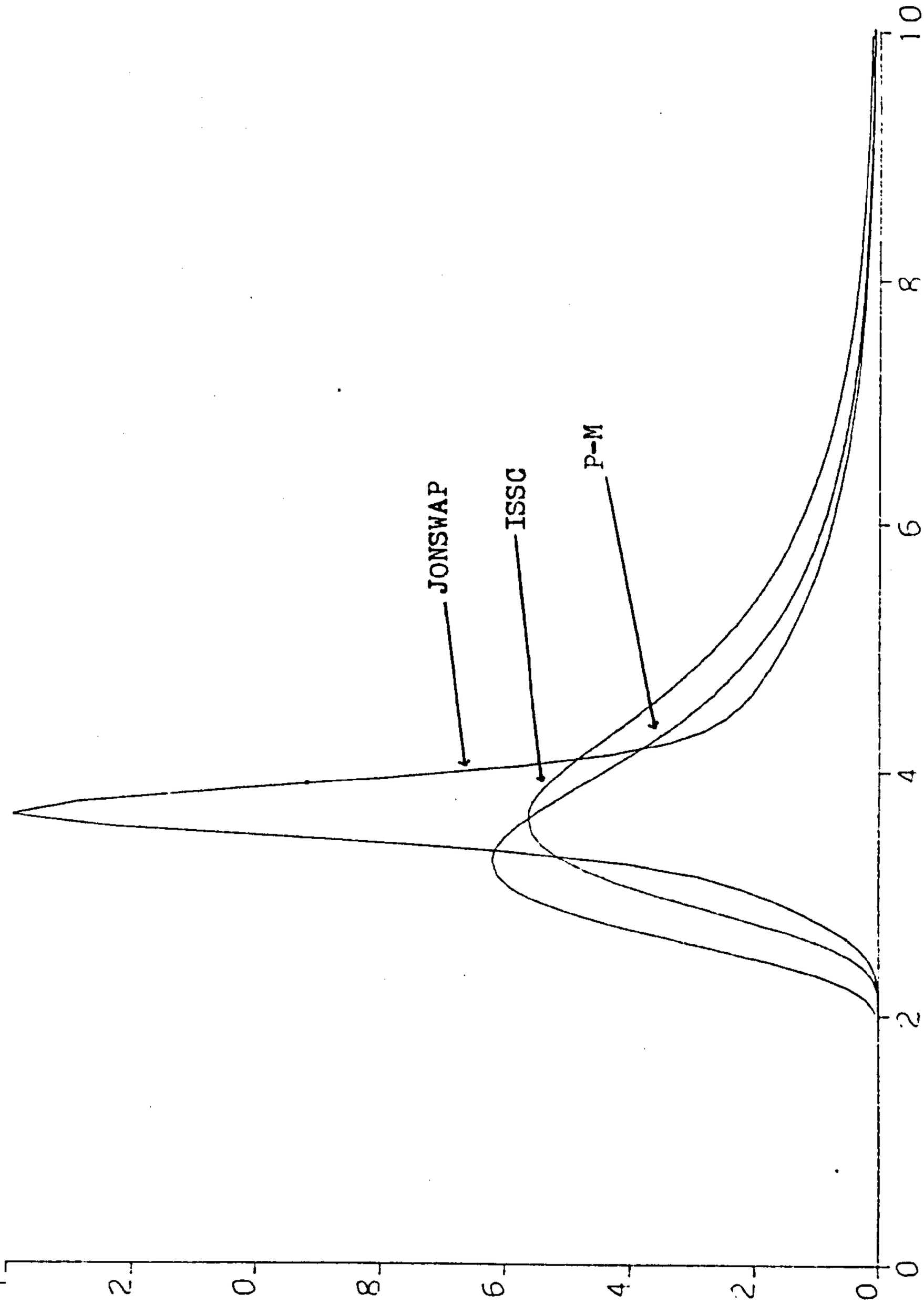

FIG. 9.30 VARIOUS SPECTRAL TYPES FOR H_S= 15M

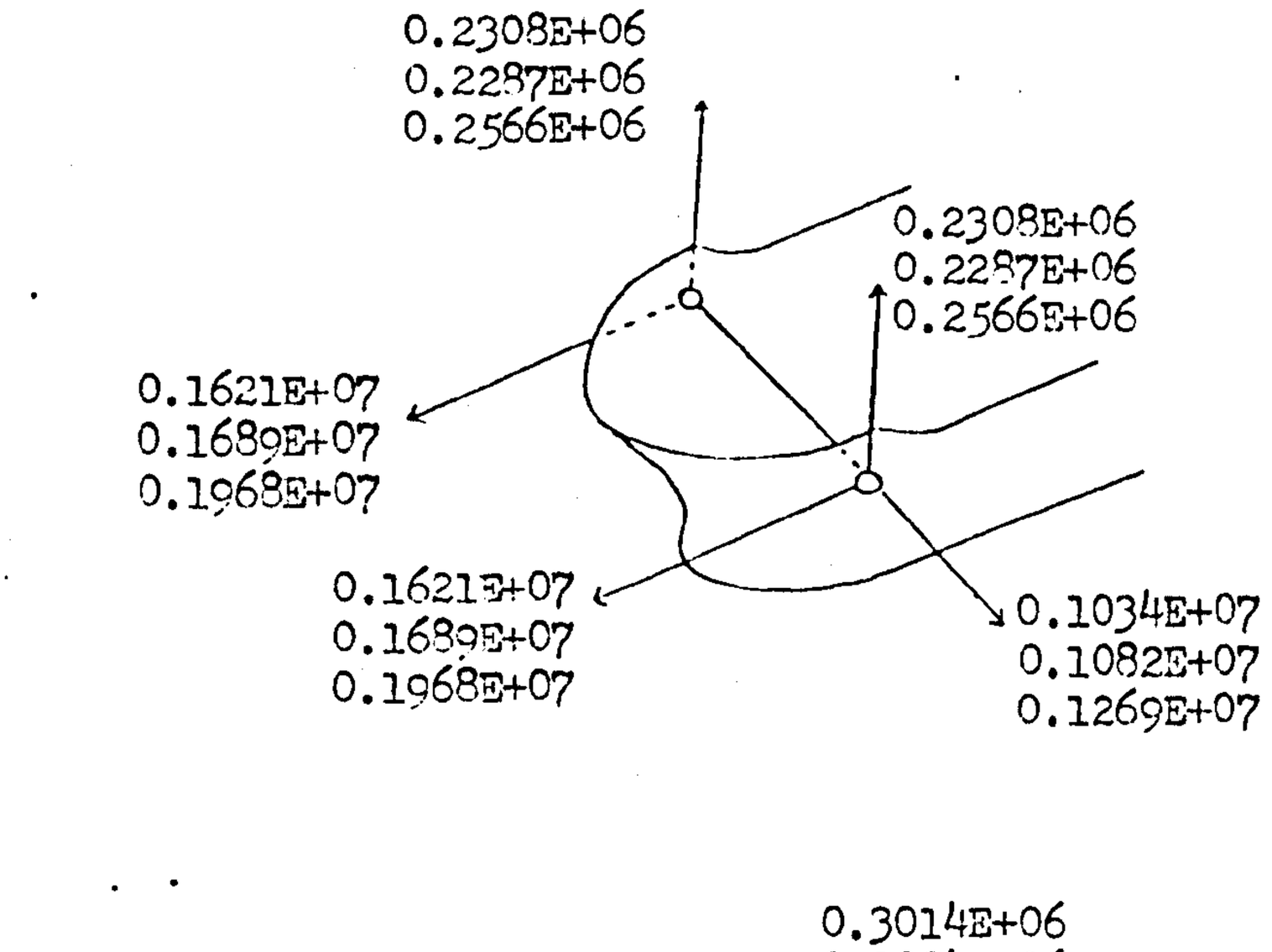

UPPER: JONSWAP
MIDDLE: P-M
LOWER: ISSC

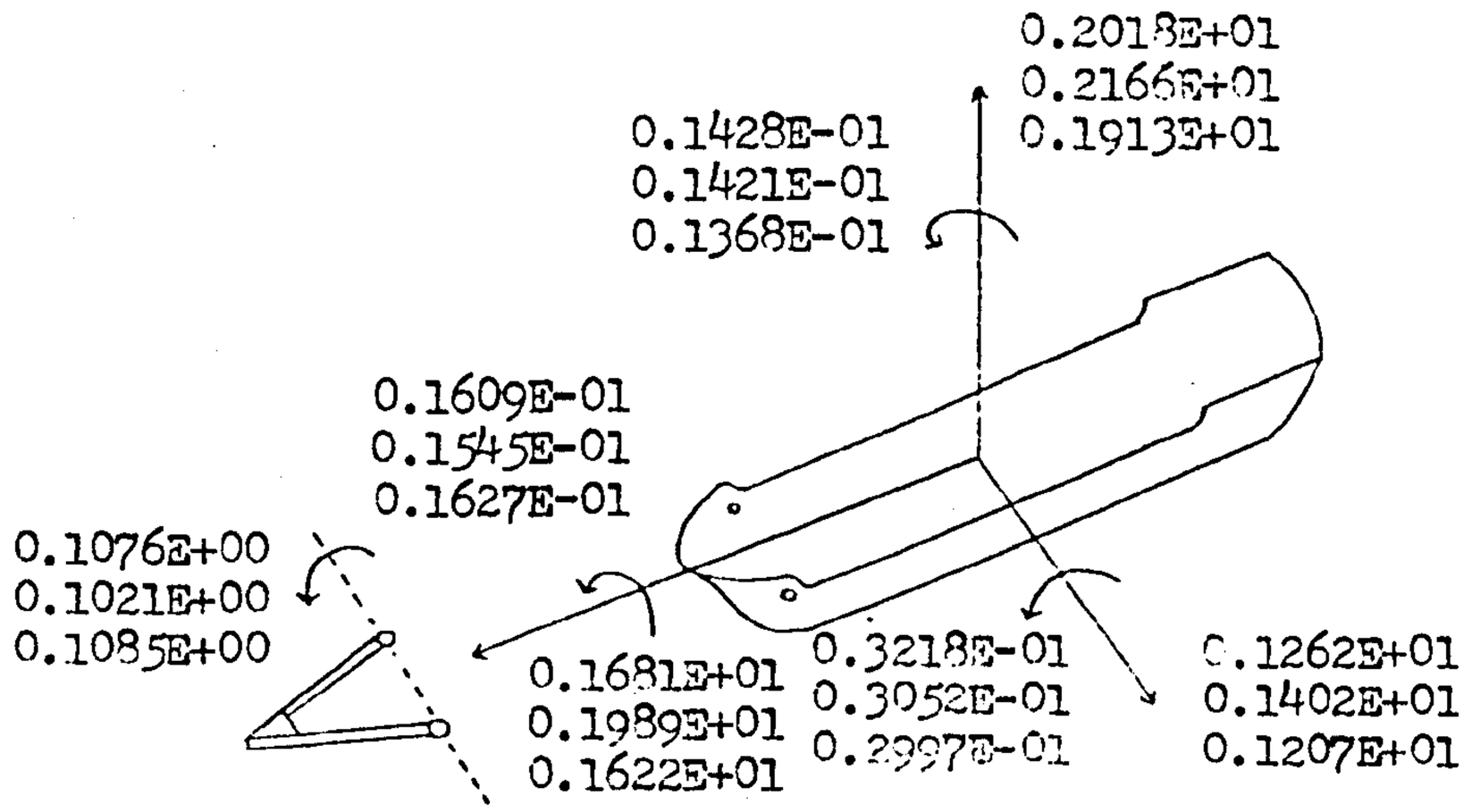

FIG 9.31 THE EFFECT OF THE SPECTRAL TYPE ON THE FIRST ORDER RESPONSE
(FOR KEY SEE FIG. 9.26)

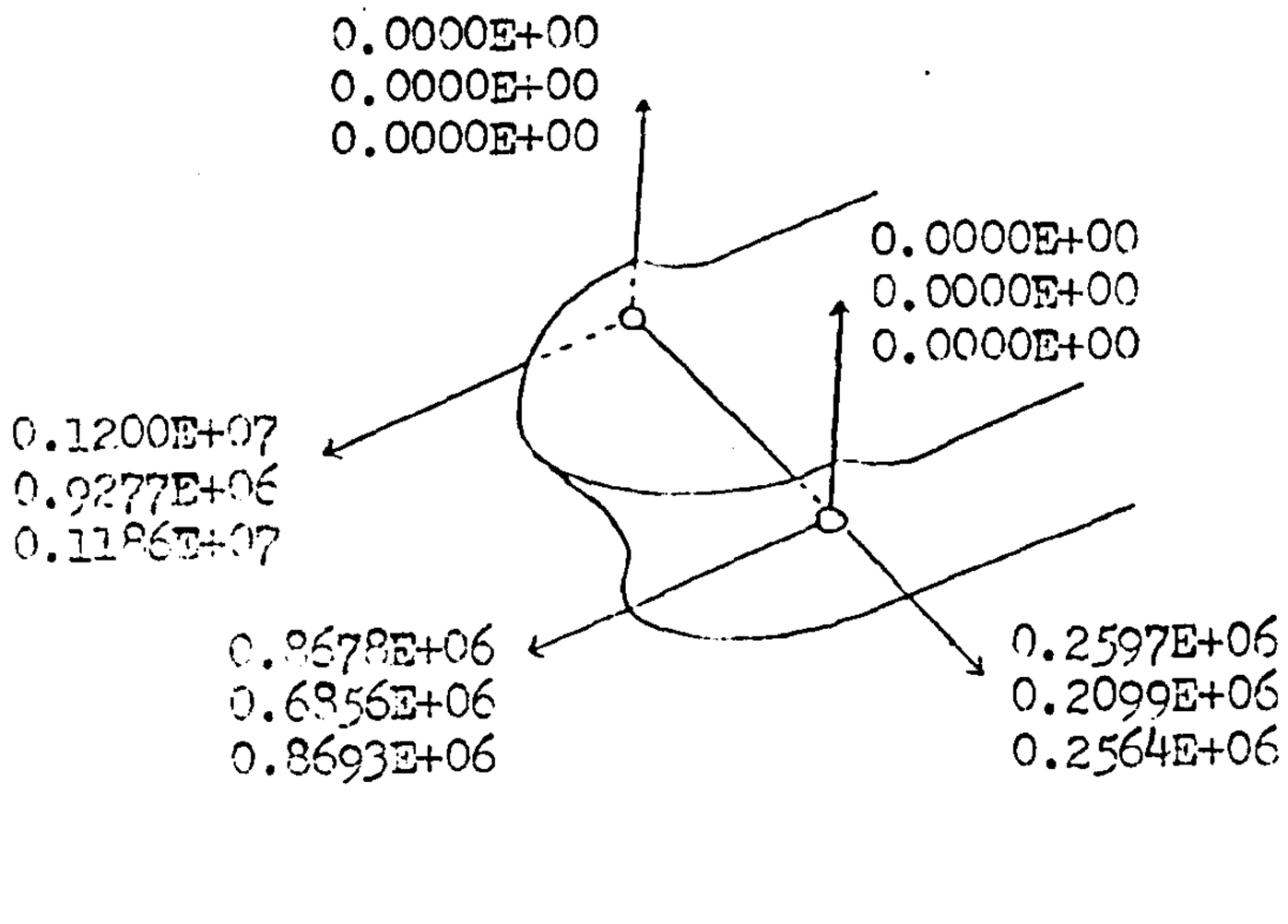

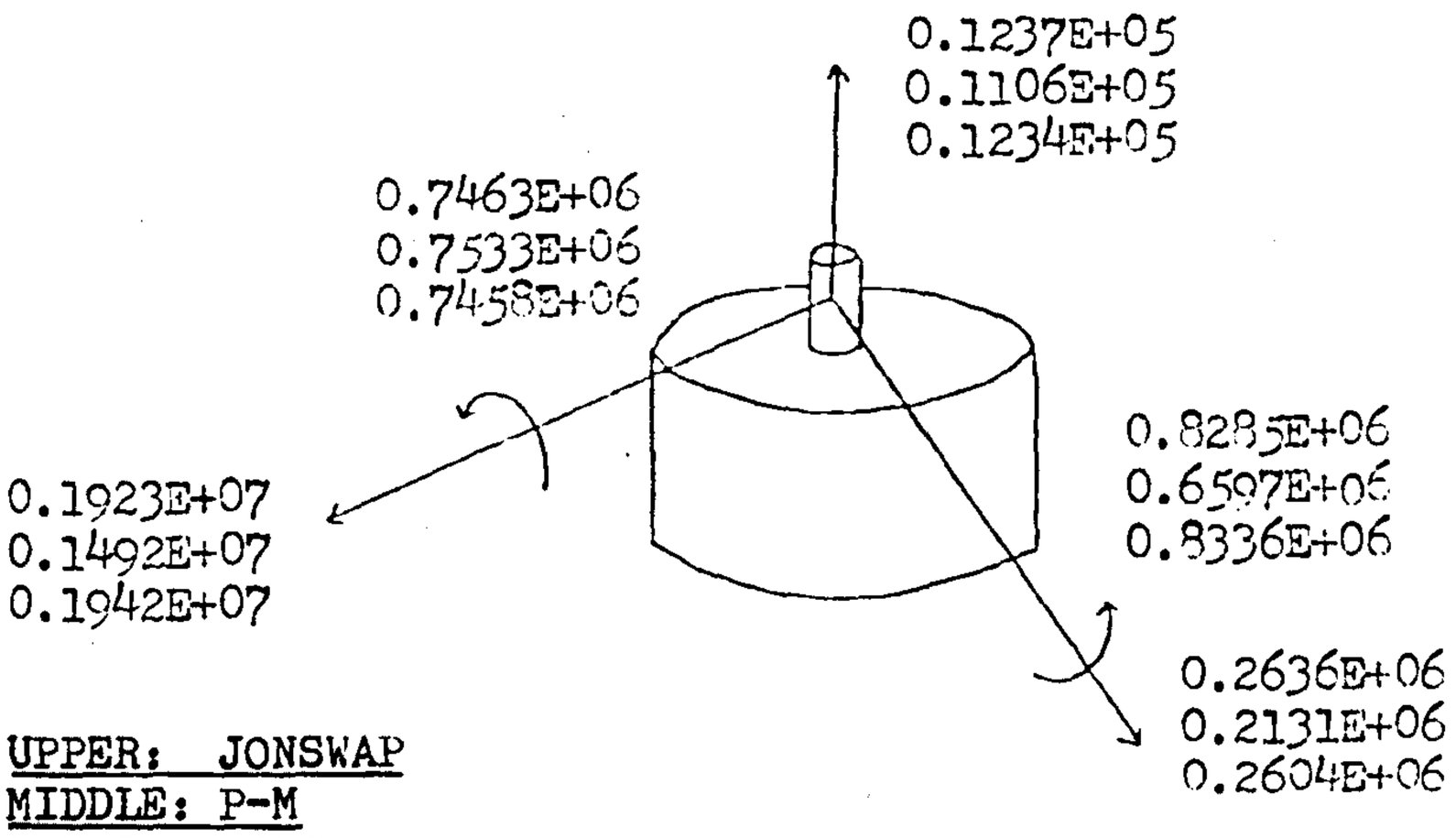

UPPER: JONSWAP
MIDDLE: P-M
LOWER: ISSC

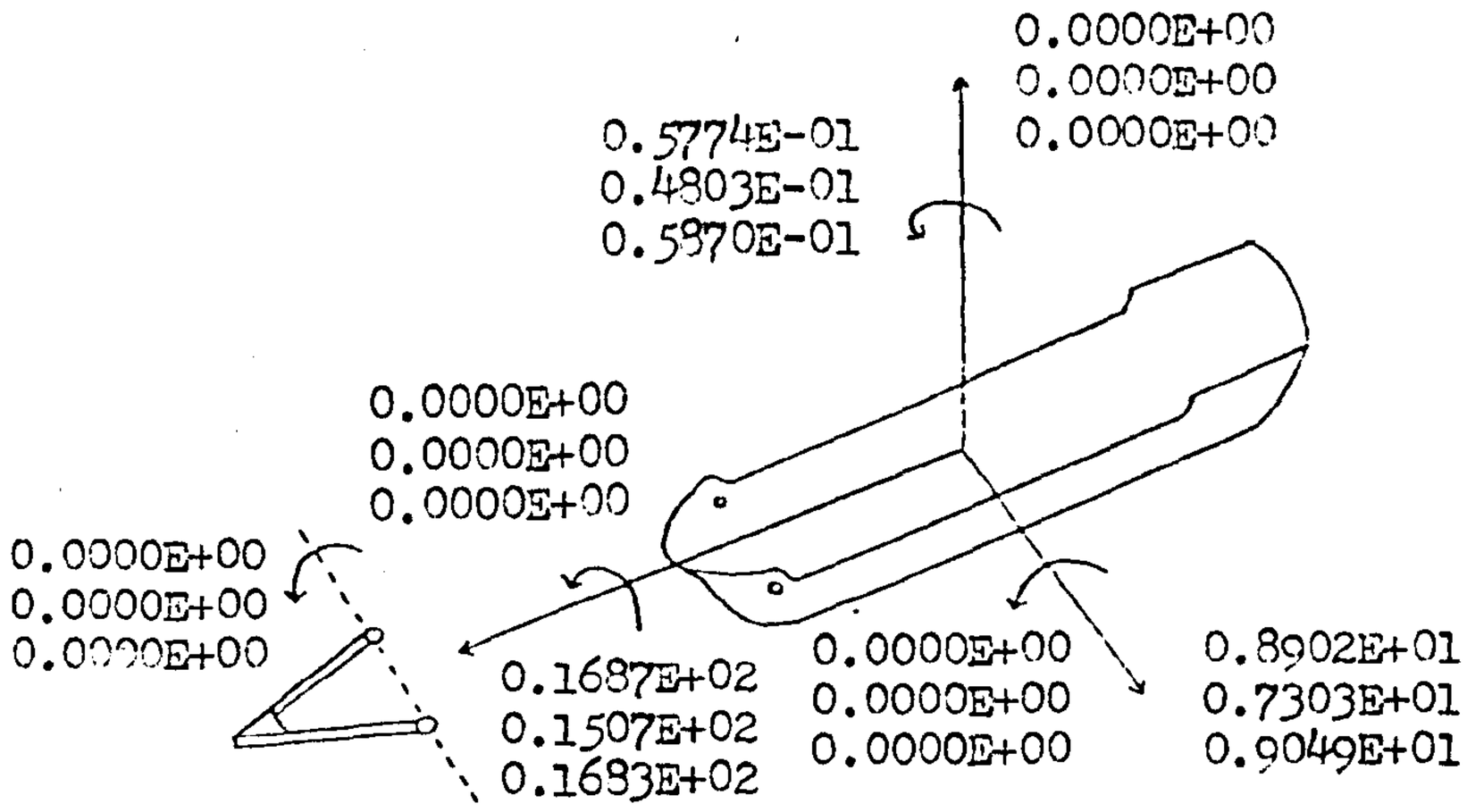

FIG. 9.32 THE EFFECT OF THE SPECTRAL TYPE ON THE SECOND ORDER RESPONSE
(FOR KEY SEE FIG. 9.26)

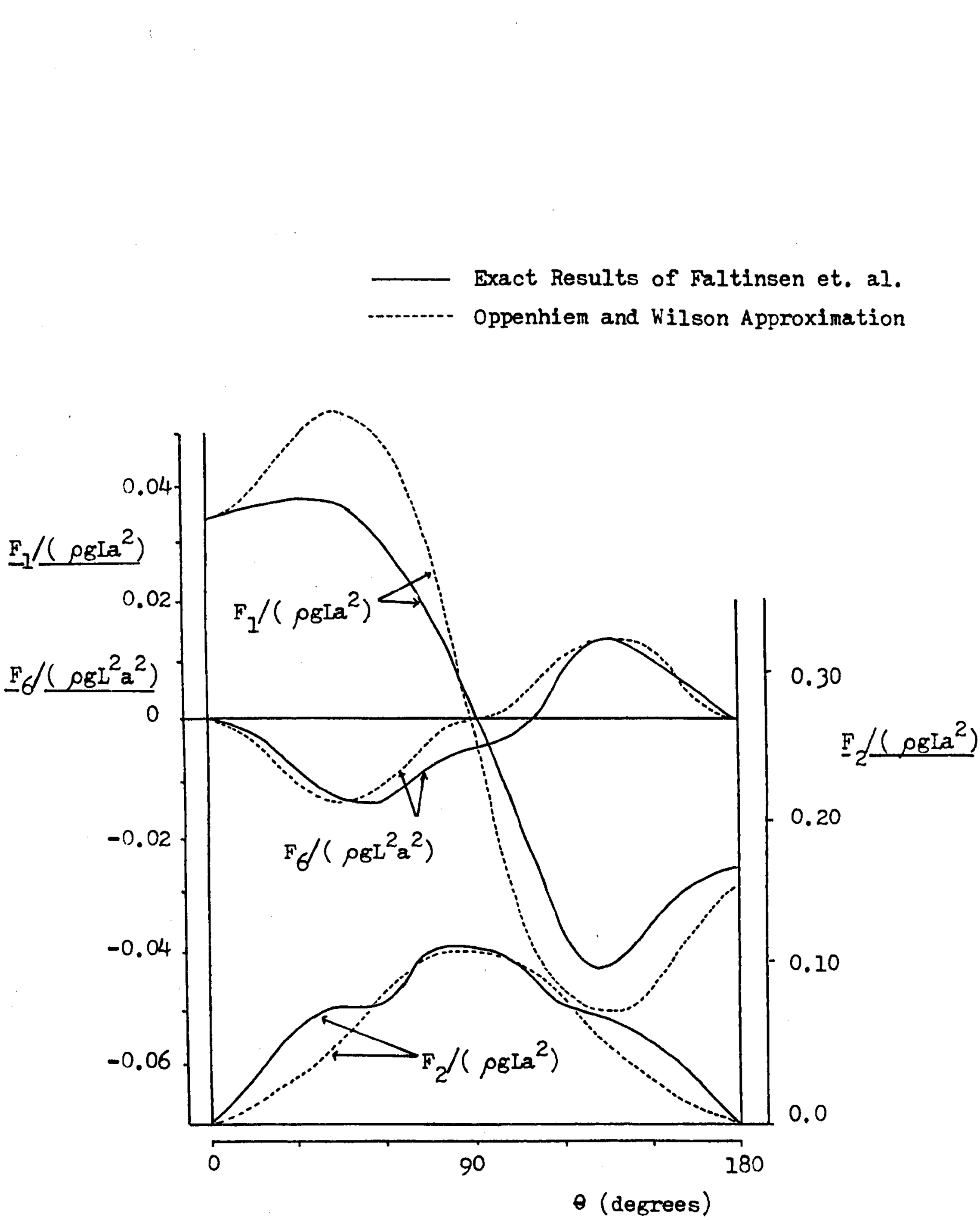

FIG. 9.33 EXACT AND APPROXIMATE REFLECTION COEFFICIENTS AT A FREQUENCY OF 0.562 RAD/SEC

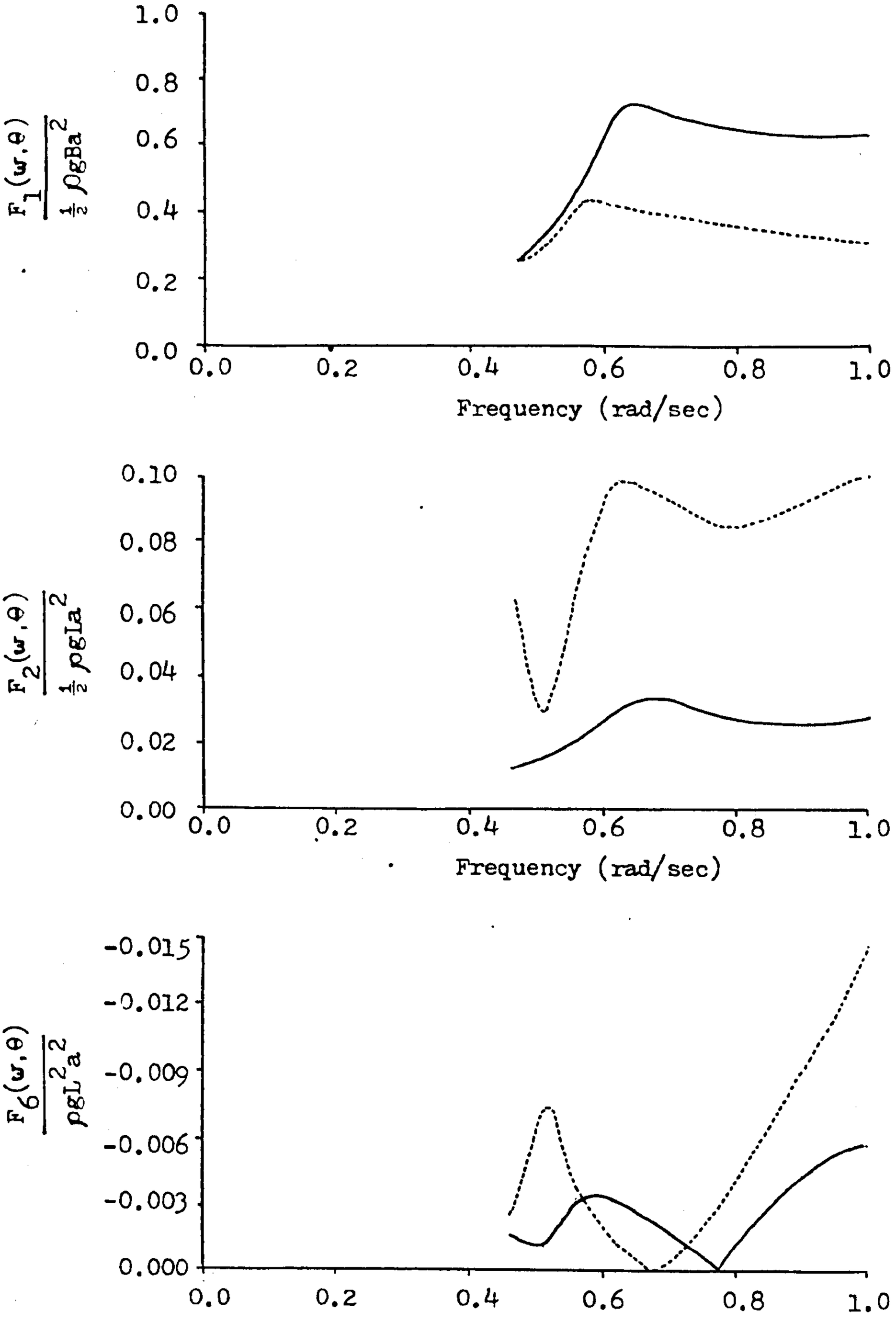

FIG. 9.34 COMPARISON BETWEEN APPROXIMATE AND EXACT REFLECTION COEFFICIENTS FOR AN INCIDENCE OF 15 DEG.

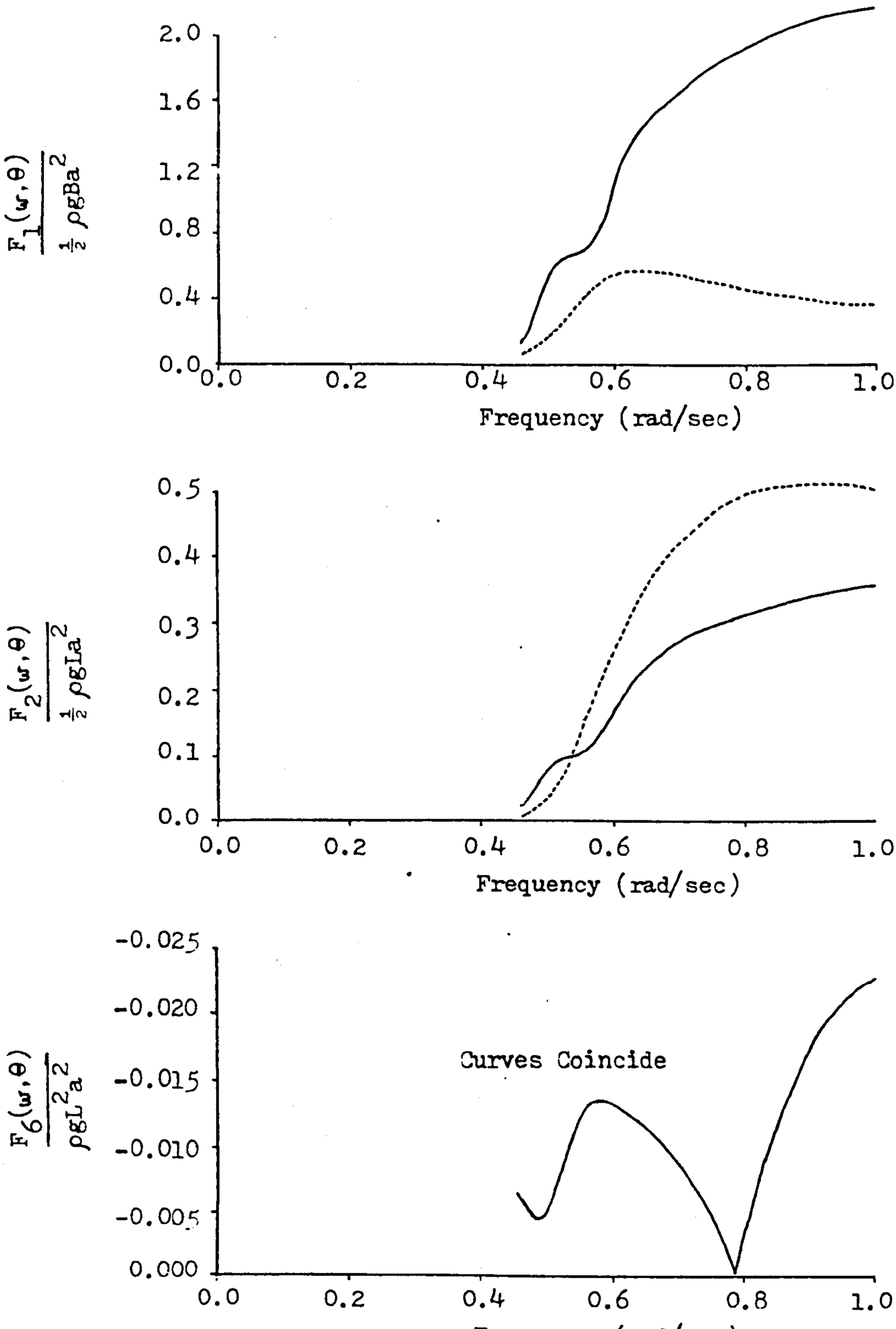

FIG. 9.35 COMPARISON BETWEEN APPROXIMATE AND EXACT REFLECTION COEFFICIENTS FOR AN INCIDENCE OF 45 DEG.

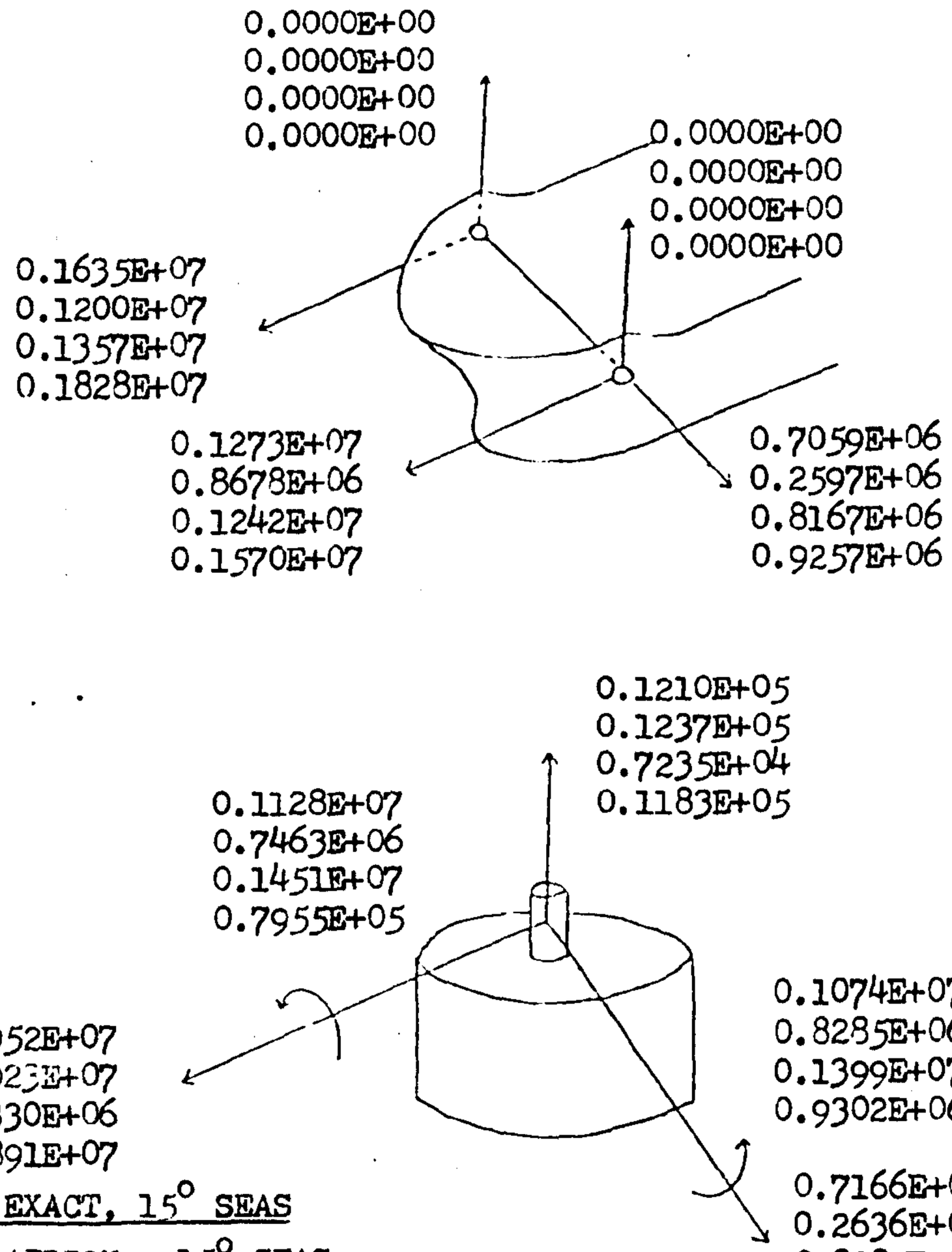

FIRST: EXACT, 15° SEAS

SECOND: APPROX., 15° SEAS

THIRD: EXACT, 45° SEAS

FOURTH: APPROX., 45° SEAS

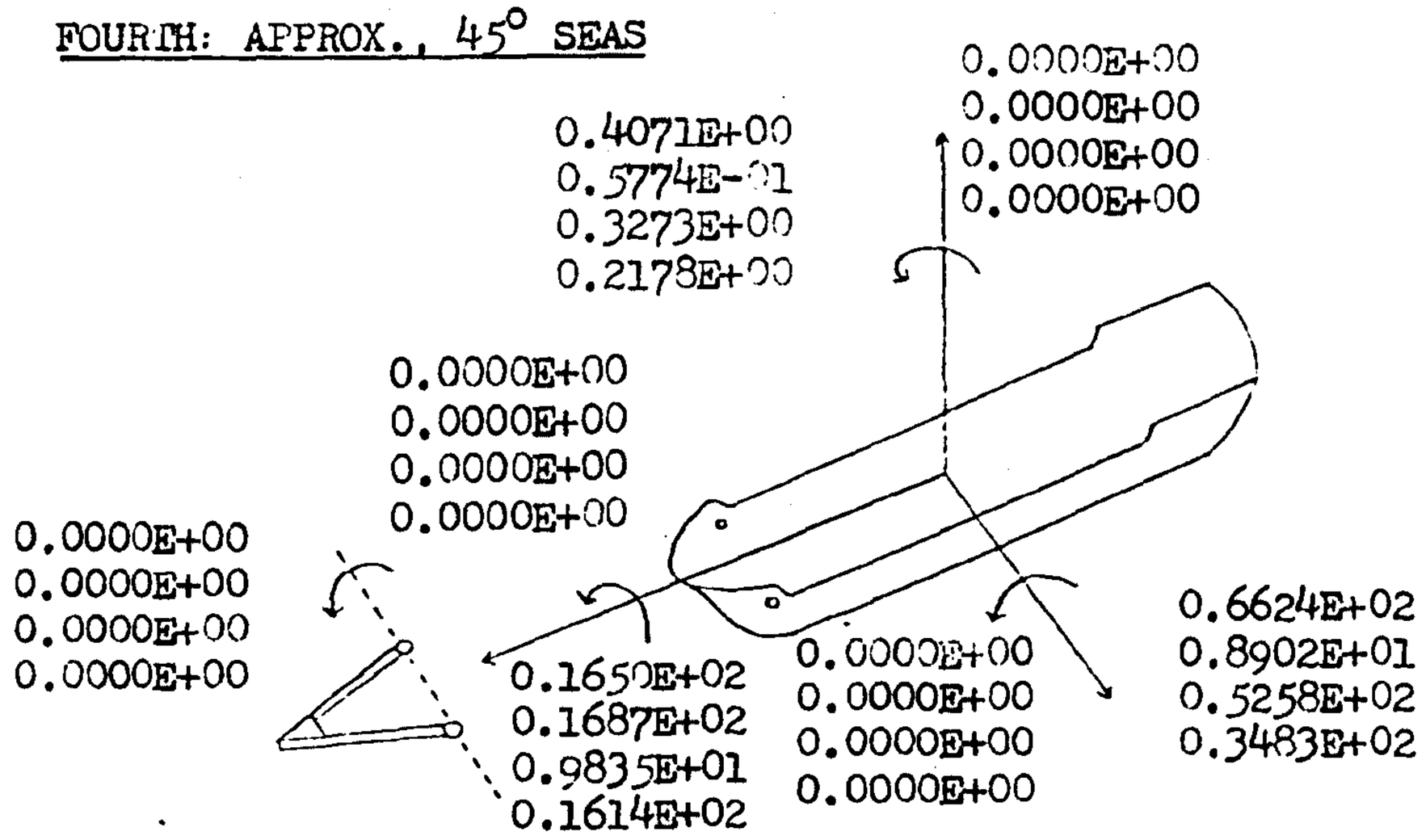

FIG. 9.36 THE EFFECT OF APPROXIMATIONS CONCERNING THE ANGULAR DEPENDENCE OF THE REFLECTION COEFFICIENTS (SECOND ORDER RESPONSE - FOR KEY SEE FIG. 9.26)

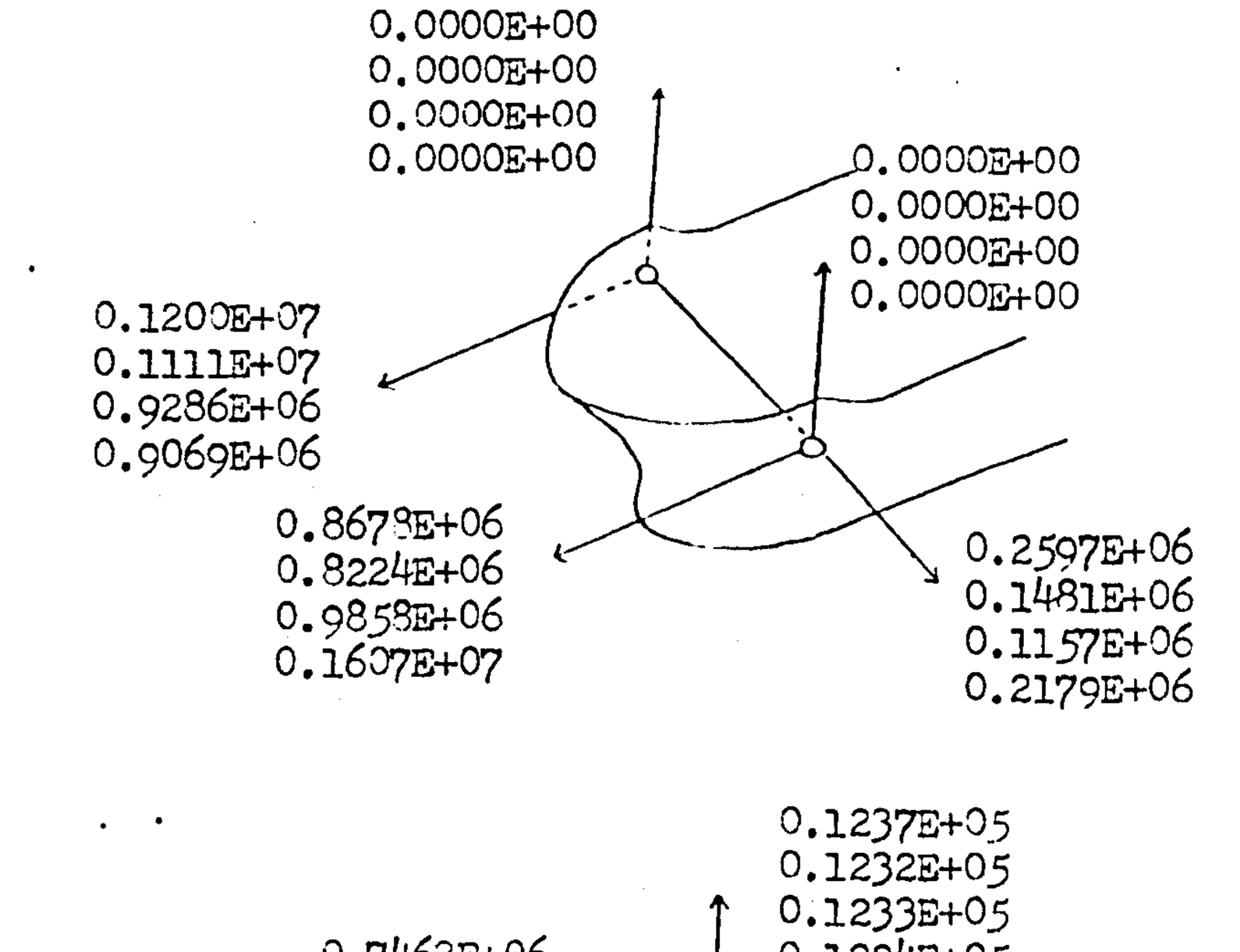

FIRST: ALL IN PHASE
SECOND: SWAY FORCE OUT OF PHASE
THIRD: YAW FORCE OUT OF PHASE
FOURTH: SURGE FORCE OUT OF PHASE

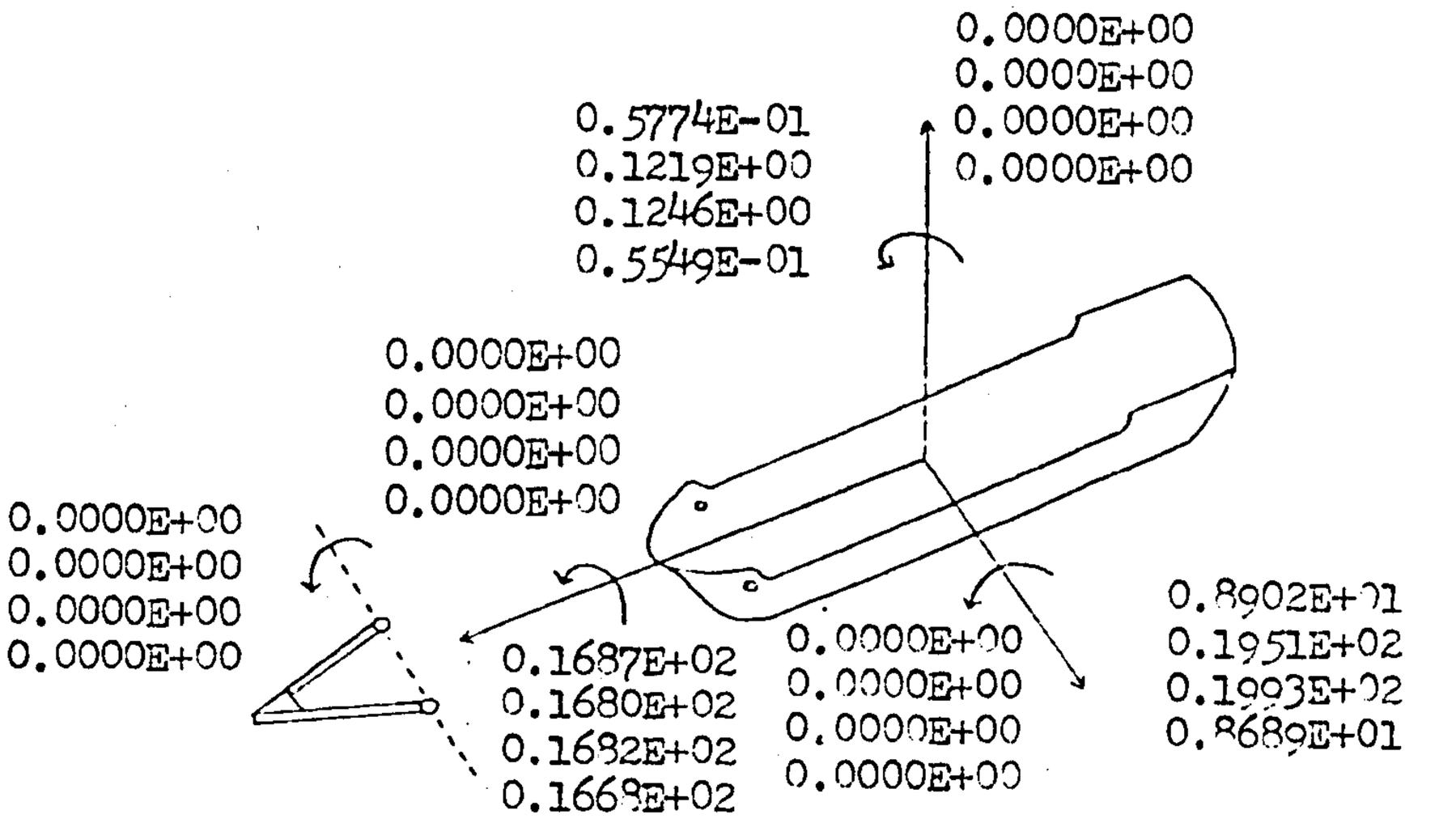

FIG. 9.37 THE EFFECT OF PHASE DIFFERENCES BETWEEN THE SLOW DRIFT FORCES
(SECOND ORDER RESPONSE - FOR KEY SEE FIG. 9.26)

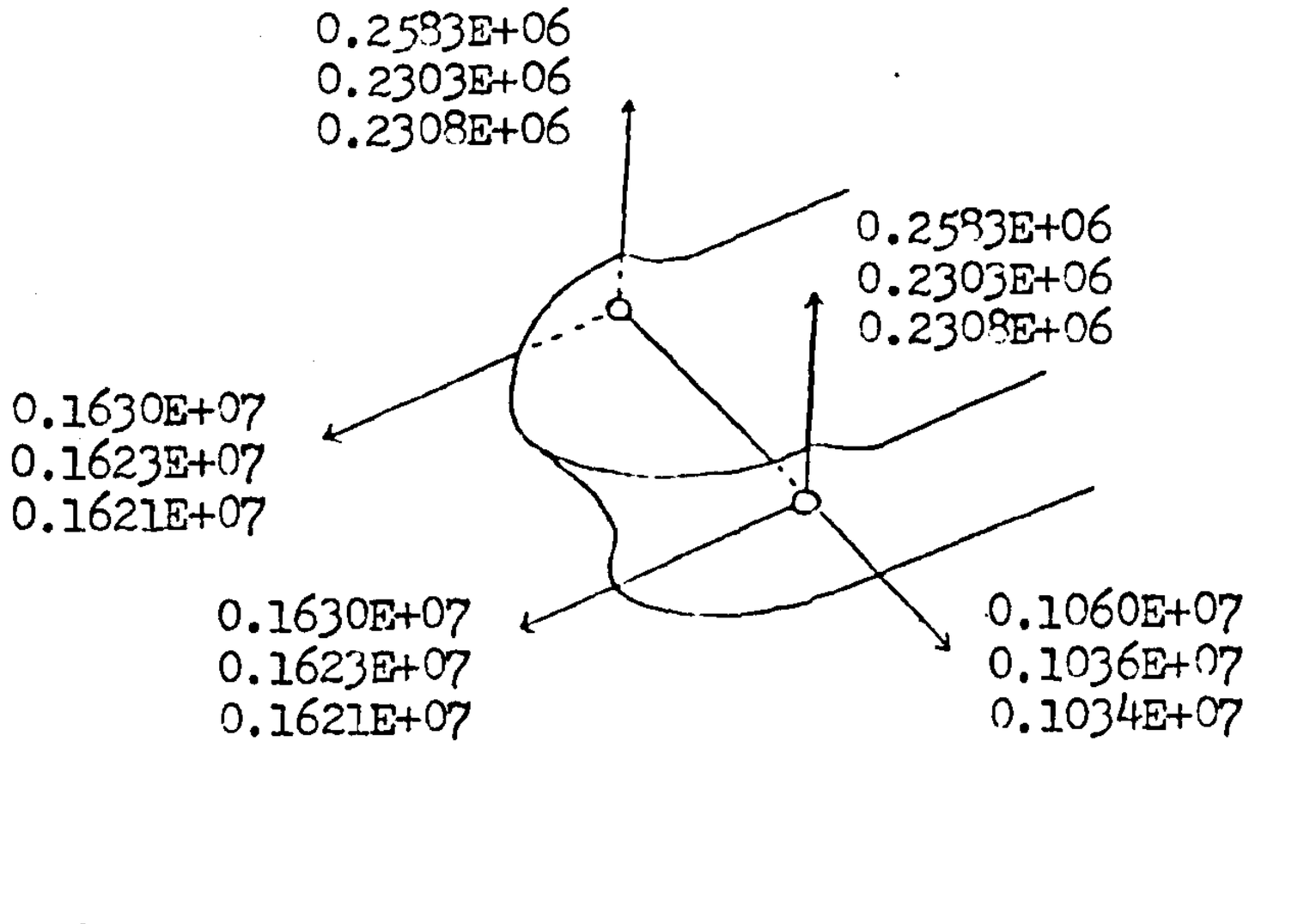

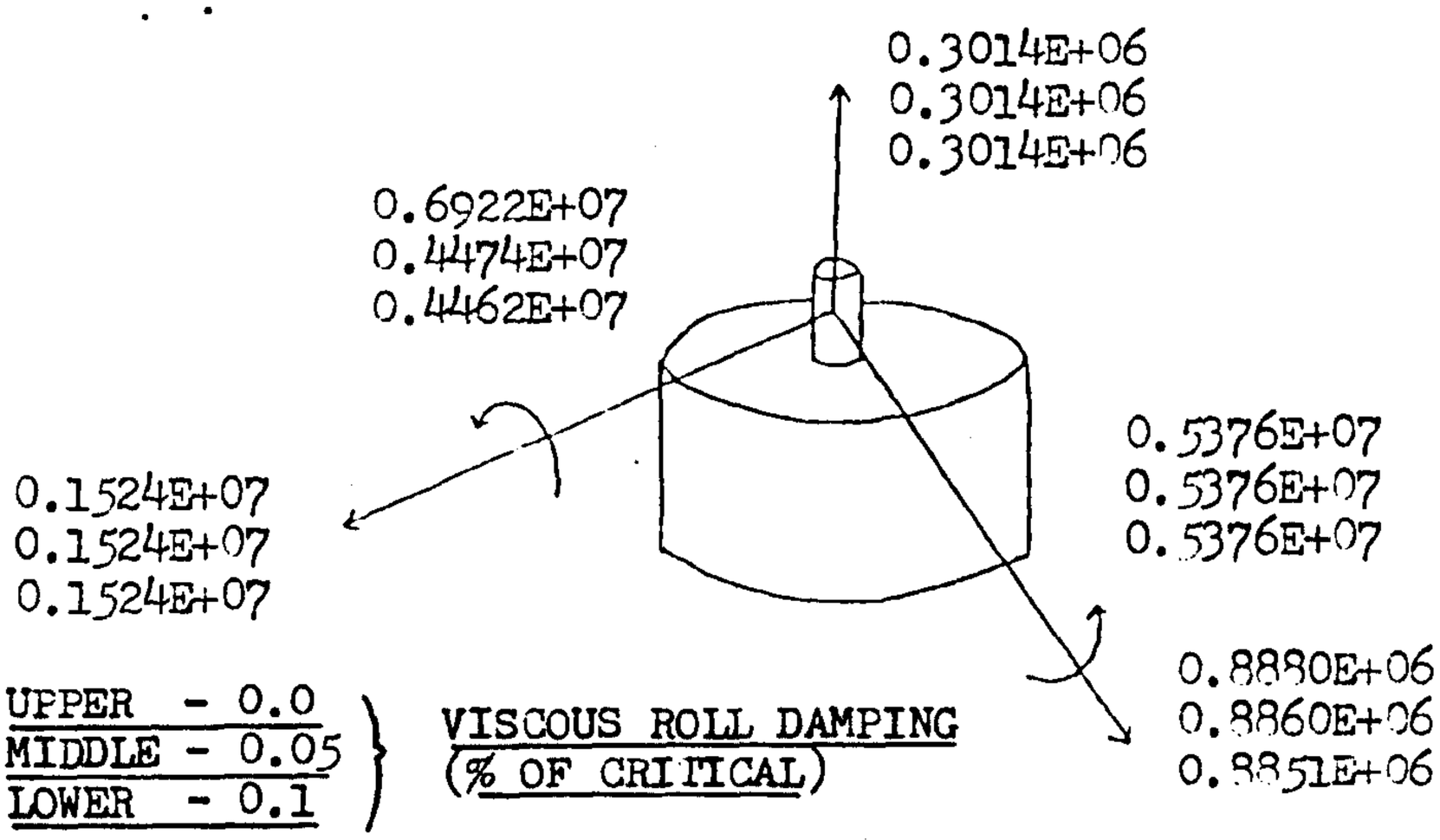

UPPER - 0.0
MIDDLE - 0.05
LOWER - 0.1

} VISCOUS ROLL DAMPING (% OF CRITICAL)

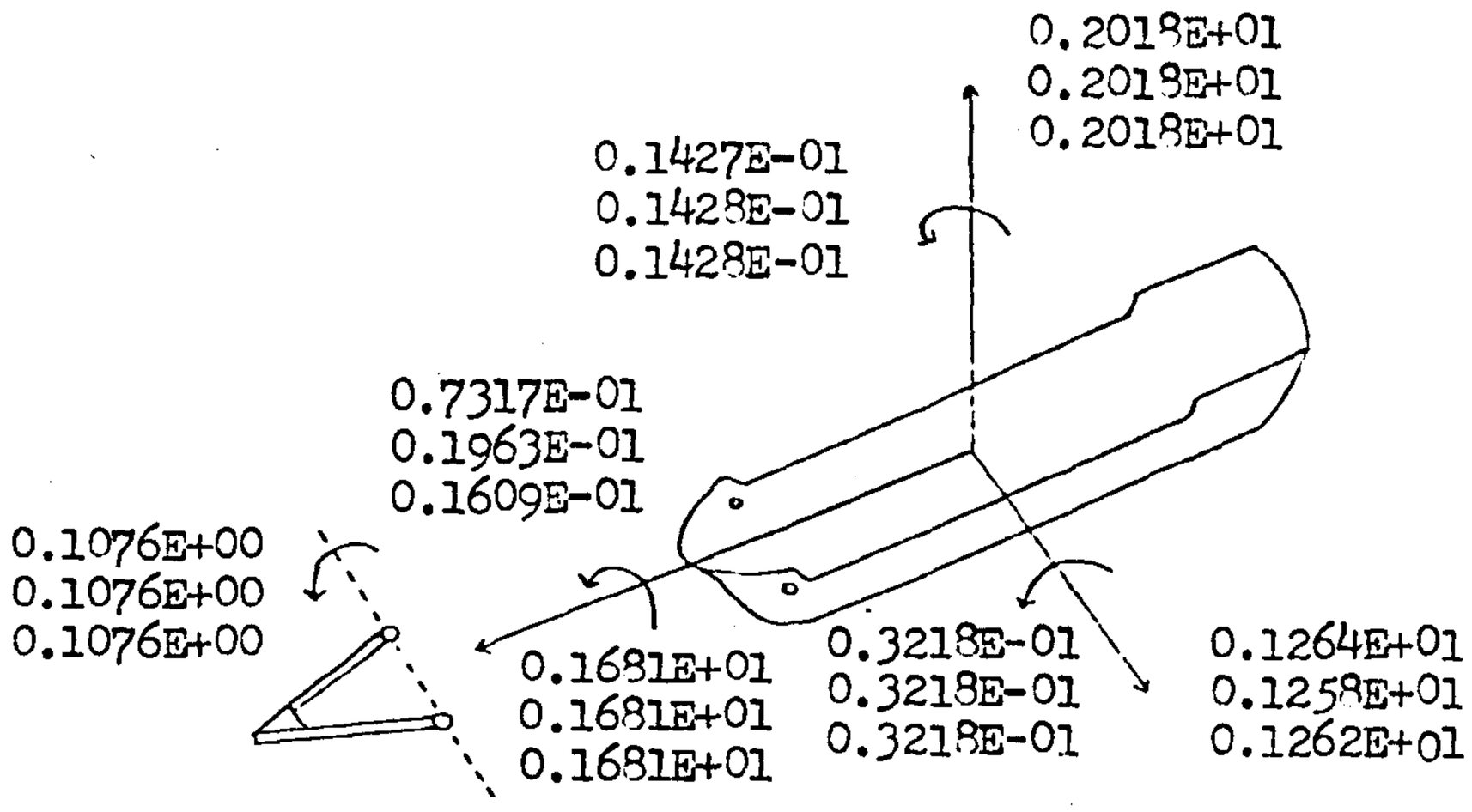

FIG. 9.38 THE EFFECT OF THE VISCOUS ROLL DAMPING COEFFICIENT ON THE FIRST ORDER RESPONSE
(FOR KEY SEE FIG. 9.26)

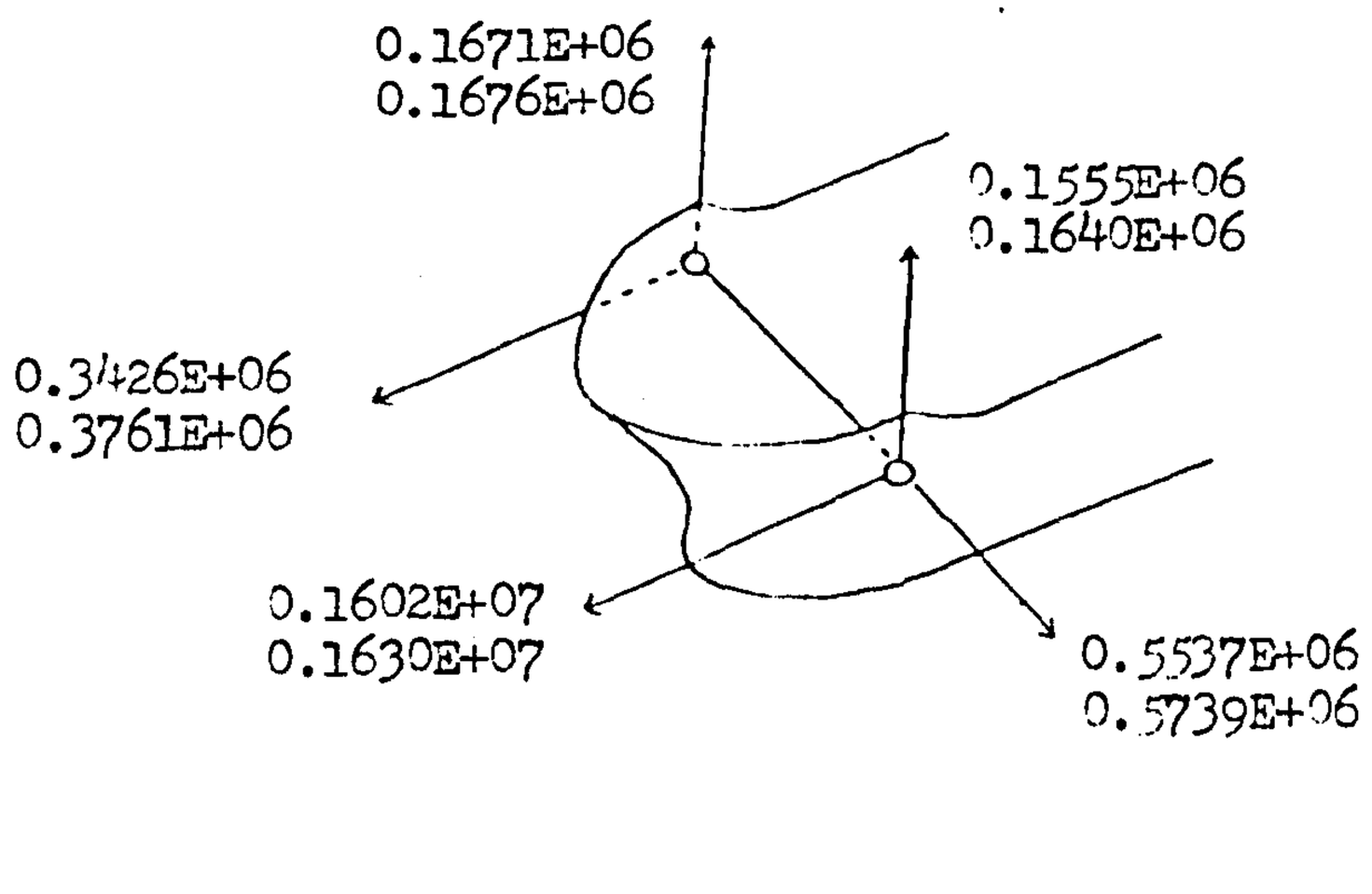

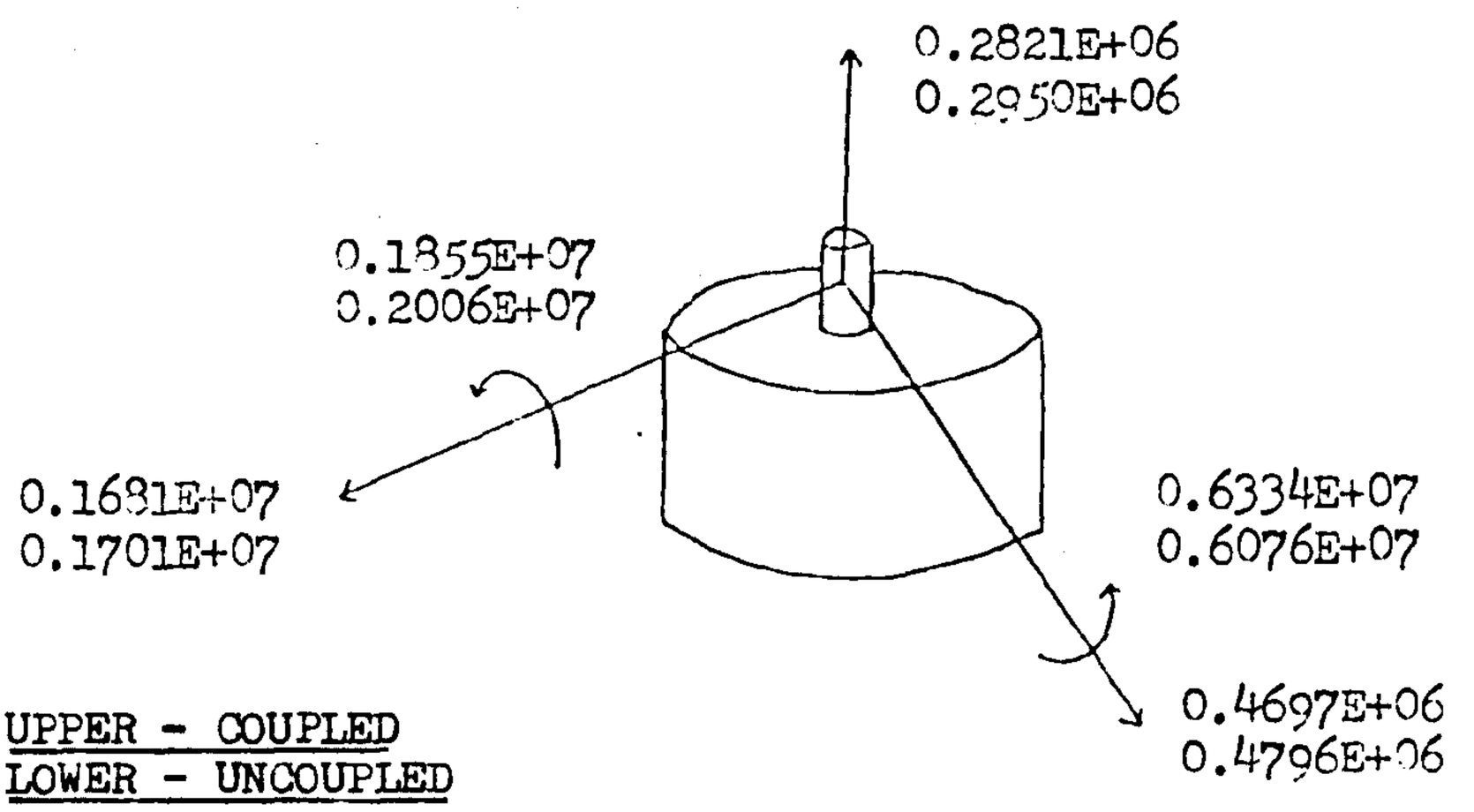

UPPER - COUPLED
LOWER - UNCOUPLED

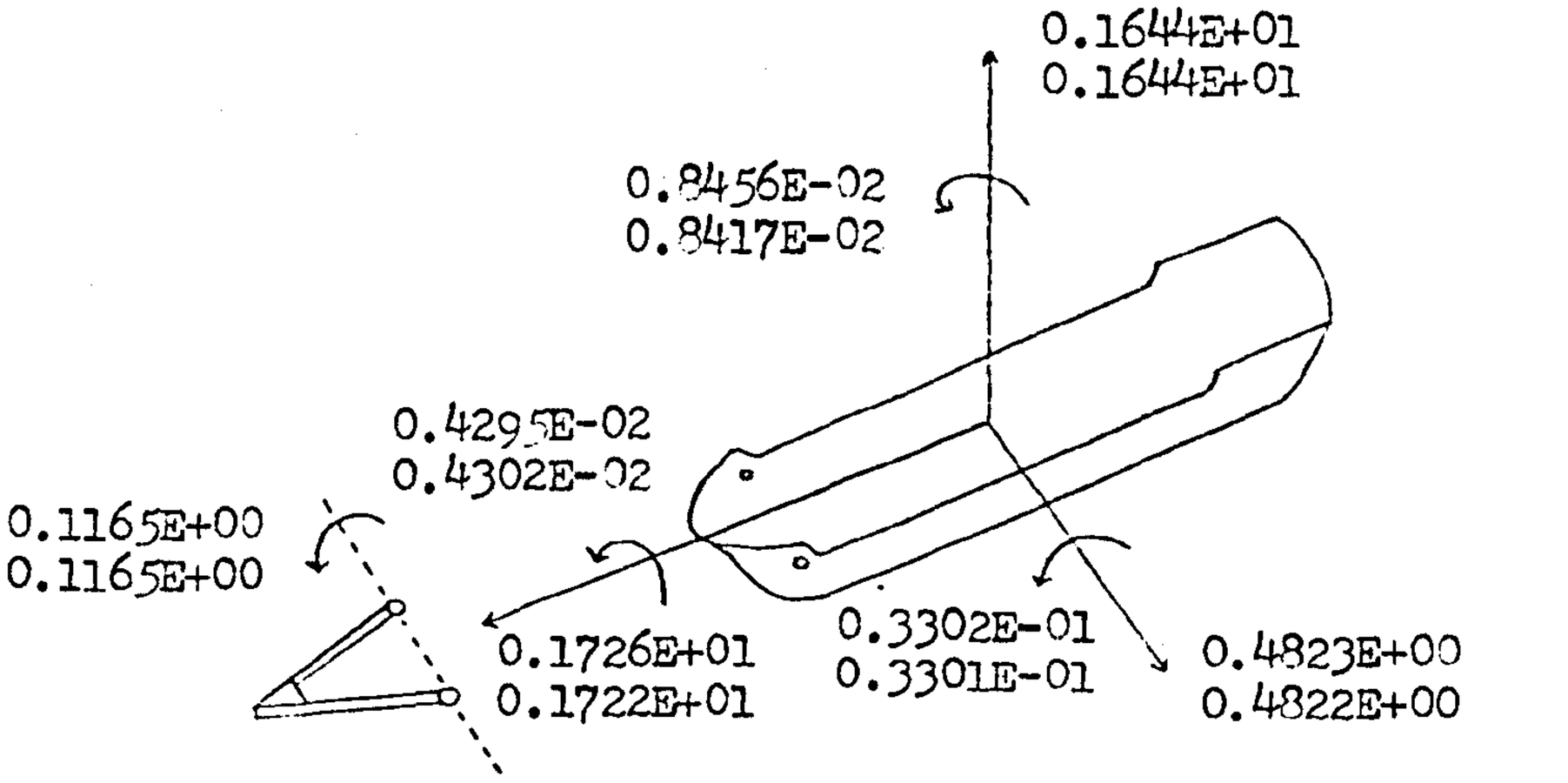

FIG. 9.39 THE EFFECT OF COUPLING BETWEEN THE FIRST AND SECOND ORDER RESPONSES ON THE FIRST ORDER RESPONSE (FOR KEY SEE FIG. 9.26)

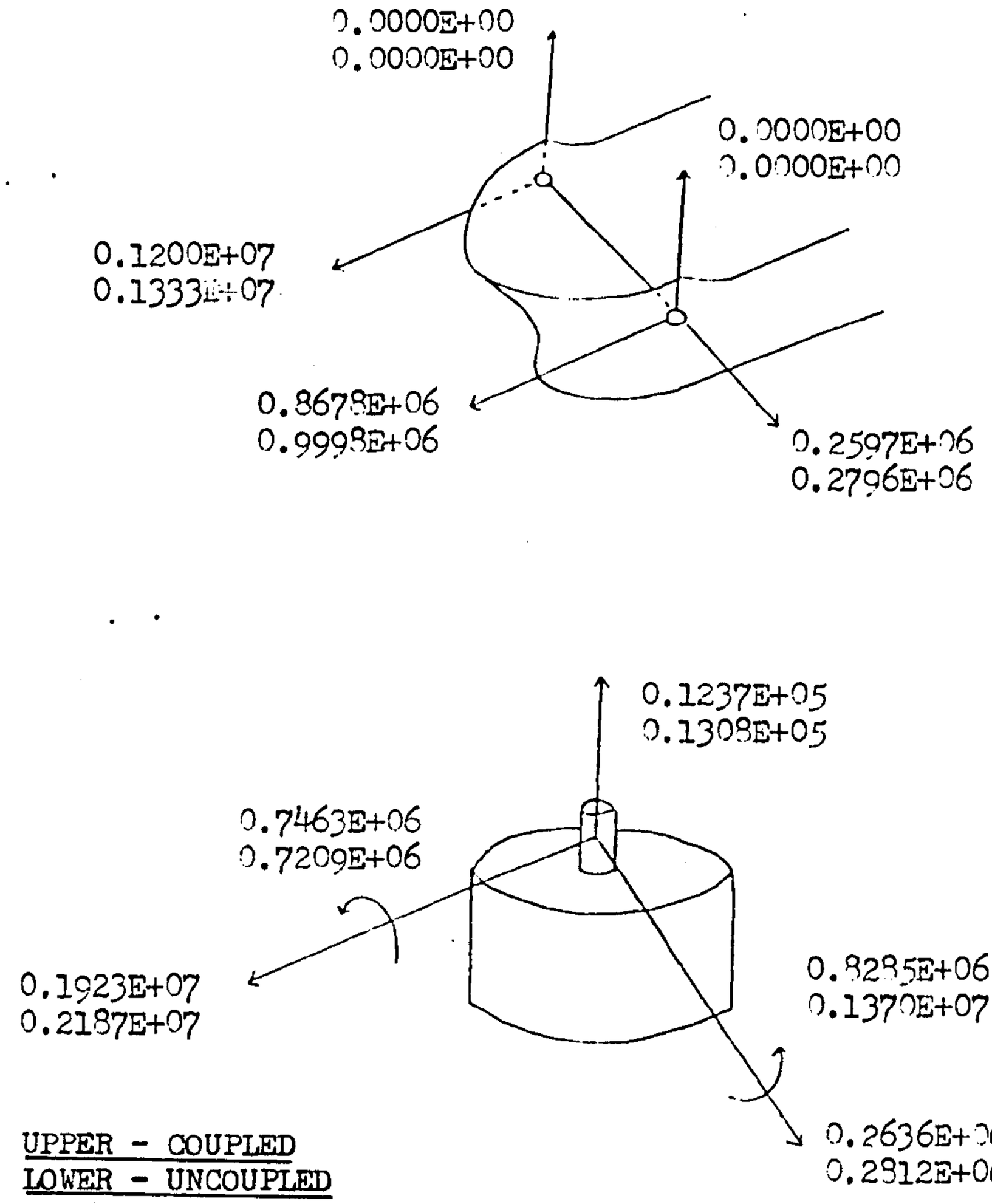

FIG. 9.40 THE EFFECT OF COUPLING BETWEEN THE FIRST AND SECOND ORDER RESPONSES ON THE SECOND ORDER RESPONSE (FOR KEY SEE FIG. 9.26)

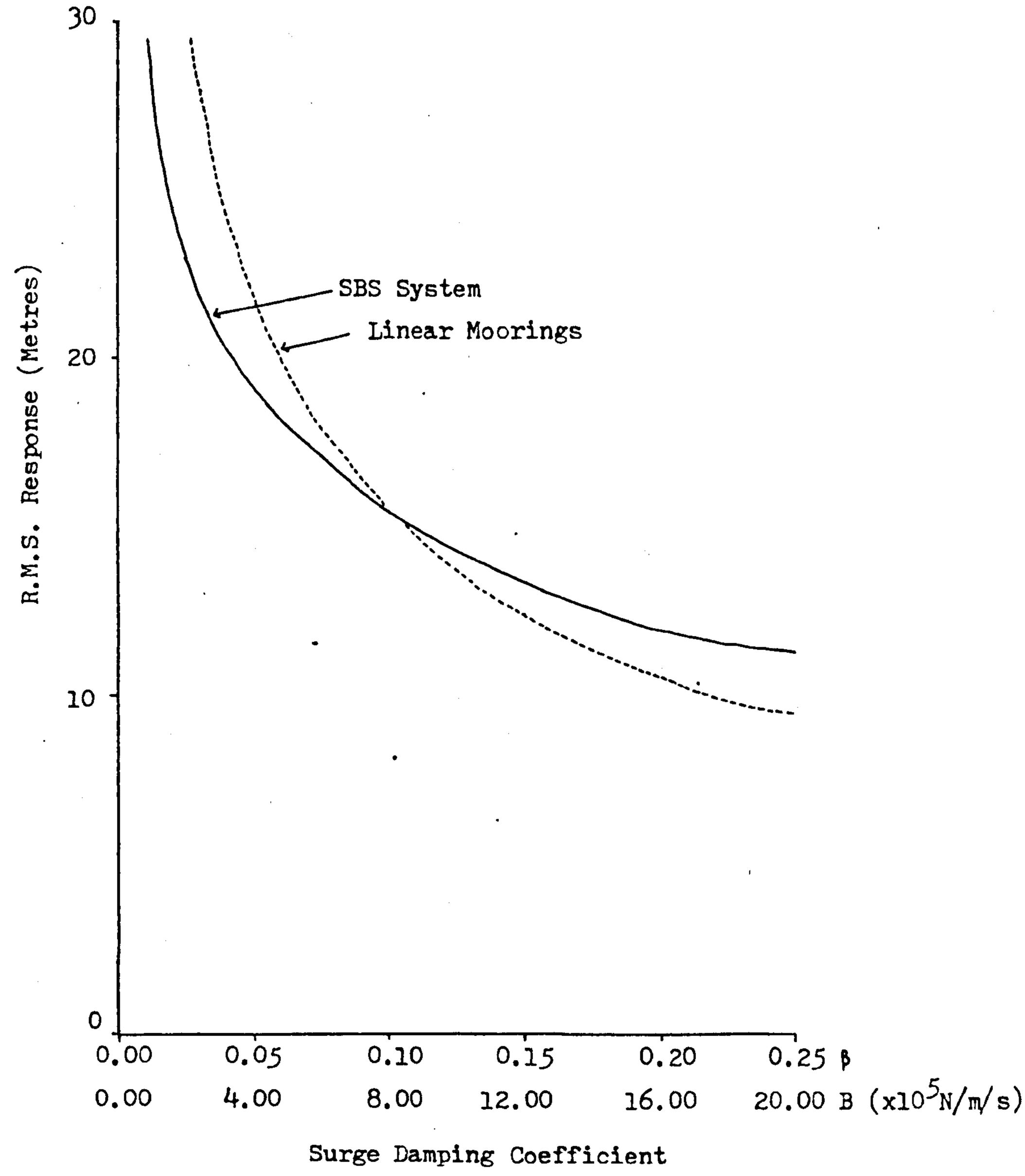

FIG. 9.41 R.M.S. SECOND ORDER SURGE RESPONSE VS SURGE DAMPING

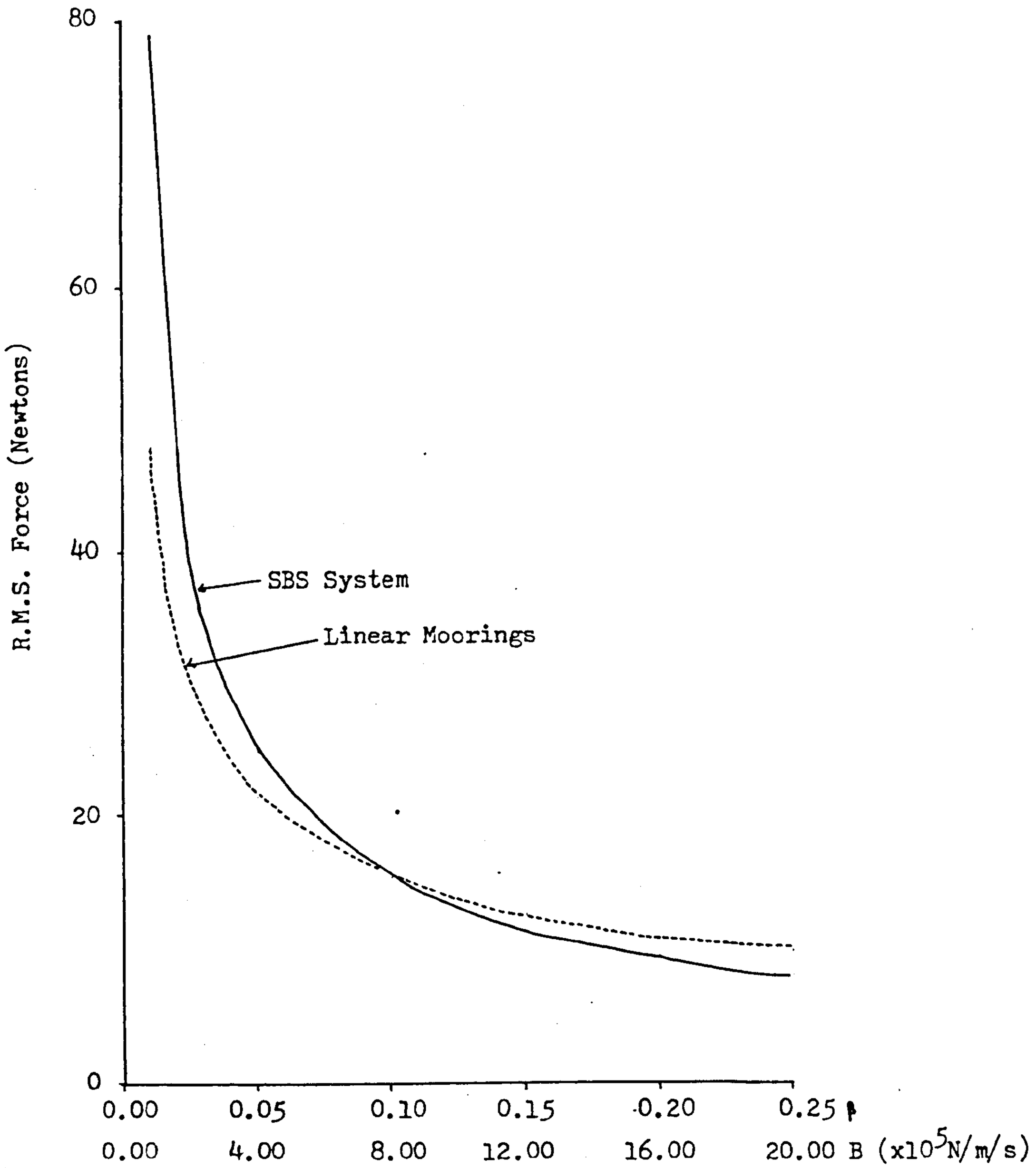

FIG. 9.42 R.M.S. SECOND ORDER SURGE RESTORING FORCE VS SURGE DAMPING

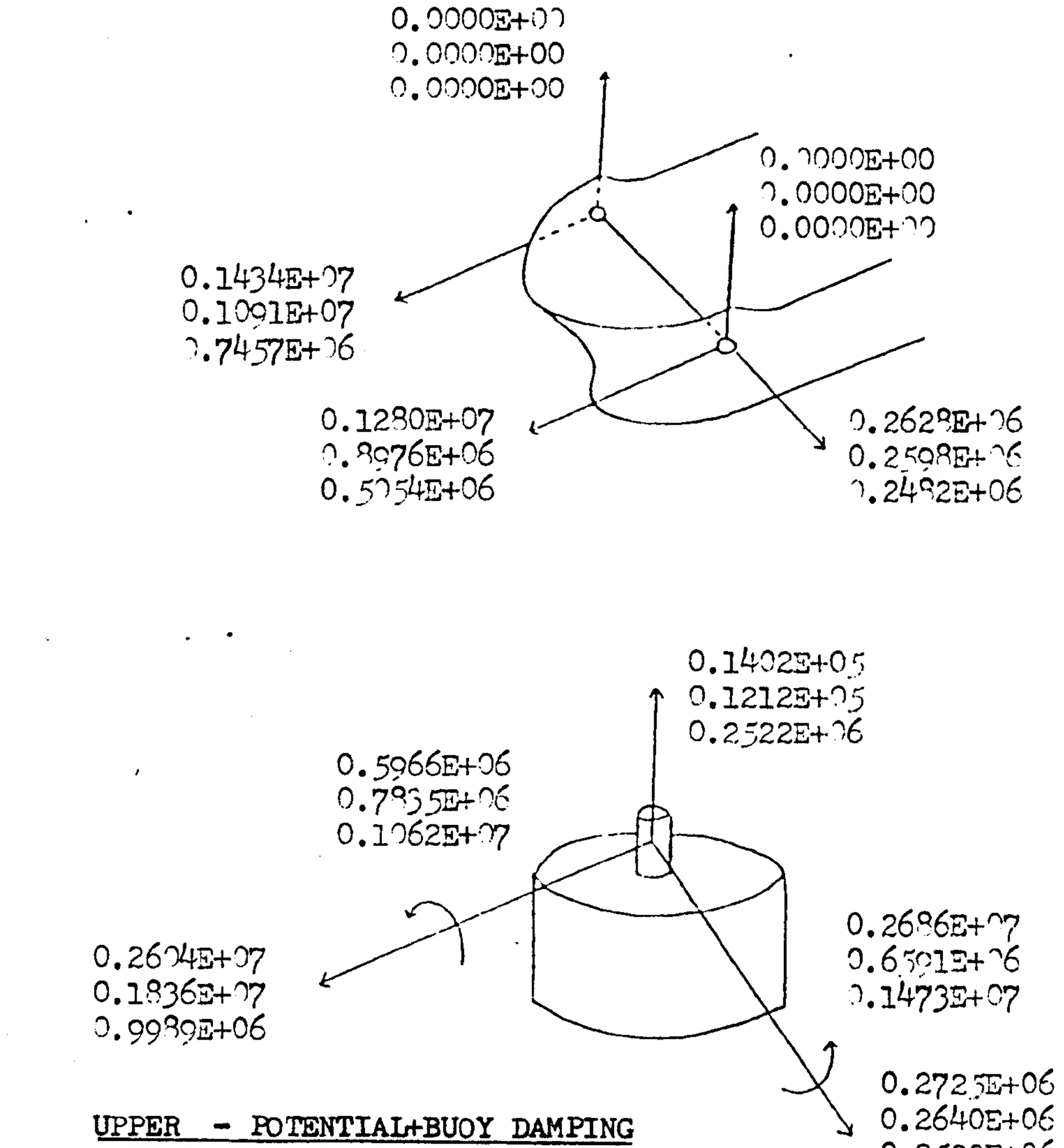

UPPER - POTENTIAL+BUOY DAMPING
MIDDLE - AS ABOVE+CURRENT DAMPING
LOWER - AS ABOVE+WAVE DAMPING

FIG. 9.43 THE EFFECT OF THE SURGE DAMPING COEFFICIENT ON THE SECOND ORDER RESPONSE
(FOR KEY SEE FIG. 9.26)

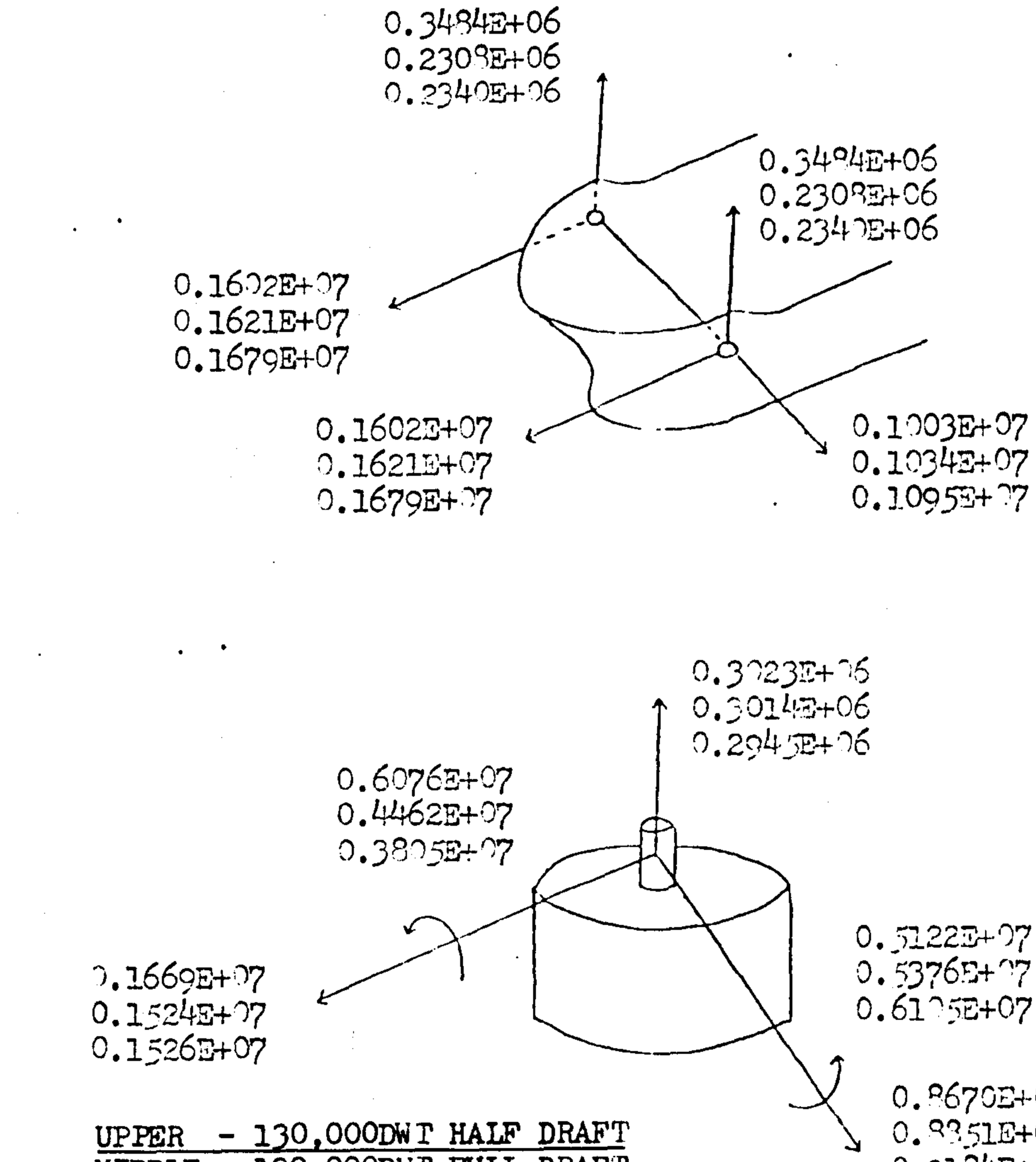

FIG. 9.44 THE EFFECT OF TANKER SIZE AND DRAFT ON THE FIRST ORDER RESPONSE
(FOR KEY SEE FIG. 9.26)

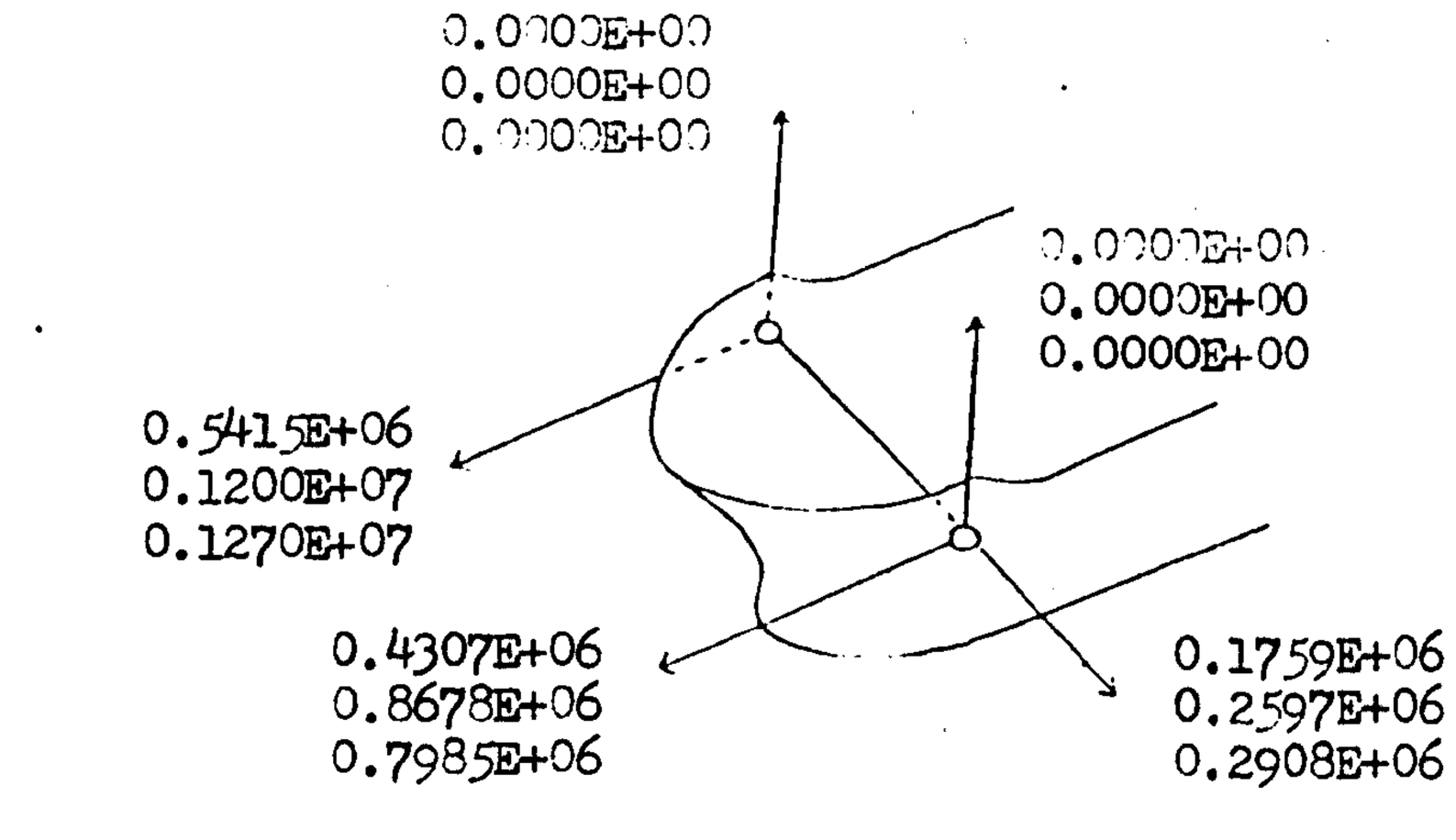

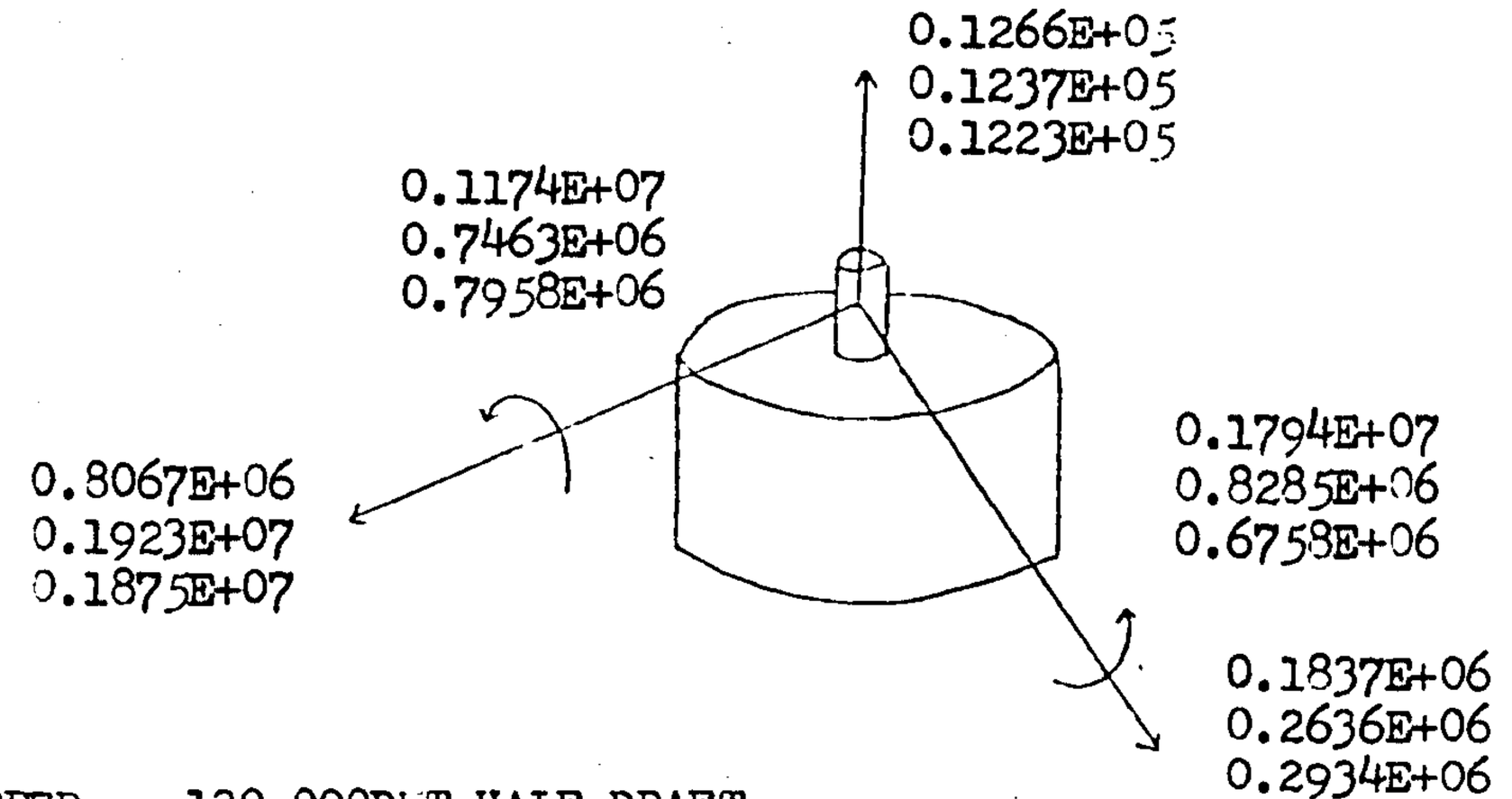

UPPER - 130,000DWT HALF DRAFT
MIDDLE - 130,000DWT FULL DRAFT
LOWER - 200,000DWT FULL DRAFT

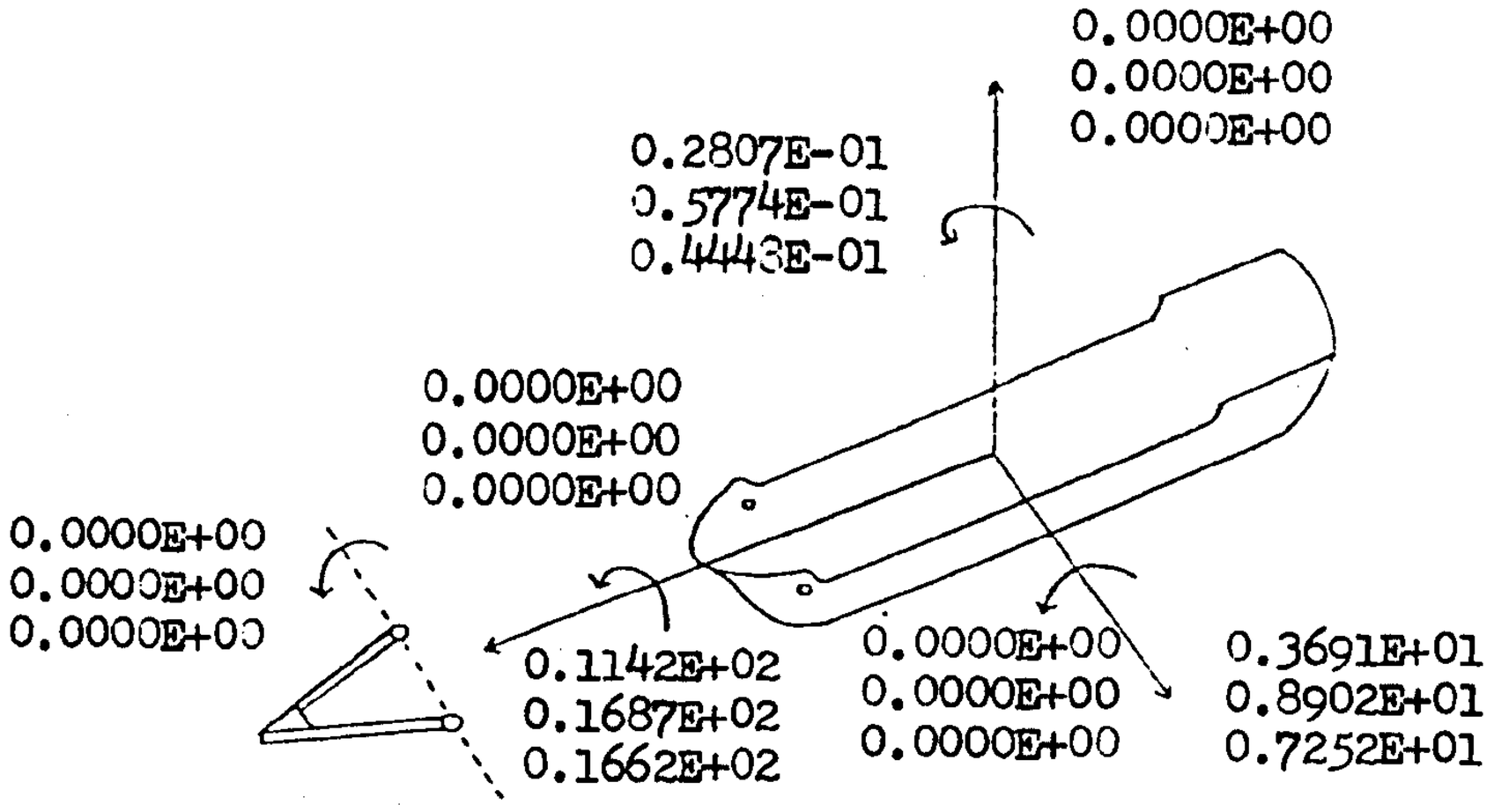

FIG. 9.45 THE EFFECT OF TANKER SIZE AND DRAFT ON THE SECOND ORDER RESPONSE
(FOR KEY SEE FIG. 9.26)

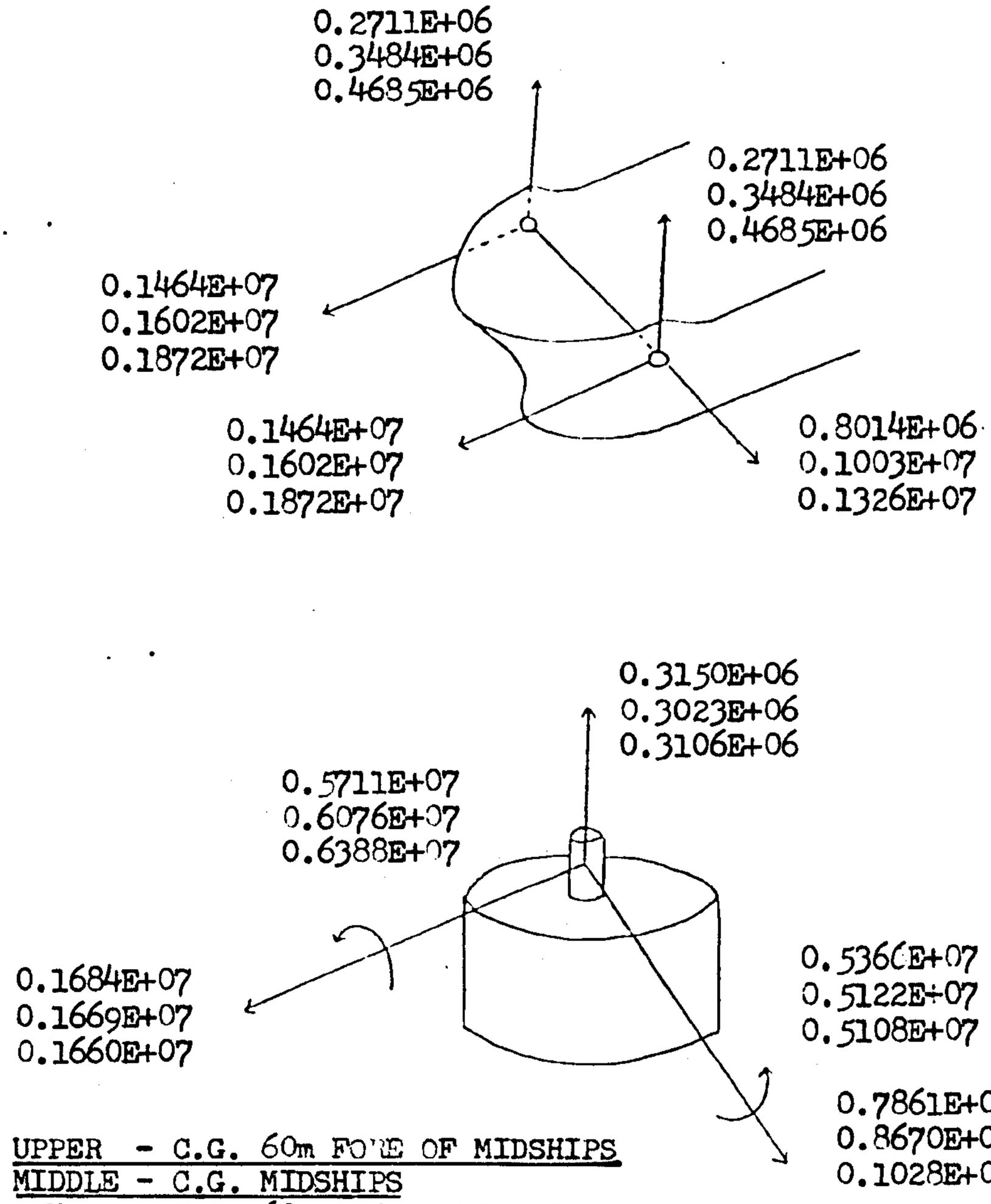

UPPER - C.G. 60m FORE OF MIDSHIPS
MIDDLE - C.G. MIDSHIPS
LOWER - C.G. 60m AFT OF MIDSHIPS

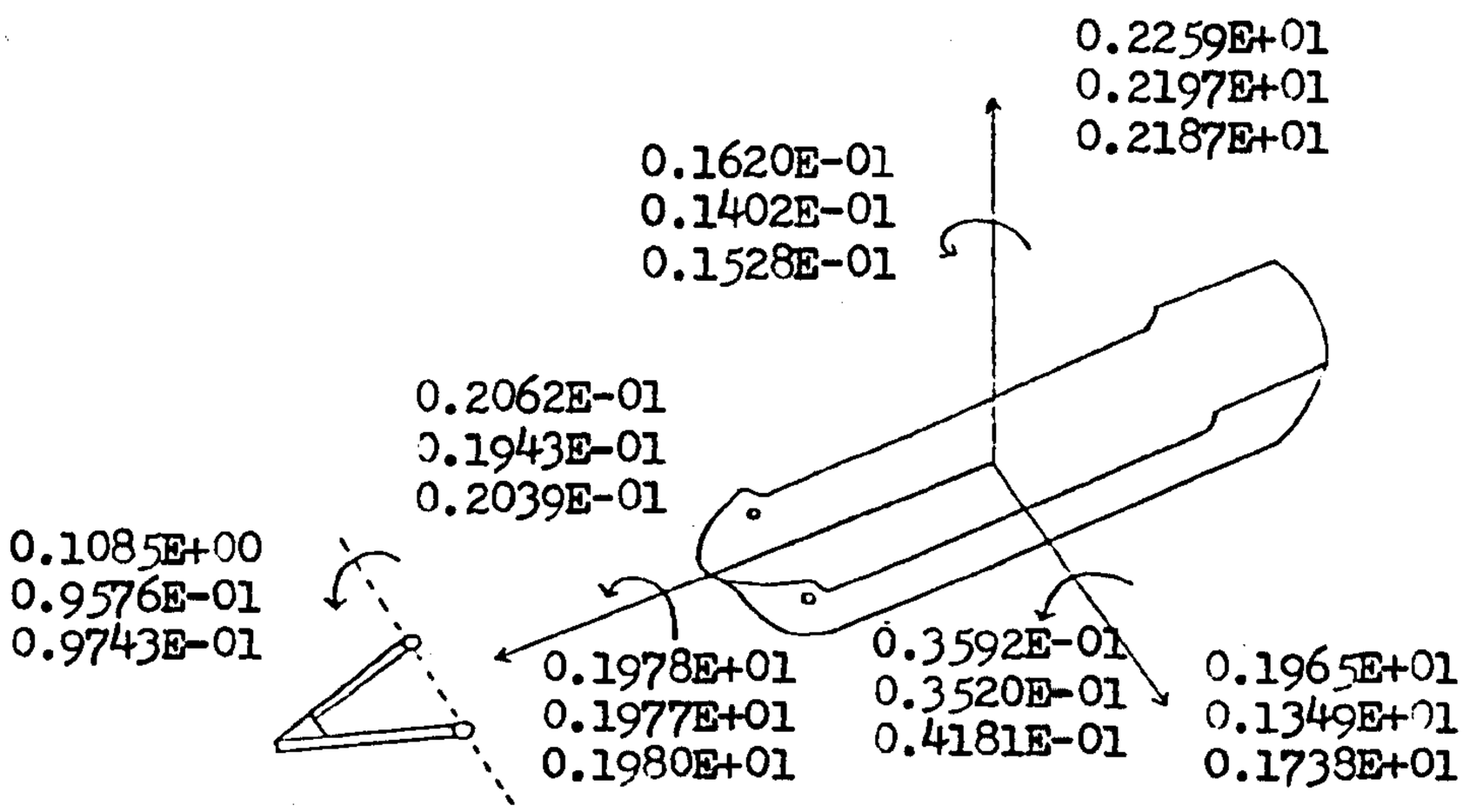

FIG. 9.46 THE EFFECT OF TANKER LOADING CONDITIONS AT HALF DRAFT ON THE FIRST ORDER RESPONSE
(FOR KEY SEE FIG. 9.26)

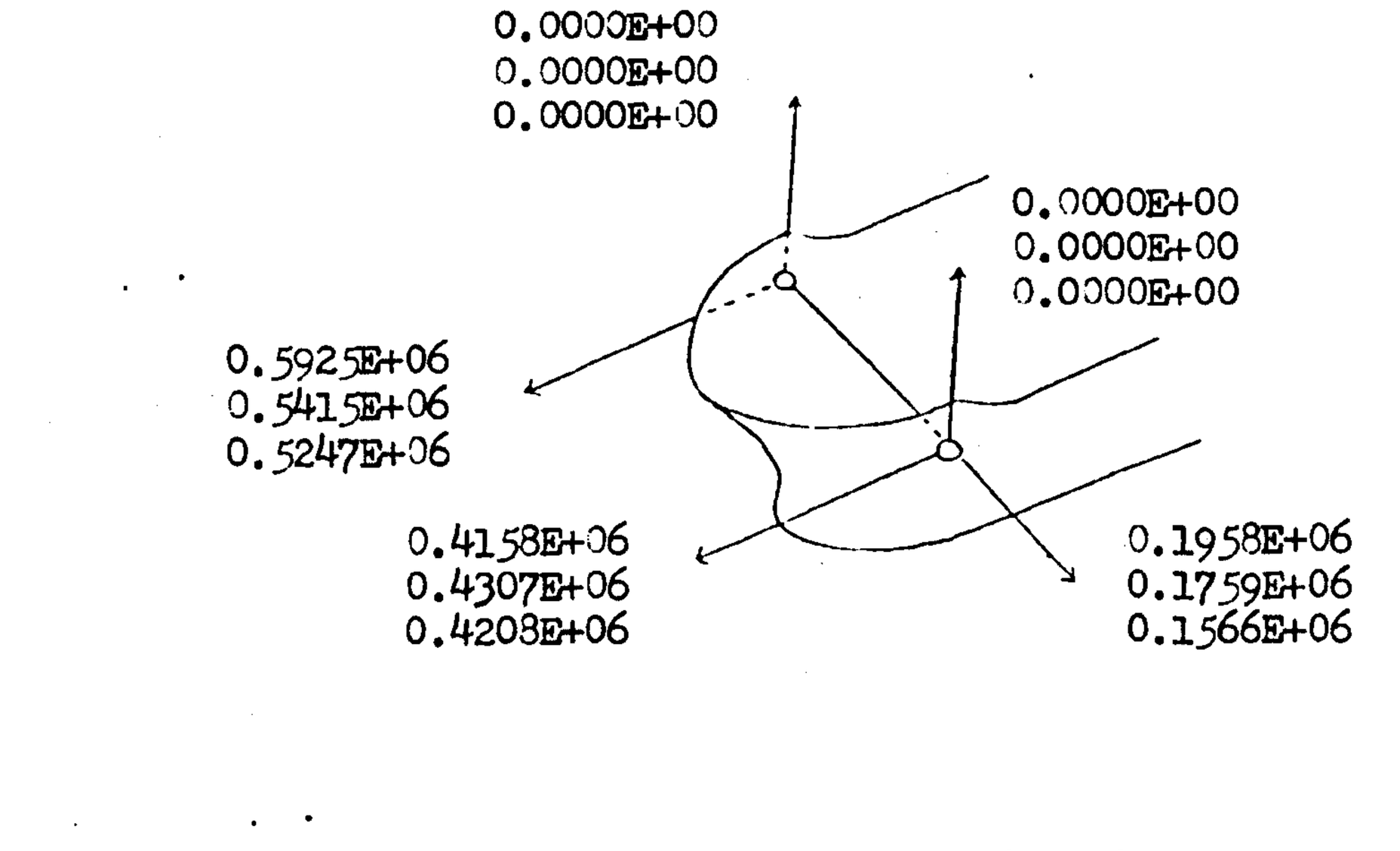

UPPER - C.G. 60m FORE OF MIDSHIPS
MIDDLE - C.G. MIDSHIPS
LOWER - C.G. 60m AFT OF MIDSHIPS

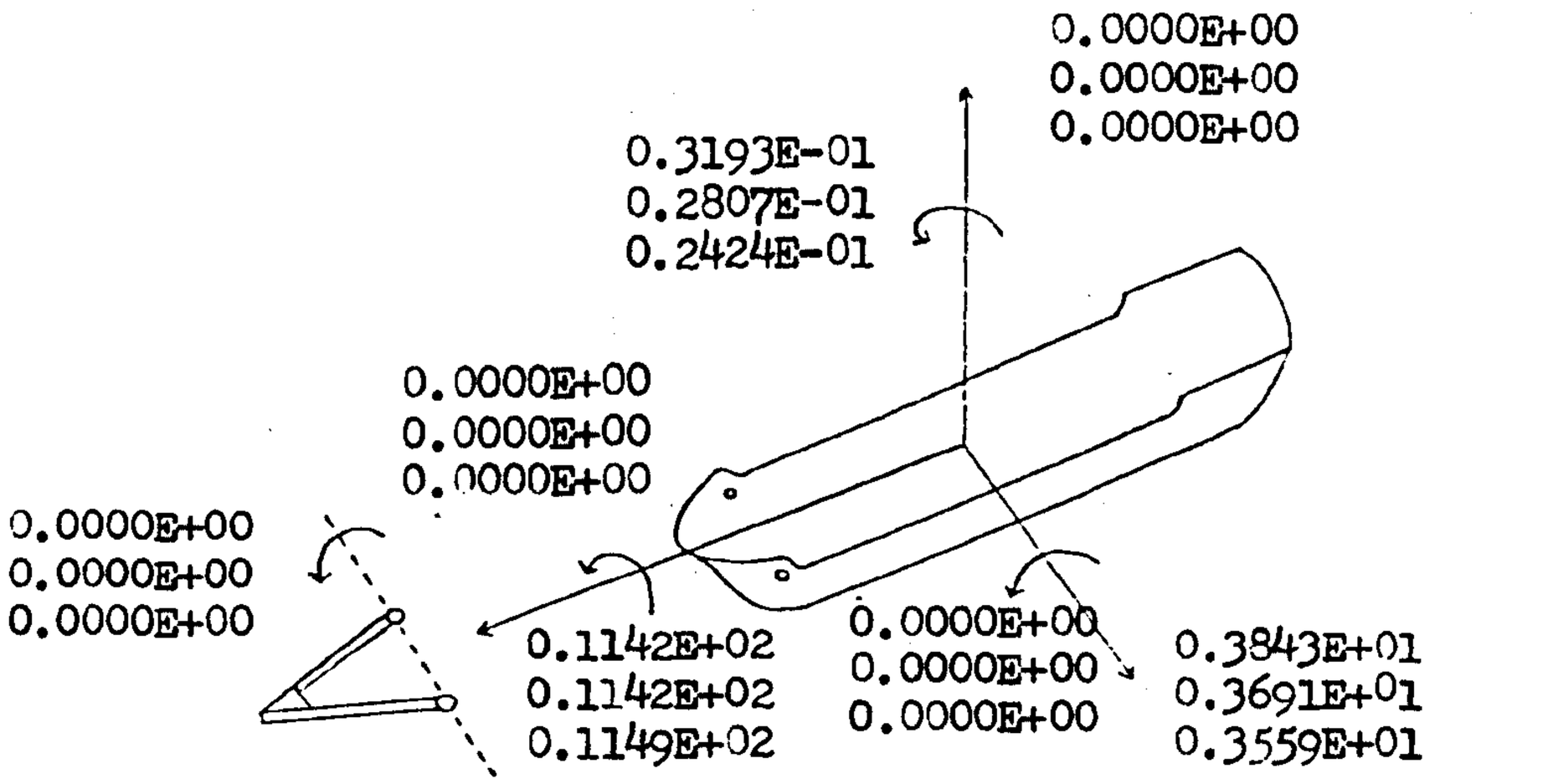

FIG. 9.47 THE EFFECT OF TANKER LOADING CONDITIONS AT HALF DRAFT ON THE SECOND ORDER RESPONSE
(FOR KEY SEE FIG. 9.26)

	CONFIGURATION OF FIG. 9.2	CONFIGURATION OF FIG. 9.3	CONFIGURATION OF FIG. 9.4
LINEAR COEFFICIENT (N/M)	9.36×10^4	3.63×10^4	1.15×10^4
CUBIC COEFFICIENT (N/M^3)	229.3	89.09	44.3
LINEARISED COEFFICIENT (N/M)	1.99×10^5	1.15×10^5	7.39×10^4

FIG. 9.48 LINEARISED STIFFNESS COEFFICIENTS FOR VARIOUS MOORING CONFIGURATIONS

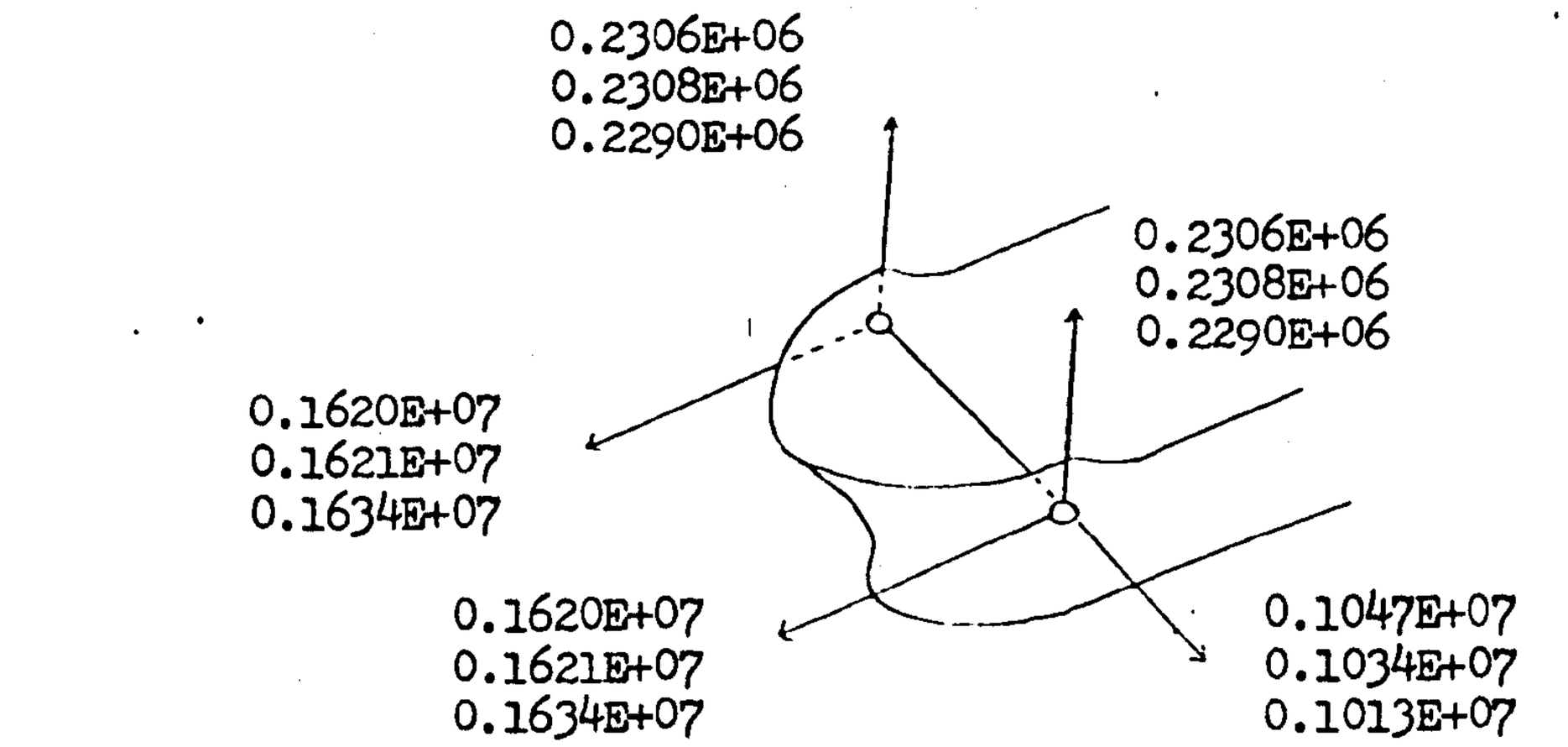

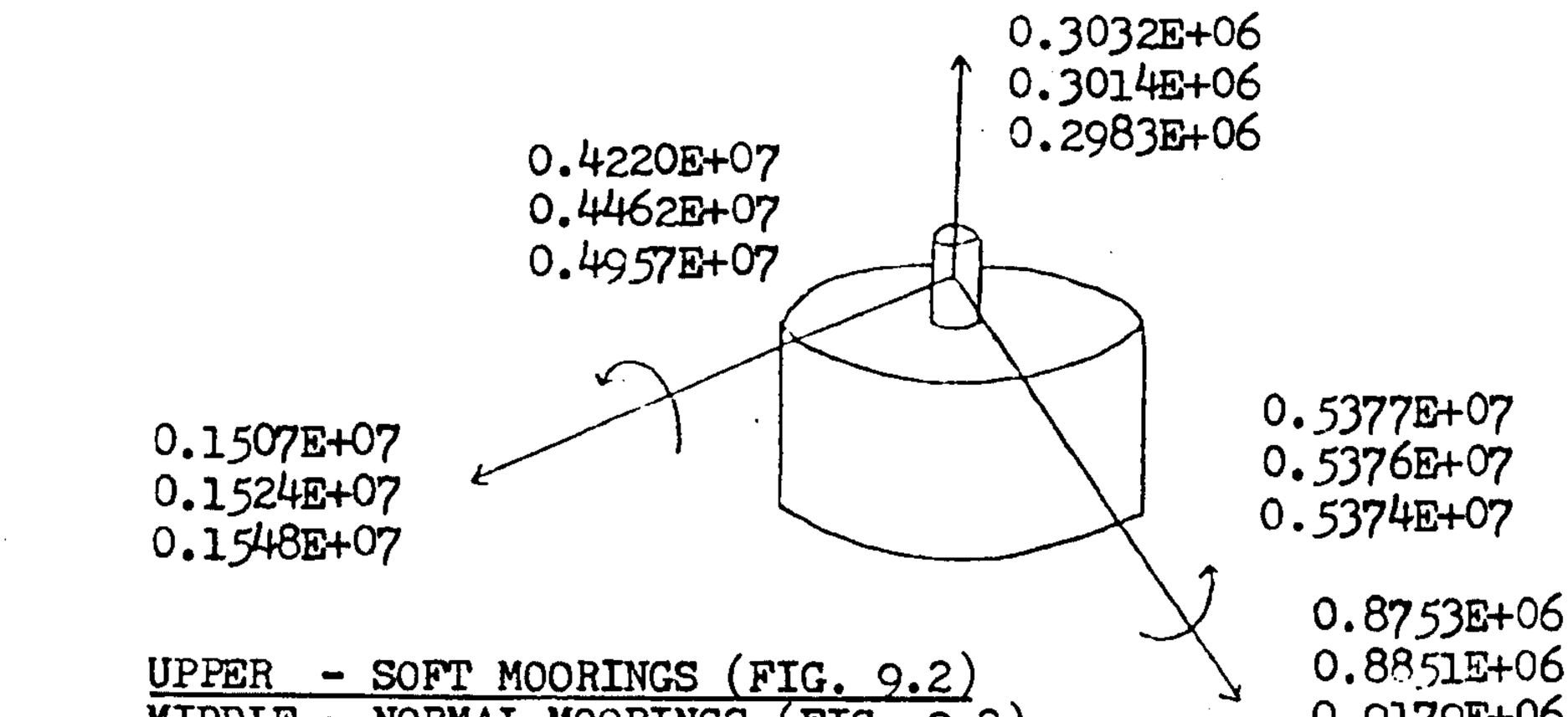

UPPER - SOFT MOORINGS (FIG. 9.2)
MIDDLE - NORMAL MOORINGS (FIG. 9.3)
LOWER - HARD MOORINGS (FIG. 9.4)

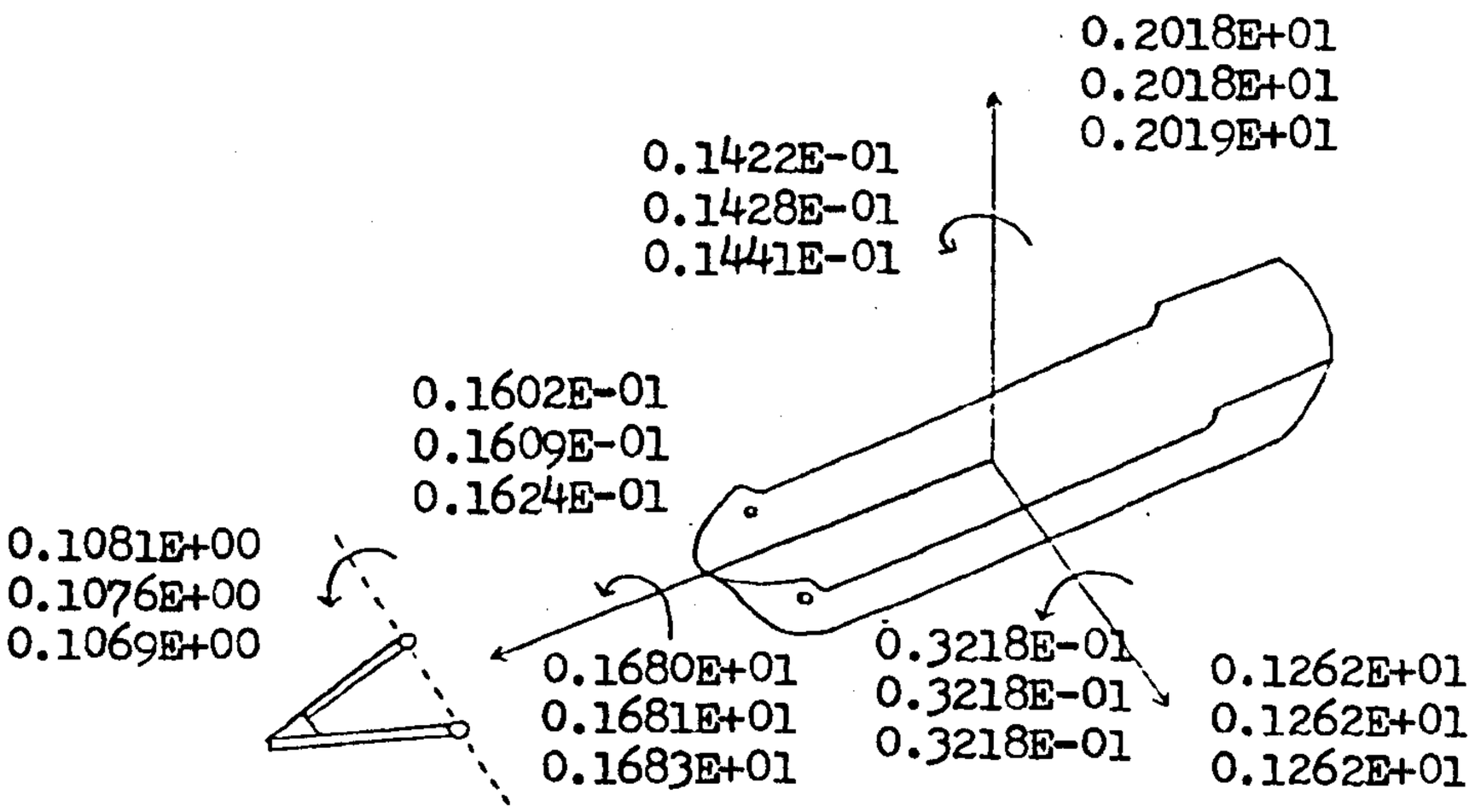

FIG. 9.49 THE EFFECT OF THE MOORING CONFIGURATION ON THE FIRST ORDER RESPONSE
(SEE FIG. 9.26 FOR KEY)

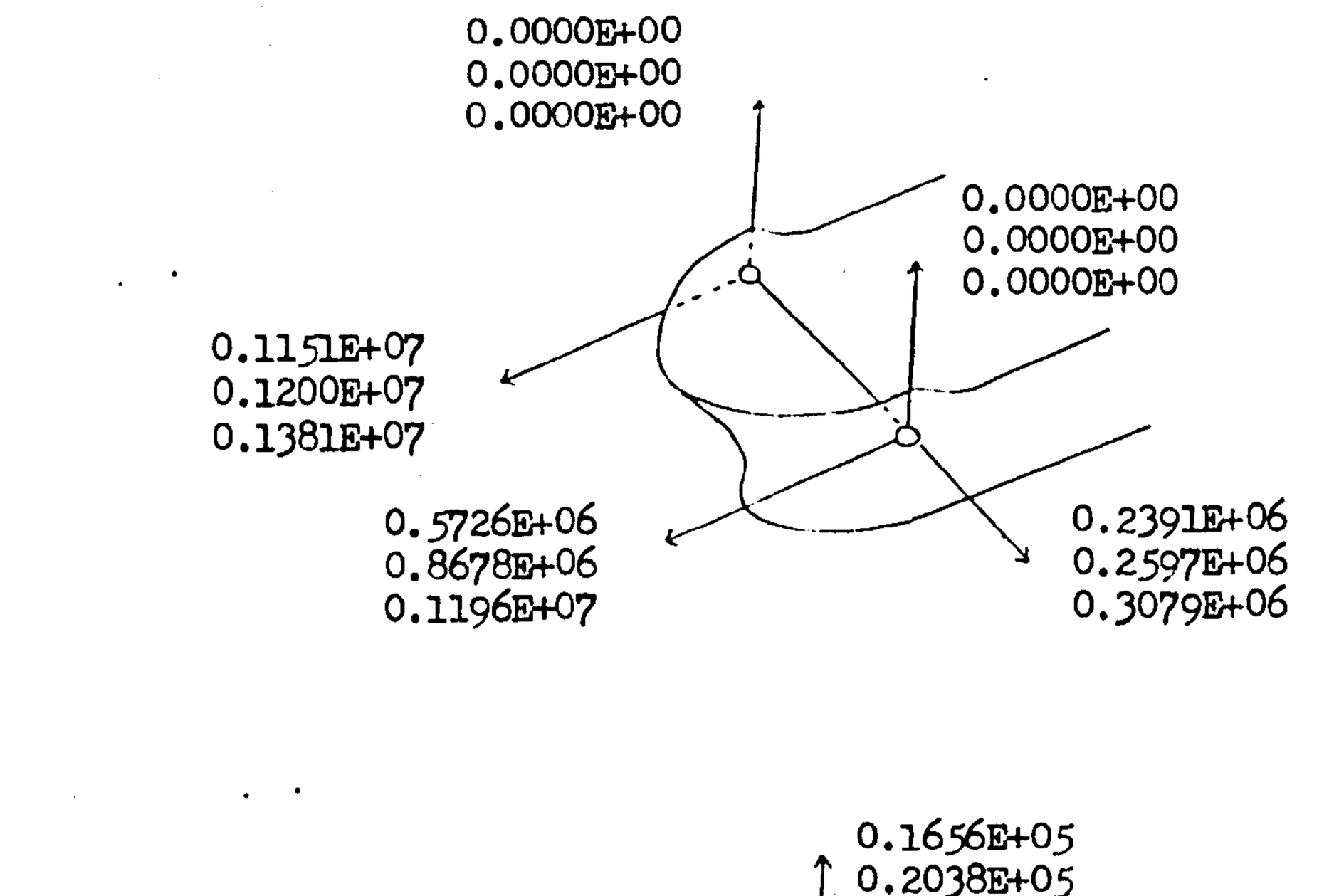

UPPER - SOFT MOORINGS (FIG. 9.2)
MIDDLE - NORMAL MOORINGS (FIG. 9.3)
LOWER - HARD MOORINGS (FIG. 9.4)

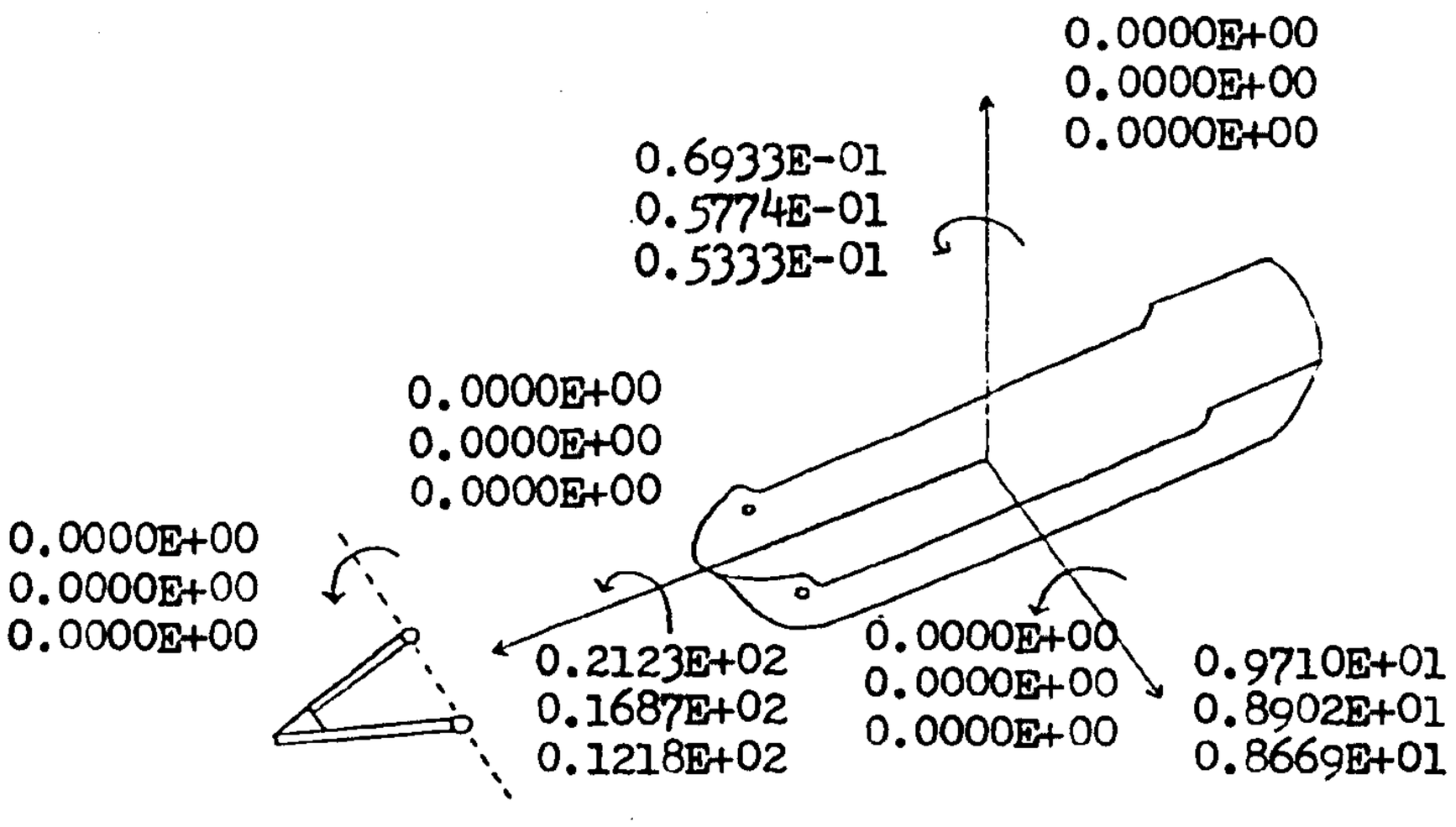

FIG. 9.50 THE EFFECT OF THE MOORING CONFIGURATION ON THE SECOND ORDER RESPONSE
(FOR KEY SEE FIG. 9.26)

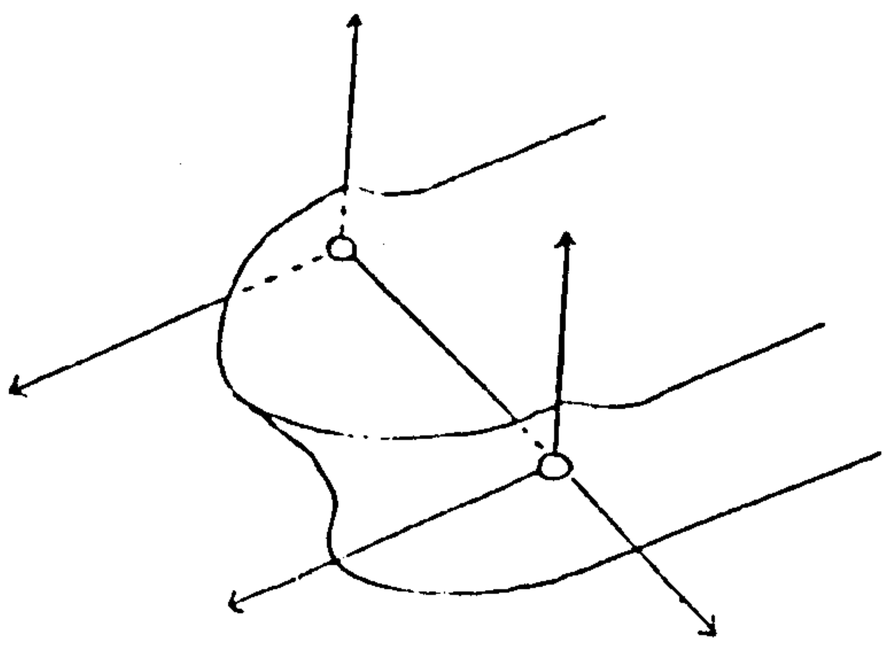

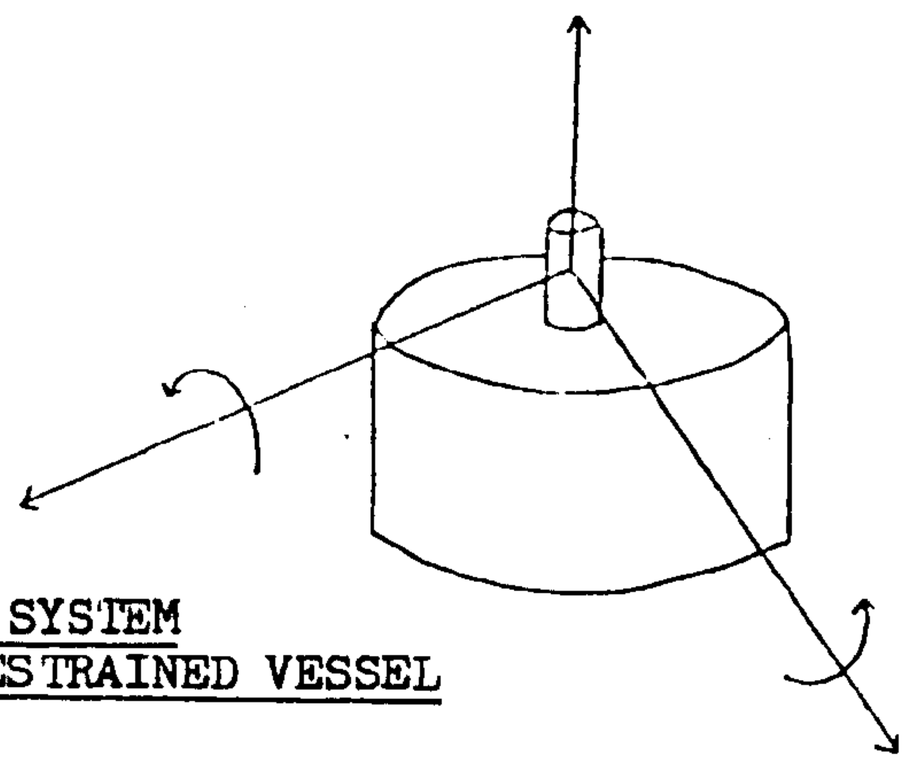

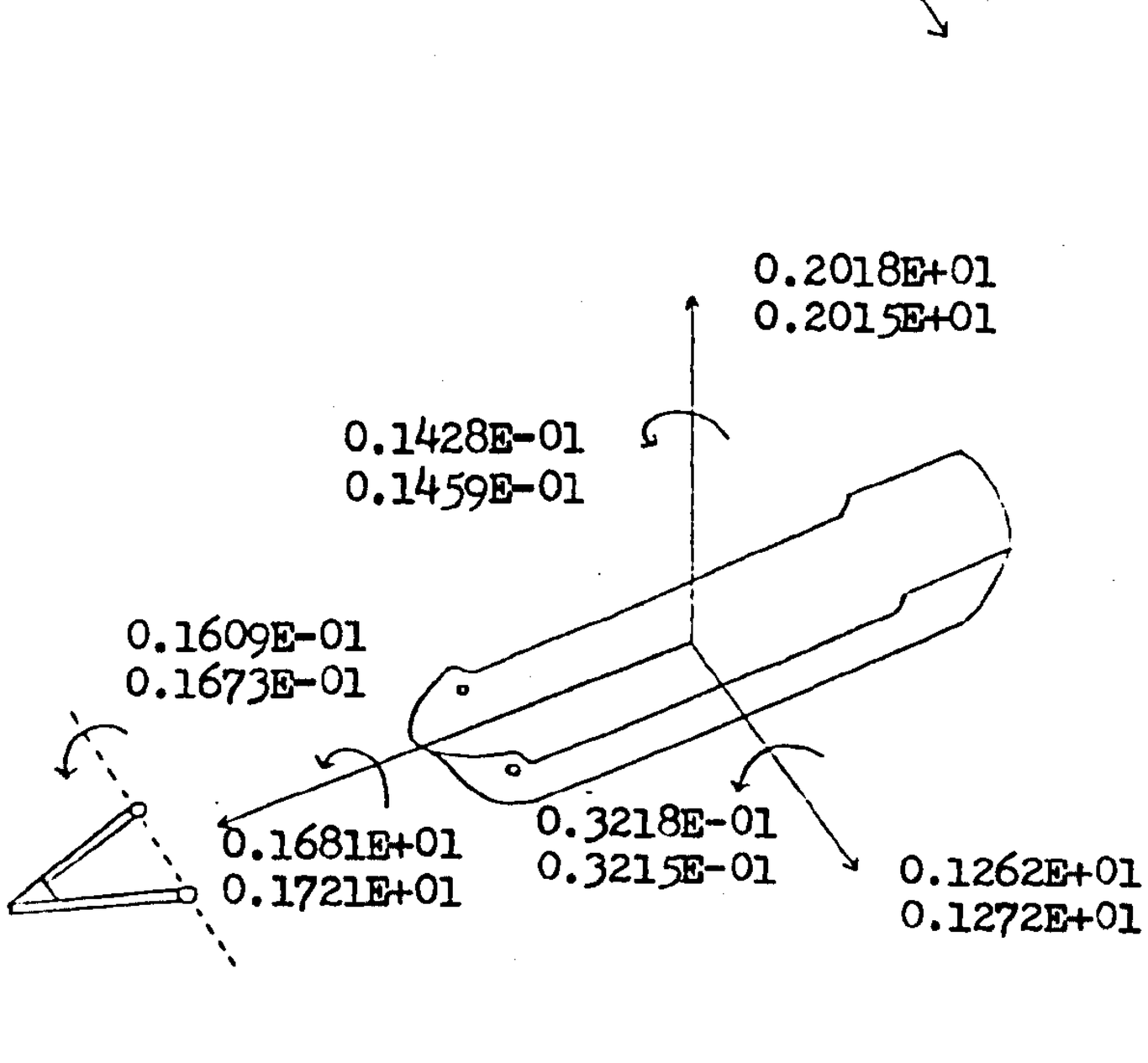

FIG. 9.51 COMPARISON TO THE FIRST ORDER RESPONSE OF AN UNRESTRAINED VESSEL
(FOR KEY SEE FIG. 9.26)

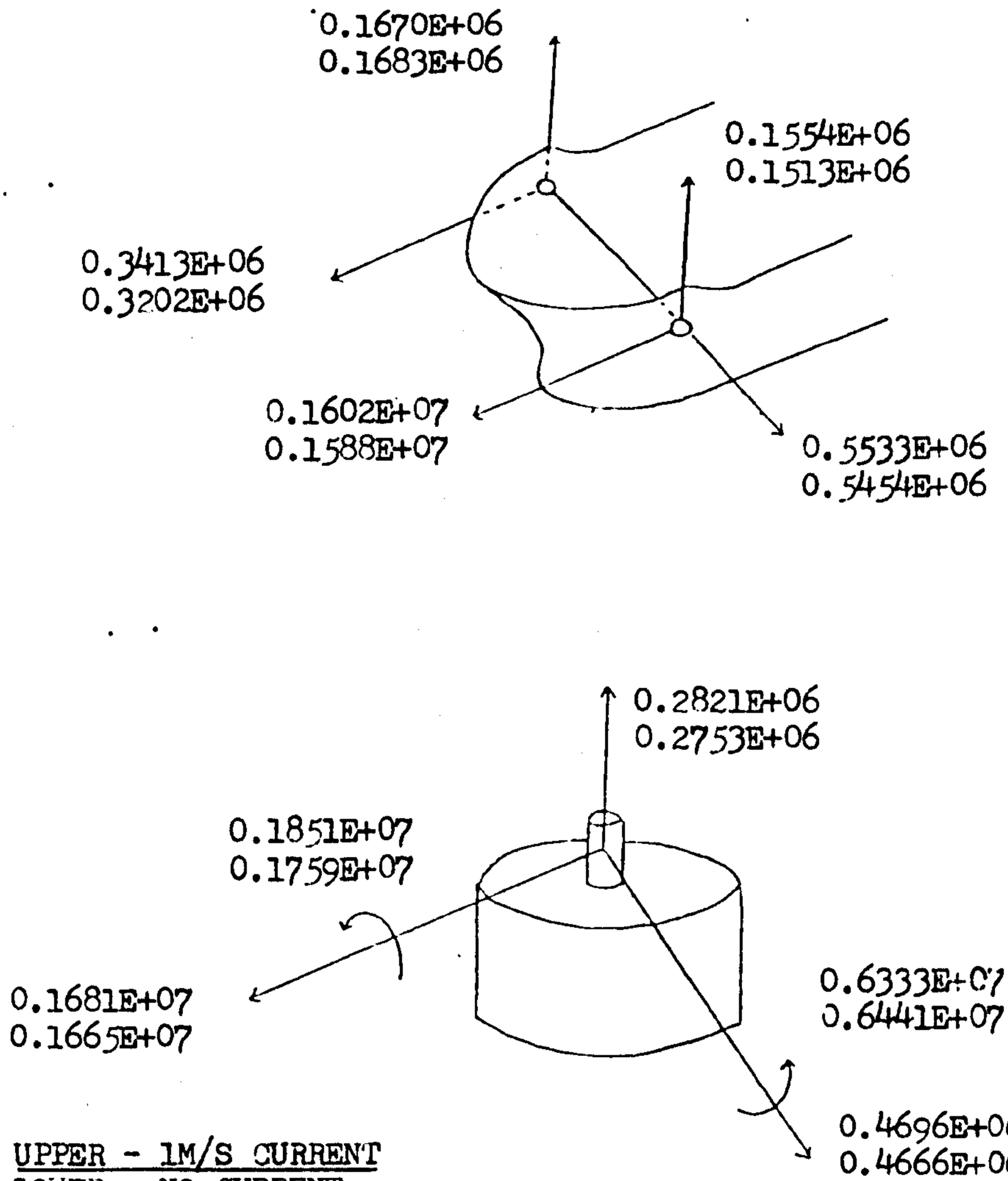

FIG. 9.52 THE EFFECT OF CURRENT ON THE FIRST ORDER RESPONSE (SEE FIG. 9.26 FOR KEY)

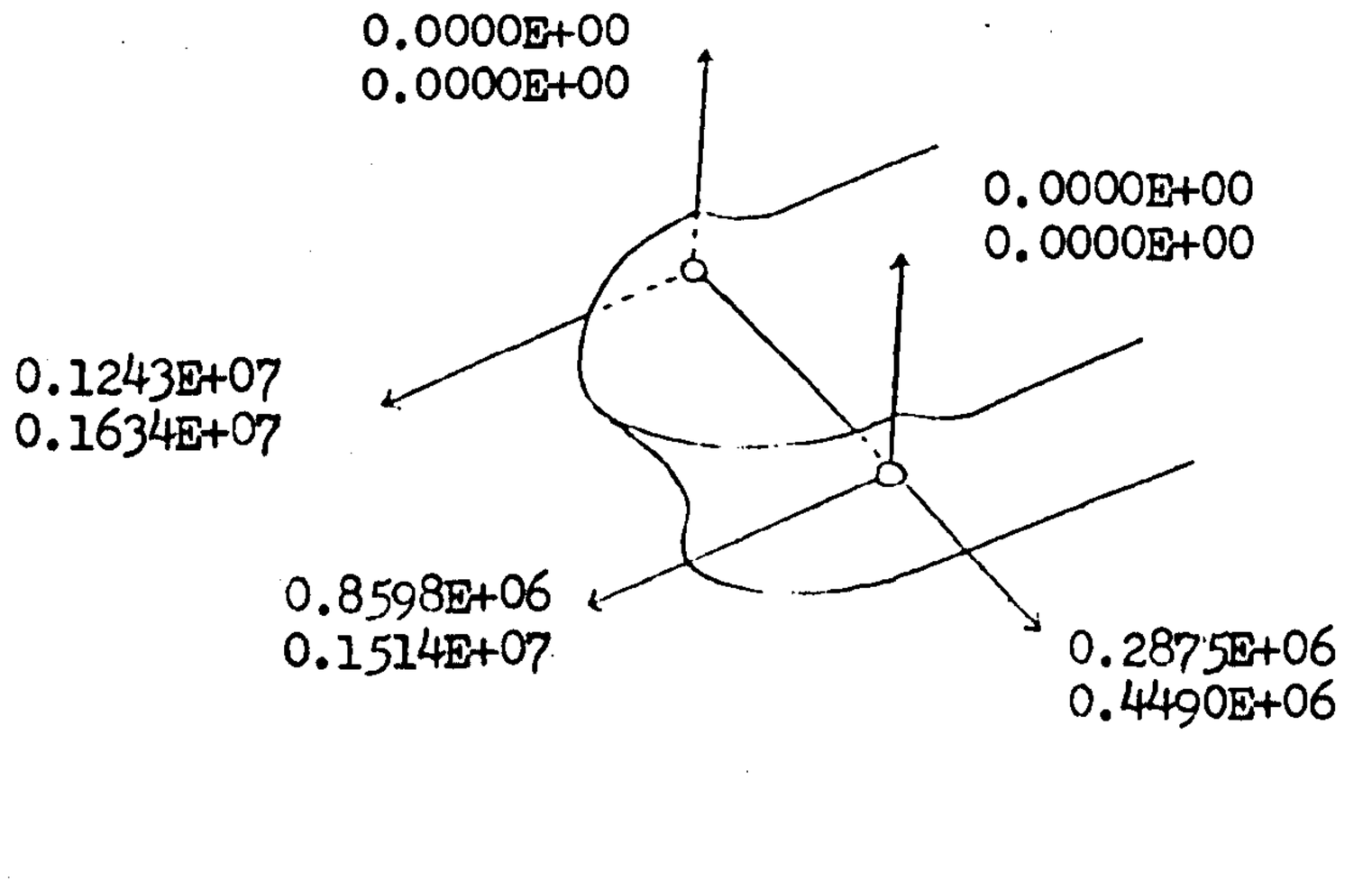

FIG. 9.53 THE EFFECT OF CURRENT ON THE SECOND ORDER RESPONSE (FOR KEY SEE FIG. 9.26)

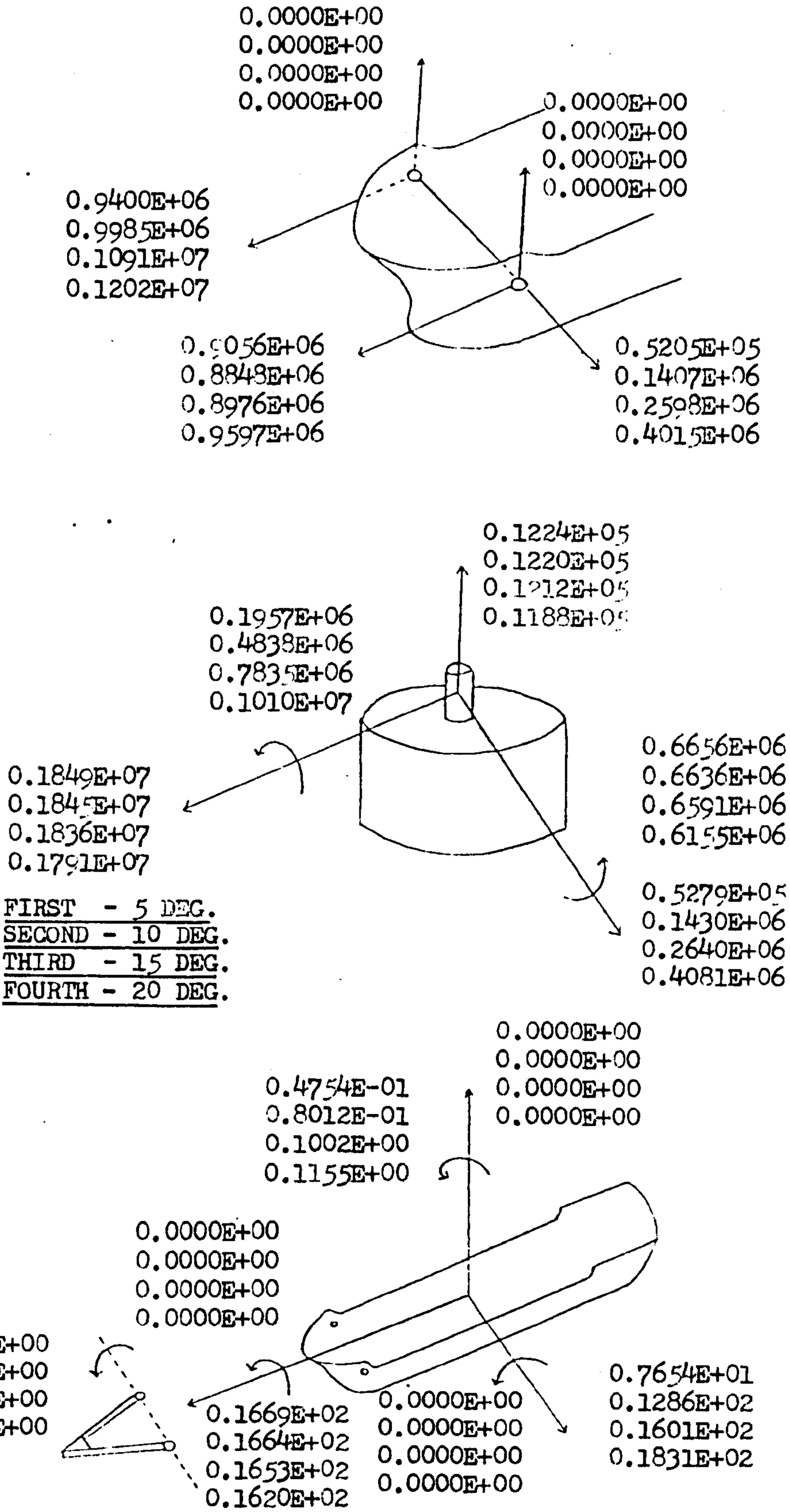

FIG. 9.54 THE EFFECT OF INCIDENCE OF SEASTATE ON THE SECOND ORDER RESPONSE
(FOR KEY SEE FIG. 9.26)

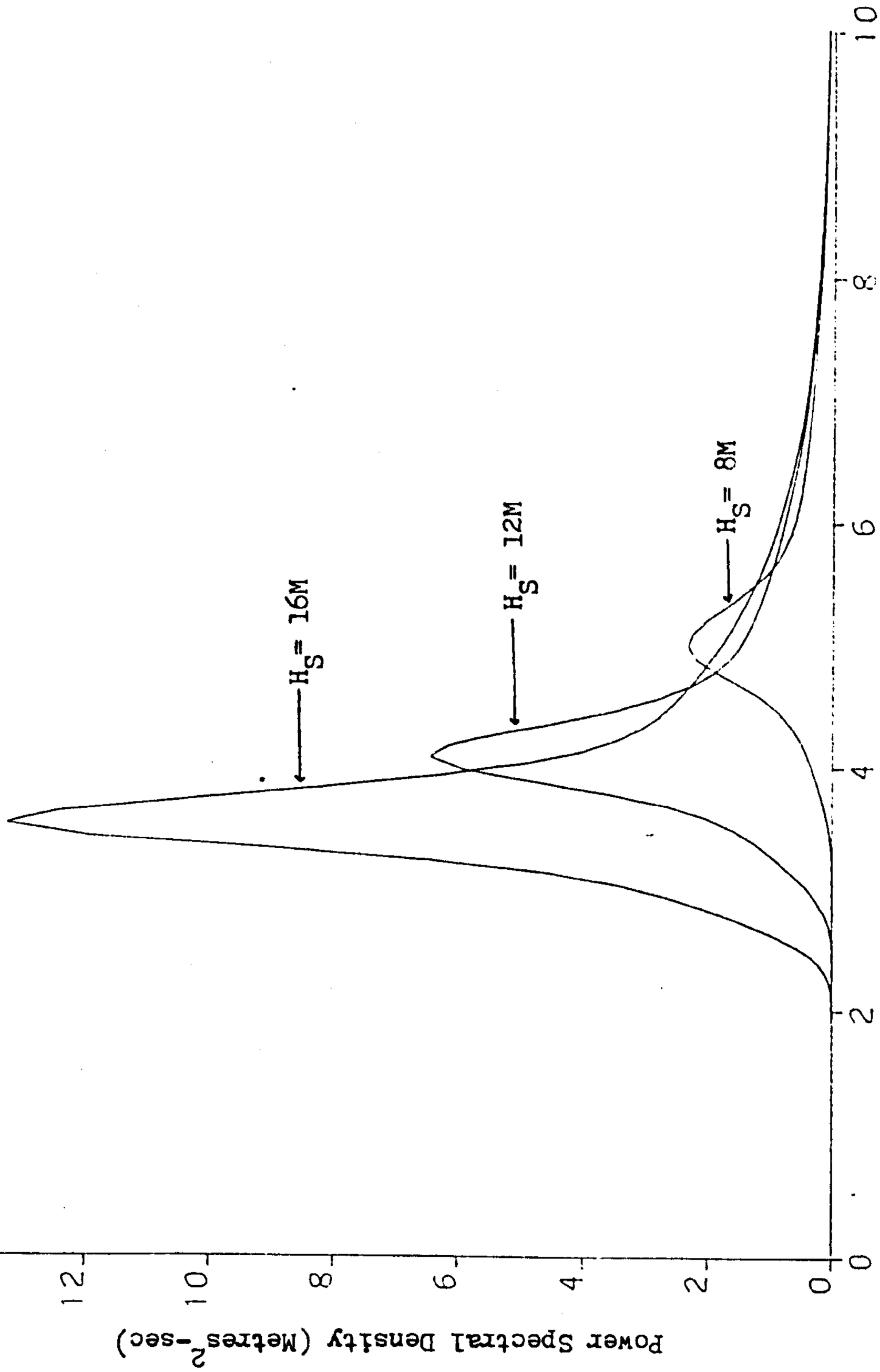

FIG. 9.55 THE JONSWAP SPECTRUM FOR VARIOUS SIGNIFICANT WAVE HEIGHTS

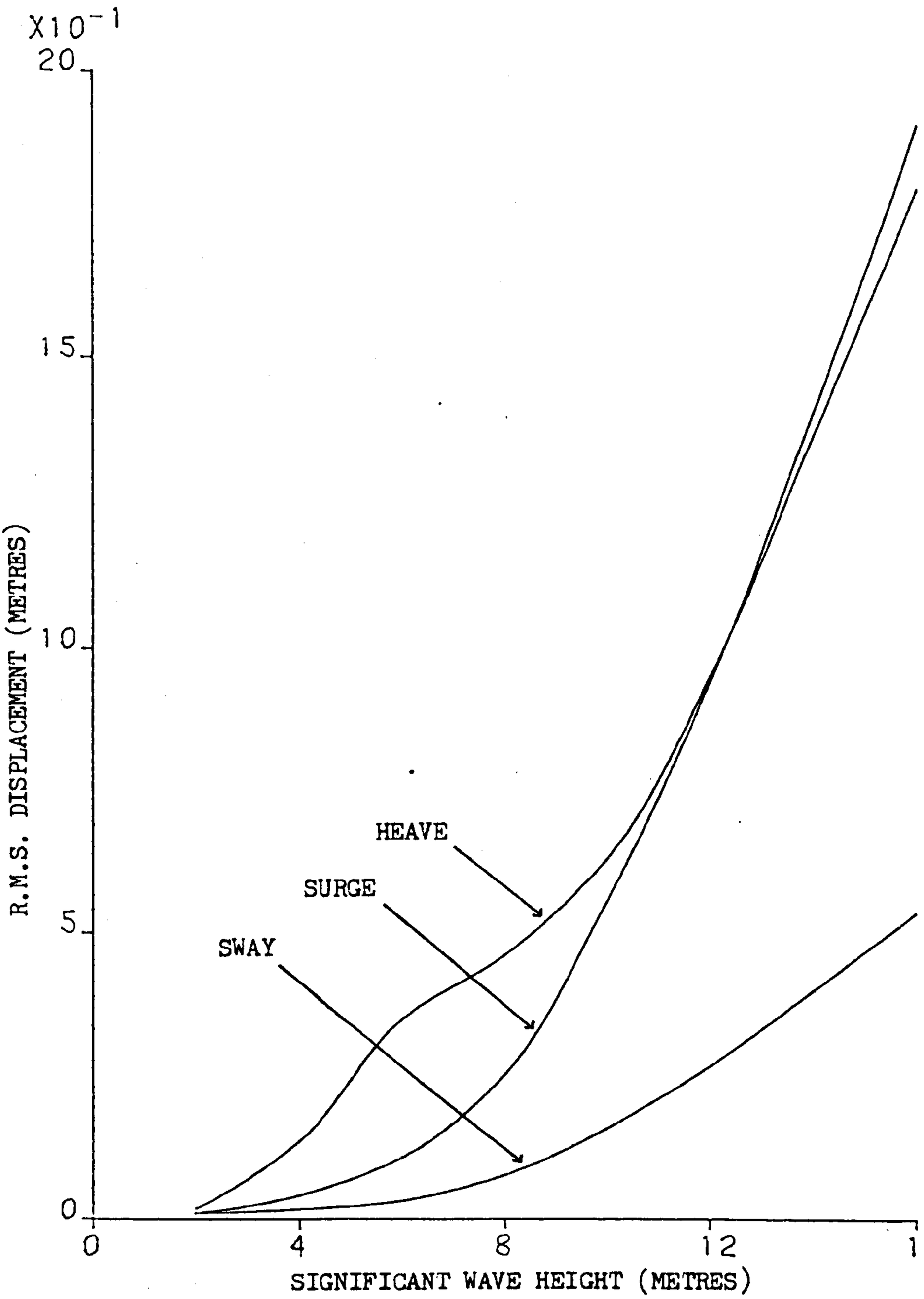

FIG. 9.56 R.M.S. FIRST ORDER TRANSLATIONAL DISPLACEMENTS VS H_S

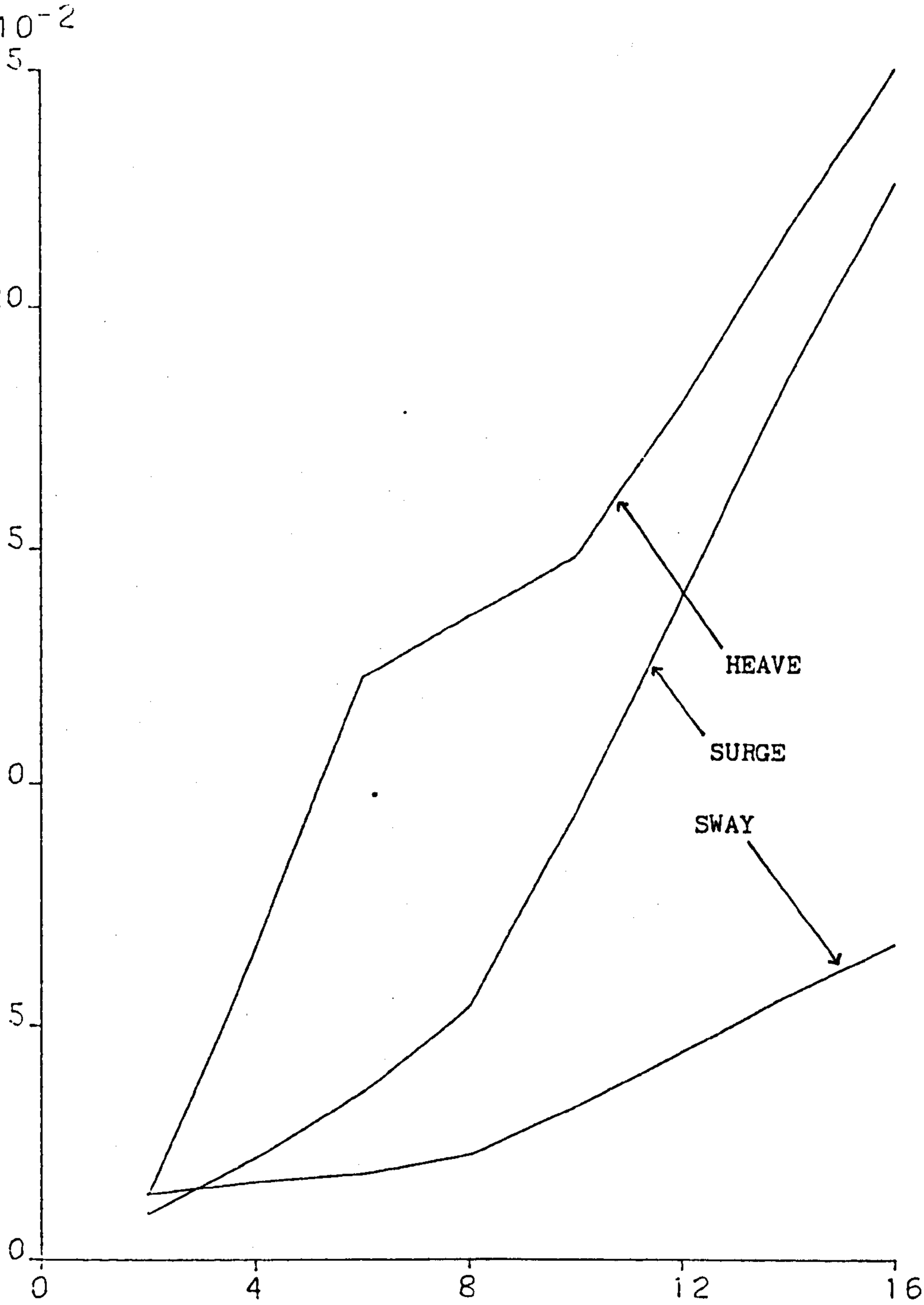

FIG. 9.57 R.M.S. FIRST ORDER TRANSLATIONAL ACCELERATIONS VS H_S

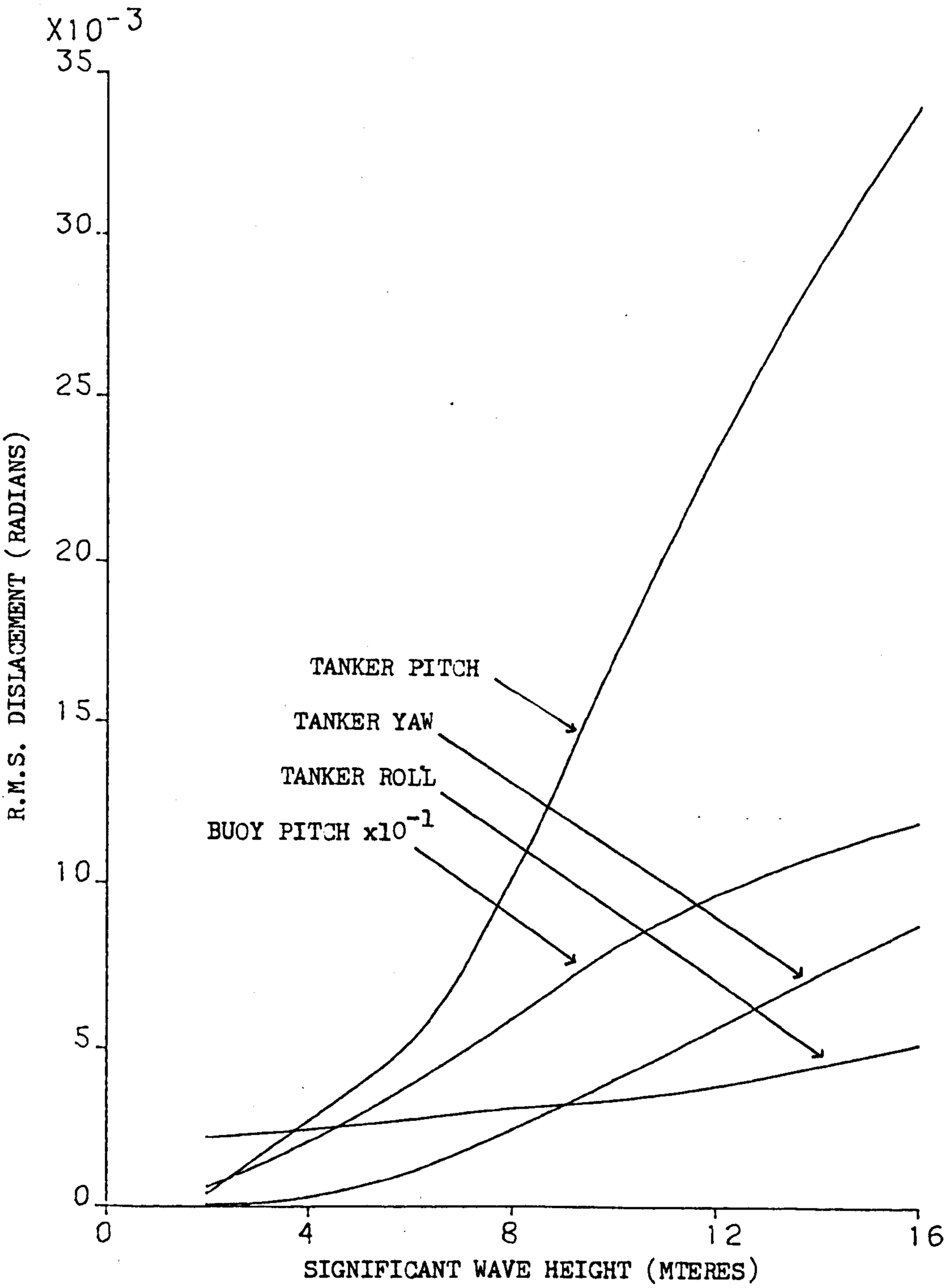

FIG. 9.58 R.M.S. FIRST ORDER ROTATIONAL DISPLACEMENTS VS H_S

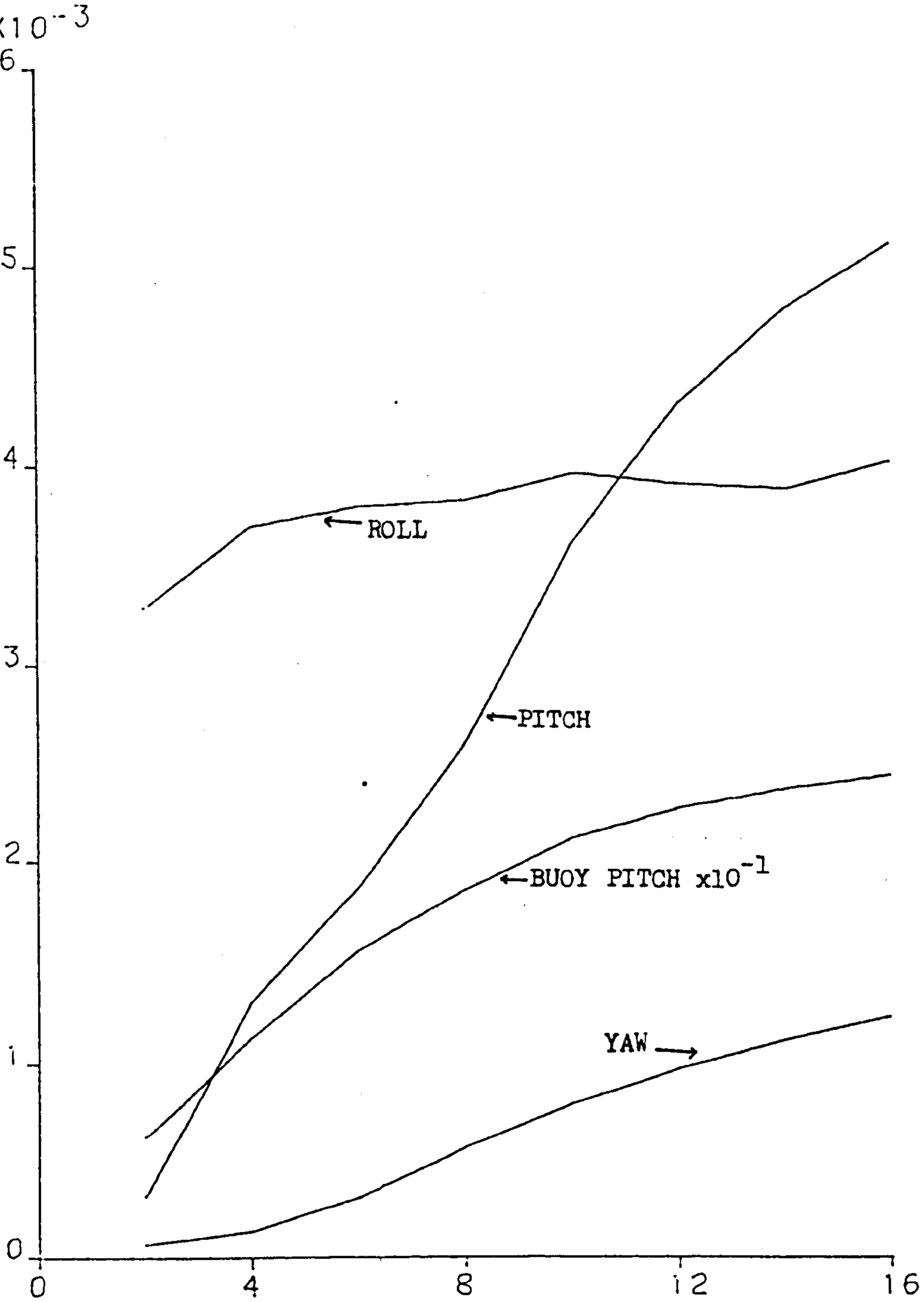

FIG. 9.59 R.M.S. FIRST ORDER ROTATIONAL ACCELERATIONS VS H_S

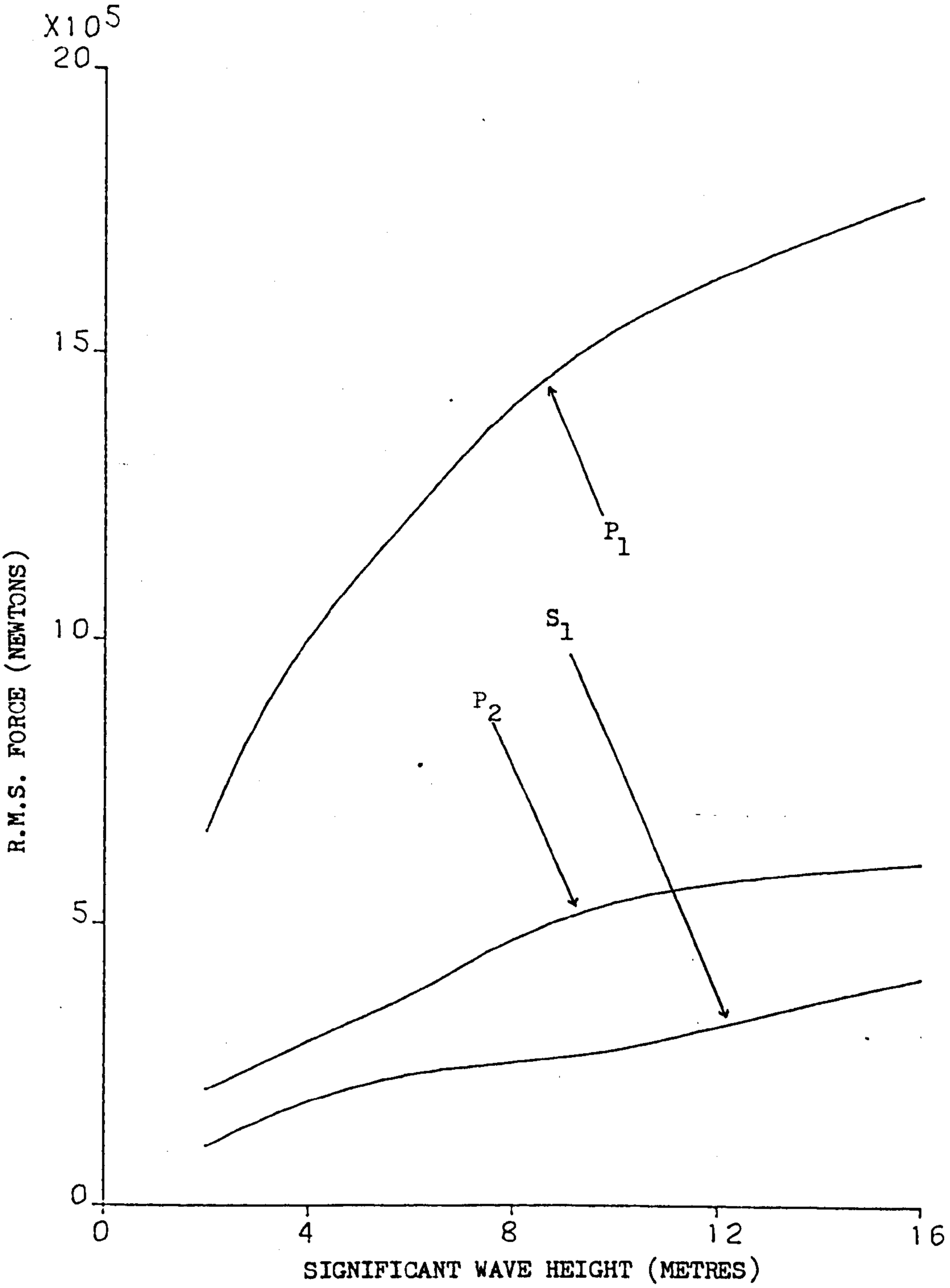

FIG. 9.60 R.M.S. FIRST ORDER LATERAL TANKER REACTIONS VS H_S

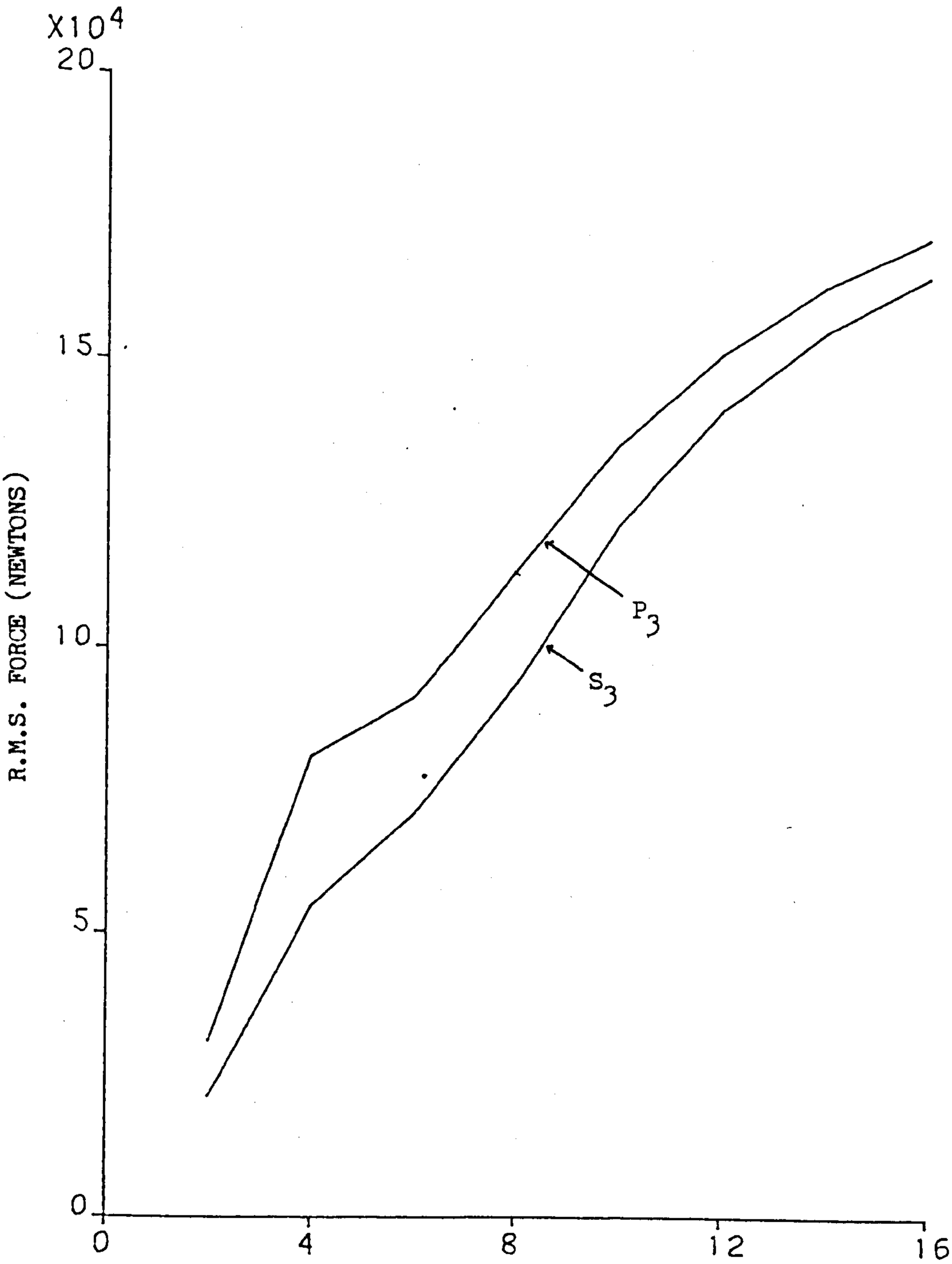

FIG. 9.61 R.M.S. FIRST ORDER VERTICAL TANKER REACTIONS VS H_S

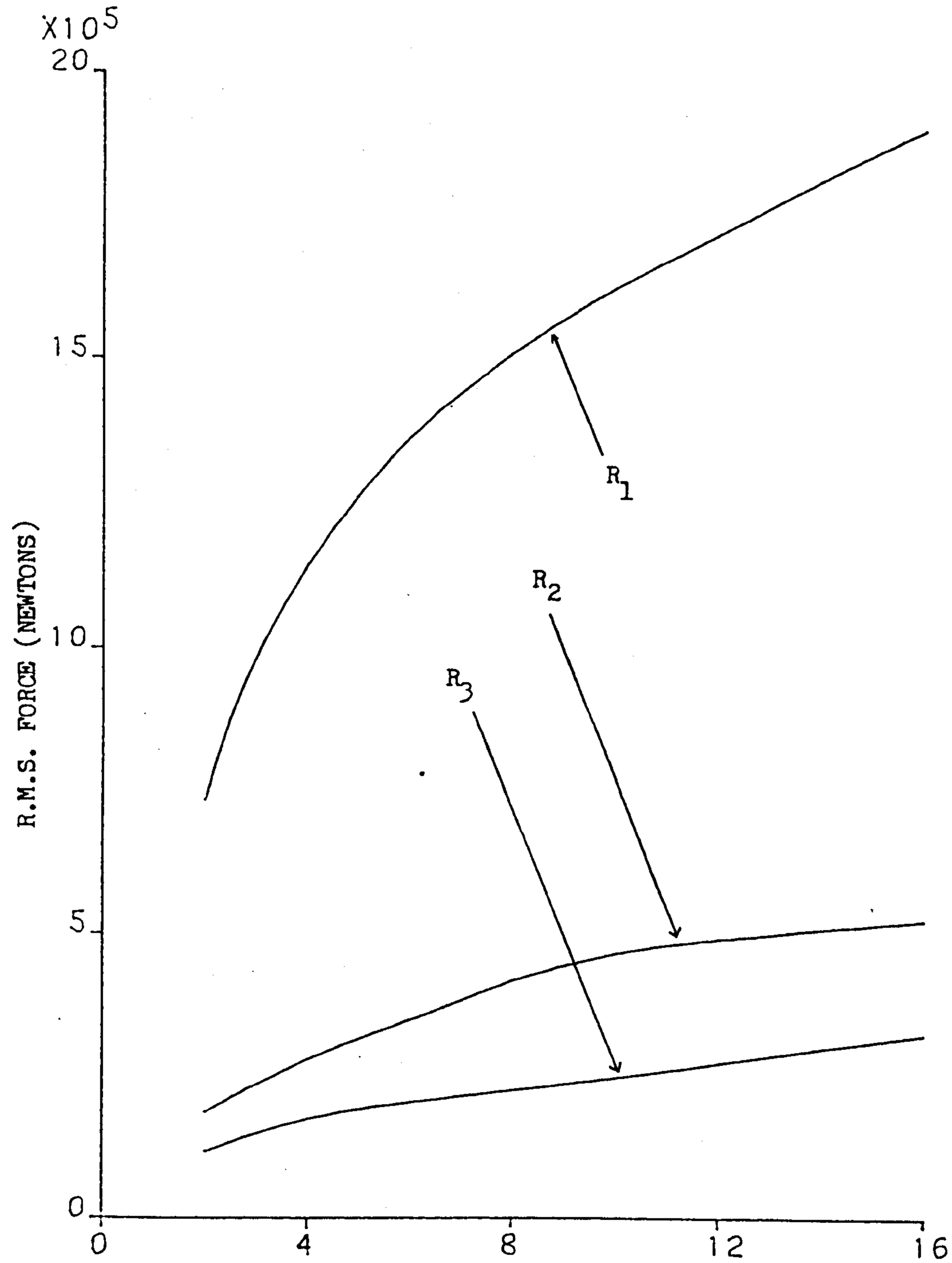

FIG. 9.62 R.M.S. FIRST ORDER BUOY REACTIONS VS H_S

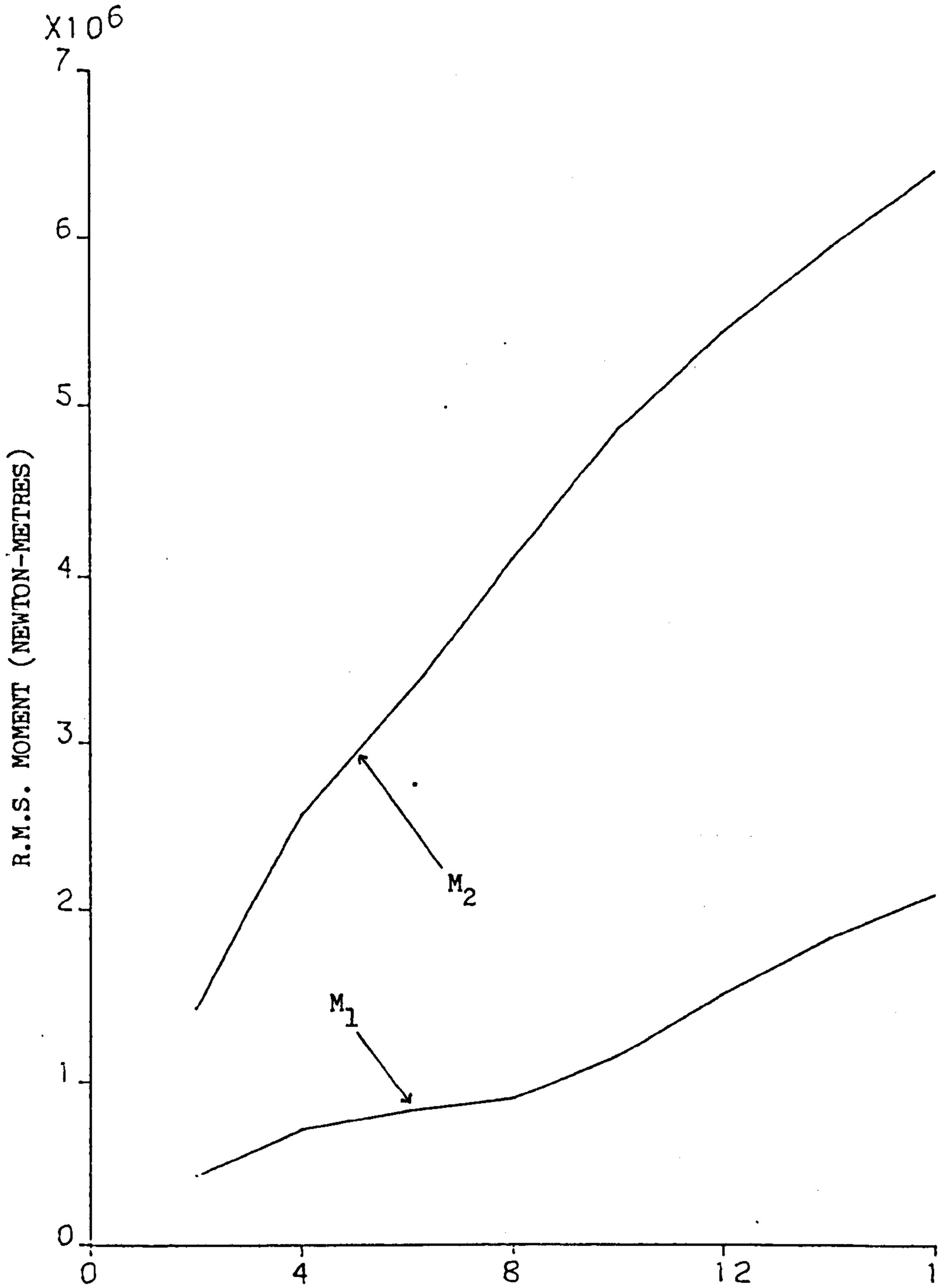

FIG. 9.63 R.M.S. FIRST ORDER BUOY MOMENTS VS H_S

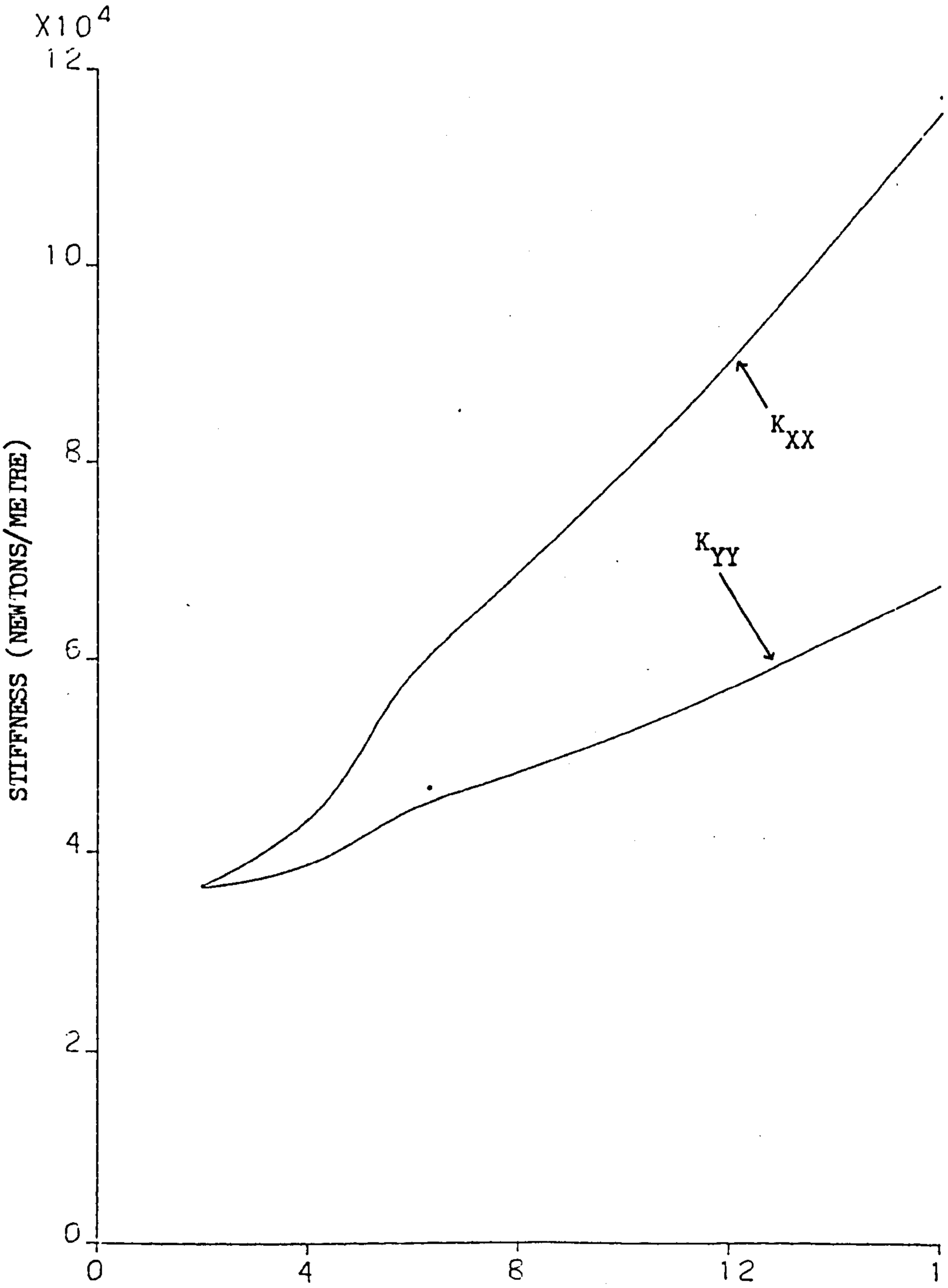

FIG. 9.64 LINEARISED HORIZONTAL PLANE STIFFNESS COEFFICIENTS VS H_S

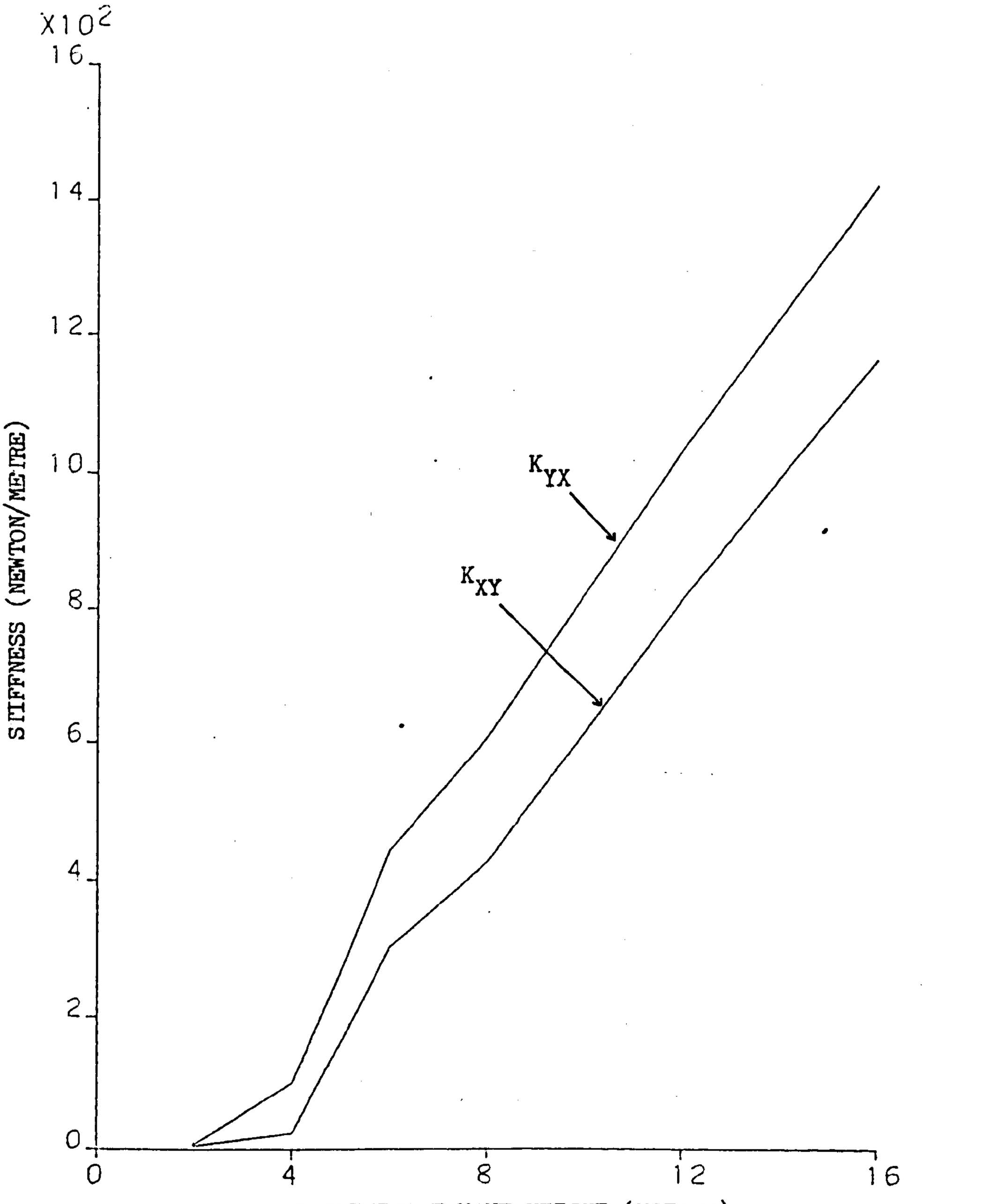

FIG. 9.65 LINEARISED HORIZONTAL PLANE STIFFNESS COEFFICIENTS VS H_S

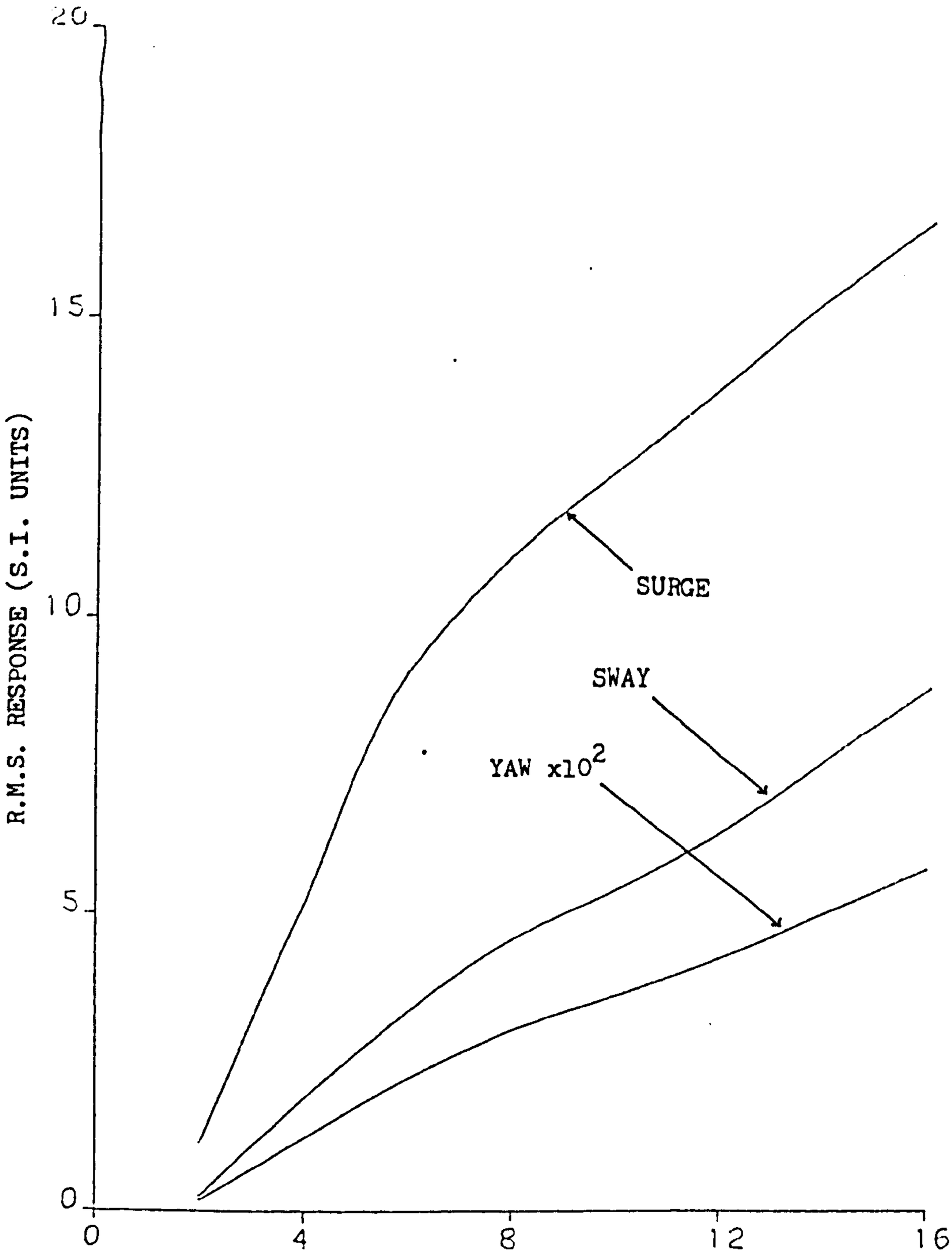

FIG. 9.66 R.M.S. SECOND ORDER RESPONSE VS H_S

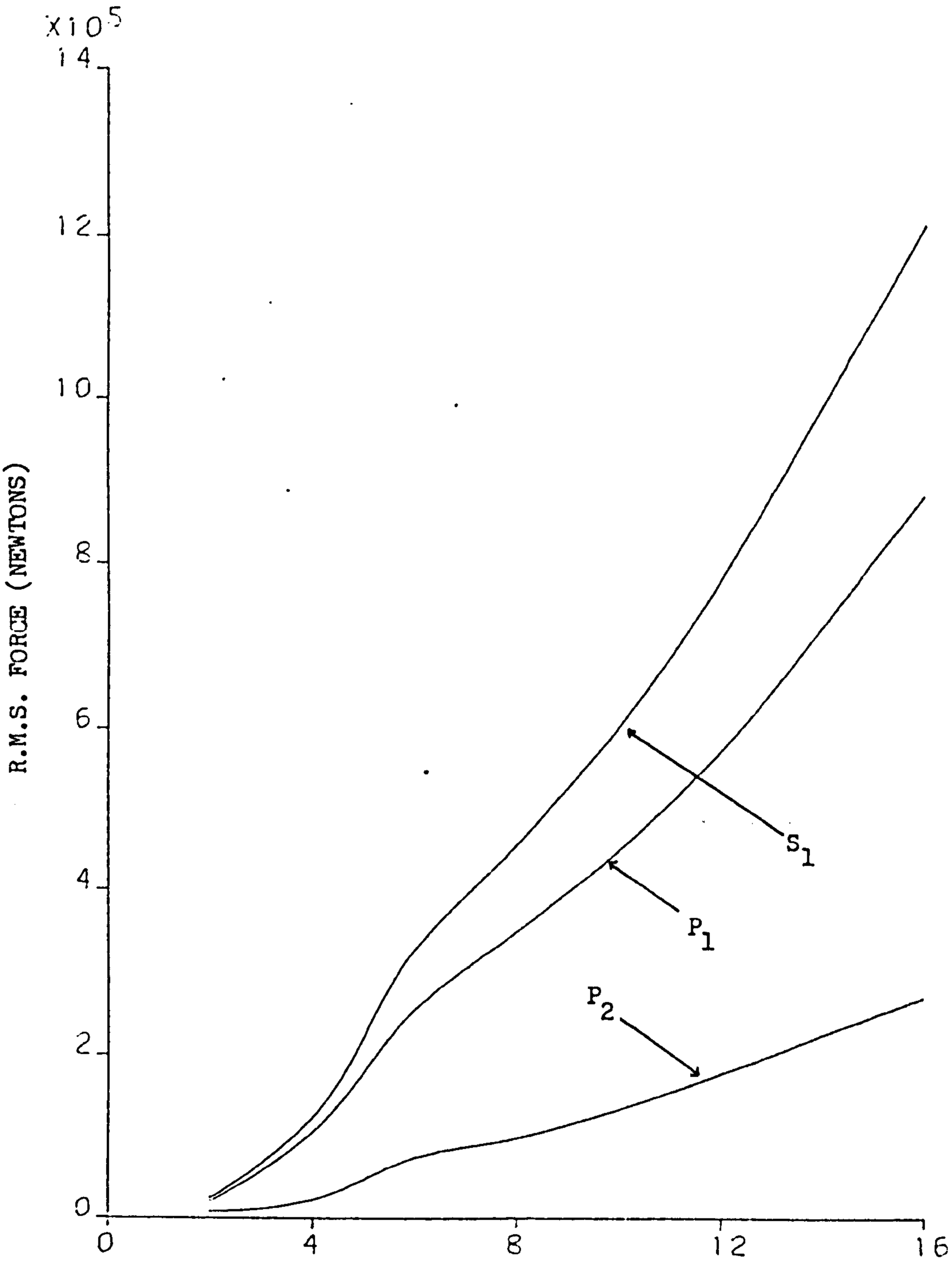

FIG. 9.67 R.M.S. SECOND ORDER TANKER REACTIONS VS H_S

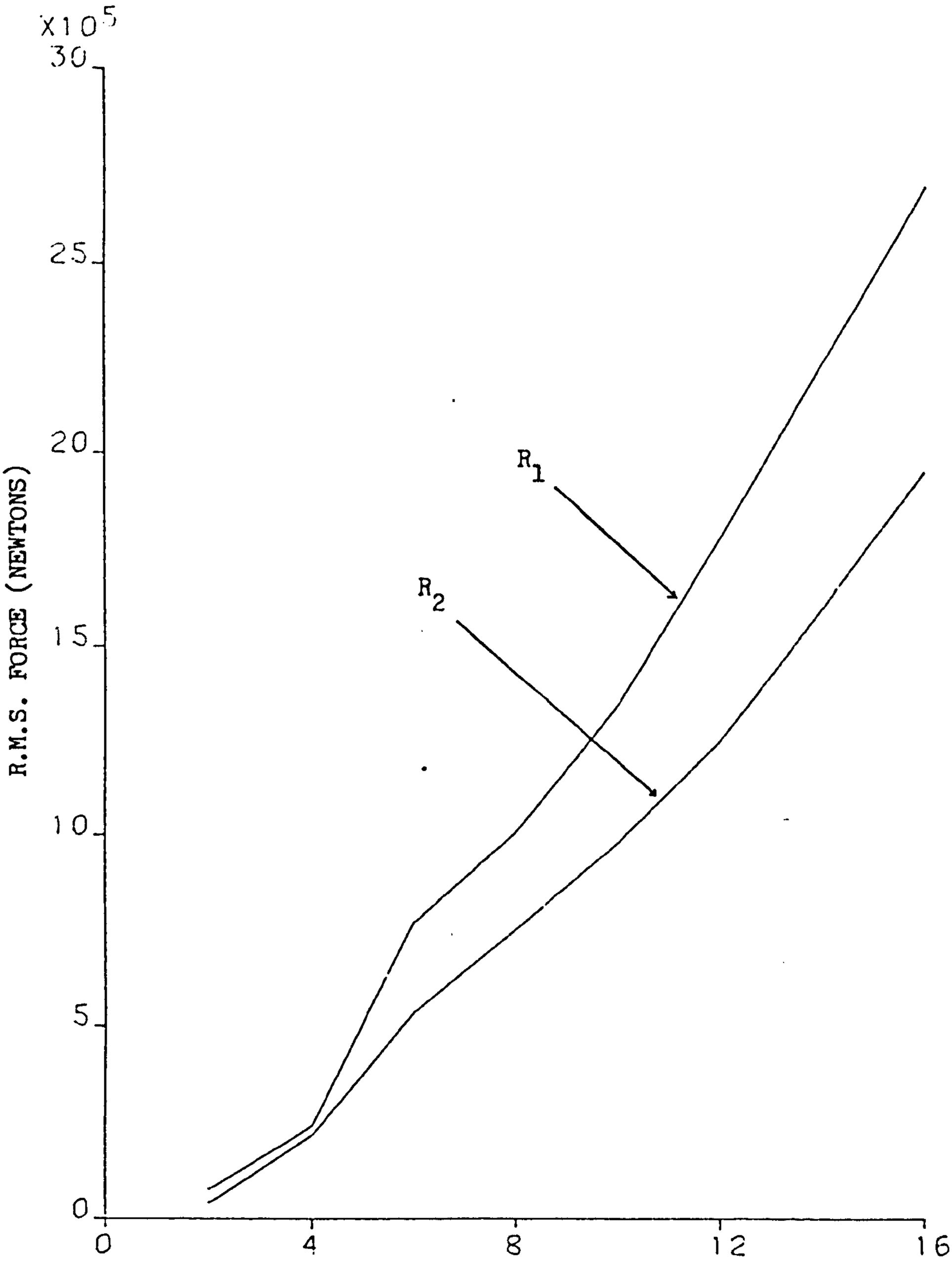

FIG. 9.68 R.M.S. SECOND ORDER BUOY REACTIONS VS H_S

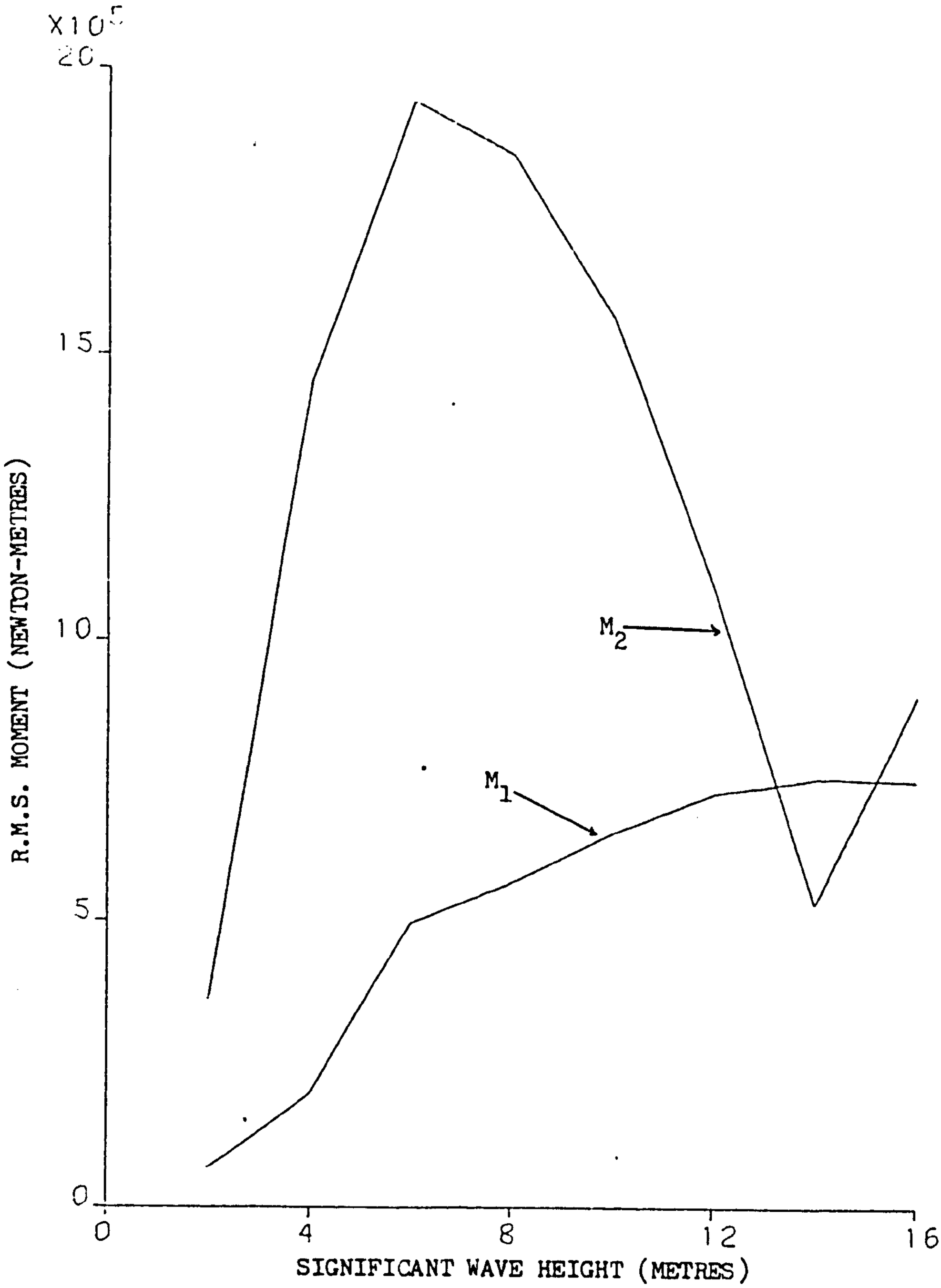

FIG. 9.69 R.M.S. SECOND ORDER BUOY MOMENTS VS H_S

	SURGE (M)	SWAY (M)	HEAVE (M)	ROLL (DEG)	PITCH (DEG)	YAW (DEG)	B. PITCH (DEG)	S1 (TONNES)	P1 (TONNES)
R.M.S. FIRST ORDER	1.91	0.53	1.79	0.29	1.95	0.49	6.79	40.08	177.70
R.M.S. SECOND ORDER	16.94	8.97	-	-	-	3.3	-	121.50	88.05
MAXIMUM EXPECTED	85.23	44.96	8.98	1.45	9.75	16.69	33.95	639.7	991.59

	P2 (TONNES)	S3 (TONNES)	P3 (TONNES)	R1 (TONNES)	R2 (TONNES)	R3 (TONNES)	M1 (TONNE-M)	M2 (TONNE-M)
R.M.S. FIRST ORDER	60.10	16.43	17.11	189.8	51.63	32.16	207.80	639.30
R.M.S. SECOND ORDER	26.55	-	-	194.6	26.96	-	75.02	90.23
MAXIMUM EXPECTED	328.52	82.15	85.55	1359.3	291.23	160.80	1104.60	3228.20

FIG. 9.70 MAXIMUM EXPECTED VALUES FOR A SBS SYSTEM IN A DESIGN STORM (H_S = 16M)

FIG. A.1 PARAMETERS FOR THE JONSWAP SPECTRUM

H_s \ T_z	4.0-4.99	5.0-5.99	6.0-6.99	7.0-7.99	8.0-8.99	9.0-9.99	10.0-10.99	11.0-11.99	12.0-12.99	13.0-13.99	14.0-14.99	15.0-15.99
2.0 - 2.49	5.490 0.0119 0.1300	4.130 0.0084 0.1440	1.260 0.0059 0.1110									
2.5 - 2.99	5.970 0.0201 0.1810	4.910 0.0094 0.1460	3.370 0.0051 0.1200	1.090 0.0032 0.0950								
3.0 - 3.49	6.350 0.0277 0.1820	5.400 0.0129 0.1470	4.260 0.0069 0.1220	1.650 0.0042 0.0950								
3.5 - 3.99	6.600 0.0359 0.1830	5.770 0.0171 0.1380	4.660 0.0092 0.1240	3.620 0.0055 0.1050	1.210 0.0035 0.0850							
4.0 - 4.49	6.850 0.0485 0.1850	6.070 0.0219 0.1490	5.710 0.0113 0.1240	4.240 0.0067 0.1060	1.560 0.0044 0.0880	1.000 0.0029 0.0750						
4.5 - 4.99		6.290 0.0267 0.1490	5.530 0.0142 0.1250	4.650 0.0083 0.1070	3.460 0.0052 0.0920	1.230 0.0036 0.0760						
5.0 - 5.49		6.490 0.0323 0.1460	5.770 0.0170 0.1250	5.040 0.0102 0.1050	4.040 0.0062 0.0930	1.770 0.0043 0.0760	1.020 0.0030 0.0680					
5.5 - 5.99		6.620 0.0390 0.1500	5.840 0.0180 0.1260	5.280 0.0119 0.1090	4.460 0.0074 0.0950	3.230 0.0050 0.0820	1.230 0.0036 0.0690					
6.0 - 6.49		6.830 0.0455 0.1500	6.170 0.0239 0.1260	5.490 0.0138 0.1090	4.800 0.0098 0.0950	3.810 0.0058 0.0830	1.560 0.0041 0.0700	1.010 0.0029 0.0620				
6.5 - 6.99		6.560 0.0523 0.1500	6.320 0.0274 0.1260	5.540 0.0143 0.1090	5.020 0.0100 0.0950	4.230 0.0067 0.0840	2.700 0.0047 0.0730	1.180 0.0035 0.0630				
7.0 - 7.49			6.490 0.0323 0.1270	5.870 0.0185 0.1090	5.220 0.0119 0.0950	4.480 0.0075 0.0840	3.220 0.0050 0.0740	1.450 0.0040 0.0640				
7.5 - 7.99			6.610 0.0353 0.1270	6.020 0.0210 0.1090	5.440 0.0133 0.0960	4.770 0.0087 0.0850	3.630 0.0059 0.0750	1.920 0.0044 0.0650				
8.0 - 8.49			6.730 0.0410 0.1270	6.150 0.0235 0.1090	5.590 0.0148 0.0960	4.950 0.0097 0.0850	4.250 0.0067 0.0760	2.550 0.0048 0.0670	1.260 0.0035 0.0580			
8.5 - 8.99			6.870 0.0475 0.1280	6.300 0.0263 0.1090	5.750 0.0165 0.0960	5.120 0.0107 0.0850	4.540 0.0074 0.0760	3.500 0.0053 0.0690	1.540 0.0041 0.0590	1.040 0.0030 0.0510		
9.0 - 9.49			6.990 0.0523 0.1290	6.410 0.0293 0.1100	5.850 0.0185 0.0960	5.330 0.0123 0.0850	4.710 0.0084 0.0770	3.910 0.0060 0.0690	2.050 0.0045 0.0600	1.140 0.0034 0.0540		
9.5 - 9.99				6.510 0.0329 0.1100	5.960 0.0193 0.0960	5.470 0.0136 0.0860	4.870 0.0092 0.0770	4.130 0.0069 0.0690	3.020 0.0048 0.0610	1.520 0.0038 0.0540		
10.0 - 10.49				6.800 0.0359 0.1120	6.110 0.0227 0.0960	5.560 0.0147 0.0860	5.010 0.0100 0.0770	4.360 0.0070 0.0700	3.450 0.0052 0.0610	1.680 0.0043 0.0550		
10.5 - 10.99				6.690 0.0334 0.1100	6.210 0.0249 0.0970	5.690 0.0160 0.0850	5.150 0.0109 0.0770	4.580 0.0079 0.0700	3.760 0.0057 0.0630	2.150 0.0045 0.0560	1.190 0.0035 0.0500	
11.0 - 11.49				6.770 0.0427 0.1120	6.300 0.0269 0.0970	5.830 0.0175 0.0860	5.260 0.0117 0.0770	4.730 0.0085 0.0700	4.000 0.0061 0.0640	2.830 0.0047 0.0570	1.290 0.0037 0.0500	
11.5 - 11.99				6.880 0.0480 0.1110	6.360 0.0290 0.0970	5.890 0.0188 0.0860	5.420 0.0132 0.0780	4.870 0.0097 0.0700	4.270 0.0068 0.0640	3.360 0.0051 0.0580	1.570 0.0042 0.0510	
12.0 - 12.49				6.950 0.0520 0.1110	6.470 0.0316 0.0970	5.980 0.0202 0.0860	5.540 0.0143 0.0780	4.970 0.0098 0.0700	4.420 0.0073 0.0640	3.710 0.0055 0.0580	2.050 0.0045 0.0520	
12.5 - 12.99					6.540 0.0339 0.0970	6.110 0.0227 0.0870	5.640 0.0154 0.0780	5.110 0.0106 0.0700	4.550 0.0078 0.0640	3.520 0.0058 0.0580	2.670 0.0047 0.0530	
13.0 - 13.49					6.610 0.0363 0.0970	6.190 0.0249 0.0870	5.730 0.0165 0.0780	5.230 0.0114 0.0700	4.650 0.0082 0.0640	4.100 0.0064 0.0590	3.120 0.0052 0.0536	
13.5 - 13.99					6.680 0.0390 0.0970	6.270 0.0261 0.0870	5.810 0.0176 0.0780	5.360 0.0126 0.0720	4.810 0.0089 0.0650	4.250 0.0069 0.0590	3.540 0.0052 0.0540	
14.0 - 14.49					6.750 0.0419 0.0970	6.340 0.0280 0.0870	5.890 0.0186 0.0780	5.460 0.0136 0.0710	4.950 0.0096 0.0650	4.350 0.0070 0.0590	3.650 0.0055 0.0540	
14.5 - 14.99					6.840 0.0450 0.0970	6.410 0.0299 0.0870	5.960 0.0198 0.0780	5.540 0.0143 0.0710	5.090 0.0105 0.0650	4.440 0.0073 0.0590	3.780 0.0057 0.0550	2.360 0.0042 0.0500

Sea state is defined in terms of H_s and T_z. Numbers in grids are:

top line : γ

second line: α

third line : f_m [sec^{-1}]

Example:

H_s = 9.0 - 9.49 m and

T_z = 9.0 - 9.99 sec

gives

γ = 5.330

α = 0.0123

f_m = 0.0850 sec^{-1}

$\bar{T}$ = 10.09 sec

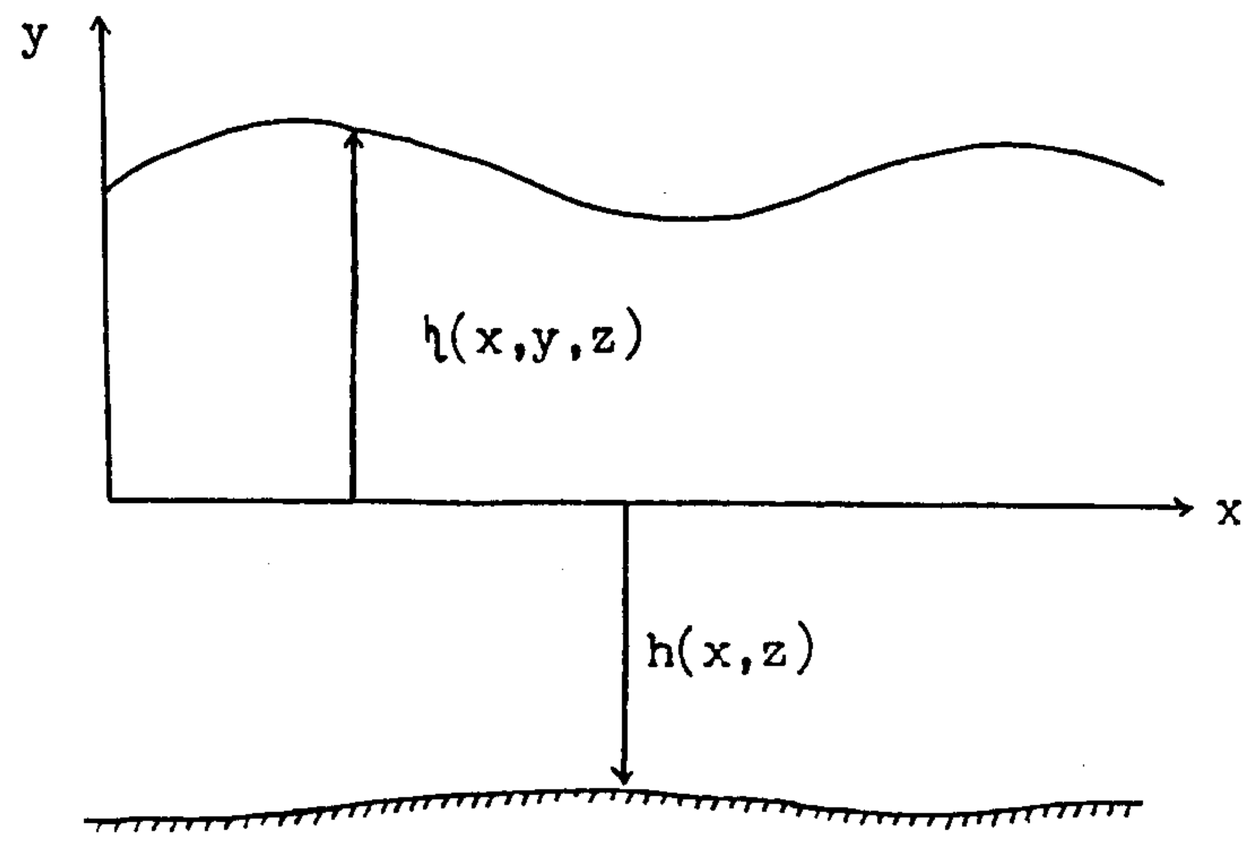

FIG. B.1 THE FLUID REGION

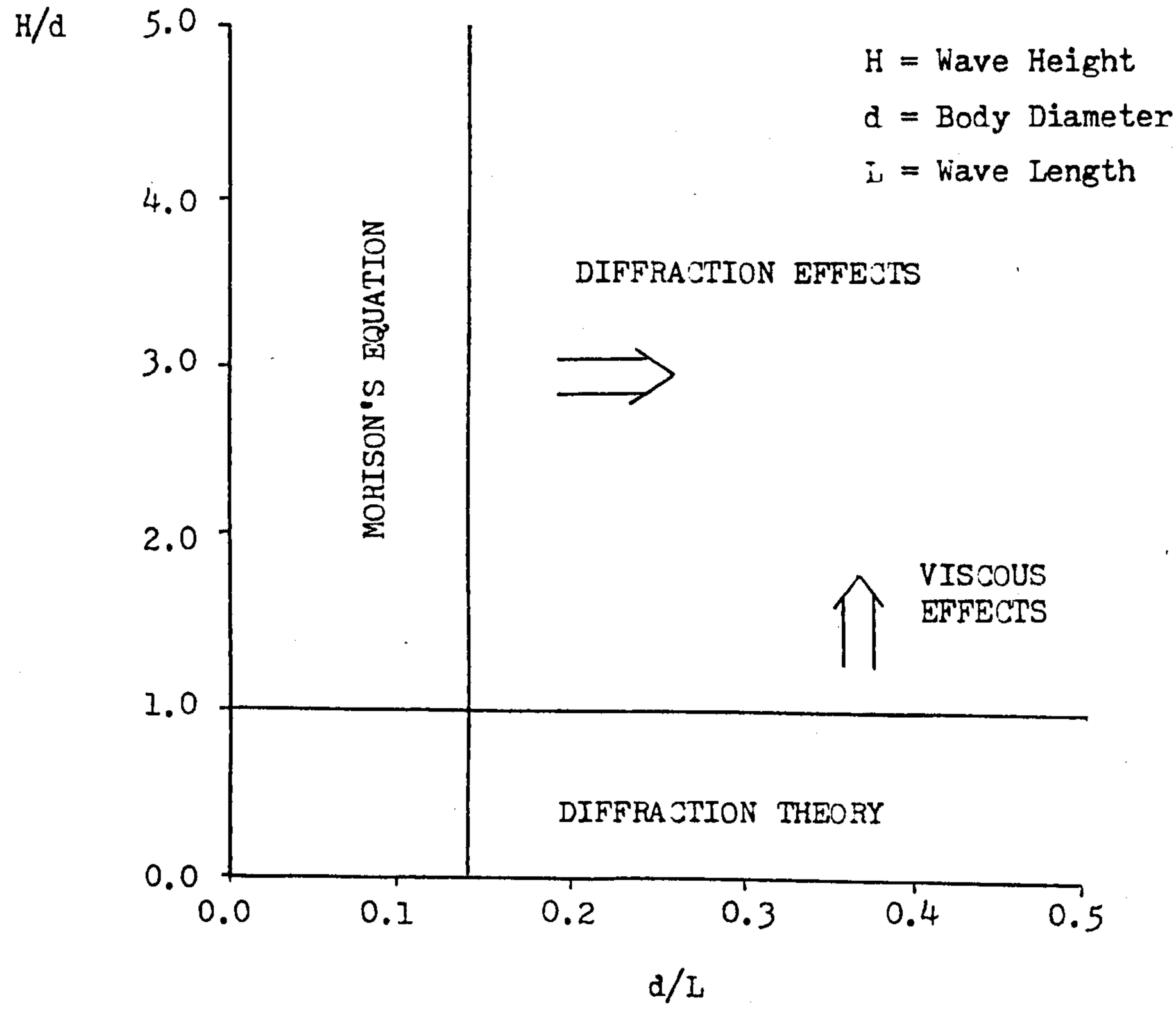

FIG. C.1 REGIONS OF VALIDITY OF METHODS OF CALCULATING THE WAVE FORCES ON A BODY

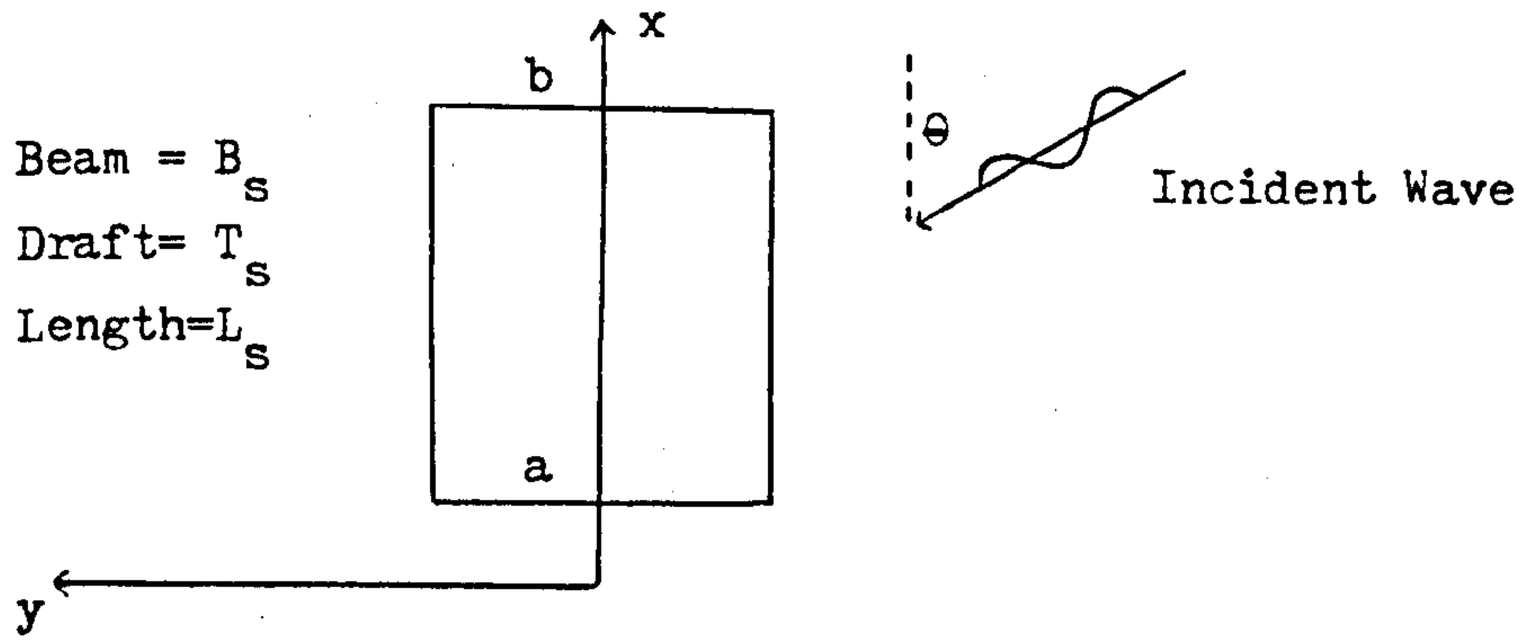

FIG. D.1 SHIP SECTION

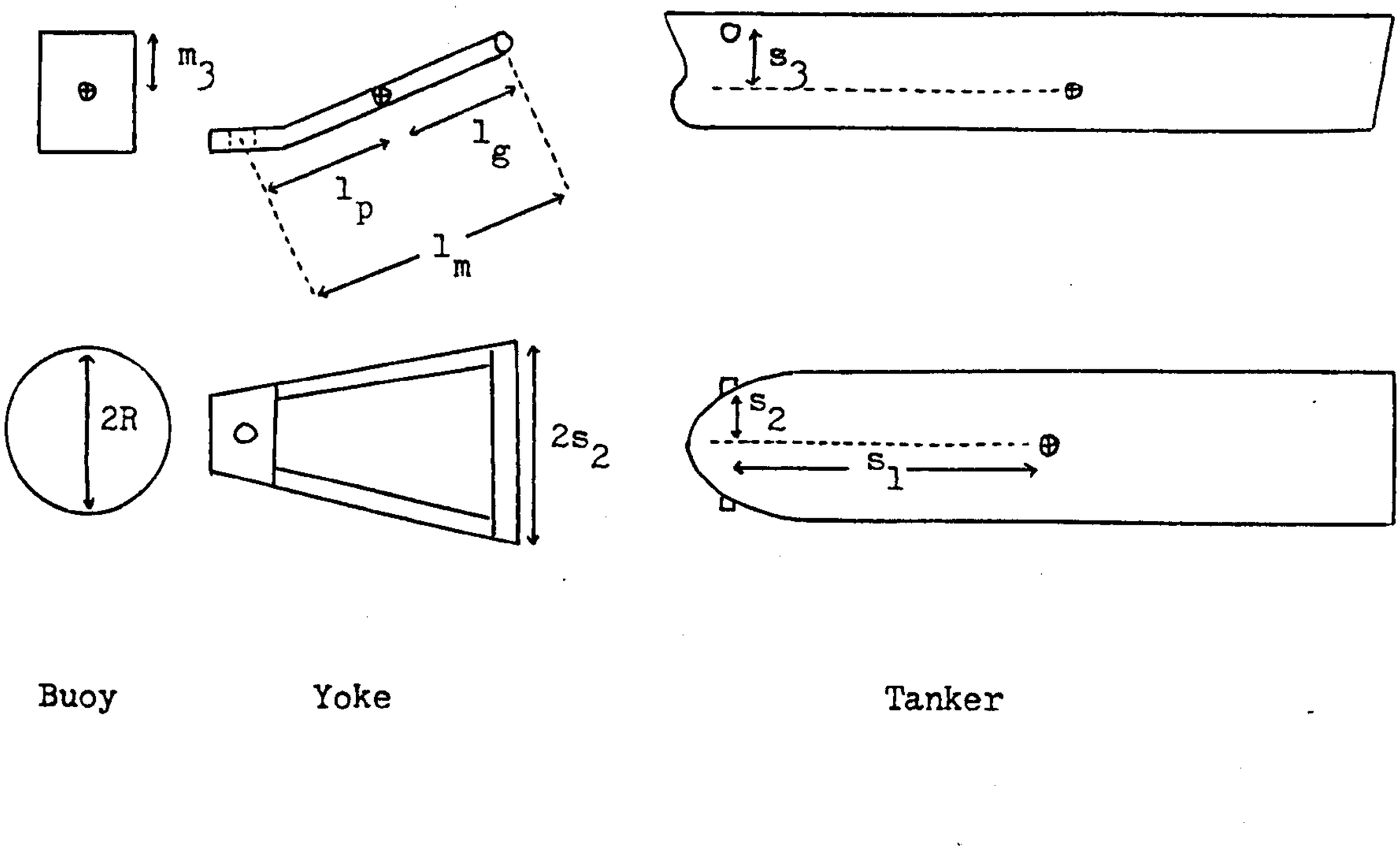

FIG. G.1 DIMENSIONS OF THE SYSTEM